STUDY AND DESIGN OF CRYOGENIC PROPELLANT ACQUISITION SYSTEMS
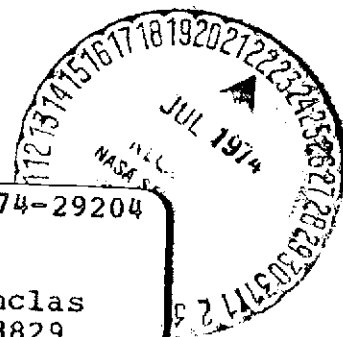
VOLUME I
DESIGN STUDIES

Final Report
December 1973

by

G. W. Burge
J. B. Blackmon, Ph.D.

McDonnell Douglas Astronautics Company
Huntington Beach, California 92647

Prepared for

NATIONAL AERONAUTICS AND SPACE ADMINISTRATION
Marshall Space Flight Center
Huntsville, Alabama
Contract NAS8-27685

MDC G5038

STUDY AND DESIGN OF CRYOGENIC
PROPELLANT ACQUISITION SYSTEMS
VOLUME I
DESIGN STUDIES

Final Report
December 1973

by

G. W. Burge
J. B. Blackmon, Ph.D.

McDonnell Douglas Astronautics Company
Huntington Beach, California 92647

Prepared for

**MCDONNELL
DOUGLAS**
CORPORATION

ABSTRACT

This program involved an in-depth study and selection of practical propellant surface tension acquisition system designs for two specific future cryogenic space vehicles, an advanced cryogenic space shuttle auxiliary propulsion system and an advanced space propulsion module. A supporting laboratory scale experimental program was also conducted to provide design information critical to concept finalization and selection. Designs using localized pressure isolated surface tension screen devices were selected for each application and preliminary designs were generated. Based on these designs, large scale acquisition prototype hardware was designed and fabricated to be compatible with available NASA-MSFC feed system hardware.

i

PREFACE

PRECEDING PAGE BLANK NOT FILMED

CONTENTS

FIGURES

TABLES

APPENDICES

SECTION 1. INTRODUCTION AND SUMMARY

To insure maximum space propulsion system performance and safe and reliable rocket engine operation, the space vehicle propellant feed system must generally be designed to provide liquid phase propellants to the engine system at startup and throughout the firing period. This is an especially critical requirement for systems which must provide multiple on-demand engine burns using cryogens with pump-fed engines. Because of the near zero gravity or adverse accelerations experienced by typical space vehicle feed subsystems, it is essential that positive means be provided for acquiring and transferring the tanked liquids to the engines. The application of essentially passive surface-tension acquisition/expulsion devices to satisfy this requirement offers significant potential advantages in terms of minimum weight, long life, high reliability, and vehicle flexibility and adaptability when compared to bladder/bellows type expulsion devices and pure acceleration settling concepts. Concepts that enhance capabilities for long life and flexibility are especially important for advanced reusable vehicles such as the Space Shuttle system.

Relatively simple surface-tension acquisition devices have been used previously in storable propellant spacecraft and missile propulsion systems, and limited research and development has been conducted to explore the design criteria for surface-tension acquisition/expulsion concepts. Although baffles, standpipe and other relatively large characteristic dimension capillary devices have been considered for achieving acquisition in very low-g and small tankage application, the more general acceleration loads and tank sizes encountered in typical advanced applications are such that very small characteristic dimension devices (10 to 1000 micron pore sizes) as those associated with fine mesh screen, are mandatory to reliably provide adequate flow. Therefore, in July 1971, an in-depth study was initiated by McDonnell Douglas Astronautics Company (MDAC) under the sponsorship of the National Aeroanutics and Space Administration, Marshall Space Flight Center (NASA-MSFC) to study and define screen surface tension acquisition systems to satisfy advanced cryogenic propulsion system requirements. It was also anticipated that this effort would expand, in general, the basic technology of in-orbit fluid acquisition and transfer.

During the study, two specific applications were addressed: (1) an advanced cryogenic Space Shuttle Auxiliary Propulsion System (CSS/APS); and (2) an advanced space propulsion module (ASPM) similar to a Space Tug. The specific requirements for these applications are summarized in Section 2 of Volume I. Detailed analytical design studies were independently conducted for each application as documented in Section 3 for the CSS/APS and Section 4 for the ASPM.

Because of the strong interactions between the various cryogenic feed subsystems such as acquisition, pressurization, and thermal control, all concept evaluations, comparisons, and selections were made on a total cryogen feed system basis. It was found that the constraints and compromises that had to be imposed on these interfacing subsystems to accommodate a particular acquisition concept had a major influence on establishing the overall desirability of a given concept. Factors considered in establishing and selecting appropriate system designs included weight, inherent reliability, operational flexibility, practicality of fabrication and assembly, availability of required design technology, and feasibility of ground-based development and design verification testing.

In addition to the extensive analytical design studies, a supporting laboratory scale experimental program was conducted to provide data necessary to support the design effort and to substantiate critical aspects of the selected system designs. All experimental efforts are documented in Volume II of this report.

In the final phase of this program, large scale test prototype acquisition hardware was designed and fabricated for the system selected for each application. This hardware was designed to be compatible with a LH_2/LO_2 auxiliary propulsion system breadboard being developed by NASA/MSFC as part of a major technology development program. Two separate prototype acquisition systems were built to be compatible with the CSS/APS and ASPM designs, both of which can be simultaneously installed in an available NASA "105-inch" LH_2 tank system. Details of the prototype hardware are documented in Section 5 of Volume I of this report.

1.1 Selected Design CSS/APS Application

The acquisition concept selected for the CSS/APS application is a localized pressure isolated and refillable screen channel (see Figure 3.4.7). The LH_2 surface tension device itself consists of two 1.6 M (5.2 ft) *diameter segmented rings intersecting at 90°. Each ring channel is made up of six straight all screen sections forming approximately a hexagon. The channel has a 17.8 cm (7 inch) circular cross-section formed by a perforated aluminum tube covered first by a coarse aluminum screen and, then, a 200 x 600 mesh stainless steel screen. The fine mesh is the retention element; the perforated tube provides structural support for the fine mesh; and the coarse mesh screen serves to reduce flow-through pressure loss. The channel sections are connected together by standard Marman V-band couplings, and the complete channel is supported within the tank by a tension cable system. The acquisition channels are installed in the aft region of the main cryogen tank within a separate 12.6 M^3 (450 ft^3) secondary tank formed by a common bulkhead within the main tank. The acquisition device supplies cryogen for engine startup and short engine burns and is refilled during long periods of high positive acceleration during the mission. This secondary tank is always pressurized with LH_2 temperature helium stored in a pressure bottle within the main tank, but the main portion of the LH_2 tank is pressurized with 111°K (200°R) GH_2 bled from the propulsion system. Thermal control

---

*All calculations in this study were generally made using English units. Conversion was then made to SI units per contractual requirements.

provisions consist of the following: (1) a helium-purged multilayer insulation (MLI) system for the LH_2 tank; (2) a non-vented LH_2 tank using an internal tank pump/mixer to eliminate temperature stratification; (3) a foam-insulated common bulkhead; (4) an LH_2 vapor shield around the aft portion of the LH_2 tank to provide acquisition device thermal protection; and (5) LH_2 vapor cooled feedlines and pumps. The LO_2 system is similar in design concept, except for smaller dimensions. The LO_2 tank also uses the hydrogen bleed fluid as a coolant in a cooling shield to maintain the LO_2 tank in a non-vented condition.

The total feed system weight, including all tankage and thermal control provisions, was estimated at 1,558 kg (3,432 lb) for LH_2 and 557 kg (1,227 lb) for LO_2.

1.2 Selected Design — ASPM

The system selected for the ASPM application also utilizes a localized and refillable pressure isolated screen acquisition concept. In this case, because of the higher destablizing accelerations, a baffled secondary tank is used, and the screen retention elements are a series of cylindrical elements using pleated mesh (see Figure 4.1.8). The LH_2 tank thermal control system in this application optimized out to be a continuously vented tank with a full vapor-cooled shield. The hydrogen vent gases are also used to cool the LO_2 tank via a cooling shield to maintain a non-vented condition. This total system, including tankage, weighs 580 kg (1,277 lb) for the LH_2 side and 355 kg (782 lb) for the LO_2 side. This selected system can be completely developed and operationally verified through ground based testing.

1.3 Supporting Experimental Program

Laboratory-class experiments were conducted in the following areas: (1) bubble point characteristics with LH_2; (2) screen flow losses; (3) multiple-screen flow behavior; (4) influence of vibration on screen retention; (5) effects of heat transfer on screen retention; (6) welding process effects on screen integrity; (7) fatigue effects on screen integrity; (8) adequacy of coupling seals for acquisition devices; (9) feasibility of screen repair patching techniques; and (10) feasibility of liquid film bubble point verification testing. Although these tests accomplished much in establishing the validity of the developed designs and to expand the technology base in the area of surface tension acquisition, several areas remain which require additional investigation emphasizing experimental research:

a.   Effects of warm pressurant gas heat transfer on screen retention capability

b.   Influence of vibration on surface tension device behavior

c.   Effects of feed system dynamics on screen device performance.

SECTION 2. REQUIREMENTS

To achieve the objectives of this program, the acquisition/expulsion systems were studied and evaluated in depth for two specific but significantly different LH_2/LO_2 space propulsion applications. These included an advanced Cryogenic Space Shuttle Auxiliary Propulsion System (CSS/APS) and a primary propulsion multiburn Advanced Space Propulsion Module (ASPM). Total system requirements were developed by drawing on other current or recently-completed system studies performed relative to these applications. The accumulated requirements then formed the basis for the feed system studies and preliminary designs reported in the subsequent sections of this report.

2.1 Cryogenic Space Shuttle Auxiliary Propulsion Application.

The CSS/APS feed system design was based on the general system design generated under contract NAS8-26248, and overall requirements were taken from the results of this study as reported in Reference 1. Some of these overall requirements are summarized in Tables 2.1, 2.2 and 2.3. Table 2.1 summarizes requirements for three representative shuttle-type missions. The APS was sized for a nominal 610 m/sec (2000 ft/sec) total ΔV with a total propellant load of 22,700 kg (49,980 lb).

In this application, the cryogenic feed system supplies subcooled cryogens for two integrated propulsion functions, including orbit maneuvering (OM) propulsion (two 66.7×10^3 Newton [15K lb] thrusters) and attitude control (AC) propulsion (4.45×10^3 [1K lb] thrusters). The feed system also stores cryogens for auxiliary power and life support functions. Table 2.2 shows the cryogen load distribution and reveals that most of the fluid is dedicated for OM functions.

Each of these functional requirements pose different conditions for the storage and feed system. In the case of the OM functions, relatively well-defined periods of high thrust with high flow rates are involved. For the AC functions, the system may be called upon to provide a low flow rate of subcooled cryogen, but the flow demand may be for one short burst or pulse or a series of short firing bursts. In this particular system, the thrusters have been ground ruled as operating off gas accumulators, as shown in the system schematic of Figure 2.1. Thus, cryogen transfer takes place from the storage tanks to the accumulators via a turbopump, rather than to the thrusters directly, and the pump does not operate with the same short pulses as would be the case with the thrusters. The discharge from the tanks is actually governed by the accumulator recharge demand, rather than the engine demand, except for the case of very long engine burn periods, such as with the OM firings. The impulse requirements which establish the feed system flow demands are shown in Figures 2.2, 2.3, and 2.4 for the three representative mission duty cycles. Gross requirements are shown in Table 2.3.

An overall picture of the cryogen demand can be obtained by summarizing the tank ullage values at critical points in the mission for the three baseline flight profiles (see Table 2.4). This shows that there is usually a large initial ullage, as high as 34 percent, and that the tank is always about 40 percent empty after the first hour. Twenty to 50 percent of the cryogen

TABLE 2-1
MISSION PARAMETERS

Parameter	Design Easterly	Polar	Resupply
ORBIT ALTITUDE, NMI	100	100	100
ORBIT INCLINATION (DEG)	28.5	90	55
PAYLOAD	29,500 KG (65,000 LB)	18,200 KG (40,000 LB)	11,350 KG (25,000 LB)
MISSION DURATION (DAYS)	7	7	7
OMS ΔV	274 M/SEC (900 FT/SEC)	198 (650)	457 (1,500)
APS PROPELLANT LOAD LH$_2$	3,220 (7,099)	4,280 (9,421)	4,106 (9,057)
LO$_2$	9,760 (21,513)	14,910 (32,854)	13,810 (30,418)
TOTAL	12,980 KG (28,612 LB)	19,190 KG (42,275 LB)	17,916 KG (39,475 LB)
DESIGN PROPELLANT LOAD (2,000 FT/SEC) LH$_2$		4,750 (10,444)	
LO$_2$		17,950 (39,536)	
		22,700 KG (49,980 LB)	

TABLE 2-2
CRYOGEN LOAD DISTRIBUTION, KG (LB)

Item	Design Easterly LH$_2$ KG (LB)	Design Easterly LO$_2$ KG (LB)	Polar LH$_2$ KG (LB)	Polar LO$_2$ KG (LB)	Resupply LH$_2$ KG (LB)	Resupply LO$_2$ KG (LB)
OMS	1,340 (2,953)	6,830 (15,054)	2,400 (5,280)	11,990 (26,420)	2,035 (4,492)	10,200 (22,463)
ACPS	256 (565)	906 (1,995)	256 (560)	895 (1,970)	447 (984)	1,585 (3,491)
AC EXPENDABLES			333 (734)	1,176 (2,591)		
IN-FLIGHT LOSSES (Preliminary)			664 (1,463)	12 (26)		
RESIDUALS			250 (551)	359 (793)		
FUEL CELLS			32 (71)	258 (569)		
AUXILIARY POWER			240 (528)	193 (425)		
ELS			105 (234)	27 (60)		
SUBTOTALS	3,220 (7,099)	9,760 (21,513)	4,280 (9,421)	14,910 (32,854)	4,106 (9,057)	13,810 (30,418)
TOTALS	12,980 (28,612)		19,190 (42,275)		17,916 (39,475)	

OMS = ORBIT MANEUVERING PROPULSION SYSTEM
ACPS = ATTITUDE CONTROL PROPULSION SYSTEM
ELS = ENVIRONMENTAL LIFE SUPPORT

TABLE 2.3
GENERAL REQUIREMENTS (CSS/APS)

ORBIT (NMI)	100
ORBIT INCLINATION ($^\circ$)	28.5
PAYLOAD	29,510 kg (65,000 lb)
ORBIT TIME (DAYS)	7
PROPELLANT LOAD	
LH$_2$	4742 kg (10,444 lb)
LO$_2$	17950 kg (39,536 lb)
DESIGN ΔV	610 m/sec (2000 ft/sec)
MAXIMUM ACCELERATION	
ON-ORBIT (G)	±0.045 (X, Y, Z)
REENTRY (G)	1.25 (Z)
	0.08 (X)
BOOST (G)	3.00 (X)
FLOW RATES	
LH$_2$	0-4.54 kg/sec (0-10 lb/sec)
LO$_2$	0-22.7 kg/sec (0-50 lb/sec)
TANK DIAMETER	
LH$_2$	3.66M (12 ft)
LO$_2$	2.44M (8 ft)
TANK VOLUMES	
LH$_2$	69.4M^3 (2450 ft^3)
LO$_2$	16.1M^3 (570 ft^3)
TANK SURFACE	
LH$_2$	89.7M^2 (967 ft^2)
LO$_2$	38.2M^2 (412 ft^2)

is used for reentry. All missions require AC propellant during coasts, which requires on-demand low-flow-rate propellant flow.

2.2 Advanced Space Propulsion Module (ASPM)

This application differs from the CSS/APS application in that the ASPM is a primary propulsion module, most of the module gross weight is usable propellant, and applied accelerations are relatively high.

Recent NASA, Air Force, and MDAC study reports were reviewed to evolve a set of design factors and operational characteristics that would be representative of an advanced spacecraft propulsion system and could serve
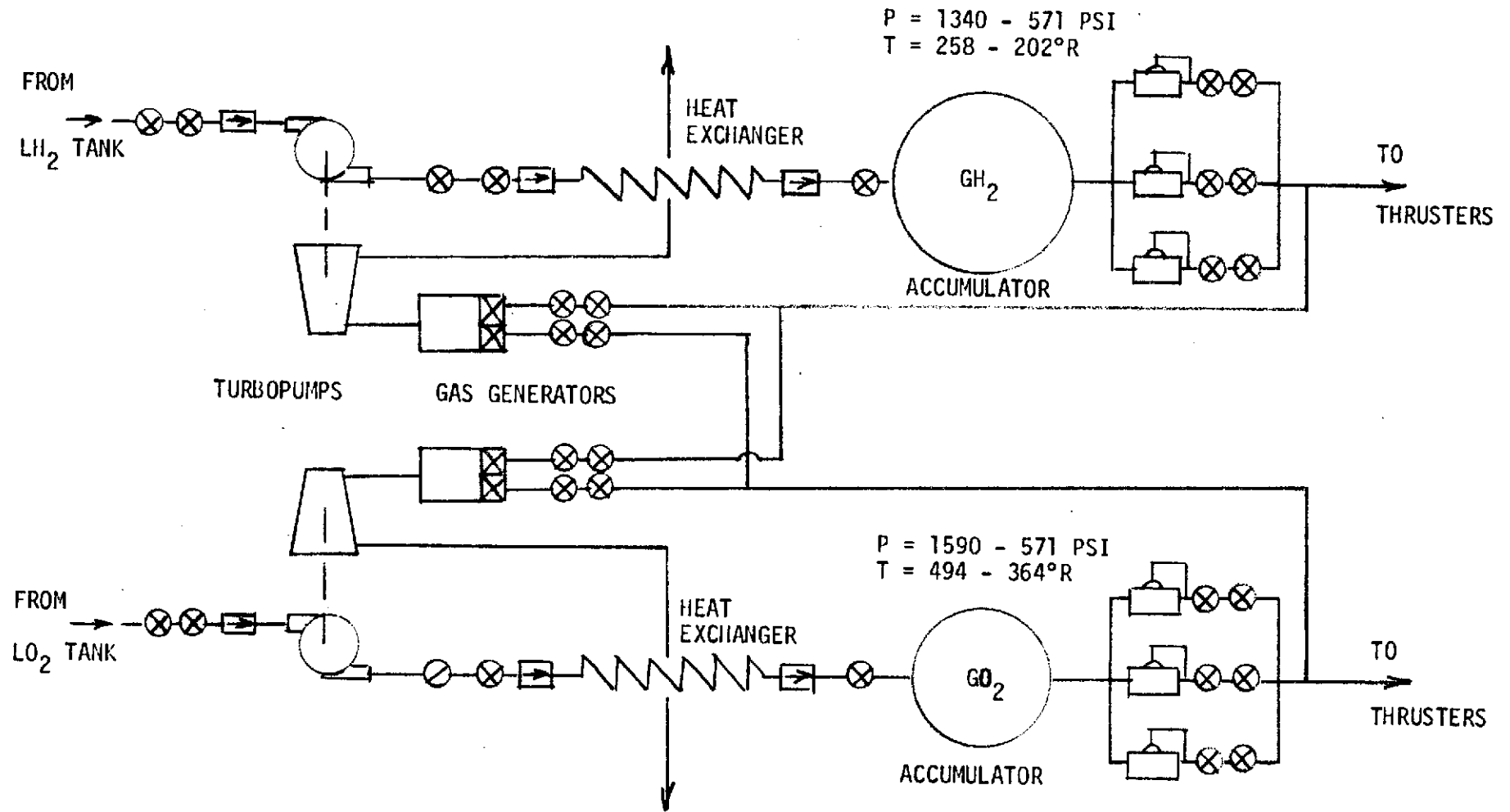
Figure 2.1. Typical CSS/APS Accumulator Conditioning System Schematic
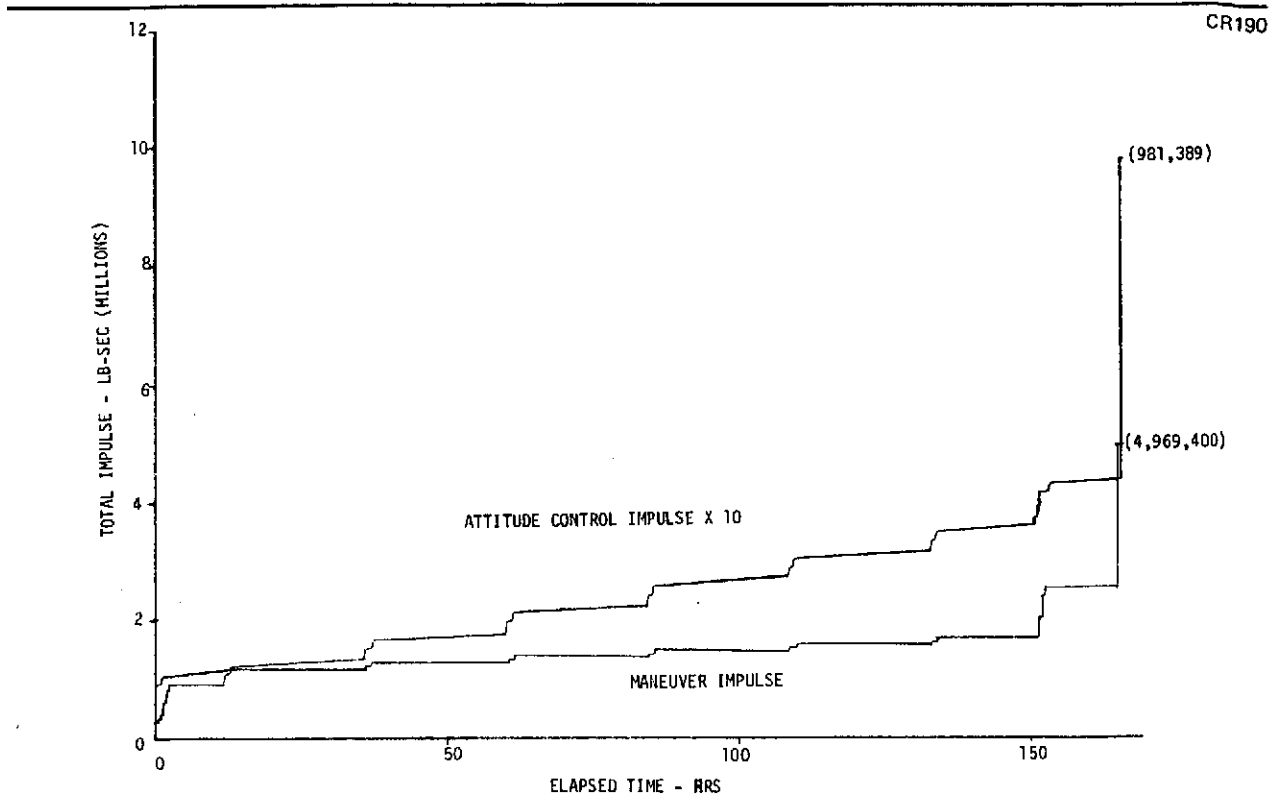
Figure 2.2. Impulse Requirements — Easterly Mission
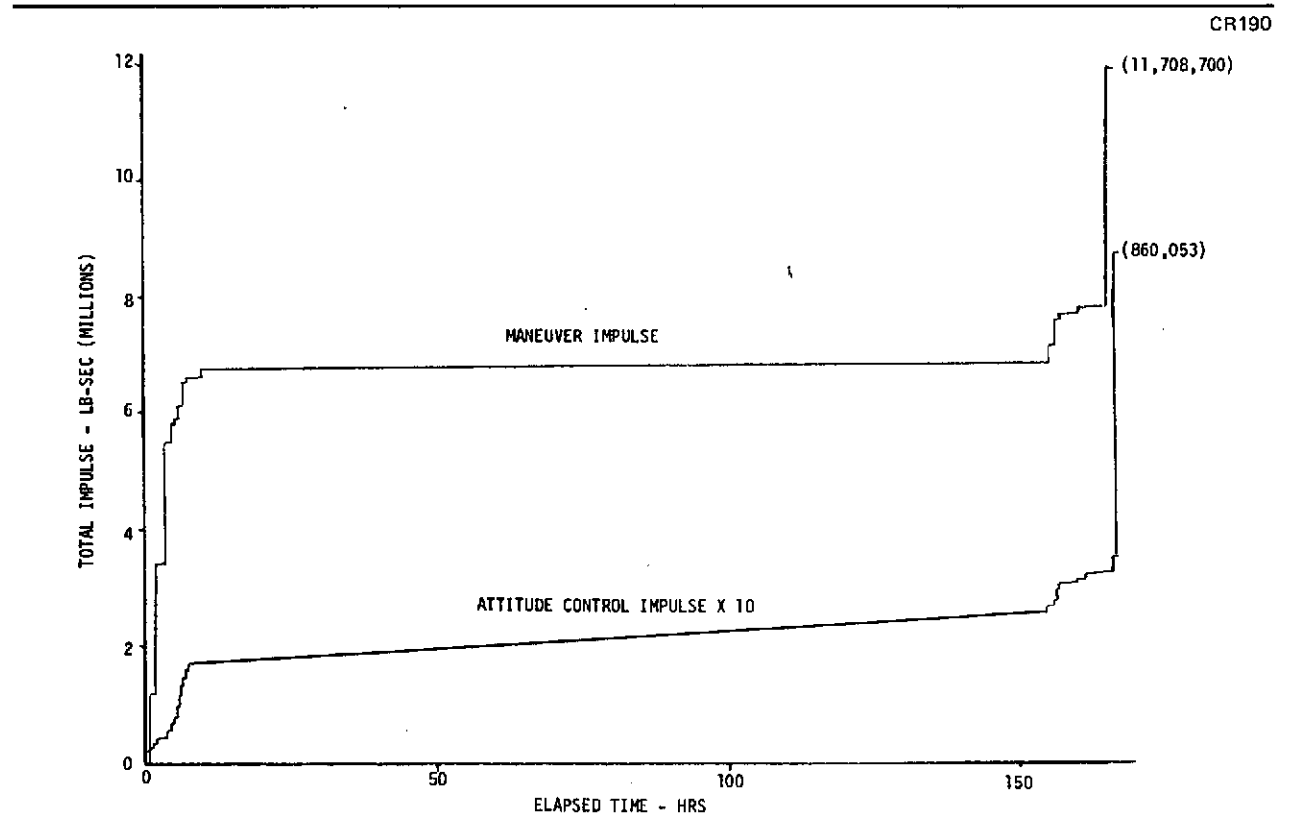
Figure 2.3. Impulse Requirements — Resupply Mission
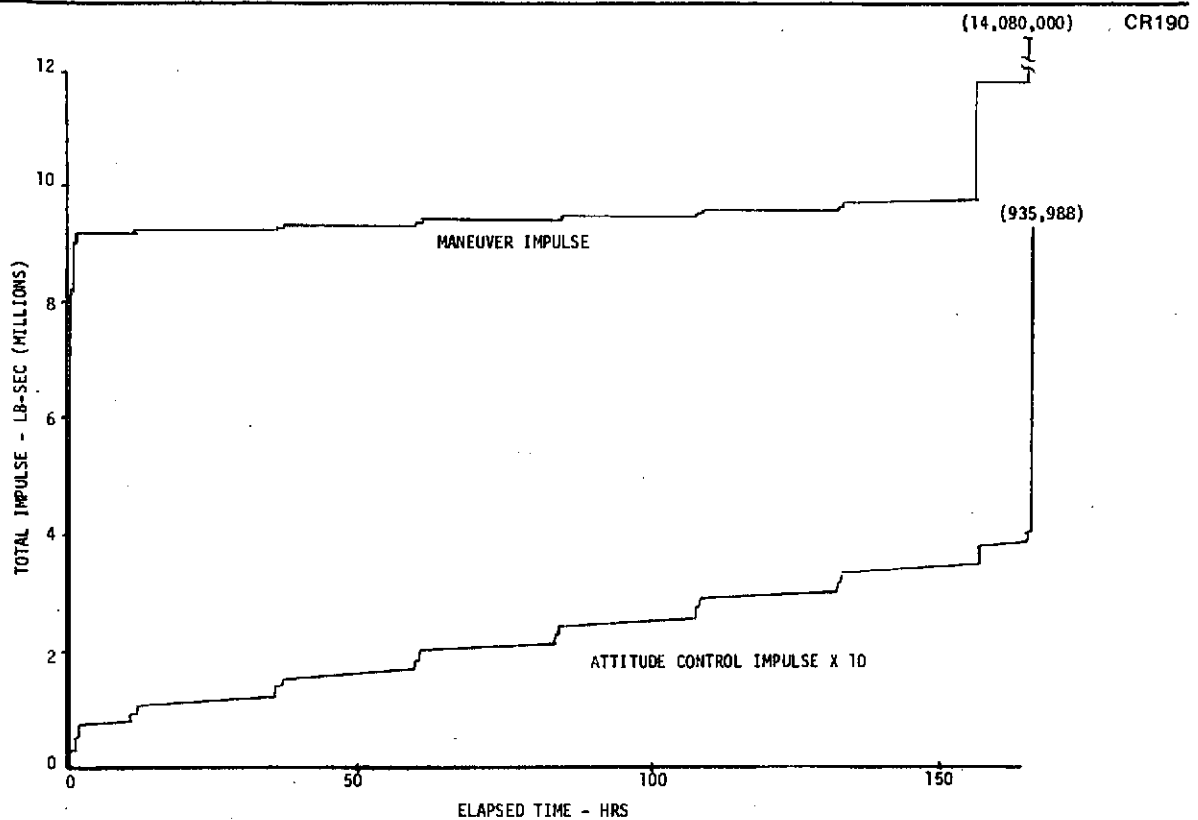
Figure 2.4. Impulse Requirements — Polar Mission

TABLE 2.4

REPRESENTATIVE ULLAGE HISTORY – SHUTTLE
CRYOGENIC APS

Mission	Easterly	Resupply	Polar
INITIAL ULLAGE (PERCENT)	34	16	12.7
ULLAGE AFTER FIRST HOUR (PERCENT)	40	41	46
ULLAGE PRIOR TO REENTRY (PERCENT)	75	50	66
FINAL ULLAGE (PERCENT)	95	95	95
MANEUVERING IMPULSES DURING COAST	YES	NO	YES
ACS IMPULSES DURING COAST	YES	YES	YES
AUXILIARY SYSTEM FLOW DURING·COAST	YES	YES	YES

as a basis for acquisition system preliminary design/comparisons. The
selected overall characteristics are summarized in Table 2.5. These parallel
very closely the baseline Space Tug requirements as defined by NASA/MSFC.
(Reference 2). The Space Tug acts as a third stage for the Space Shuttle
vehicle. Its function is to deploy and retrieve payloads in specific orbits

9

TABLE 2.5

ADVANCED CRYOGENIC SPACECRAFT PROPULSION MODULE
(ASPM) GENERAL CHARACTERISTICS

Dimensions		
Stage maximum diameter	4.57 m	(15 ft)
Propulsion module length	10.7 m	(35 ft)
Weights		
Propulsion module dry weight	2,360 kg	(5,200 lb)
Residual weights	454 kg	(1,000 lb)
Propulsion module burnout weight	2,820 kg	(6,200 lb)
Usable propellants	2,470 kg	(54,400 lb)
Propulsion module gross weight	27,500 kg	(60,600 lb)
Tug charged-interface	636 kg	(1,400 lb)
Minimum payload	1,360 kg	(3,000 lb)
Maximum stage gross weight	29,500 kg	(65,000 lb)
Engine Variables		
Main Engine Thrust	44,500 Newtons	(10,000 lb)
Main Engine I_{SP}	4,610 Newtons/kg/sec	(470 sec)
RCS Thrust per engine	134 Newtons	(30 lb)
Main Engine O/F	6	
RCS O/F	3	

originally put into near earth orbit by the Shuttle itself. The Air Force has been studying a similar vehicle, the Orbit-to-Orbit Shuttle (OOS) (Reference 3). In both cases, the stages, which use LH_2/LO_2 propellants, are carried into orbit or the payload in the Shuttle cargo bay. The empty Tug/OOS is brought back to earth in the Shuttle cargo bay after each mission. The maximum active mission duration is seven days in orbit.

The propulsion system consists of one main engine with a small RCS unit (assumed to be integrated GH_2/GO_2 thrusters). The propellants are supplied from one LH_2 and one LO_2 tank, both of which are insulated with multi-layer radiation barrier insulation to achieve the 7 days in orbit storage time. The cryogen consumption distribution is shown in Table 2.6 which shows that over 98 percent of the cryogen is used by the main engine.

Table 2.7 shows the baseline burn sequence for a typical payload deployment-retrieval mission. Each stage function is identified with respect to mission time, velocity change (ΔV), active thrusters, propellant consumed, and the applied accelerations. In terms of acquisition system design, the

TABLE 2.6

ADVANCED CRYOGENIC SPACECRAFT PROPULSION MODULE (ASPM) PROPELLANT DISTRIBUTION

	LH$_2$		LO$_2$		Total	
Main Engine	3480 kg	(7,650 lb)	20,900 kg	(45,950 lb)	24,380 kg	(53,600 lb)
RCS	56.8 kg	(125 lb)	171 kg	(375 lb)	227 kg	(500 lb)
Start/Stop Transients	22.7 kg	(50 lb)	23 kg	(50 lb)	45 kg	(100 lb)
Vented	63.5 kg	(140 lb)	0	(0)	65 kg	(140 lb)
Fuel Cell	3.0 kg	(7 lb)	24 kg	(53 lb)	28 kg	(60 lb)
	3626.0 kg	(7,972 lb)	21,118 kg	(46,428 lb)	24,744 kg	(54,400 lb)

TABLE 2.7

BASE-LINE BURN SEQUENCE (DEPLOYMENT/RETRIEVAL MISSION) – ASPM

Activity	Time (hr from launch)	ΔV (Thruster) (m/sec)	Propellant Consumed (kg)	Acceleration Level (g)
Separate from Shuttle	5	3 (RCS)	36	0.00093
Perigee burn	17	2,550 (PP)	12,260	0.154 - 0.263
Midcourse	20	15 (RCS)	91	0.00158 - 0.00159
Apogee burn	22	1,785 (PP)	5,330	0.265 - 0.383
Station keeping	22 - 47	9 (RCS)	25	0.00232
Payload deployment	47	3 (RCS)	9	0.00232 (
Intermediate phasing orbit	95	31 (TPP)	124	0.077 - 0.079
Retrieve payload	97	31 (TPP)	124	0.079
		5 (RCS)	12	0.00326
Deorbit	104	1,784 (PP)	3,540	0.395 - 0.570
Midcourse	108	15 (RCS)	43	0.0034
Perigee burn	110	2,340 (PP)	2,970	0.572 - 1.01
Circularization	112	112 (PP)	108	1.01 - 1.04
Terminal rendezvous	115	30 (TPP)	60	0.209 - 0.21
		5 (RCS)	7	0.0063
Docking	117	3 (RCS)	5	0.0063
Landing	132	–	–	–

(RCS) Reaction Control System	58	228	
(PP) Primary Propulsion	8,571	308	
(TPP) Throttle (20%) Primary Propulsion	92	24,208	
	8,721 m/sec	24,744 kg	

major difference between the ASPM and the cryogenic Space Shuttle APS application is that in the main propulsion application, the maximum acceleration is much higher and the acceleration increases during the mission. In the CSS/APS application, the system mass remains essentially constant, whereas in the ASPM application, the vehicle weight varies from 29, 500 kg (65, 000 lb) to 4, 440 kg (9, 800 lb). Burn sequences for other typical ASPM mission duty cycles are shown in Tables 2. 8, 2. 9, and 2. 10.

TABLE 2. 8

BURN SEQUENCE (DIRECT DEPLOYMENT MISSION)
(PAYLOAD WEIGHT = 4, 100 KG)

Activity	Time (hr from launch)	ΔV (Thruster)* (m/sec)	Propellant Consumed (kg)	Acceleration Level (g)
Separate from Shuttle	5	3 (RCS)	36	0. 0009
Phasing Initiation	6. 1	3 (RCS)	30	0. 001
Plane Change	13. 5	337 (PP)	1, 940	0. 157 - 0. 168
Apogee Burn No. 1	15. 3	2, 190 (PP) (RCS)	10, 100 20	0. 168 - 0. 27
Apogee Burn No. 2	20. 7	1, 795 (PP) (RCS)	5, 330 20	0. 27 - 0. 395
Rendezvous	20. 9	21 (RCS)	40	0. 0024
Deployment	26. 8	3 (RCS)	10	0. 0024
Transfer	35. 6	1, 790 (PP) (RCS)	2, 360 20	0. 6 - 0. 9
Lower Apogee Burn	40. 9	1, 615 (PP) (RCS)	1, 500 10	0. 9 - 1. 28
Mid Course	43. 1	11 (RCS)	15	0. 005
Circularization	43. 2	880 (PP)	617	1. 28 - 1. 55
Terminal Rendezvous	44. 2	22 (RCS)	30	0. 006

*(RCS) Reaction Control System
(PP) Primary Propulsion
(TPP) Throttle (20 percent) Primary Propulsion

TABLE 2.9

BURN SEQUENCE (DIRECT RETRIEVAL MISSION)
(PAYLOAD WEIGHT = 2, 050 KG)

Activity	Time (hr from launch)	ΔV (Thruster)* (m/sec)	Propellant Consumed (kg)	Acceleration Level (g)
Separate from Shuttle	5	3 (RCS)	36	0.0001
Phasing Initiation	6.1	3 (RCS)	30	0.0001
Plane Change	13.5	337 (PP)	1,820	0.166 - 0.178
Apogee Burn No. 1	15.3	2,190 (PP) (RCS)	9,650 20	0.178 - 0.283
Apogee Burn No. 2	20.7	1,795 (PP) (RCS)	5,140 20	0.283 - 0.415
Rendezvous	20.9	21 (RCS)	40	0.0053
Docking and Pickup	26.8	3 (RCS)	10	0.0031
Plane Change	35.6	1,790 (PP) (RCS)	4,130 20	0.35 - 0.51
Lower Apogee Burn	40.9	1,615 (PP) (RCS)	2,630 10	0.51 - 0.73
Mid Course	43.1	11 (RCS)	15	0.0044
Circularization	43.2	880 (PP)	1,090	0.73 - 0.89
Terminal Rendezvous	44.2	22 (RCS)	30	0.0053

*(RCS) Reaction Control System
(PP) Primary Propulsion
(TPP) Throttle (20 percent) Primary Propulsion

TABLE 2.10

BURN SEQUENCE (INTERPLANETARY VENUS MISSION)
(PAYLOAD WEIGHT = 1, 060 KG)

Activity	Time (hr from launch)	ΔV (Thruster)* (m/sec)	Propellant Consumed (kg)	Acceleration Level (g)
Separate from Shuttle	5	3 (RCS)	36	0.0009
Perigee Burn No. 1	8	2,100 (PP) (RCS)	14,050 20	0.16 - 0.316
Apogee Burn No. 2	12	2,100 (PP) (RCS)	4,560 15	0.31 - 0.505
Payload Deployment	12.2	3 (RCS)	10	0.003
Rotate Stage	12.3	1 (RCS)	5	0.003
Retro-Burn	12.4	1,800 (PP) (RCS)	2,550 10	0.58 - 0.856
Deorbit	60	1,610 (PP) (RCS)	1,875 10	0.86 - 1.22
EOS Base Rendezvous	61	1,340 (PP) (RCS)	956 10	1.22 - 1.64
Docking	62	22 (RCS)	30	0.01

*(RCS) Reaction Control System
(PP) Primary Propulsion
(TPP) Throttle (20 percent) Primary Propulsion

SECTION 3. TECHNICAL DESIGN STUDIES: CRYOGENIC SHUTTLE AUXILIARY PROPULSION SYSTEM

In approaching the design development of a surface tension acquisition subsystem for cryogenic propellants, it became obvious early in the study that this was to a high degree a total integrated feed system problem. It was found that the designs of the interfacing subsystems, such as pressurization and thermal management, interact and are greatly influenced by the acquisition device features and design criteria. Thus, valid acquisition design decisions must be made on a total feed system basis after taking all the various interactions into account. Therefore, although the study was primarily directed toward acquisition subsystems, it was necessary to give detailed attention to the design of the other interfacing subsystems.

The basic approach and results of this study are reported separately for each of the two applications, and each application is divided into four sections: (1) Acquisition Subsystem; (2) Pressurization Subsystem; (3) Thermal Management Subsystem; and (4) Feed System Integration/Comparison. In this last section, the various subsystems are brought together into an integrated feed system for each acquisition concept selected for detailed analysis and evaluation. This is concluded by making a preliminary design selection for each application. In reality, each subsystem was studied more or less in parallel with continuous feedback and interchange of information. Thus, each study area was influenced by the others as the effort progressed and a conscientious attempt was made to avoid irrelevant paths of investigation.

The CSS/APS application was investigated prior to the ASPM case, and the parametric work developed for the CSS/APS was used directly when it applied to the ASPM investigation reported in Section 4, which in its organization closely parallels Section 3.

3.1 Acquisition/Expulsion Subsystem

The basic requirement for the CSS/APS surface tension acquisition/expulsion subsystem is to provide all liquid-phase, subcooled LH_2 and LO_2 to the APS pumps on a nearly on-demand basis under the maximum destabilizing conditions that may occur during vehicle operation. To achieve this, a subsystem is normally designed for installation within the propellant tank, which consists essentially of a specially designed reservoir or communication device that transmits liquid from its location in the tank (as governed by the applied accelerations) to the tank outlet or supply line. The reservoir is maintained full of liquid by designing the device such that surface tension forces are utilized to resist the maximum pressure loads acting to force gas into the device. If, for the moment, all flow effects are neglected, the pressure, or head, that can be retained for a given fluid can be directly related to the disturbing acceleration (a) and the pore size (D_p) in the reservoir or reservoir material.

$$H = \frac{4}{a\,D_p} \left(\frac{\sigma}{\rho} \right) \tag{1}$$

Figure 3.1.1 shows this relationship and indicates, for example, that at 10^{-2} g acceleration and a required 7.6 m (25 ft) head, the required theoretical material pore size to retain LH_2 is about 80 microns. This is representative of fine mesh screen materials. Thus, although large characteristic dimension surface tension devices, such as standpipes and baffles, have been considered for small vehicles (small effective heads) in very low gravity environments ($< 10^{-4}$ g), the investigations reported here were limited to fine mesh screen materials. In addition to having the proper surface tension characteristics, the reservoir must also be in contact with the liquid wherever it may be within the tank so that the liquid can be communicated to the outlet. For this reason, surface tension acquisition devices normally take on the form of screen channels positioned along the inner tank wall, as shown in Figure 3.1.2 (a). In the limit, the screen could cover the total wall area, in which case it becomes a wall screen liner either as a double or single screen as illustrated in Figure 3.1.2 (b).

3.1.1 <u>Overall Design Approach.</u> In general, the surface tension acquisition subsystem should be designed such that the surface tension device volume remains full of all liquid-phase propellant until subsequent low-g retention will no longer be required, as during a re-entry operation or the last high acceleration burn. If the device should undergo retention breakdown such that gas enters the screen device, it will be necessary to provide capability for low-g refill. Although this is feasible in some cases, as will be discussed later, the process is generally not straightforward and should be avoided if at all possible. Therefore, the surface tension device must be designed to retain the required head against the maximum anticipated destabilizing acceleration under maximum flowrate. To accomplish this, the surface tension acquisition/expulsion device is designed such that the summation of the viscous, dynamic, and hydrostatic losses in the system do not exceed the "bubble point" pressure for the basic screen material. Bubble point is the maximum pressure difference that can be retained across the screen by surface tension forces.

The total pressure differential (ΔP_{Tot}) across the liquid/gas interface within the screen material at a specific point is given by the equation

$$\Delta P_{Tot} = \Delta P_{SCR} + \Delta P_{Device} + \Delta P_{Hydro} + \Delta P_{Dyn} + \Delta P_{Duct} \qquad (2)$$

where

ΔP_{SCR} = pressure loss accompanying flow through the screen into the screen device

ΔP_{Device} = frictional pressure drop in the screen device

ΔP_{Hydro} = hydrostatic pressure loss

ΔP_{Dyn} = dynamic pressure reduction at the critical point on the screen

ΔP_{Duct} = frictional pressure drop in the ducting

CR190

THEORETICAL STATIC HEAD – M

THEORETICAL PORE SIZE – MICRONS
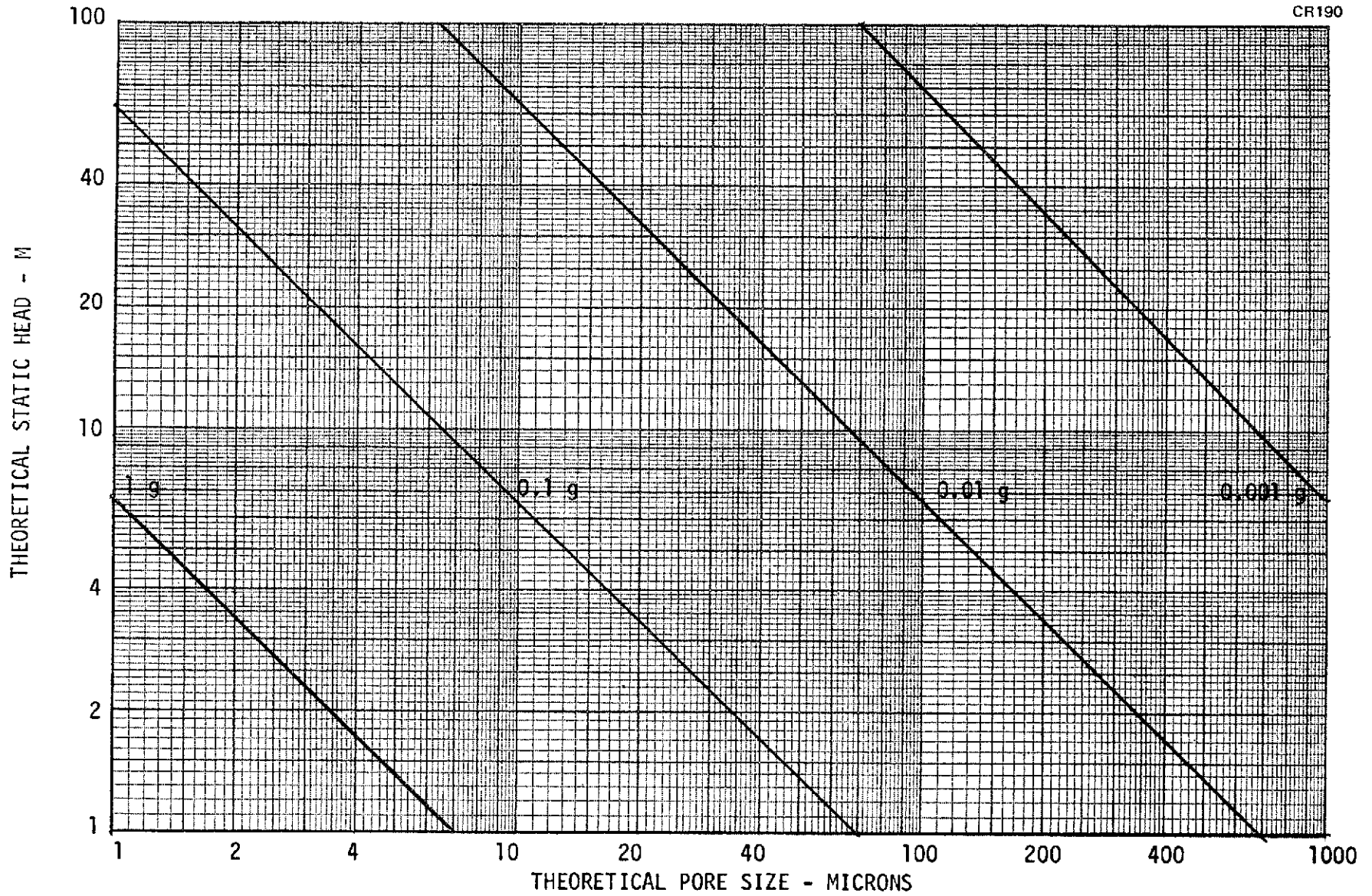
Figure 3.1.1. Influence of Pore Size on Static Head — LH_2 at 3 Atmospheres

(A) CHANNEL DEVICE CONCEPTS

SURFACE TENSION CHANNEL

A-A
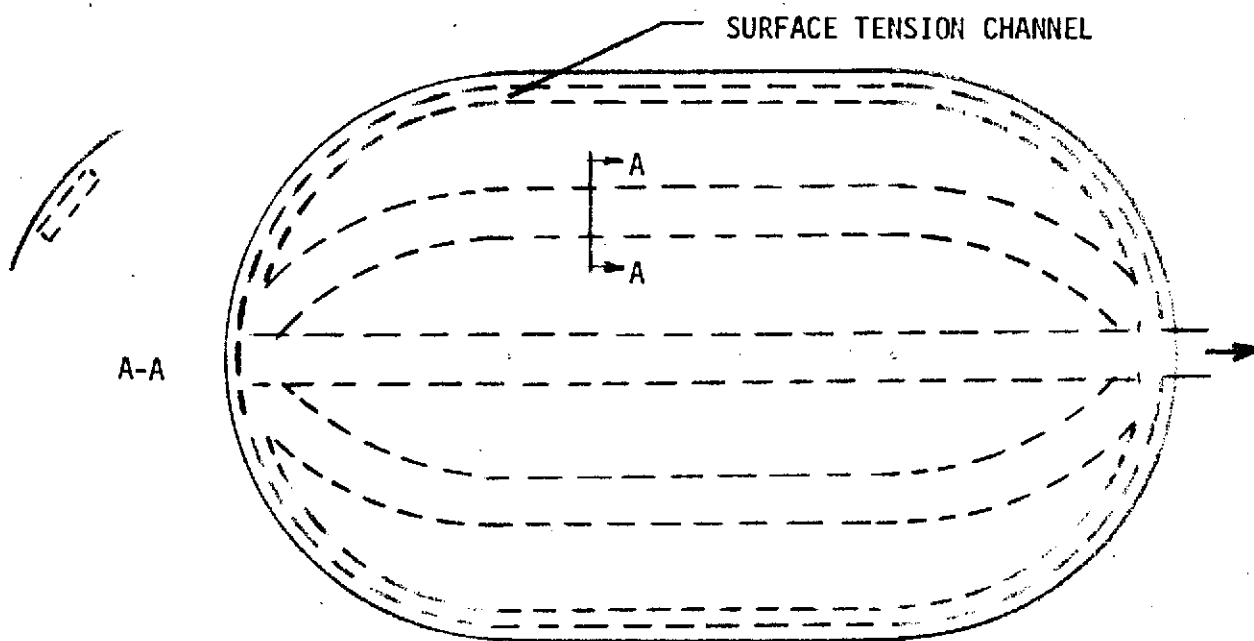
(B) FULL WALL LINER CONCEPTS

DUAL SCREEN LINER

SINGLE WALL LINER
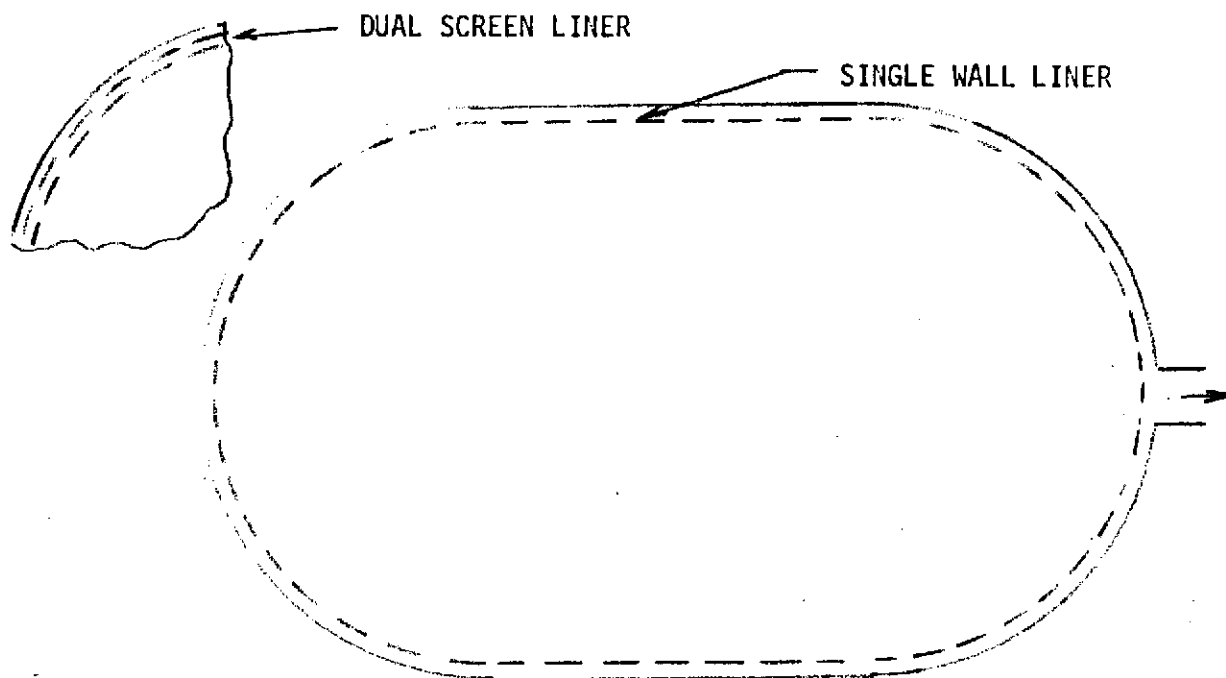
Figure 3.1.2. Basic Distributed Acquisition Concepts

Note that Figure 3.1.1 considers only the ΔP_{Hydro} term and, therefore, presents an upper limit for retention capability.

To facilitate the design and sizing of acquisition devices, Equation 2 was used as the basic element in developing a "Surface Tension Acquisition Device Sizing" code (the STADS code). This numerical code accepts as general inputs the fluid, screen mesh, acceleration, outflow rate, tank geometry, and liquid position and computes the total pressure change across the basic screen (ΔP_{Tot}).

The design variables, such as device dimensions, are iterated until the ΔP_{Tot} across the screen throughout the system remains below the screen bubble point pressure by a specific assigned design ratio, termed the retention safety factor (RSF)

$$RSF = \frac{\Delta P_{BP}}{\Delta P_{Tot}} \tag{3}$$

The fluid bubble points, usually in the form of experimentally-determined values for the specific screens under operating conditions, are supplied to the program. The bubble point is proportional to the fluid surface tension, which is strongly affected by temperature for cryogenic fluids. This dependency is shown in Figures 3.1.3 and 3.1.4, together with density for LH_2 and LO_2, respectively. Thus, it is important that the saturation temperature corresponding to tank pressure be computed and used to adjust the bubble point and surface tension used in the program.

The term ΔP_{SCR} represents the pressure loss associated with flow through the screen material into the screen channel. Several experimental programs have been conducted to relate this loss to the liquid properties and flow velocity through the porous material (References 4 and 5). The result is an empirical relationship between ΔP_{SCR} and the flow velocity, with equation constants dependent upon screen and liquid properties. Using the approach of Armour and Cannon (Reference 4).

$$f = \frac{\alpha}{Re} + \beta$$

where $Re = \frac{\rho V}{\mu a^2 D_c}$, $f = \frac{\Delta P \, \epsilon^2 D_c}{QB \, \rho \, V^2}$, α and β are experimentally determined constants (see symbols - Appendix A) and Q is a tortuosity factor (1.0 for square weave screens, 1.3 for dutch weave screens), which viscosity, μ, and density, ρ, are fluid characteristics, and V is the fluid approach velocity to the screen. For the laminar flow regime, where Re is small, β is generally much smaller than α/Re and can be ignored, resulting in $f = \alpha/Re$; substitution of f and Re gives:

$$\frac{\Delta P \, \epsilon^2 D_c}{QB \, \rho \, V^2} = \alpha \, \frac{\mu a^2 D_c}{\rho V} \qquad \text{or} \qquad \Delta P = \alpha \left[\frac{Q \, B \, a^2}{\epsilon^2} \right] \mu V \tag{4}$$
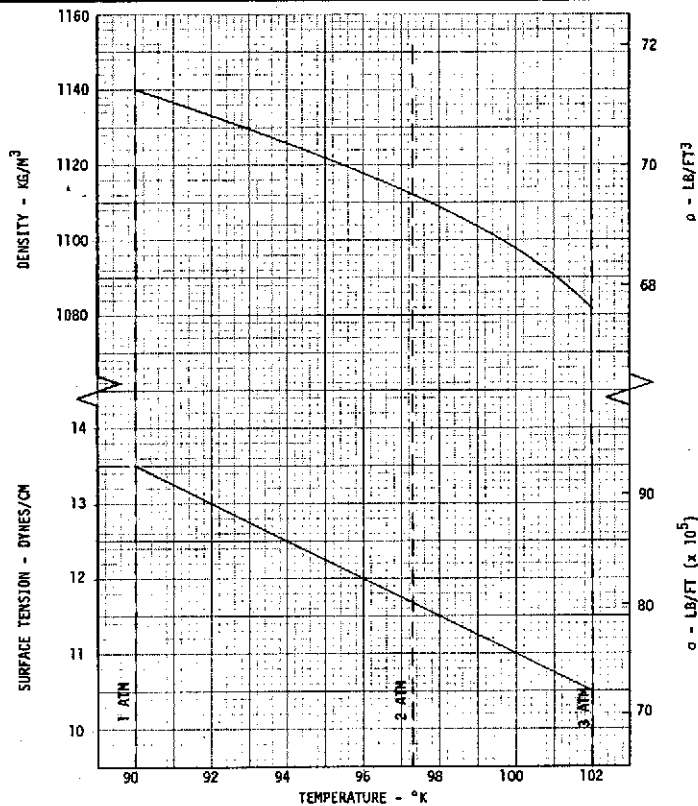
Figure 3.1.3. Properties of Saturated Liquid Oxygen
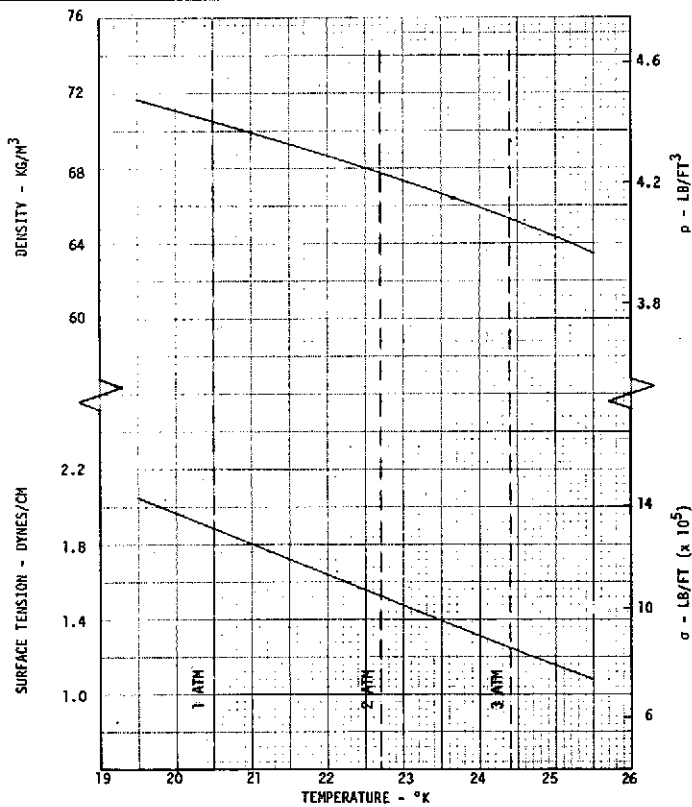
Figure 3.1.4. Properties of Saturated Liquid Para-Hydrogen

The term in parentheses is a function of screen configuration, wire size, weave, etc., and is a direct indication of screen flow loss for laminar flow. Similarly, for turbulent flow, with Re large, α/Re is much smaller than β, and

$$ f = \frac{\Delta P \, \epsilon^2 D_c}{Q B \rho V^2} = \beta \qquad \text{or} \qquad \Delta P = \beta \left[\frac{Q B}{\epsilon^2 D_c} \right] \rho V^2 \qquad (5) $$

Customarily, when applied to a retention device, the velocity entered into the empirical equation is the average flow velocity (i.e., volume flow rate/screen submerged area). However, this approach can lead to significant errors because the variation in flow velocity within the screen channel causes the flow through the screen to be nonuniform. Therefore, an analysis was made to more accurately model the actual situation (see Appendix A). The basic premise of the analysis is that ΔP_{SCR} can be expressed by

$$ \Delta P_{SCR} = K_o V $$

where K_o is an empirical constant and V is the local velocity of flow perpendicular to the screen. In terms of Armour and Cannon's findings (Reference 4), the relevant flow regime is that where

$$ 8.6/N_{Re} \gg 0.52 $$

N_{Re} being a Reynolds number. This restriction is customarily met within the retention device unless the flow area becomes very small (e.g., at propellant depletion). The analysis described in Appendix A provides a multiplying factor that corrects the ΔP_{SCR}, which is computed on the basis of an average and uniform flow through the screen. The multiplying factor is dependent upon channel and screen dimensions as well as net outflow rate. The corrected value of ΔP_{SCR} is used in the acquisition channel sizing code.

As part of the experimental program conducted under this program, screen flow loss tests, with individual screens and screen elements, were made and compared with the Armour and Cannon correlation (see Volume II). Those tests indicated significantly lower flow losses, although the characteristic trends were identical.

The term ΔP_{DYN} accounts for that portion of the total ΔP across the screen at a specific point due to the fluid velocity at that same point. Numerically, it is equal to $1/2 \rho V^2$, where the velocity V is an average value based on the flow area adjacent to the point of interest on the screen. The fluid volume flowrate is fixed by an outflow requirement imposed at the tank outlet.

The pressure drop contributions ΔP_{DEVICE} and ΔP_{DUCT} are generated by frictional losses inside the flow passages of the acquisition device. The two terms are a summation of the losses between two points. The first point is that where the screen surface rises out of the liquid pool, and the second is the location where the total ΔP is to be computed. Darcey's equation for

pipe-flow loss is used with a friction factor (f) selected on the basis of the Reynolds number and anticipated roughness factor.

$$\Delta P = f\,(L/D)\,1/2\,\rho V^2$$

$$N_{Re} = \frac{\rho V D}{\mu}$$

where D is the hydraulic diameter, and L is the passage length. Uniform flow area results in a constant Reynolds number in both the channel and duct. Sudden changes in flow direction such as occur at an elbow in the flow passage (e. g., between channel and duct) are treated by including an appropriate L/D in Darcey's equation. This L/D is selected from published data describing pipe friction losses.

In addition to satisfying the head retention requirements, the surface tension screen devices should be light in weight, have sufficient structural rigidity to resist deflection imposed by vehicle loads and the propellant flow that could damage or degrade the screens, result in minimum liquid residuals, and be practical in terms of fabrication, installation, cleaning, and servicing. These considerations tend to favor a channel or duct system, rather than a full wall liner.

In approaching the objective of evolving a practical and effective acquisition subsystem design, a full-tank distributed channel (FDC) acquisition concept was selected as a baseline, and this concept was designed to satisfy all critical CSS/APS requirements and all possible failure modes. When these objectives could not be achieved or achieved effectively (as with minimum weight or a practical design), the basic design was modified to yield the best overall solution to the problem. In fact, at the outset of the program, it was anticipated that certain feed system constraints would be necessary to satisfy FDC acquisition concept failure modes, which would result in significant weight penalties. Thus, a system using a localized pressure isolated screen channel with a refillable secondary tank was defined for preliminary design and comparative evaluation during the study.

3.1.2 Full Distributed Channel Acquisition Concept (FDC) Preliminary Design

a. General Configuration. The first task in designing a distributed channel acquisition system is to locate or position the channels so as to contact the liquid under all encountered acceleration load conditions without excess channel area or weight. This was done by surveying the propellant usage and acceleration influences for the baseline mission. Because of the relatively high boost accelerations (3g) and the fact that the tank is generally off-loaded to some degree, ring channels oriented in the y-direction (perpendicular to the tank centerline) were used. Also, because of the high-x accelerations during re-entry, a solid wall sump baffle was used over the tank outlet, which was sized to contain all of the propellant required for re-entry. This sump baffle is an integral part of the acquisition system and all the screen channels feed into the baffle, rather than into the feedline directly. The general arrangement is illustrated in Figure 3.1.5. The baffle, as well as the screen channels, will remain full of liquid up to the re-entry period, where the high re-entry acceleration causes screen

SUMP BAFFLE
REGION

CONNECTING DUCT

MAIN OUTLET LINE

PRIMARY SCREEN
ACQUISITION CHANNELS
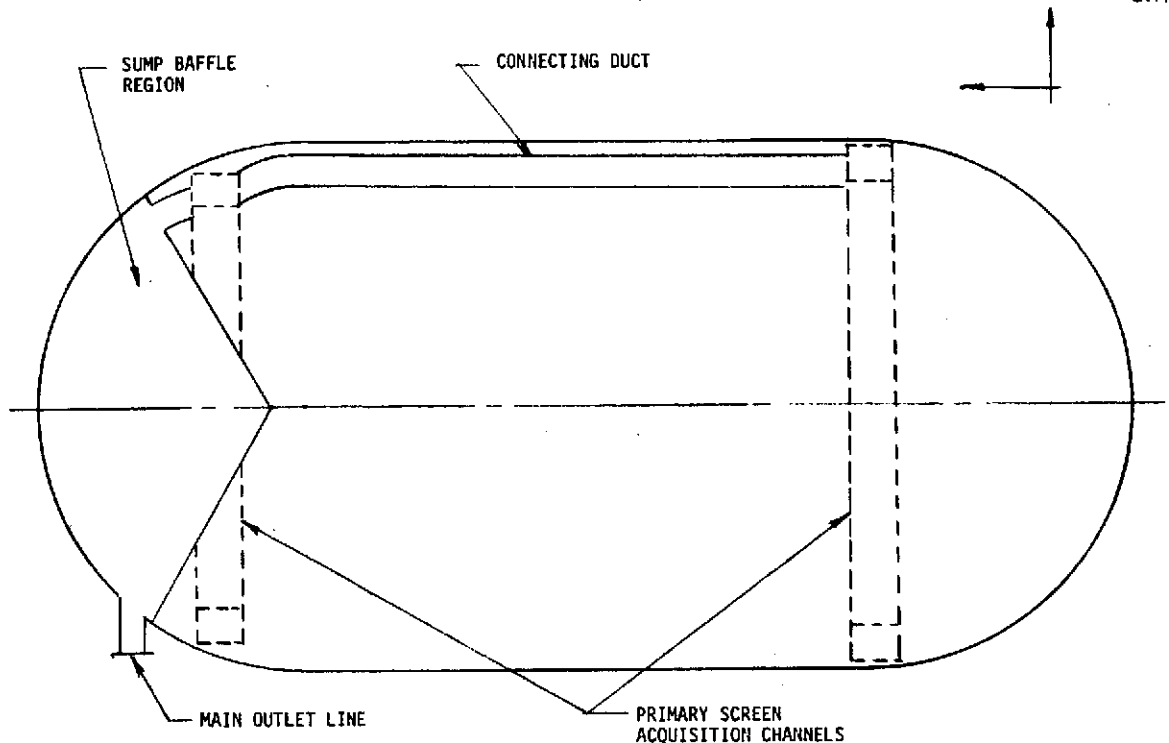
Figure 3.1.5. Conceptual Distributed Channel Arrangement (LH₂ Tank)

breakdown. Figure 3.1.6 shows the relationship between sump dimensions, volume , and baffle cone area. From the various duty cycles, a baffle liquid volume equal to 10 percent of the total tank volume is adequate for all cases. In the case of the LH_2 tank, the helium bottle will be placed within the baffle area to take maximum benefit of the surrounding cold liquid. This increased volume was taken into account when positioning the baffle. Thus, from the pressurization study of Section 3.2, the corrected LH_2 tank baffle total volume is about 7.72 M^3 (273 ft^3) and the estimated baffle cone area is 21.7 M^2 (233 ft^2). The cone shape was selected because of its simplicity and ability to distribute internal propellant loads. External loads on the cone are minimal, since the sump region is normally full of incompressible liquid which would tend to resist the forces imposed through tank propellant dynamics. Because of the conical shape of the baffle and since ground filling will be done in a vertical position, a small 1-g vent will be required at the apex of the cone. This will probably require a simple check valve discharging into the main tank or a small vent line running to the outside of the tank back through the feed line, which will be closed following ground fill. Baffle design for the LO_2 tanks is similar but with a volume of 0.81 M^3 (28.7 ft^3) per LO_2 tank.

During orbital operation, liquid will normally be positioned at either end of the tank or along the tank wall. Thus, a ring channel was placed near each end of the cylindrical section. This places the lower ring just above the sump. The upper ring is below the upper dome which is compatible with the propellant consumption and satisfies the normal off-loaded conditions for
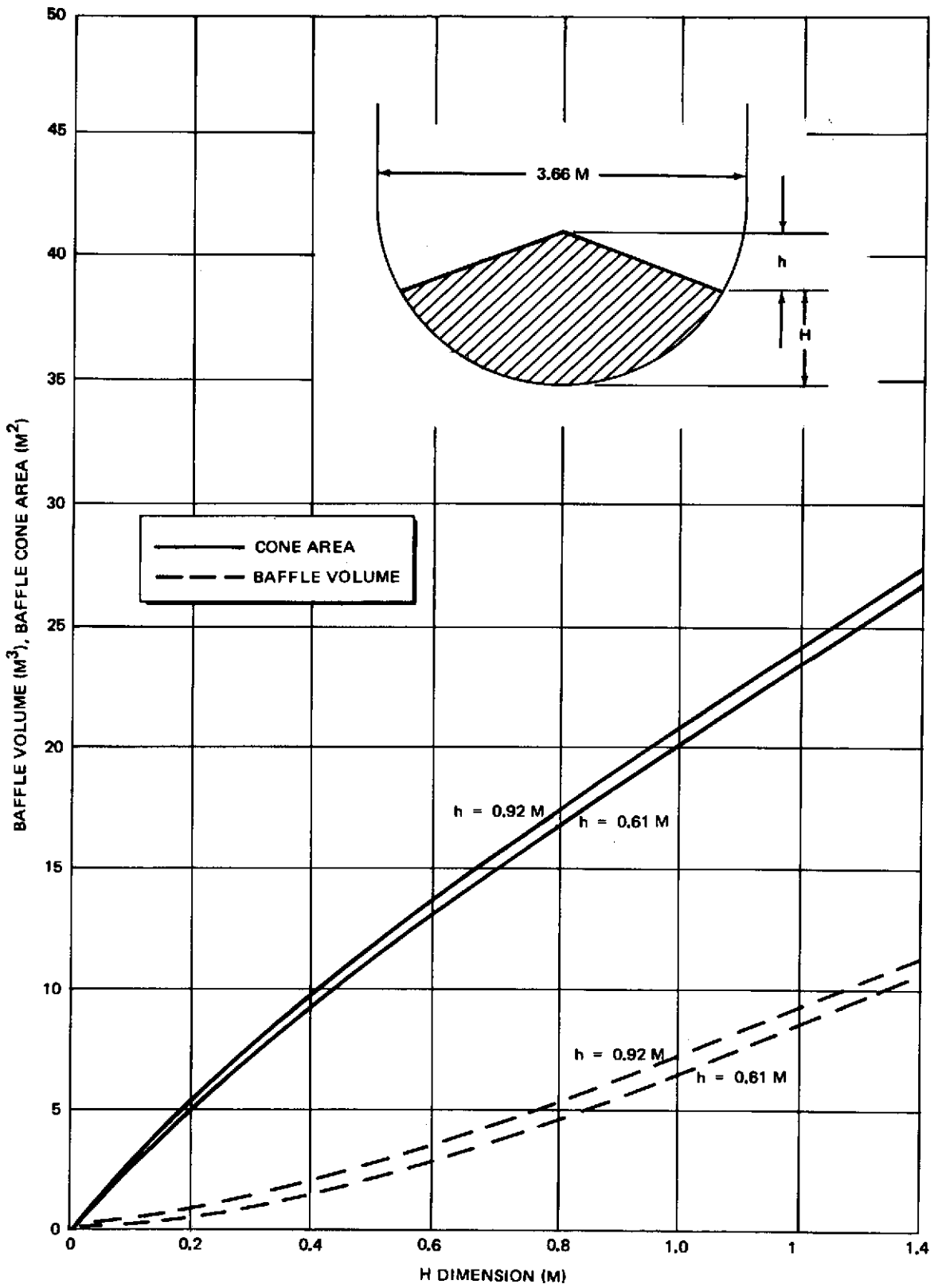
Figure 3.1.6. LH$_2$ Tank Baffle Parameters

the tank. Since the rings are near the outer periphery of the tank, on the maximum diameter, only two rings are required for the LH$_2$ tank. This is not the case with the spherical LO$_2$ tank and a third channel is required along the LO$_2$ tank equator.

   b.   Channel Design

   (1)   Fluid Dynamic Design and Mesh Selection. Calculations for evaluating the influence of channel cross section and screen mesh on retention performance were performed using the MDAC STADS code. However, before performing the final computations, all applicable results from the Bench Testing Program reported in Volume II were incorporated into the code, including new screen flow-through pressure drop data, bubble points, etc. The results are shown in Table 3.1.1 in terms of RSF for a range of screens and one specific channel rectangular cross section for LH$_2$ and LO$_2$. A range of limiting design conditions was calculated and, in each case, calculations were made assuming that screen was used either on only one face of the channel (solid-channel) or on all four faces (screen channel). Several conclusions can be drawn from these results.

   a.   The positive axial 0.45 M/sec^2 (1.5 ft/sec^2) acceleration with low screen coverage represents the most severe design condition.

   b.   Over the range investigated, the finest-mesh screen resulted in highest retention performance.

Table 3. 1. 1

INFLUENCE OF SCREEN MESH ON MAIN TANK
CHANNEL RETENTION PERFORMANCE

					Safety Factor							
					Mesh Size							
					250 x 1370		325 x 1900		325 x 2300		Top 325 x 2200 Bottom 250 x 1370	
Propellant	Channel Position	Flowrate (kg/sec)	Acceleration (m/sec^2)	Fraction Covered	Solid Channel	Screen Channel	Solid Channel	Screen Channel	Solid Channel	Screen Channel	Solid Channel	Screen Channel
LH$_2$	Top	2.04	0.292	0.50	3.11	4.17	3.42	4.74	3.84	5.16		
LH$_2$	Top	2.04	0.124	0.25	2.02	3.17	2.19	3.55	2.59	3.92		
LH$_2$	Top	2.04	0.124	0.50	2.86	3.73	3.16	4.26	3.53	4.61		
LH$_2$	Bottom	2.04	0.292	0.50	3.38	4.57	3.71	5.19	4.17	5.65		
LH$_2$	Bottom	2.70	0.457	0.25	1.12	1.49	1.25	1.70	1.41	1.84	1.38	1.83
LH$_2$	Bottom	2.70	0.457	0.50	1.40	1.64	1.59	1.89	1.73	2.03		
LO$_2$	Top	6.85	0.183	0.50	4.39	6.70	4.71	7.48	5.41	8.28		
LO$_2$	Top	6.85	0.124	0.25	2.60	4.82	2.76	5.26	3.35	5.94		
LO$_2$	Top	6.85	0.124	0.50	4.13	6.13	4.46	6.87	5.10	7.57		
LO$_2$	Bottom	6.85	0.183	0.50	4.26	7.00	4.52	7.73	5.25	8.64		
LO$_2$	Bottom	13.50	0.457	0.25	0.87	1.53	0.95	1.70	1.17	1.88	1.07	1.89
LO$_2$	Bottom	13.50	0.457	0.50	1.36	1.81	1.49	2.06	1.68	2.24		

90% Effective open area

Corrected flow properties

LH$_2$ tank has two primary rings and LO$_2$ and has three primary rings

Channel Dimensions: LH$_2$ 25.4 x 10.2 cm: LO$_2$ 20 x 8.1 cm

c. The all-screen channel produces higher retention performance than the solid channel (for the same flow cross section).

d. Use of a finer mesh on the top channel than on the bottom channel results in performance improvements.

Since it is desirable to use coarse mesh screen whenever possible from a clogging standpoint, use of two screen meshes is desirable and was adopted (325 x 2300 on top and 250 x 1370 on bottom). However, the 25.4 x 10.2 cm channel, in all cases, did not satisfy the minimum RSF requirement. Therefore, calculations were expanded to determine the channel size that would meet RSF ≥ 2 for all conditions. It was found that a 28 x 11.2 cm and 19.1 x 3.6 cm channel for LH_2 and LO_2, respectively, was needed. Resulting safety factors are shown in Table 3.1.2.

Supplementary calculations were run, and it was found that the specific geometry of the duct was not controlling in terms of safety factor. The actual criteria for the specific screen selection are as follows:

a. Duct flow area must be at least 0.0313 M^2 (48.5 in.^{2}) and 0.0145 M^2 (22.5 in.^{2}) for LH_2 and LO_2, respectively.

b. Screen actual width measured around the cross sectional perimeter must be at least 0.787 M (31 in.) and 0.533 M (21 in.).

Table 3.1.2

FINAL COMPUTED MAIN TANK CHANNEL
RETENTION PERFORMANCE

SCREENS	TOP CHANNEL	325 x 2300
	BOTTOM CHANNEL	250 x 1370

90% OPEN AREA ON ALL SIDES

Propellant	Channel Size (m x m)	Wetted Channel	Flowrate (kg/sec)	Acceleration (m/sec^2)	Fraction Covered	RSF
LH_2	0.279 x 0.112	Top	2.04	0.292	0.50	4.91
LH_2	0.279 x 0.112	Top	2.04	0.124	0.25	3.73
LH_2	0.279 x 0.112	Top	2.04	0.124	0.50	4.46
LH_2	0.279 x 0.112	Bottom	2.04	0.292	0.50	6.78
LH_2	0.279 x 0.112	Bottom	2.70	0.457	0.25	2.05
LH_2	0.279 x 0.112	Bottom	2.70	0.457	0.50	2.25
LO_2	0.190 x 0.076	Top	6.85	0.183	0.50	7.57
LO_2	0.190 x 0.076	Top	6.85	0.124	0.25	5.24
LO_2	0.190 x 0.076	Top	6.85	0.124	0.50	6.74
LO_2	0.190 x 0.076	Bottom	6.85	0.183	0.50	8.64
LO_2	0.190 x 0.076	Bottom	13.50	0.457	0.25	2.11
LO_2	0.190 x 0.076	Bottom	13.50	0.457	0.50	2.53

Thus, variations in the duct cross sectional shape within these constraints are permissible.

(2) Structural/Mechanical Design Criteria. In addition to the above fluid dynamic criteria, certain fabrication, installation, and structural criteria must also be satisfied, most of which were evolved through the supporting experimental program or as a result of MDAC experience in building and testing fine mesh screen acquisition devices. These criteria include the following:

a. 0.057 cm (0.020 in.) sheet material in either steel or aluminum, when used for basic duct structure, provides a sufficiently rigid structure (see Section 2B2, Volume II).

b. Simple riveting of duct sections should not be used when sealing against bubble point pressure is required (see Section 2B2, Volume II).

c. The composite fine mesh screen, perforated backup plate, and the edge frame can be welded together using either fusion or roll-spot welding, but the picture frame structure is recommended (see Section 2B1, Volume II).

d. In order to eliminate high flow through pressure losses, a very coarse mesh aluminum screen must be used between the fine mesh and the perforated backup plate (see Section 2A2, Volume II).

e. Compound curvature of fine mesh screen should be avoided to prevent local folding and stress points which could possibly degrade screen performance.

f. Pleated screens can be used to achieve an effective increase of a factor of three in screen area, including the effects of small changes in bubble point and flow loss (see Section 2A3, Volume II).

g. In attaching screen elements to the channel duct, screws can be used with spacing as great as 2.5 cm, if the elements are attached to a rigid duct edge and an indium-tin seal is used (see Section 2B2, Volume II).

Detail of a channel design are influenced by the size of the individual channel segments; Figure 3.1.7 shows the individual channel package size as related to the number of segments. To be practical, the design must be such that two men working within the tank can accomplish the installation with access through a conventional manhole. On this basis, an installation unit package greater than 2 M by 0.5 M would appear unrealistic. Thus, at least six segments per ring would be necessary. This would yield an installation unit package of about 1.83 M by 0.46 M. The original channel installation would occur prior to tank installation within the vehicle, but screen maintenance and repair should be possible without tank removal from the vehicle. Thus, screen installation unit package sizes would be more restrictive. If complete channel segments must be withdrawn to remove the defective screen (screen element removal is the other alternative), at least eight segments should be used, resulting in an installation unit package of 1.45 M by 0.38 M.
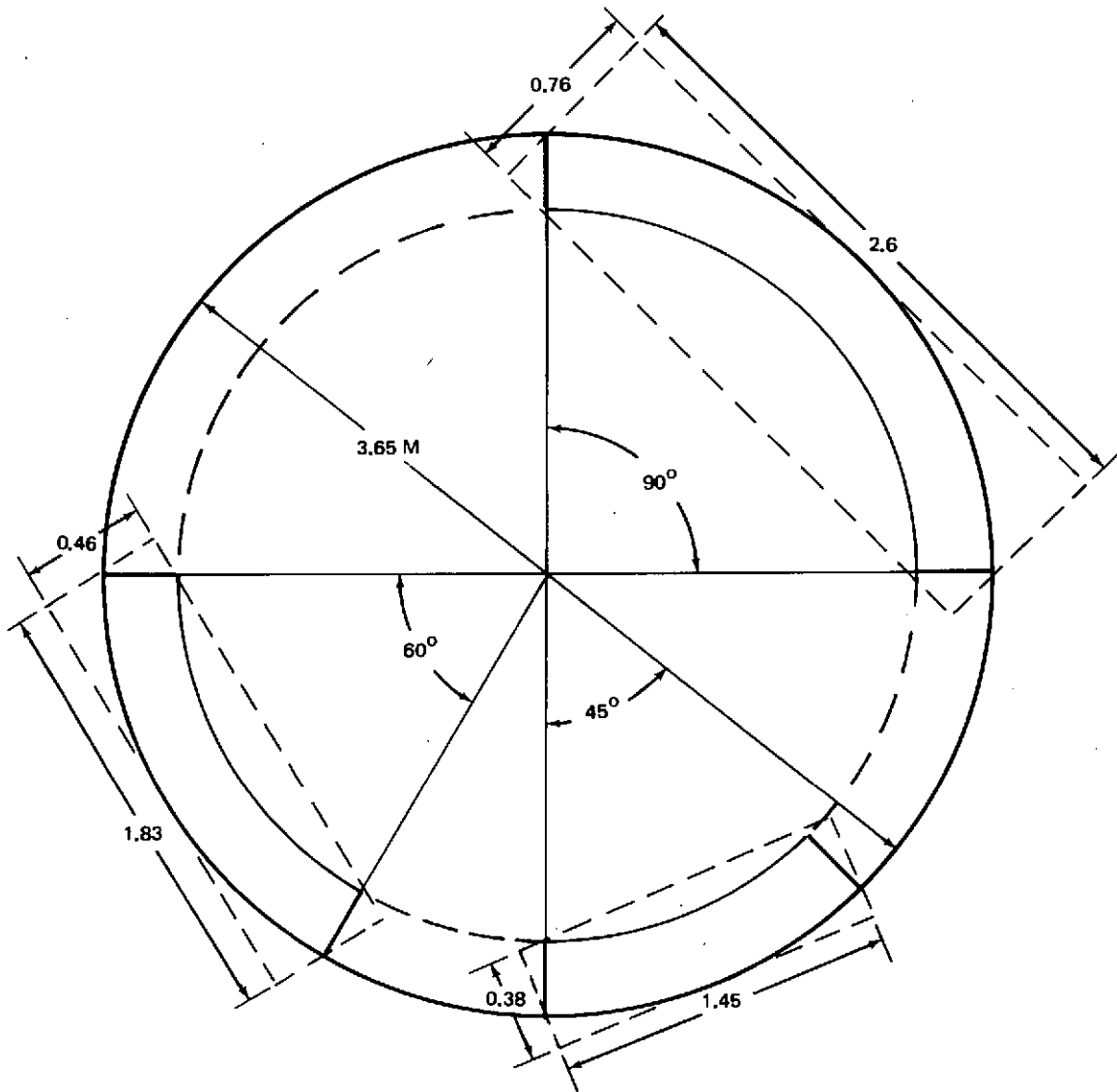
SEGMENTS	PACKAGE DIMENSIONS (M)
4	2.6 × 0.76
6	1.83 × 0.46
8	1.45 × 0.38

Figure 3.1.7. Channel Segment Sizes (LH$_2$ Tank)

In order to increase the reliability of the acquisition system, a technique for checking the bubble point performance of the system in an as-installed condition immediately after installation and at periodic times throughout the life of the vehicle appears highly desirable. This, ideally, should be accomplished without requiring access into the tank. If the test indicates a loss in bubble point, the tank can then be opened, the system inspected, and the suspected screen sections removed and repaired or replaced. Direct immersion bubble-point testing is possible with a solid duct channel which can hold fluid with pressure being applied across the single plain screen. The immersion technique is not directly applicable with an all-screen channel. However, a liquid-film technique was demonstrated during the Supporting Experimental Program, at least in terms of overall feasibility, that could be used to verify the bubble point performance of an all-screen channel. Specific test procedures using this technique are outlined in Appendix B.

Joining of the duct sections can be a critical problem. The joint must reliably provide a seal with a pressure resistance capability better than that provided by the fine mesh screen, it must be easy to install within the tank, and should not result in excessive weight penalty. Conventional bolted flanges were deemed to be too heavy and would involve complex manual operations within the tank. During our bench testing, simple riveting was checked out but did not generally prove to be adequate from a leakage standpoint. After considering various alternatives, it was concluded that the best potential solution was to use a Marman V-Band type joint coupling. This is available in a wide variety of sizes and flange details and provides a simple one- or two-bolt attachment per joint. This design requires a circular duct section at the joint, which demands either a circular duct or local transition sections from the normal duct cross section to a circular shape at the joint. This constraint does not present a problem as long as the joint is selected so that the flow area through the circular section does not drop below that required by the flow criteria. For the baseline distributed channel, a minimum diameter of 19.8 cm (7.8 in.) and 13.7 cm (5.4 in.) for LH_2 and LO_2, respectively, is required. Marman joints of several types are available in these and larger sizes. Figure 3.1.8 pictures the details of such a joint and presents a weight breakdown for an 0.204 M (8 in.) and 0.254 M (10 in.) diameter coupling assembly. Flanges are available in aluminum and stainless steel. The data shown is for a standard 4584-type design. Variations on this design to reduce weight are quite practical. During bench testing, a 17.8 cm (7 in.) diameter Marman connector with several candidate seals was leak-checked at LH_2 temperature (see Volume II, Section 2B4). As discussed, all seals worked well and the least expensive type, the Creavy Seal, was selected.

(3) Duct Cross Section Study. Three basic duct cross sections were investigated, as shown in Figure 3.1.9. Type A consists of a solid duct with the fine mesh screen on only the top surface. This design facilitates simple immersion bubble point testing, is easy to fabricate, and is adaptable to screen element removal. However, to satisfy the screen area requirement, a 0.79 M (31 in.) channel width is required, which appears impractical. This flow area problem can be avoided by using a pleated screen element which was found, during the supporting experimental program, to offer a good increase in effective screen flow area (3 times the projected area) with only minor degradation in bubble point or flow loss characteristics. With a pleated screen element, a width equal to 0.262 M (10.3 in.) would satisfy the retention criteria. The screen could be pleated in either direction but would
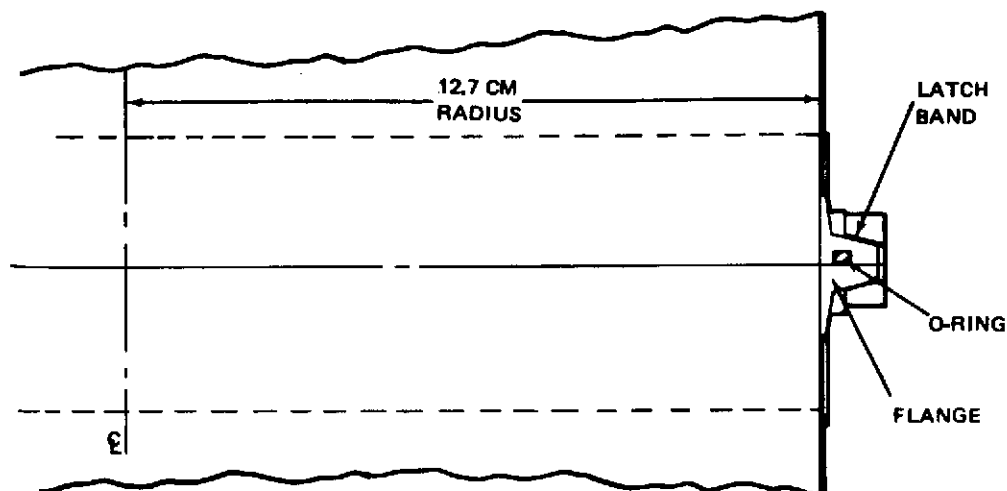
DUCT SIZE	0.254 M DIAMETER (10 IN.)		0.203 M DIAMETER (8 IN.)	
MATERIAL	STEEL	ALUMINUM	STEEL	ALUMINUM
WEIGHTS (KG)				
COUPLING	0.573	0.573	0.427	0.427
FEMALE FLANGE	0.424	0.144	0.349	0.115
O-RING FLANGE	0.555	0.168	0.397	0.134
TOTAL	1.552 KG	0.885 KG	1.173 KG	0.676 KG
NOTES	2 BOLT LATCH		1 BOLT LATCH	

Figure 3.1.8. Detail of Representative Joint Section Clamps

SOLID WALL DUCT

A

ALL SCREEN
SQUARE DUCT
B

ALL-SCREEN
CIRCULAR DUCT
C
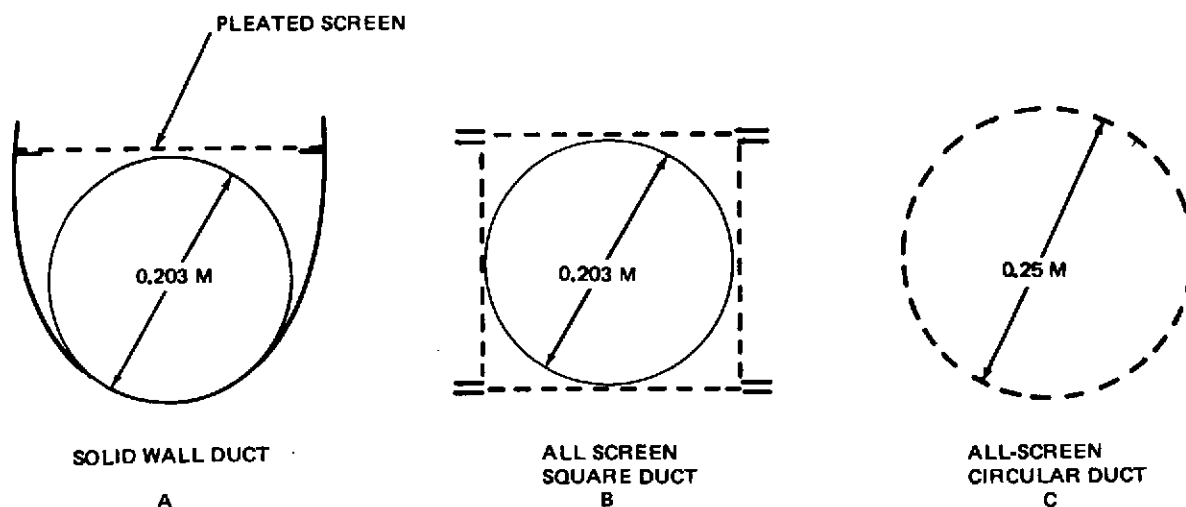
Figure 3.1.9. Candidate Acquisition Duct Design Cross Sections (LH$_2$ Tank)

provide fewer difficulties with the pleats running in a radial direction relative to the tank. To provide adequate sealing of the screen elements, the top of the channel is formed from a 2.5 by 2.5 by 0.25 cm aluminum L-section.

The remainder of the duct, including transition sections from the near hemisphere to the circular cross section at the joint, is made of 0.051 cm aluminum sheet. The screen elements which are sized for 3-to-a-duct section or 18-per-ring are about 0.31 M by 0.64 M (12 by 25 in.) and consist of the fine mesh screen in its pleated form, a very coarse mesh aluminum screen, a perforated (50 percent open area) 0.051 cm steel backup plate, and a 0.051 by 2 cm steel frame. This sandwich is welded together. Each element is attached to the duct by 60 screws, and a simple indium-tin seal is used within this joint to provide a leak path less than that of the fine mesh screen itself. Characteristics of this and the other candidate designs considered are summarized in Table 3.1.3.

The weight of a 3.67 M diameter ring is 39.5 kg. Ducts weigh 14.7 kg, screen elements weigh 20.7 kg, and joint/couplings weigh 4.1 kg.

Two variations to the above concept were considered, as noted in Table 3.1.3. In the A2 design, rather than remove the screen elements, the duct sections are removed, and the screen elements are permanently welded into the duct. (Number of duct sections is increased to 8.) This alternative primarily eliminates the tedious screw attachment operation within the tank. However, this requires an all-steel channel which results in a relatively heavy weight. To reduce this weight penalty, the A2' design was evolved; it uses a bimetallic joint just below the screen element and employs aluminum for the lower portion of the duct. This design, however, is still relatively heavy.

The other designs shown depart from the solid-wall concept and use a nearly all-screen configuration. This design requires that bubble point testing within the tank be performed using the liquid-film technique and that screen removal be accomplished by removing duct sections. In the B design, a square duct is used so that the individual screens can be attached to each of the four faces without compound curvature. This results in essentially an all-steel structure with extensive welding. The edges were specifically configured to facilitate the welding (see Figure 3.1.9). This design has a competitive weight of 42 kg composed of duct/screens, 33 kg, and joint, couplings, 9.4 kg.

Table 3.1.3

MAIN TANK DISTRIBUTED CHANNEL DESIGN COMPARISON

Type	Segments Per Ring	Weight for Maximum Diameter Ring (KG)	Screen Replacement Approach	Bubble Point Test Technique	Notes
A	6	39.5	REMOVE ELEMENT	IMMERSION	PLEATED SCREEN MUST BE USED
	8	66.3	REMOVE DUCT SECTION	IMMERSION	PLEATING ESSENTIAL; ALL STEEL CONSTRUCTION
	8	53.6	REMOVE DUCT SECTION	IMMERSION	SAME AS A2 EXCEPT THAT BIMETALLIC JOINT ALLOWS USE OF ALUMINUM FOR MOST OF DUCT
B	8	42.7	REMOVE DUCT SECTION	LIQUID FILM	ALL SCREEN CHANNEL; ALL STEEL CONSTRUCTION
C	8	40.4	REMOVE DUCT SECTION	LIQUID FILM	SIMPLE CONSTRUCTION; DUCT IS FORMED IN 16 STRAIGHT SECTIONS TO AVOID COMPOUND CURVATURE ALL STEEL CONSTRUCTION
	8	29.1	REMOVE DUCT SECTION	LIQUID FILM	USE ALUMINUM BACKUP MATERIAL TO SAVE WEIGHT

30

Design C uses a circular duct cross section but has the ring built up of straight sections to avoid compound curvature. To satisfy the fluid dynamics criteria, the duct must be at least 0.249 M (9.8 in.) in diameter. The maximum distance that the duct will be set off from the wall is a function of the number of straight sections used to form the ring (see Figure 3.1.10). To minimize this offset, at least 16 straight sections should be used. Two adjacent sections would be permanently welded, and the V-Band joint/couplings would be used at 8 points. Although the C design is all steel, it has a relatively low weight of 40.4 kg composed of ducts/screens, 28 kg, and joint/couplings, 12.4 kg. Note that the joint/coupling weight is a relatively high percentage (31 percent) of the total because of the large diameter and steel joint flanges.

A major weight savings can be effected in the C design by using an aluminum perforated tube attached by riveting to the steel end pieces. This reduces the weight by almost 10 kg per ring but complicates the fabrication. Weight could also be saved if aluminum joint flanges could be used, but this would require bimetallic joints that further complicate the fabrication and involve additional weight which would offset much of the savings. Therefore, this idea was dropped from further consideration. The only fabrication problem with this design appears to be potential damage of the aluminum from the heat generated during welding. However, this can be controlled during the welding process.

The minimum-weight A and C designs appear to be the most desirable. The C design is the lowest in weight and is relatively straightforward

CR190

NUMBER OF STRAIGHT SEGMENTS	d MAXIMUM DISTANCE FROM TANK WALL (M)
4	0.53
6	0.24
8	0.14
16	0.038

1.83 M
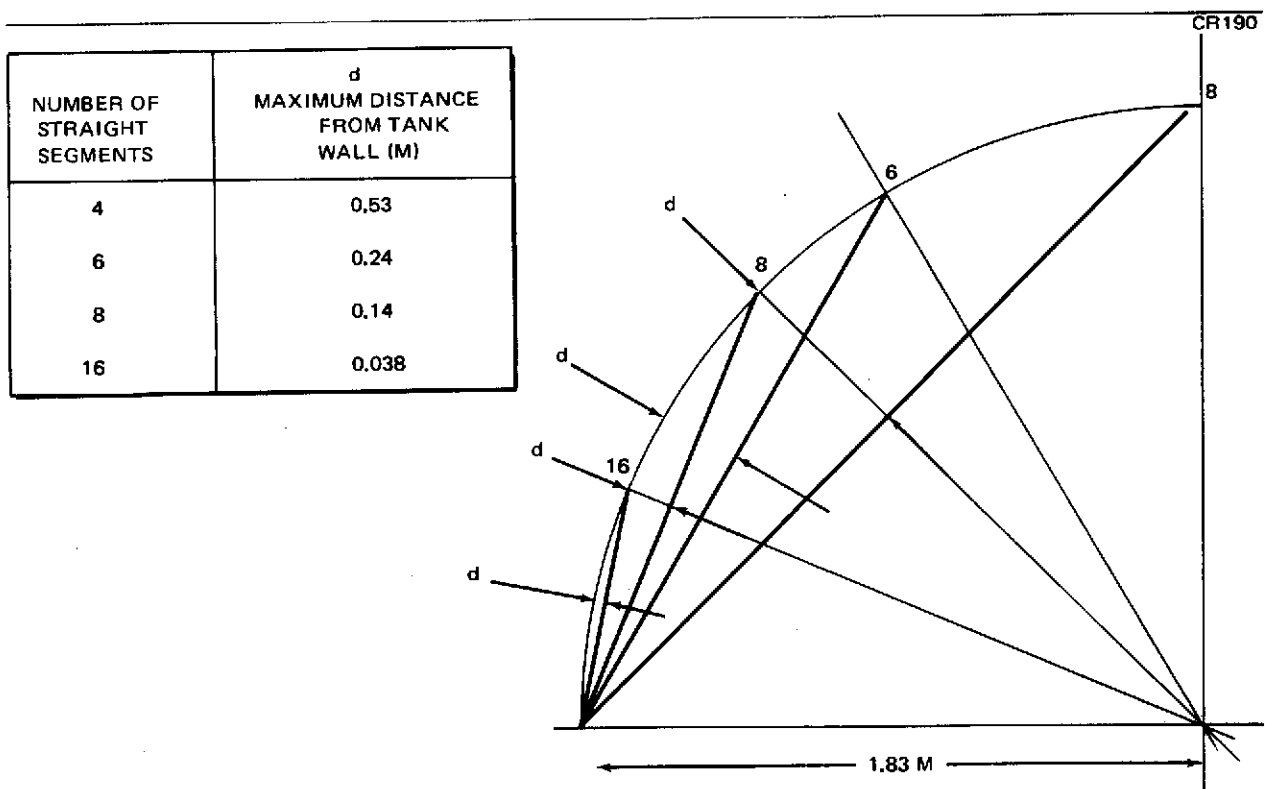
Figure 3.1.10. Influence of Straight Duct Segments on Proximity to Wall

to fabricate. A and C designs differ in the servicing philosophy and in the bubble point test approach. On balance, however, the design was selected as the main tank distributed channel preliminary design.

c. Thermal Design Criteria. As noted in the opening statement of Section 3.1, the basic requirement of the acquisition/expulsion subsystem is to provide gas-free cryogen to the feed system. Thus, the acquisition device should be free at all times of significant size bubbles. Also, bubble buildup within the screen device itself could lead to screen dry-out and to catastrophic retention breakdown in the entire acquisition device. Thus, a "bubble free" criteria must be adhered to in the design of cryogenic propellant screen surface tension acquisition devices. Ideally, it would be desirable to completely restrict all heat energy to the acquisition device that could result in vaporization. If this is not done, the designer must deal directly with the heat transfer problem, which implies that a detailed knowledge of the low-g heat loads and their impact on the acquisition device is available.

In general, there are four direct sources of acquisition device heat transfer: (1) heat by radiation or convection from the tank walls as a result of heating from the external environment; (2) heat conducted up the feed and pressurization lines into the device; (3) conduction from the tank wall through device support struts; and (4) convection from any warm gas pressurant. Theoretically, the first three sources can be controlled by using direct-GH_2-vapor cooling, or vapor-cooled shielding in the case of the tank wall; this will be discussed in detail later in this section. The pressurant heating, however, is a more formidable problem, since, by nature of the process, the pressurant heat passes across the tankage wall boundaries and can interact directly with the screen device.

(1) Basic Screen Device Heat Transfer. The selected channel design discussed previously is essentially an all-screen unit with solid walls only at the channel section joints or couplings. Thus, the basic problem, neglecting the couplings at this point, is low-g convection from a warm gas (the pressurant) to a screen surface retaining a cryogenic liquid. It has been suggested by a number of investigators that the evaporation which occurs at the screen surface is sufficient to absorb the incoming heat flux such that gas bubbles are not generated within the screen device. Such a situation is plausible if liquid is supplied to the screen at or above the rate at which it is evaporated; for example, as by wicking along the screen. The analytical assessment and evaluation of such a heat and mass transfer balance required knowledge of low-g heat transfer mechanisms and flow in surface tension devices beyond our present technology base. Thus, to further establish the retention feasibility of surface tension screen elements in the presence of a warm gas, a series of experiments was conducted.

Early in 1972, as part of the MDAC IRAD program, screen-coupon heat transfer test were conducted, in which 5-cm (2-in.) diameter screen mesh coupons were exposed to a heated gas while the screens retained a measured head of LN_2 cryogen (Reference 6). The warm gas, which simulated a warm pressurant, was electrically heated and circulated by a fan over the retention screen element as shown in Figure 3.1.11. The results (see Figure 3.1.1) indicated that the screen meshes (four varieties were tested) could sustain a high heating rate without loss of head retention capability. These results were very encouraging, and, as part of the Supporting Test Program for this project, the same apparatus with minor modifications was used with LH_2, rather than LN_2. The test results were quite different with LH_2
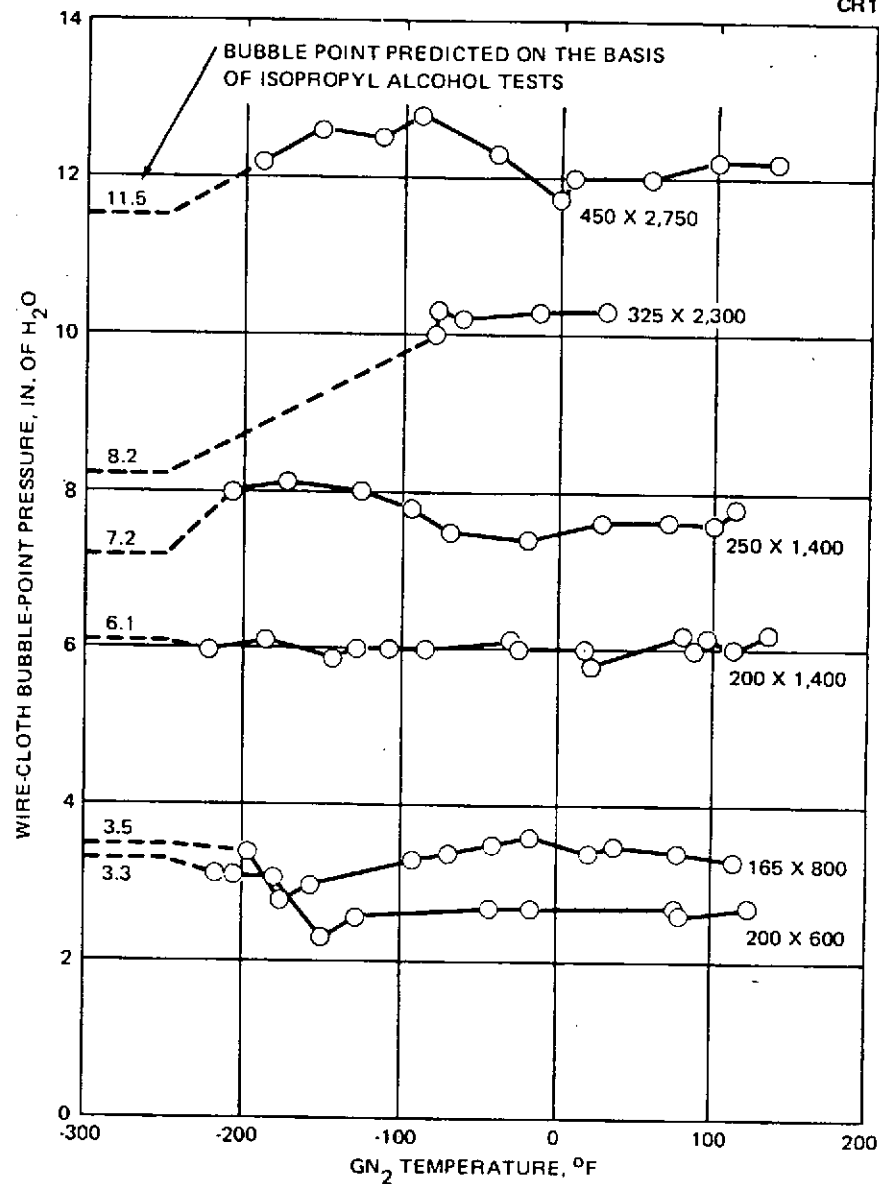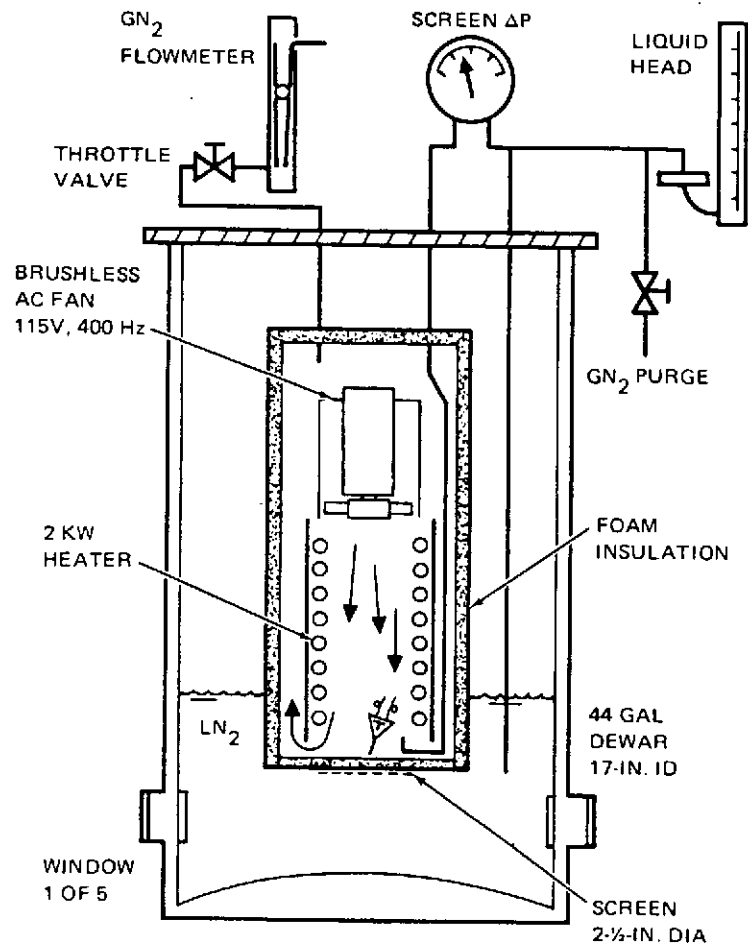
Figure 3.1.11. Heat Transfer Apparatus and Effects on Screen Bubble Point with LN$_2$ (MDAC IRAD)

as the fluid. Large reductions in head retention capability were measured (see Volume II, Section 2C1). This difference in observed behavior was attributed to the small ΔT for boiling (0.1 to 0.5°K) normally experienced with LH_2 in comparison to that for LN_2.

As reported in Section 2C1 of Volume II, another test was conducted to measure retention loss caused by local pressure decay using a movable screen device in a dewar containing LH_2. As described, the test was run by first filling the screen device with LH_2 by direct immersion and then physically moving the rectangular unit containing the LH_2 up into a warm ullage gas region (11°K to 22°K). If the ullage gas had no effect on the screen, the all-screen surface tension device (shaped much like a milk carton) should remain full of LH_2. As discussed in Appendix C, analysis also showed that a sudden tank pressure decay, as during cooldown after expulsion termination or venting, could possibly result in bubble generation and retention breakdown in a screen device exposed to these pressure changes. Therefore, the test plan called for decreasing the dewar pressure under the stable retention conditions until the head could not be retained. However, direct visual observations and movies showed that, in most cases, as soon as the screen device was moved up into the ullage, breakdown occurred even before the dewar pressure could be decreased. Ullage temperatures below 28°K were tested, and it was concluded, based on these findings, that the feasibility of using a screen device to retain LH_2 in the presence of even a moderately heated gas had not been satisfactorily demonstrated. Thus, the screen devices must be actively cooled or the system must be designed so that the screen is not exposed to warm gas - or any significant heat input, for that matter.

Additional exploratory screen heating tests were conducted at the end of the program and are reported in Section 2C1 of Volume II of this report. The objectives of this last test program were to further explore the thermal-induced retention breakdown and attempt to quantize the process by obtaining breakdown as a function of heat input. In the test, a screen supporting a head of LH_2 was subjected to a measured heat input by means of a combination heater/heat flux gage. Two screen units were tested: (1) a plain 200 x 600 mesh screen, and (2) a dual layer of 200 x 600 mesh screen. Each unit was found to retain about 33 cm (13 inches) of LH_2 with no heat input. Heat input was gradually increased up to the limits of the test setup, which was slightly above 100 watts (341 Btu/hr). Based on the screen element area, this is a heat flux of 9640 watts/M^2 (3,072 Btu/ft^{2}hr) which is, indeed, a high heat transfer level relative to that normally experienced within a cryogenic tank. However, this heat load did not result in observable screen retention breakdown in the experiments with either of the two units. Test details may be found in Section 2C1 of Volume II of this report.

Unfortunately, the results of the various heat transfer tests conducted under this program do not permit one to make a conclusive statement regarding the capability of a screen acquisition device to withstand a thermal environment without retention breakdown. Subsequent analysis has shown that, in principle at least, there is a difference in the temperature distribution imposed on a test screen such as in the "milk carton" test and the

screen heat transfer test discussed immediately above. In this last test, the liquid beneath the screen is subcooled with respect to the surface temperature, whereas in the earlier milk-carton test the liquid behind the screen is slightly superheated with respect to the saturation temperature beneath the surface. This fundamental difference between a supported column of liquid and a submerged screen with an applied pressure difference may account for the observed differences in test results. A revised series of tests to explore this area has been proposed to NASA-MSFC.

(2) Active Acquisition Device Cooling. If the feed system must be limited to a cold-helium pressurization system in order to eliminate heat input and assure satisfactory operation of the surface tension device, a significant weight penalty is incurred. Normally, a warm GH_2 pressurization approach is optimum. As evaluated in Section 3.2.2, a cold-helium pressurization system for CCS/APS LH_2 tank could be as much as 180 kg heavier than the optimum warm GH_2 pressurization system. The potentially lighter GH_2 pressurization system could be used if the acquisition device was cooled so that all incoming heat would be absorbed before it could enter the device. This is theoretically possible in the LH_2 tank if a thermodynamic vent is integrated with acquisition cooling coils in which the throttled hydrogen vent gas is passed through the coils to intercept all the potential pressurant heat. This, however, involves a coolant weight penalty which must be dumped overboard.

To assure safe operation of the acquisition device, the cooling system must be sized to absorb the heat added to the system, which is in reality the heat originally added to the pressurant above LH_2 temperature. Thus, from the pressurant inlet temperature and the mass of GH_2 added to the tank, the energy added to the tank can be estimated. This must be absorbed by the LH_2 coolant evaporation as governed by the equation

$$W_P \, \Delta H = W_C \, \Delta H_V$$

where W_P and W_C are the mass of pressurant and coolant respectively, ΔH is enthalpy change from liquid bulk to inlet temperature, and ΔH_V is the coolant heat of vaporization. The masses involved are shown in Figure 3.1.12 as a function of inlet temperature. (Pressurant mass was evaluated in Section 3.2.2.) As indicated, for the optimum pressurant inlet temperature with autogenous pressurization, 110 kg of hydrogen coolant would be required; this is a direct weight penalty. By adding tankage weight penalties and considering total ullage masses (Figure 3.2.3 in Section 3.2), a direct comparison between a cold-helium pressurization system and autogenous pressurization including screen devices cooling can be made as shown in Figure 3.1.13.

When adding this cooling penalty to the GH_2 pressurization system, Figure 3.1.13 shows that rather than a penalty of 180 kg, the cold-helium system involves a weight penalty less than 60 kg, not including any hardware required to implement the cooling. Therefore, when considering the complexities in implementing screen device cooling to assure that local dryout does not occur, the concept of screen cooling, except for very localized devices, does not appear to be particularly attractive. In reality the cooling process is effectively resulting in a cold (propellant temperature) GH_2 pressurization system. Such a system alternate is discussed in Section 3.2.
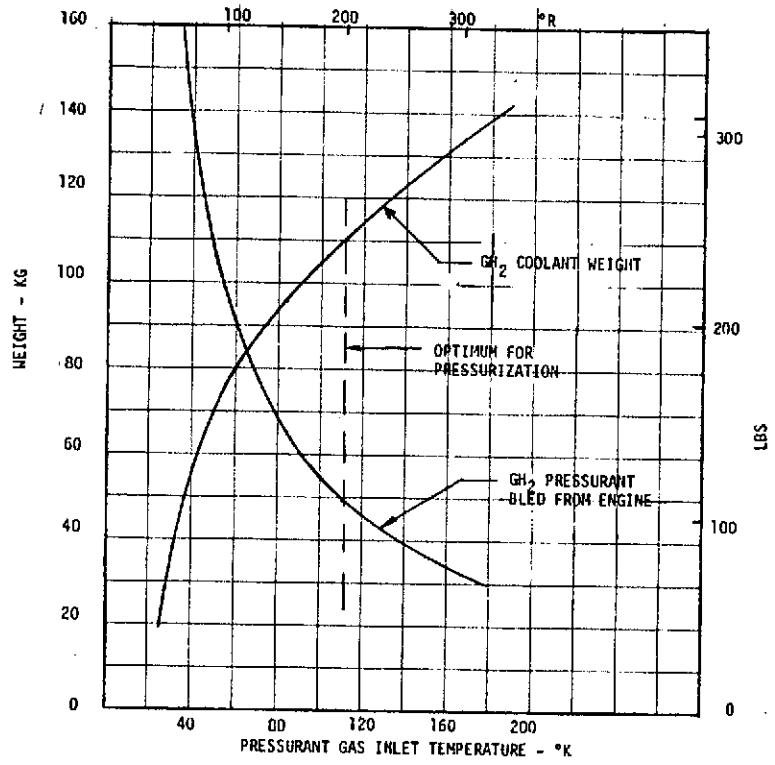
Figure 3.1.12. Comparison of GH$_2$ Pressurization With Screen Cooling and Cold Helium Pressurization
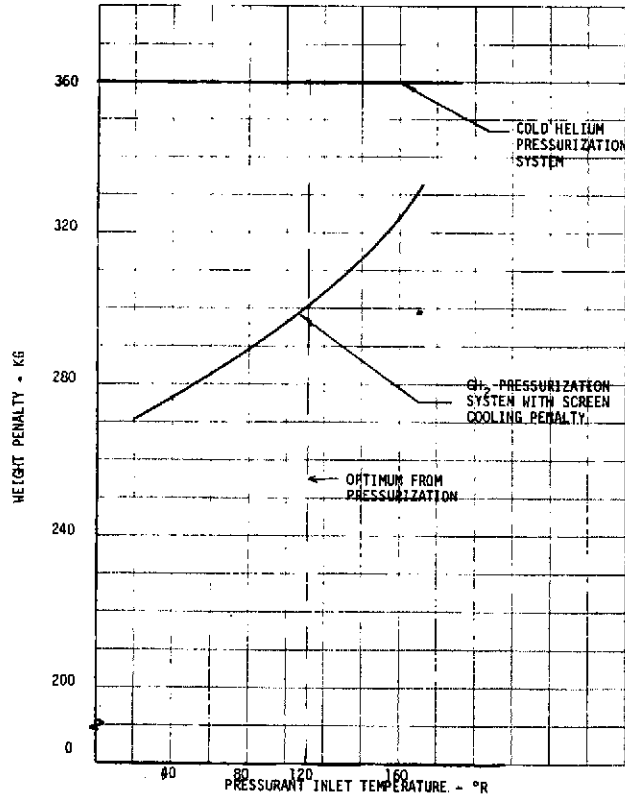
Figure 3.1.13. Comparison of Coolant and GH$_2$ Pressurant Weights

A thermal analysis was conducted for solid wall areas in the acquisition system to determine if insulation alone (without active cooling integrated with a thermodynamic vent system) can prevent boiling within the channel. Heat transfer to the channels was assumed to be by natural convection at 10^{-5} g, yielding a film coefficient of about 7.15 w/M^2°C (1.26 Btu/hr°F). A comparable film coefficient would result from forced convection at 0.3 M/sec (1 ft/sec); therefore, a combined film coefficient of 8.5 w/M^2°C (1.5 Btu/hr ft^2 °R) was chosen for this study. The film coefficient does, of course, vary with the gas temperature, composition, and pressure, and with location on the channel. However, an exact determination of these film coefficients is beyond the current state of knowledge in low-g heat transfer and fluid flow behavior.

Figure 3.1.14 shows that even with 0.15 M (6 in.) of internal foam insulation, the liquid hydrogen in the channel reaches the boiling point in 10^4 sec. This time is too short to be useful in preventing boiling in the channel. It is not likely that the situation could be improved by going to improved insulations; therefore, active cooling with a minimum of insulation must be used on significant solid wall areas that can be subjected to heat transfer. The maximum cooling weight penalty is shown in Figure 3.1.15, including the hydrogen coolant loss and the insulation weight. The insulation optimizes out to be about 0.02 M (0.79 in.). At this point, the coolant and insulation weights are about equivalent. This combined insulation and cooling requirement is not only a weight penalty but greatly complicates the design and fabrication of the system.

CR190
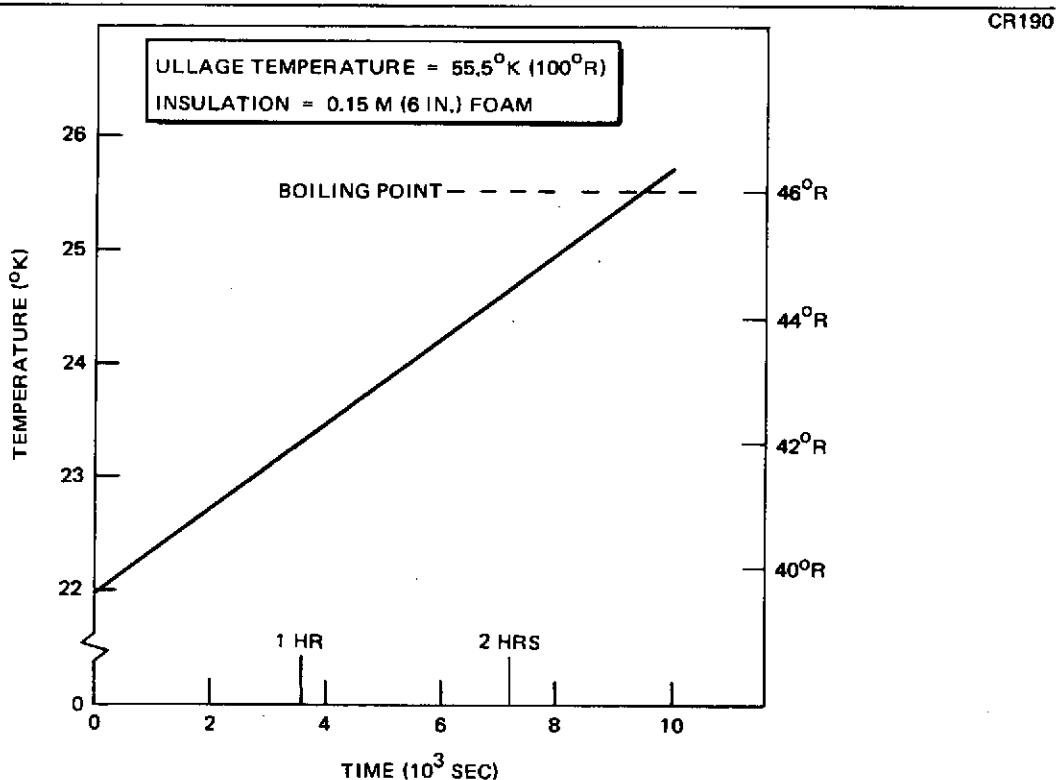
Figure 3.1.14. Transient Heating of an Uncooled Channel
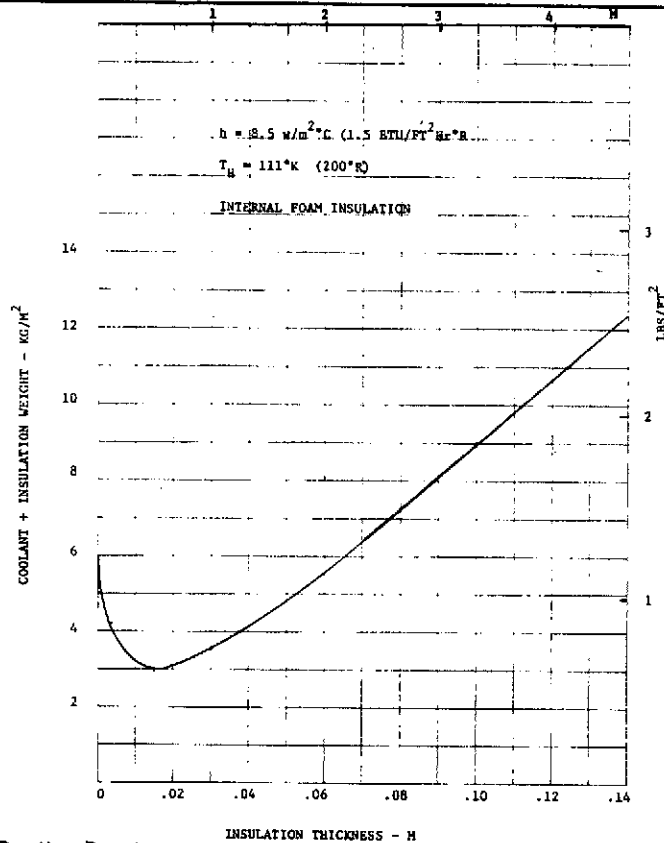
Figure 3.1.15. Solid Duct Area Cooling Penalty

As a result of the above screen acquisition device thermal control investigations, it was concluded that the feed system should be designed so that the screen device is not exposed to a source of significant heat transfer from the pressurant gas, the propellant, or the tank wall and system plumbing.

d. Feed System Transient Flow Dynamics. In the preceding section, the potentially strong impact of direct heat transfer on the operation of a distributed screen channel acquisition device was discussed, and it was shown that potential internal tank heat transfer problems, which can cause retention failure, dictate the selection of a compatible pressurization subsystem. Transient propellant flow processes in the total feed system can also lead to potential retention failure modes in the acquisition device. Some of these, such as those related to valve opening and closing transients, are common to all feed systems, and other, such as pump transients, are more unique to the specific SCC/APS application. Both of these problems are explored in the following sections.

(1) Pump Transients. In the particular ground-ruled CSS/APS application, the engines are supplied from high pressure gas accumulators which operate on a pressure control band 1103×10^4 N/M^2 (1600 psi) to 393×10^4 N/M^2 (570 psia). (See the system schematic in Figure 2.1.) However, the pump inlet is always at a low pressure, such as 17.2×10^4 N/M^2 (25 psia). Thus, when the pump undergoes startup or shutdown, there is a significant flow transient period much more severe than encountered with normal engine operation. These transients and how they are handled have a major impact on the total feed system design and weight. Two basic operational modes are possible: (1) so-called pump "dead-head" start and shutdown,

and (2) pump by-pass operation. In the "dead-head" mode of operation, the pump is started or shut down without by-pass of fluid, and the pumping action works against the existing head in the system. This results in no fluid loss from the system but is hard on the pump and could cause catastrophic pressure and backflow effects on the screen device. For example, during pump shutdown of the accumulator system, downstream pressures in the order of 1103×10^4 N/m² (1,600 psi) are possibly transmitted to the upstream feed line, screen device, and tank. Use of a tank prevalve would alleviate the pressure effects on the screen but still may present problems in terms of pump operation and sequencing. Pump shutdown also may cause a momentary backflow condition that would allow the expanding, high-pressure, two-phase fluid to pass through the screen. This effect is the most severe from the standpoint of screen acquisition device failure and could not be tolerated. Thus, "dead-head" operation was dropped from consideration from acquisition device design considerations.

In the pump by-pass approach, the heated-pump discharge fluid generated during the transient period is by-passed, partially or totally, either to an overboard dump or back to the low pressure tank. This mode of operation greatly minimizes pressure surges and backflow conditions. Dynamic analyses performed by Rocketdyne under Contract NAS 8-27794 (Reference 7) show that backflow and pressure surges are severe with no bypass, with 50 percent bypass, the pressure surge is low.

The bypass flow itself causes significant system problems. Overboard dump of the backflow is a direct weight penalty. Bypass of the fluid to the main tank introduces sufficiently warm two-phase fluid to cause significant tank pressure increases and heat load into the tank, which could cause retention breakdown. The LH_2 pump considered in this study could have a bypass flow of 0 to 2.04 kg/sec for approximately 1.5 sec for both startup and shutdown. The maximum fluid pressure would be of the order of $1,105 \times 10^4$ N/M² (1,600 psi), with the maximum fluid temperature approximately 39 to 42°K (70 to 75°R).

Based on Rocketdyne data, the approximate amount of bypassed hydrogen is of the order of 6.8 to 1.4 kg for each startup and shutdown. The effect on hydrogen tank pressure has been analyzed, and the results are plotted in Figures 3.1.16 and 3.1.17. Figure 3.1.16 illustrates the tank pressure increase resulting from the expansion of 2.72 kg of hydrogen at $1,105 \times 10^4$ N/M² (1,600 psi) and 39°K to an initial pressure of 173×10^3 N/M² (25 psia). All fluid is assumed to be expanded adiabatically into the ullage region of the tank. The APS accumulator refills may be performed consecutively for five cycles or more. Figure 3.1.16 shows that at low ullage percentages (<20 percent), pressure increases could be excessive. In this region, the bypass propellant may require positive thermal control (cooling) or overboard dump. Figure 3.1.17 shows the tank pressure increase for 3 percent ullage, which is the worst case condition.

The baseline FDC acquisition system uses cold-gas pressurization and heat flux interception at the tank wall to minimize thermal effects on screen stability. Pump bypass into the tank would violate this "no heat input" design criteria previously discussed and would introduce heat, flow patterns, and pressure changes that could affect acquisition performance. One failure mode involves the flow of the warm bypass condensate into the screen device, with subsequent tank pressure collapse. Boiling in the channel would then occur.
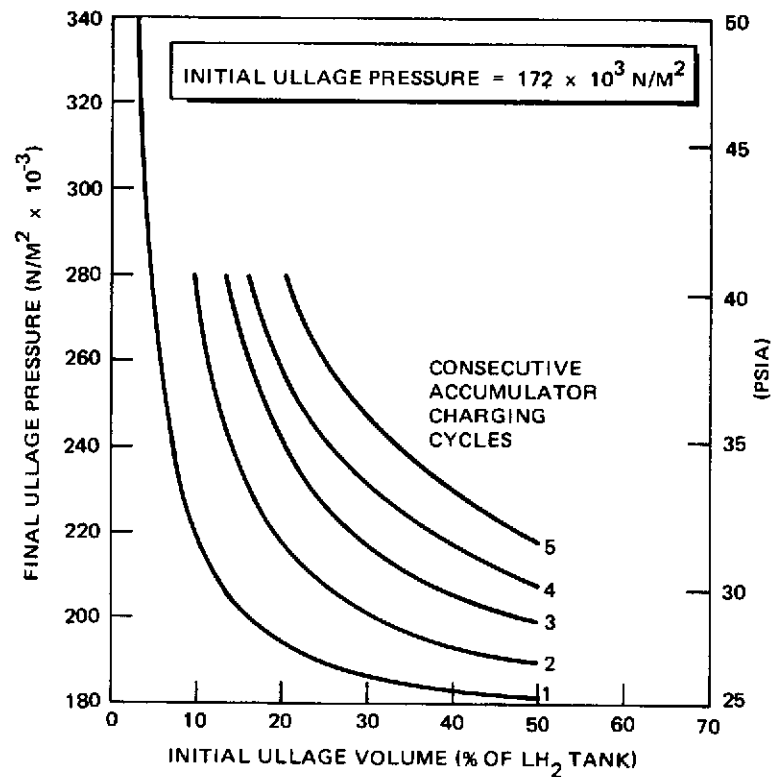
Figure 3.1.16. LH$_2$ Pump Bypass Directly Into LH$_2$ Tank — No Mixing

A general flow dynamic program, developed at MDAC, was used to estimate turbopump-induced pressure/flow surges occurring after closure of the ACPS conditioner valve with a 50-percent bypass flow back into the main tank (see Figure 3.1.18). The sequence assumes a steady flow to the ACPS conditioner and, at time zero, power is removed from the turbine, the ACPS conditioner valve is closed, and the bypass valve is opened. The pump flow decelerates rapidly, with bypass flow back into the main tank increasing rapidly. In addition, propellant surges back through the pump at a maximum rate of 0.1234 kg/sec. This negative flow, or pump backflow, constitutes one of the most significant potential failure modes associated with any screen device. The magnitude of the backflow increases as the bypass percentage decreases. With high bypass percentages, approaching 100 percent, it is probable that no significant backflow or pressure surge problem exists. At zero bypass, it is likely that backflow and pressure surges are too severe to be accommodated by the screen device. In addition to the hydrodynamic pressure surges, the liquid hydrogen downstream of the pump will be at a high pressure and will have been heated from 33°K to 40°K because of the work done by the pump on the fluid. Expansion of this fluid back through the feedline to the surface tension device is considered a serious failure.

Although these results for the feed system dynamic show that pressure differences between the screen device and ullage far exceed the maximum screen bubble point of approximately 0.69 x 10^3 N/M^2 (0.1 psi), it is not possible to determine whether the surges will, indeed, cause screen
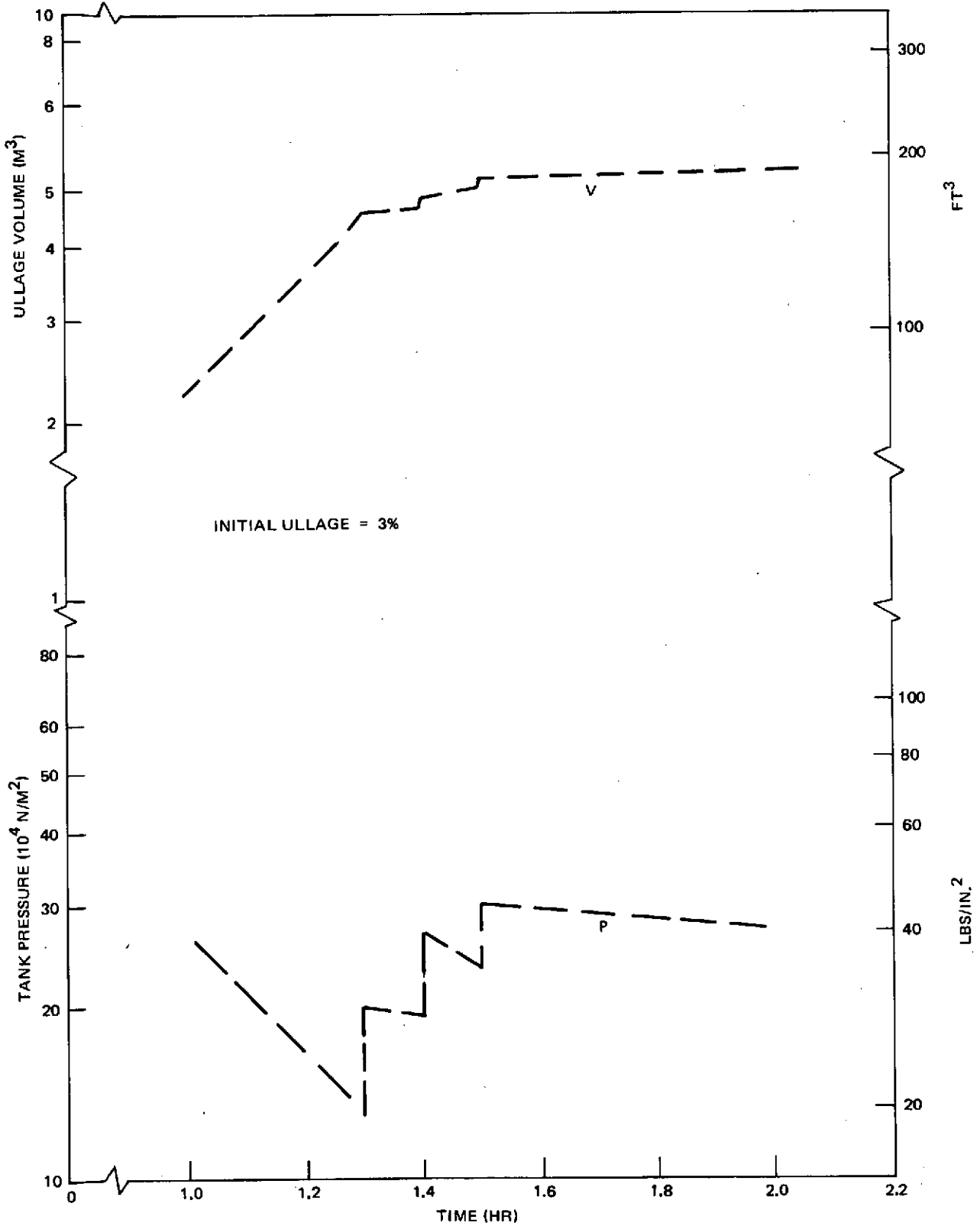
Figure 3.1.17. Estimated LH$_2$ Tank Pressure Using Pump Bypass
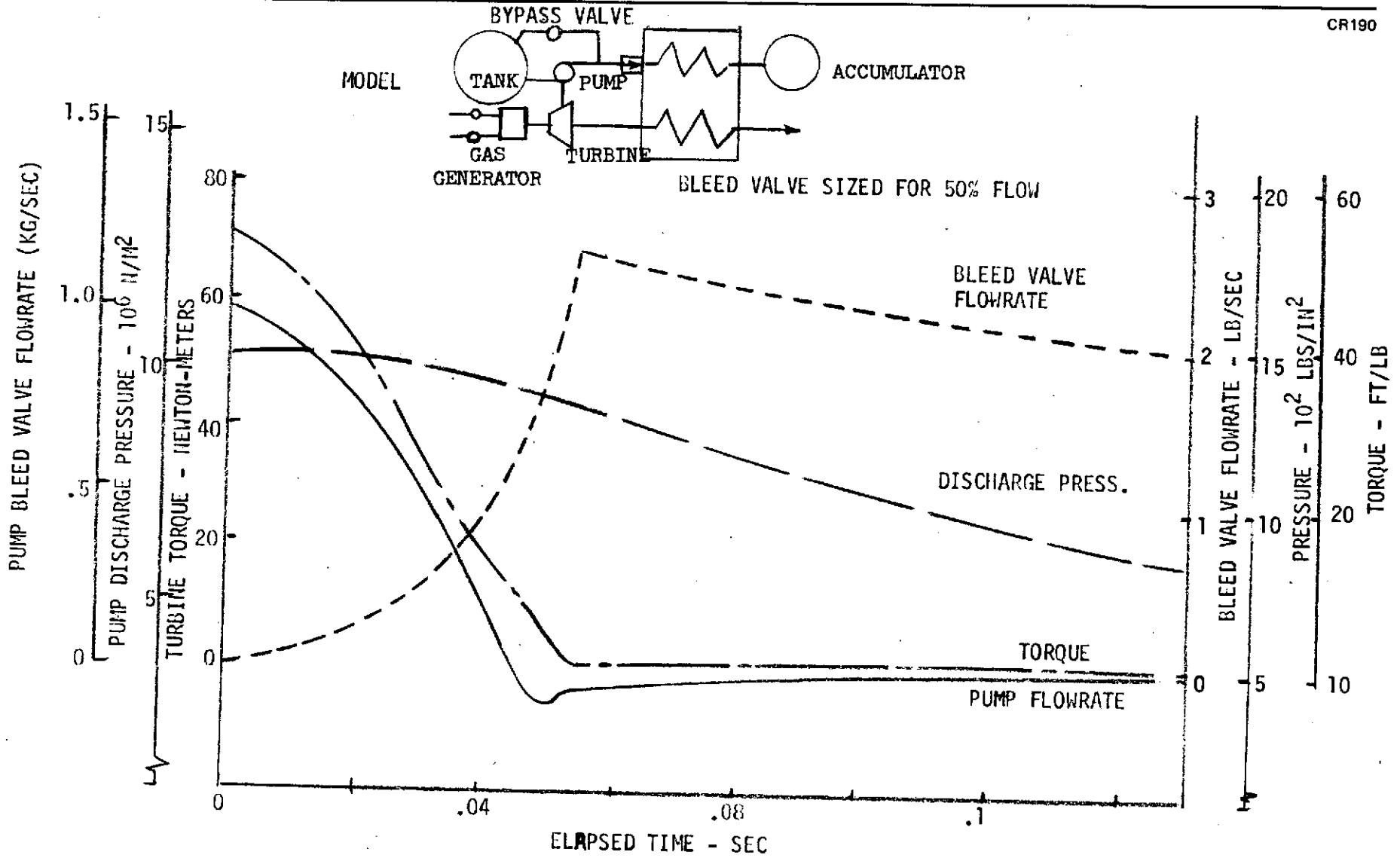
Figure 3.1.18. ACPS Turbopump Shutdown Transient

breakdown, since the screens are flexible, and this "compliance" would tend to decrease the pressure surges. This area requires additional analysis and research. However, based on current knowledge, a successful feed system design must accommodate the requirements for maintaining screen integrity during the hydraulic transient by minimizing backflow and pressure surges, while at the same time minimizing the system penalties associated with large pump bypass flowrates, as discussed in the following section.

Two approaches for managing this bypass fluid were evaluated:

(a) Dump the warm bypass fluid directly overboard until the pump comes up to design discharge pressure.

(b) Recirculate the warm bypass fluid back to the propellant tank and assume that the added heat is absorbed by boiling off tanked propellant.

Information was obtained from Rocketdyne (Reference 7) on the LH_2 and LO_2 pump transient behavior. Tabular and plotted information presented on pump bypass flow rate and temperature histories during startup and shutdown were used to evaluate impact on the feed subsystem (see Figure 3.1.19).
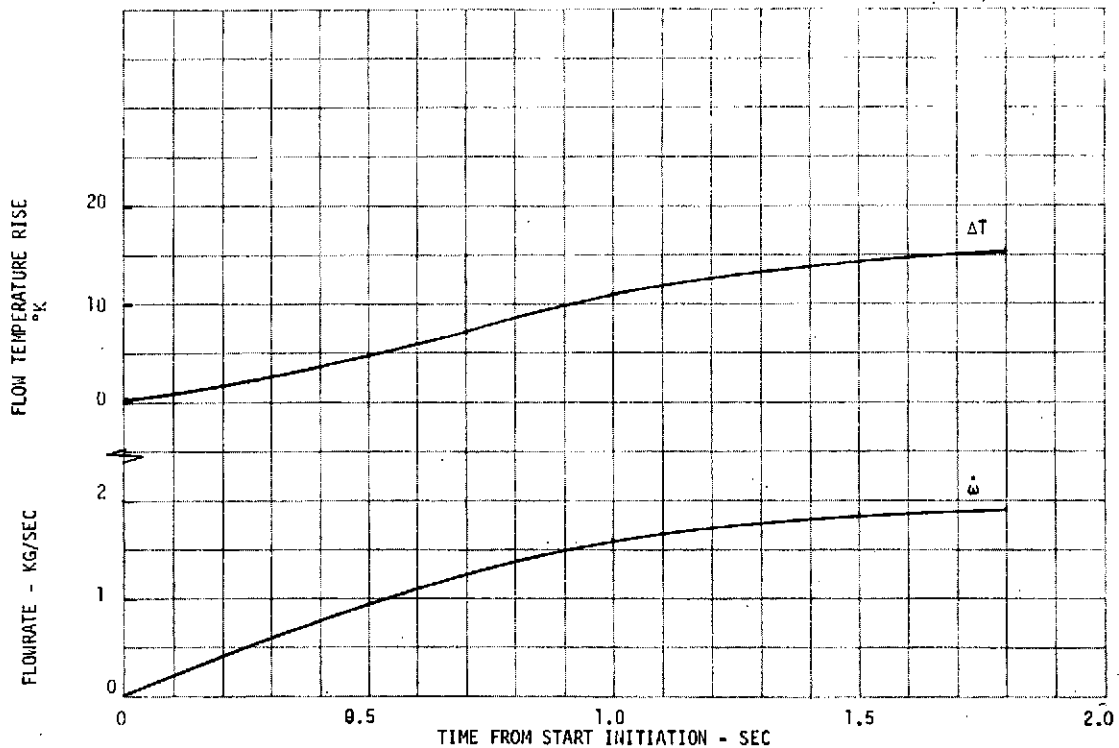
Figure 3.1.19. Pump Startup Flow Conditions

The amount of heat addition to the tank system involved in recirculating the bypass flow was estimated directly from an integration of the flow rate and ΔT histories. The results are shown in Figure 3.1.20 for the startup phase with 100 percent by-pass. From this value, the resulting tank venting or propellant loss was calculated assuming that all heat addition goes into boiling off cryogen. The boiloff losses are shown in Figure 3.1.21 and compared with the propellant losses involved in direct dumping of the startup bypass flow. Similar information is presented in Figure 3.1.22 for the shutdown phase. The 100-percent bypass case is summarized in Table 3.1.4. From these results, it can be concluded that recirculating of the bypass with subsequent tanked cryogen boiloff results in significantly less cryogen loss than direct dumping of the bypass. However, this bypass recirculation management approach requires the addition of a system to implement reliably the exchange of the heat between the by-pass and tanked fluid and tank venting in the short startup time period. This was found to be theoretically possible, but the required energy exchange rate, 221×10^3 watts (210 Btu/sec), with the low available temperature difference would result in massive heat exchangers inappropriate for this application. Thus, direct overboard dumping of the bypass was selected as the only practical approach for handling the pump transients with the losses as shown in Table 3.1.4 for each pump startup and shutdown cycle.
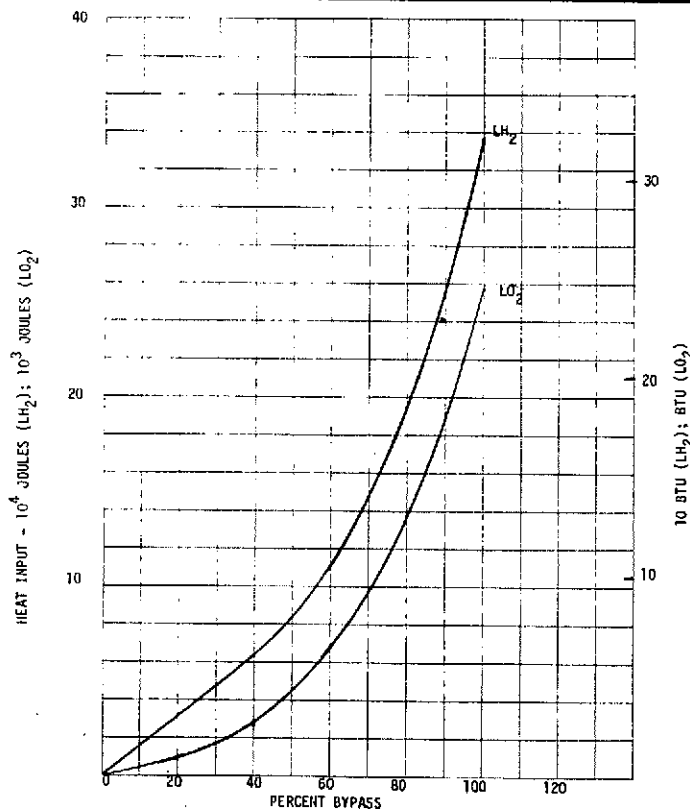
Figure 3.1.20. Potential Tank Heat Input From Startup Bypass
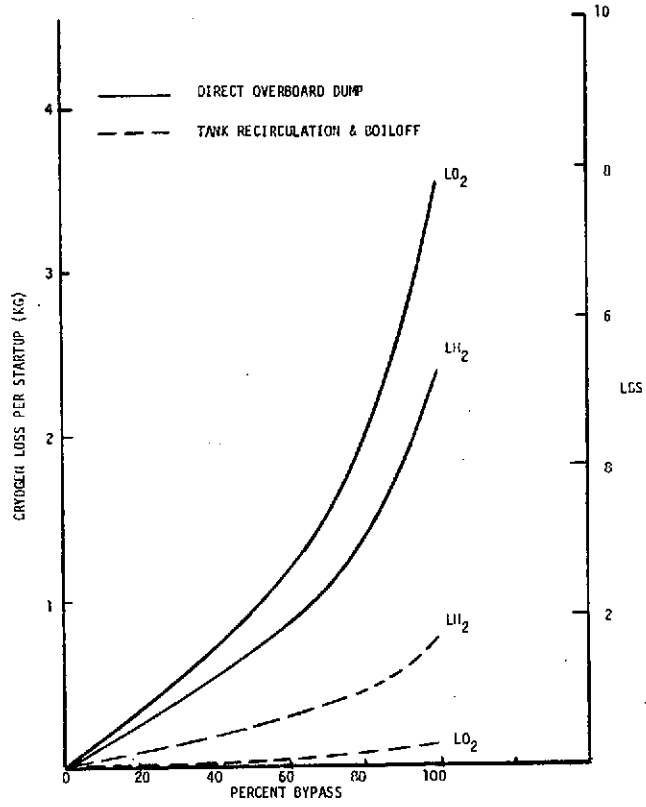
Figure 3.1.21. Startup Potential Propellant Losses
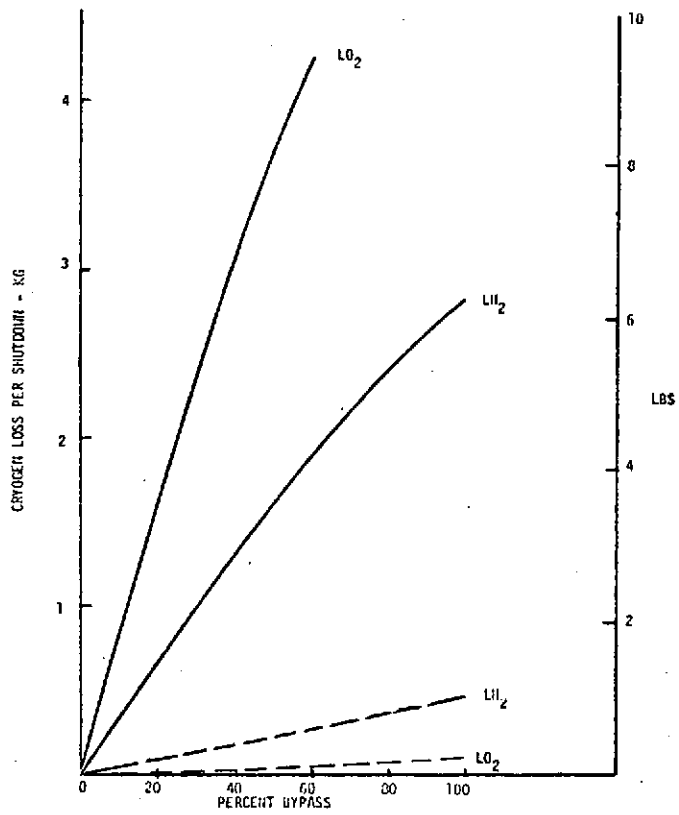
Figure 3.1.22. Shutdown Potential Propellant Losses

Table 3.1.4
PUMP BYPASS POTENTIAL PROPELLANT LOSSES
(100% BYPASS)

	Propellant Loss Per Cycle — kg (lb)		
	LO_2	LH_2	Total
Direct Dump			
Startup	3.5 (7.8)	2.4 (5.3)	5.9 (13.1)
Shutdown	6.3 (13.9)	2.8 (7.2)	9.1 (20.1)
Total	9.8 (21.7)	5.2 (11.5)	15.0 (33.2)
Tank Recirculation with Additional Boiloff			
Startup	0.136 (0.3)	0.82 (1.8)	0.95 (2.1)
Shutdown	0.091 (0.2)	0.45 (1.0)	0.54 (1.2)
Total	0.227 (0.5)	1.27 (2.8)	1.49 (3.3)

(2) Valve Opening and Closing Effects. An estimate of the importance of valve opening and closing pressure effects can be made from rigid liquid column theory. These pressure effects are often referred to as "water hammer." Parmakian (Reference 8) presents the basic equations, assuming incompressible liquid, rigid pipes, negligible hydraulic losses, and uniform flow and pressure across the pipe cross section as

$$H_a = -\frac{L}{g} \frac{dV}{dt}$$

where H_a is the head associated with the deceleration or acceleration of the liquid at the valves, L is the pipe length, and dV/dt is the rate at which the liquid velocity changes. With various pipe lengths and diameters between the liquid reservoir interface and the valve, the equation used is

$$H_a = -\frac{A_1}{g} \left(\frac{L_1}{A_1} + \frac{L_2}{A_2} + \ldots + \frac{L_n}{A_1} \right) \frac{dV_1}{dt}$$

where A_n and L_n denote the cross-sectional area and length of the nth pipe section. For liquid hydrogen flowing at 2.04 kg/sec (4.5 lb/sec) in a 0.102-M (4-in.) diameter pipe 3.05M (10 ft.) long, with a valve closure of 0.03 sec, the "water hammer" pressure is approximately 25.5×10^3 N/M^2 (3.7 psi). Although this pressure is attenuated in being transmitted from the valve to the screen device, it is clear from this single example that hydraulic transients must be considered as important system interface problems, since the pressure differences greatly exceed the screen bubble-point pressures.

As a result, the MDAC liquid propulsion feed system dynamic analysis program, H672, was applied to analyze the various types of flow situations that will be encountered. The dynamic analysis computer program is useful for determining the magnitude and duration of the pressure and flow surges as a function of geometry, valve opening and closure rates, etc. However, this information cannot be used directly to determine whether screen breakdown occurs. It will be necessary to evaluate conditions experimentally for which screen breakdown occurs, and then compare these data with the computer predictions of pressure surges within the screen device. It would also be desirable to extend the capability of dynamic analysis programs to account for flow of the liquid through screens and for surface tension effects on pressure-wave attenuation. This is beyond the scope of this project.

This computer program uses a nonlinear description of components at discrete junctions with solutions to the flow between junctions obtained by the method of characteristics. The obtained solutions are for liquid hydrogen and simulate a set of three channels in the LH_2 tank. In this configuration, it is only necessary to change the dimensions of the channels and associated tank to simulate a range of system conditions. The model cannot account for flow through the screen and, therefore, treats the screen portion as an equivalent pipe.

Figure 3.1.23 illustrates the computed pressure surges for a three-channel acquisition device configuration in the baseline LH_2 tank. Steady-state flow was not reached during the 0.015 second the valve was full open. It is seen, however, that for the low flowrate (2.05 kg/sec maximum) a high pressure surge of 690×10^3 N/M^2 (100 psi) is produced immediately upstream of the valve. This pressure wave is strongly attenuated within the screen device.

Figures 3.1.24 to 3.1.27 illustrate a higher flowrate (4.95 kg/sec) for the channel system in the LH_2 tank. (Automatic computer printout is used.) The pressure surge at the valve is a maximum of 1140 N/M^2 (165 psi) following shutdown. The pressure surge in the screen device, denoted H_4, drops a maximum of 41.5 N/M^2 (6 psi) below the ullage pressure at 0.015 second, and increases to 180 N/M^2 (26 psi) above the ullage pressure at 0.048 second. Pressure surges of this magnitude may be associated with vapor ingestion or liquid loss through the screen. Figure 3.1.25 shows that there is a short-duration negative flow following valve shutdown. Figure 3.1.27 shows that although very large pressure surges are generated at the valve when it is closed rapidly these surges are attenuated by the line restrictions, but that this attenuation is not sufficient to eliminate the possibility of breakdown at the screen device.

e. Preliminary Design. Based on the preceding channel cross section, screen mesh and element, and duct configuration selection studies, a preliminary acquisition subsystem design was developed for the FDC concept. Figures 3.1.28 and 3.1.29 show layouts of the 16-segment 3.66 M (12 ft) diameter ring system. Note that the elbow sections are designed to maintain the V-band connectors at a circular cross section. The overall duct system orientation is shown in Figure 3.1.28. Two primary acquisition rings are used. A third ring, which provides acquisition during the early portion of the reentry period and general redundancy, is positioned within the propellant trap region. The trap baffle is positioned so that the trap can contain 2.83 M^3 (100 ft^3) of LH_2. This provides propellant for all
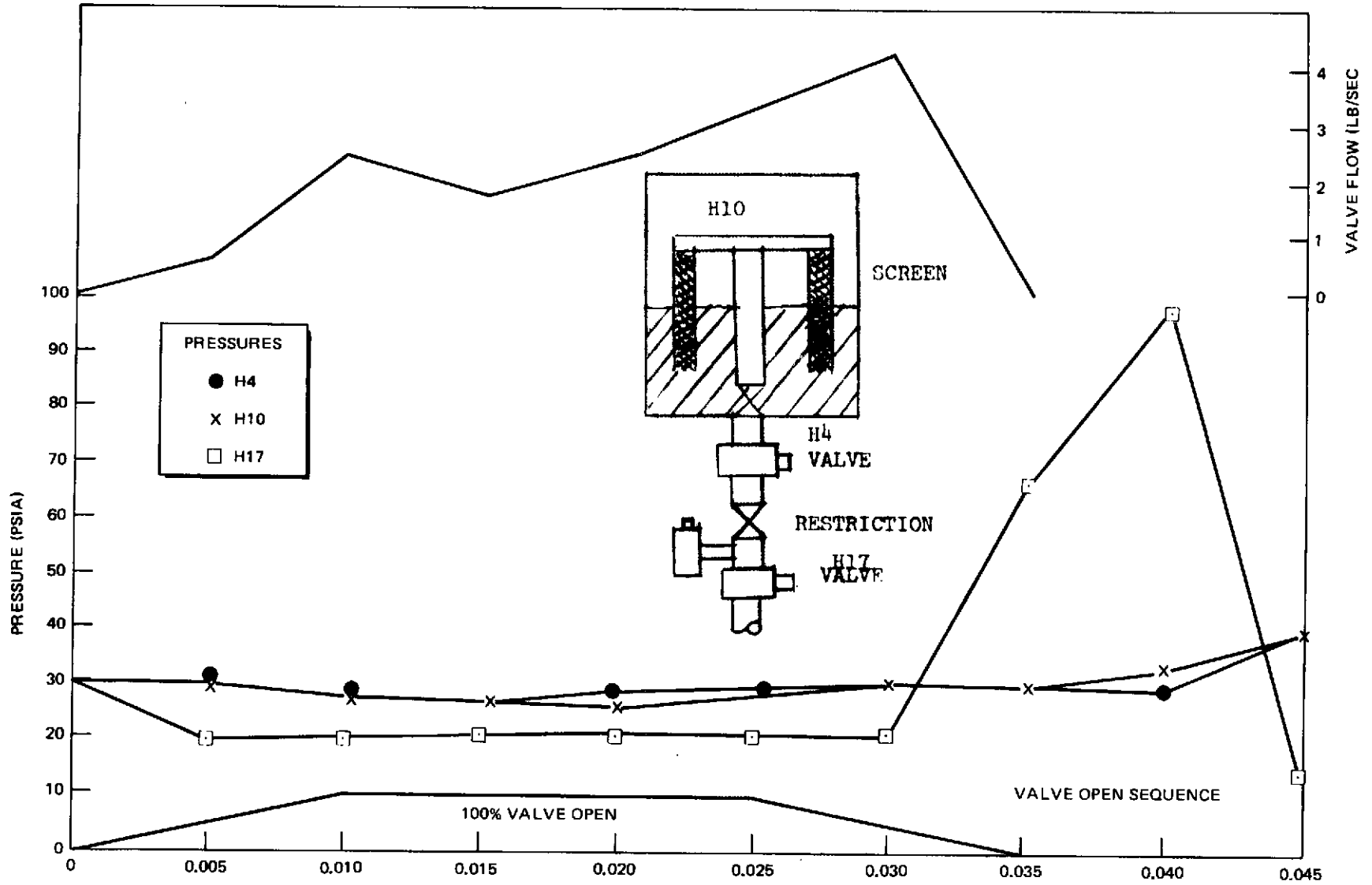
Figure 3.1.23. LH$_2$ Acquisition System Response
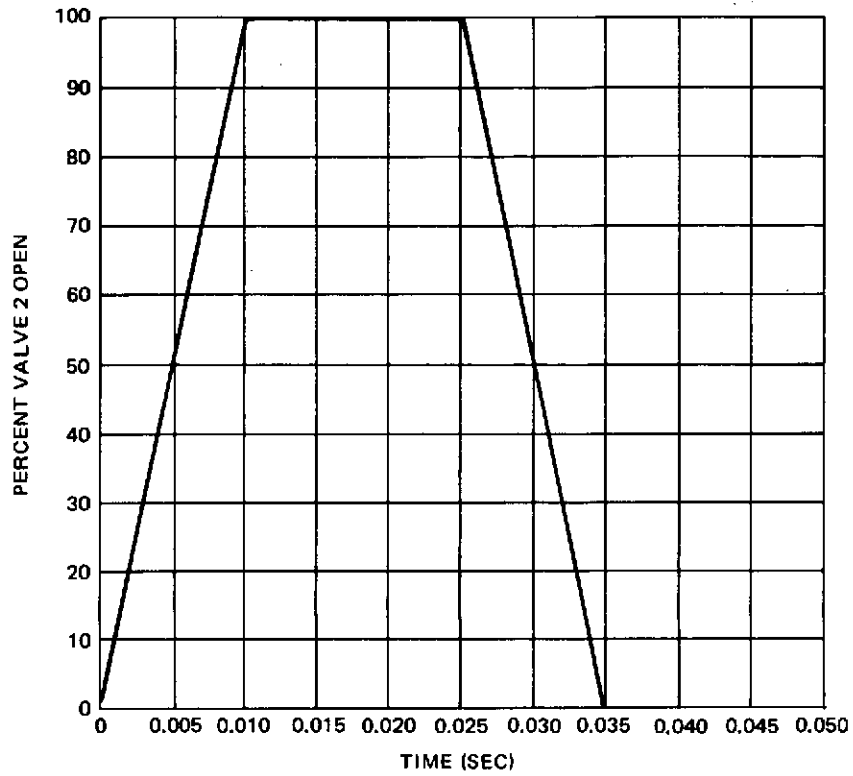
Figure 3.1.24. LH$_2$ Acquisition Subsystem
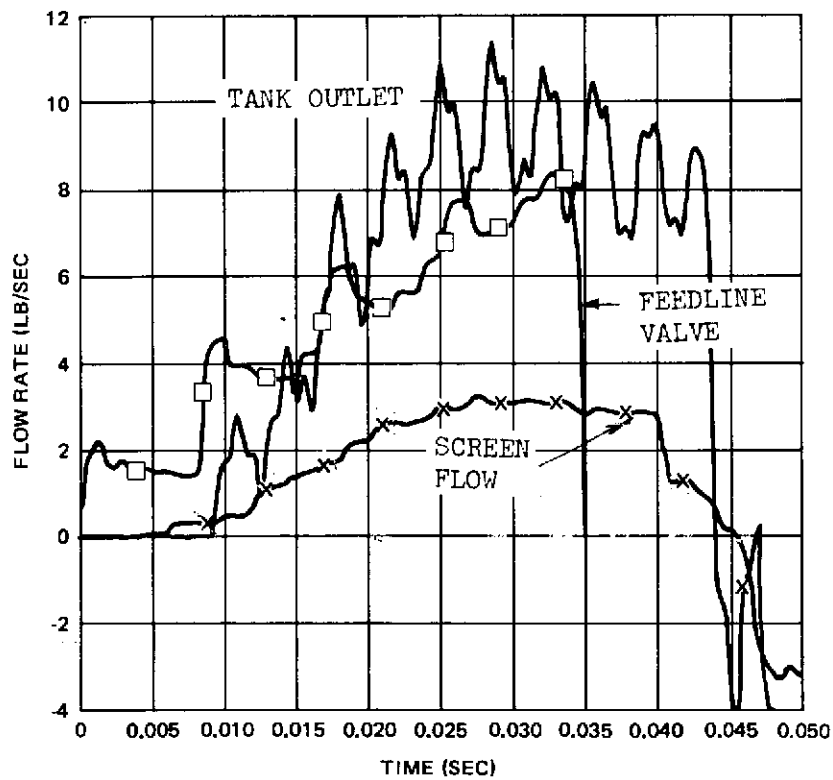
Figure 3.1.25. LH$_2$ Acquisition Subsystem
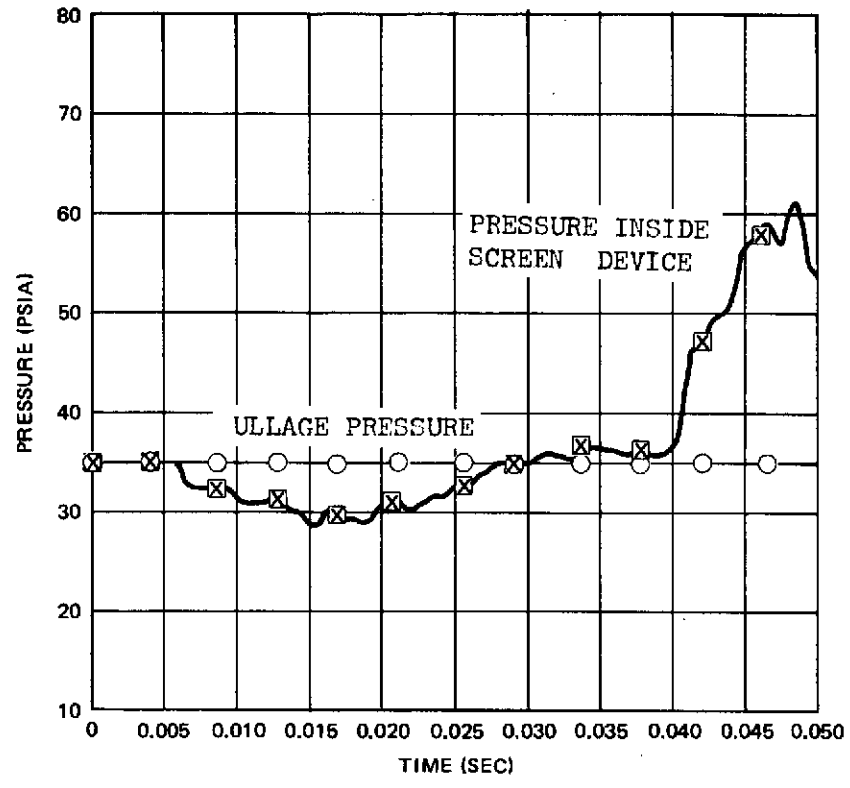
Figure 3.1.26. LH$_2$ Acquisition Subsystem
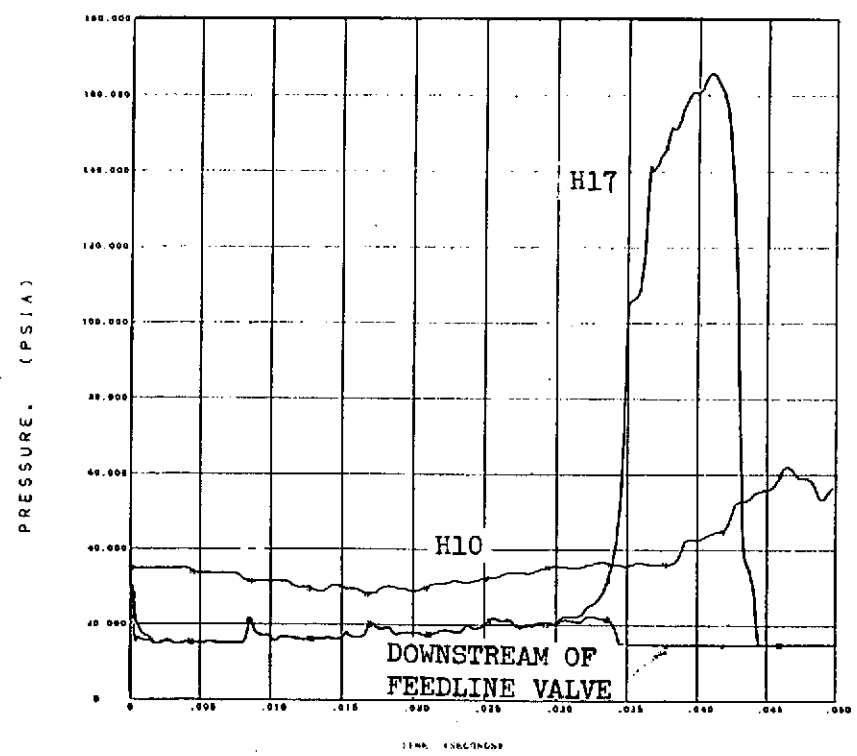
Figure 3.1.27. LH$_2$ Acquisition Subsystem
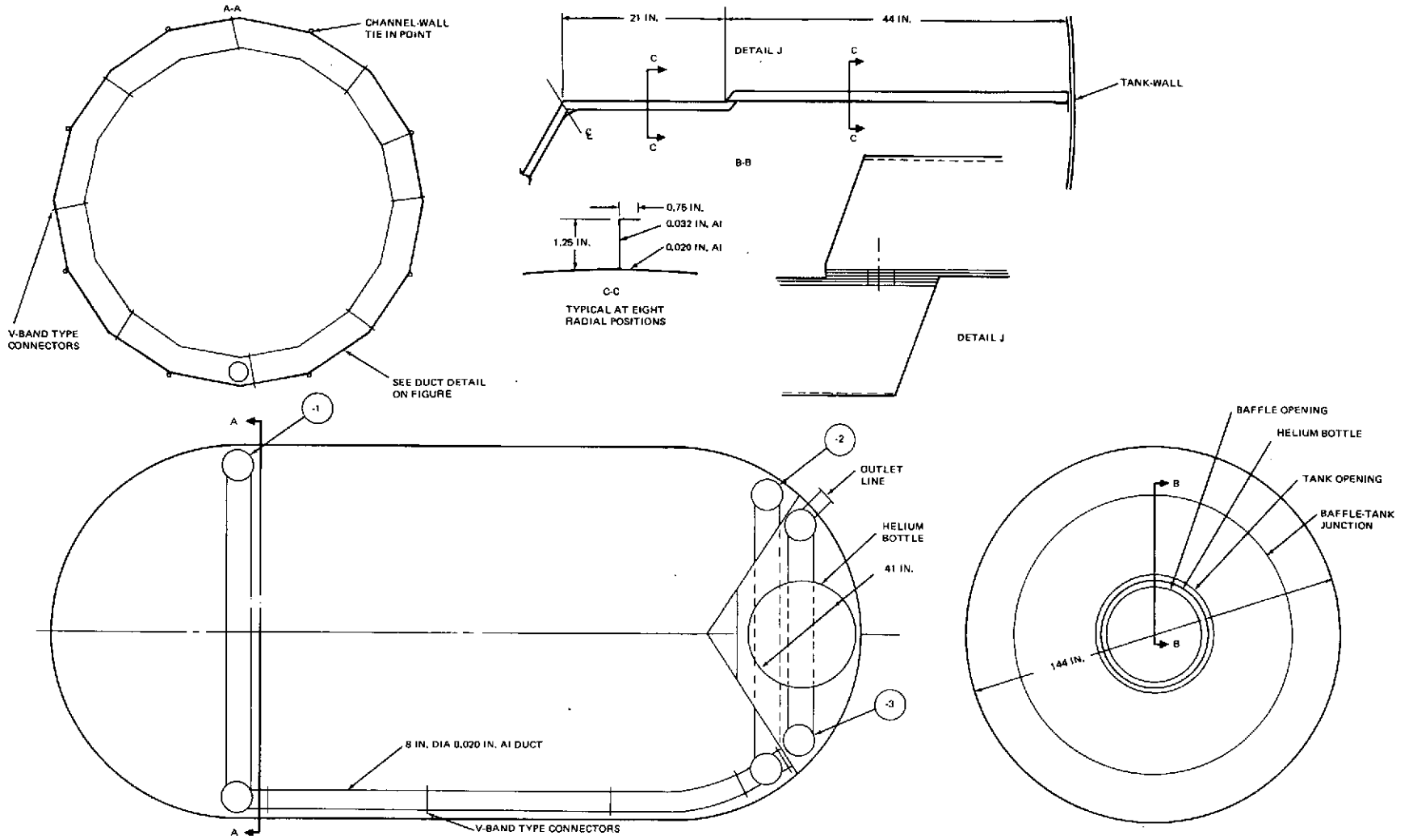
Figure 3.1.28. Distributed Channel Acquisition System Configuration (LH$_2$ Tank)

CHANNEL LOC	A	B
TOP	27.6 IN.	25.8 IN.
BOTTOM	22.8 IN.	21.0 IN.
BAFFLE	18.0 IN.	16.2 IN.

FINE MESH STEEL

WELD POINT

WELD BAND (0.010 IN.)

LATCH BAND

FLANGE

COARSE MESH ALUMINUM

RIVETS

PERFORATED ALUMINUN TUBE — 0.020 IN.

DETAIL A (1/1)

A

B

A

PERFORATED, TUBE

COARSE AI MESH

FINE MESH STEEL

B

B

B

1/4 SCALE

A

A

DETAIL A

10 IN.

A-A

0.020 IN. STEEL WELD STRIP

FINE STEEL MESH

FLUSH RIVETS

JOINT WELD

COARSE ALUMINUM MESH

0.020 IN. STEEL ELBOW

B-B (1/1)

0.020 IN. PERFORATED ALUMINUM TUBE

Figure 3.1.29. Channel Duct Det

functions during reentry. An allowance was made in the baffle volume for the helium pressurization bottle, which was sized for cold-helium pressurization requirements (see Section 3.2).

The details shown in the figures are for the C cross-section design which uses an aluminum perforated tube for structural backup. The channel is first formed by rolling the perforated aluminum into two 25.4 cm (10 in.) diameter cylinders. The two cylinders are riveted to the short steel center elbow and the steel end flanges are riveted to the aluminum tube ends to accommodate the V-band couplings. The flush rivets structurally hold the various elements together but do not provide any form of seal. The coarse mesh aluminum screen (used to reduce pressure loss) is next put into place over the perforated cylinder (no physical attachment), and the fine mesh steel screen is cut and layed in place. Thin (1.27 cm) bands are then clamped along the screen edges and the bands, screen, and steel end pieces are welded together to complete the duct section assembly. (Actual hardware details of such a system are shown in section 5 Prototype Design and Fabrication.)

The rings are connected to the sump baffle through 20.3 cm (8 in.) diameter aluminum collector ducts. Similar V-band joint/couplings are used to join the collector duct sections and to join the collector duct to the rings and the sump baffle. It should be noted that the surface area for this duct system is only 30 percent of what a full screen wall liner would be. This brings about minimum weight for the screen elements and support hardware. It is made up of 0.051 cm (0.020 in.) aluminum reinforced by eight radially-running Z-sections made of 0.091-cm aluminum. The center portion of the baffle cone is removable to provide about a 1-M access diameter into the main portion of the tank. The tank manhole itself provides sufficiently large access to accommodate the helium bottle.

Each ring channel is attached to the cryogen tank wall through local point support mechanisms. To facilitate installation of the eight channel sections, eight attachment points should be used, but these do not have to be permanent attachments, since once the ring sections are joined, the full channel could be supported by as few as three supports. The channel structure is relatively light and the support loads are small. Thus, the support structural requirements are minimum. However, the ring must be held rigid and the supports must be capable of accommodating the thermal contractions.

Two possible support approaches were devised as shown in Figures 3.1.30.1 and 3.1.30.2. In the one case, a series of hinges were conceived where the movement of the hinge would allow for contractions. This is illustrated as applied to a solid duct system. In the second case, a tension cable strut support system was used. Each support point has three cables which join at the channel and intersect at 120°. The hinge system requires the installation of cylindrical pins which could be tedious for in-tank installation and parts placement within the tank would have to be to close tolerances. The cable system, on the other hand, would use turnbuckles to allow proper alignment without highly-precise attachment pad placements in the tank. Cable attachments would use simple eye bolts to ease the in-tank installation. A three-cable support system of this type was investigated in

30° TYP

SINGLE HINGE
PLATE CENTERING
SUPPORT, 1 OF 3

TANK WALL

TANK CENTERLINE

60° TYP

COLLECTOR DUCT
LOCATION

DOUBLE HINGE
PLATE SUPPORT, 1 OF 9

JOINT BETWEEN
CHANNEL SEGMENTS

A

A

VIEW AA

HINGE PLATE
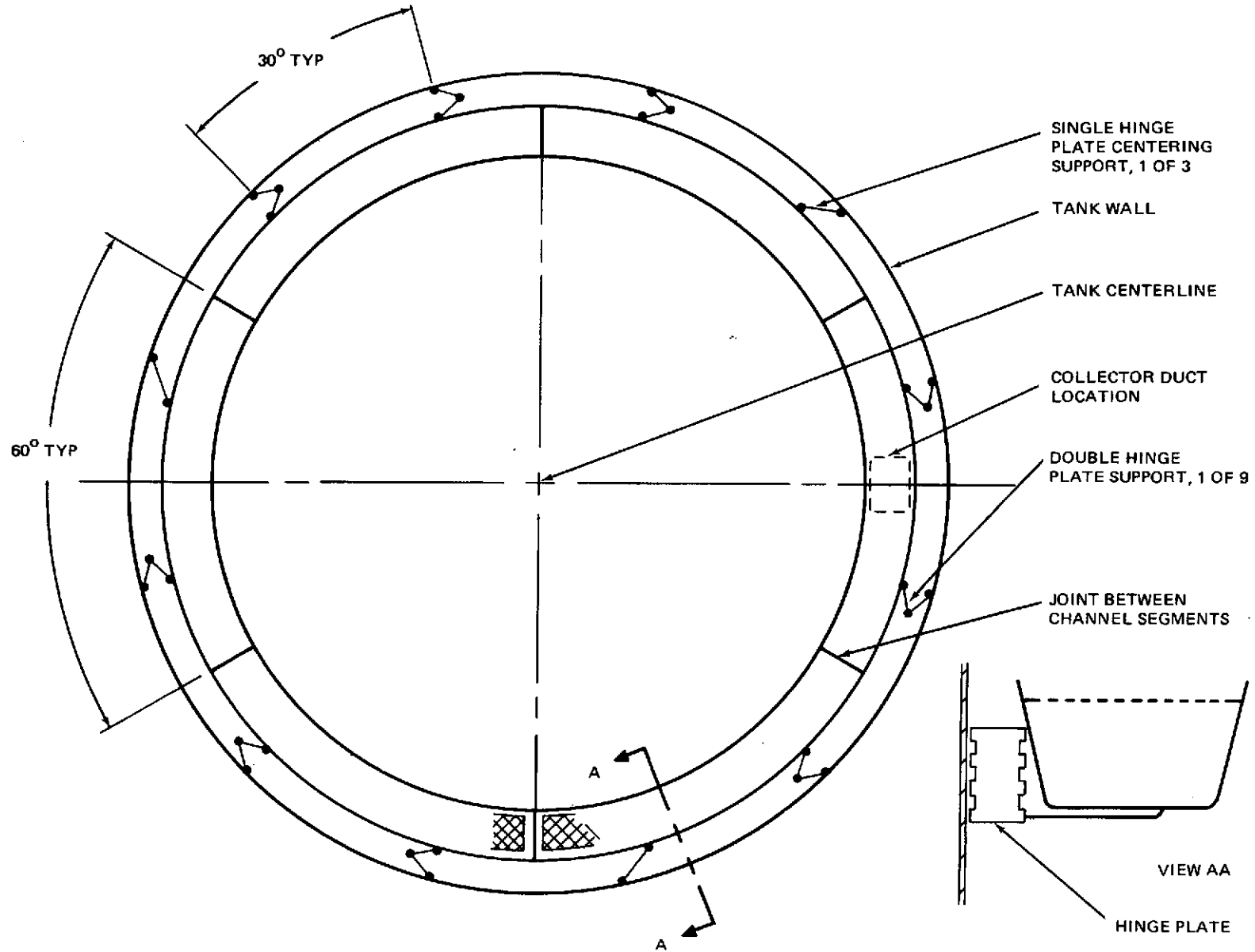
Figure 3.1.30.1. Hinge Channel Support Concept

TANK WALL

WELD PAD

SCREW-IN EYELET

DETAIL A

TURNBUCKLE

RETAINING STRAP

DETAIL B

CABLE END BALL

CABLE

CHANNEL

DETAIL A

CABLE END BALLS

RETAINER

DETAIL B
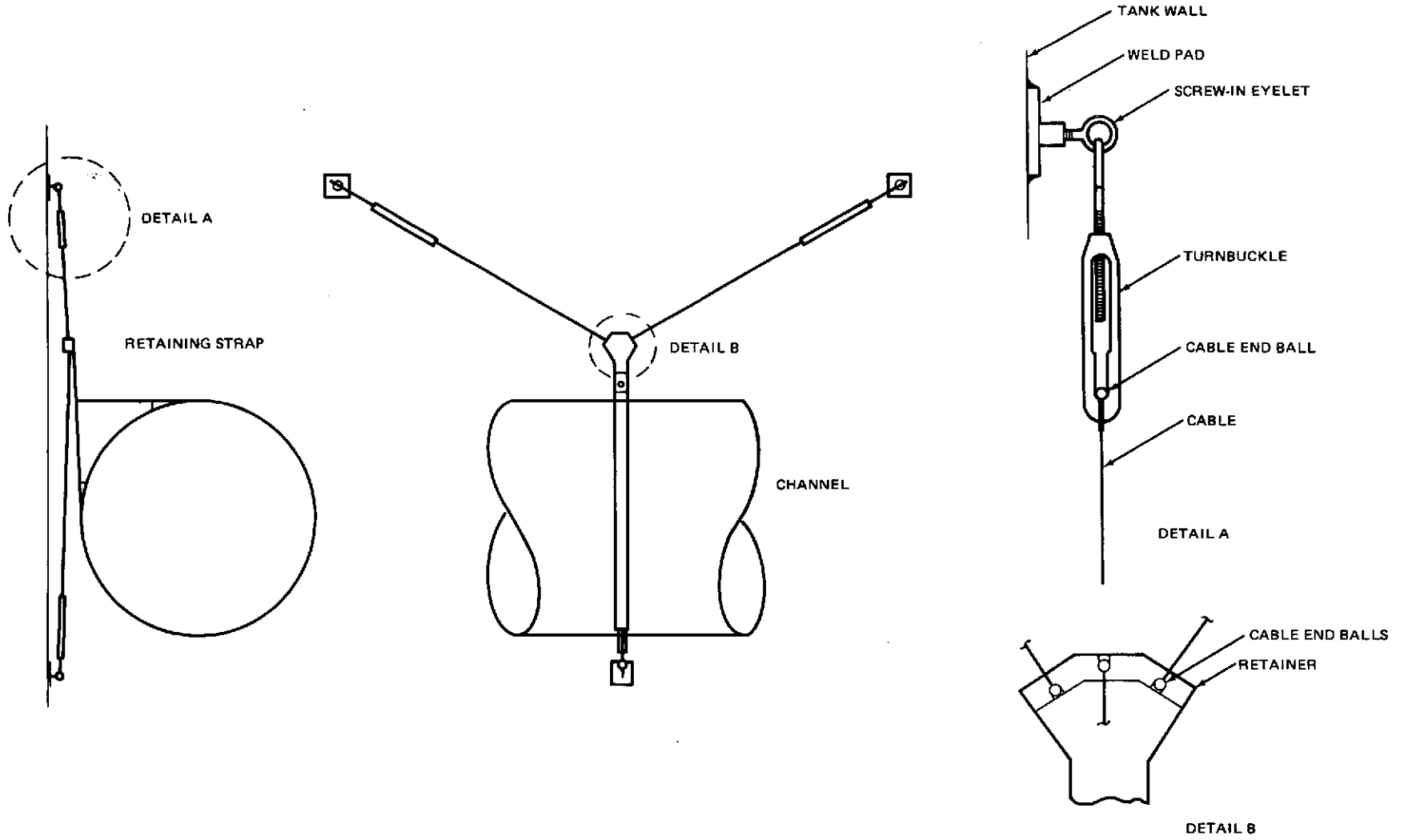
Figure 3.1.30.2. Three Cable Channel Support Concept

Reference 9 for the support of non-integral propellant tanks within a
vehicle shell structure and was shown to be highly effective in rigidly
supporting cryogenic tanks even with high loading conditions and to result
in minimum heat leak. Thus, the three-element tension member system was
selected for the channel supports using three primary supports per channel.
Design details are shown in Figure 3.1.30.1.

The channel is gripped by a thin steel band wrapped around the
channel and riveted at its ends. At the end of the band is a fixture with
sockets for retaining the end-balls on the three braided-steel support cables.
The end-balls on the other end of the cables are inserted into the turn-buckle
assemblies. During installation into the tank, the turn-buckle is screwed
into the threaded ends of the eye bolts that are attached to the tank wall.

Based on the developed preliminary design, a weight estimate
of the acquisition system was made. The breakdown is shown in Table 3.1.5.
Weights are shown for the all-stainless steel and aluminum tube designs.
The acquisition system for the LO_2 tank is similar to that for the LH_2 tank,
except that three rings are used in the main tank (see Figure 3.1.31). The
required duct cross sectional diameter to satisfy all flow requirements is
17.8 cm (7 in.). The required baffle volume is 0.623 M^3 (22 ft^3), which
means the baffle weight is much smaller than for the LH_2 tank baffle. The
weight summary for the LO_2 tank acquisition system is shown in Table 3.1.6,
(aluminum perforated tube). From the criteria developed previously in this
section, to assure satisfactory operation of this FDC preliminary design, all
heat input to the tank interiors must be minimized and, hopefully, eliminated.
To accomplish this, the following subsystem design features were established:

Propellant temperature helium tank pressurization.

Vapor-cooled shield TVS integrated with pump and
feedline cooling.

Direct overboard dump of pump bypass fluid during
startup and shutdown.

Table 3.1.5

DISTRIBUTED ACQUISITION SYSTEM WEIGHT ESTIMATES (LH_2 TANK)

	Aluminum Tube		All Steel Design	
- 1 Duct	29.5 kg	(64.9 lb)	40.8 kg	(90.0 lb)
- 2 Duct	25.9	(57.1 lb)	36.2	(79.7 lb)
- 3 Duct	23.6	(52.1 lb)	31.1	(68.4 lb)
Collection duct	8.8	(19.3 lb)	8.8	(19.3 lb)
Baffle	23.6	(52.1 lb)	23.6	(52.1 lb)
Subtotal	111.4	(245.5 lb)	140.5	(309.5 lb)
Support/attachments	6.2	(13.5)	6.2	(13.5)
Total	117.6 kg	(259.0 lb)	146.7 kg	(323.0 lb)

MARMAN CLAMPS

17.8 CM(7 IN)

-1 CHANNEL

-2 CHANNEL

BAFFLE

-3 CHANNEL
-4 CHANNEL

106.7 CM (42 IN) MANHOLE

COLLECTOR DUCT
[0 = 15.3 CM (6 IN)]
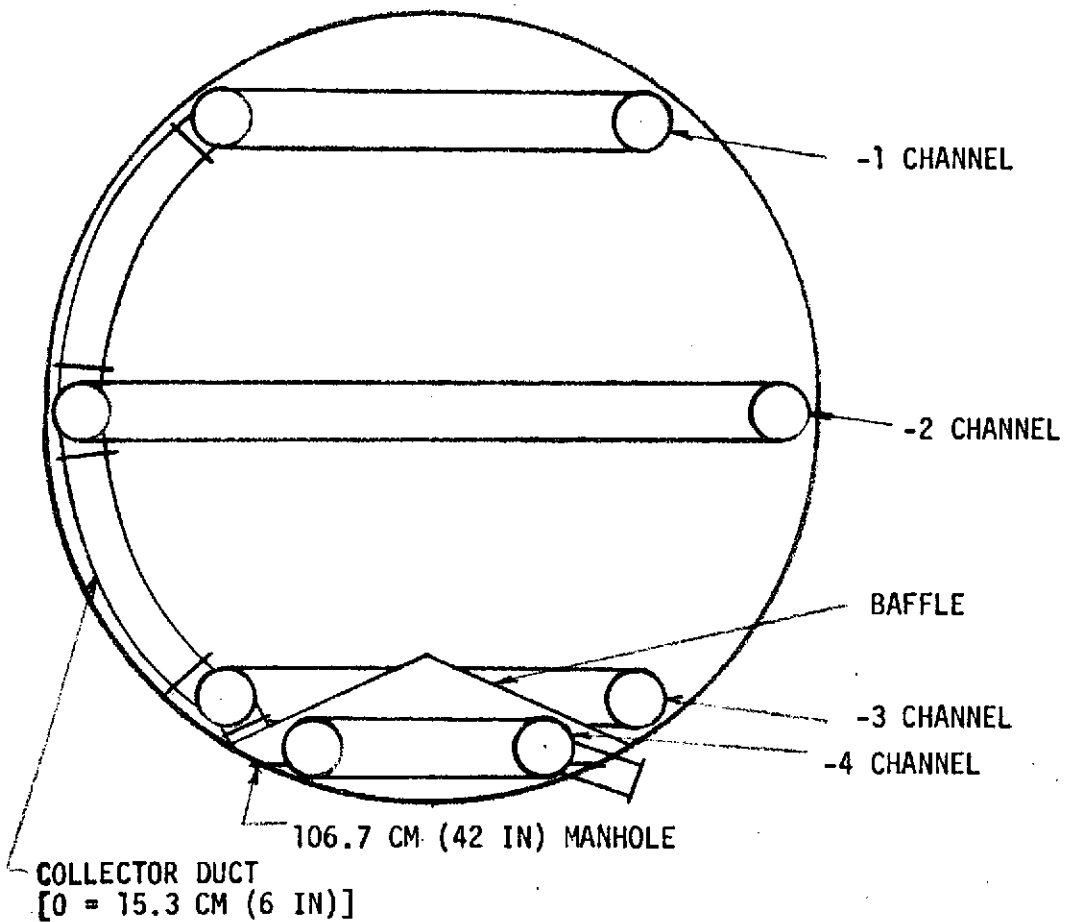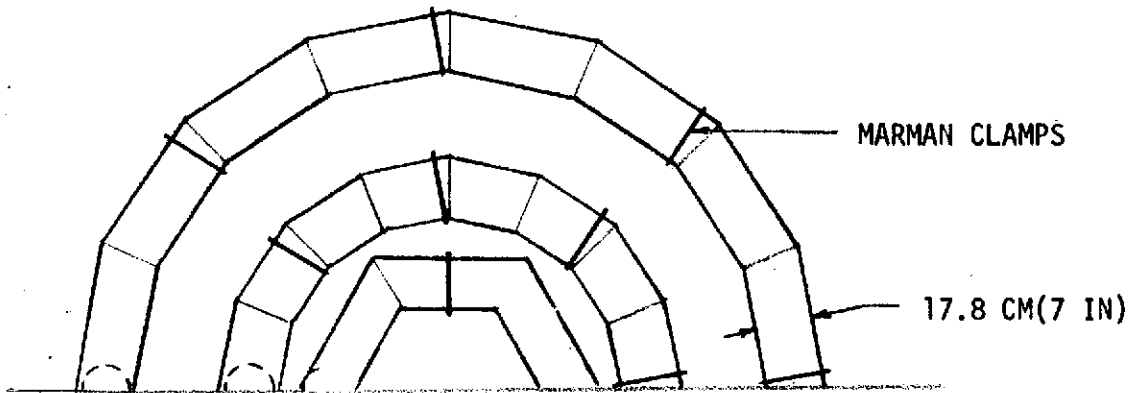
NOTE: ALL DETAIL DESIGN ELEMENTS SIMILAR
LH$_2$ SYSTEM SHOWN IN FIGURE 3.1.28

Figure 3.1.31. Distributed Channel Acquisition System Configuration (LO$_2$ Tank)

Table 3. 1. 6

DISTRIBUTED ACQUISITION SYSTEM WEIGHT ESTIMATES
LO_2 TANK

- 1 Duct	16. 3 kg	(35. 8 lb)
- 2 Duct	18. 9	(41. 7)
- 3 Duct	15. 4	(34. 0)
- 4 Duct	15. 0	(33. 0)
Collector duct	3. 7	(8. 1)
Baffle	5. 7	(12. 5)
Subtotal	75. 0 kg	(165. 1 lb)
Support/attachments	8. 3	(18. 3)
Total	83. 3 kg	(183. 4 lb)

These concepts and possible alternatives are discussed and evaluated in Sections 3. 2 and 3. 3, and the various interfacing subsystems are integrated into a total FDC feed system in Section 3. 4. This design is also compared with an alternative acquisition concept design developed in the following section.

3. 1. 3 Localized Pressure Isolated Channel (LPIC) Acquisition Concept. From the above discussion, it can be seen that the full tank distributed screen acquisition concept requires significant constraints on the design of the pressurization and thermal control subsystems when the system is designed to resist all possible failure modes. These constraints involve weight and reliability penalties which may be avoided by employing a different acquisition design approach. The basic failure modes with the FDC have their origin in the sensitivity of the surface tension screen device to heat transfer and fluid dynamics. Thus, most of these overall feed system constraints could be eliminated or greatly relieved by using a localized and thermally-isolated acquisition device as opposed to the full tank channel distribution system. The isolation principle physically separates the screen device from the critical tank thermodynamics and fluid dynamics. In this revised acquisition approach, shown in Figure 3. 1. 32, the reduced size or localized surface tension screen channel is placed within a secondary tank located within the main propellant tank. This inner tank is independently pressurized with cold helium and insulated to provide the required thermal isolation. The main tank now can be pressurized with warm GH_2 which in general results in a lighter pressurization system (see Section 3. 2). Other sources of tank energy input such as tank wall heating and pump by-pass fluid can also be tolerated with this approach since the screen is completely isolated from the fluid conditions in the main portion of the tank. The complicating factor with this and any localized acquisition concept is that the inner or secondary tank must be periodically refilled. Fortunately, in the CSS/APS application, defined long-duration Orbit Maneuvering (OM) burns are available, during which time the developed vehicle acceleration can be used to refill the secondary acquisition device tankage once the OMS is started from the propellants originally retained in the acquisition device/secondary tank. Other refill techniques are also possible, as will be discussed later.
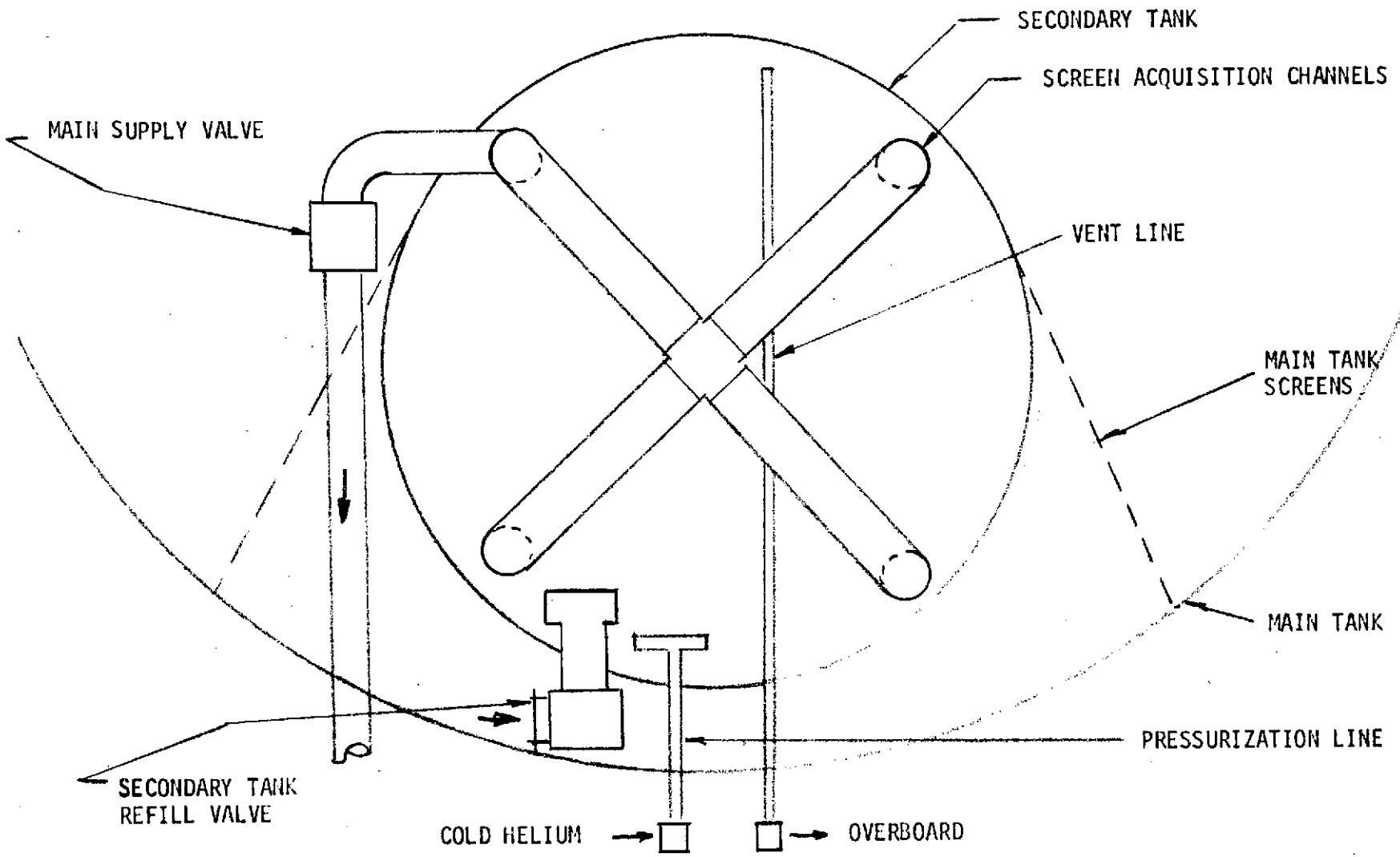
Figure 3.1.32. Localized Pressure Isolated Channel (LPIC) Concept

a. General Operation. The operation of the recommended Localized Pressure Isolated Channel (LPIC) concept, often referred to as the "start tank" concept, is as follows. During initial propellant loading, the acquisition tankage is filled immediately after main tank loading. At the first APS expulsion signal, the secondary tank is pressurized to its operating pressure with cold helium and LH_2 is discharged from the secondary tank by opening the main outlet valve. LH_2 is then expelled and transferred to the engine system at constant pressure. In the case of OMS burns, the vehicle acceleration will be relatively high (.05 g) and the main tank propellant will be reoriented by this resulting acceleration. A short period of time after OMS firing initiation (1 to 2 seconds), pressurization of the main tank is initiated and continued until the main tank is 13.8×10^3 to 20.7×10^3 N/M^2 (2 to 3 psi) higher than that in the secondary tank. When sufficient liquid bulk is positioned around the secondary tank region, the acquisition or secondary tank inlet valve is opened by a timed signal, and the resulting ΔP permits liquid to flow from the main tank into the secondary tank. As was the case with the full distributed channel concept design, the secondary tank screen device itself is not permitted to empty; only the liquid around the channel is removed. To assure proper refill, the secondary tank vent valve is activated to maintain a fixed pressure drop between the secondary and main tank. When refill is complete, the vent valve is closed, and flow continues to pass through the acquisition tank which now acts as a liquid accumulator. At expulsion termination, both outlet and refill valves are closed simultaneously, and the acquisition tank is completely full of liquid and ready for the next expulsion step.

In the case of short expulsion steps, as with low thrust ACS burns and there is insufficient time for refill, the complete burn is supplied from the secondary tank, which is then partially depleted. Thus, the secondary tank serves more than simply a start-tank function. Because of this, the secondary tank volume must be sized to provide sufficient propellant for these short burns and a subsequent OMS restart. The screen device must also be designed to provide retention under these conditions as well.

b. Preliminary Design

(1) Secondary Tank Sizing. The first step in the preliminary design of the LPIC concept is to size the volume of the secondary tank. A computer program has been developed by MDAC to size the secondary or acquisition tank volume to satisfy a specific expulsion duty cycle. This program requires as inputs, the thruster propellant consumption schedule, specified refill rate (normally twice the outflow rate), and a settling time for each major expulsion. (There is also a built-in capability for calculating a settling time.) The program iterates through the duty cycle and results in the definition of the secondary tank size to provide adequate volume to satisfy the mission requirements. The program also evaluates cold-gas pressurization requirements for the secondary tank and a variety of retention factors which will be discussed later in this section.

Several operational criteria were used in arriving at the secondary tank volume, or, more specifically, a range of volumes:

CASE A: Secondary tank is sized to contain all startup and ACS propellant, secondary fluid such as auxiliary power and life support. Only the available OM burns are used for dynamic refill.

CASE B: Secondary tank is sized to contain only
startup and ACS propellants and only
the available OM burns are used for
dynamic refill. (In this case, secondary
fluids and in-flight losses are supplied
from the main portion of the tank.)

CASE C: Same as Case A, except that specific or
dedicated periods are programmed for
secondary tank refill. (1, 2, 3, and
6 refill periods were evaluated.)

The secondary tank sizing program was used to calculate
the tank volume requirements based on the above three criteria and the gen-
eral propellant consumption histories established in Section 2 for the three
baseline missions. Other assumed conditions included a dynamic refill rate
equal to twice the nominal outflow rate and a constant settling time of
12 seconds, which was calculated to be the maximum required based on
individual settling calculations for each expulsion step in a complete mission.

Results of the sizing analysis are summarized in
Table 3.1.7, which indicates that the resupply mission dictates the secondary
tank size. Obviously, the most severe requirement from the standpoint of
secondary tank volume is Case A, with nearly continuous supply of propellant
for attitude control expendable and auxiliary supplies. A 20 percent reduction
in volume is achieved when the secondary tank is limited to supplying cryogen
only for engine start and attitude control burns. In such a case, venting and

Table 3.1.7

COMPUTED SECONDARY TANKAGE VOLUMES - M^3 (FT^3)

Sizing Criteria	LH$_2$			LO$_2$
	Easterly	Resupply	Polar	Resupply
A	15.6 (550)	15.8 (560)	15.0 (530)	2.8 (100)
B				
Refill 3rd day*	8.1 (286)	8.3 (293)	8.0 (281)	1.4 (51)
Refill 3rd and 6th days	7.6 (267)	7.5 (266)	7.1 (250)	1.1 (40)
Refill 2nd, 3rd and 6th days	5.1 (181)	5.6 (198)	4.9 (174)	0.9 (33)
Refill 1st through 6th days	2.7 (94)	3.7 (131)	2.7 (99)	0.8 (29)
C	12.5 (441)	12.7 (450)	12.1 (427)	2.4 (86)

Refill always occurs during OM burns

*Low-g refill occurs at end of day

cryogens for auxiliary functions are taken directly from the main tank region. In general, this would not appear to be a serious limitation. Therefore, the upper limit on secondary tank size was set at 12.7 M^3 (450 ft^3) and 2.4 M^3 (86 ft^3) for LH_2 and LO_2, respectively.

As indicated in Table 3.1.7, more dramatic reductions in secondary tank volume can be achieved if periods during the mission are dedicated to refilling of the secondary tank. With six such refills, the volume can be reduced to 30 percent of the maximum required value. However, special provisions must be made to accomplish this secondary tank refill. Two general approaches were investigated to obtain refill: (1) dedicated attitude control thruster firings which would settle the propellants and permit secondary tank refill while under the produced positive acceleration; and (2) a low-g vacuum vent refill technique which uses special auxiliary hardware built into the surface tension acquisition system. Both concepts involve weight penalties and operational constraints on the vehicle.

The acceleration technique is relatively straightforward and involves firing the H_2/O_2 ACS thruster to provide settling acceleration. The major weight penalty with this approach is the propellant weight that would be expended in producing the required acceleration. This was approximated by assuming a minimum ACS thrust of 4440 Newtons (1000 lb) with an I_{sp} = 400 sec at an O/F = 4.5. This yields a thruster total flowrate of 1.13 kg/sec. The thrust must be applied for a time period equal to the sum of the time for settling and the time for secondary tank refill. Settling time at 0.004 g was estimated at about 60 sec and Figure 3.1.33 shows the required secondary tank refill time as a function of tank volume and line sizes
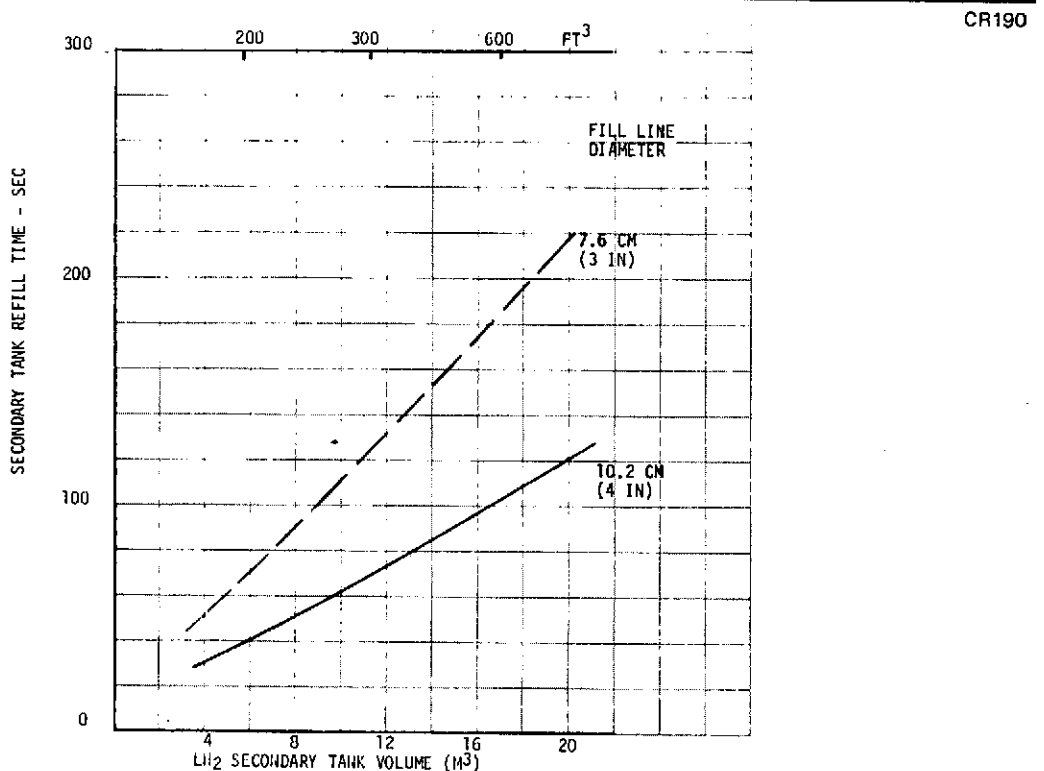
Figure 3.1.33. Secondary Tank Refill Time

for an assumed pressure differential between the main and secondary tank of 34.5×10^3 N/M^2 (5 psia). Therefore, assuming a 10.2 cm line diameter, two refills would require 240 sec of thrusting or about 270 kg of propellant and six refills would require 576 sec of thrusting or a propellant expenditure of 651 kg. Considering only the weight saved by reducing the size of a simple pressure vessel, two refills would save about 90 kg and six refills would save 135 kg. These reductions are not comparable to the propellant weight penalty. Therefore, the dedicated thruster firing approach would not result in a net savings and was dropped from further consideration.

With the low-g vacuum vent refill technique, auxiliary screen surface tension devices are used to provide liquid to the secondary tank which is vented to vacuum prior to initiating refill. This concept is discussed in detail in Appendix D and was shown to be feasible during MDAC IRAD tests (Reference 10 and 11). It was shown that a tank with liquid residual could be rapidly vented to vacuum and completely refilled with liquid. This venting method is g-level independent but involves a weight penalty in the dumped propellant. In subsequent analyses, where secondary tank volume of less than 12.7 M^3 (450 ft^3) are used, it is assumed that low-g vacuum vent refill is employed and the appropriate hardware and fluid residual weights to implement vacuum vent/refill are included as part of the acquisition subsystem weight.

(2) Basic Channel Design. Most of the channel design work performed for the FDC concept is also applicable to the LPIC acquisition system and was directly used where applicable.

The basic criteria in channel sizing is that a retention safety factor greater than 2.0 must be achieved at all orbital propellant orientations, flowrates, and acceleration levels. A minimum propellant volume of 15 percent was selected as the worst case. This condition is conservative since with the mission requirements used in this study, the system operates effectively and with no weight penalty between the limits of 100 percent full and 30 percent full or higher. In other words, there are no requirements for the propellant level in the secondary tank to drop below 30 percent until the final reentry burn when the screen device is expected to break down. Assuming that the tank must operate with a propellant load of 15 percent rather than 30 percent, one should account for propellant wave motion, which could tend to decrease the flow-through area of the screens submerged in the propellant. The minimum percentage selected is practical and results, as will be shown directly, in a system that achieves retention safety factors greater than 2.0.

Because of the spherical shape of the secondary tank, parallel plane channels, as used in the FDC concept, did not inherently provide the desired liquid communication with minimum weight. Rather, a dual intersecting channel was selected for the secondary tank. Two orientations, as shown in Figure 3.1.34 were compared. In the first case, Orientation A, the channels were oriented perpendicular and parallel to the vehicle axis such that only one channel contacted the residual liquid in the worst case propellant orientation. In Orientation B, the channels were orientated at 45 deg to the vehicle axis. In this case, two channels contacted the liquid residual. Both orientations are constrained by the requirement that the secondary tank sump be located so as to remove all of the propellant during the final reentry/landing phase when the 1-g acceleration level is in the

a = 0.457 M/SEC^2
(1.5 FT/SEC^2)
IN-X DIRECTION
ALONG VEHICLE AXIS

ORIENTATION A

PARALLEL/PERPENDICULAR ORIENTATION

ORIENTATION B
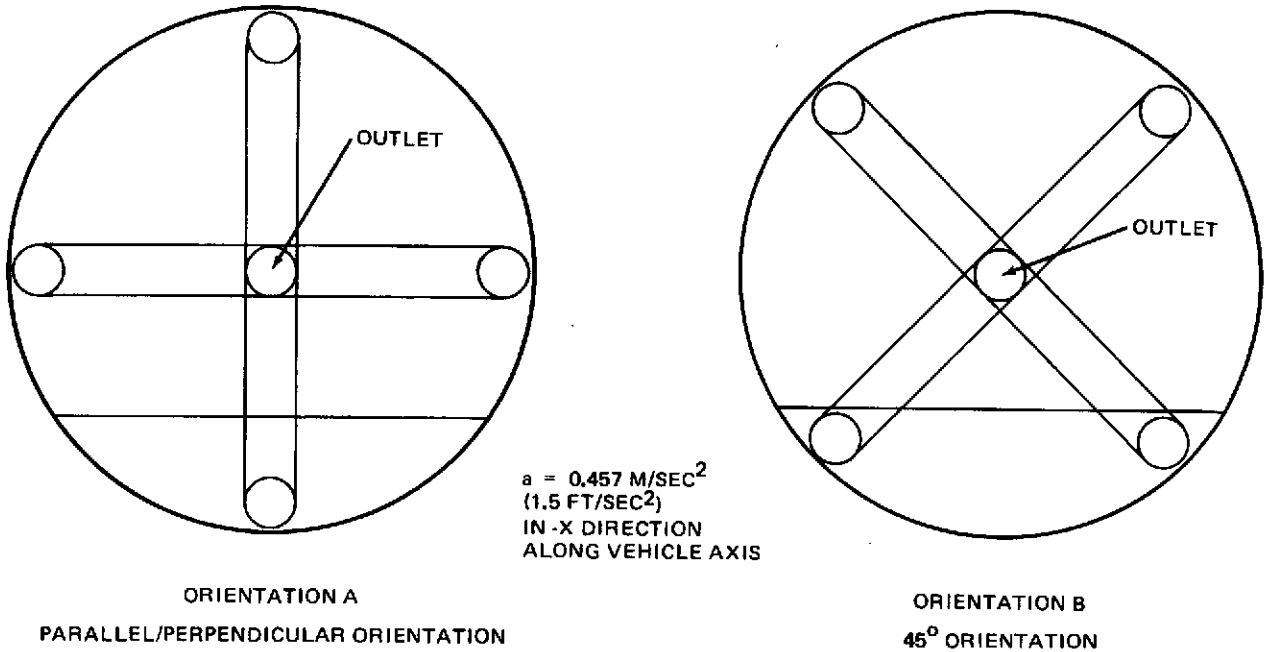
45° ORIENTATION

Figure 3.1.34. Orientations of Intersecting Channels

Table 3.1.8

EFFECT OF CHANNEL ORIENTATION ON CHANNEL LH$_2$
ACQUISITION PERFORMANCE

| Channel Orientation | System Pressure Losses, N/M^2 (lb/ft^2) | | | | | Retention Safety Factor |
	Screen Flow	Channel Flow	Velocity Head	Static Head	Total Loss	
Configuration A Parallel/ Perpendicular	27.15 (0.567)	2.78 (0.058)	52.00 (1.086)	41.33 (0.864)	123.26 (2.575)	1.48
Configuration B 45° Angle	26.33 (0.550)	1.10 (0.023)	13.02 (0.272)	35.40 (0.740)	75.85 (1.585)	2.40

Notes: (1) Acceleration — 0.457 M/sec^2 (1.5 ft/sec^2) negative parallel to vehicle axis (-x direction)

(2) LH$_2$ Flow rate — 2.7 kg/sec (5.95 lb/sec)

(3) Channel Dimensions — 17.8 x 17.8 cm (7 x 7 in.)

(4) Secondary Tank Volume — 2.8 M^3 (100 ft^3)

(5) 200 x 600 Mesh Screen —
Bubble Point Pressure = 181.9 N/M^3 (3.8 lb/ft^2)

SECONDARY TANK

CHANNEL A

CHANNEL B

COUPLINGS (8)

MAIN
FEEDLINE

NOTE

INDICATED VIEW ROTATED
45° FROM NORMAL PROJECTION
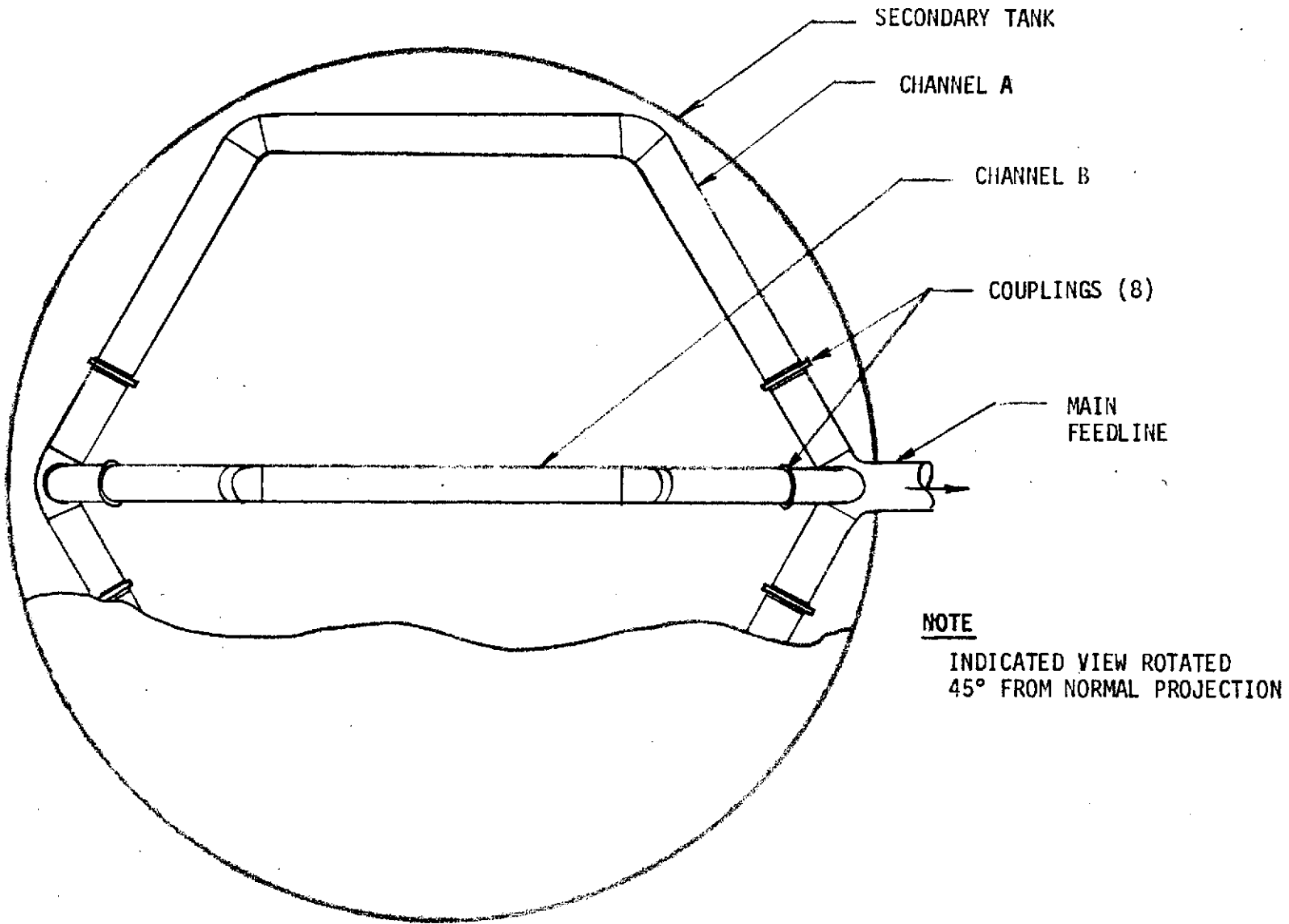
Figure 3.1.35. General LPIC Channel Arrangement in Secondary Tank

MARMAN CLAMP

FINE MESH
SCREEN

CLAMP

AUXILIARY
CHANNEL
(OPTIONAL)

AUXILIARY
CHANNEL
FITTING
(OPTIONAL)

COARSE MESH
BACK-UP
SCREEN

PERFORATED
SUPPORT
TUBE

PRIMARY CHANNEL
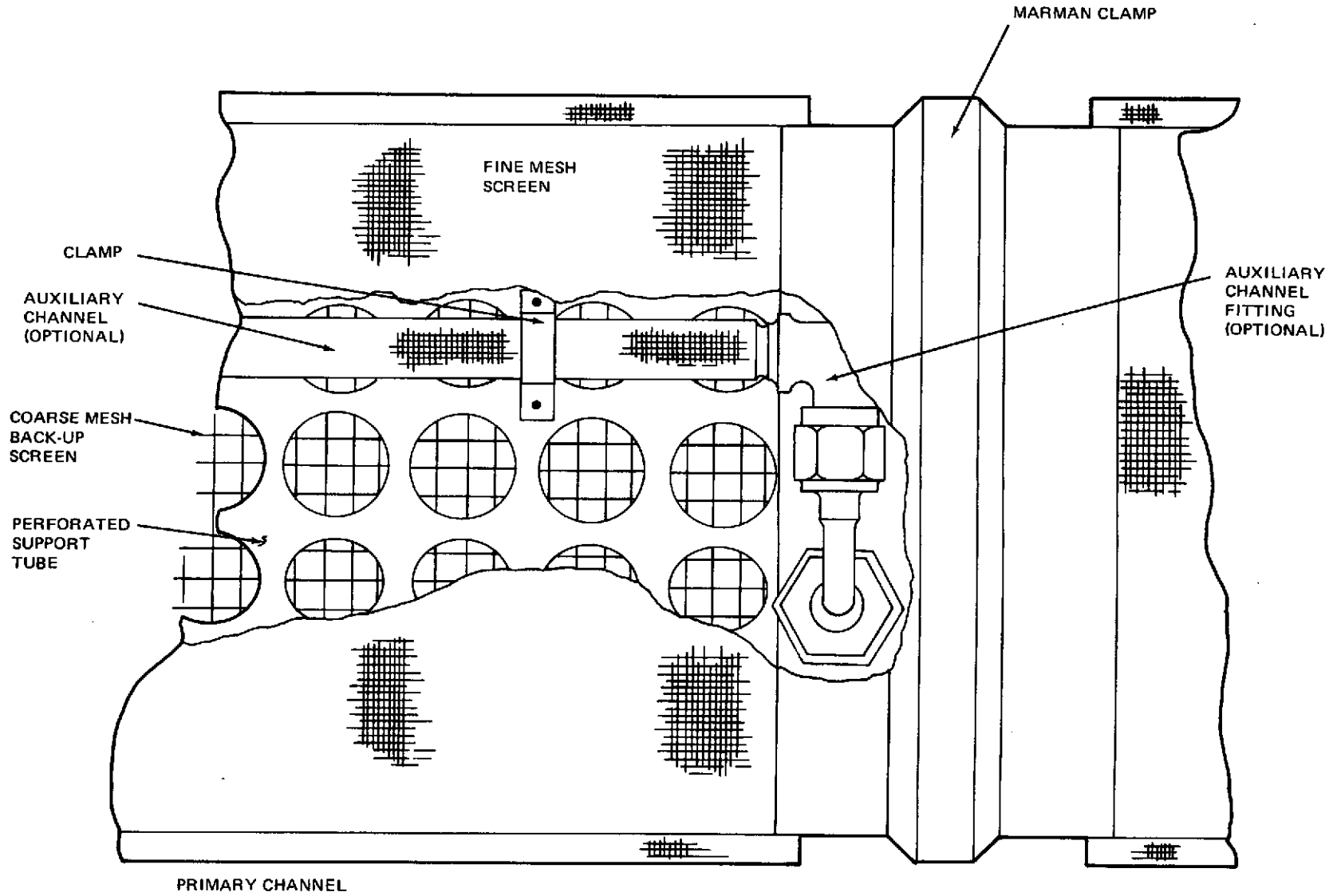
Figure 3.1.36. Channel Details

-z direction of the vehicle axis. Comparison of the retention safety factors for the two orientations (see Table 3.1.8) showed that Orientation B provides 60 percent higher retention safety factor than Orientation A. The improvement results from the fact that, with Configuration B, both channels are in contact with the liquid and the static head is decreased. With flow through two channels, the viscous pressure drop in the channel and the velocity head are both decreased, and since the wetted screen area is also increased, this contribution to pressure drop is also diminished.

The results of the duct channel cross section study conducted for the FDC concept reported in Section 3.1.2 are valid for this concept as well and showed that the all-screen circular design was preferred in terms of weight and retention performance. The channel design was also evolved to avoid compound curvature of screen surfaces, unnecessarily fine mesh screens, and complicated channel supports or duct section connections.

The resulting general channel configuration is as shown in Figure 3.1.35. It consists of two rings oriented in two perpendicular planes intersecting at their mid-points. Each ring is a hexagon formed of six nearly equal length straight screen sections. The construction features of the ducts are very similar to those adopted for the FDC concept ducting. The V-band couplings were placed so as to use the minimum possible number and still result in channel section sizes that were compatible with a two-man assembly operation within the tank. Details of the duct construction are shown in Figures 3.1.36 and 3.1.37.

The retention performance characteristics of the circular cross section all-screen channel were determined for 200 x 600 mesh screens. This is a relatively common screen material and has demonstrated favorable bubble point and flow loss characteristics. The retention safety factors are based on worst-case flow conditions in which the entire flow in the channel device follows the shortest path from the wetted screen to the outlet. In actuality, the flow would be proportioned among the four channel paths, which would decrease the dynamic and viscous flow losses. The tabulated retention safety factors are therefore somewhat low.

It had been reported, Reference 5, that a 165 x 800 mesh screen possessed the same bubble point as 200 x 600 mesh but with lower flow losses. However, comparison tests were made on the two screens as procured, and, although they were found to be comparable in terms of bubble point, the flow loss with 165 x 800 was in fact slightly higher than the 200 x 600. Thus, the 200 x 600 mesh was retained for the design.

Tables 3.1.9 through 3.1.11 present the flow losses associated for the full range of secondary tank volumes considered for the 200 x 600 mesh screen. The maximum acceleration in the -X direction is 0.457 M/sec^2 (1.5 ft/sec^2). The maximum acceleration imposed on the LH$_2$ tank in the +Z direction is 0.293 M/sec^2 (0.96 ft/sec^2). The maximum acceleration of the LO$_2$ tank is 0.188 M/sec^2 (0.6 ft/sec^2), due to the LO$_2$ tank being closer to the vehicle center of gravity, which decreases the centripetal acceleration component.

The channel weight is minimized by selection of the smallest channels which provide retention safety factors equal to or greater than 2.0 for the worst-case flow conditions. With the 200 x 600 mesh screen,

WELDMENT

FINE MESH SCREEN
SUPPORTED BY COARSE
MESH SCREEN

CLAMP
(OPTIONAL)

AUXILIARY CHANNELS
(OPTIONAL)

PERFORATED TUBE
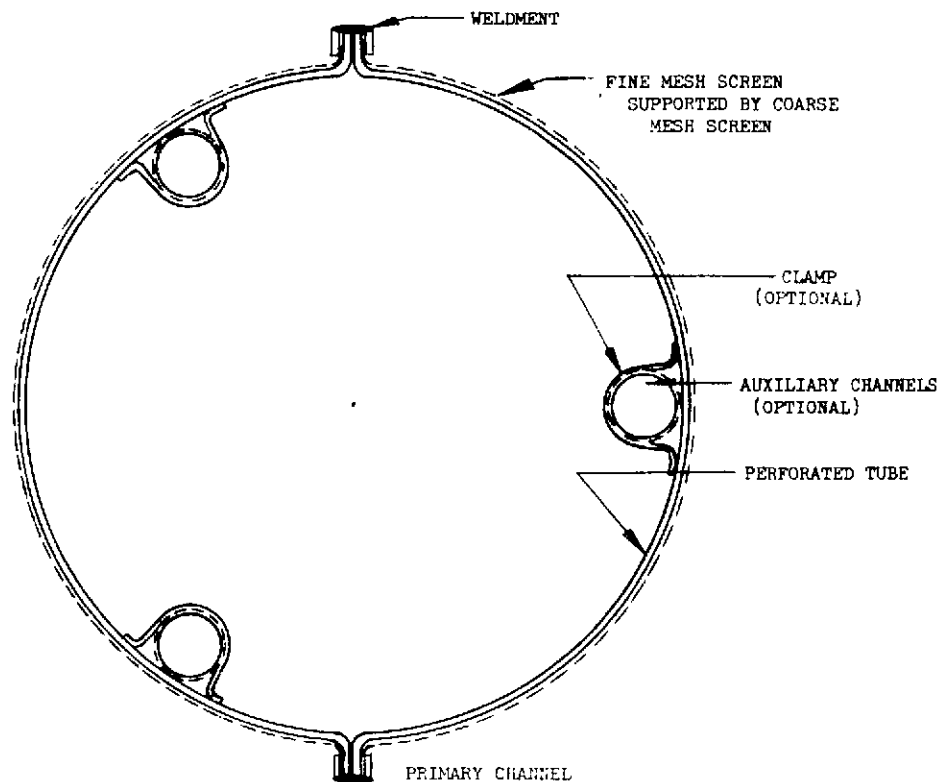
PRIMARY CHANNEL

Figure 3.1.37. Cross-Sectional View of All-Screen Channel with Auxiliary Channels

the retention safety factor in a few cases is 1.9, but since the flow losses are calculated with a conservative flow model, the actual values will be adequate. Moreover, a small increase (approximately 2 percent) in the channel diameter would decrease the flow losses to the point that the retention safety factor would be equal to or greater than 2.0

Table 3.1.11 summarizes the channel parameters for all secondary tank volume considered. Table 3.1.12 summarizes the weights for the LPIC acquistion devices. In developing these weights, it was assumed that the perforated tube is steel with a 60 percent open area, 0.508 cm (0.02 in) thick. A coarse-mesh aluminum screen is used as a standoff or backup screen; the fine-mesh screen is 200 x 600 mesh at 0.7 N/M^2 (0.16 lb/ft^2). Eight Marman V-band joints are used on the channels and a tension member system is used to join the channels to the start tank wall similar to that used in the FDC.

(3) Pressure Shell. The pressure shell represents a significant portion of the inert weight for the LPIC concept. The minimum weight tank pressure shell is a spherical isogrid structure; this design has been thoroughly analyzed and tested at MDAC and is documented in Reference 12. The weights of the isogrid with a single circumferential weld were determined from the tables of Reference 12 for the range of tank sizes considered (see Figure 3.1.38). A maximum crushing pressure of 332 x 10^3 N/M^2 (48 psi) was selected as a conservative design point. The properties of aluminum (2219-T87) were used at the appropriate cryogenic temperature (22°K for LH$_2$ and 90°K for LO$_2$). The weld seam thickness was assumed to be 2.5 times the effective thickness of the isogrid structure and the width

Table 3. 1. 9

LPIC CHANNEL DEVICE PERFORMANCE—LH$_2$ 200 x 600 MESH SCREEN—
BUBBLE POINT PRESSURE = 181. 9 N/m^2 (3. 8 lb/ft^2)

Start Tank Volume, m^3 (ft^3)	Channel Diameter, cm	LH$_2$ Flow, kg/sec	Acceleration m/sec^2 (ft/sec^2)	System Pressure Losses, N/m^2 (lb/ft^2)				Retention Safety Factor[3]
				Velocity Head	Channel Flow	Screen Flow	Static Head	
1. 42 (50)	16. 5	2. 7	0. 457 (1. 5)[1]	28. 35 (0. 592)	1. 89 (0. 039)	30. 12 (0. 630)	25. 75 (0. 538)	2. 1
		2. 04	0. 293 (0. 96)[2]	4. 05 (0. 085)	0. 58 (0. 012)	9. 96 (0. 208)	20. 67 (0. 432)	5. 2
2. 83 (100)	16. 5	2. 7.	0. 457 (1. 5)[1]	28. 35 (0. 592)	2. 50 (0. 052)	27. 55 (0. 576)	32. 20 (0. 673)	2. 0
		2. 04	0. 293 (0. 96)[2]	4. 05 (0. 085)	0. 76 (0. 016)	9. 17 (0. 192)	26. 25 (0. 549)	4. 5
12. 72 (450)	17. 8	2. 7	0. 457 (1. 5)[1]	21. 06 (0. 440)	2. 86 (0. 060)	17. 30 (0. 361)	52. 85 (1. 103)	1. 9
		2. 04	0. 293 (0. 96)[2]	3. 01 (0. 063)	0. 91 (0. 019)	6. 40 (0. 134)	43. 95 (0. 917)	3. 4
15. 85 (560)	17. 8	2. 7	0. 457 (1. 5)[1]	21. 06 (0. 440)	3. 07 (0. 064)	14. 52 (0. 304)	56. 75 (1. 186)	1. 9
		2. 04	0. 293 (0. 96)[2]	3. 01 (0. 063)	0. 99 (0. 021)	6. 36 (0. 133)	47. 25 (0. 988)	3. 2

[1] Cross-channel flow - 0. 457 m/sec^2 (1. 5 ft/sec^2) negative parallel to vehicle axis (-X direction)
[2] Four-channel flow - 0. 293 m/sec^2 (0. 96 ft/sec^2) positive normal to vehicle axis (+Z direction)
[3] Safety factor based on 15 percent LH$_2$ volume in the start tank

Table 3. 1. 10

LPIC CHANNEL DEVICE PERFORMANCE—LO$_2$ 200 x 600 MESH SCREEN—
BUBBLE POINT PRESSURE = 1, 250 N/m^2 (26. 1 lb/ft^2)

Start Tank Volume, m^3 (ft^3)	Channel Diameter, cm (in.)	LO$_2$ Flow, kg/sec (lb/sec)	Acceleration m/sec^2 (ft/sec^2)	System Pressure Losses, N/m^2 (lb/ft^2)				Retention Safety Factor[3]
				Velocity Head	Channel Flow	Screen Flow	Static Head	
0. 24 (8. 33)	12. 7 (5. 0)	13. 5	0. 457 (1. 5)[1]	125. 2 (2. 62)	6. 53 (0. 136)	293. 0 (6. 12)	229. 4 (4. 79)	1. 9
		6. 85	0. 188 (0. 6)[2]	8. 06 (0. 169)	0. 76 (0. 016)	42. 1 (0. 880)	111. 6 (2. 33)	7. 7
0. 47 (16. 67)	12. 7 (5. 0)	13. 5	0. 457 (1. 5)[1]	125. 2 (2. 62)	7. 18 (0. 150)	171. 8 (3. 59)	287. 7 (6. 01)	2. 1
		6. 85	0. 188 (0. 6)[2]	8. 06 (0. 169)	1. 02 (0. 021)	29. 7 (0. 621)	142. 8 (2. 98)	6. 9
1. 84 (65)	15. 2 (6. 0)	13. 5	0. 457 (1. 5)[1]	60. 4 (1. 26)	4. 93 (0. 103)	75. 4 (1. 57)	451. 0 (9. 44)	2. 1
		6. 85	0. 188 (0. 6)[2]	3. 89 (0. 081)	0. 68 (0. 014)	13. 2 (0. 275)	228. 7 (4. 78)	5. 1

[1] Cross-channel flow - 0. 457 m/sec^2 (1. 5 ft/sec^2) negative parallel to vehicle axis (-X direction)
[2] Four-channel flow - 0. 188 m/sec^2 (0. 6 ft/sec^2) positive normal to vehicle axis (+Z direction)
[3] Safety factor based on 15 percent LO$_2$ volume in the start tank

Table 3.1.11
CHANNEL SIZING PARAMETERS

	Tank Volume, M^3 (ft^3)	Tank Radius, M	Main Channel Diameter, M	Length of Straight Section M	Straight Section Surface Area, M^2	Straight Section Volume, M^3	Propellant Mass in Section, kg
LH$_2$	1.42 (50)	0.695	0.165	0.506	0.262	0.0108	0.76
	2.83 (100)	0.877	0.165	0.690	0.357	0.0147	1.03
	12.72 (450)	1.450	0.178	1.250	0.697	0.0309	2.17
LO$_2$	0.236 (8.33)	0.383	0.127	0.231	0.0922	0.0029	3.32
	0.471 (16.67)	0.483	0.127	0.330	0.132	0.0042	4.76
	1.84 (65)	0.760	0.153	0.582	0.279	0.0106	12.05

Table 3.1.12
LPIC ACQUISITION DEVICE WEIGHTS (KG)

LH$_2$ SYSTEM	Secondary Tank Volume		
Item	1.4 M^3 (50 ft^3)	2.8 M^3 (100 ft^3)	12.6 M^3 (450 ft^3)
Primary Channels (two)			
Perforated Steel Tube	8.9	11.4	22.4
Steel Screen (200 x 600)	2.5	3.4	6.6
Aluminum Backup Screen	0.8	1.0	2.0
Welding Joints	0.4	0.5	0.9
Total	12.6	16.3	31.9

LO$_2$ SYSTEM	Secondary Tank Volume		
Item	0.236 M^3 (8.33 ft^3)	0.47 M^3 (16.67 ft^3)	1.84 M^3 (65 ft^3)
Primary Channels (two)			
Perforated Steel Tube	3.1 kg	4.2 kg	12.0 kg
Steel Screen (200 x 600)	0.9	1.3	3.0
Aluminum Backup Screen	0.3	0.4	1.0
Welding Joints	0.2	0.2	0.5
Total	4.5	6.1	16.5
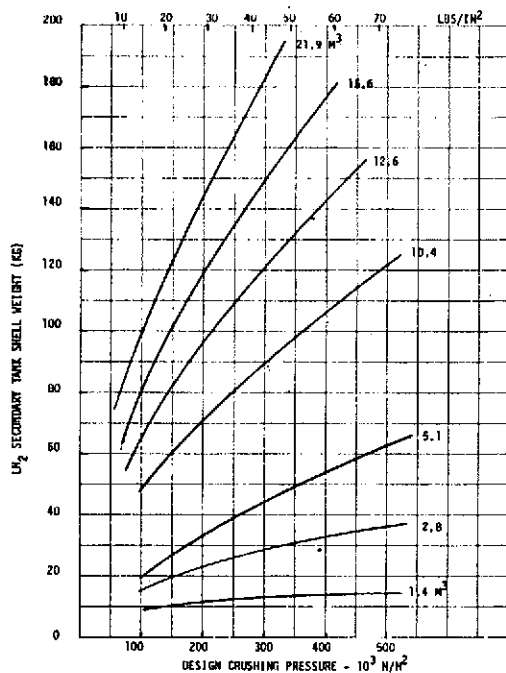
Figure 3.1.38. LH$_2$ Secondary Tank Weight

was assumed to be 7.5 cm (3 inches) for all start tank sizes. The lightest and most practical design is composed of two hemispheres joined by a single circumferential weld. The tank support weight was assumed to be approximately 8 percent of the basic tank shell weight.

For the larger start tanks, a manhole is used to provide access for screen device servicing. Thus, installation and removal of the channels would be accomplished by technicians working within the tanks. The manhole cover design is based on that used on the Saturn S-IVB. The total weight penalty is essentially proportional to the manhole circumference. The flange weight penalty for a 0.9 M (3 ft) diameter flange is 16.8 kg (37 lb) and 1.9 kg (4.2 lb) for the bolts.

Installation of the large start tank within the main propellant tank would probably have to be accomplished during main tank assembly. However, in the case of the small LO$_2$, the entire secondary tank can be inserted through the normal manhole access of the liquid oxygen main tank. It is only necessary that the structural supports of the LO$_2$ secondary tanks be easily detachable.

Tables 3.1.13 and 3.1.14 summarize the acquisition hardware weights for the LH$_2$ and LO$_2$ tanks. The pressure shell data were taken from Figure 3.1.38 and the channel weights were taken from Table 3.1.12. The foam insulation weights are compatible with the insulation requirements identified in Figure 3.3.16 of Section 3.3.3. In addition to the basic acquisition hardware, weights are also presented for vacuum vent/refill provisions which are mandatory for the small secondary tanks and optional for tank volume of 12.6 M^3 LH$_2$ and 1.84 M^3 LO$_2$ tanks or larger.

Table 3.1.13

LPIC ACQUISITION SYSTEM WEIGHTS
(LIQUID HYDROGEN)

SYSTEM WEIGHT PENALTIES	Start Tank Size			
	1.4 M^3 (50 Ft^3)	2.8 M^3 (100 Ft^3)	12.6 M^3 (450 Ft^3)	15.6 M^3 $(550 \text{ Ft}^2$
ACQUISITION HARDWARE				
PRESSURE SHELL (SPHERICAL ISOGRID) (See Figure 3.1.38)	14.6 Kg	29.3 Kg	132.0 Kg	163.0 Kg
SUPPORT STRUCTURE FOR SECONDARY TANK (8% of shell)	1.2	2.4	10.5	13.0
ACCESS MANHOLE (1M ID)	18.7	18.7	18.7	18.7
PRIMARY CHANNEL (Table 3.1.12) SCREEN DEVICE	12.6	16.3	31.9	36.0
MARMAN CLAMPS (8 STAINLESS STEEL)	7.6	7.6	8.1	8.1
FOAM INSULATION[1]	5.0	8.2	18.0	19.5
MAIN TANK SCREENS	18.1	18.1	18.1	18.1
CHANNEL SUPPORTS	0.4	0.7	1.0	1.1
	78.2	101.3	238.3	277.5
VACUUM VENT/REFILL PROVISIONS				
AUXILIARY CHANNEL	1.0	1.3	2.6	2.7
AUXILIARY ANNULAR SCREEN	3.5	4.5	12.4	14.3
MAIN TANK REFILL CHANNEL	6.3	8.2	16.0	18.0
RESIDUAL IN CHANNEL	2.4[2]	1.5[3]	0.4[4]	0.4[4]
ANNULAR RESIDUAL	20.4[2]	15.0[3]	5.7[4]	6.8[4]
	33.6	30.5	37.1	42.2

(1) TAKEN FROM FIGURE 3.3.16

(2) CALCULATED FOR 15 VACUUM VENT/REFILL CYCLES

(3) CALCULATED FOR 7 VACUUM VENT/REFILL CYCLES

(4) RESIDUAL BASED ON ONE SCREEN BREAKDOWN CORRECTION PROCEDURE

Table 3.1.14

LPIC ACQUISITION SYSTEM WEIGHTS
(LIQUID OXYGEN)

	Start Tank Size		
	0.236 M^3 (8.33 Ft^3)	0.47 M^3 (16.67 Ft^3)	1.84 M^3 (65 Ft^3)
ACQUISITION HARDWARE			
PRESSURE SHELL (SPHERICAL ISOGRID)	2.5 Kg	5.0 Kg	19.3 Kg
SUPPORT STRUCTURE FOR START TANK	0.2	0.4	1.5
ACCESS MANHOLE (3 FT ID)	0	0	18.7
PRIMARY CHANNEL SCREEN DEVICE	4.5	6.1	15.5
MARMAN CLAMPS (11 STAINLESS STEEL)	0	0	8.1
FOAM INSULATION	0	0	0
CHANNEL SUPPORTS	0.4	0.7	1.4
MAIN TANK SCREENS	9.0	9.0	9.0
	16.6	21.2	73.5
VACUUM VENT/REFILL PROVISIONS			
AUXILIARY CHANNELS (STAINLESS STEEL)	0.4	0.5	1.1
AUXILIARY ANNULAR SCREEN	1.4	1.9	4.5
MAIN TANK REFILL CHANNEL	2.2	3.1	8.2
RESIDUAL WITHIN CHANNELS	17.8[1]	12.0[2]	3.0[3]
RESIDUAL WITHIN ANNULAR SCREEN	59.0[1]	19.7[2]	4.1[3]
	81.8	37.5	20.9

(1) CALCULATED FOR 15 VACUUM VENT/REFILL CYCLES

(2) CALCULATED FOR 7 VACUUM VENT/REFILL CYCLES

(3) RESIDUAL BASED ON ONE SCREEN BREAKDOWN CORRECTION PROCEDURE

These weights will be combined into a total integrated LPIC feed system in section 3.4 and compared with the FDC feed system developed in section 3.1.2.

3.2 Pressurization Subsystem

The pressurization subsystem, in general, represents a significant portion of the weight of a cryogenic feed system, and it can also involve an appreciable cryogenic tank heat input, since the pressurant gas is normally heated before injection into the tank. Cryogenic propellant tanks are normally pressurized with: (1) helium stored in high pressure tanks located within the cryogen to minimize storage volume: (2) by bleeding gaseous propellants from the engine to the tanks, or (3) combination of these two techniques. In all cases, during engine operation some finite pressure must be maintained in the tank above the propellant saturation pressure (generally termed net positive suction pressure - NPSP). The controlling factor in sizing the pressurization system is the amount of pressurant gas that must be supplied to the tank to satisfy the design NPSP for a given expulsion flowrate schedule, tank geometry, including internal hardware, and gas inlet temperature. An available MDAC pressurization analysis computer program, Code H431, was used to evaluate the relatively complex thermodynamic processes that occur within the tank and to predict the pressurant usage.

3.2.1 <u>Analytical Technique</u>. The H431 Pressurization Analysis Computer program is based on a one-dimensional flow model. Spatial variations in the system variables are permitted only along the vertical tank axis; there are no radial or circumferential variations. Tank pressurization computer programs based on this type of model have been compared extensively with experimental data and found to be valid (Reference 13). The thermal system for this analysis consists of the tank wall of specified geometry, internal hardware, propellant liquid, and ullage gas. The ullage gas may be pure propellant vapor or a mixture of vapor with helium. Tabulated variable properties are used to describe the thermodynamic behavior of all materials.

The computations are based on a finite-difference representation of the physical system. The tank wall, internal hardware, propellant, and ullage are each divided by horizontal planes into a number of nodes, the properties within each node being uniform. The gas and liquid are divided into nodes whose thickness and location can vary with time. The tank wall and hardware nodes are of equal axial thickness and are stationary.

The volume of each liquid and gas node is bounded by the top and bottom boundary planes and by the solid surface of the tank wall and the internal hardware. Heat transfer takes place between each gas node and the solid surface with which it is in contact. The physically simultaneous processes of heat transfer and pressure change are assumed to take place sequentially as isobaric heat transfer and isentropic pressure change. The numerical solution is obtained by calculating the change in the state of each node in the system during each successive time step throughout the total solution time.

Expulsion duty cycle control data is input to the program in time-variable tables. These include propellant outflow rate, vehicle acceleration, pressurant inlet temperature and composition, tank pressure, and pressurant inflow rate. Heat transfer coefficients may be input or calculated internally

from free convection relationships. The solution may be computed in two modes: either the tank pressure schedule is specified and the required pressurant flow rate is calculated, or the pressurant flow rate is specified and the pressure is calculated. Initial conditions specified at the start of the duty cycle are the ullage fraction, tank pressure, and all temperature distributions.

This basic computer program has been further developed into two modified versions with added capabilities for analyzing complete missions. The "multistep expulsion" version, generally used in this study, treats the mission as a series of discrete expulsion steps separated by coast periods during which complete thermal equilibration occurs within the tank. The "continuous" version analyzes the transient heat transfer processes throughout the entire mission as a single continuous computation.

In the multistep analysis, the mission is assumed to consist of discrete periods of expulsion, each starting with a prepressurization to specified operating pressure followed by a propellant outflow at a specified rate and duration. From the temperature distributions at the end of the first step, the temperature and pressure are calculated that would result from a complete equilibration of the complete system, including the tank wall, liquid, and ullage gas.

The coast phase may be specified in two ways: by the total heat leak into the tank or by liquid outflow from the tank (to feed a thermodynamic vent device that intercepts the heat input). Following this heat addition or mass removal, the equilibrium tank conditions are again calculated. These values are then used by the program input routines as initial conditions for the subsequent expulsion step. Each step is calculated in sequence as a separate input case, but in one computer submission.

Three options are available for specifying the operating pressure for the second and subsequent steps: a fixed pressure, a fixed pressure increment over the initial pressure, or a fixed pressure increment over the initial vapor pressure of the propellant (defined as true NPSP control). When the ullage is pure propellant vapor (no helium), the latter two options are identical. The operating P or ΔP may be changed for individual steps during the mission. Under some conditions, the tank pressure at the start of expulsion may be greater than the specified outflow pressure; in this case, the outflow begins with no pressurant addition and continues until the pressure falls to the specified level, when the pressurant flow begins at the required rate.

The multistep analysis described above assumed that complete thermal equilibrium is attained after each expulsion. There is one limiting case where heat transfer occurs sufficiently rapidly to always attain equilibrium. Another limiting case is to permit only the minimum heat transfer rates between gas, liquid, and wall. To do this, thermal conduction equations were added to the program for one-dimensional heat transfer axially down the tank wall, the liquid, and the ullage gas. The propellant remains settled, and heat is transferred between the gas and wall by free convection. Heat conducted down the wall to the liquid surface level is transferred directly to the surface liquid node. With these assumptions, the tankage system is virtually always in a transient, nonequilibrium state when prepressurizations and propellant outflow

events occur. The case of continuous pressure control can also be analyzed, giving pressurant requirements to maintain tank pressure throughout the mission under these assumed conditions of minimum heat transfer.

These computer programs have been used to analyze the pressurant requirements and the pressurization system behavior for typical mission conditions. The hydrogen tank has been extensively studied with the multiburn program, using both autogenous and helium pressurant. Data curves and a discussion of results are presented below. A more thorough discussion of the thermodynamic behavior of the pressurization system is given in Appendix E.

3.2.2 <u>Multistep Expulsion Parametric Analysis</u>. For the generation of parametric performance data, the mission was approximated by a number (6, 12, and 18) of equal duration burns spaced evenly over the seven-day mission. During the coast periods, propellant was withdrawn from the tank to supply a thermodynamic vent system at a rate sufficient to remove the incoming heat. The initial ullage volume fraction was 5 percent, and propellant was expelled to depletion in the last burn. The initial pressure was 15 psia. The tank volume is 75 M^3 (2,650 ft^3) for these calculations. Although the final system configuration tank volume is now 69.3 M^3 (2,450 ft^3), the larger value was used in the initial parametric study. A general pump NPSP requirement of 34.5 x 10^3 N/M^2 (5 psi) was assumed. This choice was arbitrary but was considered to be representative of a typical APS system.

a.   <u>LH$_2$ Tank Pressurization Study</u>. A detailed study was conducted for the LH$_2$ tank pressurization including evaluation of autogenous and helium pressurization, and the influences of pressurant inlet temperature, tank pressure control logic, and expulsion duty cycle variation. This level of detail is essential in order to perform realistic overall or total propellant feed system comparisons.

b.   <u>Autogenous (GH$_2$) Pressurization</u>. Autogenous pressurization requirements were evaluated in terms of the total ullage mass at the end of the mission, since this represents the total unusable fluid weight penalty against the system. The results for pressurization at a fixed outflow pressure of 173 x 10^3 N/M^3 (25 psi) as computed with the H431 code are shown in Figure 3.2.1 as a function of inlet temperature. This shows the ullage mass to be insensitive to pressurant inlet temperature above 111°K (200°R). This insensitivity to inlet temperature results from the nature of the multistep expulsion operation in which the system reaches equilibrium after each expulsion with the gas cooling down to near LH$_2$ temperature. With an infinite number of equal steps there would be no advantage at all in heating the pressurant.

The use of a fixed or constant outflow pressure throughout the mission to maintain required NPSP for all expulsion steps results in high tank pressures as shown in Figure 3.2.2. The required tank pressure increases as the number of expulsion steps and NPSP increases and inlet temperature decreases. A fixed ΔP pressurization control mode can be used to ensure that the required NPSP is efficiently attained. This control logic is termed "true NPSP control". At the start of each burn, the tank pressure is
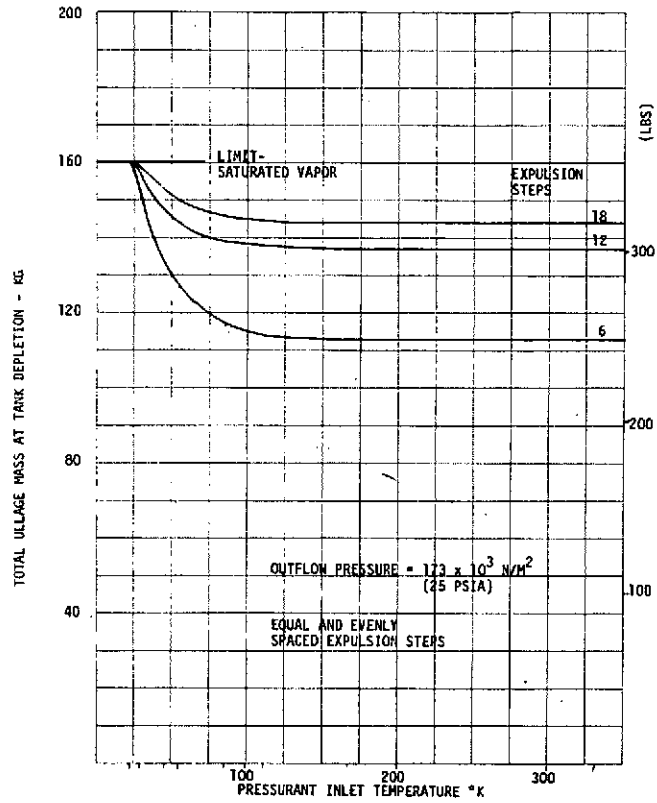
Figure 3.2.1. Ullage Mass with GH_2 Pressurant-Fixed Tank Pressure Control
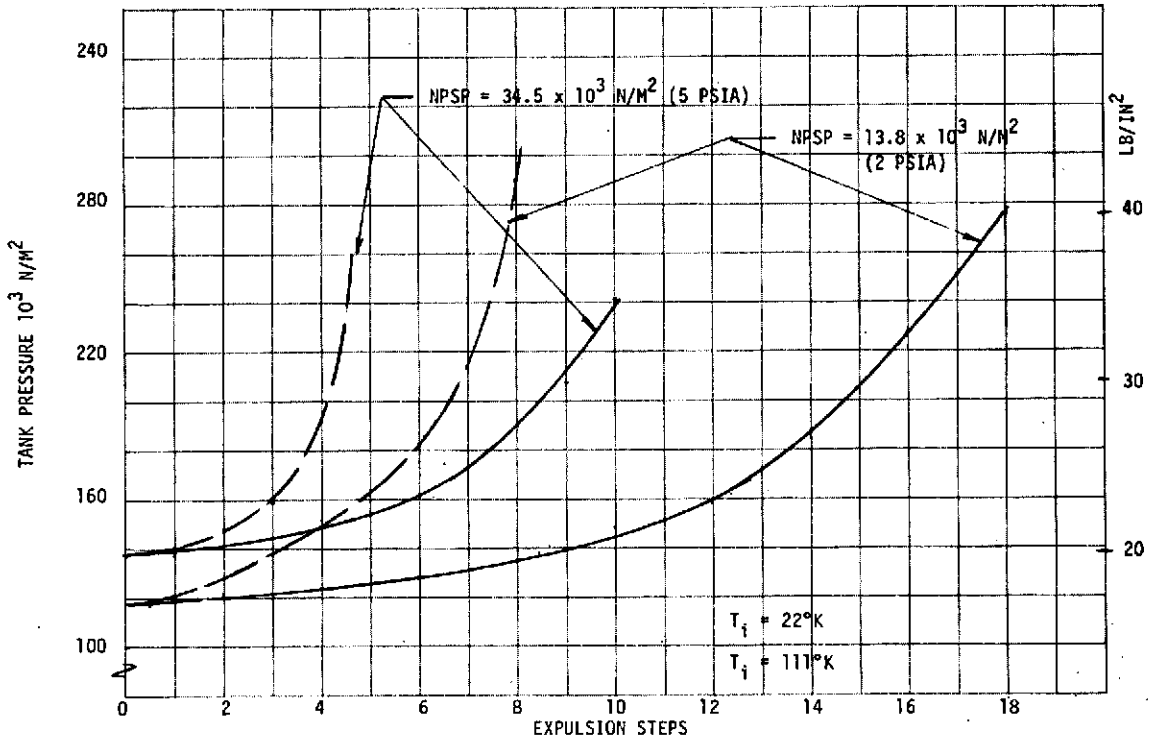
Figure 3.2.2. Tank Pressure Requirements with Fixed Pressure Control

increased to the required 34.5×10^3 N/M^2 (5 psi) above the initial pressure, so that the outflow pressure increases for each expulsion step throughout the mission. The resulting pressurant requirements are shown in Figure 3.2.3. Since there is no limiting pressure in this operating mode, the mass curves continue to increase with increasing number of expulsion steps. The tank pressures attained at the final expulsion step is also shown in Figure 3.2.3 and the resulting tank pressures attained for a given NPSP are compared for the two control logics in Figure 3.2.4. The comparison in terms of pressurant mass is also shown in Figure 3.2.5 for the optimum inlet temperature value. The concept of true NPSP tank pressure control was shown to be completely feasible in an MDAC/NASA-LeRC technology program (see Reference 14) and in subsequent MDAC LH$_2$ feed system IRAD tests. Thus true NPSP control was assumed throughout the rest of this study.

    c.   <u>LH$_2$ Tank Helium Pressurization Requirements.</u> LH$_2$ tank pressurization requirements were computed with the H431 computer code using helium gas pressurization. Figure 3.2.6 presents the resulting final helium and propellant vapor mass with true NPSP control as a function of expulsion steps and helium inlet temperature. A cursory examination and comparison of Figures 3.2.6 and 3.2.3 reveals that for the same NPSP, the total ullage mass with helium pressurization is slightly less than with GH$_2$ pressurization. However as will be shown directly, when the tankage and helium bottle penalties are considered, the helium system is significantly heavier as would be expected.
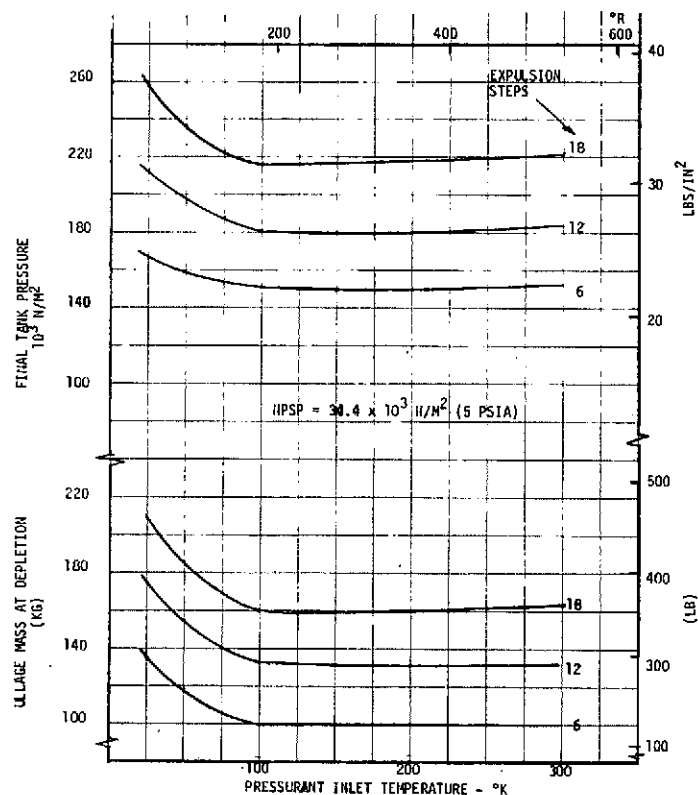
Figure 3.2.3. LH$_2$ Tank Autogenous Pressurization — True NPSP Control
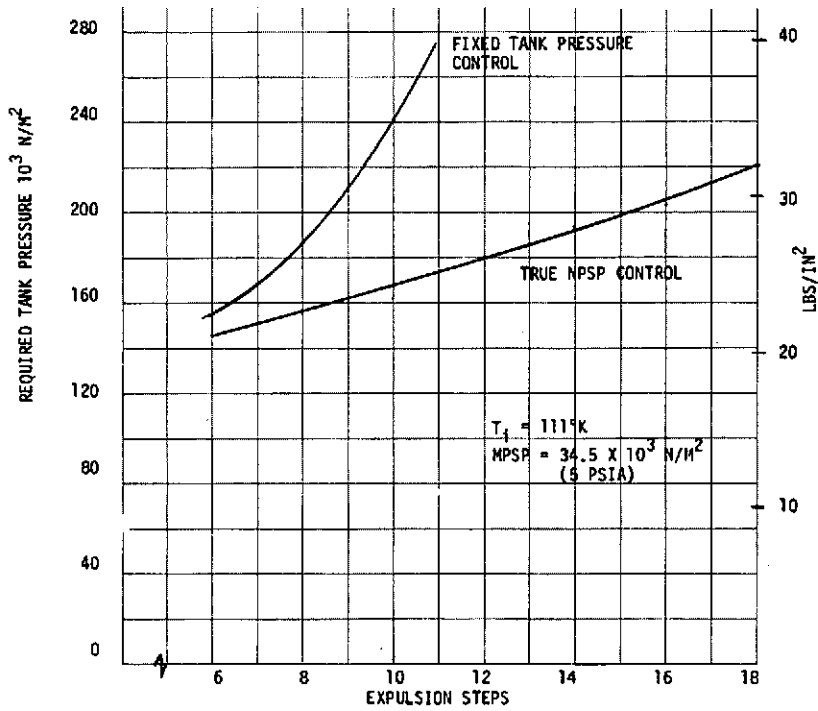
Figure 3.2.4. Influence of Pressure Control Logic on Tank Pressure
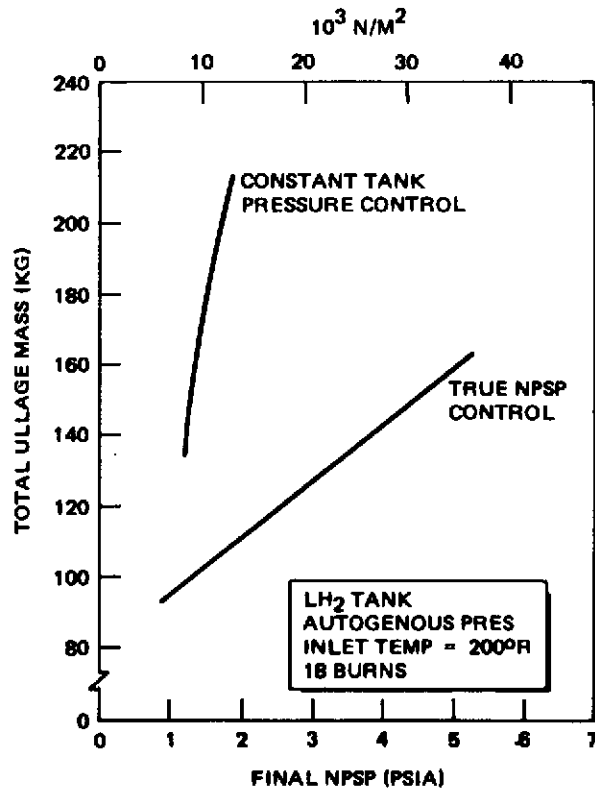
Figure 3.2.5. Influence of Control Logic on LH_2 Tank Pressurant Mass (Autogenous Pressurization)
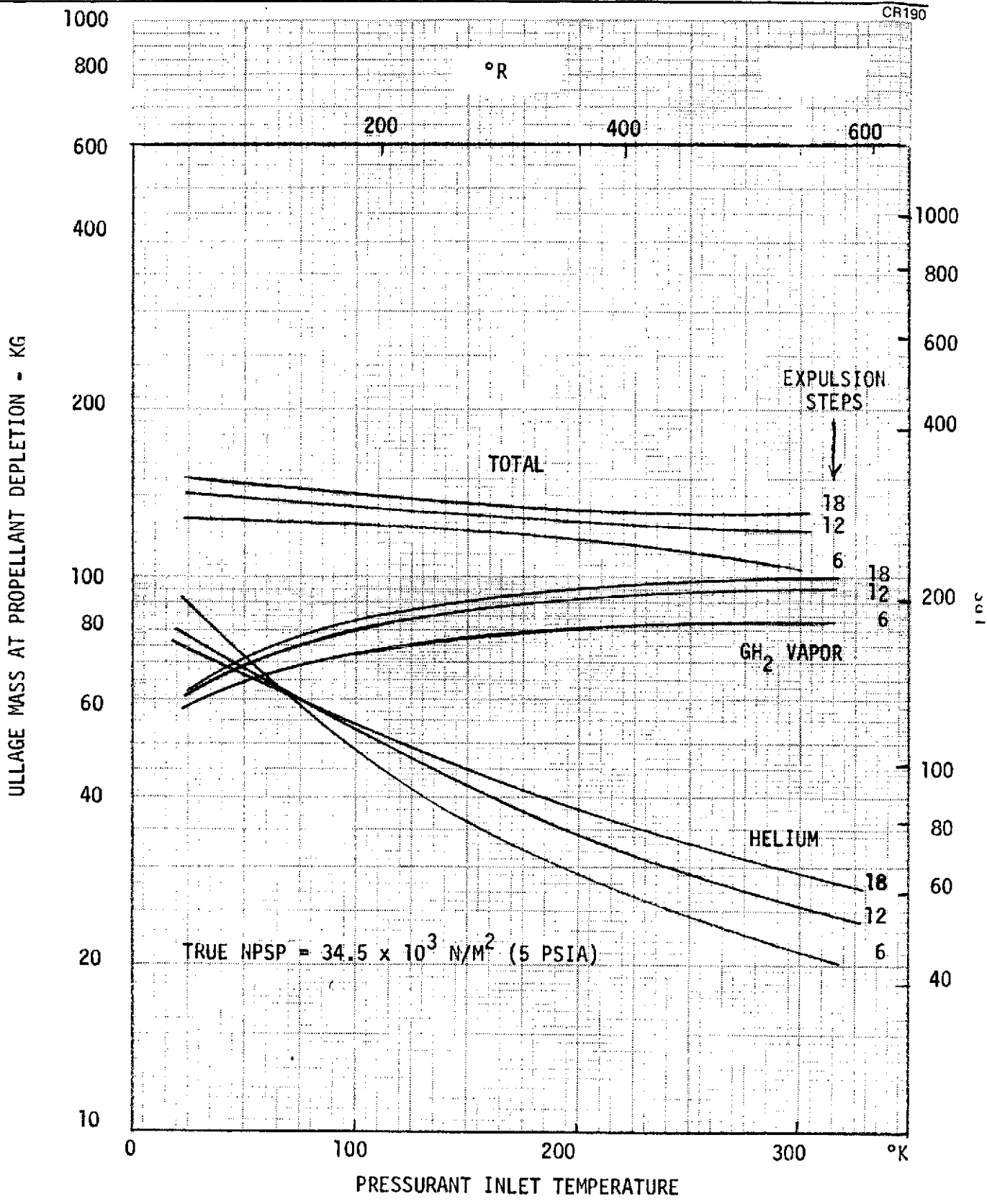
Figure 3.2.6. Ullage Mass With Helium Pressurization — True NPSP Control

d. Expulsion Duty Cycle Variations. The pressurization system analysis to this point has been conducted with the assumption that the expulsion duty cycle could be adequately represented by a series of identical expulsion steps (same flowrate and expulsion time) equally spaced throughout the mission (equal coast time between expulsion steps). This was a completely arbitrary assumption, and a limited-scope parametric study has been performed to assess the variation in pressurization system design resulting from duty-cycle differences. The duty cycle for a space propulsion module generally involves the consumption of a larger quantity of cryogen during the first and last hours of the mission with a series of small expulsion steps distributed over the coast operational period. For the groundrule conditions, there is always a rather large initial ullage (12 to 35 percent) for the baseline missions. (See section 2.)

To define the impact of these variations on the system design, the pressurization requirements were evaluated for a range of conditions for near-optimum LH_2 tank pressurization using heated ($200°R$) GH_2 and cold-helium pressurants.

Results with GH_2 are shown in Table 3.2.1, while results with cold helium are shown in Table 3.2.2. As can be seen from these tables, combinations of two expulsion duty cycles and initial ullage values were studied.

Table 3.2.1

INFLUENCE OF DUTY CYCLE ON PRESSURANT REQUIREMENTS
(LH_2 PRESSURIZATION WITH GH_2 AND TRUE NPSP CONTROL)

Case	Number of Expulsion Steps	Expulsion Step Distribution	Initial Ullage (Percent)	Final Ullage Mass (kg)	Final Tank Pressure (10^3 N/M^2)
A	18	Equal*	5	160	214
B		Equal	30	190	248
C		Weighted**	5	110	203
D		Weighted	30	145	240
A'	6	Equal	5	100	150
B'		Equal	30	110	157
C'		Weighted	5	80	150
D'		Weighted	30	95	160

*Assumes all steps to be equal in total expulsion and equally spaced during the mission.

**Assumes that first expulsion consumes 40 percent of liquid and occurs at beginning of mission, the final burn at the end of the mission consumes 40 percent of the initial propellant and that the rest of the steps are equal and equally distributed during the seven-day coast.

Table 3.2.2

INFLUENCE OF DUTY CYCLE ON PRESSURANT REQUIREMENTS (LH$_2$ PRESSURIZATION WITH HELIUM AND TRUE NPSP CONTROL)

Case	Number of Expulsion Steps	Expulsion Step Distribution	Initial Ullage (Percent)	Final Ullage Mass (kg)†	Final Tank Pressure (10^3 N/M^2)
A	18	Equal*	5	75 + 59 = 134	100
B		Equal	30	73 + 67 = 140	106
C		Weighted**	5	134 + 50 = 184	117
D		Weighted	30	102 + 60 = 162	121
A'	6	Equal	5	96 + 58 = 154	104
B'		Equal	30	88 + 66 = 154	108
C'		Weighted	5	130 + 50 = 180	116
D'		Weighted	30	109 + 60 = 169	120

*Assumes all steps to be equal in total expulsion and equally spaced during the mission.

**Assumes that first expulsion consumes 40 percent of liquid and occurs at beginning of mission, the final burn at the end of the mission consumes 40 percent of the initial propellant and that the rest of the steps are equal and equally distributed during the seven-day coast.

†Given as helium mass + vaporized H$_2$ mass = total

The duty cycles included the baseline, consisting of equivalent expulsion steps equally distributed over the seven-day mission, and a weighted cycle in which it was assumed that 40 percent of the loaded cryogen was consumed both at the very beginning and end of the mission with 20 percent of the cryogen being expelled in equivalent steps equally distributed over the seven-day mission. The combination of weighted distribution and 30-percent ullage would most clearly approach the representative Shuttle APS groundrules. By studying various combinations for both 18 and 6 expulsion steps, a relatively clear picture of the impact can be seen. In the case of GH$_2$ pressurization, the combination of the equal distribution expulsion steps and 30-percent ullage, Cases B and B', results in the heaviest pressurization system. However, this is not a very realistic combination. On the other hand, Cases A and A', which have been the baseline throughout the study, represent a conservative design condition relative to the most likely operating conditions (Cases D and D').

This same trend does not carry over into the cold helium system. In this instance, the weighted expulsion duty cycle with large ullage which is in accordance with SS/APS requirements produces a heavier pressurization system (about 20 percent greater) than the assumed A/A' baseline. In

summary, for an LH_2 autogenous pressurization system, the system should be sized for a minimum (5 percent) ullage and a duty cycle consisting of 18 identical expulsion steps equally distributed over the seven-day mission. This will result in a slight over capacity of 10 percent for a representative mission. For a LH_2 pressurization system using cold helium, sizing should be based on a maximum ullage (30 percent) with a weighted burn distribution. The pressurization system weights were computed, based on these design points. Other assumptions included: (1) true NPSP control logic with a 34.5×10^3 N/M^2 (5 psi) ΔP, (2) 18 expulsion steps, (3) inlet temperatures of 111°K and 22.2°K for GH_2 helium respectively.

  e. <u>Hardware Weight Estimates</u>. Except for control components, including valves, regulators, etc. which will be considered later as part of the integrated system, the major hardware weight items in the pressurization system are pressurant gas bottles and propellant tank volume increases required to store the pressurant. These weight penalties are particularly high for the helium system.

  Total LH_2 pressurization system weight (W_{pst}) is given by

$$W_{pst} = \text{helium + propellant vapor + helium bottle + helium bottle residual + bottle tank weight penalty + propellant tank weight penalty + insulation/vent system penalty} \quad (1)$$

$$= W_{HU} + W_{PV} + W_B + W_R + \Delta W_{TB} + \Delta W_{TV} + \Delta W_i$$

  Values of W_{HU} and W_{PV} are taken from the pressurant requirements curves such as Figures 3.2.3 and 3.2.6. W_B is the total helium bottle structural weight and W_R is the gas bottle helium residual. ΔW_{TB} is the increase in LH_2 tank weight required to accommodate the gas bottle volume while ΔW_{TV} is the propellant tank penalty required to store the propellant vapor in its original liquid state.

  In the helium pressurization system, W_B is generally the largest penalty. The helium storage bottle is treated in a thin walled pressure vessel and the relation defining the operating stress in a thin-walled spherical shell is:

$$\text{Operating stress} = s = \frac{Pd}{4t}$$

where

  P = operating pressure

  d = diameter

  t = wall thickness

The weight of a spherical shell can be expressed as:

  Shell weight = W = $t \rho_m S$

where

ρ_m = metal density

S = surface area

Bottle weight = W_B = $F_1 F_2 W$

where

F_1 = beefup factor for bosses, outlets, etc.

F_2 = support structure factor

Combining the above equations with bottle volume $\left(V_B = \dfrac{\pi d^3}{6}\right)$ and surface
($S = \pi d^2$) equations

$$\frac{W_B}{V_B} = 1.5 \, \rho_m \, \frac{P}{s} \, F_1 F_2 \tag{2}$$

Since the weight of helium used (W_{HU}) for propellant tank pressurization is equal to the helium weight at bottle initial conditions before pressurization begins minus the residual helium weight at propellant tank depletion,

$$\rho_{H_i} - \rho_{H_f}$$

where

ρ_{H_I} = density of helium at bottle initial conditions

ρ_{H_F} = density of helium at bottle final or residual conditions

$$\frac{\text{Bottle weight + total helium weight}}{V_B} = \frac{W_B}{V_B} + \rho_{H_i}$$

and

Helium storage efficiency, ζ_B, = $\dfrac{\text{Helium weight used}}{\text{Bottle weight + total helium weight}}$

$$\zeta_B = \frac{\rho_{H_1} - \rho_{H_F}}{\dfrac{W_B}{V_B} + \rho_{H_1}} \tag{3}$$

The criterion that defines the allowable operating stress in the pressure vessel for this application is based upon a procedure that utilizes

static fracture and cyclic fracture test data to empirically determine the allowable stresses and ultimate design and proof test factors for a given minimum-pressure cyclic life. The criterion is shown in Figure 3.2.7 for titanium alloy 6AL-4V at liquid hydrogen temperatures. For this study and the discussion and figures that follow, unless otherwise noted, 1,000 cycles and a proof stress of 13.70 x 10^8 N/M^2 (200,000 psi) were chosen, which yields an operating stress of 6.2 x 10^8 N/M^2 (90,000 psi). The set of bottle design parameters is defined as:

$$F_1 = 1.11$$

$$F_2 = 1.08$$

$$\rho_m = 4,429.21 \text{ N/M}^3 \ (276.48 \text{ lb/ft}^3)$$

$$s = 6.2 \times 10^8 \text{ N/M}^2 \ (90,000 \text{ psi})$$

and using the above equation:

Operating Pressure, P		W_B/V_B	
N/M^2	(lb/in.^{2})	Kg/M^3	(lb/ft^3)
6.895 x 10^6	(1,000)	88.494	5.524
13.790 x 10^6	(2,000)	176.989	11.048
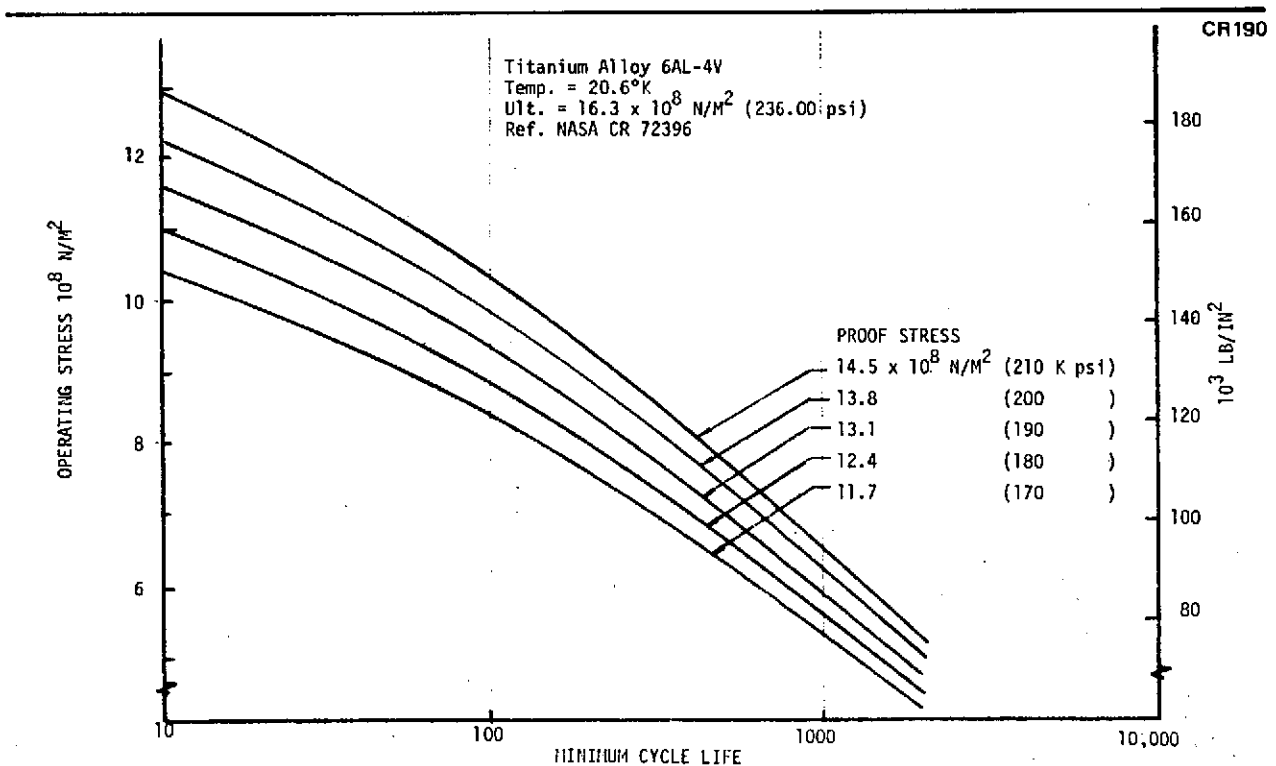
Figure 3.2.7. Allowable Operating Stress

| 20.685 x 10^6 | (3,000) | 265,483 | 16.572 |
| 27.580 x 10^6 | (4,000) | 353.978 | 22.096 |

Utilizing these W_B/V_B values and a range of initial and final helium densities, the helium storage efficiency, and helium weight used divided by bottle volume can be parametrically displayed, as in Figures 3.2.8 through 3.2.11. Two values of final bottle pressure are shown, 6.895 x 10^5 N/M^2 (100 psia) and 13.790 x 10^5 (200 psia), which illustrate the sensitivity of the weight and volume parameters to the initial and final bottle pressures. The range of final helium temperatures shown, 22.2°K (40°R) and 11.1°K (20°R), cover the. range from isothermal to isentropic for the gas processes within the bottle. The bottle weight and volume parameters are strongly affected by the final bottle temperature. For the duty cycles of interest, a final ullage temperature of 11°K was found to be appropriate and for satisfactory regulator functions a final tank pressure of 6.5 x 10^5 N/M^2 (100 psia) is practical.

Although the optimum gas storage parameters vary slightly for specific application, in general the following conditions have been found to be representative for multi-step expulsion low heat input feed systems:

Initial helium bottle pressure = 13.790 x 10^6 N/m^2 (2,000 psia)

Final helium bottle pressure = 6.895 x 10^5 N/m^2 (100 psia)

Initial helium temperature = 20.8°K (37.5°R)

Final helium temperature = 11.1°K (20°R)

Thus, from Figure 3.2.10, W_{Hu}/V_B = 123 Kg/M^3 and W_B/V_B = 177 Kg/M3. Therefore,

$$\left(\frac{W_B}{V_B}\right)\left(\frac{V_B}{W_{Hu}}\right) = \frac{177}{123} = 1.44$$

and

$$W_B = 1.44\, W_{Hu} \tag{4}$$

The helium bottle gas residual, W_R, is also a significant weight in low temperature systems.

$$W_R = V_B\, \rho_{H_F}$$

$$V_B = \frac{W_B}{(W_B/V_B)}$$
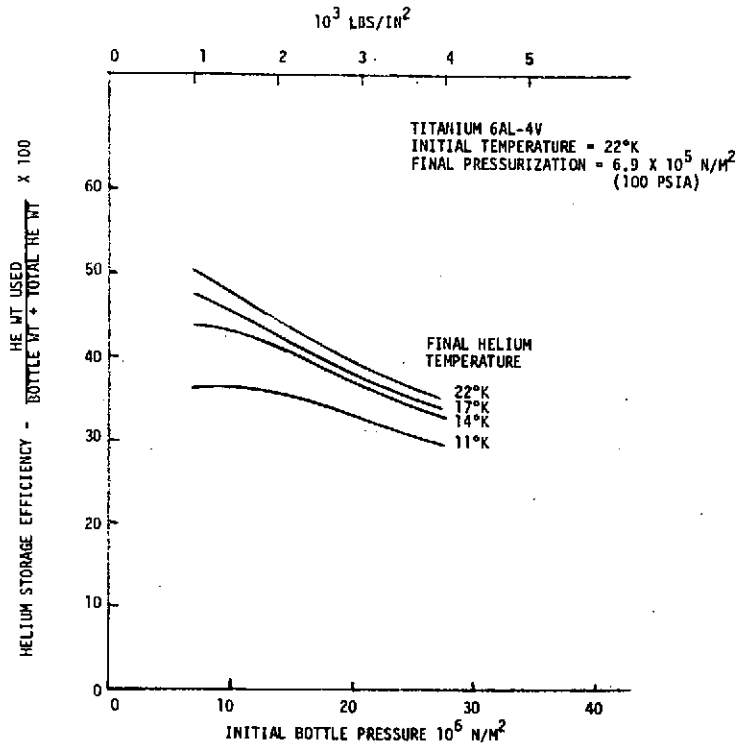
Figure 3.2.8. Helium Bottle Optimization
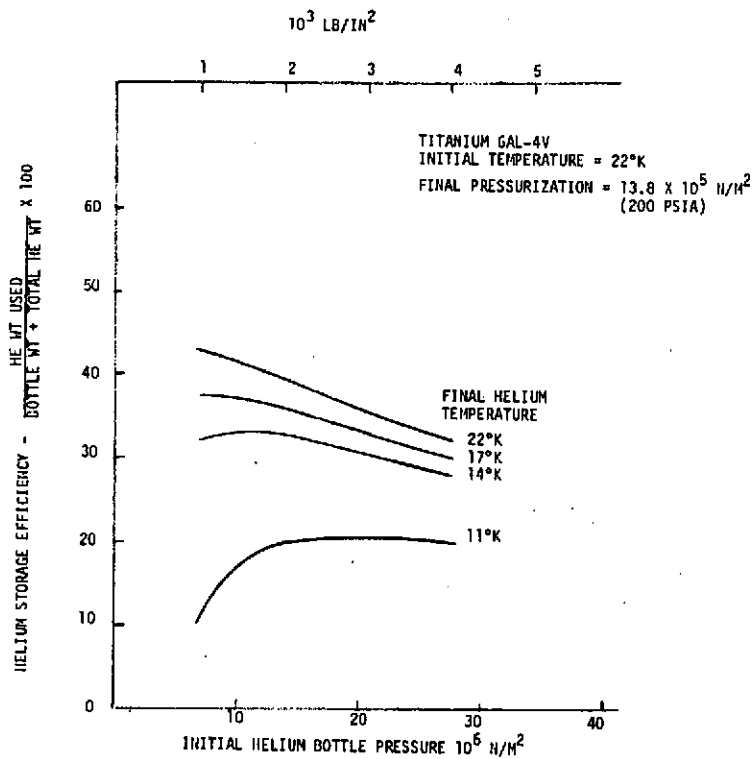
Figure 3.2.9. Helium Bottle Optimization
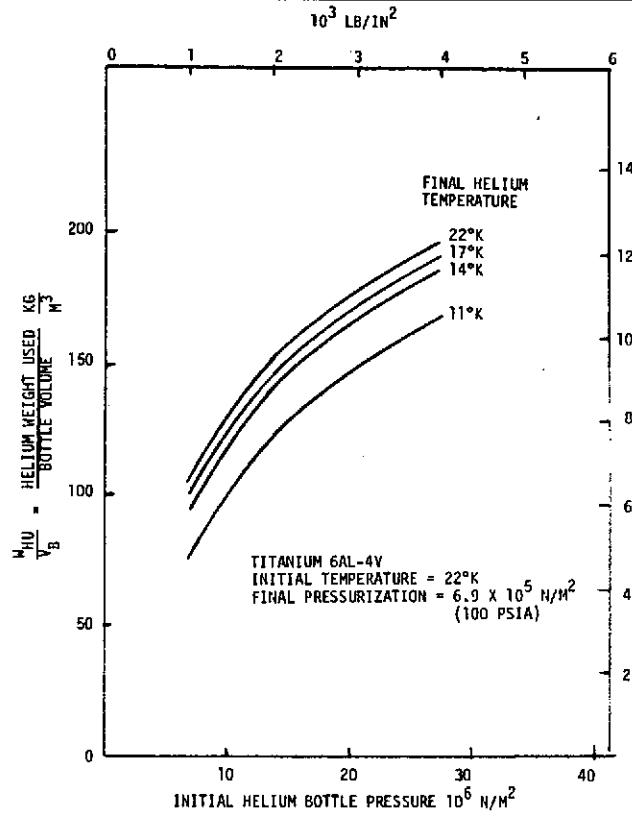
Figure 3.2.10. Helium Bottle Volume Parameter
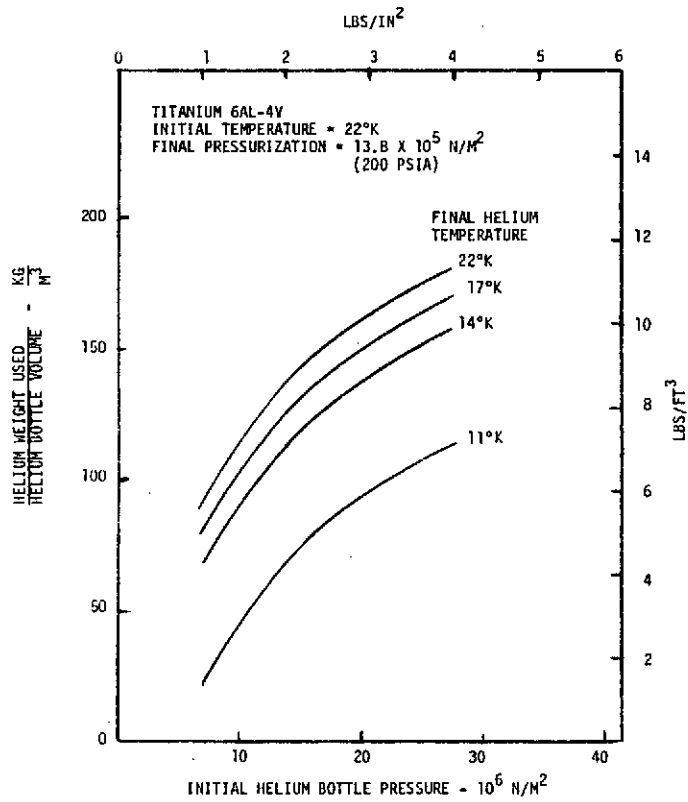
Figure 3.2.11. Helium Bottle Volume Parameter

From equation (4), $W_B = 1.44\ W_{HU}$

$$V_B = \frac{1.44\ W_{HU}}{(W_B/V_B)}$$

and

$$W_R = \frac{1.44\ W_{HU}\ \rho_{H_F}}{(W_B/V_B)} \tag{5}$$

For the assumed conditions

$$W_B/V_B = 177\ Kg/M^3\ (11.05\ lb/ft^3)$$

$$\rho_{H_F} = 41.7\ Kg/M^3\ (2.6\ lb/ft^3)$$

Thus

$$W_R = \frac{1.44 \times 41.7}{177}\ W_{HU} = 0.34\ W_{HU} \tag{6}$$

The increase in propellant tank weight to accommodate the helium bottle and the additional liquid that must be carried to account for vaporization is derived from the volume increase and the weight per unit length for the tank cylindrical section $(dW/dL)_T$

$$\Delta W_T = (dW/dL)_T\ \Delta L$$

$$\Delta L = \frac{\Delta V}{A_c}$$

where A_c is the tank cross-sectional area at its equator and $A_c = \pi D_T^2/4$

Thus

$$\Delta W_T = \frac{4\Delta V}{\pi D_T^2}\ \left(\frac{dW}{dL}\right)_T$$

For the helium bottle,

$$\Delta W_{T_B} = \frac{4V_B}{\pi D_T^2}\ \left(\frac{dW}{dL}\right)_T$$

From the above

$$V_B = \frac{1.44\ W_{HU}}{(W_B/V_B)} = \frac{1.44\ W_{HU}}{177} = 0.00814\ W_{HU}$$

For the specific tankage

$$D_T = 3.66 \text{ M: and } (dW/dL)_T = 57.9 \text{ Kg/M:}$$

$$\Delta W_{T_B} = \frac{4 \times 0.00814 \, W_{HU} \times 57.9}{3.14 \times 3.66^2} = 0.044 \, W_{HU} \tag{7}$$

$$\Delta W_{T_V} = \frac{4 \, V_{VP}}{\pi D_T^2} \left(\frac{dW}{dL}\right)_T$$

$$V_{PV} = W_{PV}/\rho_L \qquad \rho_L = 72.14 \text{ Kg/m}^3$$

Thus

$$\Delta W_{T_V} = \frac{4 \times W_{PV} \times 57.9}{3.14 \times 3.66^2 \times 72.14} = 0.076 \, W_{PV} \tag{8}$$

The insulation system weight penalty is generally small and is expressed as

$$\Delta W_i = \left(\frac{dW}{dL}\right)_i \left[4\left(\frac{V_B + V_{PV}}{\pi D_T^2}\right) \right]$$

Generally $(dW/dL)_i = 28.4 \text{ Kg/m}$

$$\Delta W_i = 28.4 \left[4\left(\frac{0.00814 \, W_{HU} + 0.0139 \, W_{PV}}{3.14 \times 3.66^2}\right) \right]$$

$$= 28.4 \, (0.000774 \, W_{HU} + 0.00132 \, W_{PV})$$

$$\Delta W_i = 0.022 \, W_{HU} + 0.037 \, W_{PV} \tag{9}$$

Now combining equations 1, 4, 6, 7, 8, and 9

$$W_{PST} = W_{HU} + W_{PV} + 1.44 \, W_{HU} + 0.34 \, W_{HU} + 0.044 \, W_{HU}$$

$$+ 0.076 \, W_{PV} + 0.022 \, W_{HU} + 0.037 \, W_{PV}$$

$$W_{PST} = 2.846 \, W_{HU} + 1.113 \, W_{PV} \tag{10}$$

    f. Comparison of Autogenous and Helium LH$_2$ Tank Pressurization. The gas requirements and hardware weights can now be combined to obtain a comparison of the pressurization system weights for a given value of NPSP. As was shown above, the optimum autogenous system uses a pressurant inlet temperature of 111°K (200°R); however, the helium system cannot be optimized strictly on gas requirements. Figure 3.2.12 shows the total helium
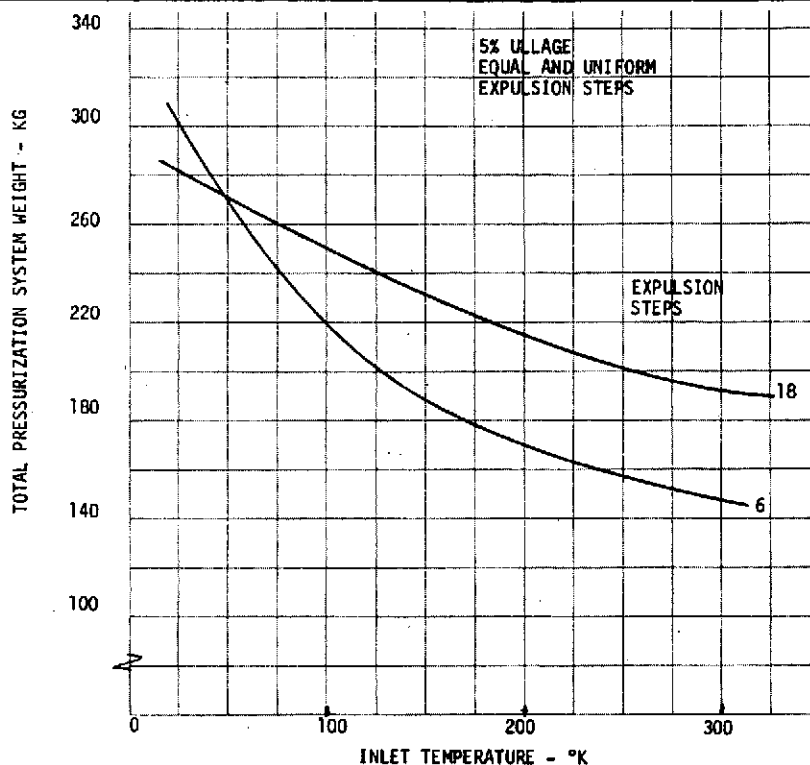
Figure 3.2.12. Influence of Inlet Temperature on Helium Pressurization of LH$_2$ Tank

pressurization system weight as a function of inlet temperature. Because of the driving nature of the helium bottle and residual weights this does not have a clear optimum but something on the order of 300°K is reasonable since beyond this level, gas heating penalties (not considered in this study) would begin to cause a hardware weight penalty. This figure clearly shows the penalty imposed by restricting the helium system to no heat inlet (22°K inlet temperature).

The total pressurization system weights are compared in Figure 3.2.13 for two general conditions: (1) The recommended design points based on the expulsion duty cycle effects study and on the basis of identical and uniformly spaced expulsion steps. Note that in all cases, the heated GH$_2$ approach is the lightest and cold helium is the heaviest approach. Also note that a very low temperature hydrogen system is slightly lighter than cold helium.

Figure 3.2.14 shows the influence of NPSP on the total pressurization system weight for the recommended 111°K GH$_2$ and cold helium pressurization systems.

g.   System Implementation.   From a system implementation standpoint, the cold helium system is simple and straight-forward.   The helium is stored in a high pressure bottle within the LH$_2$ tank and regulated to a low pressure significantly above maximum LH$_2$ tank pressure.   The pressurant supply to the LH$_2$ tank is controlled by an on-off or modulating value controlled by the true NPSP controller, which senses tank pressure and critical propellant temperature (as in the outlet of the acquisition device).

RECOMMENDED
DESIGN POINTS

111°K GH₂

22°K He

TRUE NPSP
5 PSIA NPSP

18 EQUAL AND UNIFORMLY
SPACE EXPULSION STEPS

111°K GH₂

25°K GH₂

333°K He

22°K He

0	100	200	300	400	500

TOTAL PRESSURIZATION SYSTEM WEIGHT - KG
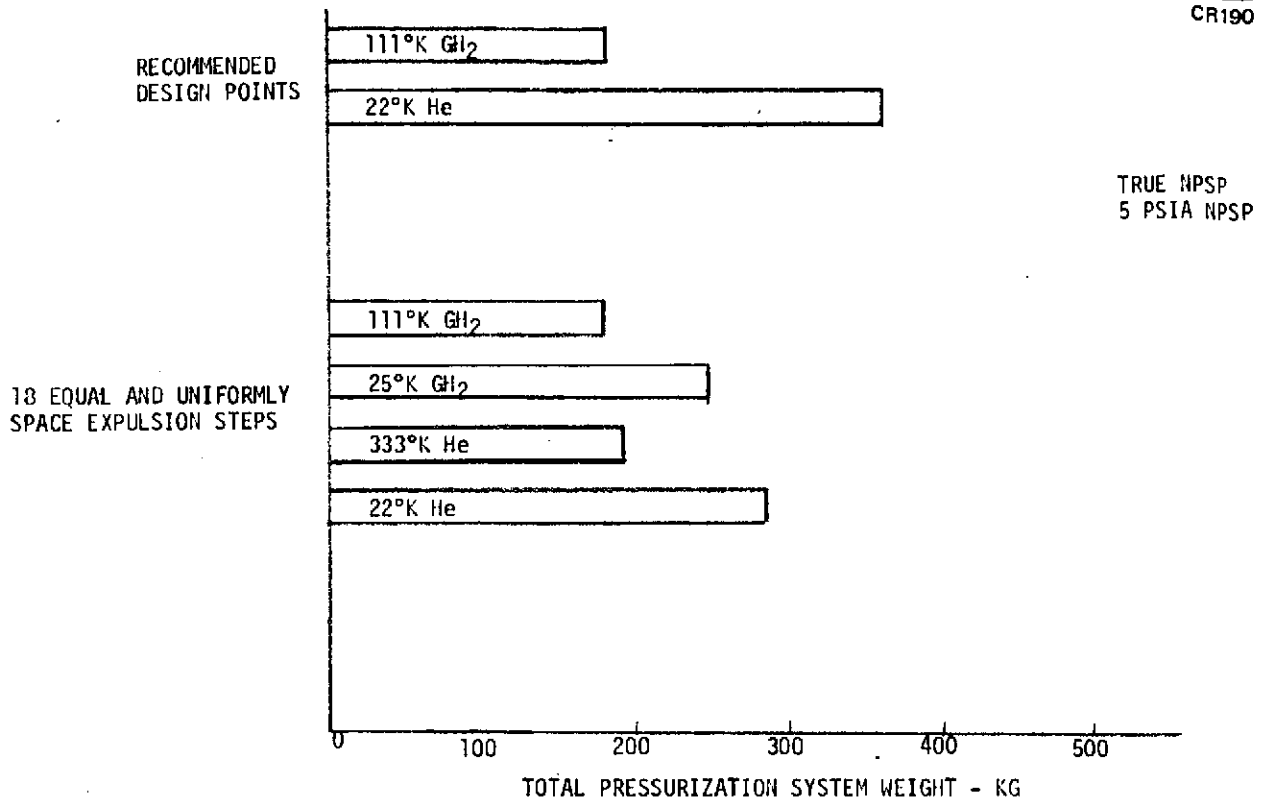
Figure 3.2.13. LH₂ Tank Pressurization System Weight Comparison

The system becomes more complicated if the helium is heated in that thermal energy must be added to the gas prior to entry into the tank. In the baseline propulsion system, gas accumulators are used and these provide a convenient heat source for moderate inlet temperatures. For very high temperatures, a separate combustor/heat exchanger such as used on the Saturn SIV stage would be required. The helium pressurization systems are illustrated in Figure 3.2.15.

With the baseline accumulator system, the 111°K GH₂ system is also quite simple to implement in that the pressurant can be bled directly from the accumulator. In doing so, there would be some inlet temperature variations but these would be of little consequence.

As indicated by the weight comparisons of Figure 3.2.13, the cold GH₂ system is a viable candidate. This could save about 115 kg as compared to the recommended cold helium design. From a mechanical standpoint, some means must be provided for supplying low-temperature hydrogen gas. The APS accumulators provide a high-pressure gas source, but this gas is at too high a temperature (110 to 170°K) and it must be cooled. Using the accumulator as the high-pressure GH₂ source, at least 135×10^3 watt (128 Btu/sec) must be removed from the GH₂ before entering the tank at close to LH₂ temperatures. If a heat exchanger were submerged in the LH₂ tank utilizing free convection, 560 m²
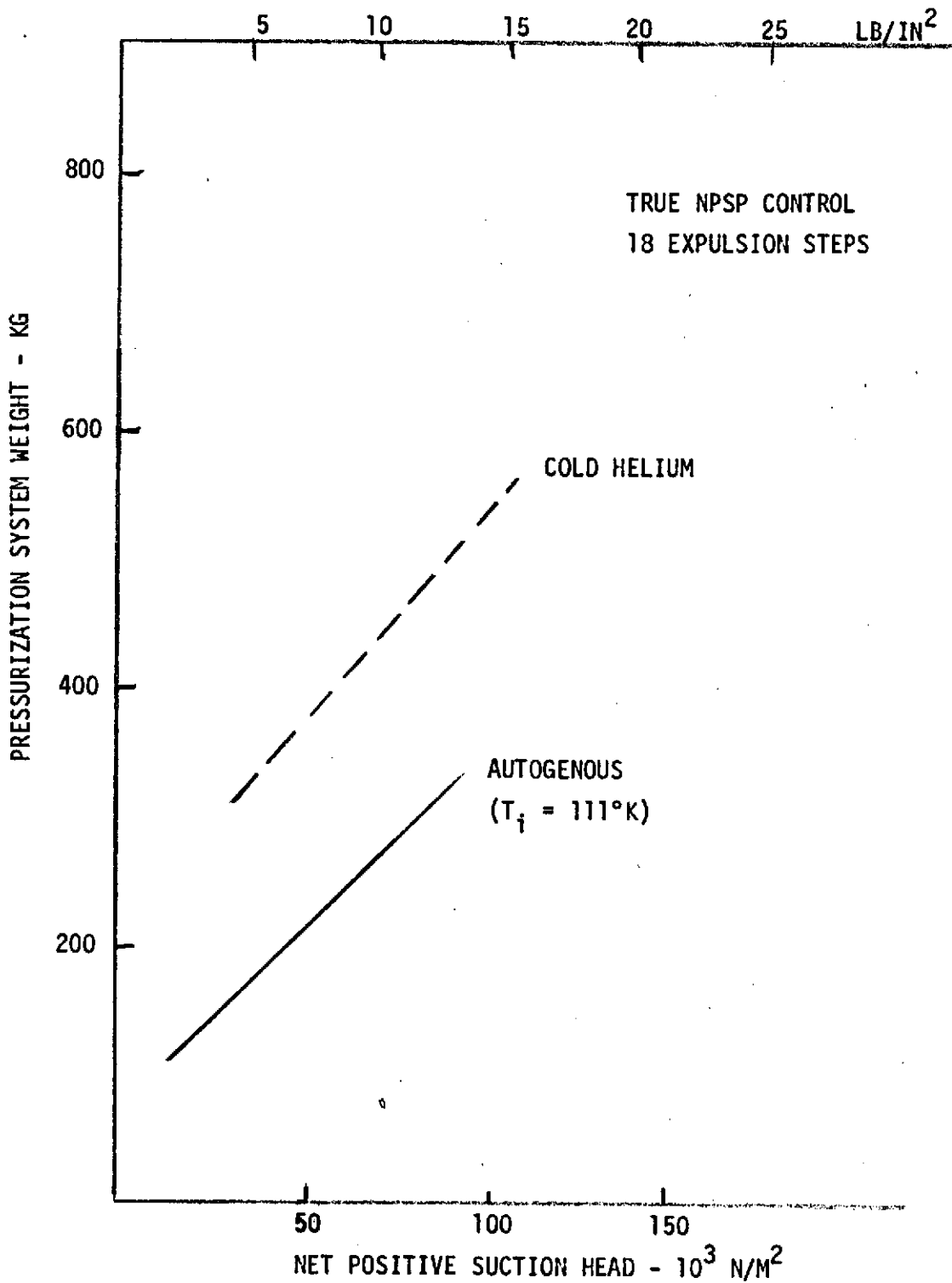
Figure 3.2.14. Influence of NPSP on Pressurization System Weight

COLD HELIUM SYSTEM

HELIUM BOTTLE

TRUE NPSP
CONTROLLER

REGULATOR

CONTROL VALVE

HEATED HELIUM SYSTEM

HEAT
EXCHANGER

APS
ACCUMULATOR

HELIUM

HELIUM

COMBUSTOR

GH$_2$ GO$_2$
FROM ACCUMULATORS
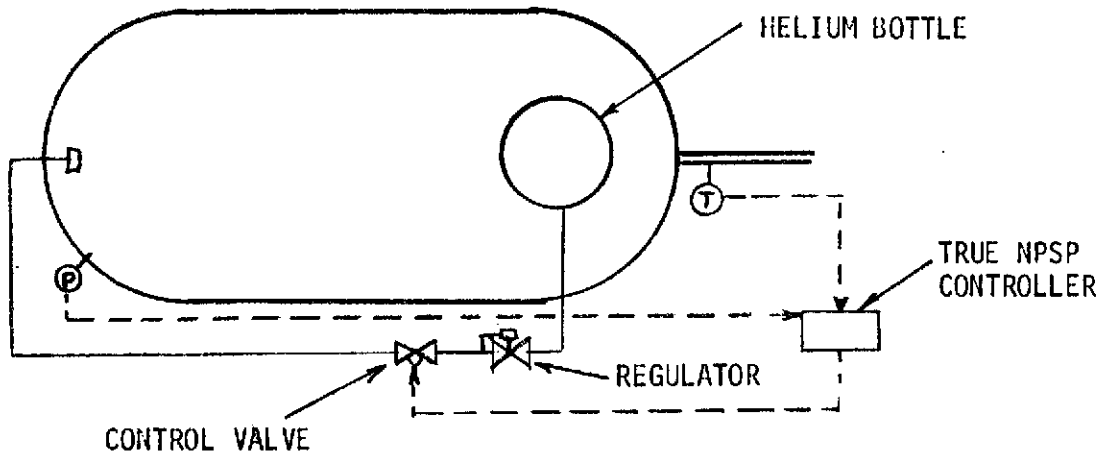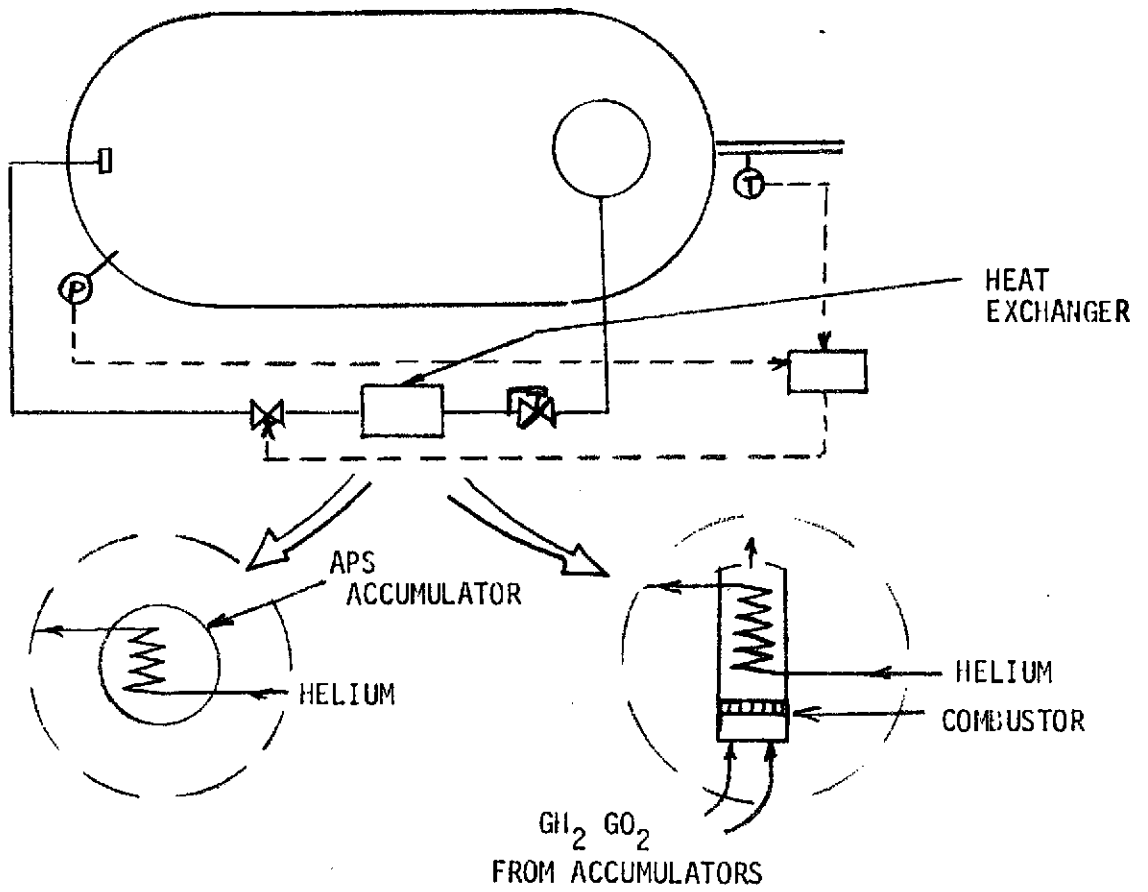
Figure 3.2.15. Helium Pressurization Systems

(6,000 ft^2) of heat transfer area would be needed; which is impractical. A more reasonable approach is to use a compact heat exchanger which uses pumped LH$_2$ taken from the acquisition device to cool down the GH$_2$ being supplied from the accumulator. In the process the liquid flow will vaporize. Of course, a booster type pump must be used to feed the LH$_2$ from the acquisition device into the heat exchanger. Furthermore, to conserve fluid, both flows are mixed upon leaving the heat exchanger to form the actual pressurant stream entering the tank. For a specific accumulator gas temperature, the ratio of the LH$_2$ flow through the heat exchanger to the gas flow has a certain theoretical value as shown below

$T_{accumulator}$	$\dfrac{\dot{W}_{liquid}}{\dot{W}_{gas}} = \dfrac{C_p \Delta T_G}{H_v}$
111°K (200°R)	2.53
139°K (250°R)	3.31
117°K (300°R)	4.11

For the 111°K case, 37 x 10^3 watt (36 Btu/sec) must be removed from the GH$_2$ thus requiring about 7.17 M^2 (72 ft^2) of heat exchanger area which is more reasonable but would still be heavy (about 18 to 20 kg). A simpler and potentially more efficient approach is to intimately mix the LH$_2$ and warm GH$_2$ in a vaporizer/cooler. This vaporizer/cooler should weigh only about 3 to 5 kg. Schematics for the two GH$_2$ conditioning concepts are shown in Figure 3.2.16.

The pump must be capable of providing about 0.086 kg/sec with a pressure rise of 173 x 10^3 N/M^2 (25 psi) which is essentially governed by injector differential pressure. Assuming a pump efficiency of 65 percent, this requires a 324-watt pump and about a 540-watt motor.

Based on preliminary conservative weight numbers, the vaporizer/cooler GH$_2$ conditioning device should have the following weights.

Pump	2.0 kg
Motor	2.0
Vaporizer/Cooler	4.0
Supports, etc.	0.8
	8.8 kg

This compares favorably with the 115 kg savings afforded by the cold GH$_2$ system relative to the cold helium.

h. <u>LO$_2$ Tank Pressurization</u>. Pressurization requirements for the LO$_2$ tank were estimated in the same manner as for the LH$_2$ tank. Figure 3.2.17 depicts the parametric pressurant requirements for helium
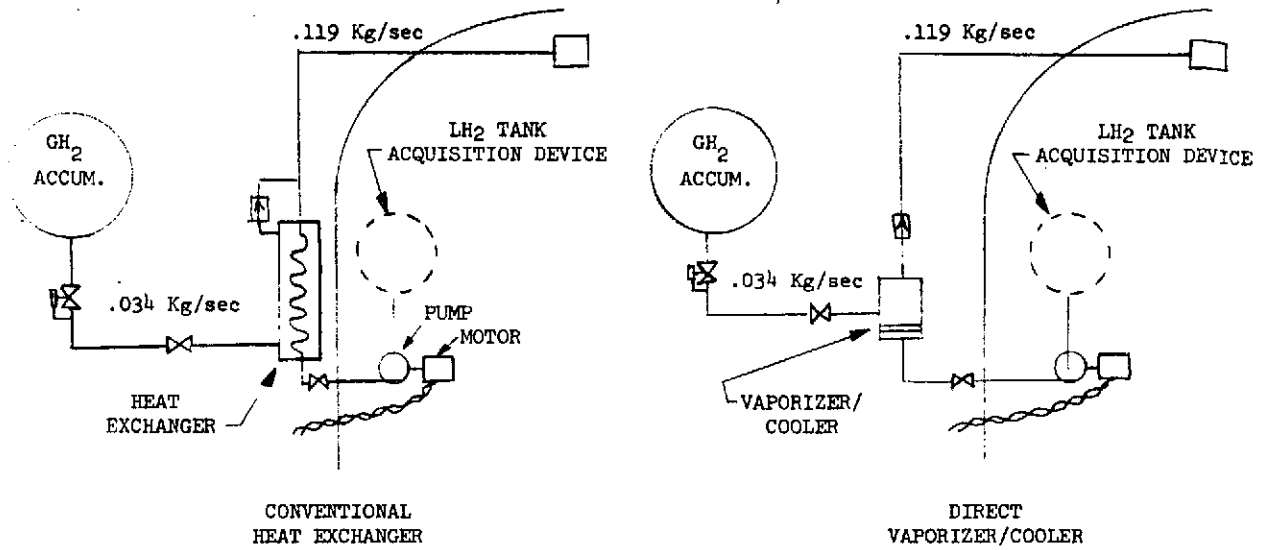
Figure 3.2.16. Cold GH$_2$ Conditioning Concepts
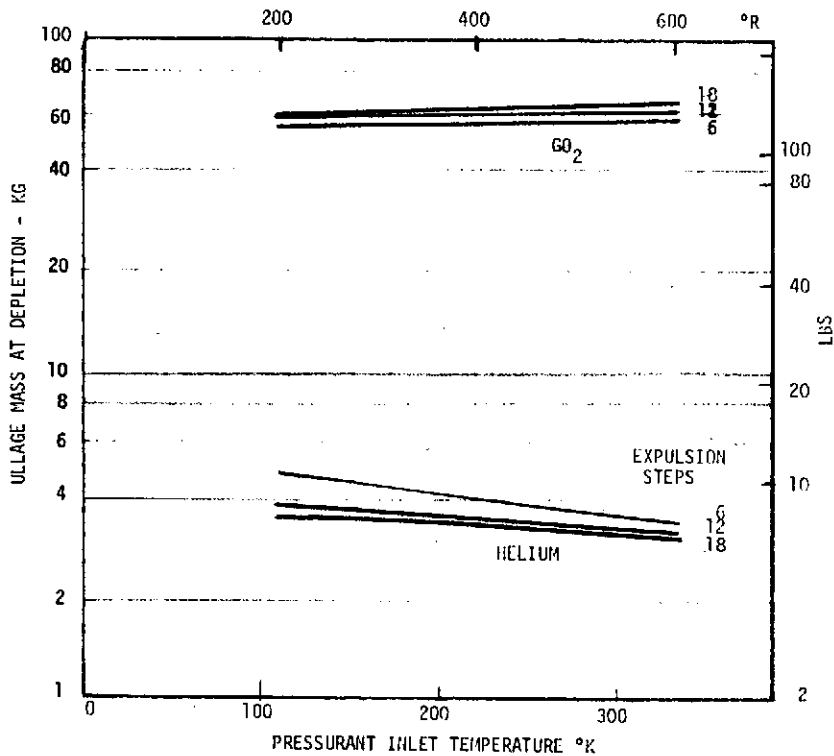
Figure 3.2.17. LO$_2$ Tank Pressurization with Helium True NPSP (3.45 X 10^4 N/M^2)

pressurization assuming true NPSP control with a NPSP of 3.45×10^4 N/M^2 (5 psia). This shows that the bulk of the ullage is primarily GO$_2$ and that very little helium is required. It also shows that the system is very insensitive to pressurant inlet temperature. Based on these results, a helium pressurization system with an inlet temperature equal to LO$_2$ temperature (111°K) was used. With this choice, the influence of control logic, was evaluated as shown in Figure 3.2.18. Based on these results, a true NPSP control logic was selected.

To pressurize the LO$_2$ tank, additional helium will be stored in the main helium bottle in the LH$_2$ tank. A helium bottle could also be placed in the LO$_2$ tank but this would not be as efficient from a storage standpoint and the use of structurally efficient titanium bottles in a LOX environment is not recommended. Because of the small gas flow requirements, there should be adequate passive heat sink in the lines and structure to allow the helium to be heated to LO$_2$ tank temperature prior to entry into the tank.

Hardware weight penalties are derived in a similar manner to those for the LH$_2$ tank.

$$W_B = 1.44\ W_{HU} \text{ (from equation 2)}$$

$$W_R = 0.34\ W_{HU} \text{ (from equation 6)}$$

(Since the helium is stored in the LH$_2$ tank, the O$_2$ vapor is stored as liquid in the LO$_2$ tank)
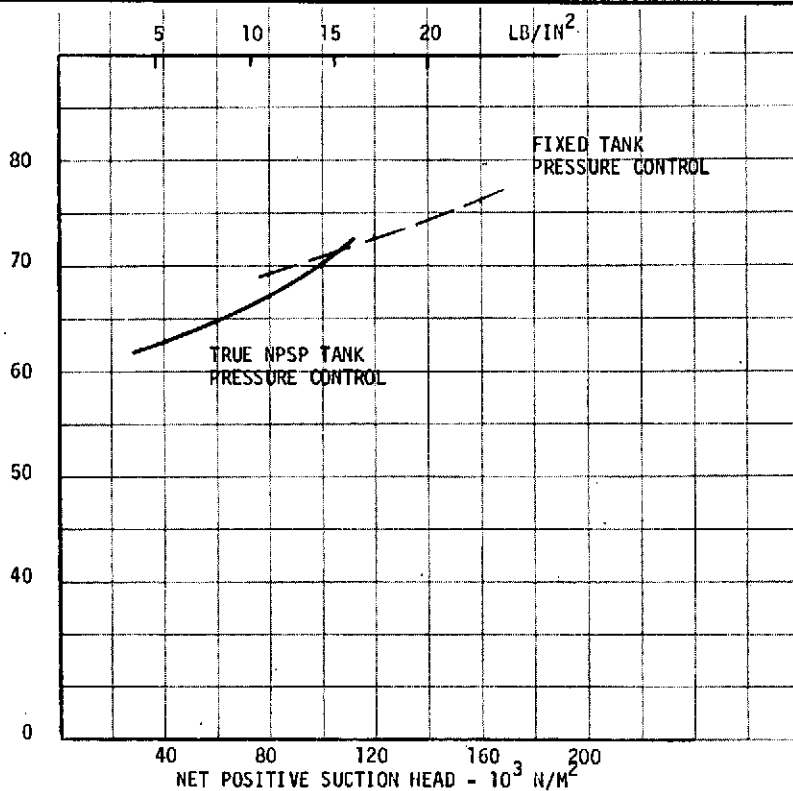
Figure 3.2.18. Influence of Control Logic on Ullage Mass (LO$_2$ Tank)

$$\Delta W_{T_B} = 0.044\ W_{HU}\ \text{(from equation 7)}$$

Thus,

$$\Delta W_{T_V} = \frac{4V}{\pi D_T^2}\left(\frac{dW}{dL}\right)_T = \frac{4V_{PV}}{\pi D_T^2}\left(\frac{dW}{dL}\right)_T$$

$$\left(\frac{dW}{dL}\right)_T = 39\ \text{kg/m}$$

$$V_{PV} = W_{PV}/\rho_L = \frac{W_{PV}}{1123} = 0.00089\ W_{PV}$$

$$\Delta W_{T_V} + \frac{4 \times 0.00089\ W_{PV} \times 39}{2.14 \times 2.442} = 0.0074\ W_{PV}$$

$$\Delta W_i = \left(\frac{dW}{dL}\right)_{i_H}\left(\frac{4\ V_B}{\pi D_T^2}\right)_H + \left(\frac{dW}{dL}\right)_{i_0}\left(\frac{4\ V_{PV}}{\pi D_T^2}\right)_0$$

$$= 28.4\left[4\left(\frac{0.00814\ W_{HU}}{3.14 \times 3.66^2}\right)\right] + 19\left[4\left(\frac{0.0089\ W_{PV}}{3.14 \times 2.44^2}\right)\right]$$

$$= 0.022\ W_{HU} + 0.0036\ W_{PV}$$

Combining the above

$$W_{pst} = W_{HU} + W_{PV} + 1.44\ W_{HU} + 0.34\ W_{HU} + 0.044\ W_{HU}$$
$$+ 0.0074\ W_{PV} + 0.022\ W_{HU} + 0.0036\ W_{PV}$$

$$W_{pst} = 2.846\ W_{HU} + 1.011\ W_{PV}$$

Thus for the baseline system

$$W_{pst} = 2.846\ (3.6) + 59\ (1.011) = 10.2 + 59.6 = 69.8\ \text{Kg}$$

The LO_2 tank pressurization system is, clearly, not a driving factor in the overall storage/transfer system.

3.3 Thermal Management Subsystem

To efficiently store cryogens in orbit for seven days, it is essential to minimize the heat entering the storage/expulsion system and to properly manage the heat that does enter. In recent years, intensive research has been conducted to develop non-integral tankage, multi-layer radiation barrier type insulation (MLI), low heat leak tank supports, and low heat leak fluid transfer lines which can be integrated to produce a lightweight low heat load cryogen storage system. With such concepts, it is possible to obtain heat leaks of 1.58 to 0.63 watts/M^2 (0.5 to 0.2 Btu/Ft^2Hr) and insulation weight penalties of about 2.44 to 1.47 kg/M^2 (0.5 to 0.3 lb/ft^2). However, in designing and optimizing the total thermal control subsystem, detailed consideration must be given not only to heat input minimization but proper management of the finite heat that does enter the feed system. Also, as discussed in Section 3.1, the acquisition concept may place considerable constraints on the thermal management subsystem. Thermal management of propellants can be achieved by three general techniques: (1) direct venting, where the incoming heat all goes to propellant vaporization and boiloff from the system; (2) non-venting with pressure rise, where all the incoming heat goes to increasing tank pressure and propellant temperature; and (3) non-venting with cooling, where a lower temperature fluid extracts or intercepts the incoming heat. If tank venting is used, positive provisions must be made to assure that liquid phase venting does not occur in the low-g environment. Numerous studies (such as References 9, 15 and 16 have shown the superiority of a thermodynamic vent system (TVS) for this low-g venting function. With the TVS concept, the vent fluid leaving the tank is throttled to a pressure and temperature below that of the tanked propellant and is then passed through a heat exchanger where it vaporizes and extracts heat from the stored propellant or intercepts the heat before it enters the propellant. Both internal tank mixer-heat exchangers and external cooled-shield TVS concepts are feasible for this application. The TVS also has the capability of performing limited cooling functions in the feed system, as for heat shorts such as supports and fluid lines and acquisition hardware. Studies (Reference 17) have also been conducted to investigate the use of surface tension screen-wall-liners to provide an all gas zone in the tank for low-g venting.

3.3.1 <u>Basic Insulation System.</u> The major factors in determining the effectiveness of an insulation system are the effective thermal conductivity (K_e) and the insulation density (ρ_i). Figure 3.3.1 shows the approximate influence of the product of these characteristics ($K_e\rho_i$) on the required number of multi-layer sheets and the boiloff or vented weight. The optimum is based on achieving the highest ratio of mass of cryogen transferred after seven-day storage to the initial tank system gross weight, including loaded propellant, insulation, and tank structure. The basic $k_e\rho$ for typical MLI ranges from 100-300 joule-kg and is orders of magnitude lower than other classes of insulation such as foams. The indicated boiloff includes only equilibrium space operation and does not consider launch or reentry effects. Based on these considerations, MLI type insulation was accepted as mandatory for the required tank sizes and the 7-day in-orbit storage times.
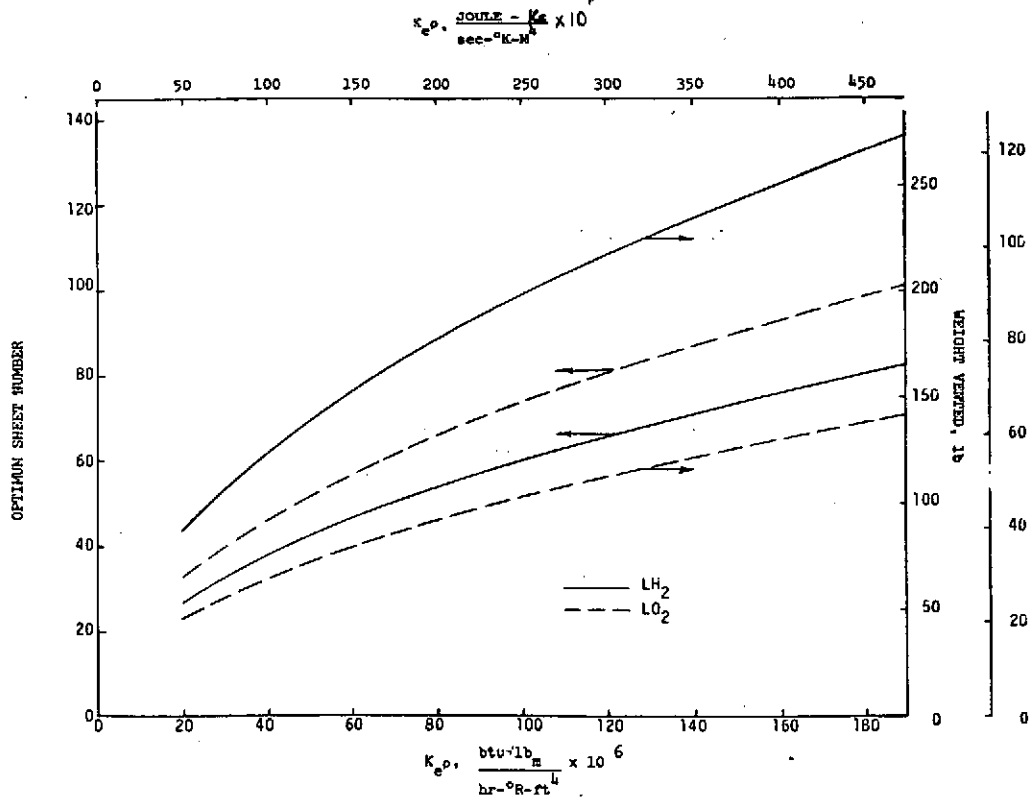
Figure 3.3.1. Space MLI Optimization

Insulation systems of this class for similar tankage application were studied in depth by MDAC under contract NAS8-26006 (Reference 18). This analytical and experimental study resulted in the selection of an insulation system consisting of alternating layers of goldized Kapton and Dacron B4A net separators formed into blankets attached to the tank by low conductivity attachments. This system was selected as the basic insulation system for this study with the characteristics as summarized in Table 3.3.1.

In establishing the design effective conductivity values, the conductivity obtained from calorimeter type tests on the basic MLI layup was downgraded by 75% to account for performance losses due to joints, attachments, and perforations. This 75% was arrived at by calorimeter experimental results where a basic layup was progressively altered to account for these potential sources of degradation. (See Reference 19.)

A further factor in the selection of the goldized Kapton system, as opposed to the more common aluminized mylar, is the requirement for reusability. Conventional aluminized mylar is susceptible to moisture damage during temperature cycling which results in loss of the aluminum coating and degradation of thermal performance (see Reference 13). Although there are potential solutions to this problem, such a study was beyond the scope and objectives of this program.

Table 3. 3. 1

INSULATION CHARACTERISTICS FOR DOUBLE GOLDIZED
KAPTON WITH DACRON B4A SEPARATORS (DGK/B4A)

EFFECTIVE THERMAL CONDUCTIVITY

$$LH_2 \quad K_e \;=\; 2.68 \times 10^{-5} \; \frac{Joules}{M\text{-}Sec\,°K} \left(1.55 \times 10^{-5} \; \frac{BTU}{Ft\text{-}Hr\,°R} \right)$$

$$LO_2 \quad K_e \;=\; 3.51 \times 10^{-5} \; \frac{Joules}{M\text{-}Sec\,°K} \left(2.03 \times 10^{-5} \; \frac{BTU}{Ft\text{-}Hr\,°R} \right)$$

WEIGHT

DGK $=$ 0.0066 Kg/M^2

B4A $=$ 0.0095 Kg/M^2

	0.0161 Kg/M^2 _ Layer
Attachments* =	0.0380 Kg/M^2
Face Sheets (4)** =	0.3900 Kg/M^2
Purge Bag*** =	0.404 Kg/M^2

Total Weight $=$ (0.794 + 0.0161 N) Kg/M^2

or (0.162 + 0.0033 N) Lb/Ft^2

LAYER DENSITY

35 Pairs/Cm (90 Pairs/In)

---

*Includes attaching studs, thread and tape
**Nomex face sheets, 2 per blanket, 2 blankets
***Kapton purge bag.

3.3.2 Space Insulation Optimization. The results depicted in Figure 3.3.1
are based on an overly simplified optimization criteria where boiloff weight
loss is directly balanced against insulation weight. In reality, the boiloff weight
does not have to be accelerated for the entire mission and, therefore, does
not have the same impact on stage velocity change as inert weight. This
difference is accounted for by the Multiburn Space Propulsion Module Sizing
Computer Program, H109, specifically developed by MDAC for such system
optimization. The insulation optimization was performed using this code
which takes the entire propulsion module into account and optimizes any
selected design variable on the basis of either minimum stage gross weight
or maximum stage velocity change. The program was set up using the base-
line CSS/APS vehicle overall geometry, specific insulation parameters, and
overall design factors; the vehicle gross weight was evaluated as the number
of insulation layer-pairs on the LH$_2$ tank was varied. Rather than using total
vehicle weight, results are presented in terms of vehicle gross weight value
minus 123,000 kg termed the gross weight datum. Other important assump-
tions for this analysis are as follows: (1) easterly launch mission; (2) a
three-blanket, double goldized, kapton/dacron (B4A) net insulation (effective

design thermal conductivity = 2.68 x 10^{-5} Joules/M-Sec °K; (3) a 9-burn duty cycle; (4) tankage size based on the data of Table 2.3 in Section 2.1; (5) initial ullage of 35%; (6) true NPSP tank pressure control maintaining 34.5 x 10^3 N/m^2 (5 psi) above propellant saturation pressure during expulsion and a hot boundary temperature for the vehicle of 278°K (500°R).

The standard easterly launch mission was selected because this requires storing the smallest amount of propellant in a given tank size for the longest period of time, thus maximizing the difficulty of thermal storage. Thermal management involves a significant interaction between the insulation and pressurization systems since the pressurant represents a significant tank heat input. Since different pressurization systems are used with each acquisition system concept, the thermal management optimization was conducted independently for cold helium and 111°K GH$_2$ pressurization subsystems.

a. LH$_2$ Tank Optimization Study. In the first case, it was assumed that the LH$_2$ tank is pressurized with 111°K (200°R) inlet temperature GH$_2$ taken from the APS accumulators. This was found in Section 3.2 to be more efficient than cold and/or heated helium. However, the warm GH$_2$ represents a significant tank heat input; it is about twice that which enters through the insulation. To optimize this total system problem, the MDAC H109 propulsion system sizing and optimization computer program was used. This program analyzes the thermal interactions for a typical space propulsion module including insulation heat input, pressurant heating, thermal shorts, etc., and optimizes the various critical module design variables in terms of system weight or stage velocity changes.

Results from the program computations are shown in Figure 3.3.2 in terms of MLI layers versus vehicle gross weight datum. Two thermal management options were examined: (1) nonvented tanks with the heat being absorbed by uniform temperature rise in the system; and (2) in-orbit venting with all heat transfer through the insulation resulting in direct boiloff loss. For these computations, insulation parameters identical to those used previously were retained and it was assumed that true net positive suction pressure (NPSP) control with an NPSP = 34.5 x 10^3 N/M^2 (5 psia) was used in all cases. Another important assumption is that thermal equilibrium is attained in the tank shortly after each major expulsion step, as would be provided by internal tank mixers or by the mixing of the liquid and vapor following engine shutdown.

From Figure 3.3.2, it can be seen that for the LH$_2$ tank, the optimum multilayer insulation (MLI) layer-pairs are 21 and 25 for nonvented and continuous venting operation, respectively. For the nonvented case, a limiting tank pressure of 207 x 10^3 N/m^2 (30 psi) is reached, which is about compatible with tank wall minimum gage limits (see Section 3.3.4). Another important observation from Figure 3.3.2 is that the nonvented/mixed fluid mode of operation is considerably lighter than the vented case. This weight comparison is broken down and computed more precisely in Table 3.3.2. A weight difference of about 85 kg has been estimated. The nonvented tank saves about 7 kg in insulation, 101 kg in boiloff, and 5 kg in mixer/heat exchanger hardware; however, it requires about 30 kg more gas residual because of the higher final tank pressure. Nonventing theoretically would also result in a tank weight increase except that operation is within the minimum gage limit.
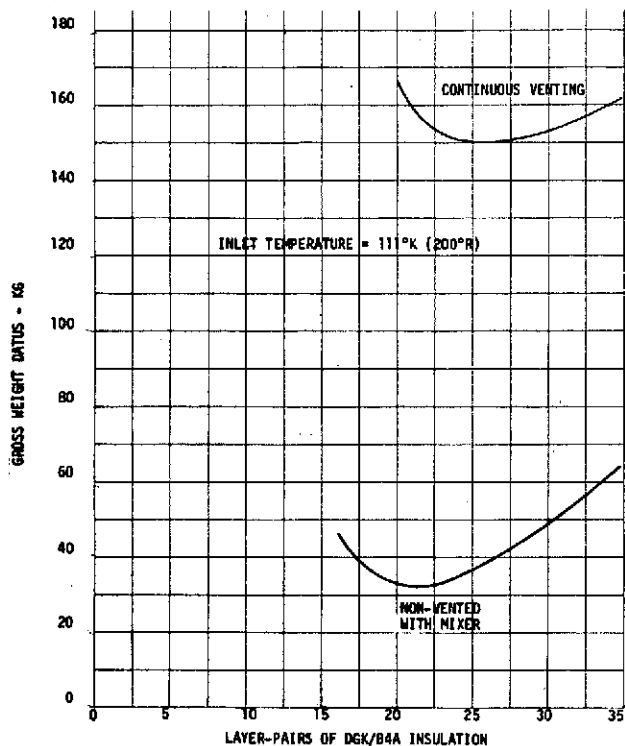
Figure 3.3.2. LH$_2$ Tank Insulation Optimization — GH$_2$ Pressurization

Table 3.3.2

WEIGHT COMPARISON OF VENTED AND NONVENTED LH$_2$ TANK
(111°K GH$_2$ PRESSURIZATION)

	Continuous Venting During Coast	Nonvented with Uniform Tank Heating
Purge bag	36.3 kg	36.3 kg
Face sheets	35.2	35.2
MLI layers	35.8	27.8
Insulation attachments	1.0	1.0
Tape and thread	2.4	2.4
In-orbit boiloff	101.0	0
Final ullage mass	81.0	110.0
Mixers/heat exchangers	10	5.0
	302.7 kg	217.7 kg

LPIC system - autogenous 110°K (200°R) pressurization of main tank:
true NPSP control - 34.5 x 10^3 N/m^2 (5 psia): 7-day easterly mission

Figure 3.3.3 shows the pressure-time history for the optimum nonvented LH$_2$ system. The technical acceptability of the nonvented tank rests on the adequacy of the internal tank mixers to reliably and properly distribute the incoming heat uniformly in a reduced-gravity environment. This will be explored later in this section.

The second case investigated assumes cold helium pressurization of the LH$_2$ tank where there is negligible heat contributed by the incoming pressurant. The H109 sizing and optimization code was again used to perform this analysis and the results are shown by the solid line in Figure 3.3.4. This indicates an optimum insulation consisting of 48 layer-pairs. An alternate thermal management technique using a nonvented tank with a mixer to assure uniform temperature distribution was also optimized for comparison. This optimization result is shown by the dashed line in Figure 3.3.4 that indicates an optimum insulation consisting of 25 layer-pairs. The maximum LH$_2$ tank pressure is about 188×10^3 N/m^2 (27.4 psia) as shown in Figure 3.3.5. This also shows that the nonvented system is lighter than that concept using continuous in-orbit venting. Detailed weights are presented in Table 3.3.3 indicating a weight difference of about 99 kg. However, use of an internal mixer to uniformly distribute tank heat does not assure that heat entering the system does not interact with the acquisition device before being redistributed by the mixer.

b. LO$_2$ Tank Optimization. As discussed in Section 3.2, the LO$_2$ tank is always pressurized with cold helium. The LO$_2$ tank insulation was optimized on this basis and on the assumption of nonventing operation using internal tank mixers. Such a concept was investigated by General Dynamic/Convair and found to be feasible (Reference 20). The results are shown in Figure 3.3.6 indicating 11 as the optimum number of layer-pairs of MLI. This results in a maximum tank pressure of 186.2×10^3 N/M^2 (27 psia) as shown in Figure 3.3.7

A number of other options also are possible for the LO$_2$ tank thermal management including direct boiloff and LH$_2$ cooling. These are compared in Table 3.3.4. As shown direct boiloff is relatively heavy and was not considered further. GH$_2$ cooling is attractive especially when the LH$_2$ tank is vented and the GH$_2$ coolant is essentially "free" to the LO$_2$ tank. This approach should also be quite the same when using a cooled shroud around the LO$_2$ tank. (The cooled shroud or shield concept will be discussed later in this section.)

3.3.3 In-Atmosphere Thermal Protection. In Section 3.3.2, the MLI requirements were analyzed and optimized based on in-orbit operation only. Although this is generally a valid approach, the final insulation subsystem must be compatible with in-atmosphere operation including ground-hold, boost phase flight, reentry, and landing. For the CSS/APS, the reentry and landing phase is important since cryogen must be available for control during these periods.

Multilayer insulation of the type discussed previously is primarily compatible with space operation where the system is evacuated and the primary mode of heat transfer through the insulation is radiation. If gas is present between the reflector sheets or the sheets are compressed together, conduction will dominate and the heat transmission will increase by orders of
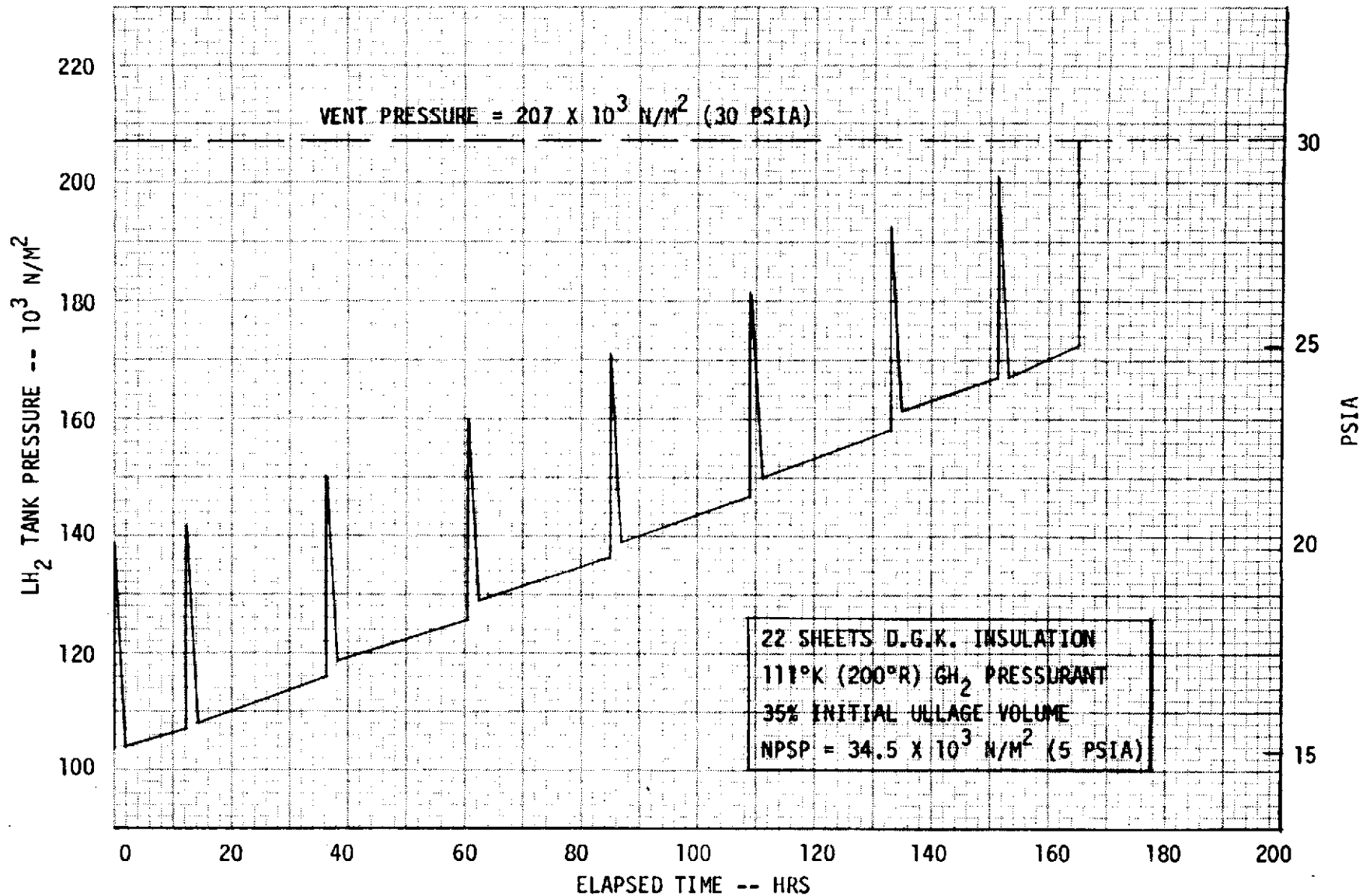
Figure 3.3.3. Optimum LH$_2$ Tank Pressure History — Easterly Mission
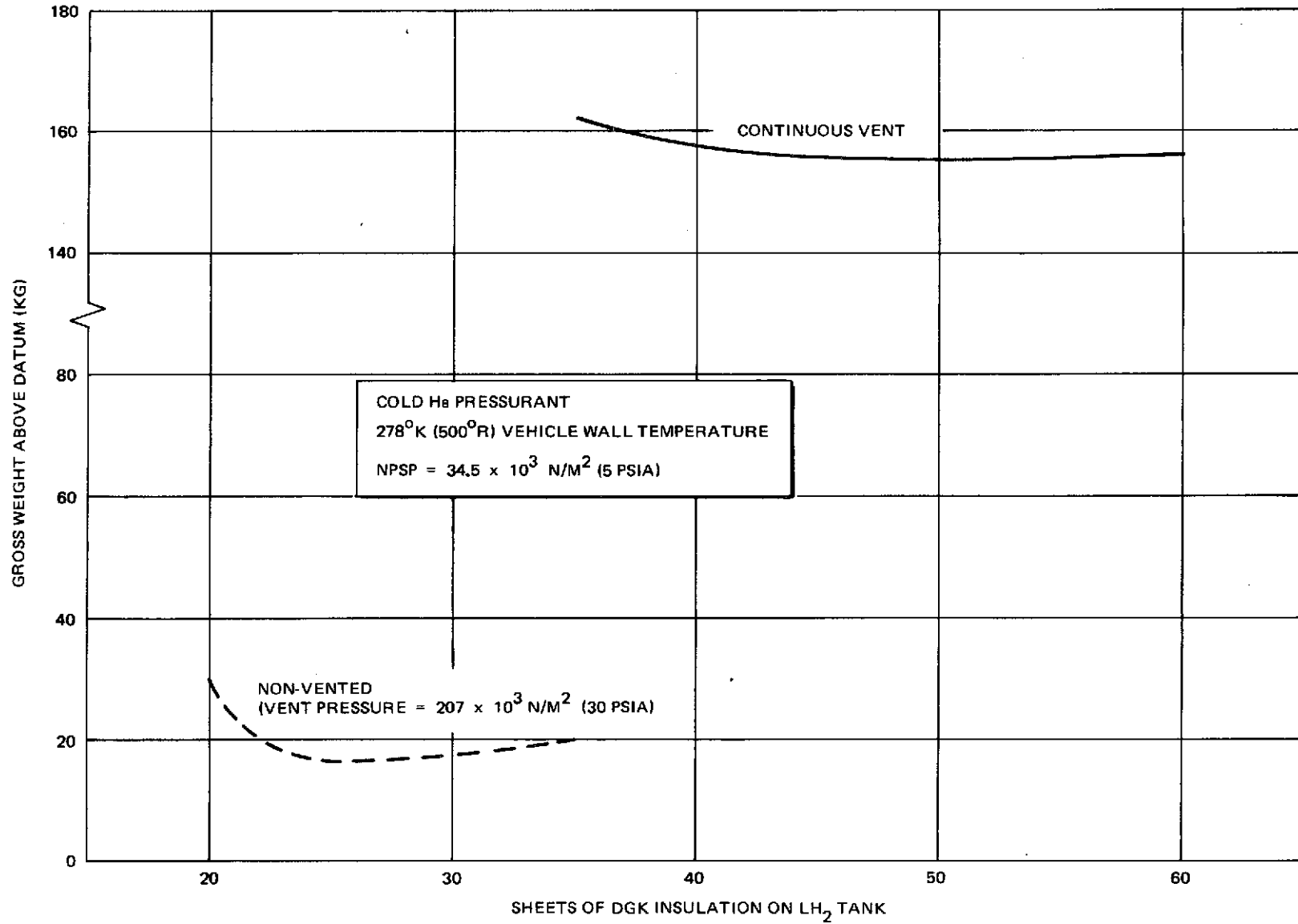
Figure 3.3.4. Effect of LH$_2$ Insulation on Stage Gross Weight — Easterly Mission
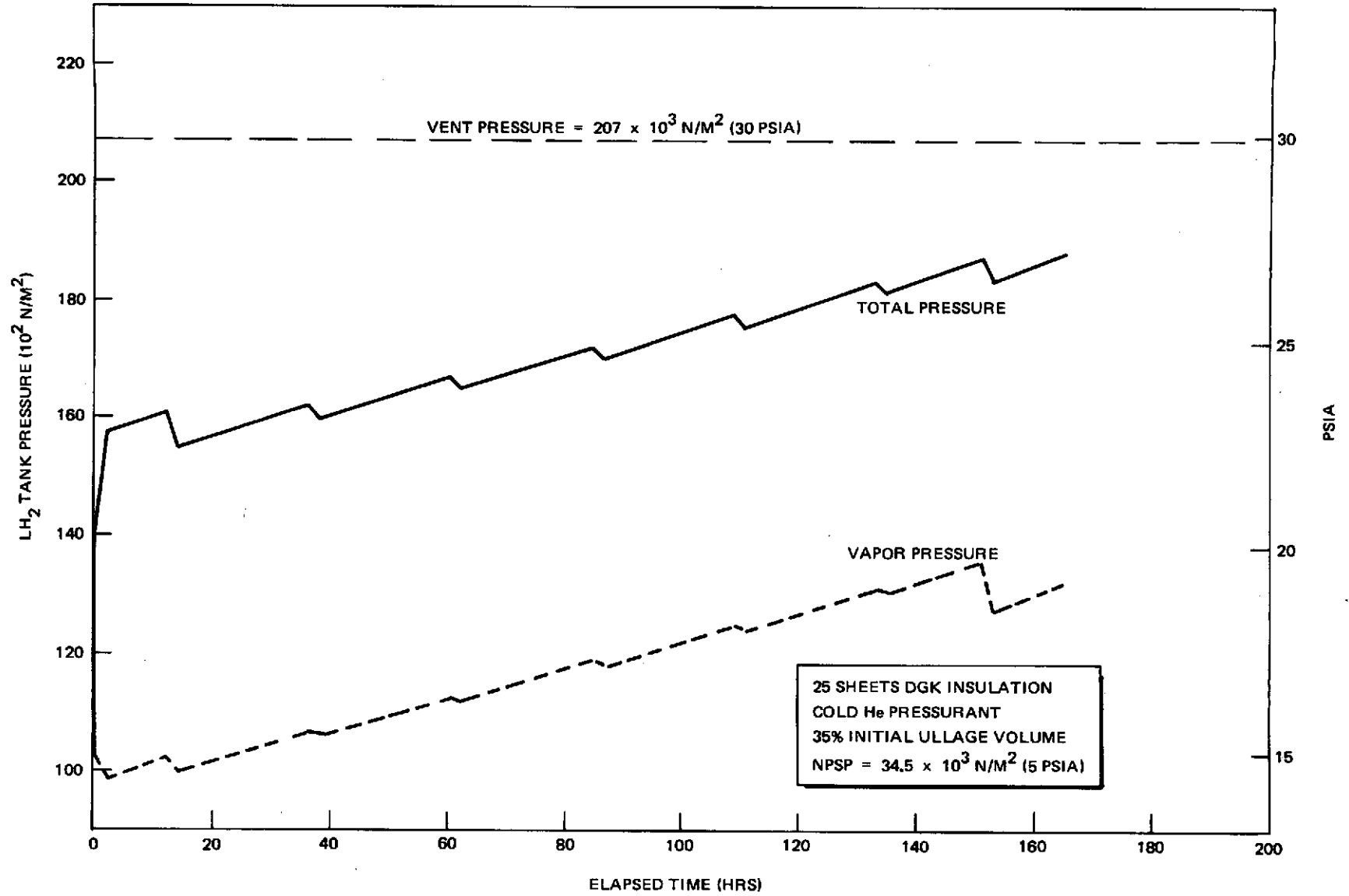
Figure 3.3.5. Optimum LH$_2$ Tank Pressure History — Easterly Mission

Table 3.3.3

WEIGHT COMPARISON OF VENTED AND NONVENTED LH$_2$ TANKS
(COLD HE. PRESSURIZATION)

	Continuous Venting During Coast	Nonvented with Uniform Heating
Purge bag	36.3 kg	36.3 kg
Face sheets	35.2	35.2
MLI layers	63.5	33.1
Insulation attachments, tape, and thread	3.4	3.4
In-orbit boiloff	60.5	0
Final ullage mass	173.0	199.0
Mixers	0	5
Cooling shields	34.5	0
	411.4	312.0

CR190
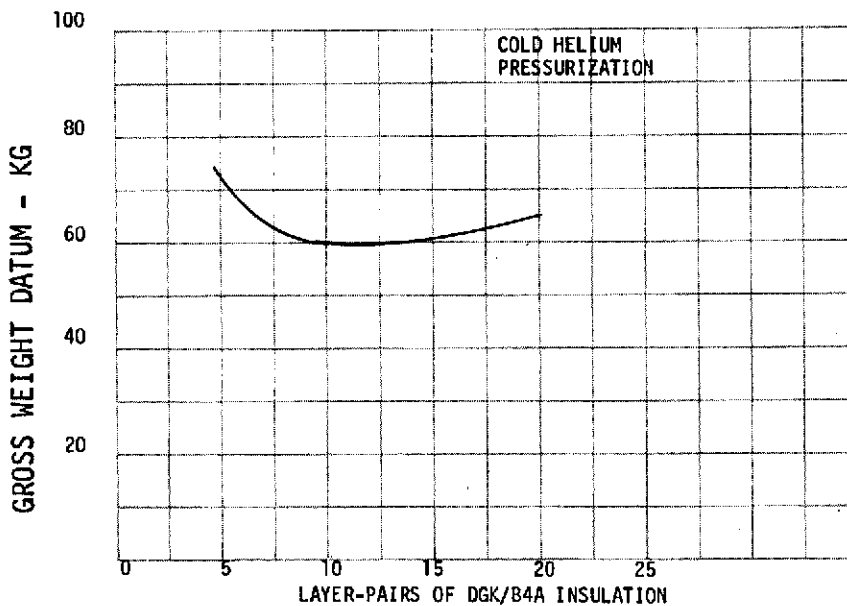
Figure 3.3.6. LO$_2$ Tank Insulation Optimization
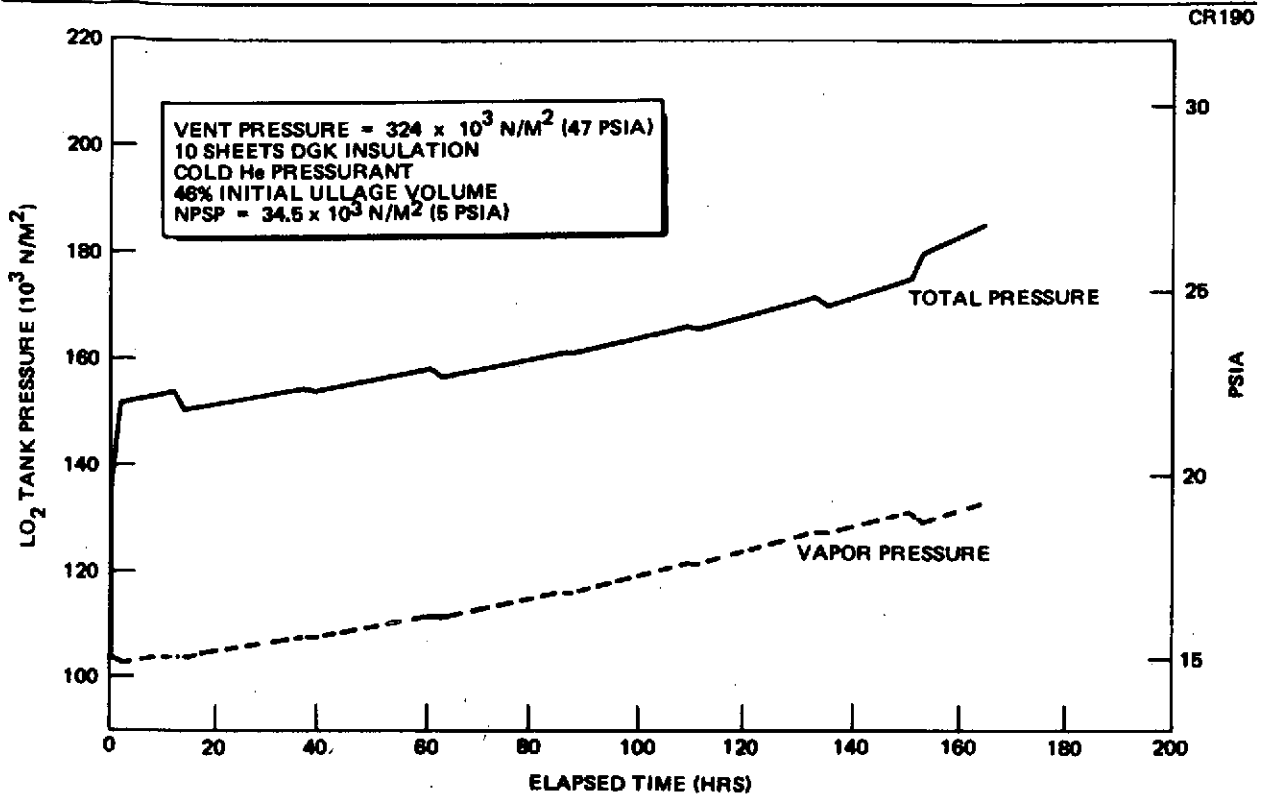
Figure 3.3.7. Optimum Non-Cooled LO_2 Tank Pressure History — Easterly Mission

Table 3.3.4

LO_2 TANK THERMAL MANAGEMENT TECHNIQUES WEIGHT COMPARISON

	Simple Boiloff[2]	GH_2 Heat Interception[3]	GH_2 Heat Interception (Free GH_2)[4]	Nonventing with Mixing
Purge bag	16.8 kg	16.8 kg	16.8 kg	16.8 kg
Face sheets	15.0	15.0	15.0	15.0
Insulation attachments	2.1	2.1	2.1	2.1
MLI (Layer-pairs)	36.1 (64)	28.2 (50)	12.4 (22)	6.2 (11)
LO_2 boiloff	40.0	0	0	0
LH_2 coolant loss	0	29.0	0	0
Mixer weight penalty	10	0	0	10
Final ullage mass	56.5	56.5	56.5	68.2
Cooling shroud	0	20.9	20.9	0
	176.5 kg	168.5 kg	123.7 kg	118.3 kg

[1] Baseline conditions - True NPSP control. NPSP = 34.5 x 10^3 N/m² (5 psia)
   LO_2 temperature helium pressurization

[2] Assumes all heat input goes to LO_2 boiloff

[3] The optimum GH_2 is directly extracted and used as a coolant for the LO_2 tank

[4] Applies to the case where 66 kg of GH_2 is being used for other purposes and can be diverted for LO_2 tank cooling before overboard dumping.

magnitude. Moisture and subsequencing freezing within the MLI must also be avoided. Several concepts have been researched for adopting an MLI system for acceptable in-atmosphere performance. They are as follows:

    a.   Prior to in-atmosphere operation, purge and pressurize the MLI with helium and/or nitrogen gas. Studies have shown that if this is done properly, the gas between the layers will approach stagnant conditions and the system will exhibit an overall conductivity equal to that of the filler gas. Condensation of the purge gas must, of course, be avoided.

    b.   A low conductivity foam insulation substrate can be installed between the tank and the MLI and the MLI is purged with dry gas.

    c.   A vacuum jacket is used over the MLI thus maintaining the MLI is a constant vacuum environment.

The vacuum jacket achieves the lowest total heat load by a wide margin but also involves a high inert weight penalty equal to the weight of the vacuum jacket. The all gas purge results in the highest heat load, especially for the LH_2 tank, since helium, which has a relatively high thermal conductivity, must be used to prevent condensation within the MLI. The weight and complexity of the active purge system must also be considered. The MLI/foam composite falls between the other two concepts in heat load and permits the use of mostly dry nitrogen purge gas since the foam thickness is sized to limit the MLI temperature to above the GN_2 condensation point. The foam conductivity is much higher than that of helium and its density is relatively low. To analyze properly the candidate insulation concept alternates, an efficient transient thermal analysis computer program is required. Such a code for computing the transient and accumulated heat input into a general cryogen tank over a total flight profile was prepared as part of the MDAC IRAD program. This code was applied to evaluating the overall heat input into the baseline LH_2 tank including ground hold, launch, space coast, reentry, and landing. This program can accommodate either a purged MLI system or a composite foam/MLI system with various purging options. The physical geometry and an insulation time-pressure history are input into the code. For the initial computations, the pressure histories for launch and reentry were taken from Figure F1 of Appendix F, which in turn was taken from Reference 18. In addition, a two-minute ground hold and a ten-minute landing period (both with a one atmospheric insulation pressure) were assumed. Nominal shuttle tank compartment temperature histories were assumed as presented in Appendix F.

Figures 3.3.8, -9 and -10 present the results of the thermal computations for helium-purged MLI, an external foam/MLI composite, and in internal foam/MLI composite insulation, respectively, All helium or combined helium/GN_2 reentry purges were evaluated for the composites. The presented curves are for the optimum (minimum weight penalty) insulation thicknessed for each thermal protection concept. For example, Figures 3.3.11 and 3.3.12 show the in-atmosphere weight penalty and optimum design points for the purged MLI and external foam/MLI composite, respectively. The weight penalty does not include any tank weight penalty required to load additional propellant for boiloff.
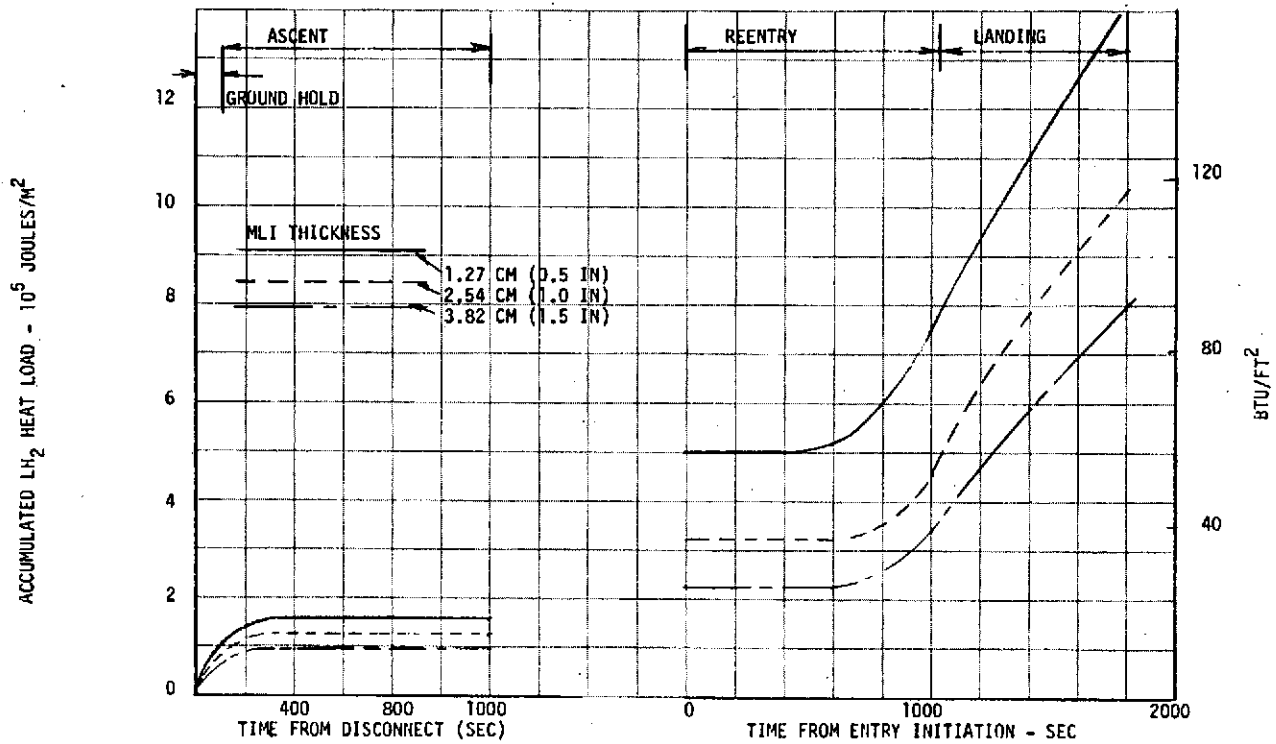
Figure 3.3.8. Typical Mission LH$_2$ Tank Accumulated Heat Load — Helium Purged MLI
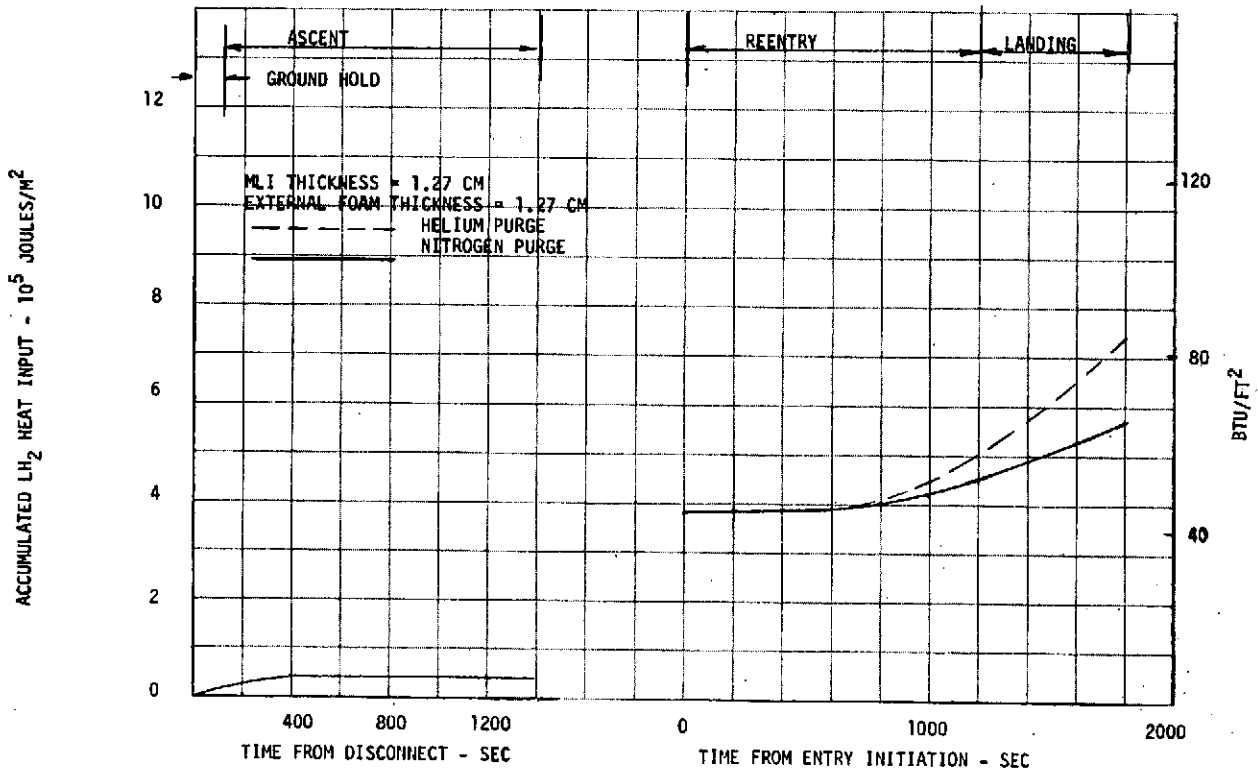
Figure 3.3.9. LH$_2$ Tank Thermal Analysis — External Foam/MLI
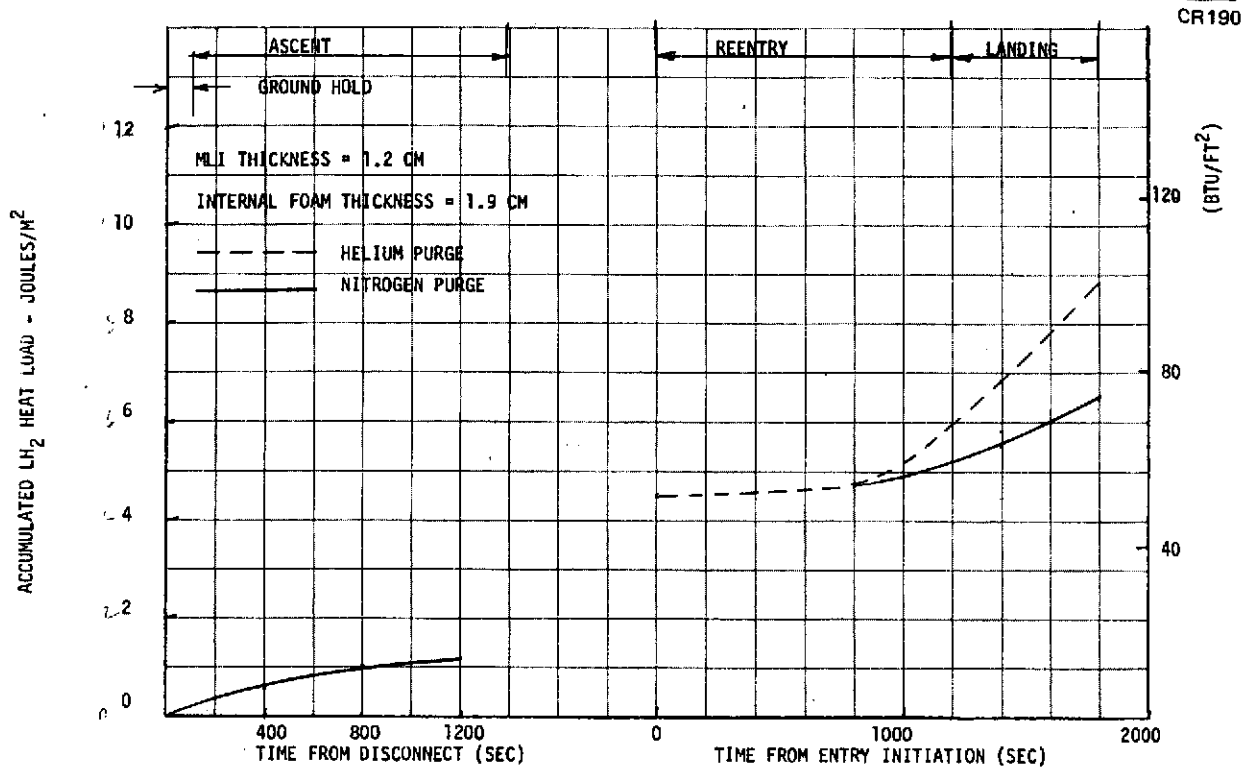
Figure 3.3.10. LH₂ Tank Mission Thermal Analysis — Internal Foam/MLI
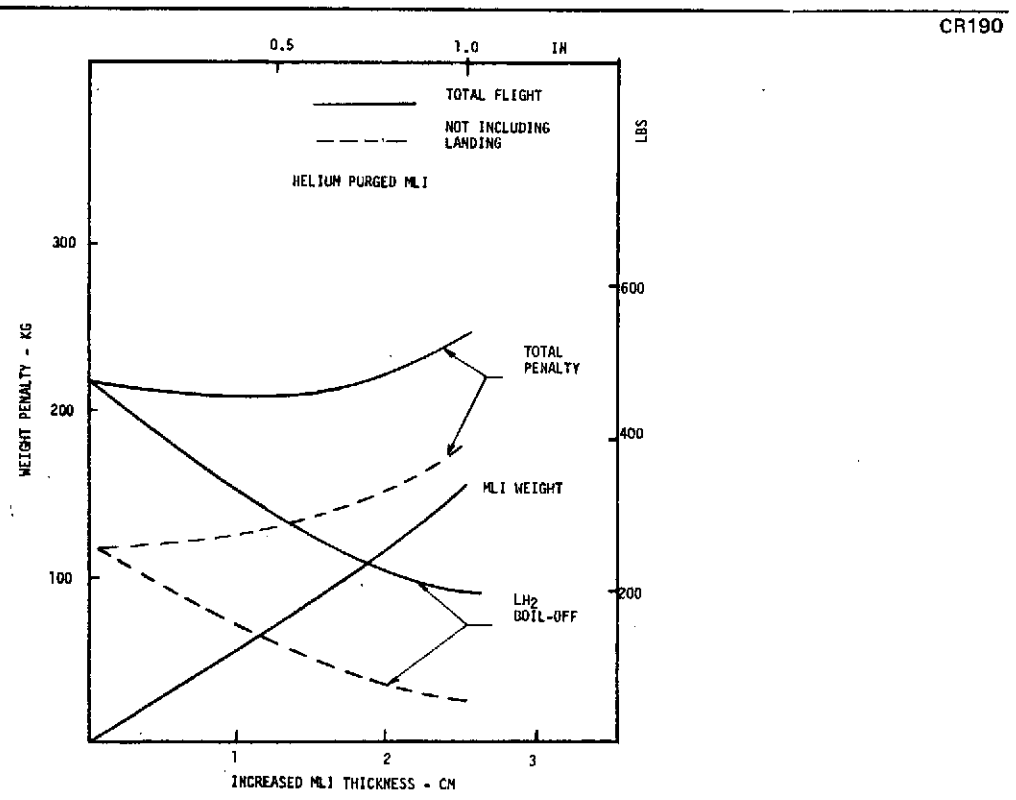
Figure 3.3.11. Total In-Atmosphere Weight Penalty
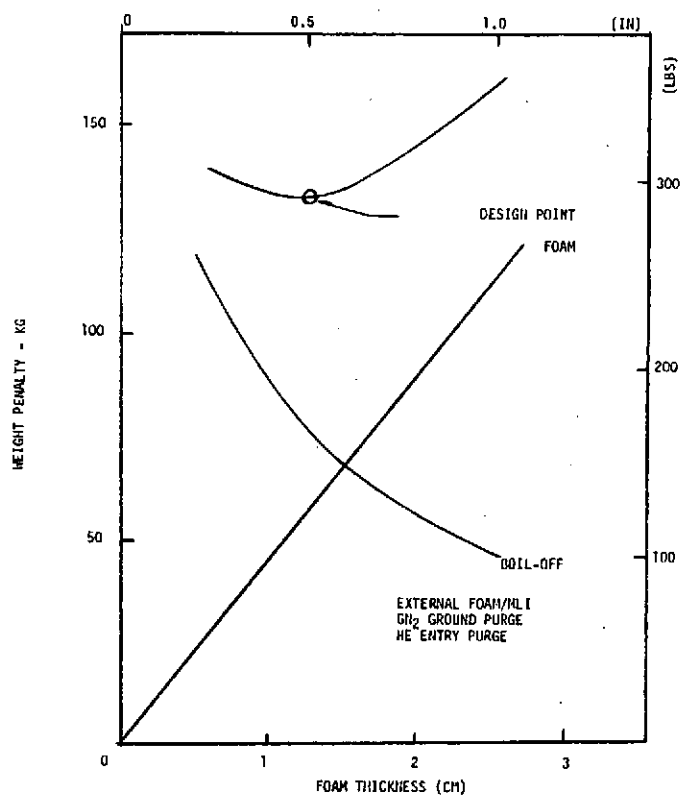
Figure 3.3.12. In-Atmosphere Insulation Optimization

Figure 3. 3. 13 presents the thermal conductivity and density design factors assumed for the foam systems. The internal foam represents a near state-of-the-art material such as that used in the S-IVB Saturn stage. The external foam is in reality an advanced technology insulation system, such as Klegecell currently being developed in Europe (Reference 21).

A vacuum jacket concept was also investigated for the LH_2 tank. In this case, the thermal performance of the system was assumed to be constant throughout the mission and equal to the established space level. The jacket weight was obtained by using the data reported in Reference 22 (curve from this report is shown in Figure 3. 3. 14). This applies to a 56. 6 m³ (2,000 ft³) LH_2 tank with a jacket clearance of 11. 4 cm. Based on surface area alone, the reported jacket weight would have to be increased by a factor of 1.27 for our baseline tank and cylindrical L/D = 1. 4. The weight was thus estimated at 517 kg and corresponds to a jacket structure using 5056 aluminum honey-comb flex core with boron/epoxy and titanium face sheets. This was the lightest reported design. Other vacuum jacket designs are possible, some of which may involve lower weight than that shown here; however, it is unlikely that these will be closely competitive in terms of total weight with the other insulation concepts, even for a full mission storage requirement.

A comparison of the various concepts is made in Table 3. 3. 5 considering three required levels of cryogen storage: (1) only through boost; (2) only through entry; and (3) completely through landing. The following conclusions can be drawn from the summarized results.
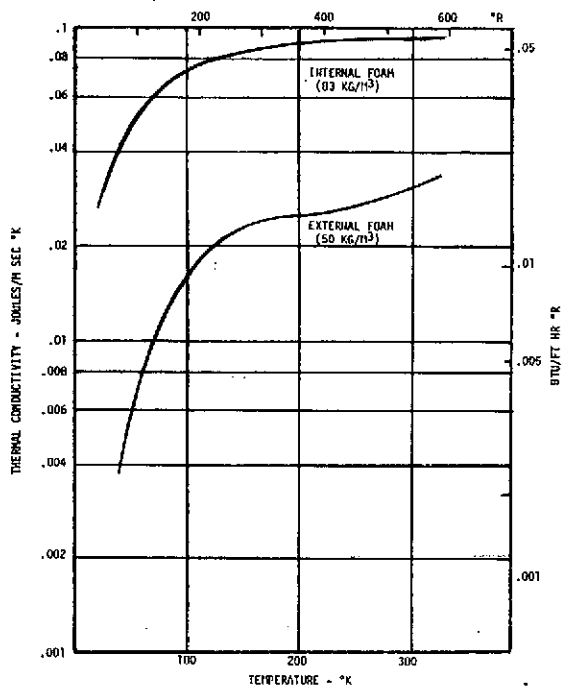
Figure 3.3.13. Foam Insulation Characteristics
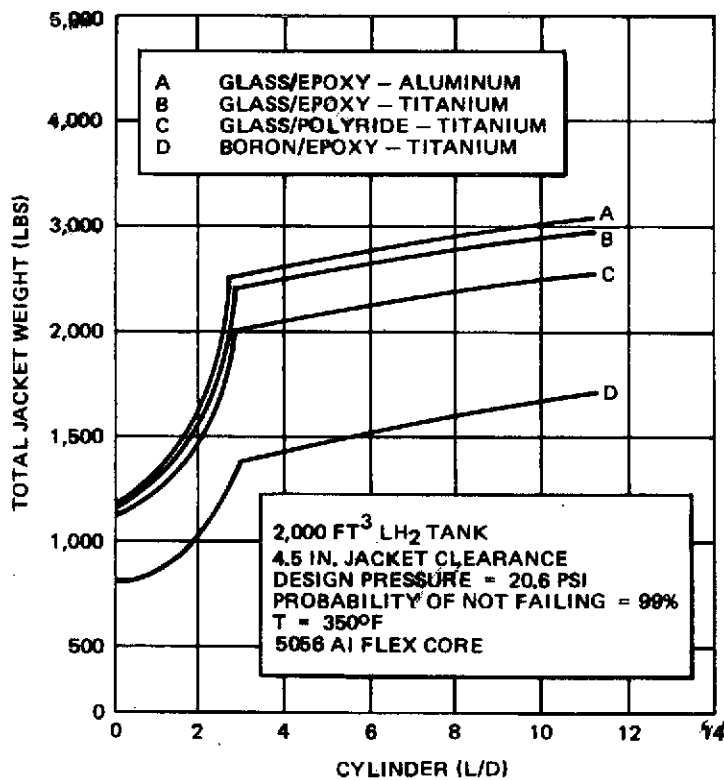
Figure 3.3.14. Vacuum Jacket Weight — Honeycomb Structure

Table 3.3.5

COMPARISON OF INSULATION CONCEPTS FOR IN-ATMOSPHERE OPERATION DISTRIBUTED CHANNEL ACQUISITION SYSTEM

Required LH$_2$ Storage	Insulation Type	Insulation Thickness (cm)	ΔWeight Insulation (kg)	ΔWeight Boiloff (kg)	Total Weight (kg)
Through boost	Excess helium-purged MLI	0	0	33	33
	Internal foam	1.9 (1)	143	27	170
	External foam	0.64(4)	29	11	40
	Vacuum jacket	0	517(2)	0	517
Through entry	Excess helium-purged MLI	0	0	118	118
	Internal foam	1.9	143	39 or 49(3)	182 or 192
	External foam	0.64	29	31 or 56	60 or 85
	Vacuum jacket	0	517(2)	0.5	517
Through landing	Excess helium-purged MLI	1.27	99	136	235(5)
	Internal foam	1.9	143	61 or 104	204 or 247
	External foam	1.27	57	45 or 79	102 or 136
	Vacuum jacket	0	517(2)	1	518

1. Minimum thickness of internal foam to restrict temperature below LN$_2$.
2. Outer vacuum jacket weight (Reference 22).
3. First value GN$_2$/He repressurization: Second value GHe purge only.
4. Minimum layup of insulation.
5. Corrected value in ( ) to account for performance improvement during coast.

a. Internal foam provides no weight advantage relative to simple helium-purged MLI although the foam would permit use of all GN$_2$ ground purging.

b. The external foam results in minimum weight except for the case of storage only through boost where it is 7 kg heavier than the simple helium-purged MLI. However, being able to use GN$_2$ rather than helium is probably worth the 7 kg of added weight.

In the case of simple helium-purged MLI for LH$_2$ storage over the entire mission, the MLI thickness is increased over that required for space to yield the optimum-purged MLI. This in turn improves the space performances of the system by reducing the in-space boiloff by about 32 kg. Thus, the effective weight penalty is actually 235 - 32 = 203 kg as indicated. In no other case does the in-atmosphere storage provision have a significant influence on in-orbit behavior. However, the helium-purged MLI is still not as light as the optimum external foam. Therefore, the external foam insulation with a GN$_2$ purge, augmented with helium for the initial reentry purge, was selected as the

preferred system. This represents some advancement in the state-of-the-art for the foam insulation itself but the concept has been shown to be feasible (Reference 21).

It should be noted that a GN_2 purge cannot be used for all phases of the mission because the foam/MLI interface drops to below the condensation point of nitrogen. This is clearly indicated in Figure 3.3.15. Thus during the initial MLI pressurization prior to reentry, helium purge gas must be used until the foam/MLI interface exceeds 178°K (320°R). Then the purge can be supplied from the GN_2 system.

Based on the analyses for the LH_2 tank, it can be concluded that a simple GN_2 purge system would be quite adequate for the LO_2 tank. No further analysis was conducted for the oxidizer tank.

In a feed system where the cryogen for reentry is stored in a separate secondary tank within the main propellant tank, the reentry/landing cryogen heating problem is not as severe. In this situation the effective area for propellant heat transfer is well defined and is the surface area of the secondary tank rather than the entire propellant tank. As an example, for a 10% volume secondary tank, the heat transfer area would be reduced to about 30% of the value for the primary tank. This reduction in heat transfer area reduces the potential cryogen losses during reentry and landing and would shift the overall system optimization.

CR190
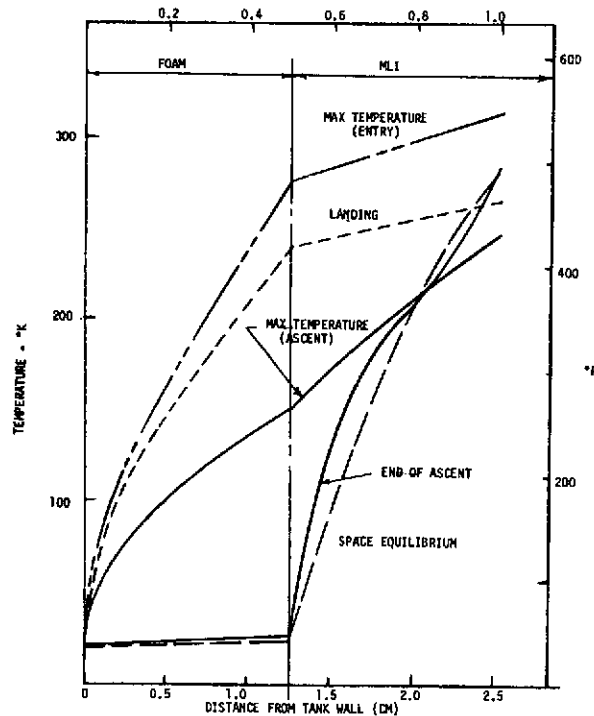
Figure 3.3.15. Representative LH_2 Insulation Temperature Profiles During Mission

To evaluate the possible savings by using a secondary tank, a detailed thermal analysis of such a system was conducted using the developed MDAC transient thermal analysis computer code. The following assumptions were made:

a. A 21.9 M³ (773 ft³) secondary tank was assumed (this is the very maximum size that would be anticipated).

b. A conventional S-IVB type foam insulation with a density of 0.832 x 10² kg/M³ (5.2 lb/ft³) was used on the start tank.

c. A helium-purged MLI optimized for space operation alone was used on the main tank.

d. The external environment used in the previous insulation system analysis was used and it was assumed that the LH_2 had to be stored through reentry and landing.

e. During reentry, the main tank was assumed to be vented to 1 atmosphere.

For these conditions, the integrated heat load for the total mission up to reentry is about 44 x 10⁶ joules (41,700 Btu) for 1.27 cm of MLI. For the entry and landing period, the integrated heat load into the reentry propellant contained in the secondary tank, with no foam insulation on the secondary tank, is about 46.6 x 10⁶ joules (44,500 Btu) as compared to 86.4 x 10⁶ joules (82,000 Btu) to the reentry propellant contained within the main tank with 1.27 cm of MLI. The total weight penalty of the basic thermal storage system for the secondary tank system is shown in Figure 3.3.16 as a function of secondary tank foam thickness. The weight penalty includes the total usable boiloff, including in-orbit losses from both the main tank and the secondary tank, and the foam weight. The computed values shown in Figure 3.3.16 indicate an optimum secondary tank foam insulation of 0.635 cm (0.24 in.), yielding a total weight penalty of 263 kg broken down as shown in Table 3.3.6. Also shown are weights for a single tank system, including one using an optimum thermal protection system consisting of a composite external foam/MLI and another using a simple helium purged MLI. The secondary tank does result in a minimum thermal storage system weight penalty but has about the same weight as the optimum single tank system. There is a savings of about 83 kg over a single tank system using a simple helium-purged MLI.

From this analysis it is concluded that there probably is no significant advantage, in terms of thermal storage improvement, by using a secondary tank unless the selected MLI/external foam composite cannot achieve the expected performance or is not used for any other reason. However, use of a small secondary tank will result in more thermal improvement, and a decrease in overall hardware weight. The effects of secondary size was investigated and it was found that the optimum secondary tank insulation thickness remained essentially constant at 0.75 cm with variation in secondary tank volume. However as shown in Figure 3.3.17, the secondary tank boiloff plus insulation weight decreases as secondary tank size decreases.
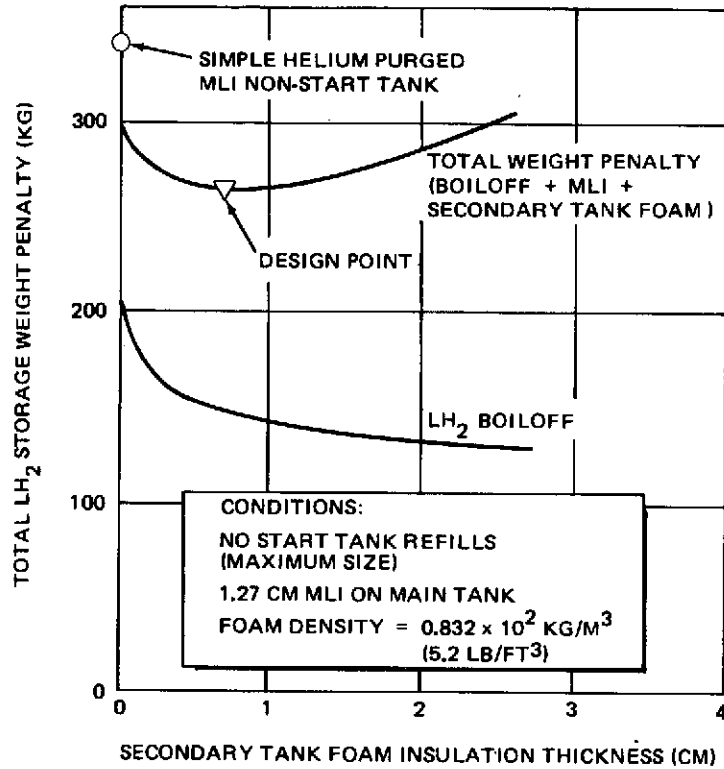
Figure 3.3.16. LH$_2$ Storage Characteristics with Integrated Secondary Tank

Table 3.3.6

LH$_2$ THERMAL STORAGE WEIGHT PENALTY BREAKDOWN

	Maximum Secondary Tank with Optimum Foam Insulation Thickness (kg)	Conventional Single Tank	
		Optimum* (kg)	Simple Helium-Purged MLI (kg)
Main tank total LH$_2$ boiloff	100	112	170
Secondary tank boiloff	43	0	0
MLI	99	99	176
Secondary tank foam	21	0	0
Main tank foam	0	57	0
Total weight penalty	263	268	346

*1.27 cm external foam with 1.27 cm of MLI on main tank.

118
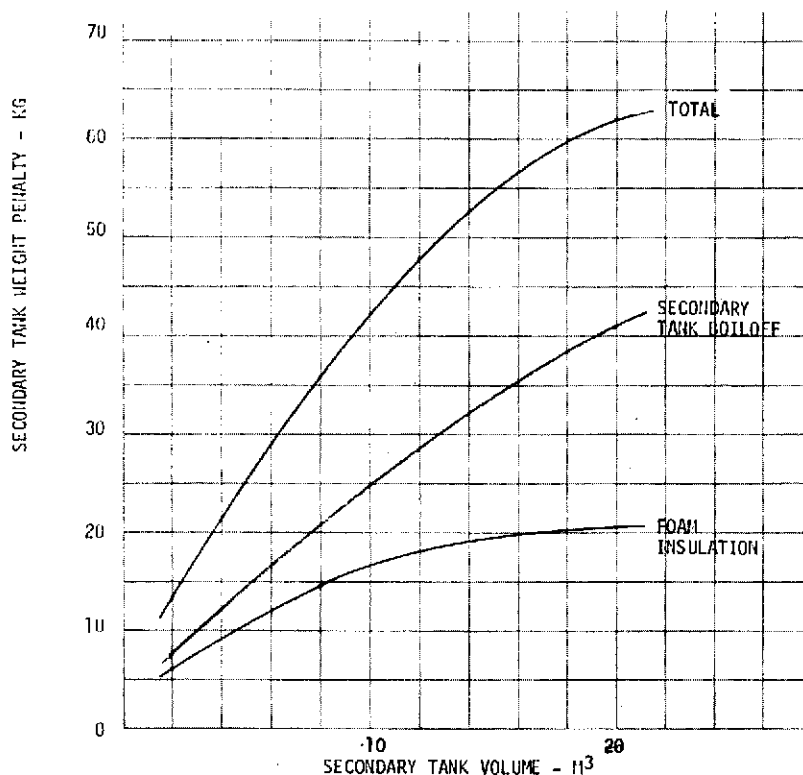
Figure 3.3.17. Influence of Secondary Tank Size on Weight Penalty

3.3.4 In-Orbit Venting. As discussed previously in this section, to effectively control tank pressure buildup as a result of propellant heating during extended space coast, a vent system that can function in zero gravity and provide liquid free venting is required for most space cryogenic storage and expulsion systems. Numerous studies have shown the superiority of the thermodynamic vent system (TVS) for this application. In this general concept, the vent fluid leaving the tank is throttled to a lower pressure and temperature and is then passed through a heat exchanger that extracts heat from the stored cryogen or intercepts the heat before it enters the cryogen. In the heat exchanger, the vent fluid is completely vaporized, thus providing tank pressure control with gas-phase venting. The concept is illustrated in Figure 3.3.18. Conveniently, the TVS also has the capability of performing limited cooling functions in the feed system, such as for local heat shorts, pumps, acquisition devices, and the warmer cryogen tanks (such as cooling of the LO_2 tank with GH_2 vent gases).

Several variations of the TVS have been studied in recent years:

    a.   Direct Tank Wall Cooling. In this approach, the TVS heat exchanger is a cooling coil mounted directly on the cryogen tank wall and it can theoretically intercept heat coming into the tank through the insulation and remove heat from the tank contents. Work on this approach has been reported in References 23 and 24.

To auxiliary cooling

Regulator

Overboard

$\dot{q} \rightarrow$ Heat
Exchanger

P_v B

Throttling Valve

Vent
Inlet

P_T

A

C

T

P_T

A

B P_v C

S
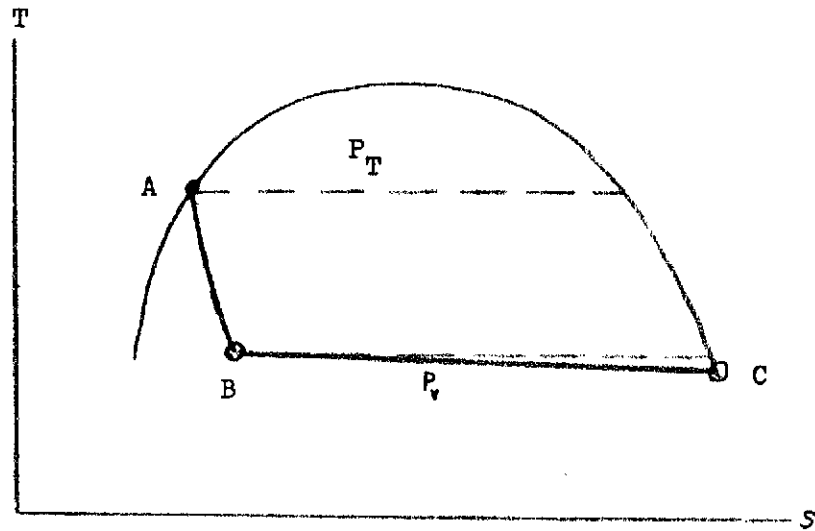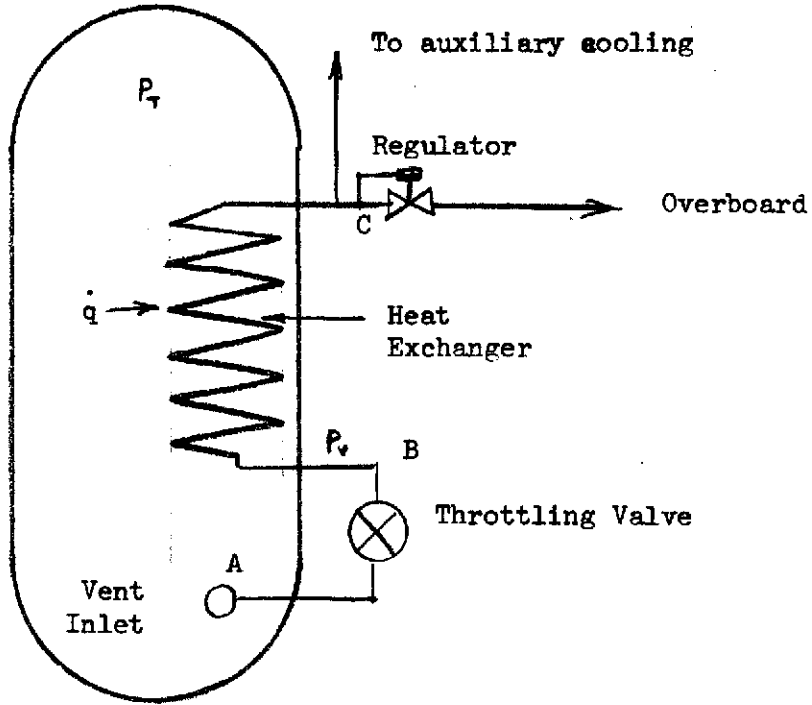
Figure 3.3.18. Thermodynamic Vent System Principle

b. Internal Tank Mixer/Heat Exchanger. In this concept, which has been studied in depth (References 15 and 16), the heat exchanger is a compact design located inside the cryogen tank. The throttled vent fluid flows through one side of the unit and exchanges heat with the tank contents, which are forced through the other side of the heat exchanger by a pump-mixer fan unit.

c. Externally Cooled Shield. In this concept, the heat exchanger is a cooled shield or shroud which surrounds the outside wall of the cryogen tank but is set off from the tank wall. In this passive system, the shield intercepts the heat entering through the insulation and can theoretically result in "zero" net heat leak into the cryogen.

Another approach to achieving low-g tank venting is to use a surface tension screen device to provide a gas region within the tank which is directly vented. This concept does not utilize the TVS principle.

In assessing these concepts for the ground-ruled applications, a number of factors are of importance:

a. The system should be simple with as few moving parts as possible to be compatible with a long life reusable manned application.

b. The design of the system should be relatively straightforward with a minimum reliance on gravity dependent heat transfer and fluid dynamic processes. One-g checkout would be highly desirable.

c. The concept should not involve severe compromises to the tank structure.

d. The concept should be weight competitive.

e. The concept must be compatible with the acquisition and pressurization system.

In our initial evaluation of the concepts, it was judged that the direct tank wall cooling concept did not adequately meet criteria b and c itemized above. The design of this system requires detailed knowledge of the low-g heat transfer processes occurring on the inside tank wall and the installation of the cooling coils on the tank wall is quite likely to result in undesirable constraints on the tankage design. This approach was, therefore, not considered further. However, the internal tank mixer/heat exchanger and external cooled shield TVS concepts were considered in detail and a comparative evaluation was made with the surface tension device low-g venting approach.

a. Internal Tank Mixer/Heat Exchanger TVS. This concept, as illustrated in Figure 3.3.19, provides tank pressure control with gas-phase venting and may be operated continuously or intermittently. Extensive
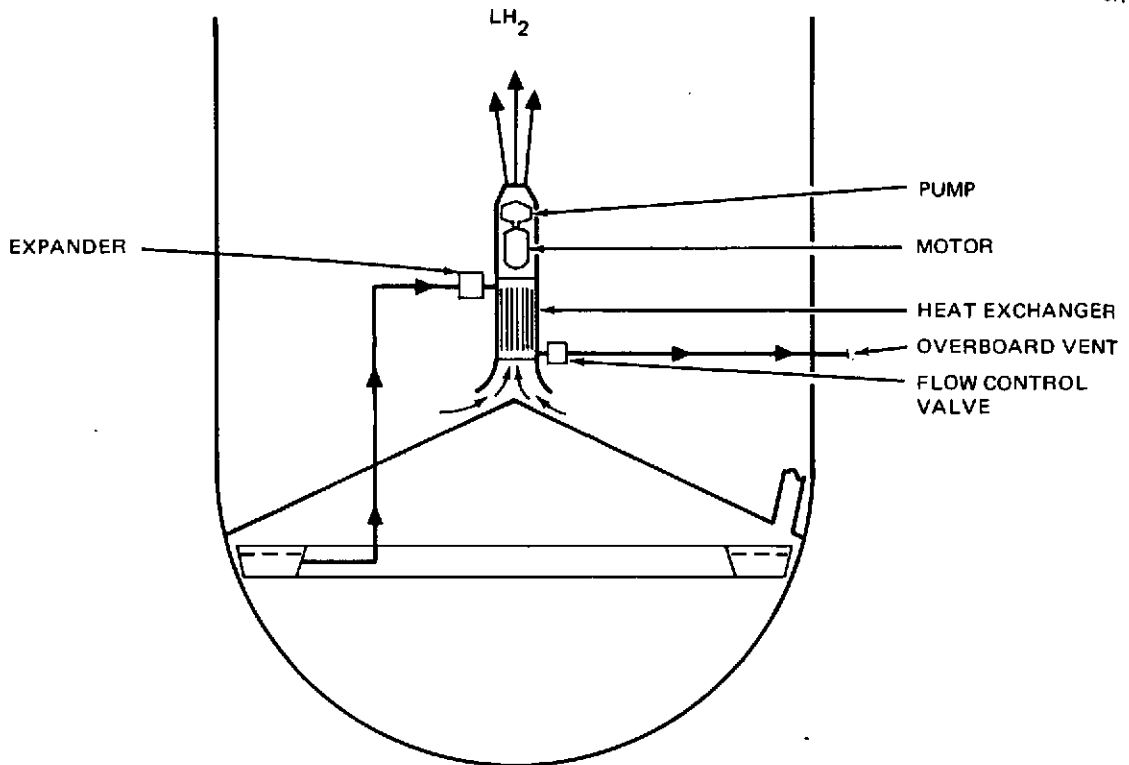
Figure 3.3.19. Internal Tank Pump/Mixer TVS Concept

research has been conducted on this concept, as reported in References 15 and 16, and information was extracted from these sources to generate design factors for this concept as applied to this specific study application.

The mixer provides a positive means of supplying the warm LH_2 to the heat exchanger where it heats and vaporizes the vent fluid prior to discharge. It is essential that the warm, possibly stratified, cryogen in the tank be drawn into the pump inlet. Thus, the pump must have sufficient power to disrupt and circulate the warm layer of liquid at the liquid-gas interface. An axial jet, positioned at the bottom central position in the tank with a discharge velocity sufficient to break through the interface, can satisfy the mixing requirements.

The analysis of the internal tank pump mixer/heat exchanger TVS was conducted in detail. Two design accelerations were considered: (a) 10^{-4} g which corresponds to the steady-state, in-orbit operation, and (b) 10^{-2} g which is representative of attitude control accelerations. The low 10^{-4} g level should be an adequate design criteria for the TVS, from simply a venting standpoint.

Basic equations for sizing the mixer pump for a TVS of this type are given in Reference 25. From this reference, the velocity at the liquid-

gas interface required to penetrate the interface and to thus mix the propellant is given by:

$$V_i = \frac{0.057}{b^2} \left\{ \frac{\beta \Delta T_{MAX} P}{\left[1 - \left(\frac{V_{MAX}}{V'_{MAX}} \right)^2 \right] (P + 1)(P + 3)} \right\}^{1/2} a^{1/2} Z^{1/2}$$

where

$$b = 0.25$$

$$V_{MAX}/V'_{MAX} = 0.9$$

$$P = 1.0$$

$$a = \text{acceleration}$$

$$Z = \text{distance to the interface (tank length)}$$

Also, the product of the jet exit diameter (D_O) and velocity (V_O) is given by

$$V_O D_O = \frac{1}{2} \left\{ \frac{\beta \Delta T_{MAX} Z^3 aP}{\left[1 - \left(\frac{V_{MAX}}{V'_{MAX}} \right)^2 \right] (P + 1)(P + 3)} \right\}^{1/2}$$

The mixer volumetric and weight flow are given respectively by

$$\dot{V}_O = A V_O = \frac{\pi D_O^2}{4} V_O = \frac{\pi}{4} D_O (V_O D_O)$$

$$\dot{w}_O = \dot{V}_O$$

The required time to mix the tank contents, θ, is given by

$$\theta = \frac{N D_t^2}{0.456 \, V_O D_O}$$

where $N = 6.0$, and D_t = tank diameter.

The theoretical pump head is approximated by $H = V_O^2/2g$, which gives

$$\dot{V}_O = \frac{(V_O D_O)^2 \pi}{4 \sqrt{2gH}}$$

Pump power input = $\dot{P}_{IN}$:

$$\dot{P}_{IN} = \frac{H\dot{V}_o\rho}{\eta}$$

Small axial pump/motors have efficiencies, η, as shown in Figure 3.3.20 from Reference 15. Part A of Table 3.3.7 summarizes the sizing parameters for the two design accelerations based on the above equations.
Considering the internal thermodynamics of the tank, the rate of pressure change, dP/dt is

$$\frac{dP}{dt} = \frac{dP}{dT}\frac{dT}{dt}$$

The rate of temperature change, for mixed tank contents, is

$$\frac{dT}{dt} \qquad \frac{\dfrac{dQ_{net}}{dt}}{W_P C_P} = \frac{\dot{w}_v H_v - (\dot{Q} + \dot{P})}{W_P C_P}$$

CR190

FIGURE TAKEN DIRECTLY FROM GD/C REPORT GDC-DDB67-006 (REFERNCE 6)

DATA POINT REPRESENT DIFFERENT MOTOR DRIVEN AXIAL FLOW PUMPS AT THEIR ESTIMATED NORMAL OPERATING CONDITION IN LH_2
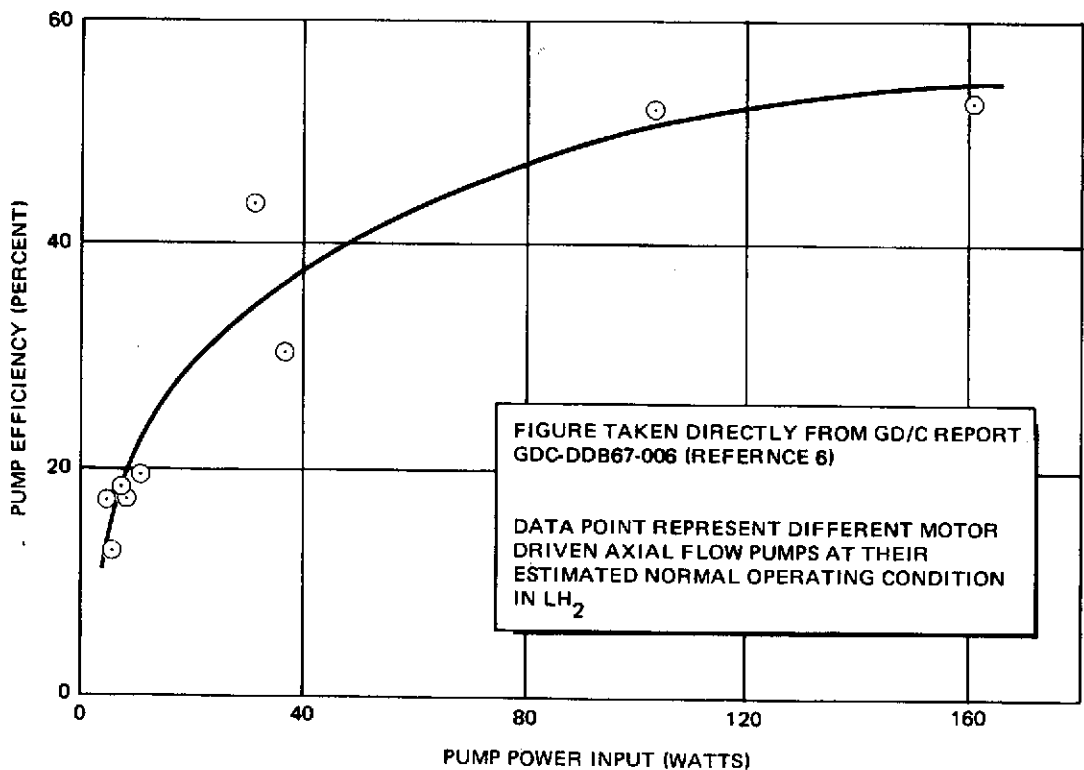
Figure 3.3.20. Influence of Power on Effiency for Small LH_2 Pumps

Table 3.3.7

PUMP-MIXER/HEAT EXCHANGER TVS SIZING PARAMETERS

A-Pump/Mixer Sizing Factors	Design Acceleration		
	10^{-2}	g's	10^{-4}
Required interface velocity	0.061 (0.2)	m/sec ft/sec	0.0061 (0.02)
Mixing time	0.2	hr	2.0
Exit diameter x velocity	25.5×10^{-2} (2.74)	m^2/sec ft^2/sec	2.55×10^{-2} (0.274)
Pump outlet diameter	5.1 (2.0)	cm in.	2.54 (1.0)
Volumetric flow	1.02×10^{-2} (21.6)	m^3/sec ft^3/min	0.05×10^{-2} (1.07)
Weight flowrate	0.72 (1.58)	kg/sec lb/sec	0.035 (0.08)
Pump outlet velocity	5.0 (16.4)	m/sec ft/sec	1.0 (3.3)
Pump head	1.28 (4.18)	m ft	0.052 (0.17)
Pump fluid power	8.9	watts	0.018
Pump efficiency	33	%	2.3*
Pump input power	27	watts	0.78*
Estimated pump weight	0.57	kg	0.27
LH_2 loss from pump heat input per cycle	0.044	kg	0.0127
B-Vent Cycle Factors			
Vent time per cycle	0.5	hr/cycle	5.0
Vent flowrate	18.2 (40)	kg/hr lb/hr	2.6 (5.7)
Vent cycles	8	-	7

*Minimum practical pump/mixer size is 5 watts at 12-percent efficiency which would require resizing of the mixer and vent system characteristics

where H_v is heat of vaporization, $\dot{Q}$ is heat input, $\dot{P}$ is power in, and W_P = propellant weight.

$$\therefore \frac{dP}{dt} = \left(\frac{dP}{dT}\right)\frac{\dot{w}_v H_v - (\dot{Q} + \dot{P})}{W_P C_P}$$

the term dP/dT is evaluated from the Clapeyron equation

$$\frac{dP}{dT} = \frac{\Delta H_{fg}}{\Delta V_{fg} T}$$

where ΔH_{fg} is the enthalpy change for vaporization, and ΔV_{fg} is the specific volume change during vaporization.

The number of vent cycles, N_v is

$$N_v = \frac{\dfrac{\dot{Q}_{in} t}{H_v}}{\dot{w}_v t_v - \dfrac{\dot{P} t_v}{H_v}} = \frac{\dot{Q}_{in} t_t}{(\dot{w}_v H_v - \dot{P}) t_v}$$

where t_t = total mission time, $\dot{w}_v$ = venting flow rate, and t_v = total venting time.

Figure 3.3.21 shows the vent time per cycle and vent cycles for a 0.5-psi pressure change. For a practical design, propellant mixing should occur well within the duration of the venting cycle. For 10^{-4} g design acceleration, propellant mixing requires about 20 hr (see Table 3.3.7). This is
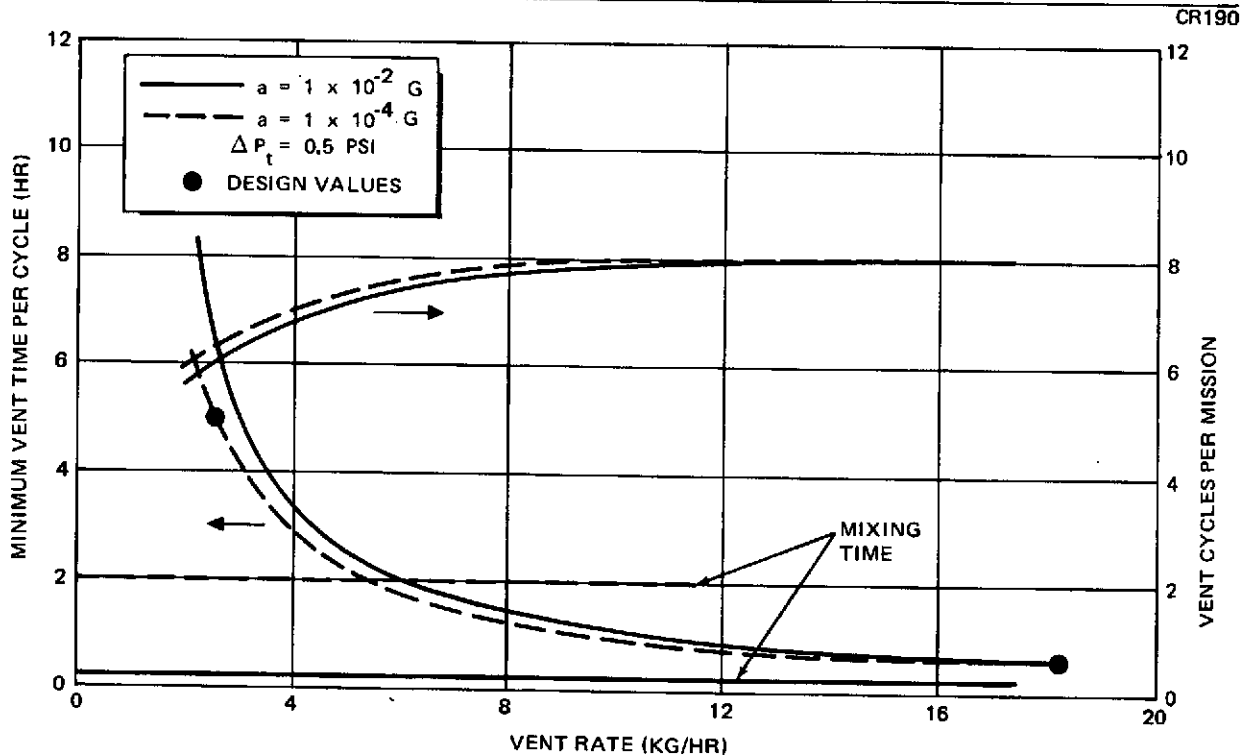
Figure 3.3.21. LH$_2$ Tank Venting Parameters with Pump Mixer TVS

noted on Figure 3.3.21. To permit adequate margins, it has been assumed that venting time must be 2.5 times the mixing time. Thus, for 10^{-4} g acceleration, a venting time of 5.0 hr with a vent flow of 2.7 kg/hr is required. These and corresponding values for 10^{-2} g are summarized in Part B of Table 3.3.7.

Compact counterflow heat exchangers were designed, based on the design data of Reference 16 and the requirements of Table 3.3.8. Because of helium pressurization of the tank, the critical design requirement for the heat exchanger is to transfer sufficient heat when flowing helium on the hot side, since the heat transfer coefficient with helium is much less than for liquid hydrogen. The design of the heat exchanger is also based on expansion across the throttle valve (cold side) from 117 to 23.4 x 10^3 N/m^2 (17 to 3.4 psia) (heat exchanger cold side pressure), to ensure staying above the triple point. The heat excahnger effectiveness was assumed to be 0.9 which strikes the proper balance between pumping power and heat exchanger size. The heat exchanger core weight (based on stainless steel) and size are shown parametrically in Figures 3.3.22 and 3.3.23. The helium and LH$_2$ pressure drop (hot side) are shown in Figures 3.3.24 and 3.3.25. Table 3.3.8 summarizes the pertinent design characteristics of the heat exchangers designed for 10^{-2} and 10^{-4} g's. The weights shown assume aluminum heat exchangers with a 25 percent factor added for manifolds.

The general heat exchanger/pump package configuration and location in the tank is shown in Figure 3.3.19. The unit is situated in the main tank so that the bulk of the propellant is available for cooling.

From the above analyses it was concluded that the pump mixer/heat exchanger concept was feasible and that it could be provided to the system for less than 10 kg including complete double redundancy and support hardware weight.

b. Cooled Shield TVS Concept. The cooled-shield TVS integrated with the MLI system is shown schematically in Figure 3.3.26. The basic operation of the system is that LH$_2$ is expanded at constant enthalpy through an orifice system (for example, a "viscojet") to a lower pressure and temperature (Point A to Point B in Figure 3.3.26). The saturated LH$_2$, upon expansion, also partially vaporizes to a quality of 0.1 to 0.2, depending on conditions. This low-temperature, mixed-phased fluid is the coldest part of the storage system and thus can intercept all incident heat flux through the MLI. The insulation heat is intercepted by using a thin (0.005 inch) 1100 aluminum foil shield between the MLI and the tank wall. The shield is set off from the tank wall and cooled by passing the throttled hydrogen flow through cooling coils brazed to the foil. The shield thickness is determined by the required conduction path to transmit heat to the cooling coils. The coolant flow is adequate to absorb the insulation heat by evaporation of the coolant and, by maintaining the shroud at a temperature less than that of the stored LH$_2$, no heat will enter the stored cryogen. (In addition to the cooled shield, all tank supports and lines must also be cooled to keep all heat out of the propellant.) The requirement to intercept all heat through the MLI necessitates that the shield be at or below the tank because a temperature gradient must be established in the shield to
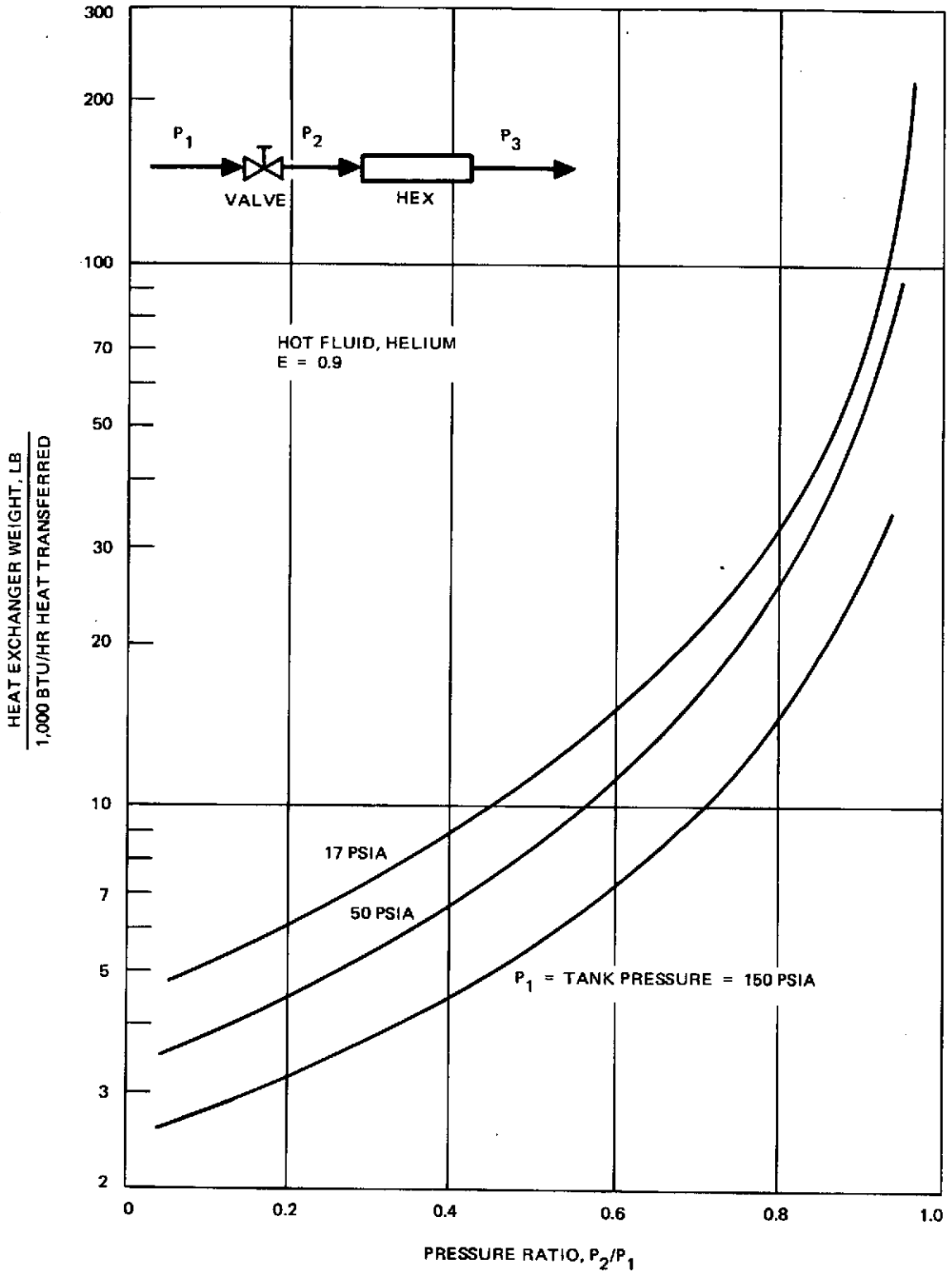
Figure 3.3.22. Heat Exchanger Weight
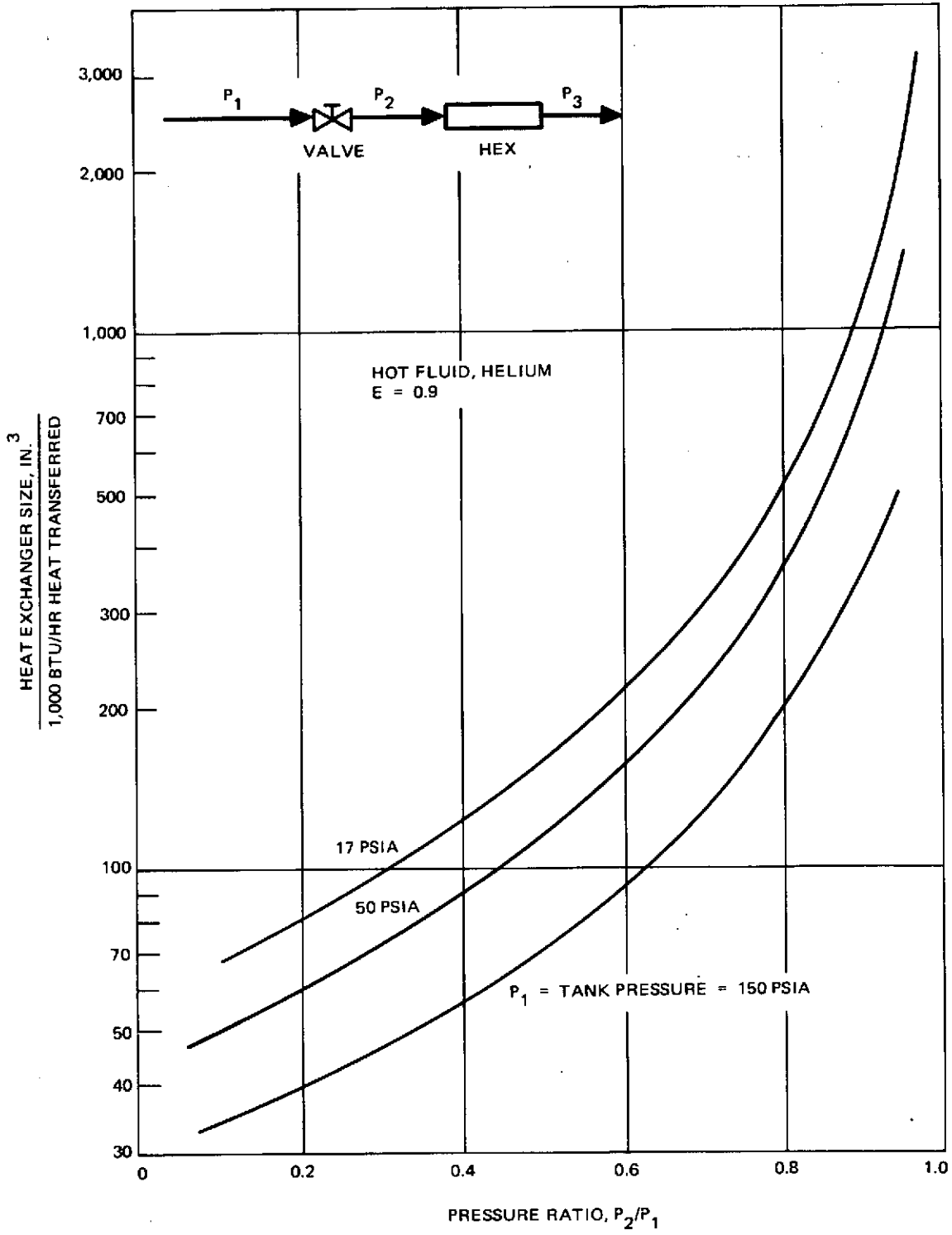
Figure 3.3.23. Heat Exchanger Size
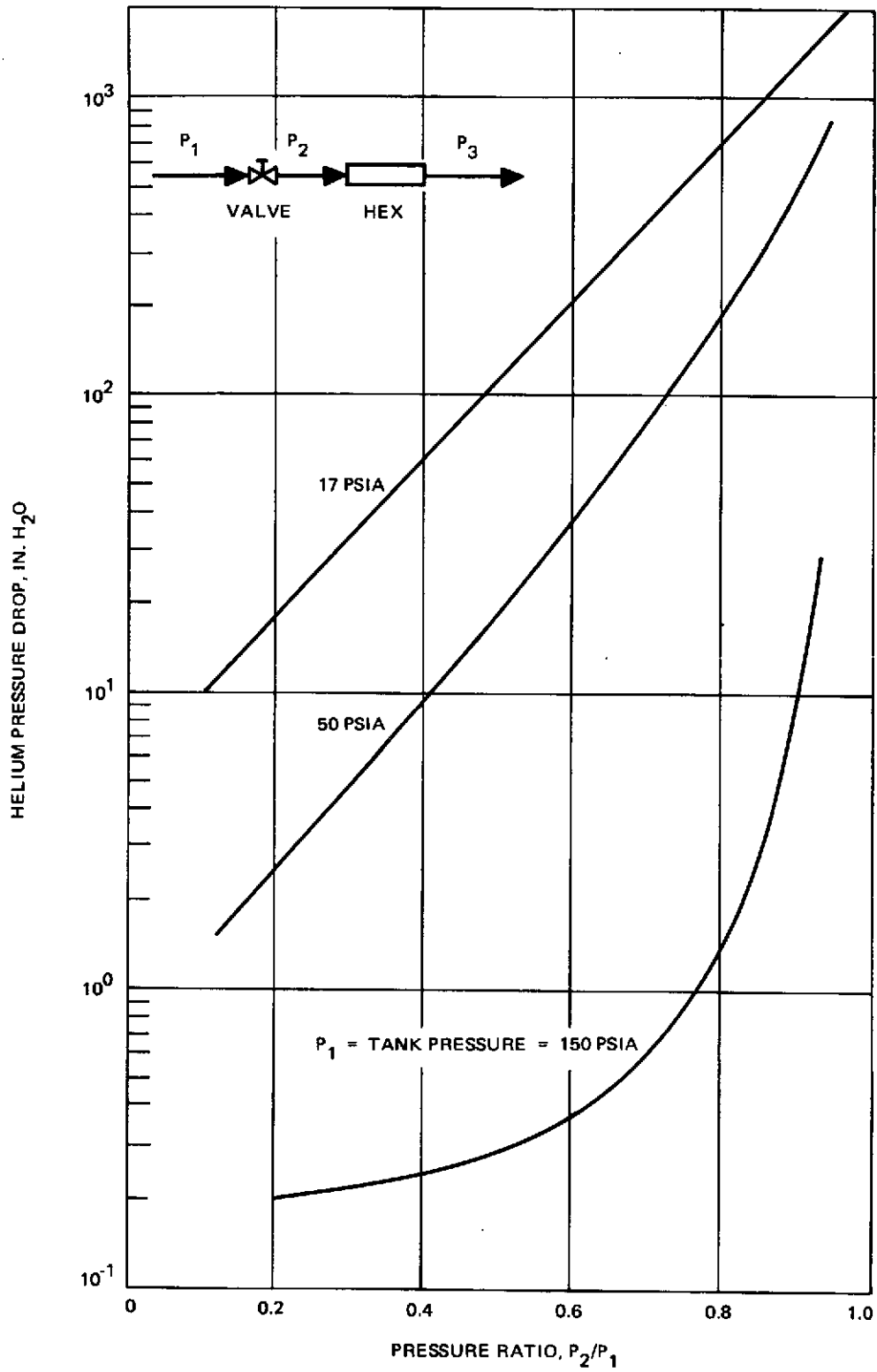
Figure 3.3.24. Heat Exhcanger Hot Side Pressure Drop with Helium
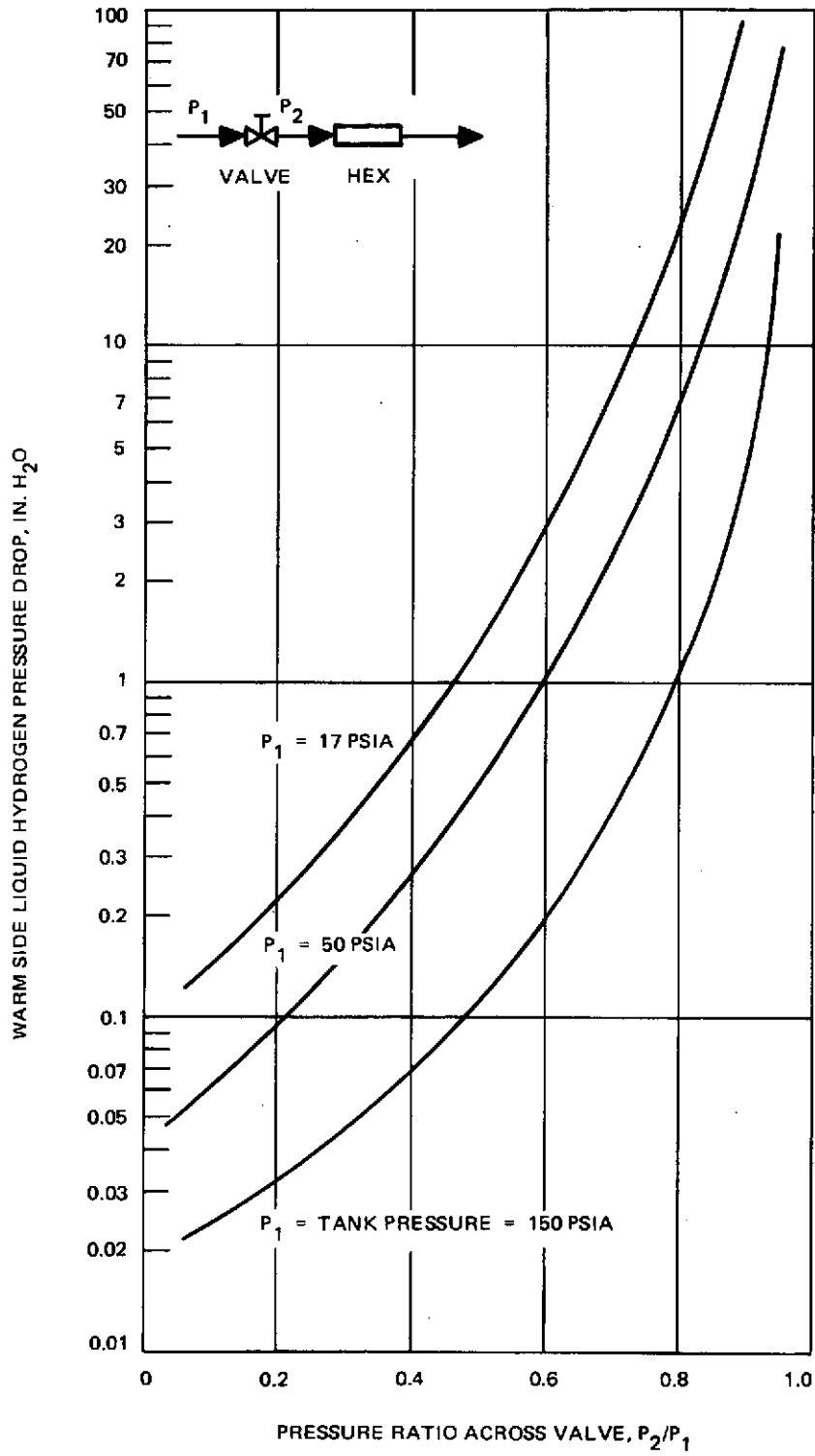
Figure 3.3.25. Heat Exchanger Warm Side Pressure Drop with LH₂

Table 3.3.8

TVS COMPACT HEAT EXCHANGE PARAMETERS

	Design Acceleration		
	10^{-2}	g's	10^{-4}
Vent flow	18.2 (40)	kg/hr (lb/hr)	2.6 (5.7)
Heat transfer rate	2,290 (7,800)	watts (Btu/hr)	325 (1,110)
Weight (Aluminum)	9.4 (20.7)	kg (lb)	1.35 (3.0)
Size (frontal area)	0.152 x 0.152 (6 x 6)	m x m (in. x in.)	0.076 x 0.076 (3 x 3)
Length	0.435 (17.5)	m (in.)	0.254 (10)
Helium ΔP (warm side)	4.73×10^3 (0.685)	N/m^2 (psi)	4.73×10^3 (0.685)
LH_2 ΔP (warm side)	57.2 (0.0083)	N/m^2 (psi)	57.2 (0.0083)
H_2 ΔP (cold side)	1.27×10^{-4} (1.84)	N/m^2 (psi)	2.35×10^3 (0.34)

CR190
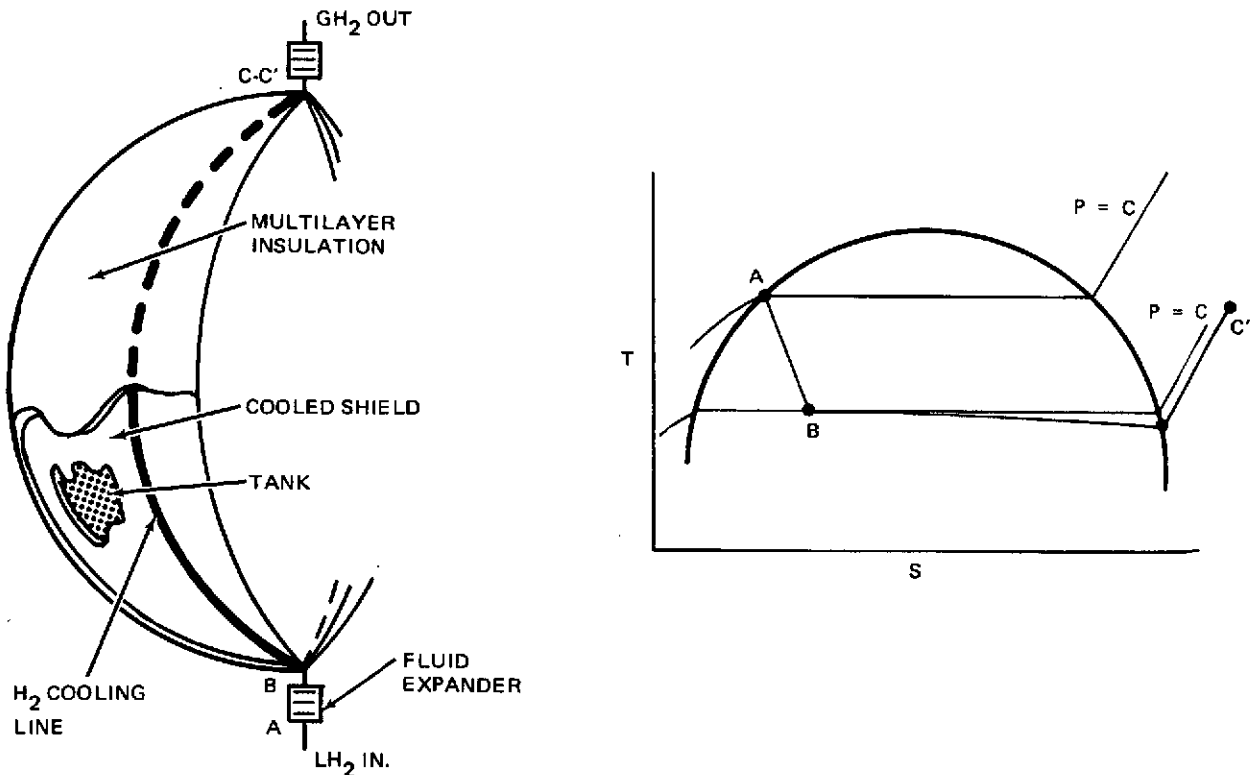
Figure 3.3.26. Cooled Shroud TVS Concept

transfer heat to the vent fluid. Because the shield is colder than the tank, a small amount of heat will be radiated from the tank to the shield. This amount can be kept very small if a few layers of MLI are placed between the shield and the tank. This should minimize any propellant cooling.

The heat flux vaporizes the remaining LH$_2$ flowing through the shield at essentially constant pressure and temperature until the conditions of Point C are reached. The simplest basic configuration is a single-point design for a steady flowrate of just enough vented LH$_2$ so that the heat of vaporization equals the nominal heat flux to the shield. The only heat transfer mechanisms in the shield are assumed to be conduction along the shield, radiation through the MLI (independent of shield temperature), and forced convection to the vented fluid. The appropriate equations for steady-state heat flow in the configuration shown in Figure 3.3.27. The heat balance is:

$$q_o \Big|_x = q_i \Big|_{x+dx} + q_r \Big|_{dx}$$

The conductive heat flux out is:

$$q_o \Big|_x = KA \frac{dT}{dx}$$

The conductive heat flux in is:

$$q_i \Big|_{x+dx} = KA \frac{dT}{dx} + \frac{d}{dx}\left(KA \frac{dT}{dx}\right) dx$$

The external radiative heat flux is assumed to be independent of the temperature (differences) in the wall. This is a conservative assumption, even for conductive heat transfer through insulation.

$$q_r \Big|_{dx} = q_r \frac{dx}{D_o/2}$$

Substitution gives

$$K\ Lt \frac{d^2 T}{dx^2} = -\frac{q_r}{D_o/2}$$

The heat flux per unit area q' is constant over the shield or

$$q' = \frac{q_r}{L\ D_o} = CONSTANT$$
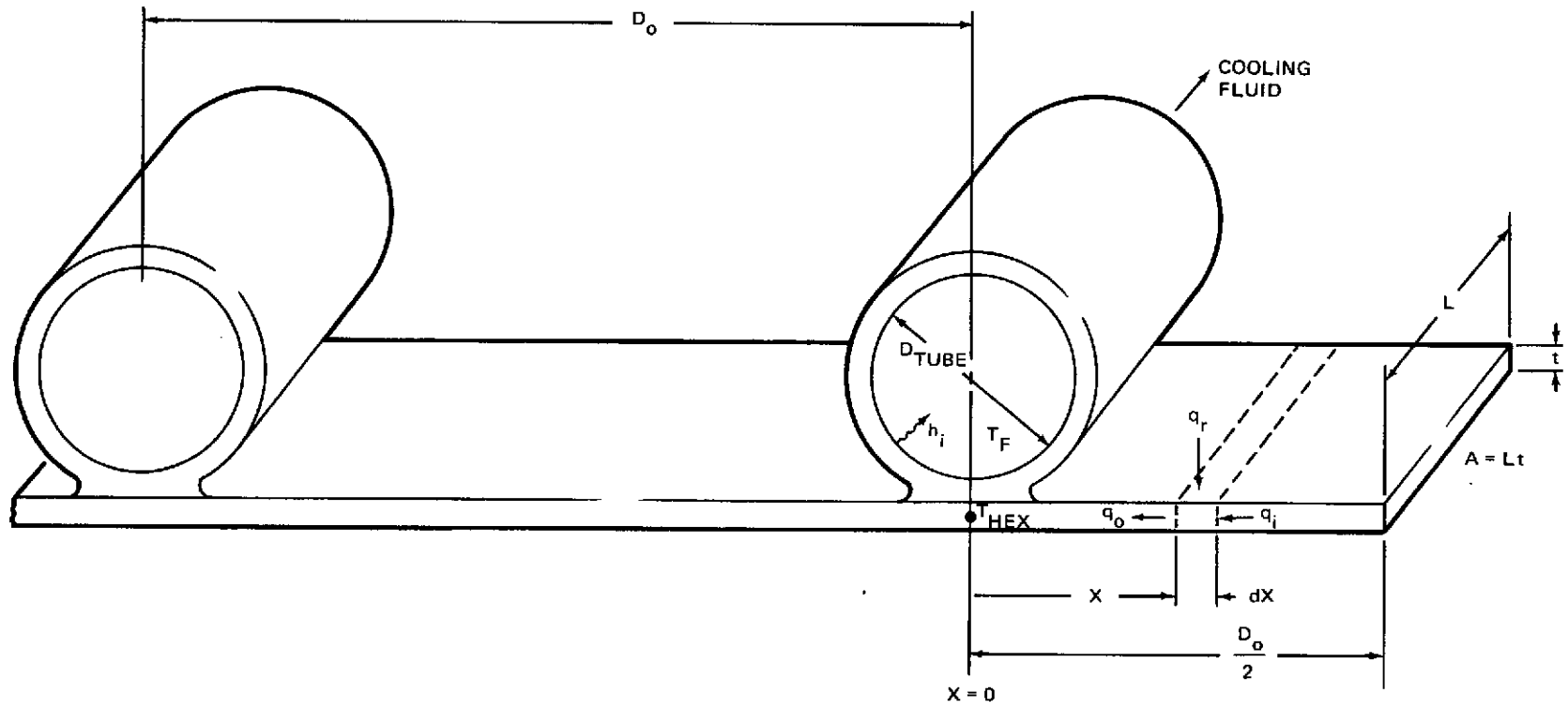
Figure 3.3.27. Shield Heat Exchanger Configuration

Combining the last two equations gives

$$\frac{d^2 T}{dx^2} = -\frac{q'2}{Kt}$$

Integrating gives:

$$\frac{dT}{dx} = -\frac{q'2}{Kt} x + B$$

Integrating again gives:

$$T = -\frac{q'}{Kt} x^2 + Bx + C$$

where B and C are constants of integration.

Imposing the boundary conditions:

at $x = D_o/2$ $\qquad\qquad\qquad$ $dT/dx = 0$

at $x = 0$ $\qquad\qquad\qquad\qquad$ $T = T_{HEX}$

gives

$$B = \frac{q'}{Kt} D_o \qquad\qquad\qquad C = T_{HEX}$$

so that

$$T - T_{HEX} = -\frac{q'}{Kt} x^2 + \frac{q' D_o}{Kt} x$$

All of the heat incident on the fin must be transferred to the cooling fluid:

$$q' L D_o = h_i L \pi D_{TUBE} (T_{HEX} - T_F)$$

or

$$(T_{HEX} - T_F) = \frac{q' D_o}{h_i \pi D_{TUBE}}$$

and

$$T - T_F = -\frac{q' x^2}{Kt} + \frac{q' D_o}{Kt} x + \frac{q' D_o}{h_i \pi D_{TUBE}}$$

For a fin length $x = D_o/2$, the $T - T_F = \Delta T$

$$\Delta T = \frac{q' (D_o/2)^2 \, 2}{Kt} - \frac{q' (D_o/2)^2}{Kt} + \frac{q' D_o}{h_i \pi D_{TUBE}}$$

$$= \frac{q' (D_o/2)^2}{Kt} + \frac{q' D_o}{h_i \pi D_{TUBE}}$$

or

$$D_o^2 = \frac{4Kt \Delta T}{q'} - \frac{4Kt}{h_i \pi D_{TUBE}} D_o$$

In order to maximize D_o and minimize the length of vent tubing, the ΔT should be maximum. It is usual practice to expand the vent fluid to low pressure 34.5×10^3 N/M^2 (5 psia) and temperature $7.2\,^\circ$ K ($13\,^\circ$R) to maximize ΔT and D_o. The constraint on the expansion pressure is the pressure drop along the vent tubes (including LH$_2$ shield, connecting tube, and LO$_2$ shield), which must be such that the H$_2$ exits the LH$_2$ tank shield at a pressure above the triple-point pressure of 6.895×10^3 N/M^2 (1 psia). The tubes on the shield should be as small as possible (commensurate with ΔP restrictions) to obtain the maximum h_i, which also maximizes D_o.

Because the shield weight varies at its thickness, t, with the vent tubing giving only a second-order weight effect, the thickness should be minimized and the conductivity of the shield maximized. To avoid differential expansion problems with the aluminum tankage, the shield should also be made from aluminum. Commercially pure aluminum, Type 1100, has K = 311 joules/Msec$\,^\circ$K (180 Btu/hr-ft$\,^\circ$R) at 22$\,^\circ$K and K = 259 joules/Msec$\,^\circ$K (150 Btu/hr-ft-$\,^\circ$F) at 97$\,^\circ$K. MDAC, under its IRAD program, has fabricated a cooled shield from 0.005 inch thick 1100 aluminum sheet brazed to 0.125 inch diameter by 0.015 inch wall tubing, as shown in Figure 3.3.28, and has tested this shield on a 260 gallon LH$_2$ tank in conjunction with a high performance thermal protection system (MLI, low-conductivity fiber glass supports, cooled lines, etc.). It was found that the tank could be essentially kept at constant pressure using the cooled shield technique, and that the required vent rate could be correlated with analytical predictions.

Since the cooled shield acts as a boiler for vented LH$_2$, the flow in the LH$_2$ shield is two-phase. Following expansion through the viscojet, the flow in the tubing of the shield is assumed to be in the annular regime, up to the annular-mist transition, which occurs at a quality of 0.8 to 0.9. In the annular and annular-mist regime, the heat transfer coefficient, h_i, is determined from the correlation of Chen (Reference 27). Chen uses Forster and Zuber's microconvective heat transfer relation for boiling and the Dittus-Boelter macroconvective heat transfer relation for forced convection, and obtains:

$$h_i = h_{MIC} + h_{MAC}$$

Figure 3.3.28. MDAC IRAD Zero-Heat-Leak Shield Test Article

or

$$h_i = S \, (0.00122) \, \frac{K_L^{0.79} \, C_L^{0.45} \, \rho_L^{0.49} \, g_e^{0.25} \, \Delta T^{0.24} \, \Delta P^{0.25}}{\sigma^{0.5} \, \mu_L^{0.29} \, H_{fg}^{0.24} \, \rho_v^{0.24}}$$

$$+ \, F \, (0.023) \, (Re)_L^{0.8} \, (Pr)_L^{0.4} \, \frac{K_L}{D}$$

where S and F are empirically determined dimensionless functions which allow for variations in the boiling and forced convection components, respectively. The value of S and F are given in Figures 3.3.29 and 3.3.30.

From the above equations, and the geometric consideration that

$$L \, D_0 = A_{SHIELD}$$

the shield tube spacing D_0, and required tubing length, L, under nominal conditions of heat flux, g', can be determined.

Because of uncertainties in the basic heat flux through the insulation and variations due to orbital thermal parameters, the operation of the shroud system under nonnominal conditions is of interest. For the TVS shown, the quality (vapor mass fraction) of the expanded LH_2 results in a vapor volume fraction of 0.80 to 0.95, depending on conditions. The fluid resistance (and thus flow rate) through the "viscojet" is determined by the sum of liquid resistance times the liquid volume fraction plus the vapor resistance times the vapor volume fraction. Because of the large vapor volume fraction, the vapor phase dominates the resistance in and flow through the "viscojet," so that the flow is proportional to the tank pressure, P_T, and is choked through the "viscojet" because, generally, the pressure in the shroud, P_S, is much less than $0.5 \, P_T$. Of course, the flow through the "viscojet" at the shroud outlet, exhausting to vacuum, is also choked and is proportional to $P_S / \sqrt{T_S}$. The flow through the shield is thus controlled by P_T, while P_S adjusts to provide the same flow through the outlet "viscojet."

For the condition where the incident heat flux to the shield is less than the nominal (equivalent design flow rate) value, not all of the LH_2 flow is vaporized. However, the vapor fraction is still very nearly 1.0, and the flow through the outlet "viscojet" is essentially unaffected: P_S and T_S are the same, and both "viscojets" remain choked at the same flow values.

For the condition where the incident heat flux to the shield is higher than the nominal value, the vent flow will heat up to a temperature above Point C in Figure 3.3.26. If the shield is in good thermal contact with the LH_2 tank, the maximum temperature the vent flow will reach an essentially tank temperature, T_T. If, on the other hand, the shield is not thermally connected to the tank (except by radiation), the vent fluid temperature can rise substantially above the tank temperature. For example, the fluid-shield temperature could reach 50 °K before the radiation interchange to the tank through the two layers of MLI between the tank and the shield reaches
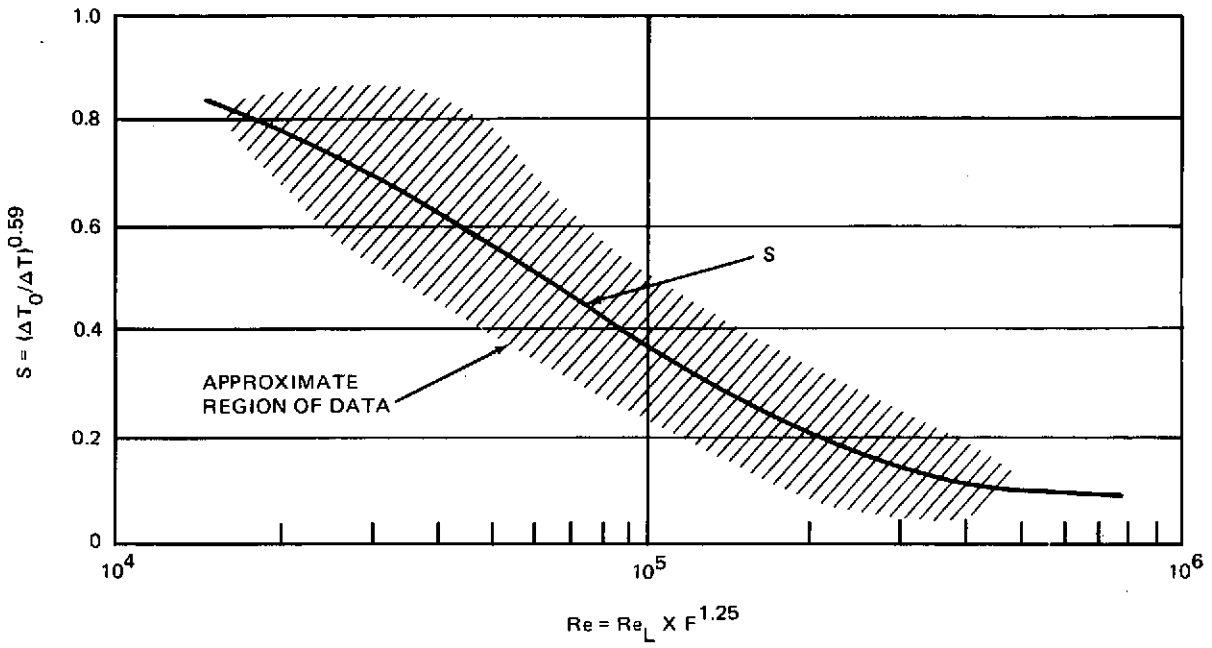
Figure 3.3.29. Suppression Factor, S
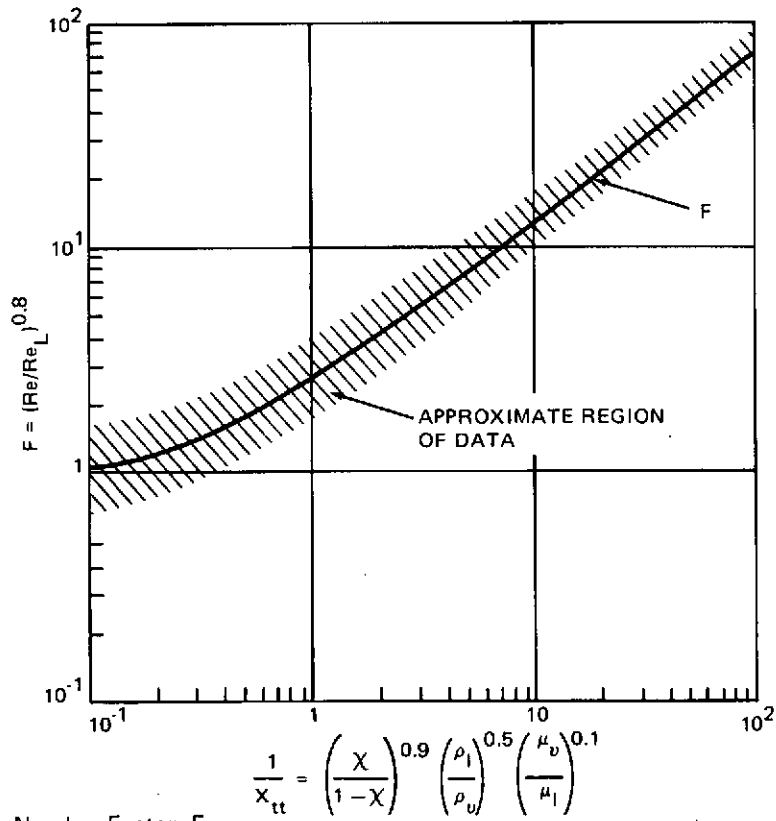
Figure 3.3.30. Reynolds Number Factor, F

3 to 5 percent of the incident heat flux. The vented fluid at 50°K has twice the enthalpy of the fluid at Point C, thus giving a 2:1 margin in allowable incident heat flux. As the temperature in the shield rises, the shield pressure must also rise to keep the ratio $P_S / \sqrt{T_S}$ constant and provide steady flow in the shroud. In general, the P_S will not rise sufficiently to unchoke the inlet "viscojet" and reduce flow. Conversely, the few percent or less of incident heat flux transmitted through the shield to the tank will tend to increase tank pressure, and thus flow rate through the shield. The increased flow rate will tend to reduce the final shield temperature and transmitted heat flux, and thus provides a limited self-regulatory effect.

For the total integrated system, the vent flow will be taken on a continuous basis from the acquisition device and split into several parallel legs or loops. The cooling loops are shown in Figures 3.3.31 and 3.3.32 with the estimated flow rates, including those for pump cooling, tank support cooling, and feed line cooling. As noted, another circuit may be required for acquisition device cooling. Pump cooling is based on providing an equivalent flow rate continuously to each of the three pumps that is adequate to absorbe pump heat input by vaporization. For the hot pump, the additional heat input is taken up as sensible temperature rise in a counterflow heat exchanger. The resulting temperature rise is quite tolerable. Pump cooling requires additional LH_2 loss from the system, compared to normal tank venting. This loss, based on the heat inputs shown in Figure 3.3.32, is about 41 kg for the seven day
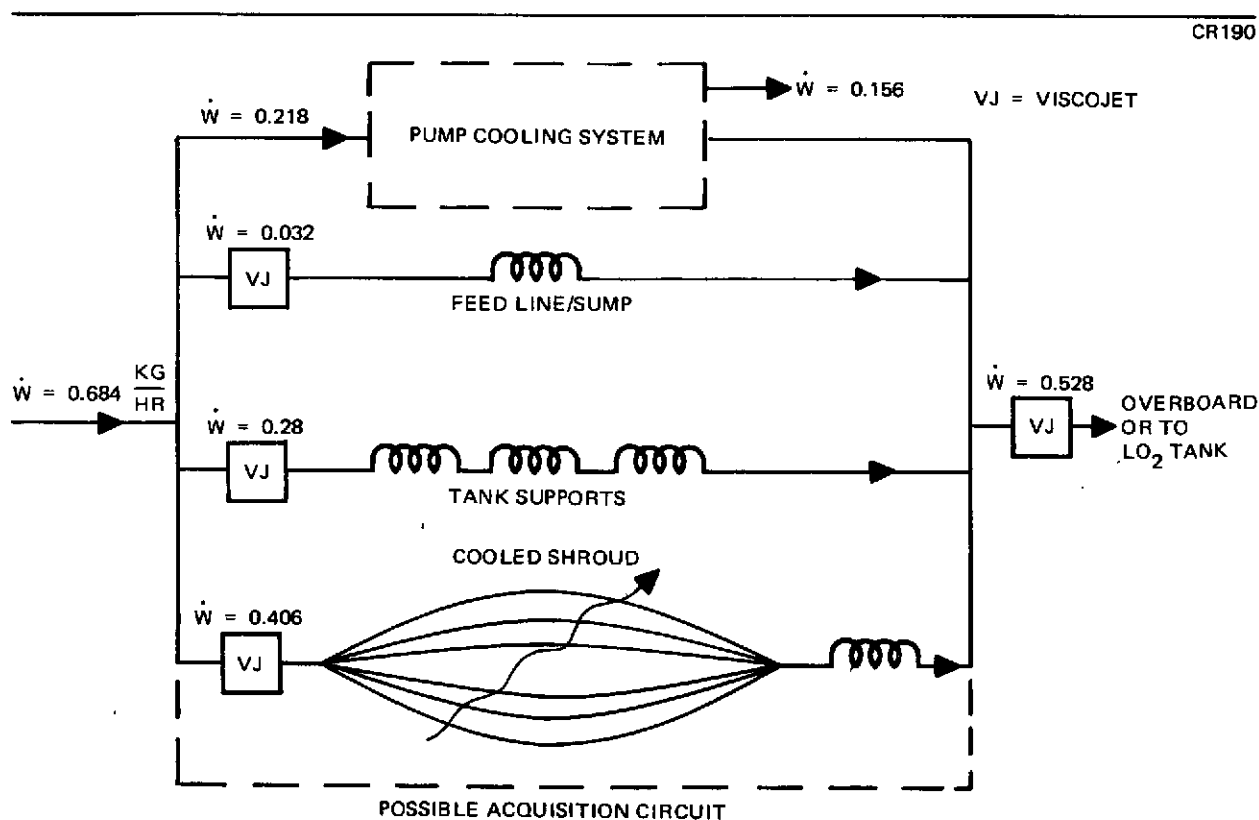
Figure 3.3.31. Integrated Thermodynamic Vent and Cooling System

LH$_2$ TANK

ACQUISITION DEVICE

MLI

PUMPS*

TURBINES*

Q (WATTS)

	9.08	21.9 (LH$_2$)
	7.03	16.7 (LO$_2$)

*THREE UNIT FOR REDUNDANCY,
ONE HOT AND TWO COLD
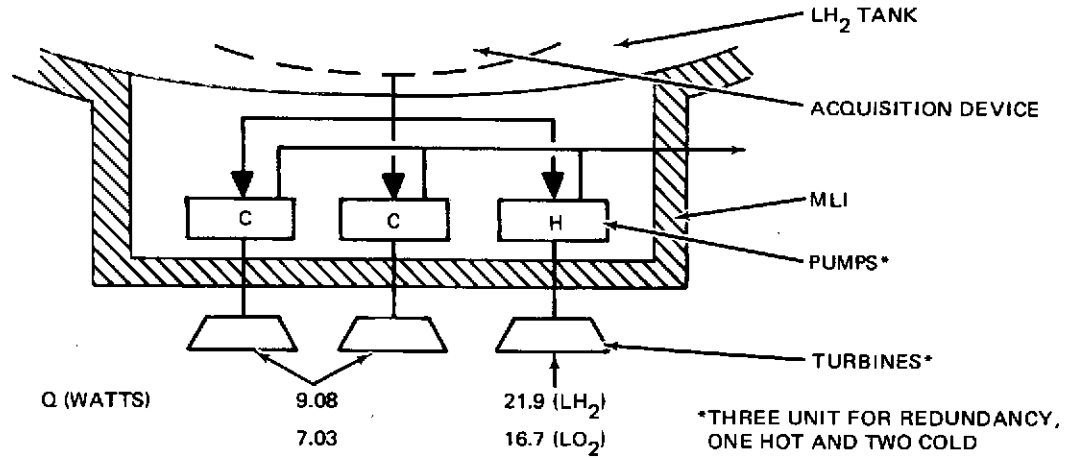
DESIGN CRITERIA - SUPPLY LH$_2$ (22°K) TO ABSORB "COOL PUMP" HEAT INPUT BY VAPORIZATION
AND ABSORB INCREASE HEAT INPUT FROM HOT PUMP BY SENSIBLE ΔT

SHAFT $\dot{W}$ = 0.052

$\dot{W}$ = 0.073

HOUSING

COOL

W = 0.021   21°K

$\dot{W}$ = 0.218 $\dfrac{KG}{HR}$

21°K

COOL

21°K

$\dot{W}$ = 0.063

34°K

HOT

123°K
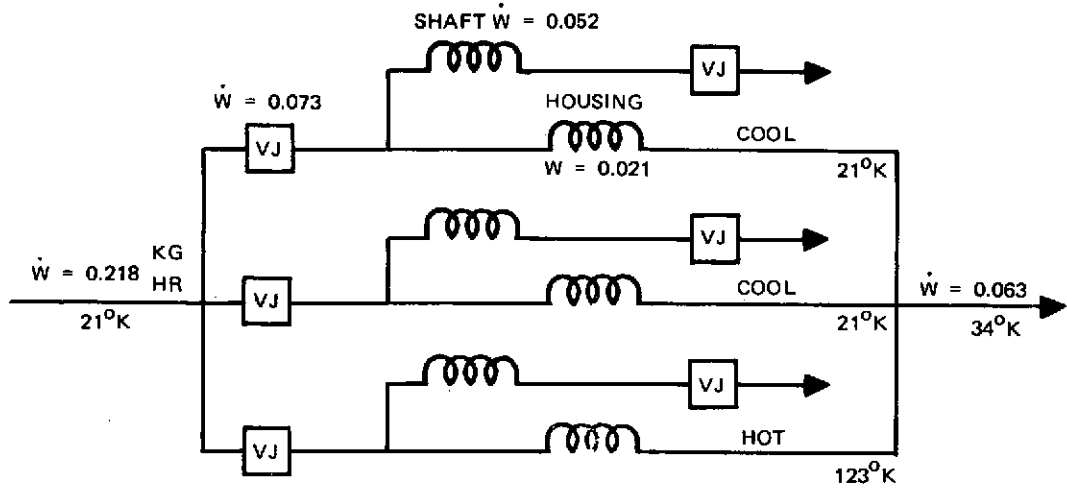
Figure 3.3.32. Preliminary Pump Thermal Parameters

141

mission. Heat loads were taken from Reference 1. The GH$_2$ leaving the LH$_2$ system can be used to cool the LO$_2$ system. In fact, the LO$_2$ system can be maintained in a nonvent condition with a saving in vented LO$_2$ and MLI. This requires routing the GH$_2$ up to and around the LO$_2$ tank (again using the offset thin-foil cooled shield).

It has been proposed that a wall screen liner can be used within a cryogenic tank to provide a gas annulus that can be directly vented while in orbit without using a TVS. Assuming that this is feasible, although low-g demonstration would probably be required, the concept would be relatively heavy and would present a significant installation problem. For example, assuming a 89.7 m^2 (969 ft^2) tank surface, a 325 x 2300 single mesh aluminum screen would weigh about 16 kg. This must be backed up by a support structure which would weigh about 63 kg (assuming 0.05 cm thick perforated aluminum sheet) yielding a total weight of 79 kg plus an additional 10% for attachments totaling 87 kg. The TVS cooling shield weighs only 40 kg and including the internal mixer the total weight is still much less than for the wall screen liner. Therefore, the screen liner approach as a venting concept does not offer any advantage. This simple comparison neglects any liquid loss incurred in initially emptying the annular space between the tank wall and the screen liner which would make the weight difference even larger.

3.4 Feed System Integration and Comparison

From the information generated in section 3.1, 3.2 and 3.3, total integrated feed system designs were evolved based on the FDC and LIPC acquisition concepts.

3.4.1 Basic Propellant Tankage. Although the basic tankage itself is not strongly influenced by the particulars of the acquisition system design, the tankage does represent a significant portion of the total feed system. Therefore, a preliminary tankage design and weight analysis was conducted for a configuration using dual LO$_2$ tanks with either single or dual LH$_2$ tanks. In all cases, the tanks were assumed to be cylinders with hemispherical ends. Internal frames were used for stiffness and point support load distribution.

Selection of an operational stress level is an important aspect in the design of space vehicle tankage. In May 1970, NASA published a structures design criteria document, NASA SP-8040, entitled "Fracture Control of Metallic Pressure Vessels." That document outlines design approaches to assure long-life structure. Analyses were completed using the techniques outlined in that document, and final design recommendations were made.

The results of long-life analyses that follow the recommendation of SP-8040 are shown in Table 3.4.1. These data indicate that selection of an operating stress based on a room temperature proof test results in a very low parent material operating stress. Furthermore, use of the proof factor attendant to the weld toughness properties would result in a drop of parent material operating stress.

Table 3.4.1

FRACTURE TOUGHNESS OPERATING STRESS—2219-T87 ALUMINUM

Material	Temperature (°K)	Tensile Yield		Proof Factor	(0.95 x TY)/PF	
		N/m^2	(ksi)		N/m^2	(ksi)
Parent Metal	294	3.59×10^8	(52)	1.85	1.84×10^8	(26.7)
Weld Metal	294	1.8×10^8	(26)	2.30	0.75×10^8	(10.8)
Parent Metal	77	5.17×10^8	(75)	1.68	2.94×10^8	(42.4)
Weld Metal	77	2.14×10^8	(31)	1.86	1.09×10^8	(15.8)
Parent Metal	20	5.87×10^8	(85)	1.96	2.84×10^8	(41.2)
Weld Metal	20	2.07×10^8	(30)	2.67	0.74×10^8	(10.7)

Notes: Parent material thickness is 0.102 to 0.127 cm (0.04 to 0.05 in.)
Weld material thickness is approximately 0.508 cm (0.20 in.)

References:

NASA CR72606, "Investigations of Deep Flaws in Thin Wall Tanks,"
J.M. Masters et al.; MDC E 0375, "Space Shuttle Data—Airframe—Part 3,"
Booster Appendices C and D; MIL HDBK-5

Two recommendations are made for the design of the propellant tanks:
(1) that cryogenic proof tests be planned and (2) that special, non-destructive
evaluations be made of a sample weld to allow use of the parent material
proof factors.

From Table 3.4.1, using these two ground rules, operating allowables
are 2.94×10^8 N/M^2 (42.4 ksi) for the LOX tanks and 2.84×10^8 N/M^2
(41.2 ksi) for the LH$_2$ tanks. For this analysis, a level of 2.76×10^8 N/M^2
(40.0 ksi) is chosen for a slight measure of conservatism.

The following criteria have been assumed for the tanks:

    A.   Life - 100 missions, which is assumed to be a total of
        600 operating pressure cycles.

    B.   Material - 2219-T87 sheet

    C.   Proof test of 95 percent of yield

    D.   Internal volume (total)

        1.   LH$_2$ = 69.2 m^3 (2450 ft^3)

        2.   LO$_2$ = 16.2 m^3 (573 ft^3)

E. Minimum gages

1. 0.1015×10^{-2} m (0.040 in.) hemisphere

2. 0.1525×10^{-2} m (0.070 in.) cylinder

Other parameters are given in Table 3.4.2 with size data being taken from Table 2.3 of section 2.

Estimated weights for the baseline tankage as a function of design pressure are plotted in Figures 3.4.1 and 3.4.2. It will be noted that the assumed minimum gage leads to a minimum tank weight and a critical pressure below which the weight no longer decreases significantly. The limits are shown in Table 3.4.2. Another important parameter required for trade studies is the change in tank weight for increases in tank length $(dW/dL)_T$. As discussed in section 3.2.2, this weight parameter is required to assess weight penalties associated with LH tank volume increases required to accommodate pressurant storage. In (2) the case of a single LH_2 tank,

$$\left(\frac{dW}{dL}\right)_{T_H} = \pi D_T\, T_w\, \rho_m = (3.14)(3.66)(0.001778)(2840) = 58 \text{ kg/m}$$

In the case of dual LH_2 tanks

$$\left(\frac{dW}{dL}\right)_{T_H} = (3.14)(2.44)(0.001778)(2840) = 39 \text{ kg/m}$$

CR190
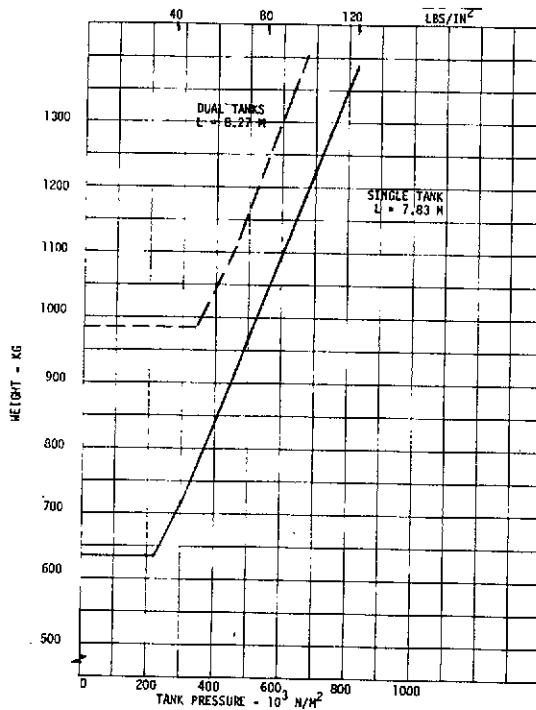
Figure 3.4.1. LH2 Tank Basic Structural Weight
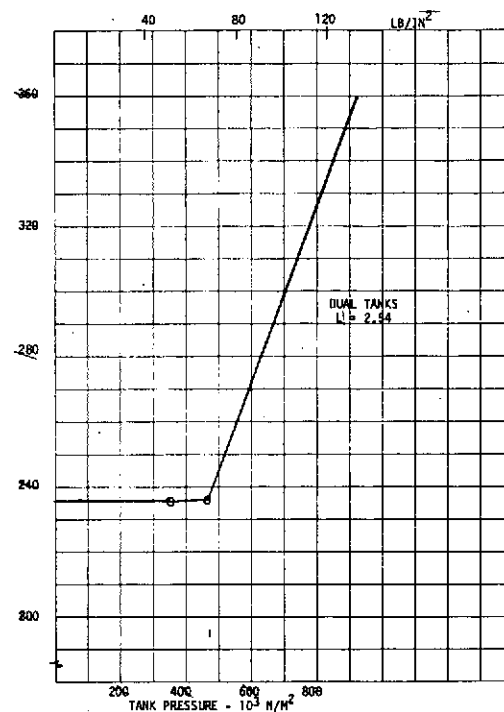
Figure 3.4.2. LO$_2$ Tank Basic Structural Weight

This information was used in the pressurization trade studies and optimizations.

For extended on-orbit storage of cryogens, point support systems made of low-conductivity, high-strength fiberglass struts have been found to be efficient in terms of low weight and minimum heat transfer (Reference 9). During the study reported in Reference 1, a support system of this type was designed for a representative shuttle APS. Table 3.4.3 summarizes the characteristics of such a system based on extending this previous design to the conditions of this study. The tank support system itself is a relatively small part of the APS and of secondary impact on the acquisition system. Therefore, further analysis in this area was not decreed to be necessary. The total basic tankage weight including support structure is 679 kg for a single LH$_2$ tank and 265 kg for dual LO$_2$ tanks.

3.4.2 FDS Feed System Integration. Table 3.4.4 summarizes the weight for the final integrated feed system for the FDC concept. The FDS acquisition subsystem weights as given in Tables 3.1.5 and 3.1.6 for the lightest design, using aluminum perforated tubing, are 118 kg and 83 kg for the LH$_2$ and LO$_2$ tanks respectively. These include the screen channels, sump baffles, and support/attachment provisions. For tank pressurization, cold (propellant temperature) helium is assumed for both tanks with the helium storage bottle placed in the LH$_2$ tank. This yields a total pressurization system weight of 357 kg for the LH$_2$ tank as shown in Figure 3.2.13 which includes 102 kg of usable helium, 60 kg of GH$_2$ (see Table 3.2.2), 147 kg for the helium bottle, 35 kg of helium residual and 13 kg for other

Table 3.4.2

BASELINE TANKAGE PARAMETERS

| Parameter | LH$_2$ | | LO$_2$ |
	1 Tank	2 Tanks	2 Tanks
Tank Volume, M^3 (ft^3)	69.2 (2,450)	69.2 (2,450)	16.2 (573)
Tank Diameter, M (ft)	3.66 (12)	2.44 (8)	2.44 (8)
Tankage Length, M (ft)	7.83 (25.7)	8.27 (27.1)	2.5 (8.2)
Tank Pressure Corresponding to Minimum Gage			
Cylinder, N/M^2 (psi)	228 x 10^3 (33)	345 x 10^3 (50)	345 x 10^3 (50)
Dome, N/M^2 (psi)	303 x 10^3 (44)	455 x 10^3 (66)	455 x 10^3 (66)
Minimum Tank Weight, kg (lb)	645 (1,420)	985 (2,170)	236 (520)

Table 3.4.3

TANK SUPPORT SYSTEM CHARACTERISTICS

| Tank | Weight | | Heat Rate | |
	kg	(lb)	watts	(Btu/hr)
LH$_2$ Tank				
Single tank	34.0	(75)	0.322	(1.1)
Dual tank	54.5	(120)	0.644	(2.2)
LO$_2$ Tank				
Single tank	18.1	(40)	0.235	(0.8)
Dual tank	29.0	(64)	0.470	(1.6)

tankage penalties as taken from the equations given in section 3.2.2. Similarly for the LO$_2$ tank, the total LO$_2$ pressurization system weight is 70 kg with 3.6 kg of usable helium, 59 kg of GO$_2$, 5.2 kg for the helium bottle, 1.2 kg of helium residual and 1 kg for other tankage penalties.

146

With respect to thermal management for the FDC concept, the principle of restricting all heat to the interior of the cryogen tank was rigidly adhered to in the integration. Thus, continuous venting with a vapor cooled shield TVS was used for the LH_2 tank. Thus, an in-orbit insulation system with 48 layer pairs of MLI was used. Based on the data presented in Table 3.3.3, this yields an insulation system weight of 138.4 kg and an in-orbit boil-off loss of 60.5 kg. As discussed in section 3.3.3, a foam sub-strat is optimum for in-atmosphere boil-off loss of 45 kg (see Table 3.3.5). Thus the total LH_2 tank insulation weight is 195.4 kg and the total boil-off loss is 105.5 kg. To affect the continuous low-g venting, a cooled shroud system as required was estimated at 40 kg and auxiliary cooling losses were estimated at 60.2 kg. This includes cooling for tank supports, feed lines and pumps.

For the LO_2 tank, a GH_2 vent gas cooled shield used to maintain zero heat leak to the LO_2 was found to be low in weight (see Table 3.3.4) and to satisfy the no heat input design criteria. This requires an MLI with 22 layer-pairs and results in an insulation weight of 46.3 kg. The cooled shield weighs 21 kg and of course there is no cooling loss incurred with the shield because the GH_2 is "free" from the LH_2 tank vent system. The in-atmosphere losses for the LO_2 tank are negligible.

To retain the no heat input design criteria, the pump by-pass required for turbopump system start-up and shut-down was dumped directly overboard with the FDC design as discussed in section 3.1.2. Thus, the 5.2 kg and 9.8 kg weight loss per cycle for LH_2 and LO_2 respectively as given in Table 3.1.4 was taken along with 50 cycles of operation giving a total pump by-pass weight loss of 260 kg for LH_2 and 490 kg for LO_2.

Figures 3.4.3 and 3.4.4 show schematics for the LH_2 feed system using cold helium and cold GH_2 pressurization. From these, component listings and weights were assembled as shown in Tables 3.4.4, 3.4.5 and 3.4.6. For the cold helium pressurization system components weights were estimated at 26.2Kg and 53.5Kg for the LH_2 and LO_2 systems respectively.

3.4.3 LPIC Feed System Integration. In the preceding subsections of Section 3.1.3, the various elements of the LPIC acquisition concept preliminary design have been detailed. These elements were taken and integrated into a total LH_2/LO_2 storage and feed system.

In Table 3.1.13 and 3.1.14, the LPIC acquisition subsystem weights are presented as a function of secondary tank volume ranging from 1.4 to 15.6 M^3 (50 to 560 ft.^{3}) for the LH_2 and 0.24 to 2.4 M^3 (8.3 to 85 ft.^{3}) for LO_2.

In the LPIC concept, the secondary tanks are pressurized with cold helium stored in a high pressure bottle located within the main LH_2 tank. This eliminates the possibility of thermal induced retention breakdown of the acquisition screen device. However, the main tank is pressurized with optimum (111°K) GH_2 bled from the high pressure accumulators (see Section 3.2).

The total propellant which is expelled directly from the secondary tank, using the cold helium system alone, has been determined to be 22 m^3 (780 ft^3) for the LH_2 system, independent of the size of the secondary tank.
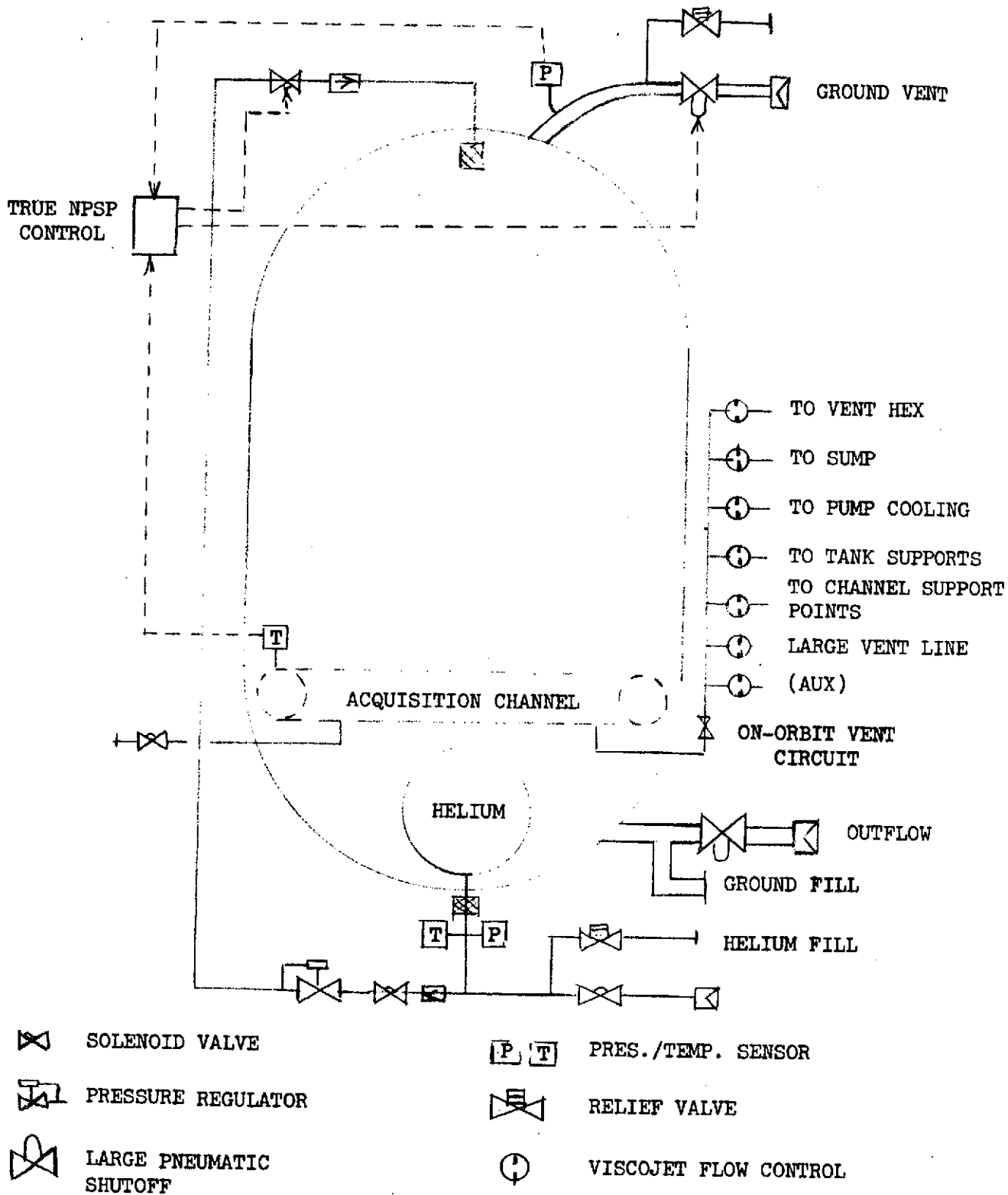
Figure 3.4.3. Cold Helium Pressurization System Schematic (Distributed Channel Acquisition System)
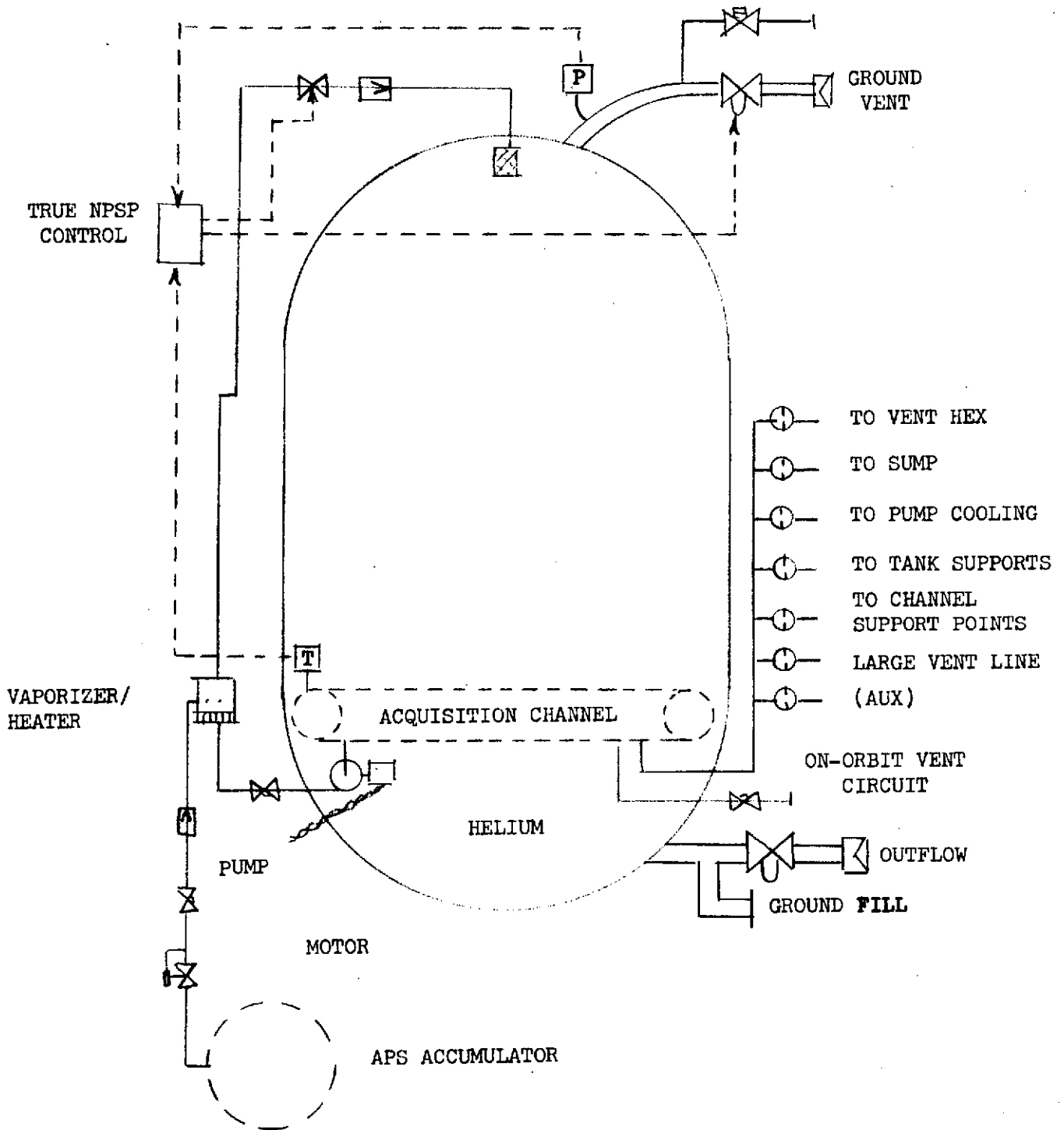
Figure 3.4.4. Cold GH₂ Pressurization System Schematic (Distributed Channel Acquisition System)

Table 3.4.4

TOTAL INTEGRATED FEED SYSTEM WEIGHT (kg)
Full Distributed Channel Acquisition Concept

	LH_2 Tank	LO_2 Tank
Acquisition Subsystem		
Hardware	118	83
Residuals	0	0
	118.0	83
Pressurization Subsystem		
Helium (usable)	102	3.6
Vapor	60	59
Helium bottle	147	5.2
Helium residual	35	1.2
Tankage penalties	13	1.0
	357.0	70
Insulation Subsystem		
MLI	138.4	46.3
Foam	57.0	0
	195.4	46.3
Boil-off Losses		
In-orbit	60.5	0
In-atmosphere	45	0
	105.5	0
Low-g Venting		
Cooled shields	40.0	21.0
Cryogen Cooling Loss	60.2	0
Basic Tankage	679.0	265
Feed System Components	86.2	53.5
	1641.3 kg (3615 lb)	538.8 kg (1187 lb)
Pump By-pass	260.0 kg (573 lb)	490 kg (1079 lb)

Table 3.4.5 (a)

LH$_2$ SYSTEM COMPONENT WEIGHTS
(COLD HELIUM PRESSURIZATION)

Quantity	Item	Weights	
		kg	lb
1	Outlet shutoff valve (2-inch ball)	6.35	(14)
1	2-inch quick-disconnect	2.27	(5)
1	4-inch vent valve	9.10	(20)
1	4-inch gas quick disconnect	2.72	(6)
2	Pressure sensors	0.68	(1.5)
1	Pressurization diffuser	0.45	(1.0)
2	Check valves (1 inch)	1.36	(3)
2	Solenoid valves (1 inch)	1.82	(4)
1	Pressure controller (split with LO$_2$ tank)	3.18	(7)
2	Solenoid valves (1/2 inch)	0.73	(1.6)
2	Temperature sensors	0.45	(1.0)
1	Filter	1.36	(3.0)
7	Viscojets	0.32	(0.7)
1	High-pressure relief (1 inch)	2.72	(6.0)
1	High-pressure solenoid (1 inch)	1.82	(4.0)
1	1-inch quick-disconnect	0.91	(2.0)
1	High-pressure regulator	2.27	(5.0)
	Component support hardware	4.54	(10.0)
		52.15	(113.8)
	Feed lines (2 inch)	0.91	(2.0)
	Vent lines (4 inch)	5.90	(13.0)
	Pressurization lines (1 inch)	10.45	(23.0)
	Miscellaneous lines	3.18	(7.0)
	Fittings	2.27	(5.0)
	Supports and miscellaneous hardware	2.27	(5.0)
		24.98	(55.0)

Table 3.4.5 (b)
LH$_2$ SYSTEM COMPONENT WEIGHTS
(COLD GH$_2$ PRESSURIZATION)

Quantity	Item	Weights kg	lb
1	Outlet shutoff valve (2-inch ball)	6.35	(14)
1	2-inch quick-disconnect	2.7	(5)
1	4-inch vent valve	9.10	(20)
1	4-inch relief valve	9.10	(20)
1	4-inch gas quick-disconnect	2.72	(6)
2	Pressure sensors	0.68	(1.5)
1	LH$_2$ boost pump	2.00	(4.4)
1	Electric motor	2.00	(4.4)
1	Vaporizer/cooler	4.00	(8.8)
1	Pressurization diffuser	0.45	(1.0)
2	Check Valves (1 inch)	1.36	(3.0)
1	Solenoid valves (1 inch)	0.91	(2.0)
1	Pressure controller (split with LO$_2$ tank)	3.18	(7.0)
2	Solenoids (1/2 inch)	0.73	(1.6)
2	Temperature sensors	0.45	(1.0)
7	Viscojets	0.32	(1.1)
1	High-pressure solenoid (1 inch)	1.82	(4.0)
1	High-pressure regulator	2.27	(5.0)
	Component support hardware	4.60	(10.0)
		54.31	(119.8)
	Feed lines (2 inch)	0.91	(2.0)
	Vent lines (4 inch)	5.90	(13.0)
	Pressurization lines (1 inch)	10.45	(23.0)
	Miscellaneous lines	3.18	(7.0)
	Fitting	2.27	(5.0)
	Support and miscellaneous hardware	2.27	(5.0)
		24.98	(55.0)

Table 3.4.6

LO$_2$ SYSTEM COMPONENT WEIGHTS
(COLD HELIUM PRESSURIZATION)

		Weights	
Quantity	Item	kg	lb
1	Outlet shutoff valve (2 inch ball)	6.35	(14)
1	2-inch quick-disconnect	2.27	(5)
1	3-inch vent valve	5.45	(12)
1	3-inch gas quick-disconnect	2.72	(6)
1	Pressure sensor	0.36	(0.8)
1	Pressurization diffuser	0.45	(1.0)
1	Check valve (1 inch)	0.68	(1.5)
2	Solenoid valves (1 inch)	1.82	(4)
1	Pressure controller (split with LO$_2$ tank)	3.18	(7)
2	Solenoid valves (1/2 inch)	0.73	(1.6)
1	Temperature sensor	0.23	(0.5)
7	Viscojets	0.32	(0.7)
1	High-pressure solenoid (1 inch)	1.82	(4.0)
	Component support hardware	3.63	(8.0)
		29.92	(66.1)
	Feed lines (2 inch)	0.91	(2.0)
	Vent lines (3 inch)	4.50	(10.0)
	Pressurization lines (1 inch)	10.45	(23.0)
	Miscellaneous lines	3.18	(7.0)
	Fittings	2.27	(5.0)
	Supports and miscellaneous hardware	2.27	(5.0)
		23.58	(52.0)

As a highly conservative estimate, it is assumed that the total pressure in the secondary tank is 1.52×10^5 N/m^2 at 22°K (22 psia) prior to venting, and that the partial pressure of hydrogen vapor is negligible.

Based on these assumptions, the cold helium pressurization system weight is 220 kg (485 lb), including gas, pressure bottles, supports, and a main tank weight penalty associated with the additional volume. As a comparison the system weight associated with an equilibrium mixture of hydrogen

and helium is 110 kg (242 lb). The assumption of equilibrium conditions is, therefore, possibly conservative by a factor of two. The system weights for both the main and LH_2 tank using warm GH_2 and the secondary tank are shown in Figure 3.4.5 as a function of secondary tank volume. The warm GH_2 weight was taken from the data presented in Section 2.3 but corrected for main tank volume. The warm hydrogen gas weight decreases with increasing secondary tank volume since less LH_2 is displaced from the main tank as the secondary tank becomes larger.

Figure 3.4.6 shows the overall feed system schematic for the LH_2 tank LPIC system including vacuum vent/refill provisions. The LO_2 tank system is similar. The various required mechanical control components compatible with this schematic are listed along with their weights in Tables 3.4.7 and 3.4.8. The main tank insulation was taken from Table 3.3.2 of Section 3.3 for a non-vented LH_2 tank and cooled LO_2 tank. This LH_2 insulation consists of 21 layer pairs of insulation or an 0.6 cm thickness. From Figure 3.3.8 of Section 3.3, 0.6 cm of helium purged MLI would result in a heat load during ground hold and launch of about 3.2×10^5 Joules/M^2 (28 Btu/Ft^2) which would thus result in 63 kg (139 lb) of boiloff during this period. The reentry and landing boiloff and the secondary tank foam weight was taken from Figure 3.3.17 of Section 3.3.

CR190
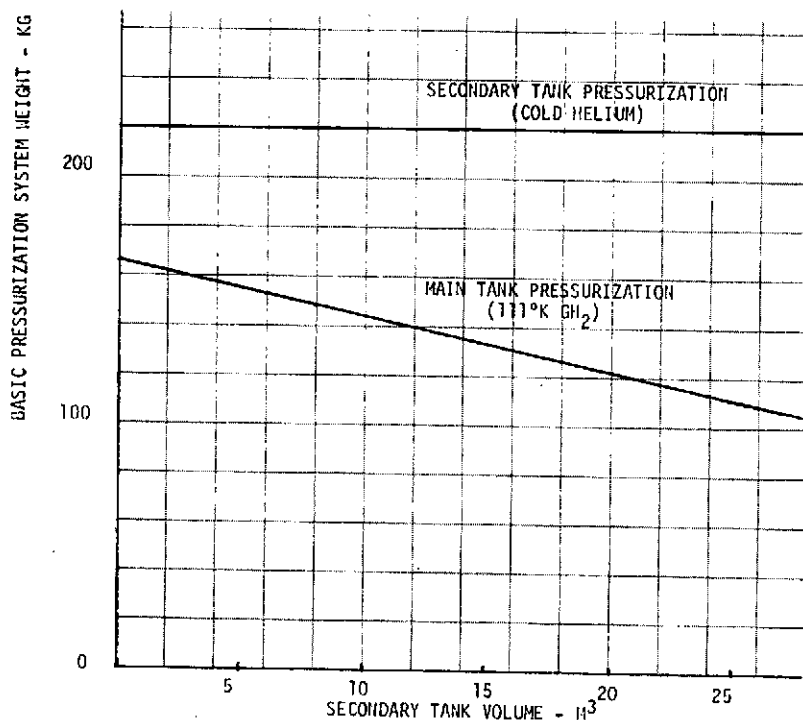
Figure 3.4.5. LPIC Concept Pressurization System Weight
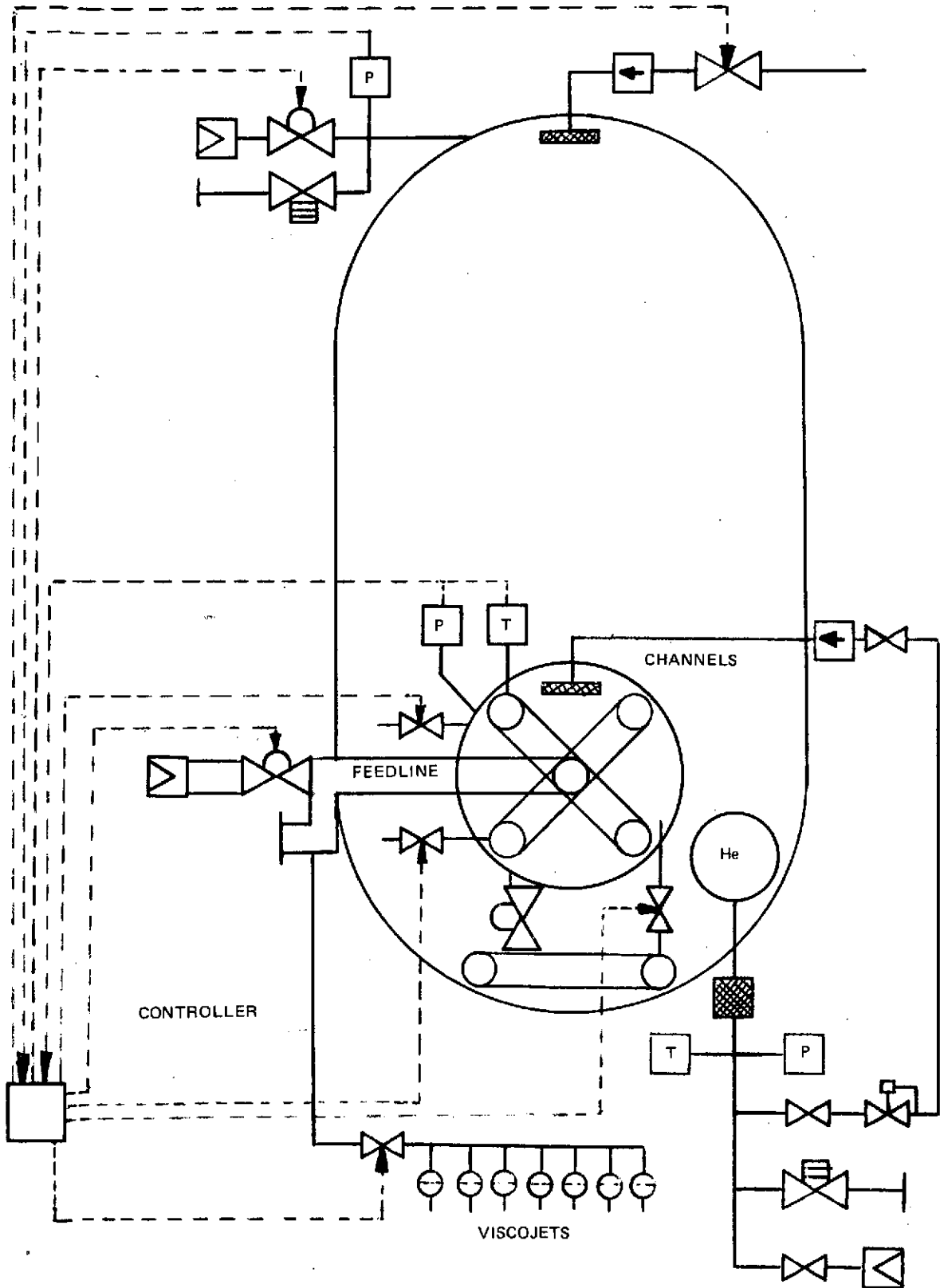
Figure 3.4.6. Schematic Diagram of LH$_2$ LPIC System

Table 3.4.7

LH$_2$ START TANK SYSTEM COMPONENT WEIGHTS
VACUUM VENT/REFILL DESIGN*

Quantity	Component		
2	Outlet shutoff valves (2-inch ball)	12.70 kg	(28.0 lb)
1	Filter	1.36 kg	(3.0 lb)
1	2-Inch quick-disconnect	2.70 kg	(5.0 lb)
1	4-Inch vent valve	9.10 kg	(20.0 lb)
1	4-Inch relief valve	9.10 kg	(20.0 lb)
1	4-Inch gas quick disconnect	2.72 kg	(6.0 lb)
3	Pressure sensors	1.00 kg	(2.2 lb)
2	Pressurization diffusers	0.90 kg	(2.0 lb)
2	Check valves (1 inch)	1.36 kg	(3.0 lb)
2	Solenoid valve (1 inch)	1.82 kg	(4.0 lb)
1	Pressure controller (split with LO$_2$ tank)	3.19 kg	(7.0 lb)
1	Logic Controller	4.54 kg	(10.0 lb)
4	Solenoids (1/2 inch)	1.46 kg	(3.2 lb)
2	Temperature sensors	0.45 kg	(1.0 lb)
7	Viscojets	0.32 kg	(1.1 lb)
2	High-pressure solenoid (1 inch)	3.64 kg	(8.0 lb)
1	1-Inch gas Q-D	0.91 kg	(20.0 lb)
2	High-pressure regulator	4.52 kg	(10.0 lb)
1	High-pressure relief (1 inch)	2.72 kg	(6.0 lb)
	Component support hardware	4.60 kg	(10.0 lb)
		77.00 kg	(169.0 lb)
	Feed lines (2 inch)	0.91 kg	(2.0 lb)
	Vent lines (4 inch)	5.90 kg	(13.0 lb)
	Pressurization lines (1 inch)	10.56 kg	(23.0 lb)
	Miscellaneous lines	3.18 kg	(7.0 lb)
	Fittings	2.27 kg	(5.0 lb)
	Support and miscellaneous hardware	2.27 kg	(5.0 lb)
		24.99 kg	(55.0 lb)

*Dynamic refill design does not require three
1/2-inch solenoid valves tabulated above.

Table 3.4.8

LO$_2$ START TANK SYSTEM COMPONENT WEIGHTS
VACUUM VENT/REFILL DESIGN*

Quantity	Component		
2	Outlet shutoff valves (2-inch ball)	12.70 kg	(28.0 lb)
1	2-Inch quick disconnect	2.70 kg	(5.0 lb)
1	4-Inch vent valve	9.10 kg	(20.0 lb)
1	4-Inch relief valve	9.10 kg	(20.0 lb)
1	4-Inch gas quick disconnect	2.72 kg	(6.0 lb)
3	Pressure sensors	1.00 kg	(2.2 lb)
2	Pressurization diffusers	0.90 kg	(2.0 lb)
2	Check valves (1 inch)	1.36 kg	(3.0 lb)
2	Solenoid valve (1 inch)	1.82 kg	(4.0 lb)
1	Pressure controller (split with LH$_2$ tank)	3.18 kg	(7.0 lb)
1	Logic Controller	4.54 kg	(12.0 lb)
3	Solenoids (1/2 inch)	1.10 kg	(2.4 lb)
2	Temperature sensors	0.45 kg	(1.0 lb)
1	High-pressure regulator	2.26 kg	(5.0 lb)
	Component support hardware	4.60 kg	(10.1 lb)
		57.10 kg	(125.7 lb)
	Feed lines (2 inch)	0.91 kg	(2.0 lb)
	Vent lines (4 inch)	5.90 kg	(13.0 lb)
	Pressurization lines (1 inch)	10.45 kg	(23.0 lb)
	Miscellaneous lines	3.18 kg	(7.0 lb)
	Fittings	2.27 kg	(5.0 lb)
	Support and miscellaneous hardware	2.27 kg	(5.0 lb)
		24.99 kg	(55.0 lb)

*Dynamic refill design does not require three
1/2-inch solenoid valves tabulated above.

The tankage weight is taken from the data presented in Table 3.4.2. These values cover only basic tank weight. Penalties such as due to the pressurization system are included in the pressurization system weight. The weight shown under low-g tank pressure control includes two internal tank mixer units for maintaining near uniform propellant temperature. Cooling loss weight is taken from data presented in Section 3.3. .

With the LPIC concept, pump by-pass can be sent back to the main tank and there is no direct propellant dump loss as with the FDC concept.

Total integrated feed system weights for the LIPC system are shown in Tables 3.4.9 and 3.4.10.

These tables show that there is no weight advantage in using secondary tank sizes below 12.6 m^3 (450 ft^3) and 2.4 m^3 (85 ft^3) for LH$_2$ and LO$_2$ respectively. Thus, these sizes were selected for the secondary tanks.

Table 3.4.9

LPIC LH$_2$ FEED SYSTEM WEIGHT ESTIMATES (KG)

	Secondary Tank System					
	2.8 m^3 (100 ft^3)		12.6 m^3 (450 ft^3)		15.6 m^3 (560 ft^3)	
Acquisition System						
Hardware	107.1		220.3		258.0	
Residuals	16.5		0		0	
		123.6		220.3		258.0
Pressurization System						
Secondary Tank	220.0		110.0		110.0	
Main Tank	160.0		138.0		133.0	
		380.0		248.0		243.0
Feed System Components		102.0		101.0		101.0
Insulation System						
Main Tank	102.7		102.7		102.7	
Secondary Tank	8.2		18.0		19.5	
		110.9		120.7		122.2
Thermal Induced Boiloff						
Through Launch	63.0		63.0		63.0	
In-Orbit	0		0		0	
Reentry and Landing	9.1		30.6		34.5	
		72.1		93.6		97.5
Basic Tankage		678.0		678.0		678.0
Low-g Tank Pressure Control		5.0		5.0		5.0
Cryogen Cooling Loss		60.2		60.2		60.2
		1531.8 kg		1526.8 kg		1564.9 kg
Pump Bypass		0		0		0

Table 3.4.10

LPIC LO$_2$ FEED SYSTEM WEIGHT ESTIMATES (KG)

	Secondary Tank System			
	0.47 m^3 (16.67 ft^3)		1.84 m^3 (65 ft^2)	
Acquisition System				
Hardware	26.7		73.5	
Residuals	31.7		0	
		58.4		73.5
Pressurization				
Start Tank	9.1		9.1	
Main Tank	77.6		71.0	
		86.7		80.1
Feed System Components		82.1		82.1
Insulation System				
Main Tank	46.3		46.3	
Start Tank	0		0	
		46.3		46.3
Thermal Induced Boiloff		0		0
Basic Tankage		265.0		265.0
Low-g Tank Pressure Control		10.0		10.0
Cryogen Loss for Cooling		0		0
		548.5 kg		557.0 kg
Pump Bypass		0		0

3.4.4 _System Comparison_. At this point, a comparison of the FDC and LPIC concepts can be made. Table 3.4.11 shows the weight comparisons broken down into subsystems. This indicates that the weights, neglecting pump bypass losses, are very close. For all practical purposes, the LO$_2$ tank systems weight are the same while for the LH$_2$ tank, the LPIC system is about 114 kg (251 lbs.) lighter. This represents a savings on the LH$_2$ system of about 7% for the LPIC over the FDC design. This is significant but probably not controlling. An examination of the breakdown is of interest. Note that the LPIC acquisition subsystem is actually heavier than for the FDC, but to assure proper operation of the FDC system, weight penalties had to be taken in the pressurization, insulation, and low-g vent subsystems. These penalties more than compensated for the heavier LPIC acquisition subsystem weight.

When the pump bypass losses are included, the weight balance swings very heavily in favor of the LPIC system with the total system (LH$_2$ and LO$_2$) weight difference being as much as 846 kg. A comparison of the system features are tabulated in Table 3.4.12.

Table 3.4.11

TOTAL FEED SYSTEMS WEIGHT COMPARISON (KG)

Concept ——→	FDC		LPIC	
Tank ——→	LH$_2$	LO$_2$	LH$_2$	LO$_2$
Acquisition	118	83	220	74
Pressurization	357	70	248	80
Insulation	195	46	121	46
Boil-off	106	0	94	0
Low-g Venting	40	21	5	10
Cryogen Cooling Loss	60	0	60	0
Basic Tankage	679	265	679	265
Feed System Components	86	54	101	82
Subtotal	1641	539	1527	557
Pump Bypass	260	490	0	0

Table 3.4.12

OVERALL BASIC CONCEPT COMPARISON

	Distributed Channel	Pressure Isolated Channel
	Cooled Shield TVS: Cold Helium Pressurization:	Internal Mixer Thermal Control: 111 °K GH$_2$ Pressurization
Weight	Higher weight	Minimum weight
Reliability	Fewer Parts	Uses rotating machinery for propellant mixing
	Completely passive	Has potential retention breakdown correction capability (+30 to 45 kg)
G-independent	All thermal aspects and critical flow characteristics can be tested on the ground	Internal mixer and refill involves some potential low-g uncertainties
Technology status	In hand	Internal mixer involves some potential log-g uncertainties
Head potential for required screen mesh	About at limit of finest available mesh	Good safety factor with relatively coarse mesh
Fabrication capability	Must have access to all interior tank wall	Tank within a tank fabrication
Pump bypass compatibility	Must dump all pump bypass	Could be handled with minimum or no dumping
Offloading	Severely limited capability	Complete flexibility

As can be seen, each system has its strong points. The distributed channel system is completely passive, its design is g-independent and all technology is basically in hand. The LPIC system is relatively light, can accommodate pump bypass without significant propellant loss, has good head safety factor with relatively coarse mesh screens, and can accommodate a high range of offloading.

The pump bypass problem is of particular concern for shuttle class application since it may involve an additional weight penalty of 750 kg (LH_2 plus LO_2 loss) for the distributed channel system or any similar concept that does not involve a pressure-isolated screen device. The FDC type device is not capable of reliably accepting the warm high-pressure pump bypass flow without screen breakdown. Bench tests of the sensitivity of the screen devices to heating and pressure decays have shown significant effects (see Section 2C1, Vol. II). All attempts to handle the bypass flow with heat exchangers, separate tanks, etc., were found to be ineffective for the distributed channel system. Therefore, unless pump bypass flow can be proven not to affect a specific screen device in the main tank, it must be assumed that all of this flow must be dumped overboard

The LPIC system operation is not sensitive to heat transfer and pressure fluctuations in the main tank. Thus, it is permissible for all of the missions studied to accept all pump bypass flow into the main tank. For a mission requiring a completely full tank delivered to orbit, followed by a series of short-duration burns, the pump bypass could cause significant pressure increases, until the ullage volume reached approximately 15 percent. In this case, a small pump bypass weight penalty would be assessed against the LPIC concept. Since this case does not occur for the missions considered, no pump bypass weight penalty is assessed against the LPIC design.

Offloading, or the ability to launch with a partially loaded cryogenic tank, may be important for vehicles that fly a large variety of missions, and is required for the three missions considered in this study. The distributed channel concept and all known distributed screen acquisition concepts have severely limited tank offloading capability. Unless the tanks are full during launch, the screen devices are exposed to excessive hydrostatic pressures which cause screen retention breakdown due to the combination of screen height above the liquid surface and the high launch accelerations. These problems appear to be significantly increased by launch vibrations. The LPIC design is not affected by the percentage of propellant in the main tank during launch. Furthermore, the secondary tank screen devices are completely submerged in liquid during the high launch acceleration periods; this design is immune to problems of high launch accelerations or vibrations.

Tank offloading could be achieved for a specific volume by separating the main tank into compartments, but this concept adds additional weight. Changing the offloading volume would require additional tank compartments. This approach has not been considered further in this study.

Another approach that could be used to provide offloading capability is to design the acquisition channels such that they will refill by capillary forces in a low-g environment. A pressure induced flow could also be used to assure refill after the initial high acceleration breakdown during launch. Although

this refill is theoretically possible, it would require a significant expansion of technology and would require extensive in-orbit verification testing which was not in line with the overall objectives of this program. Thus, this idea was not pursued further.

Both FDC and LPIC systems have been designed to provide retention safety factors in excess of 2.0, but in order for the distributed channel to meet this requirement, it was necessary to use the finest available mesh screens. The LPIC design, however, uses relatively coarse mesh screen (200 x 600) which should be less prone to clogging and bubble point degradation.

The FDC concept is independent of propellant orientation and zero-g effects, principally because its thermal management system, based on the heat interception shroud, is independent of these effects. The LPIC system used with autogenous pressurization in the main tank and propellant mixers to control tank pressure, poses some questions regarding mixing efficiency in low gravity. These problems may be significant with small amounts of propellant, since mixers might not be immersed in liquid and thus would pump vapor. Incomplete mixing would lead to increased tank pressure and the necessity for venting. Although pure vapor venting can be provided by the mixers, coupled with a forced convection thermodynamic vent system, an additional weight penalty could be incurred. Extensive analytical and 1-g experimental work has been conducted on internal mixers for destratification and tank pressure control (References 15 and 16) and they would appear to be feasible. But mixers have not been tested under actual reduced-g conditions; thus there is an area of uncertainty especially for large ullage conditions.

The desirability of achieving g-independence for the final system suggests a combination of system features to yield an optimum hybrid design. One such arrangement is to use the basic LPIC acquisition system and autogenous main tank pressurization, but to use low-g venting with a vapor-cooled shield rather than the mixer for tank pressure control and thermal management. In this case the insulation system uses the FDC design but no tank foam substrat. Weights for this system are shown in Table 3.4.13 along with comparison weights for the basic LPIC and FDC systems. This combination of subsystems retains the pressurization and pump bypass handling advantage of the LPIC, achieves complete low-g independency, and eliminates the rotating machinery for the mixer system. This combination is about equal in base system weight to the basic distributed channel system but has no dump penalty for pump operation.

Theoretically, with a cooled-shield TVS, heat is not transferred from the tank wall to the liquid. Thus a retention screen can be adjacent to or connected directly to the main tank wall with no risk of thermally induced screen retention breakdown. Thus, when using a cooled-shield TVS, it is feasible to consider the integration of the secondary tank and the main tank lower dome. This integrated tankage (IT) is shown in Figure 3.4.7 assuming a 12.6 M^3 (450 ft^3) secondary tank volume.

A preliminary structural analysis was made to determine the weight difference between the independent and integrated tankage designs. This analysis revealed that significant bending loads are imposed at the point

Table 3.4.13

WEIGHT COMPARISON OF HYBRID LH_2 FEED SYSTEM
WITH BASIC FDC AND LPIC (KG)

	Basic FDC	Basic LPIC	Hybrid
Acquisition	118	220	220
Storage	361	275	351
Pressure Control	40	5	40
Components	86	101	101
Pressurization	357	248	248
	962	849	960
Pump Bypass	260	0	0

CR190

COMMON DOME (INSULATED)

MAIN TANK SECONDARY SCREEN

CHANNEL

1.6M (5.2 FT)

1M (6 FT)

FEEDLINE

REFILL VALVE

COOLING SHIELD

MAIN TANK DOME

PRESSURIZATION/VENT LINES
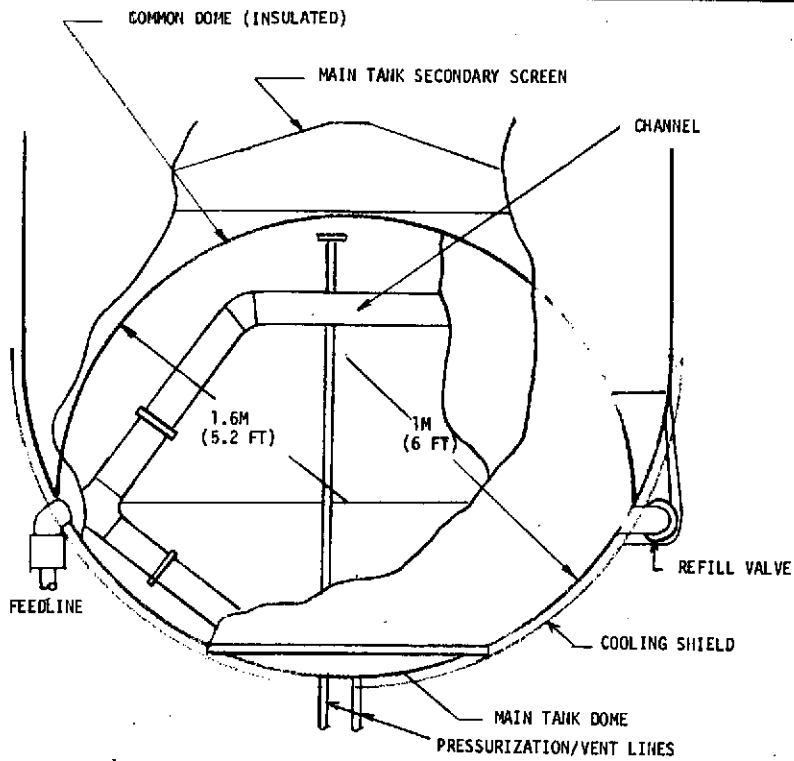
Figure 3.4.7. LPIC With Integrated Tankage

where the main and common tank domes intersect. To accommodate these loads, about 40.4 kg (89 lb) of structural buildup material must be added to the secondary tank hemispherical dome weight of 87 kg (192 lb); the total integrated secondary tank pressure shell weight penalty becomes 127.4 kg (281 lb). The independent tank pressure shell base weight is 132 kg (291 lb). To this base weight must be added the support system weight of 10.5 kg for a total installed tank weight of 142.5 kg (314 lb). Thus, integration saves about 15.1 kg (33 lb). The hybrid system weight can be reduced to 945 kg by integrating the tankage structure but this design is still 96 kg heavier than the basic LPIC system because of the increased thermal management system weight associated with the heat interception shield. The resulting fabrication and structural simplifications, g-independence of the venting system, and the passive nature of the cooled shield TVS with integrated tankage may offset this weight penalty.

A further system variation using the LPIC concept with integrated tank structure is possible. The main LH_2 tank can be maintained non-vented with a mixer and the cooled shield can be used only on the lower half of the tank around the acquisition device. In this approach, all of the features of the LPIC concept are retained, including autogenous pressurization of the main LH_2 tank, nonvented LH_2 tank operation with an internal LH_2 tank mixer, and recirculated pump by-pass fluid. The LH_2 bled from the tank to supply coolant to the local shield is strictly an additional coolant loss much like that required for the feed lines and pump cooling. Using the LPIC tank insulation requirements, 21 layer-pairs, this results in a tank wall heat flux of 1.26 watts/M^2 (0.4 BTU/Ft^2Hr) and, therefore, requires 35 kg of LH_2 coolant. The shield structural weight will be about 10 kg.

All of the alternates are compared on a common weight basis in Table 3.4.14. To obtain the installation simplicity of the integrated tankage, a weight penalty of 30 kg must be incurred by the LPIC system. To further obtain complete g independence, an additional 66 kg weight penalty must be incurred. Since the internal mixer concept has been relatively well developed,

Table 3.4.14

ALTERNATE LH_2 FEED SYSTEM WEIGHT COMPARISONS (KG)

	Basic FDC	Basic LPIC	Hybrid	Hybrid/IT	LPIC/IT
Acquisition	118	220	220	205	205
Storage/Cooling	361	275	351	351	310
Pressure Control	40	5	40	40	15
Pressurization	357	248	248	248	248
Basic Tankage	679	679	679	679	679
Components	86	101	101	101	101
Pump Bypass	260	0	0	0	0
Total Weight	1901 Kg	1528 Kg	1639 Kg	1624 Kg	1558 Kg

the low-g problems with its operation are not considered severe and it was accepted for the design. However, the installation simplification afforded by the integrated tankage is worth the small weight penalty. Thus, the LPIC with integrated tankage was accepted for the LH_2 tank feed system.

Using the same rational as above, the LPIC with integrated tankage was also adopted for the LO_2 feed system. Because of the small size of the LO_2 secondary tank, little total feed system weight change was found for this system.

Because of the uncertainty still remaining as to the feasibility of using warm gas pressurization with a full distributed screen acquisition device, a final weight comparison was made between the selected LPIC system and a FDC system using a $111^{\circ}K$ $(200^{\circ}R)$ inlet temperature GH_2 tank pressurization system. This weight comparison is shown in Table 3.4.15 and indicates that if pump bypass is not considered, the FDC/AP concept is significantly lighter but when pump bypass overboard dump is still used, which is most likely, the selected system is only slightly heavier.

Table 3.4.15

WEIGHT COMPARISON OF SELECTED LH_2 FEED SYSTEM AND AN FDC SYSTEM USING AUTOGENEOUS PRESSURIZATION

	LPIC/IT	FDC/AP
Acquisition	205	118
Storage/Cooling	310	265
Pressure Control	15	5
Pressurization	248	180*
Basic Tankage	679	679
Components	101	86
Sub-Total	1,558	1,333
Pump By-Pass	0	260
Total	1,558 kg	1,593 kg

Section 4. TECHNICAL DESIGN STUDIES
ADVANCED SPACE PROPULSION MODULE

The second class of application addressed in this study was a LH_2/LO_2 multi-burn space propulsion module. Like the previous CSS/APS application, it involves the use of LH_2 and LO_2, requires long operational times in orbit, reusability and requires large tankage. In fact from the data summarized in Section 2, the propellant loading is very similar: 24,744 kg to 22,700 kg for the ASPM and CSS/APS respectively. The major differences are that with the ASPM, the propellant represents a much higher percentage of the gross weight than in the CSS/APS case and that the ASPM must be designed for higher destabilizing accelerations (about 1 g as compared to 0.05 g). However, because of the similar tank sizes, much of the parametric data and conclusions developed for the CSS/APS, particularly with respect to pressurization, are directly applicable and such analyses were used wherever possible in the design development for the ASPM.

4.1 Acquisition Subsystem

Tables 2.7 - 2.10 of Section 2 reveal that the ASPM experiences disturbing accelerations in excess of 1 g. This consideration, when combined with the high flow rates and large tank sizes, makes distributed screen acquisition devices impractical for the ASPM class application. This point can be appreciated by an examination of Figure 4.1.1 which shows the ideal hydrostatic LH_2 head that can be supported by a range of available screen meshes as a function of disturbing acceleration. At 1 g the LH_2 head is limited to about 1 meter, whereas the tank dimensions for the ASPM are greater than 4 meters.

When consideration is given to the additional pressure losses associated with flow through the screen, flow along the screen channels, inertial effects, and the necessity for a retention safety factor of at least 2.0, it is clear that the ASPM tanks and g-level constraints combine to make distributed device concepts unworkable.

Much attention has recently been directed to the use of multiple screens "sandwiched" together to increase the total bubble point pressure. This concept, which was investigated by MDAC under an IRAD program (Reference 28), is reputed to be applicable to large tanks and high g-levels. However, as has been shown in bench tests reported in Volume II, Section 2.9.3, multiple screens do not appear practical for increasing bubble point since the vapor region built up between the screens block the flow passages until breakthrough occurs, which leads to loss of liquid retention.

Because of the factors discussed above, only localized screen retention acquisition concepts were considered for the ASPM application. Furthermore, in view of the significant weight savings achieved by the LPIC concept used for the CSS/APS application, efforts were primarily directed toward the LPIC concept as applied to ASPM mission requirements.
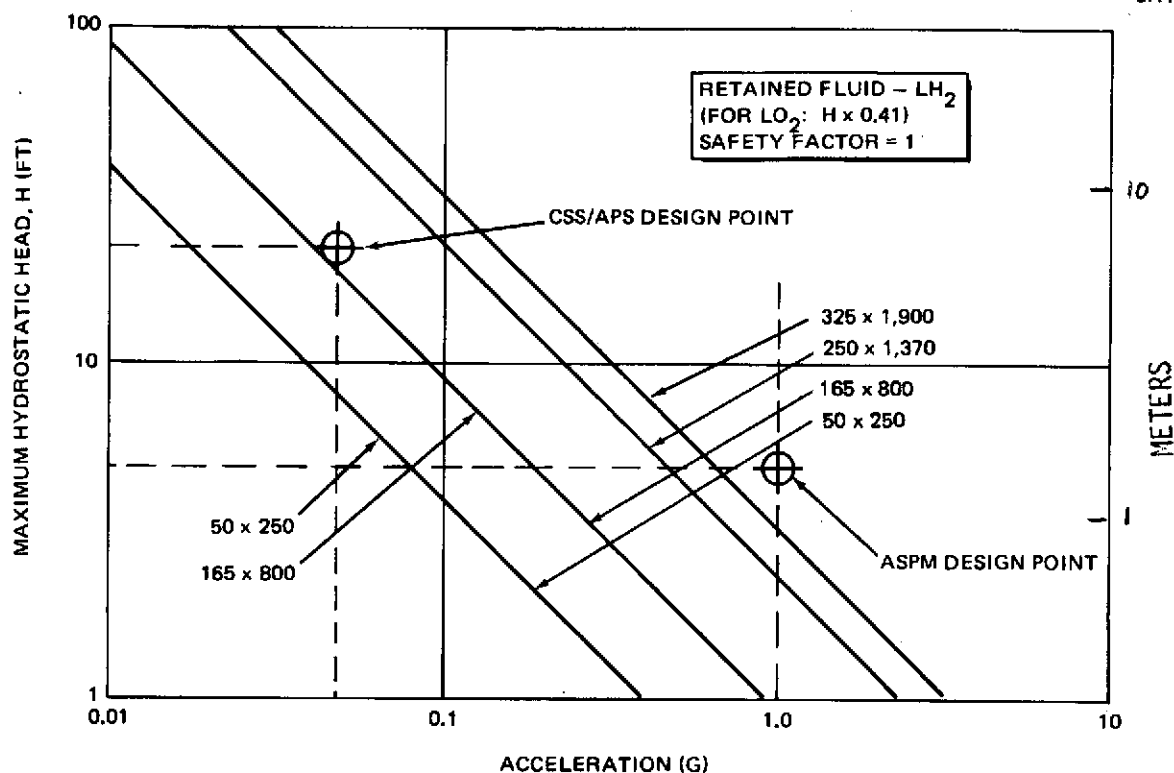
Figure 4.1.1. Ideal Hydrostatic Retention Capabilities for Fine Mesh Screens

4. 1. 1 Secondary Tank and Device Sizing. The design of a LPIC acquisition system for the ASPM was conducted, based on the requirements described in Section 2. The Acquisition Device Sizing Program (H574) was used to generate propellant usage curves for the baseline mission defined by Table 2. 7. These curves are instrumental in determining the secondary tank size, screen device location and configuration, and the resulting retention safety factors (RSF).

Figures 4. 1. 2 through 4. 1. 5 present the propellant usage curves for two types of secondary tanks: the baseline design with dynamic refill during main engine burns, and an alternate design, with the additional capability of vacuum vent/refill (the vacuum vent/refill concept is described in Appendix D). Figures 4. 1. 2 and 4. 1. 3 apply to the baseline designs for LH$_2$ and LO$_2$. In order to obtain the necessary retention safety factors, the secondary tank volumes are selected as 0. 735 m^3 (26 ft^3 for LH$_2$ and 0. 17 m^3 (6 ft^3 for LO$_2$. These volumes are sufficiently large to prevent the liquid levels from dropping to the point where screen breakdown failure would occur during the burn sequences.

The resulting secondary tank volumes are relatively small with diameters of 1. 11 and 0. 68 m, and thus the screen heights are approximately compatible with the large total flow losses and hydrostatic pressures associated with the high acceleration levels (1g) of the ASPM.
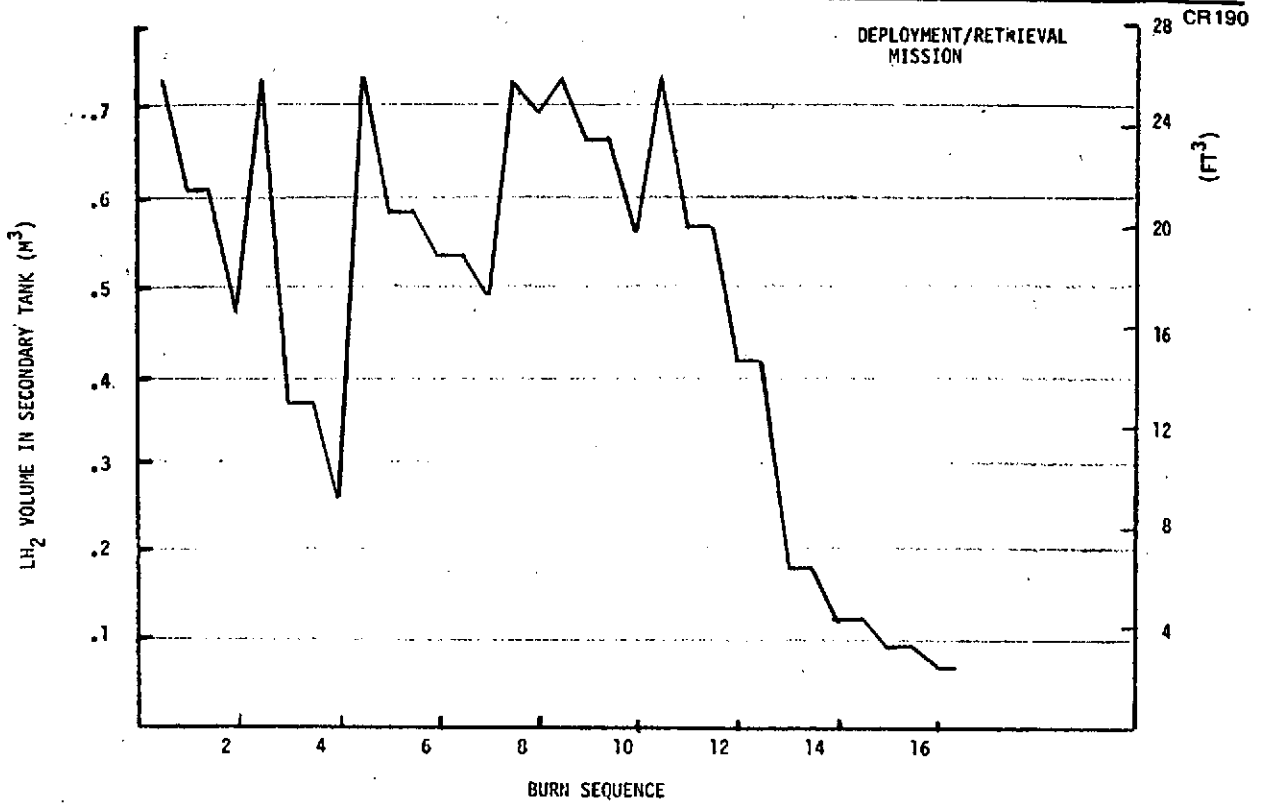
Figure 4.1.2. Secondary LH$_2$ Volume During Mission (Dynamic Refill)
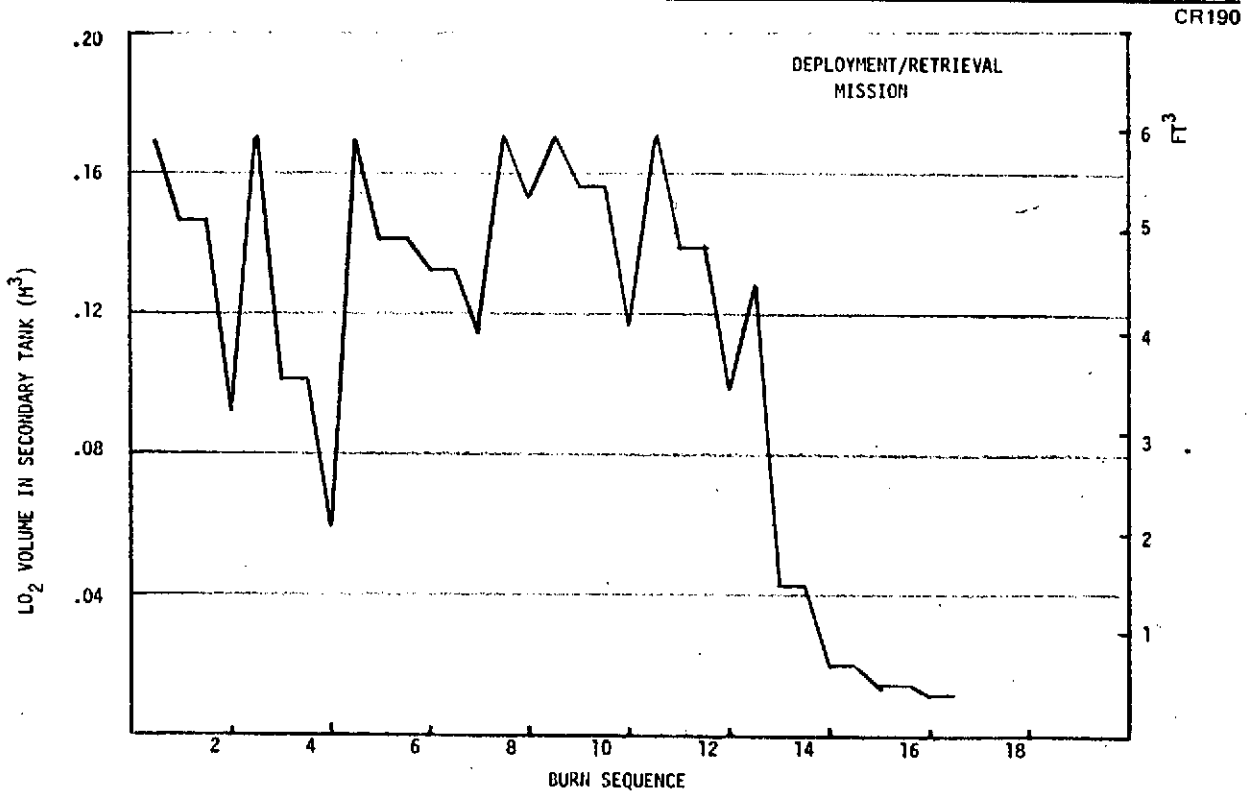
Figure 4.1.3. Secondary Tank LO$_2$ Volume During Mission — Dynamic Refill
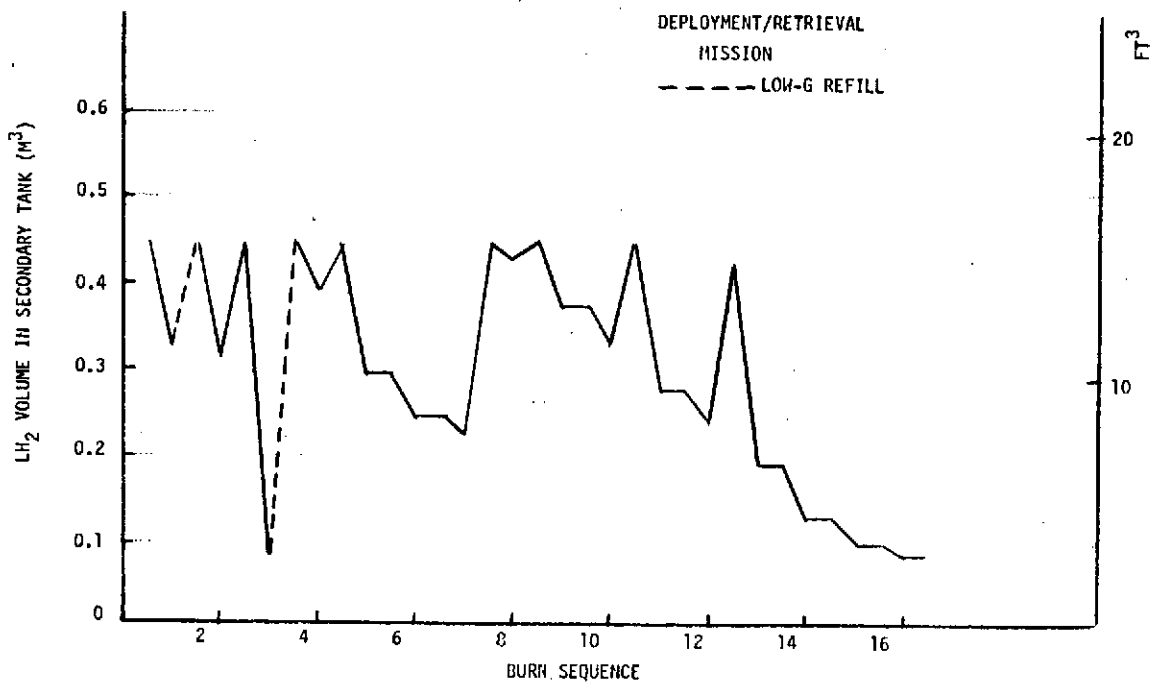
Figure 4.1.4. Secondary Tank LH$_2$ Volume During Mission — Vacuum Vent/Refill
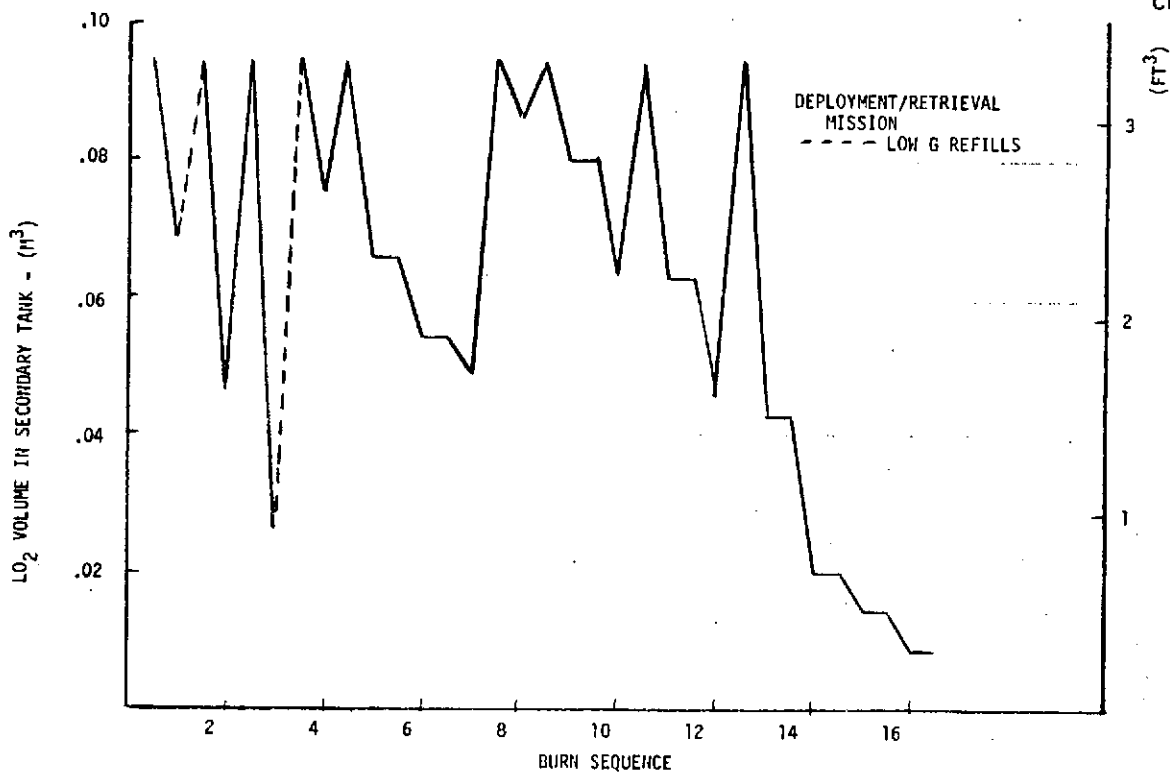
Figure 4.1.5. Secondary Tank LO$_2$ Volume During Mission — Vacuum Vent/Refill

Figures 4.1.4 and 4.1.5 apply to the vacuum vent/refill concept. The corresponding secondary tank volumes are 0.48 m^3 (17 ft^3) and 0.096 m^3 (3.4 ft^3) for LH$_2$ and LO$_2$, respectively. The vacuum vent/refill capability allows the secondary size to be minimized since refill is accomplished in zero g prior to high acceleration burns. However, based on results of the CSS/APS study this size reduction would not make a significant difference in the overall system and the vacuum vent/refill technique was not considered further.

The curves of Figures 4.1.2 through 4.1.5 should be interpreted as follows. For each burn sequence, the secondary tank volume is shown decreasing from its initial volume to some minimum volume. For the RCS maneuvers, there is no dynamic refill, and therefore at the end of the burn, the minimum and final tank propellant volumes are equal, as denoted by the short horizontal line connecting to the next burn sequence. For primary propulsion system burns, there is sufficient time to settle the propellant in the main tank and refill the secondary tank. In these cases, the liquid level drops to a minimum volume, refill is initiated, the secondary tank is completely refilled, and propellant flow from the main to the secondary tank and then to the engines is continuously maintained for some period following refill. For the mission shown, refill is accomplished in periods of the order of 10 seconds, whereas all continuous engine burns are maintained for at least several minutes.

Selection of the secondary tank size and configuration requires that the minimum liquid level not be permitted to drop below a critical level associated with a retention safety factor of 2.0, under conditions corresponding to the maximum total flow loss. This can be achieved by compartmentizing the secondary tank with each compartment having its individual screen elements of selected size so that all breakdown criteria are satisfied. This arrangement is shown schematically in Figure 4.1.6.

The system design illustrated in Figure 4.1.6 is divided into three regions: a top region, a primary trap region, and a secondary trap region. The primary screen channels directly connected to the outlet line as located beneath the primary screen/baffle. Near the circumference of the primary screen/baffle are a series of liquid communication screen channels. It should be noted that the maximum hydrostatic head associated with each of the channels is determined by the maximum g-level applied and the height of these channels measured along the vehicle axis. Two separate channels are used, rather than one set of primary channels which reach the same level as the communication channels; this reduces the hydrostatic head. Since it is assumed that the 134 N (30 lb) thrust RCS maneuvers result in the acceleration being applied in an arbitrary direction, the effects of lateral accelerations are also considered in the design. However, even with the relatively large effective height (i.e., approximately 2 meters) associated with lateral accelerations, the hydrostatic head imposed across the set of channels is very much smaller than that imposed along the vehicle axis during the primary propulsion system burns.

Figure 4.1.7 shows the conceptual design for the acquisition subsystem to satisfy the criteria established above and the mission requirements for the deployment/retrieval mission summarized in Table 2.7.
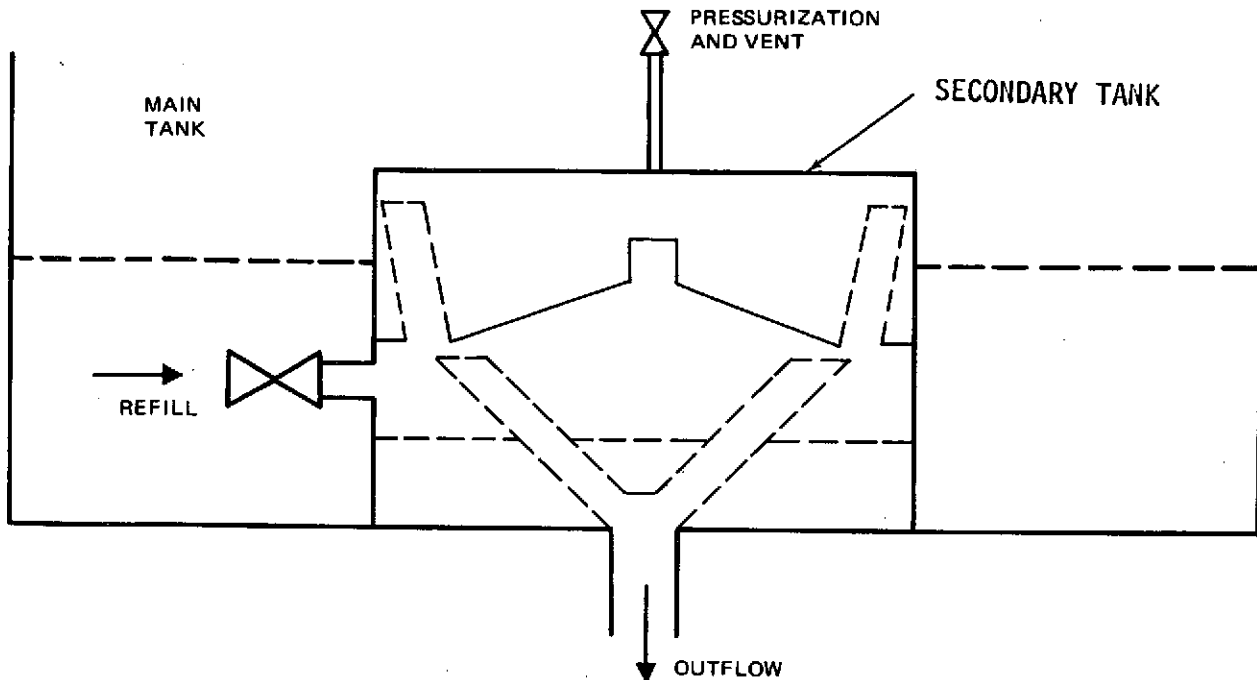
Figure 4.1.6. ASPM Secondary Tank Schematic

The secondary tank thermal management system consists of foam insulation on the top of the common dome and a heat interception shield situated along the bottom of the tank. This provides thermal protection of the screen devices and allows integration of the main secondary structure. The main tank screen retains some liquid in the bottom of the main tank above the secondary tank to minimize settling time and heat transfer to the start tank. Thermodynamic vent system coils attached to the shield are routed around local areas of high heat flux, such as the feedline connection, or across the top of the secondary tank beneath the foam insulation, to further decrease any heat transfer into the secondary tank.

The configuration shown in Figure 4.1.7 minimizes the hydrostatic head, and therefore provides high retention safety factors with relatively coarse mesh screen. A screen/baffle is depicted at the main tank sump to minimize vapor pull-through and vortex motion of the propellant. The screen also forms a barrier against bubble entrainment during the refill operation. The refill line and valve are located outside the main tank for access during checkout and refurbishment. However, the valve and line could be located inside the main tank/start tank to minimize heat transfer through the main feedline and the refill valve.

To demonstrate the adequacy of the concept shown in Figure 4.1.7, the conditions corresponding to each burn sequence for the retrieval/deployment are described chronologically below.

COMMON DOME

CYLINDRICAL
SCREEN ELEMENTS

VENT

TOP REGION

PRIMARY TRAP

SECONDARY TRAP

REFILL VALVE

COOLED SHIELD
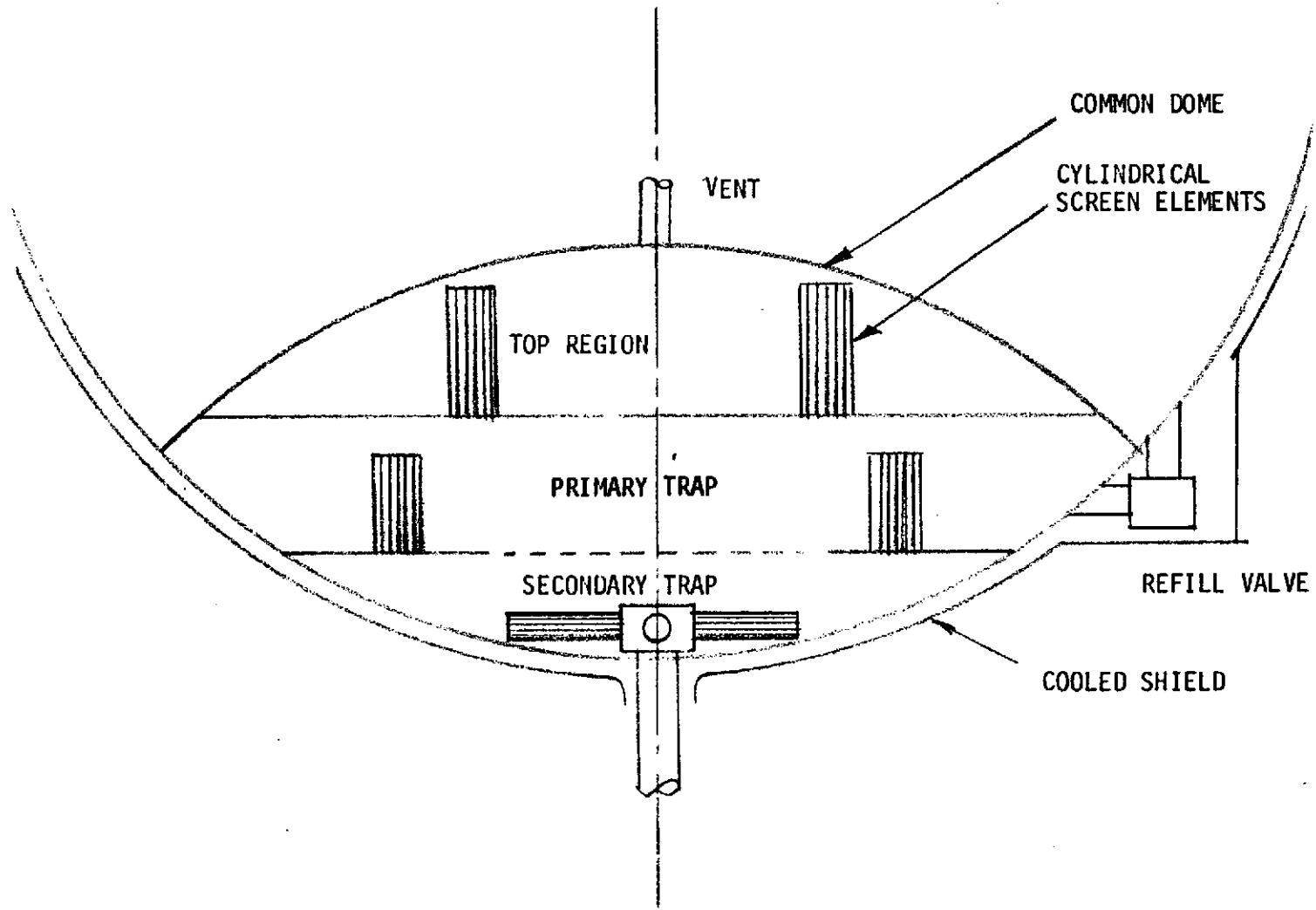
Figure 4.1.7. ASPM Acquisition Subsystem Conceptual Design

Referring to Table 2.7, it is seen that burn sequence 1 involves a RCS maneuver to separate the ASPM from the Shuttle Orbiter. In all cases, the secondary tank is assumed to be full of liquid during the boost into orbit to avoid any possibility of screen failure due to high launch loads, vibrations, or handling of the ASPM during preparation for separation. For the first burn, Figure 4.1.2 shows that the LH_2 volume drops from 0.735 m^3 (26 ft^3) to approximately 0.62 m^3 (22 ft^3) at a flow rate of 0.27 kg/sec (0.59 lb/sec) and an acceleration level of 0.00093 g's. Liquid flows from the top region through the communication channels to the primary regions, and from these through the primary screen channels to the feedline. At the end of the first burn, the secondary tank ullage of 0.113 m^3 (4 ft^3) would occupy the top region of the device. Since, as a conservative design require-ment, the orientation of the acceleration during this burn sequence is assumed to be in any direction 0.255 m^3 (9 ft^3) of LH_2 would remain above the primary and secondary trap regions, which retain the remaining propellant. It is necessary at this point that the communication channels be long enough to at least reach the remaining 0.255 m^3 (9 ft^3) of LH_2 in the top region.

The second burn involves the primary propulsion system with a flow rate of 1.34 kg/sec (2.955 lb/sec) and an acceleration of 0.154 to 0.263 g. Assuming a worst-case condition, propellant would be located at the top of secondary tank and initially would be transferred to the primary trap region through the communication channels. After a few seconds, settling of this liquid would occur and thus flow into the primary trap region would also occur through the primary screen. When the secondary tank LH_2 volume reaches 0.467 m^3 (16.5 ft^3), refill is initiated. After approximately 10 to 12 seconds, the secondary tank is refilled and flow is continued for approximately 1,300 seconds.

Note that the refill inlet to the secondary tank enters the primary trap region, above the secondary screen. During refill, liquid flows into the primary region and bubbles rise to the top of the conical bulkhead which supports the communication screen channels and the primary trap region vent screen. Gas passes through these screens during the overboard vent operation, but a small amount of gas will be entrapped when the combined effects of hydrostatic head and drag forces due to flow through the screen exert insufficient pressure to cause breakthrough. Although this refill pro-cedure is satisfactory, an improvement was evolved and is discussed in Section 4.1.2.

The third burn sequence is another RCS maneuver which drops the LH_2 volume to 0.360 M^3 (13 ft^3) at a g-level of 0.00158 to 0.00159 and a flow rate of 0.0085 kg/sec (0.0187 lb/sec). The top region is emptied of all propellant during this maneuver.

The fourth burn involves the primary propulsion system. Initially, all liquid is contained in the primary and secondary trap regions. The initial g-level is 0.265 g and thus the communication channels can easily be designed to support the hydrostatic head. However, breakdown could occur in the communication channels without in any way adversely affecting the propellant retention, since liquid is settled beneath the primary screen/baffle. After approximately 0.113 M^3 (4 ft^3) of LH_2 has been transferred to the engine, leaving 0.071 m^3 (2.5 ft^3) in the primary trap region, the refill valve is opened and the secondary tank refilled. At the initiation of

refill, the acceleration imposed is still approximately 0.265 g, but since flow is maintained for approximately 575 seconds, the vehicle mass is decreased, resulting in an increase in acceleration level to 0.383 g. The primary screen channels must be capable of supporting approximately 10.1 cm (4 inches) of LH_2 at 0.265 g with a retention safety factor of 2.0 or greater; this is not the most critical condition and therefore has no impact on screen selection.

Burn sequence 5 is an RCS maneuver which removes approximately 0.141 m^3 (5 ft^3) from the top region. This is followed by the sixth burn, another RCS maneuver, which removes an additional 0.0565 M^3 (2 ft^3) of LH_2, leaving 0.17 m^3 (6 ft^3) in the top region. The seventh burn sequence involves the throttled primary propulsion system with an acceleration of 0.079 g at a flow rate of 0.272 kg/sec (0.6 lb/sec). The secondary tank LH_2 volume drops from 0.537 m^3 (19 ft^3) to 0.48 M^3 (17 ft^3) and refill is initiated.

The communication screen channels can easily be designed to support approximately 15.2 cm (6 inches) of LH_2 at 0.079 g, but again there is no adverse effect resulting from their breakdown, since propellant is settled and the secondary tank completely refilled prior to the following zero-g coast. The total burn time for this maneuver is 40 seconds. The refill time is 7 seconds, and the settling time is approximately 12 seconds. Burn sequence 8 also involves a throttled primary propulsion system burn at 0.079 g and 0.272 kg/sec (0.6 lb/sec) of LH_2. The burn time, refill time, and settling time are equal to those for the preceding burn.

Burn sequence 9 is an RCS maneuver which removes 0.071 M^3 (2.5 ft^3) of LH_2 from the top region.

A design modification should be noted at this point. The total LH_2 expelled in the preceding three burns is approximately 0.41 M^3 (14.5 ft^3), whereas the secondary tank initially contained 0.837 M^3 (19 ft^3). With a start tank size of 0.735 M^3 (26 ft^3), it would not be practical to accomplish the three preceding burns with no refill during the throttled primary propulsion burns, since only 0.127 M^3 (4.5 ft^3) of propellant would remain in the tank, and the secondary trap region must hold approximately 0.184 M^3 (6.5 ft^3) of propellant to accomplish the very last burn sequences. However, by increasing the secondary tank size from 0.735 M^3 (26 ft^3) to 0.85 m^3 (30 ft^3), the two throttled primary propulsion burns, followed by the RCS maneuver, could be accomplished without refill. The increase in tank size is small enough not to significantly affect the screen breakdown criteria, whereas the pressurization weight penalty is decreased by avoiding two tank prepressurizations. In addition, the sequencing requirements for the refill valves, tank prepressurization, and start tank venting are decreased. Finally, a larger start tank, although slightly heavier, has a greater mission flexibility.

At this point, the dynamic refill design based on refill during throttled as well as full thrust primary propulsion system burns will be assumed.

The tenth burn accomplishes deorbit and involves the primary propulsion system. The LH_2 volume is reduced from 0.66 M^3 (23.5 ft^3) to 0.565 M^3 (20 ft^3) at which time refill is initiated. The acceleration level imposed

prior to refill is approximately 0.395 g and thus breakdown of the communication screen devices does not occur, although breakdown could occur without affecting the mission. The total burn time is approximately 387 seconds, the refill time is 9 seconds, and the settling time is 5.5 seconds. Again, the refill time is a small part of the total burn time.

Burn sequence 11 is another RCS maneuver which decreases the LH$_2$ volume to 0.565 M^3 (20 ft^3).

In all of the previous burns, there is no combination of liquid volume, liquid position, flow rate, acceleration level, or direction which constitutes a problem from the standpoint of the screen device design. The important screen device sizing criteria are determined from the following burn sequences.

Burn sequence 12 involves the primary propulsion system at an initial acceleration of 0.572 g. The liquid volume decreases from 0.565 M^3 (20 ft^3) to approximately 0.41 M^3 (14.5 ft^3) immediately prior to initiation of refill. The primary screen channels can be designed to support approximately 20.2 cm (8 inches) of LH$_2$ at 0.572 g with a retention safety factor greater than 2.0. However, as before, breakdown of the communication channels at this time poses no problem. The settling time for this burn sequence is 5.7 seconds, the refill time is 9 seconds, and the total burn time is 328 seconds. All remaining propellant [0.41 M^3 (14.5 ft^3)] is now contained in the secondary tank.

Burn sequence 13 is the final high-thrust primary propulsion system burn. The top region is emptied into the primary region, and the primary trap region is nearly emptied, leaving over 0.17 M^3 (6 ft^3) of the propellant in the secondary tank. The primary screen channels must support a maximum of approximately 10.1 cm (4 inches) of LH$_2$ at 1.04 g without breaking down. Since the acceleration is positive, the only adverse pressure to be considered during this period is hydrostatic head. Thus, a 200 x 600 or 165 x 800 mesh screen, each of which supports approximately 25.4 cm (10 inches) of LH$_2$ at 1 g, would be sufficient, yielding a retention safety factor greater than 2.0.

Burn sequence 14 involves throttled primary propulsion system with a LH$_2$ flow rate of 0.272 kg/sec (0.6 lb/sec) and a maximum acceleration of 0.21 g. The liquid volume drops to approximately 0.113 M^3 (4 ft^3), exposing the primary screen channels to a maximum of 15 to 20 cm at 0.21 g. This condition is easily met by the 200 x 600 or 165 or 800 mesh screens, with a retention safety factor of approximately 6.

The two remaining burn sequences are both RCS maneuvers which involve no appreciable flow loss and hence no retention safety factor design problems.

a. Alternate Mission Requirements. The acquisition sub-system design generated above was based on the deployment/retrieval mission summarized in Table 2.7.

Through consultation with personnel in the MDAC Space Tug/OOS system design group, three other missions were identified and critical information was then generated for each of these. The new missions included a deployment, a retrieval, and an interplanetary launch. These complemented the baseline deployment/retrieval roundtrip mission. Pertinent data for these mission duty cycles are summarized in Section 2. These missions are similar to one another and to the baseline in their general sequence of events and arrangement and magnitudes of the various burns. All three new mission time periods are shorter than the baseline period. Because of the manner in which payload is handled, the maximum acceleration varies for the different missions, going as high as 1.64 g in the case of interplanetary missions.

These duty cycles were used in conjunction with the MDAC acquisition device sizing program to generate secondary tank size and other design values for each mission. The size results are summarized in Table 4.1.1. The first three sets of sizing values apply to the baseline roundtrip deployment/retrieval mission. The first set of size values is that directly generated by the computer program and is essentially based on volume usage demands with no influence of screen retention limits. The second set of sizing numbers shows the adjusted baseline values with the secondary tank size increased to prevent the liquid level from dropping to the point where screen retention breakdown might be possible during the burn sequence. The third set of values is the baseline size adjusted so that a fixed settling time can be used which would permit the use of a simple fixed start-up control logic. The resulting volumes are 0.952 m^3 (33.6 ft^3) for LH$_2$ and 0.244 m^3 (8.6 ft^3) for LO$_2$. The last three sets of sizing numbers which apply to the other three duty cycles, are the volumes directly computed from the sizing program. The results from Table 4.1.1 and supporting retention-head analyses show that the baseline roundtrip mission results in the largest volume secondary tank, and its size is therefore compatible for the other missions considered.

Table 4.1.1

ASPM SECONDARY-TANK SIZES

	Start-Tank Volume m^3 (ft^3)	
	Fuel	Oxidizer
1. Baseline (Round Trip)	0.518 (18.3)	0.119 (4.2)
2. Baseline (Adjusted Size)	0.762 (26.9)	0.173 (6.1)
3. Baseline (Fixed Settling Time)	0.952 (33.6)	0.244 (8.6)
4. Direct Deployment	0.504 (17.8)	0.105 (3.7)
5. Direct Retrieval	0.49 (17.3)	0.104 (3.7)
6. Interplanetary	0.241 (8.5)	0.065 (2.3)

4.1.2 Preliminary Design

a. LH2 System. The operation of the ASPM acquisition design is discussed in Section 4.1.1 along with the development of a conceptual design. This concept was then detailed to evolve the preliminary design shown in Figure 4.1.8.

The ASPM LH2 acquisition design is divided into three regions: a top region, a primary trap region, and a secondary trap region. The screen tubes in the top region communicate propellant to the primary region under all propellant configurations encountered in the low-g or high-g level conditions. The primary screen tubes are designed to retain liquid under the worst-case conditions which correspond to a high positive g level (e.g., 1.6 g) under maximum propellant outflow.

Since it is assumed that the 134 N (30 lb) thrust RCS maneuvers result in the acceleration being applied in an arbitrary direction, the effects of lateral accelerations are also considered in the design. However, even with the relatively large effective height (i.e., 1 meter) associated with lateral acceleration, the hydrostatic load imposed across the set of channels is much smaller than that imposed along the vehicle axis during the primary propulsion system burns.

Comparison of Figure 4.1.7 and 4.1.8 shows several minor differences. The design in Figure 4.1.8 has a flat plate supporting the communication screen tubes, not a conical plate, and there is no separate provision for a vent screen. Instead, during the secondary tank vent/refill operation, gas passes from the primary trap region through the screen tubes in the top region until, as before, the combination of hydrostatic head and drag forces exerted on the gas is insufficient to drive it through the screens into the top region. The volume of gas entrapped, even if the screen tubes were essentially filled with gas, is negligible compared to the primary trap region volume (i.e., 5 percent). Special provision for venting all of the gas from the primary trap region was therefore considered unnecessary. Another design modification is that the screen tubes in the primary trap region are separate from the screen tubes in the secondary trap region. This change diminishes the total hydrostatic head supported by the primary trap region screen tube, and in addition, the secondary trap region screen tubes have no opportunity for retention failure since they are never exposed to gas. Therefore, effects of engine startup and shutdown pressure transients will be strongly attenuated on passing through the secondary trap region screens, and the possibility of breakdown is greatly diminished.

Consideration of Figure 4.1.8 reveals that all of the screen devices can be installed by one man with access through a conventional manhole. The screen tubes in the top and primary trap regions are placed in the tank and bolted into place. A compatible metallic seal would be used. The flat screen element, perhaps temporarily supported by flat stock, is then placed into position and bolted into place, and its temporary support removed. The manhole cover, containing the four additional screen tubes connected directly to the sump, is then brought into position and sealed. The feed line can then be joined to the tank with a Marman flange.

FLANGE
PRESS & VENT
LEVEL SENSOR - CAPACITANCE

COMMON DOME

SCREEN TUBE (PLEATED) (8-TYPICAL)

HIGH PRESSURIZATION HELIUM

(2000 PSIA)

PLATE
SCREEN (PLEATED)
SCREEN TUBE (PLEATED) (8-TYPICAL)
BAFFLE

41.3 R

28 ft³

SUMP

TOP REGION (16.8 FEET³)

REGULATOR
TO LO₂ START TANK

12 IN. R

SOLENOID VALVE

PRIMARY TRAP REGION
(10.8 FEET³)

11 FT³

6.5 FT³

VISCOJET

17 IN. R

PRESS & VENT
COMPONENTS

SECONDARY TRAP
REGION

VENT VALVE

FLANGE

SCREEN TUBE (PLEATED)

DIFFUSER

PORT FOR SCREEN TUBE

REVILL VALVE

MARMAN FLANGE

FEED LINE

35.1 IN.

Figure 4.1.8. ASPM LH₂ Acquisition System Preliminary Design

The secondary tank pressurization system as shown in Figure 4.1.8 consists of a helium bottle, a 500-psi regulator, two solenoid valves, a high flow rate orifice and a low flow rate orifice (e.g., VISCO jets). Two separate pressurization rates are used because of the low RCS flow rates and the high flow rates associated with the main engine operation. Cold helium is used of course to prevent thermal induced screen retention failure.

A capacitance probe liquid-level sensor is included as a backup determination of the propellant quantity. The probe would be used in conjunction with a timed circuit to control the secondary tank refill.

b. Acquisition Screen Selection. With the conservative LH_2 secondary tank volume associated with a fixed settling time, the appropriate sizing and placement of the screen tubes was determined, which meets the requirements of a retention safety factor (RSF) of at least 2.0. The tank configuration has also been selected to minimize the dome weight. This in turn affects the placement, length, and mesh size of the screen tubes. Figure 4.1.9 shows the generalized geometrical relationships for the secondary tank design based on a design volume of 0.95 m³ (33.6 ft³). A preliminary study was conducted to determine the tank structural-weight penalty including the common dome (isogrid) weight and the main-tank dome weight increase to accommodate load distribution at the bulkhead juncture. This is shown in Figure 4.1.10 which illustrates that the weight penalty decreases as the total secondary-tank height increases. Thus, it is desirable to use a smaller radius on the common dome than on the main-tank dome (maintaining constant volume). However, going beyond a total height of 0.7 m results in only a minor weight savings. (This corresponds to a secondary-tank diameter of 1.8 m.) Also, increasing height either limits retention-head capability or requires a finer screen mesh. The change from 0.56 to 0.7 m necessitates only a slight change in mesh size and does not have a significant impact on the acquisition device design or its overall capabilities.

The baseline system was originally designed to use relatively coarse mesh screens (200 x 600). Such screens were found to be adequate for the accelerations encountered in the baseline mission with a main-engine thrust of 44,500 Newtons (10,000 lb). However, thrust levels of 66,700 Newtons (15,000 lb) or even 89,000 Newtons (20,000 lb) have been discussed in independent studies. (Reference 3). Increases in acceleration level above those previously reported have resulted with the additional missions considered. The maximum acceleration is 1.64 g, assuming a 44,500 Newtons (10,000 lb) thrust engine for the Interplanetary Mission. The secondary tank size and configuration selected above is compatible with all of these missions.

The appropriate screen mesh has been increased to 200 x 1,400, instead of 200 x 600, to meet broader mission requirements with the higher accelerations (1.64 g).

Considering the overall design shown in Figure 4.1.8, the primary screen tube and flat screen between the primary and secondary trap regions is seen to be the critical region for flow-loss calculations. The flow losses associated with the primary trap region are composed of hydrostatic head and pressure drop through the screen, with the propellant flowing through
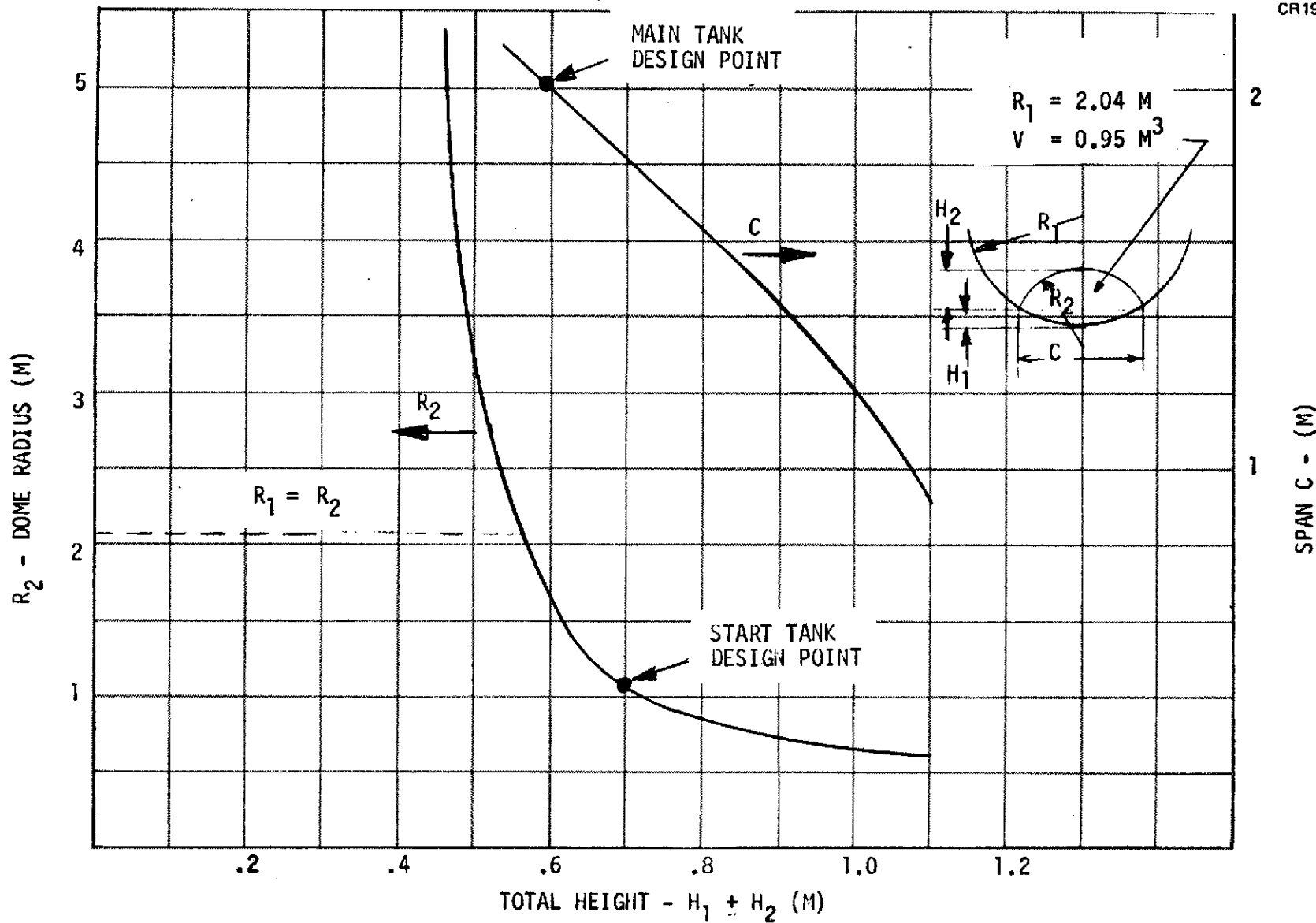
Figure 4.1.9. Secondary Tank Geometrical Relationships (ASPM LH$_2$ Tank)
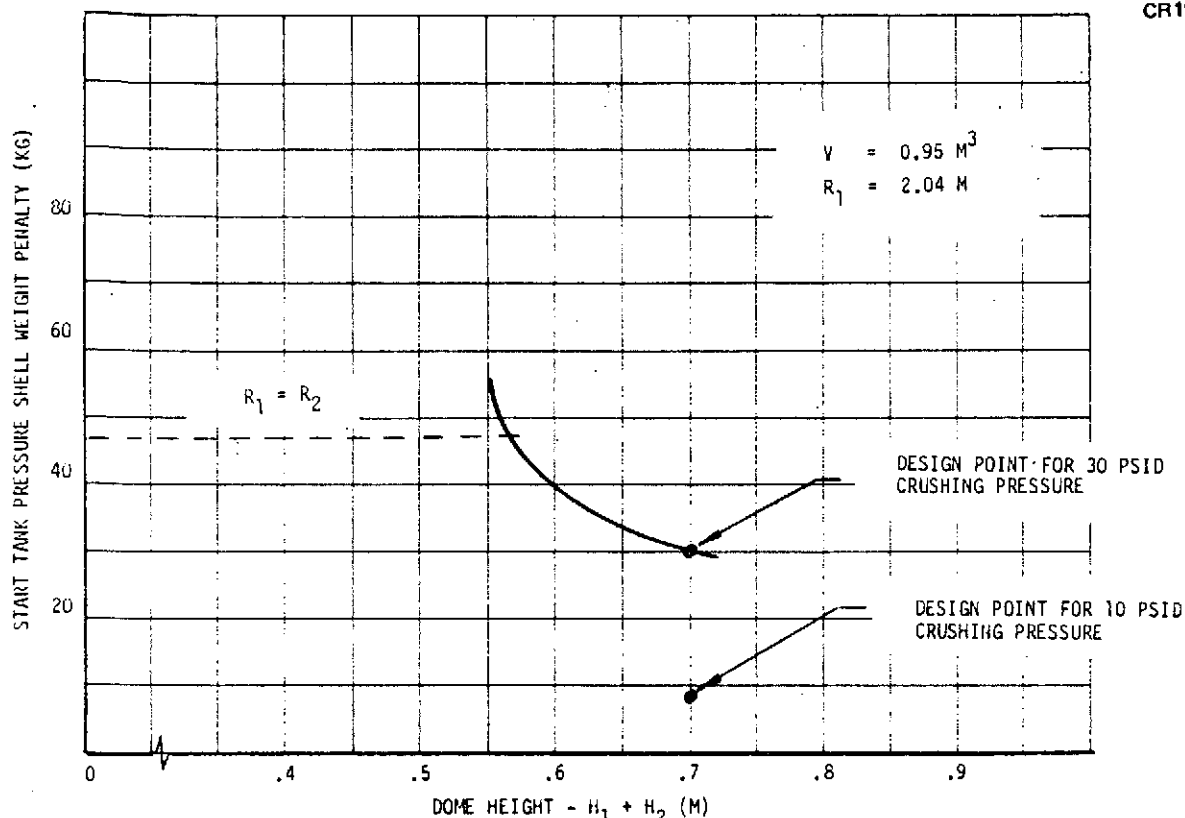
Figure 4.1-10. Secondary Tank Structural Weight Penalty (ASPM LH$_2$ Tank)

the screen at 1.64 g. The LH$_2$ volume flow rate is 0.0213 M^3/sec (0.75 ft^3/sec). The flat screen is assumed to be pleated with a factor of three in area; the screen diameter is 0.71 M (28 in.). Eight pleated screen tubes with a pleating factor of three, two inches in diameter and five inches long, are used. Pleating tests reported in Volume II, Section 2.A.3 indicated that the plating concept was acceptable both from a bubble point and flow-loss considerations. The hydrostatic head is based on a submerged depth of 6.35 cm (2.5 in.)., which is conservative compared to the operating conditions. The pressure drop due to flow loss through the screen tubes and the flat screen is 46.7 N/M^2 (0.975 lb/ft^2). The hydrostatic head is 93.1 N/M^2 (0.95 lb/ft^2). The total pressure loss is 140 N/M^2 (2.925 lb/ft^2). With 200 x 1,400 mesh screens, having a bubble point of 335 N/M^2 (7.0 lb/ft^2), the retention safety factor is 2.4. This design is flexible in several ways in terms of providing increased capability. The pressure drop through the screen can be decreased by increasing the pleating factor to 4, increasing the number of screen tubes, and increasing the flow area of the flat screen. An increased hydrostatic head requirement due to an increase in the vehicle acceleration from 1.6 to 3.2 g could be met by use of a finer mesh screen.

Based on the hydrostatic head associated with the low-g levels of the RCS system, and the negligibly small pressure drops due to flow, very coarse mesh screens (30 x 30) would be workable. However, extraneous impact acceleration may be present as a result of docking, etc., which implies the need for finer mesh screens. One such impact acceleration has been estimated based on a typical ASPM docking mechanism.

The Space Tug docking mechanism described in subsection 4.2.2.5 of the NASA-MSFC Baseline TUG Definition Document, Rev A, June 26, 1971, consists of a square frame supported by eight pneumatic/hydraulic shock absorbers/actuators. During docking, the frame moves from its deployed position to its retracted position, a distance of 1.18 M (46.3 in.), absorbing the docking impact energy. The maximum approach velocity prior to docking is 0.305 M/sec (1.0 ft/sec). Thus, during docking the acceleration on the vehicle could be of the order of 0.004 g. This allows for nonlinear deceleration during docking and additional effects of misalignment and lateral motion which would increase the maximum acceleration imposed on the screen devices. Therefore, even though a 30 x 30 mesh screen is adequate to maintain retention during the 0.005-g acceleration, a finer mesh screen is recommended to avoid any change of breakdown due to docking. There are no adverse affects in using a finer mesh screen, such as 50 x 250 or even 165 x 800, and the retention capability is increased by a factor of 10 or more over the 30 x 30. Thus, a screen such as the 50 x 250 or 165 x 800 will be used.

c. Secondary Tank Weight. The LH_2 secondary tank weight was determined, including components, screens, the common dome, and an access manhole.

The LH_2 secondary tank dome weight has been estimated, assuming a spherical isogrid tank shell welded to the main-tank dome. The weight of the isogrid has been determined, based on the curves of Reference 12 for a crushing pressure of 69 x 10^3 and 207 x 10^3 N/M^2 (10 and 30 psid). The welded joint weight has also been estimated for these two cases; results are shown in Table 4.1.2. To use the lower weights associated with the lower pressure, a relief valve must be used to assure that the secondary-tank pressure does not fall more than 69 x 10^3 N/M^2 (10 psi) below the main-tank pressure. Under normal operating conditions, the secondary-tank pressure would be less than 13.8 x 10^2 N/M^2 (2 psi) below main-tank pressure, and there is no requirement to penalize the tank dome weight by unnecessarily high pressure loads. The 69 x 10^3 N/M^2 (10 psid) is thus considered to be conservative.

Accessibility provisions were also studied. Using a conservative manhole weight penalty of 23 kg/m of diameter, the weight of 0.81 m (32 in.) diameter manhole would be 18 kg. This would provide good access to the secondary tank interior. Integration of the tank manhole flange buildup and the beef-up zone on the main-tank bottom is probably not advisable since undesirable seal loadings may be encountered. If the complete secondary tank were to be removed, the manhole would have to be placed above the dome intersection at a diameter of about 2.13 m (7 ft). This would weigh approximately 49 kg, which is 31 kg heavier than the smaller access hatch in the main-tank bottom. Thus, the common dome will be welded into the main tank and a tank-bottom manhole will be used for secondary tank access.

The weight of the screen tubes has been determined, assuming that each is composed of a support screen, (e.g., 10 x 10 mesh, 0.028 inch wire) fittings (as shown in Figure 4.1.8) and the appropriate mesh screen (200 x 1,400) for primary screen tubes and 200 x 600 for top and secondary trap region screen tubes); a pleating factor of 3.0 is used. The flat screen element is formed from pleated 200 x 1,400 stainless steel screen 0.782 kg/M^2 (0.16 lb/ft^2) with a bolted flange-type fitting 2.54 cm wide and

Table 4.1.2

LH$_2$ SECONDARY TANK DOME WEIGHT

Item	Weight	
	(kg)	(lb)
Spherical Isogrid Dome (10 psid)	5.2	(11.5)
Welded Ring (10 psid)	4.0	(8.8)
Total	9.2	(20.3)
Spherical Isogrid Dome (30 psid)	10.5	(23)
Weld Ring (30 psid)	20.0	(44)
Total	30.5	(67)

0.25 cm thick. The top and bottom plates are ribbed aluminum with nominal thickness of 0.0635 cm (0.025 in.). The flat screen is pleated with an area factor of 3.0. These weights are summarized in Table 4.1.3.

d. LO$_2$ System. The acquisition system for the LO$_2$ tank is identical in operation and design concept to that for the LH$_2$ tank and the preliminary design was approached in the same manner. The preliminary design with a 0.244 M^3 (8.6 ft^2) secondary tank is detailed in Figure 4.1.11 and weights are summarized in Table 4.1.4.

Table 4.1.3

ASPM LH$_2$ TANK ACQUISITION SYSTEM WEIGHTS

Item	Weight	
	(kg)	(lb)
Pressure Shell (Common Dome, Spherical Isogrid, Crushing ΔP = 10 psid)	9.2	(20.3)
Access Manhole Penalty (32-in. ID, Plus Bolts)	18.0	(40.0)
Top Region Stainless Steel Screen Tubes (8)	2.2	(4.7)
Primary Region Stainless Steel Screen Tubes (8)	1.6	(3.5)
Secondary Region Stainless Steel Screen Tubes (4)	0.6	(1.3)
Stainless Steel Flat Screen	2.6	(5.8)
Aluminum Top Plate (Nominal 0.025-in. Thick)	3.7	(8.0)
Aluminum Bottom Plate (Nominal 0.025-in. Thick)	1.2	(2.8)
	39.1	(86.4)
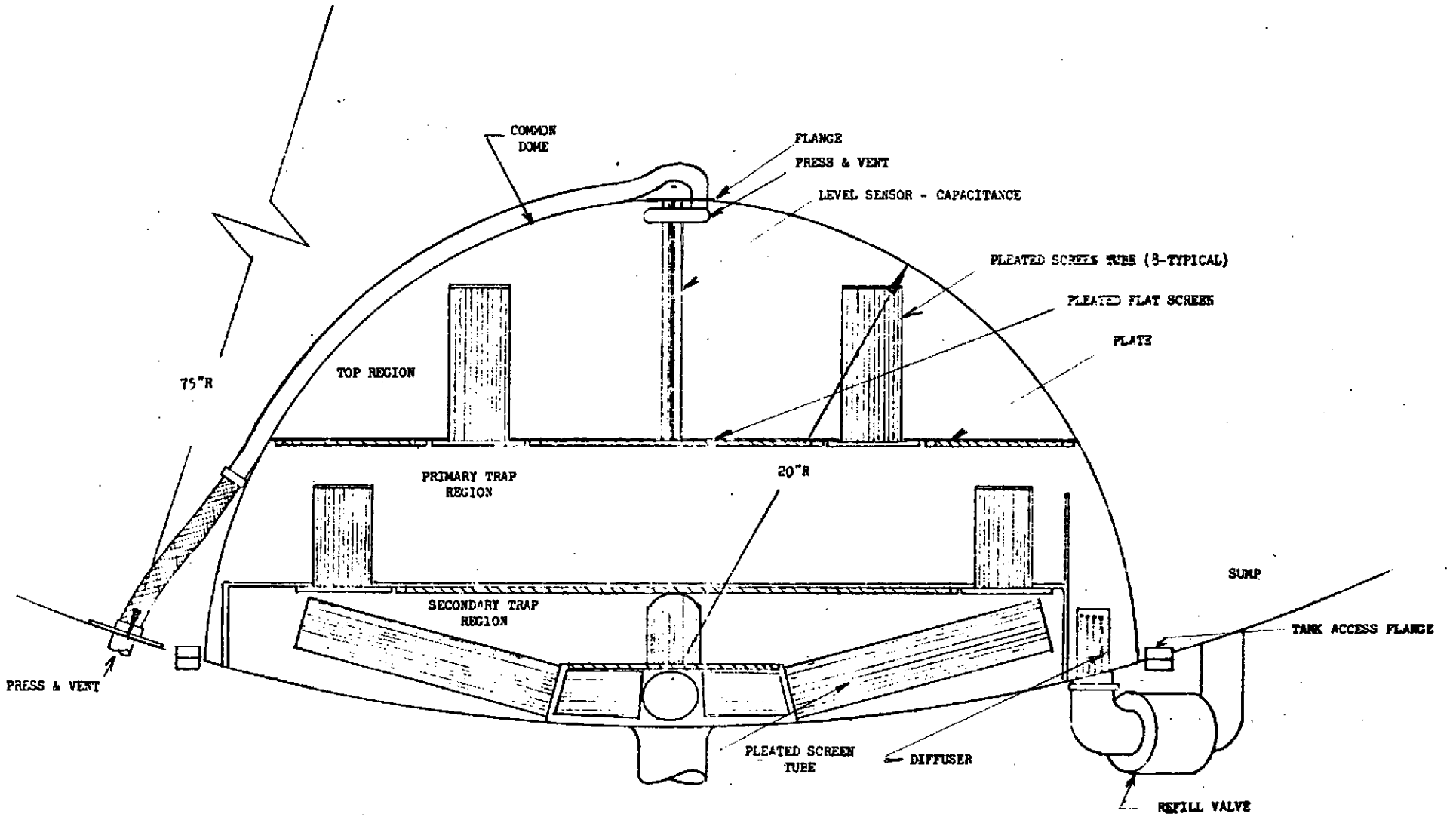
Figure 4.1.11. ASPM LO$_2$ Tank Acquisition System Preliminary Design

Table 4.1.4

ACQUISITION SYSTEM WEIGHT - ASPM LO$_2$ TANK

	kg	(lbs)
Pressure Shell (ΔP = 10, R = 18")	4.08	9
Manhole	22.70	50
Top Screen Tubes	2.27	5
Middle Screen Tubes	2.09	4.6
Bottom Screen Tubes	1.22	2.7
Flat Screen	2.32	5.1
Al. Top Plate	5.45	12.0
Al. Bottom Plate	2.73	6.0
Al. Cyl. Support for Bottom Plate	.91	2.0
Refill Diffuser	.91	2.0
	44.68	98.4

4.2 Pressurization System

As discussed in Section 4.1, a basic refillable pressure-isolated surface tension acquisition system has been selected for the ASPM application. A LH$_2$ secondary tank size of 0.95 m^3 (33.6 ft^3) was also defined. With this size and the baseline duty cycle, the overall LH$_2$ tank pressurization system was analyzed. This included the pressurization of the secondary tank with cold gaseous helium and pressurization of the main tank with 111°K (200°R) GH$_2$. This inlet temperature was arrived at from the optimization reported in Section 3.2.2. The various weight elements are summarized in Table 4.2.1. Main-tank penalties include the effects of increased tank volume to accommodate the pressurants and increase in tank-wall thickness over minimum gage to withstand maximum tank pressure, 147 x 10^3 N/m^2 (22.3 psia). A 0.52 m (1.69 ft) diameter helium bottle will be required for the LH$_2$ side.

The LO$_2$ tank pressurization system was also analyzed assuming an LO$_2$ secondary tank volume of 0.244 m^3(8.6 ft^3) (based on values presented in Section 4.1). Main LO$_2$ tank pressurization calculations are summarized in Table 4.2.2 for a range of helium inlet temperatures. This table shows that pressurant weights are only slightly affected by the inlet temperature for the baseline ASPM duty cycle. However, the maximum tank pressure at low inlet temperatures does tend to increase over the minimum gage pressure level of 158 x 10^3 N/m^2 (23 psi). Therefore, it would be desirable to use an inlet temperature of about 222°K (400°R) that could probably be provided by a simple passive structural heat sink-type heat exchanger. The resulting weights are summarized in Table 4.2.3. If the LO$_2$ tank helium were stored in a separate high pressure bottle within the LH$_2$ tank, volume of 0.43 m^3 (1.53 ft^3) with a diameter of 0.44 m (1.44 ft) would be needed. In practice, the LH$_2$ and LO$_2$ tank helium supplies would be incorporated into a single

Table 4.2.1

ASPM LH$_2$ TANK PRESSURIZATION SYSTEM WEIGHT ESTIMATES
0.95 m^3 SECONDARY TANK VOLUME
34.5 x 10^3 N/M^2 TRUE NPSP CONTROL

	(kg)
Secondary Tank Usable Helium	8.4
Helium Residual	2.8
Helium Bottle and Supports	13.6
Main Tank GH$_2$	76.0
Main Tank Penalties	10.0
TOTAL	110.8

Table 4.2.2

INFLUENCE OF INLET TEMPERATURE
ON ASPM LO$_2$ TANK PRESSURIZATION

(0.244 m^3 SECONDARY TANK VOLUME)
(34.5 x 10^3 N/m^2 (5 psi) TRUE NPSP CONTROL)

Inlet Temperature (^{O}K)	Ullage Mass - (kg)	Helium Mass - (kg)	Maximum Tank Pressure 10^{3}N/m^2 (psia)
111	73	6.1	210 (30.4)
222	74	4.9	166 (24)
333	76	4.4	153 (22)

Table 4.2.3

ASPM LO$_2$ TANK PRESSURIZATION SYSTEM WEIGHT ESTIMATES
(0244 m^3 SECONDARY TANK VOLUME, 34.5 X 10^3 N/m2 TRUE NPSP
CONTROL, 222°K INLET TEMPERATURE)

	(kg)
Secondary Tank Helium	0.4
Main Tank Helium	4.9
Helium Bottle and Supports	8.5
Main LO$_2$ Tank GO$_2$	69.1
Main Tank Penalities	0.4
	83.3

high-pressure bottle. This would be 0.111 m^3 (3.93 ft^3) in volume with a diameter of about 0.61 m (2 ft) which is quite reasonable. This combined bottle would weigh about 22.1 kg including support provisions.

A GO$_2$ pressurization system for the LO$_2$ tank was also analyzed. In this case, the optimum inlet temperature was about 333°K (600°R) and the total system weight was estimated at 116.4 kg. This is about 33 kg heavier than the helium system and was, therefore, dropped from consideration.

4.3 Propellant Thermal Management

A propellant thermal management study was conducted for the ASPM in a similar manner to that conducted for the CSS/APS. This included consideration of both in-orbit and in-atmosphere operation. However, in the case of the ASPM, active cryogen storage during reentry and landing was not required except that the insulation had to be compatible with a reusability requirement.

4.3.1 In-Orbit Propellant Thermal Management. A detailed analysis of the basic in-orbit propellant thermal management concepts for the ASPM was conducted. Vehicle performance values in terms of stage gross weight were computed, using the MDAC multi-start space propulsion system sizing and optimization program (H109), for three options: (1) both nonvented LH$_2$ and LO$_2$ tanks; (2) both vented (to 102 x 13^3 N/M^2 (14.7 psi)) LH$_2$ and LO$_2$ tanks; and (3) a vented LH$_2$ tank and a nonvented LO$_2$ tank cooled by using GH$_2$ vent gases to intercept incoming heat. All calculations were made for the baseline duty cycle (Table 2.7 of Section 2) and are summarized in Figure 4.3.1. In the case of vented or cooled tanks, vapor-cooled shields

CR190
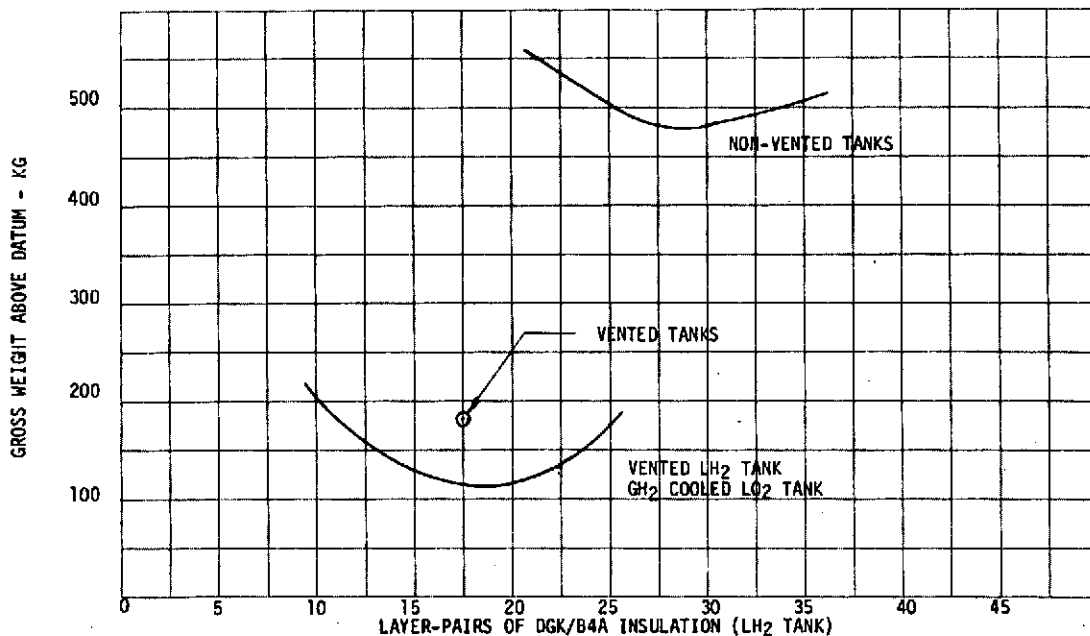
Figure 4.3.1. LH$_2$ Tank In-Orbit Insulation Optimization

were assumed and for locked-up nonvented tanks, internal mixers that would prevent temperature stratification were assumed.

Figure 4.3.1 shows that, for the ASPM application, a significant reduction in gross weight results by using vented and/or cooled tanks rather than a nonvented system. The optimum amount of insulation also shifts significantly for the various thermal management approaches. For nonvented tanks, the optimum LH_2 insulation consists of 30 pairs of DGK/B4A MLI and results in a gross weight above datum of 480 kg. With a vented LH_2 tank and a cooled LO_2 tank, the optimum LH_2 tank insulation is 18 layer-pairs of MLI and the gross weight above datum is 115 kg. Venting of the LO_2 tank rather than cooling results in a gross weight increase of 65 kg. Table 4.3.1 which lists the weights of the thermal management concept affected items provides insight into how the gross-weight changes come about. As shown in the table, the vented system results in a lighter burnout weight (by about 76 kg) but requires venting 80 kg of LH_2. However, the burnout weight has a stronger influence on stage performance (produced velocity change) than the boiloff loss which does not have to be accelerated for the full stage ΔV. Thus, less propellant is required to produce the needed ΔV with the vented tank approach. The 365 kg gross weight change is primarily a difference in required propellant mass. This strong impact of small inert weight changes on gross weight and the distinction between true inert and consummable weight illustrates the need for careful overall system weight comparisons. This type of performance sensitivity, which is common to high-energy propulsive stages, was not evident in the CSS/APS application because the APS weights had very little effect on the weight of the relatively massive Space Shuttle orbiter vehicle.

Table 4.3.1

THERMAL MANAGEMENT CONCEPT WEIGHT (kg) COMPARISON
ASPM (LH_2 TANK)

	Vented (kg)	Nonvented (kg)
Purge Bag	28.4	28.4
Face Sheets	27.6	27.6
MLI Layers [1]	20.6	34.4
Attachments	3.0	3.0
Tank Basic Structure	173.0	222.0
Cooling Shroud	25.5	0.0
Internal Mixers	0.0	5.0
Final Ullage Gases (GH_2) [3]	78.0	112.0
Tank System Burnout Weight	356.1	432.4
In-Orbit Boiloff	80.0 [2]	0.0
Total	436.1	432.4

[1] 18 and 30 layers for vented and nonvented, respectively.

[2] 117-hr coast for baseline mission.

[3] Tank Pressure = 147×10^3 N/m² (21.3 psia) vented.

= 200×10^3 N/m² (29 psia) nonvented.

Based on the above results, the selected propellant thermal management concept consists of a vented LH_2 tank and a LO_2 tank cooled by the vent gases from the LH_2 tank. A cooled shield or an internal tank mixer/heat exchanger TVS could be used to effect the LH_2 venting. The cooled shield would be about 20 kg heavier than the mixer case but is desirable because of its passive nature, g independence, and that continuous venting provides a convenient coolant supply. As discussed in Section 3.3, the cooled shield also serves to provide the thermal protection essential for the acquisition screen device. Therefore, the cooled shield TVS was selected as the best choice for this application. A cooled shield using GH_2 vent gases will also be used on the LO_2 tank to maintain it in a nonvented condition and to thermally protect its acquisition device.

4.3.2 <u>In-Atmosphere Propellant Thermal Protection</u>. The study discussed in the preceding section dealt only with in-orbit propellant storage. Provisions are also required to limit propellant losses during ground hold and launch, and reentry and landing under certain conditions. This was investigated for the CSS/APS application (see Section 3.3.) and this work has been extended to this application.

Figure 4.3.2 shows the heat load associated with each operational regime as a function of MLI thickness, assuming a simple helium-purged insulation concept. These values agree with the data presented for the CSS/APS, but have been extended to smaller MLI layups by using the MDAC transient thermal analysis program.

The weight penalty for in-atmosphere propellant thermal storage for a simply helium-purged MLI system concept is shown in Figure 4.3.3 for three operational requirements. The weight of added MLI and the summation of the added MLI and the resulting hydrogen boiloff are shown. These results indicate that increasing MLI thickness does not result in a weight saving except possibly for the case where LH_2 must be stored completely through landing. For the ASPM, storage through landing is a requirement only for abort operation where thermal performance is not critical. Therefore, one candidate approach to providing in-atmosphere storage capability would be to purge the MLI insulation, sized for orbital storage, with helium. This would result in the weight penalties indicated in Figure 4.3.3 at "zero" increased MLI thickness.

Calculations were made to substantiate that condensation of the GH_2 purge used in the Space Shuttle payload bay during ground hold will not be a significant problem, even with helium purged MLI layups as small as 18 layer-pairs.

An alternate concept was analyzed and compared with simple helium purging. This alternate concept involved using a minimum layer of external foam between the tank wall and the MLI with the MLI being purged with GN_2 rather than helium during ground hold. A foam thickness of 0.4 cm was used, which results in a MLI/foam insulation temperature well above the nitrogen and/or air condensation points. This foam insulation is discussed in Section 3.3 and would weight 17.8 kg as installed on the entire ASPM LH_2 tank. The corresponding LH_2 boiloff for ground hold and boost operation is 12.3 kg resulting in a total weight penalty of 30.1 kg.
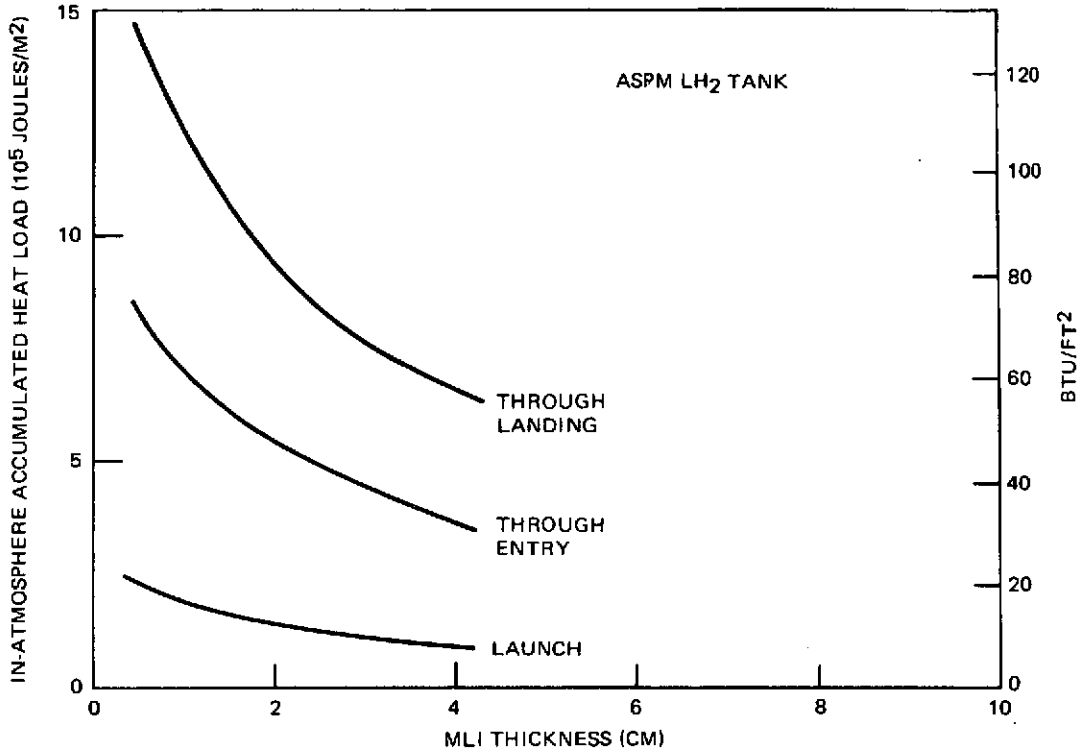
Figure 4.3.2. In-Atmosphere Accumulated Heat Load (Helium Purged MLI Concept)
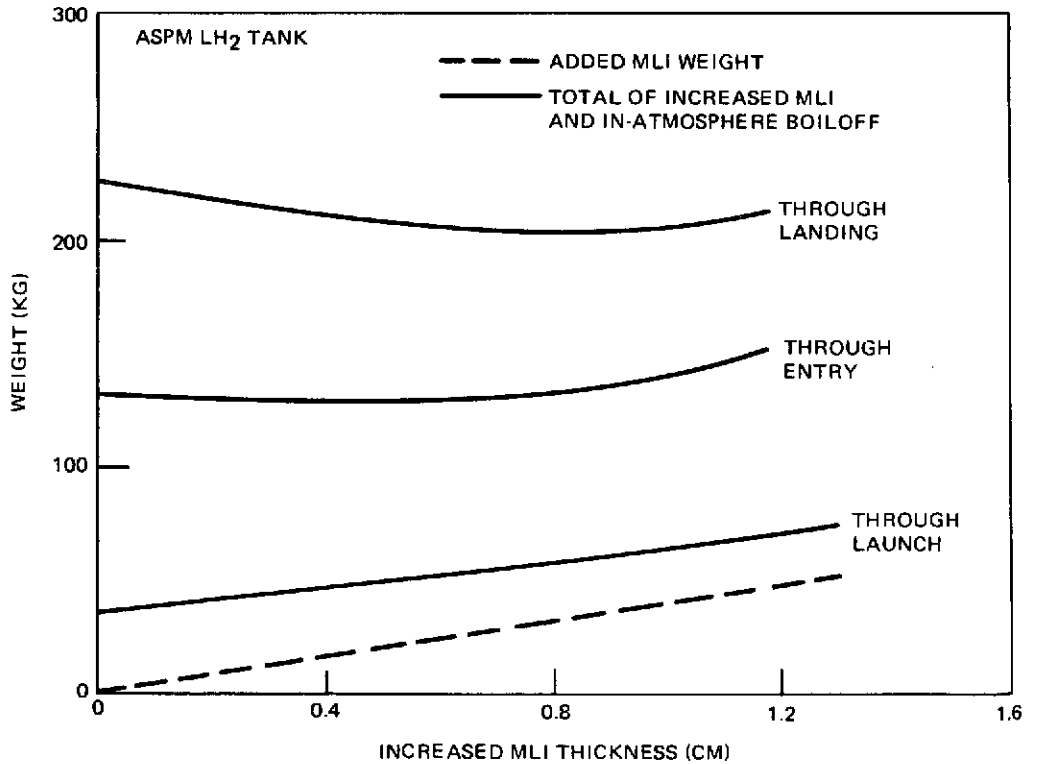
Figure 4.3.3. Weight Penalty — In-Atmosphere Propellant Storage (Simple Helium Purged MLI Concept)

Table 4.3.2 shows the weight penalties for all operational regimes although the reentry storage requirement does not require optimum storage since it is needed only during an abort situation. As can be seen, the foam substrate always results in some weight savings. The foam system also permits a simpler GN2 ground purge system.

Table 4.3.2

COMPARISON OF SIMPLE HELIUM-PURGED MLI AND
A GN2-PURGED MLI/FOAM SUBSTRATE

| | Weight Penalty* (kg) | |
Operation	Foam Substrate	Simple Helium Purge
Launch Only	30.1	35
Complete Mission Through Entry	84	130
Complete Mission Through Landing	138	225

*Foam insulation weight + in-atmosphere boiloff weight

4.4 Integration

The elements or sub-systems of the ASPM discussed previously in this section were integrated together to form the total ASPM feed system.

Basic tankage weight estimates were obtained by conducting preliminary sizing analyses based on the requirements presented in Table 2.5 and using, as a check point, data generated by MDAC under Space Tug/OOS studies reported in References 3 and 30. The computed parameters are summarized in Table 4.4.1. Lower minimum tank wall gages were assumed for the ASPM than in the case of the CSS/APS. For the LH_2 tank, which was assumed to be a cylinder with spherical ends, wall thicknesses of 0.051 cm (0.020 in.) and 0.114 cm (0.045 in.) were assumed for the domes and cylinders respectively. Minimum gage for the LO_2 tank of 0.076 cm (0.030 in.) was assumed. Figure 4.4.1 shows the influence of tank pressure on tank weight. These data were used in the pressurization and thermal control studies reported previously in Section 4.

Feed system mechanical components are listed along with their weights in Table 4.4.2 and 4.4.3 for the LH_2 and LO_2 systems respectively.

The above weights are combined with the acquisition, pressurization and thermal control subsystem weights computed previously to yield the total ASPM feed systems as summarized in Table 4.4.4. Acquisition hardware weights were taken from Tables 4.1.3 and 4.1.4; pressurization weights from Table 4.2.1 and 4.2.3; and thermal control subsystem weights from Tables 4.3.1 and 4.3.2.

Table 4.4.1

ASPM BASELINE TANKAGE PARAMETERS

	LH$_2$	LO$_2$
Tank volume, m^3	53.8	19.45
(ft^3)	(1900)	(687)
Tank diameter, m	4.17	3.79
(ft)	(13.67)	(12.5)
Tank length, m	4.38	2.55
(ft)	(17.61)	(8.33)
Total surface area, m^2	70.2	35.3
(ft^2)	(757)	(380)
Tank pressure corresponding to minimum gage		
cylinder, N/m^2	152 x 10^3	—
(PSI)	(22)	—
dome, N/m^2	134.5 x 10^3	159 x 10^3
(PSI)	(19.5)	(23)
Minimum tank weight, kg	165.5	109
Support weight, kg	25	42

CR190
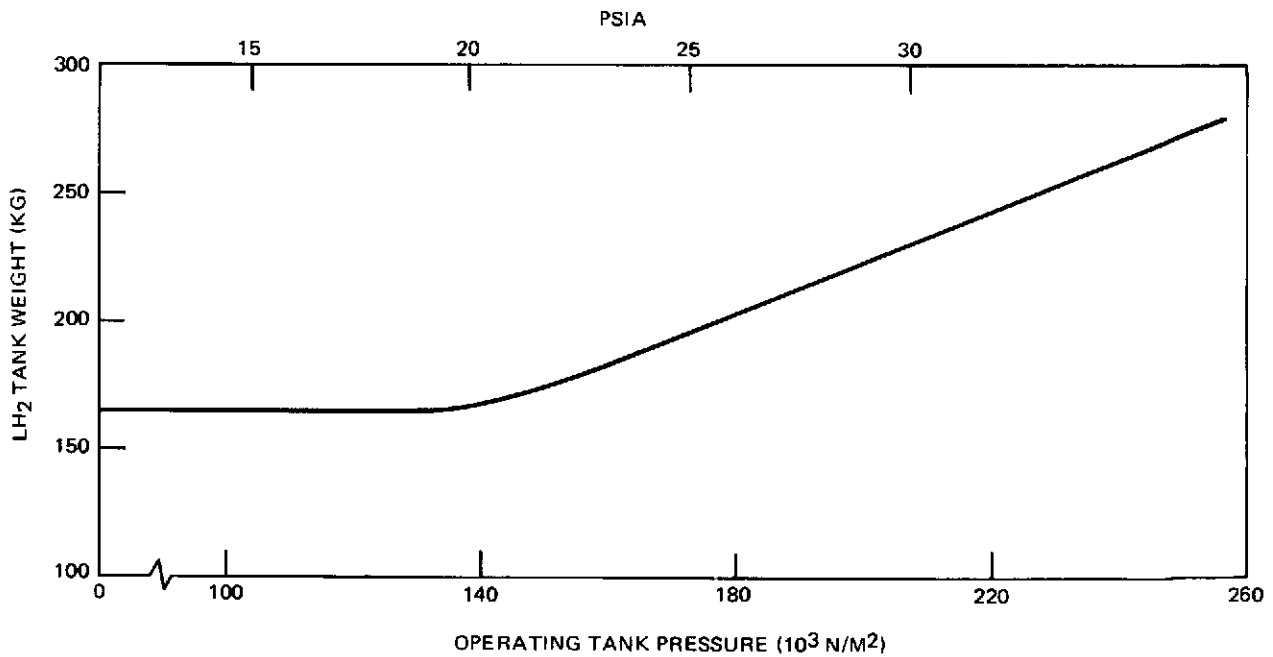
Figure 4.4.1. LH$_2$ Tank Weight — ASPM

Table 4.4.2

ASPM LH$_2$ TANK SYSTEM COMPONENT WEIGHTS*

Quantity	Component	Weight (kg)	(lb)
1	Refill Valve (2-in. Ball)	6.38	(14.0)
1	Main Feed Line Valve (2-in. Ball)	6.38	(14.0)
1	Vent Valve (1-in.)	0.91	(2.0)
2	Viscojets	0.11	(0.25)
1	Regulator (Helium Bottle)	2.25	(5.0)
4	Solenoid Valves (1/2-in.)	1.46	(3.2)
1	Quick Disconnect 1/2-in. Helium Bottle Fill)	0.45	(1.0)
1	High Pressure Relief Valve (Helium Bottle)	0.91	(2.0)
1	Low Pressure Relief Valve	0.22	(0.5)
1	Pressure Controller (Split With LO$_2$ Tank)	2.25	(5.0)
1	Pressurization Diffusers	0.45	(1.0)
1	Capacitance Probe	0.91	(2.0)
1	Pressure Sensor	0.32	(0.7)
2	Temperature Sensor	0.22	(0.5)
1	Marman Flange	1.36	(3.0)
	Total	24.18	(54.15)

*Principal components associated with main-tank pressurization, expulsion, and fill and drain are not included. (86.2 kg)

Table 4.4.3
ASPM LO$_2$ TANK COMPONENT WEIGHT

	Kg	LBM
1 Refill Valve	6.36	14
1 Feedline Valve	6.36	14
1 Vent Valve	0.91	2
2 Viscojets	--	--
1 Regulator	2.27	5
4 Solenoid Valves	1.45	3.2
1 QD for GHe Fill	0.45	1
1 High Pressure Relief	0.91	2
1 Low Pressure Relief	0.23	0.5
1 Pressure Controller	1.14	2.5
1 Pressure Diffuser	0.45	1.0
1 Capacitance Probe	0.68	1.5
1 Pressure Sensor	0.32	0.7
1 Temperature Sensor	0.23	0.5
1 Marman Flange	1.36	3.0
	23.12	50.9

Table 4.4.4
ASPM FEED SYSTEM WEIGHTS (KG)

	LH$_2$	LO$_2$
Acquisition		
Pressure Dome	9.2	4.1
Manhole Penalty	18.0	22.7
Screen Elements	7.0	7.9
Baffles	4.9	10.0
	39.1	44.7
Components	110.4	76.6
Pressurization	110.8	83.3
Thermal Control		
ML1	79.6	40
Cooling Shield	25.5	13
In-Orbit Boil-Off	80.0	0
In Atmosphere Protection	30.1	0
	215.0	53.0
Basic Tankage	190.5	151.0
Pump By-Pass Last	0	0
	665.8 kg	408.5 kg
	(1466.5 lb)	(899.8 lb)

SECTION 5. TEST PROTOTYPE DEVELOPMENT

In Sections 3 and 4, preliminary designs were evolved for two propellant surface tension acquisition/expulsion subsystems to satisfy requirements of two different cryogenic propulsion system applications. The two recommended designs differ significantly in comparison to previously fabricated and tested surface tension devices. Thus in conformity with the original program study plan, test prototypes were developed for future experimental evaluation by NASA. This prototype hardware was to be compatible with an existing (105") NASA owned LH_2 tank being integrated into an APS breadboard at NASA-MSFC.

Philosophically, the test prototypes should provide the capabilities to investigate all critical design, operational, and fabrication aspects of the recommended acquisition system concepts for both the CSS/APS and ASPM applications. Although some compromises may be required because of overall test operations, available hardware, and cost constraints, the above statement was clearly the design goal. Because of the differences between the acquisition device designs recommended for the CSS/APS and the ASPM applications, two prototype acquisition devices are mandatory. These include (1) a screen ring channel installed within the 105-in. tank representing the CSS/APS application, and (2) a smaller screen device located within a small pressure vessel within the 105-in. tank representing the ASPM application. Ideally, these should be compatible with simultaneous installation within the test tank.

5.1 **CSS/APS Test Prototype.** The NASA 105-in. tank has a volume about equal to that of the full scale CSS/APS secondary tank, 12.7 M^3 (450 ft^3). Thus, it was concluded that a circular all-screen ring channel, incorporating all major system design features, could be installed into this tank to represent the CSS/APS system. This installation would represent the same class of practical installation problem posed by the actual system. Limiting flow tests could be run, even at 1-g, to establish fluid performance capability. As conceived, the "105-in." tank represents the LH_2 secondary tank. The prototype is also representative of a full distributer channel system as well, at reduced scale of course.

Figure 5.1.1 shows the basic configuration of the flight vehicle LPIC acquisition channel design for the CSS/APS application. This has a 17.8 cm (7 in.) diameter duct channel using 200 x 600 mesh screen with installation details essentially as illustrated in Figure 3.4.7 of Section 3. This uses a minimum of 8 joint/couplings which divides the rings into segments that can be reasonably handled by two mechanics working in the tank to install the acquisition system.

Figure 5.1.2 shows the general layout of the prototype system selected to represent the CSS/APS case. This is very close to full scale for the acquisition device itself. For the test prototype only one of the two required channel-rings was designed and fabricated to minimize cost. The ring was designed, fabricated, and will be installed in a manner very similar to that required for the flight vehicle. A small channel element of the second ring was incorporated to permit the experimental assessment of head capability for the basic device and to simulate the two-channel intersection point. The channel uses the flight vehicle screen mesh size and near flight weight hardware wherever practical.

195
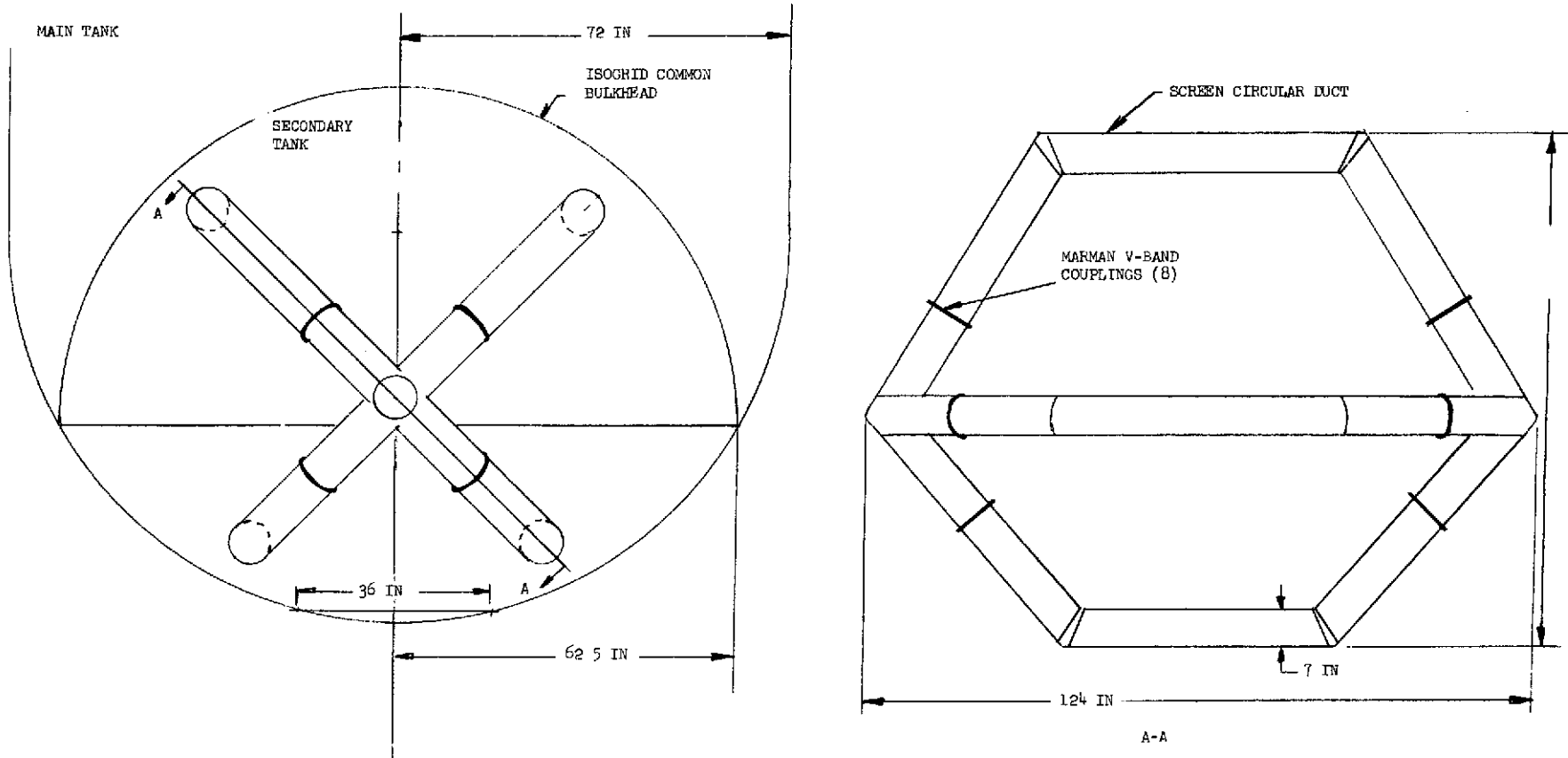
Figure 5.1.1. CSS/APS Flight Vehicle Acquisition Design

SPECIAL TEST
SCREEN SECTION

EXISTING TANK
RINGS TO
SUPPORT DUCT

SHEET METAL
COLLECTOR DUCT

A

MARMAN
V-BAND
COUPLINGS

SHEET METAL ENDS

105 IN

88 IN

7 IN

ALL SCREEN
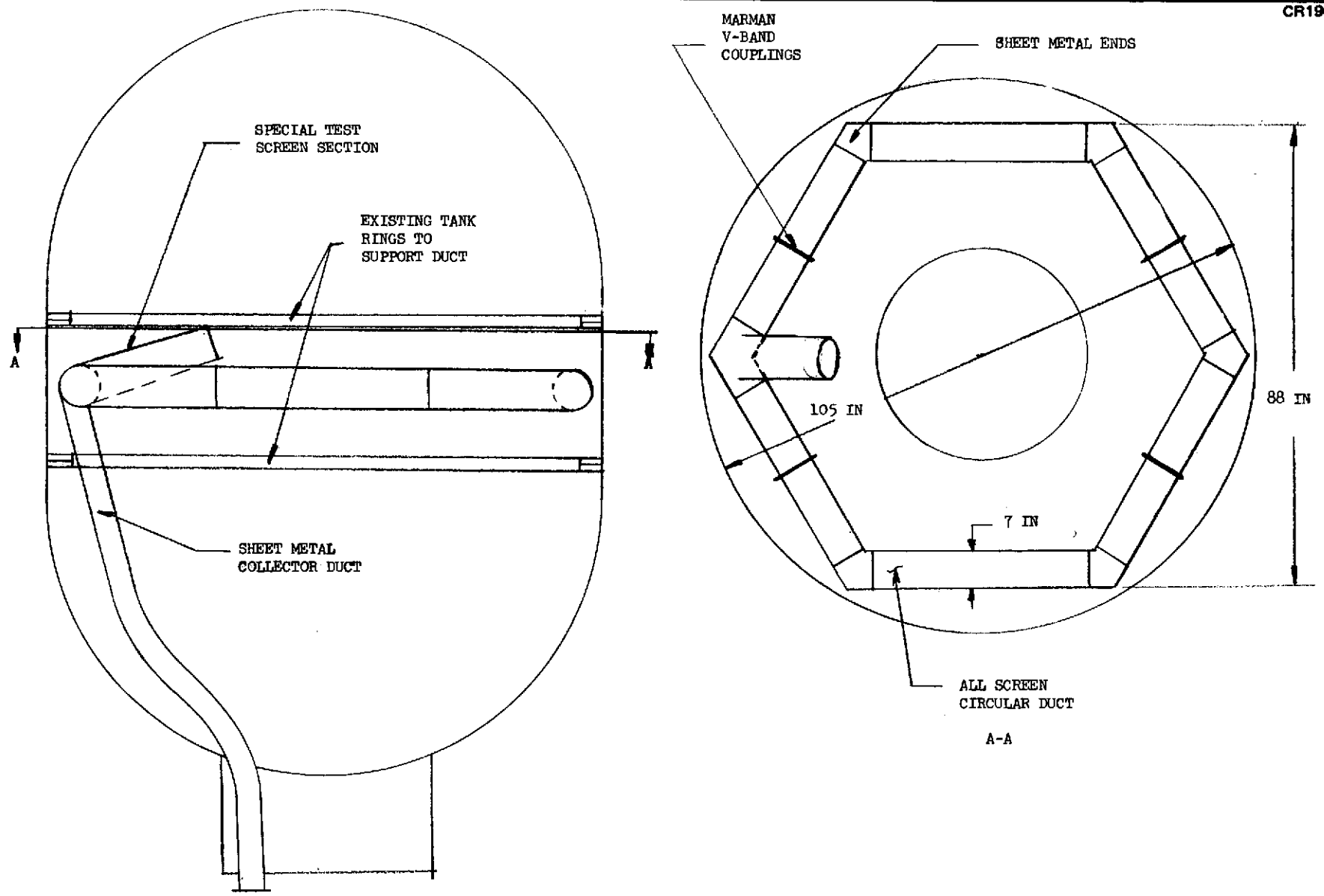CIRCULAR DUCT

A-A

Figure 5.1.2. Conceptual Prototype Design — CSSI APS Application

The number and general locations of the couplings is the same in the flight vehicle and prototype designs which will thus pose a similar channel installation and hookup problem. The couplings include female flange (Aeroquip Part 4560-700-5), O-Ring flange (Aeroquip Part 4570-700-5), coupling (Aeroquip Part 4583-700) and a Creavy O-ring seal element. In the prototype, the ring device will be supported by aluminum support struts from an existing internal ring in the 105-in. tank. This differs in detail from the flight vehicle design because of the limits posed by the available tank design.

A detailed design of the ring channel system including supports and feed lines was conducted and the components were made in MDAC fabrication facilities and at various local fabrication shops. The critical screen channel welding and assembly were performed by Western Filter Incorporated who has had extensive experience in handling fine mesh screen device fabrication.

The channel system consists of six major parts as indicated in Figure 5.1.: two large side channel sections, one four-way junction channel, one two-way junction channel, one straight test channel, and one feedline with shutoff valve. All screen channels are of similar construction consisting of a 200 x 600 dutch twill 304L stainless steel mesh layed over a coarse 16 x 16 mesh 5056 aluminum screen in turn backed up by a 6061-T1 aluminum perforated tube. The tube is 0.020 in. thick with 3/16 in. holes placed in a staggered pattern on 1/4 in. centers. This perforated backup tube is split and spring loaded to assure a tight fit. Channel end elbows and the end cross are formed from 0.036 thick 304L stainless steel. Design details are shown in Figures 5.1.3, 5.1.4, and 5.1.5. Some of the fabricated components are shown in Figure 5.1.6.

In assembly, the fine mesh steel is cut and welded into a cylinder by making a longitudinal weld along the screen. The screen cylinder is then welded to the stainless steel end pieces which may be an elbow cross (see Figure 5.1.7) or flange. In each of the long channel sections, a stainless steel bellows is welded into the duct for expansion and misalignment correction (see Figure 5.1.8). In a separate operation, the perforated tube is cut, bent and rolled into a tube as shown in Figure 5.1.9. A specially designed leaf spring is installed to provide a constant load against the fine mesh screen (see Figure 5.1.10). The coarse mesh is layed over the perforated tube (see Figure 5.1.11), the leaf spring is compressed and this combination is inserted into the fine mesh cylinder. When positioned, the springs are released and the elbow section is riveted to the perforated tube to provide added rigidity to the structure. A protective cover for each steel screen was provided consisting of an aluminum sheet and a layer of foam rubber (see Figure 5.1.12).

The channel support struts are made from 0.049 in. 3/8 O.D. 6061 aluminum tubing. The attachment of these struts and a complete installation procedure are covered in Appendix G. The complete unit, except for the feed line is shown in Figure 5.1.13. The illustrated installation was prepared in a specially designed mock-up of the 105-in. NASA tank. The metal band to which the channel is attached in an exact simulation of the existing stiffening ring within the tank. The installation was completed by two mechanics in less than one day.

Page intentionally left blank

NOTES:
UNLESS OTHERWISE SPECIFIED:

1. WELD PER MPD 164, TYPE II

2. BUBBLE POINT TEST -3 THRU -9 PER SAE ARP301 INSPECTION TEST
   PROCEDURE. 7 INCHES OF WATER MINIMUM ACCEPTABLE.

3. NOTIFY CUSTOMER 24 HOURS IN ADVANCE OF BUBBLE POINT TEST

4. SCREEN MAY BE REPAIRED USING STA-BOND U-35 AND EC301 PRIMER.
   MAXIMUM AREA THAT MAY BE PATCHED IS 2 SQUARE INCHES PER
   ASSEMBLY.

5. PROCESS 2, -3 THRU -9 FOR FUEL SERVICE PER MSFC-SPEC-164 AFTER
   BUBBLE POINT TEST.

6. PROVIDE REUSABLE WOODEN SHIPPING CONTAINERS.

7. SHIP -11 ASSEMBLIES AS LOOSE ITEMS.

MS20470AD6 RIVET 2 REQD
(SEE INSTL IN VIEW B)

-9 SCREEN ASSY

-11 SCREEN ASSY

IT44577-11 SCREEN
IT44499-509 SUPPORT ASSY
IT44493-579 SUPPORT ASSY

-5 SCREEN ASSY

MS20470AD6 RIVET
6 EA REQD

IT44517-5 SCREEN
IT44499-503 SUPPORT ASSY
IT44499-513 SUPPORT ASSY
2 EA REQD
SEE VIEW A-A FOR INSTL.

IT44514-1 CROSS

-7 SCREEN ASSY

IT44517-9 SCREEN
IT44499-507 SUPPORT ASSY
IT44499-517 SUPPORT ASSY
2 EA REQD

IT44499-577

MS20470AD6 RIVET
2 REQD
PICK UP HOLES IN
IT44499-507,
OPPOSITE SPRINGS

.75 MIN

IT44499-507

VIEW B
TYP 2 PLCS

1.00 (ON SURFACE OR PART)

IT44517-3 SCREEN
2 REQD

IT44517-7 SCREEN

-3 SCREEN ASSY
2 REQD

IT44517-3

IT44499-511 SUPPORT ASSY
2 REQD

.75 TYP

IT44499-501 SUPPORT ASSY
2 REQD

IT44499-515 SUPPORT ASSY

IT44499-505 SUPPORT ASSY

MS20470AD6 RIVET 3 REQD
PICK UP 3 HOLES IN LINE IN IT44499
TYP 3 PLACES

VIEW A-A SCALE 1/1

Figure 5.1.4. Screen Assembly (CSS/APS)

NOTES

UNLESS OTHERWISE SPECIFIED.

1. ANODIZE PER MIL-A-8625, TYPE I.
2. BREAK ENDS OF -3 THRU -11. SHARP EDGES NOT PERMITTED.

-23 SHEET 2 REQ'D

7.00 DA

XXX TYP

STEEL RIVETS MAY BE USED AS ALTERNATE

45° TYP

.75
.70
.44
.30

-13 SCREEN
-15
-17
-19
-21

-25 SPACER, 2 REQ'D PER SPRING. ADJUST THICKNESS TO COMPRESS SPRING 0.3

.30
.75

.05R TYP

.31 TYP

9K21673 SPRING 4 REQ'D

6.93 DA

$L^{+.06}_{2}$

1.50 TYP

.50 TYP

PICK UP HOLE THAT MATCHES IN -3 THRU -11

MS20670-8 RIVET 2 REQ'D 4 PLACES

-9 TUBE
-11

30°

L_1 (-3-5-7)

$L^{+.06}_{1}$ (-9-11)

-3 TUBE
-5
-7
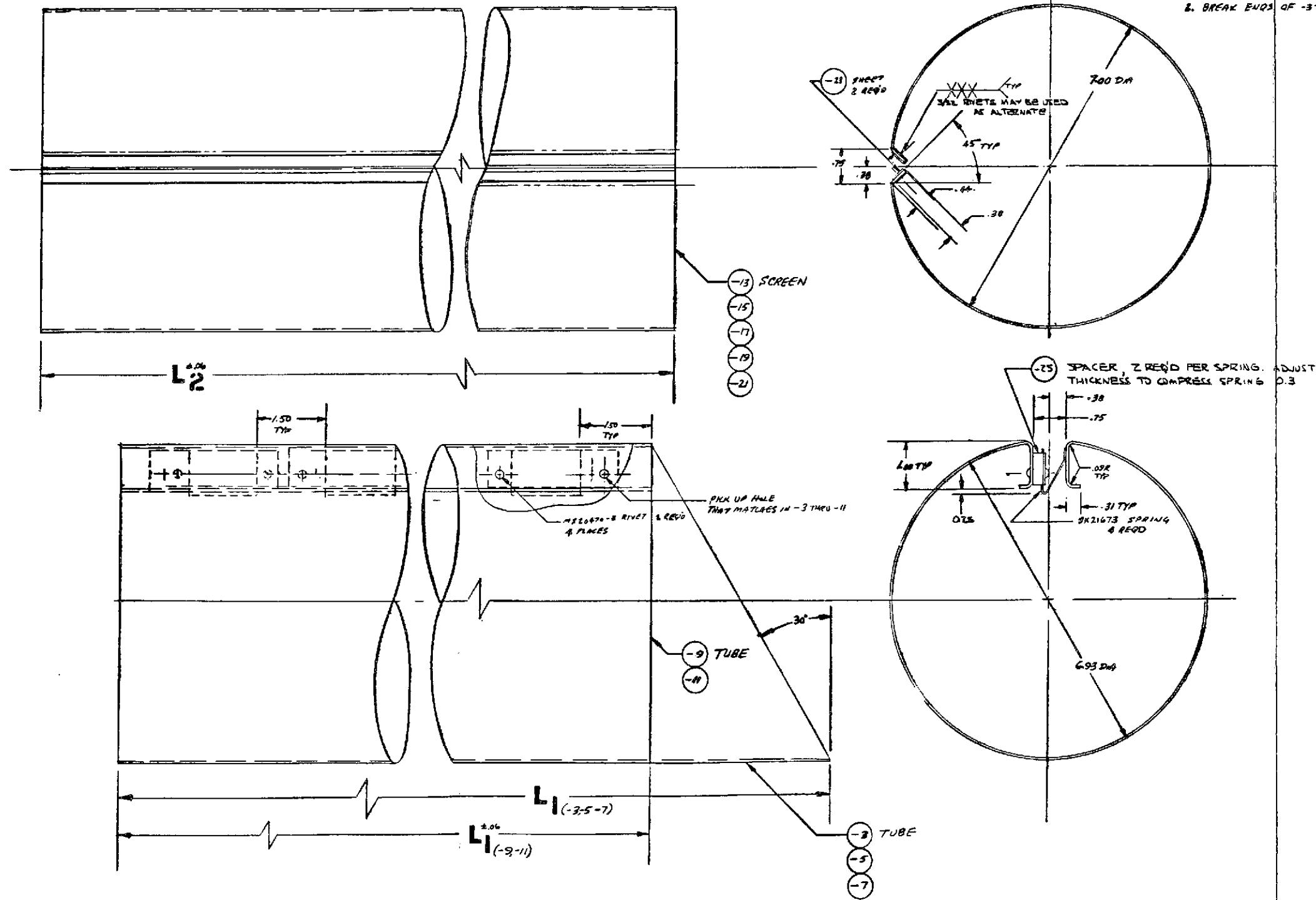
Figure 5.1.5. Screen Support Design (CSS/APS)
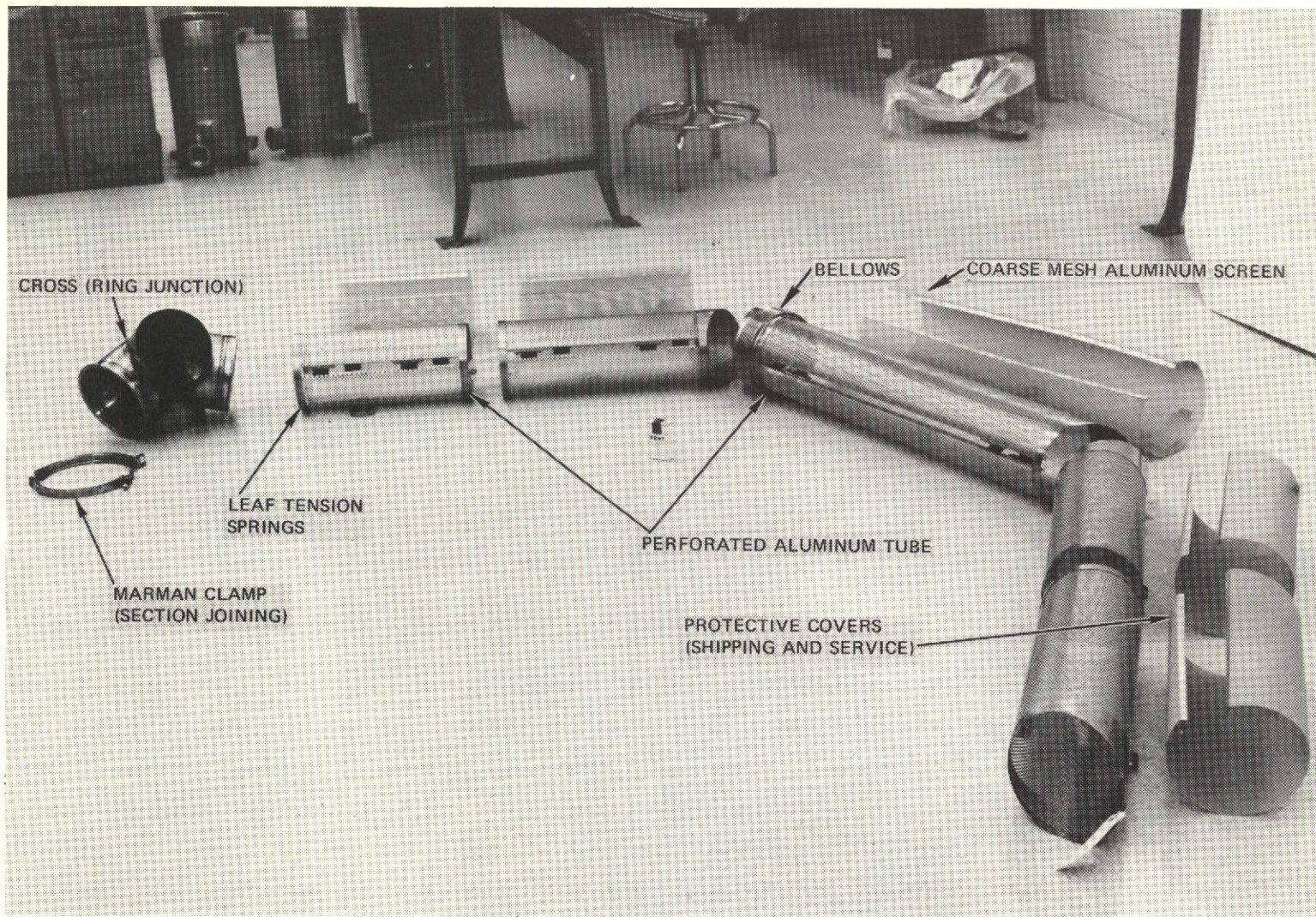
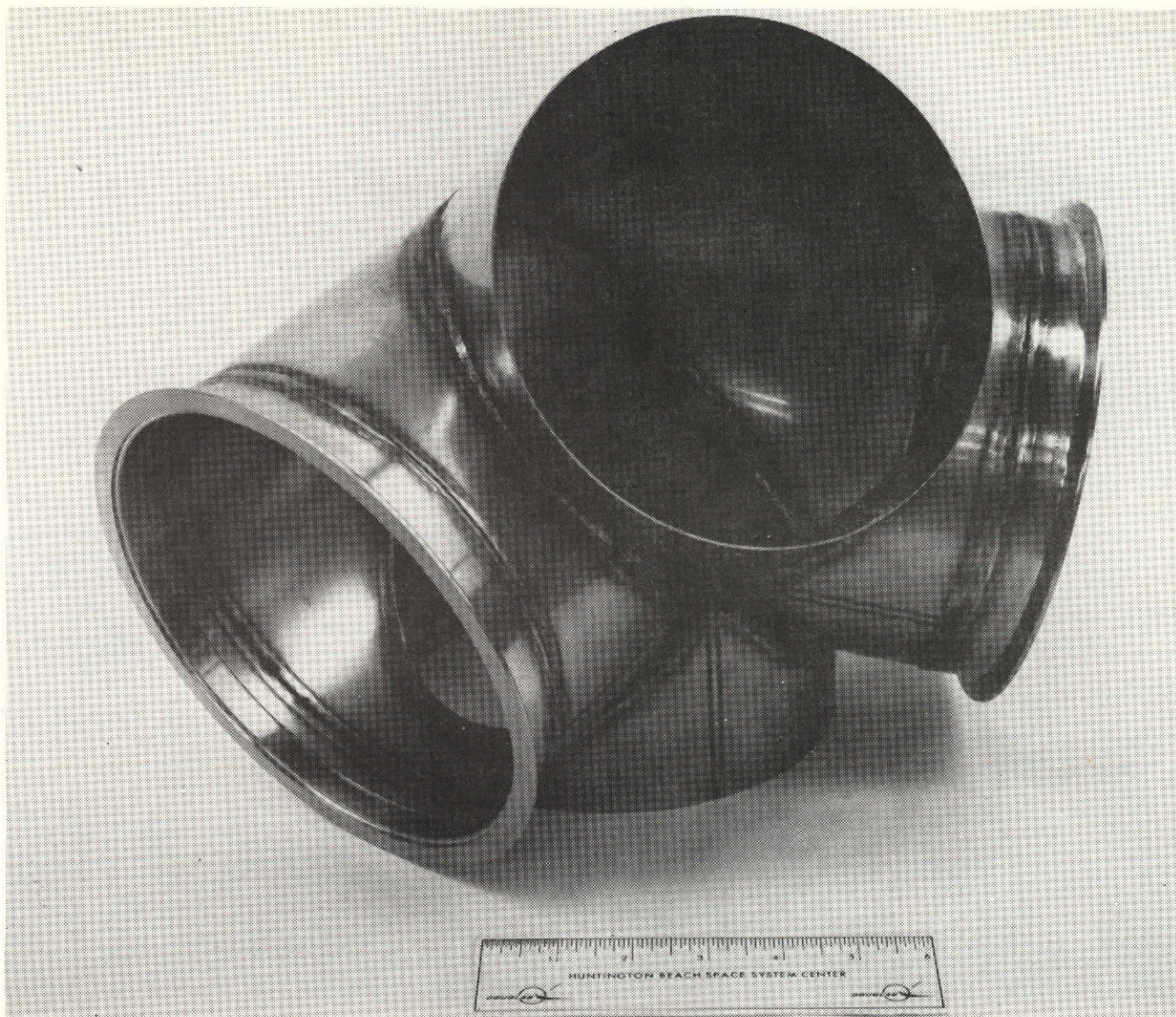Figure 5.1.6. Ring Channel Component Parts (Not Including Fine Mesh)

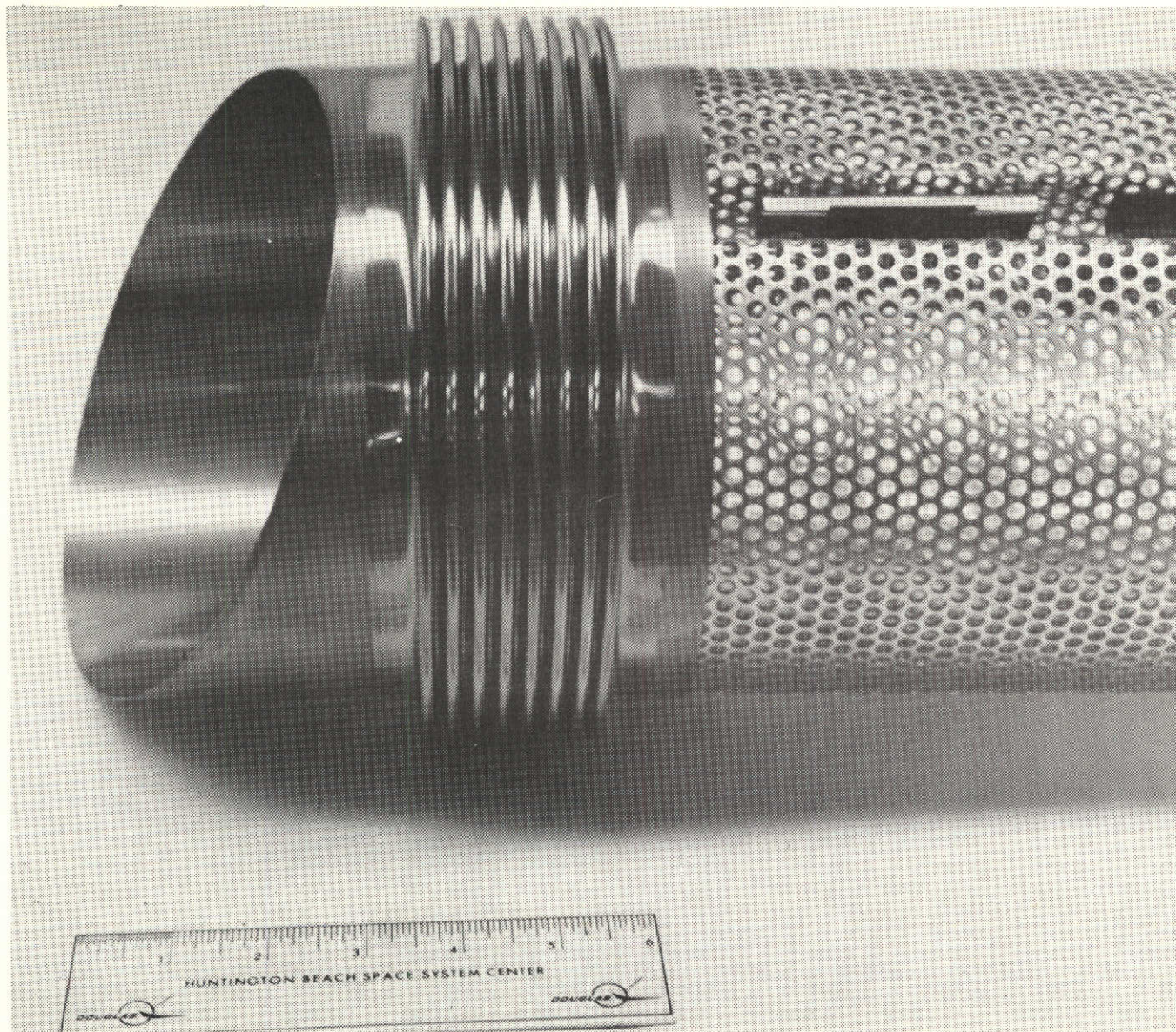Figure 5.1.7. Channel System Cross Assembly
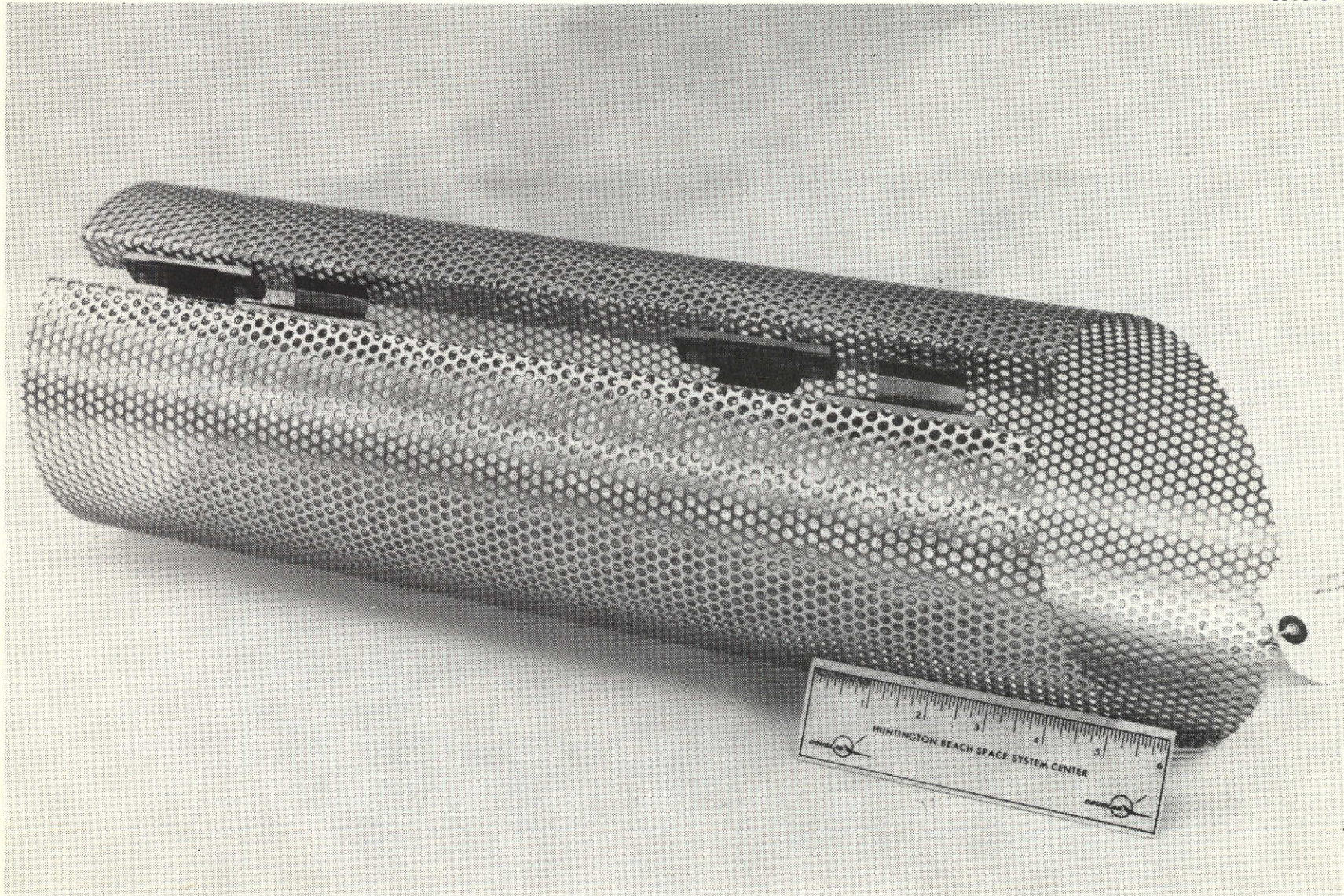
Figure 5.1.8. Channel Bellows
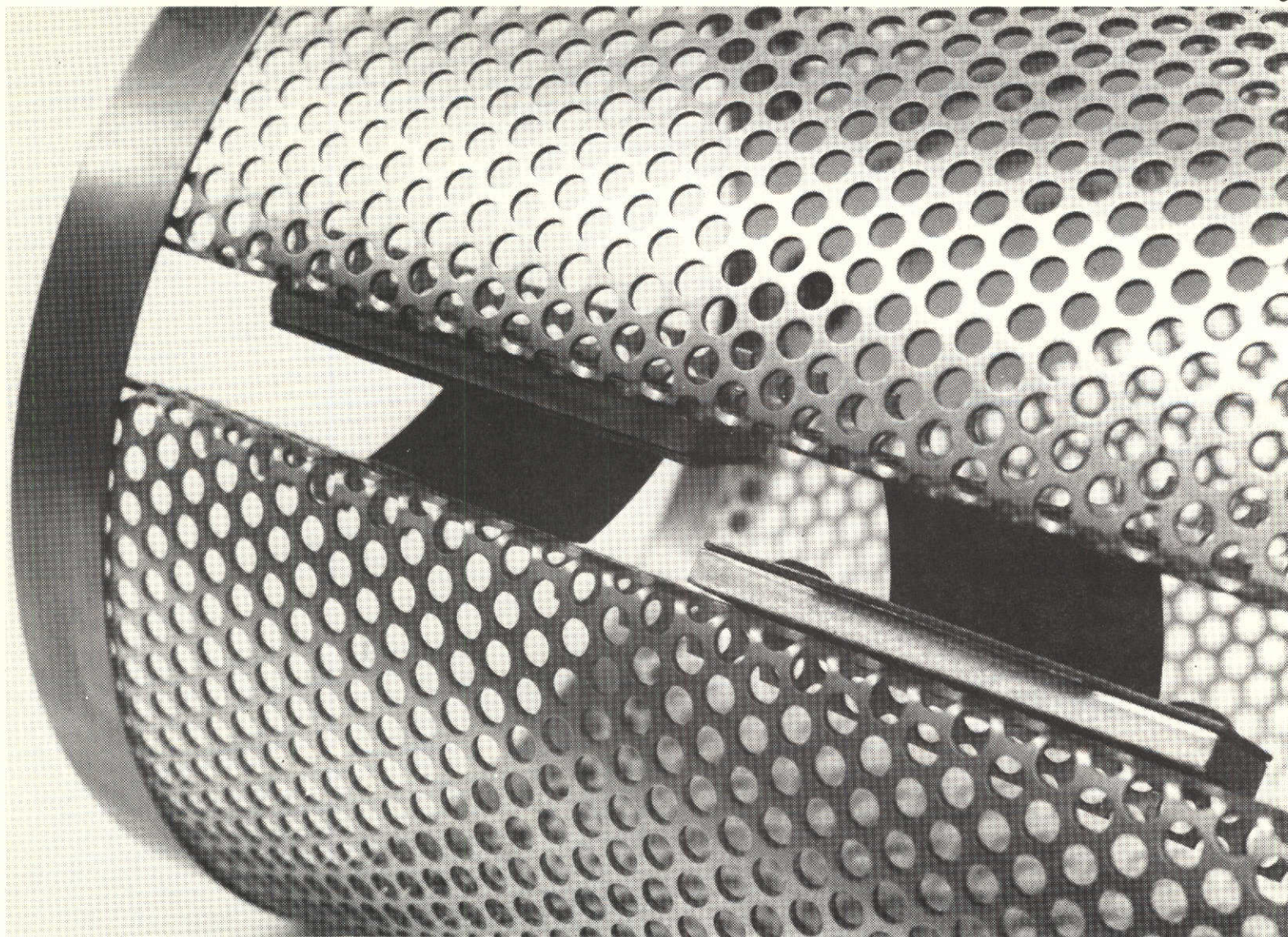
Figure 5.1.9. Completed Perforated Tube

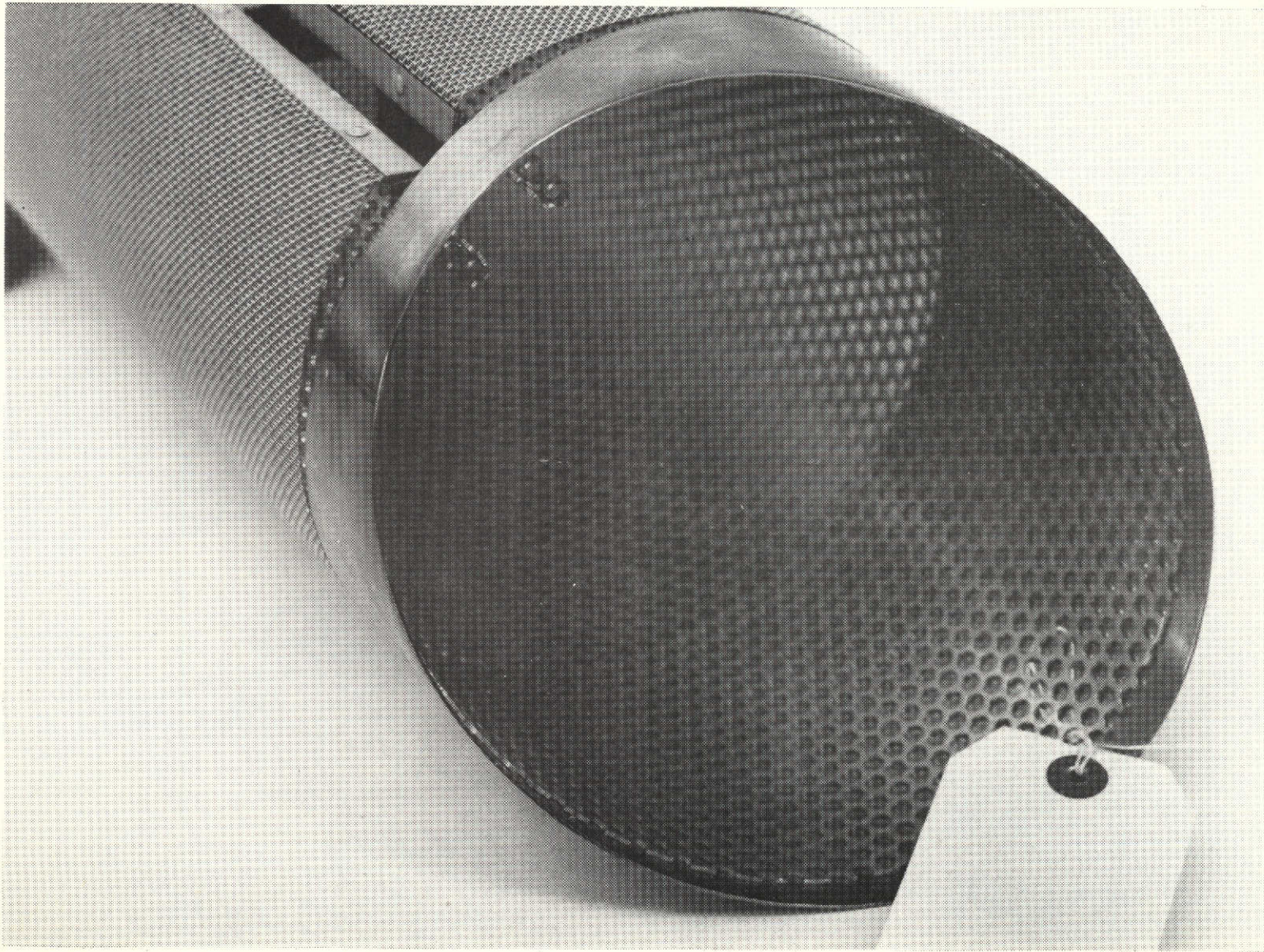Figure 5.1.10. Perforated Tube Leaf Spring Close-up

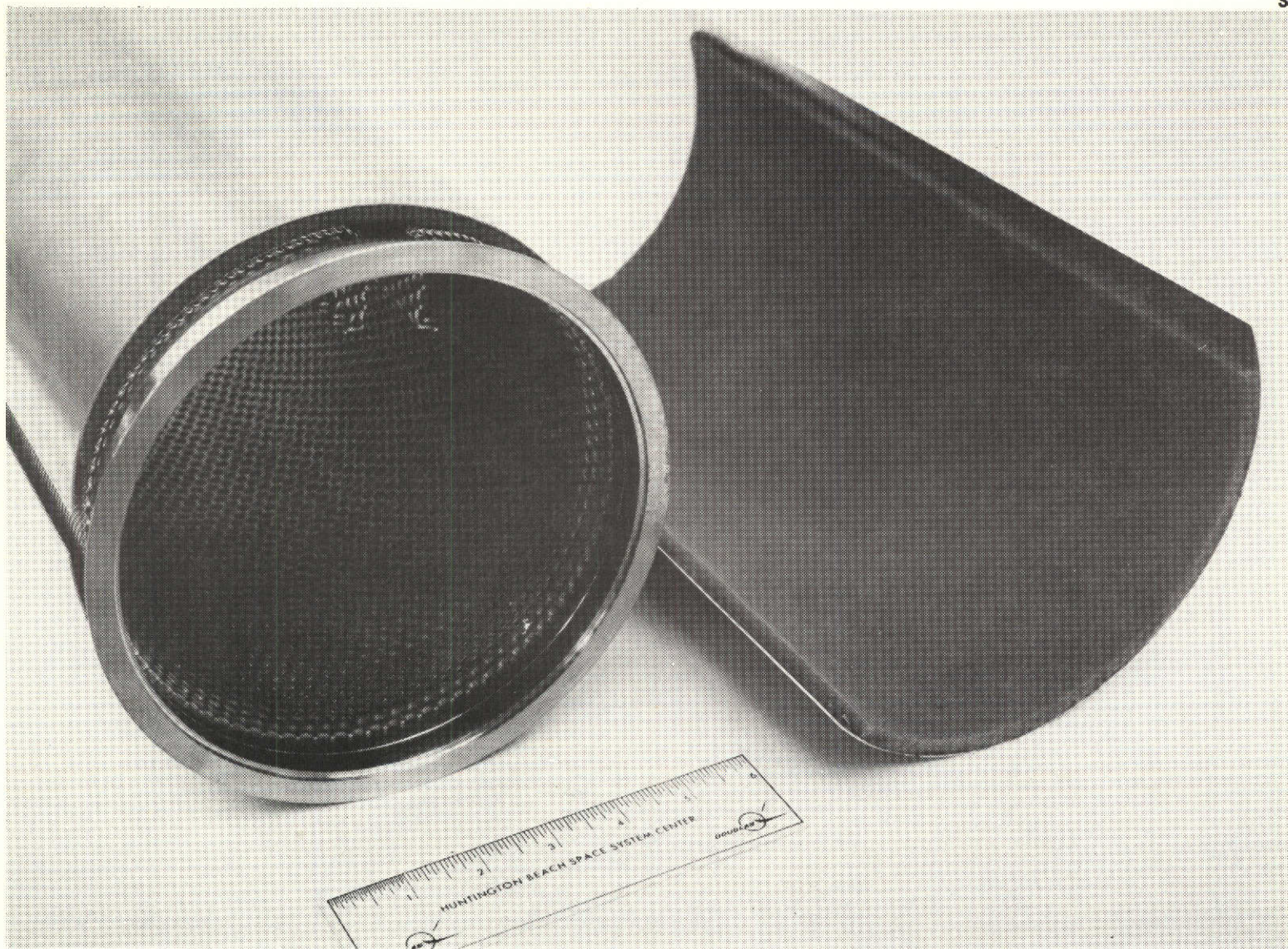Figure 5.1.11. Coarse Mesh Application Over Perforated Tube
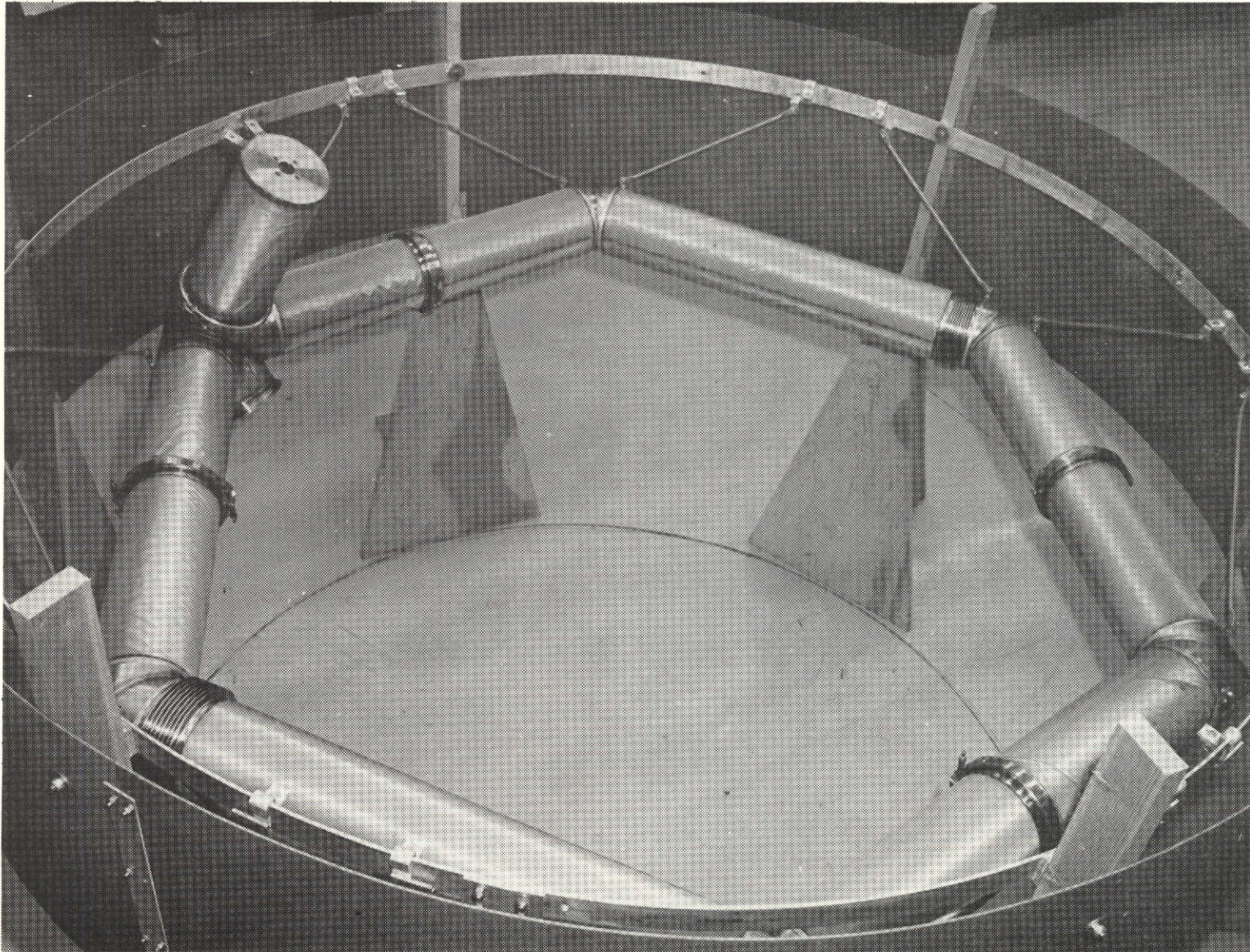
Figure 5.1.12. Channel Protective Cover

Figure 5.1.13. Completed Prototype (CSS/APS)

The bubble point characteristics of the device were checked with alcohol at two points during the buildup: Immediately after screen cylinder welding and after complete section assembly for which a special tank had to be built. Tests showed all units to meet the bubble point specification requirement of 7 in. of water. However, it was necessary to apply some small amount of polyurethane adhesive to close up several small holes near the weld area.

Details of the construction are shown in the photos of Appendix G.

The completed units were weighed and compared to the predicted weights in Table 3.1.13. The table indicates a weight, including Marman clamps of 40 kg. The actual weights for the prototype hardware including the additional sections to make up the two ring design would be 40.3 kg as indicated in Table 5.1 which is exceptionally close to the predicted value.

Table 5.1

ACTUAL CHANNEL COMPONENT WEIGHTS

T-Section	4.72 kg x 2 =	9.44 kg
Main Sections	7.04 x 4 =	28.10
V-Bands	0.34 x 8 =	2.72
		40.26

5.2 ASPM Test Prototype. The volume of the LH_2 secondary tank for the ASPM acquisition system was set at 0.952 M^3 (33.6 ft^3), about 7.3% of the "105-in." tank volume. Thus to satisfy ASPM conditions, a secondary tank containing baffles and individual screen elements must be used within the "105-in." tank. MDAC is currently developing for NASA under contract NAS6-27571 another experimental acquisition system for installation within the same "105-in." tank. This involves a 13 ft^3 pressure vessel containing an annular screen device with all control components including an auxiliary TVS cooling system. Although this is only 38% of the required ASPM secondary tank volume, it is adequate to accommodate full size screen elements and represents an extremely cost effective design approach. Thus the selected approach was to retain the pressure shell and control components developed under contract NAS8-27571 and to provide a new retention system representative of that required for the ASPM to replace the existing annular screen. This approach is conceptually illustrated in Figure 5.2.1.

In developing the ASPM prototypes, the base plate with control components and the outer pressure shell from the IDU built under contract NAS8-27571 were retained. Two internal baffles and three sets of screen elements were designed to simulate the ASPM design. The elements are of the size and screen mesh recommended for the ASPM design and the baffles provide flow operation as anticipated in the ASPM which can be verified in 1-g testing. Detailed designs of the new parts are shown in Figures 5.2.2-5.2.4.

The cylindrical screen elements are of similar design but vary in length and screen mesh. Each uses pleated screen backed up by a perforated tube. Although acceptable bubble point characteristics were obtained as verified
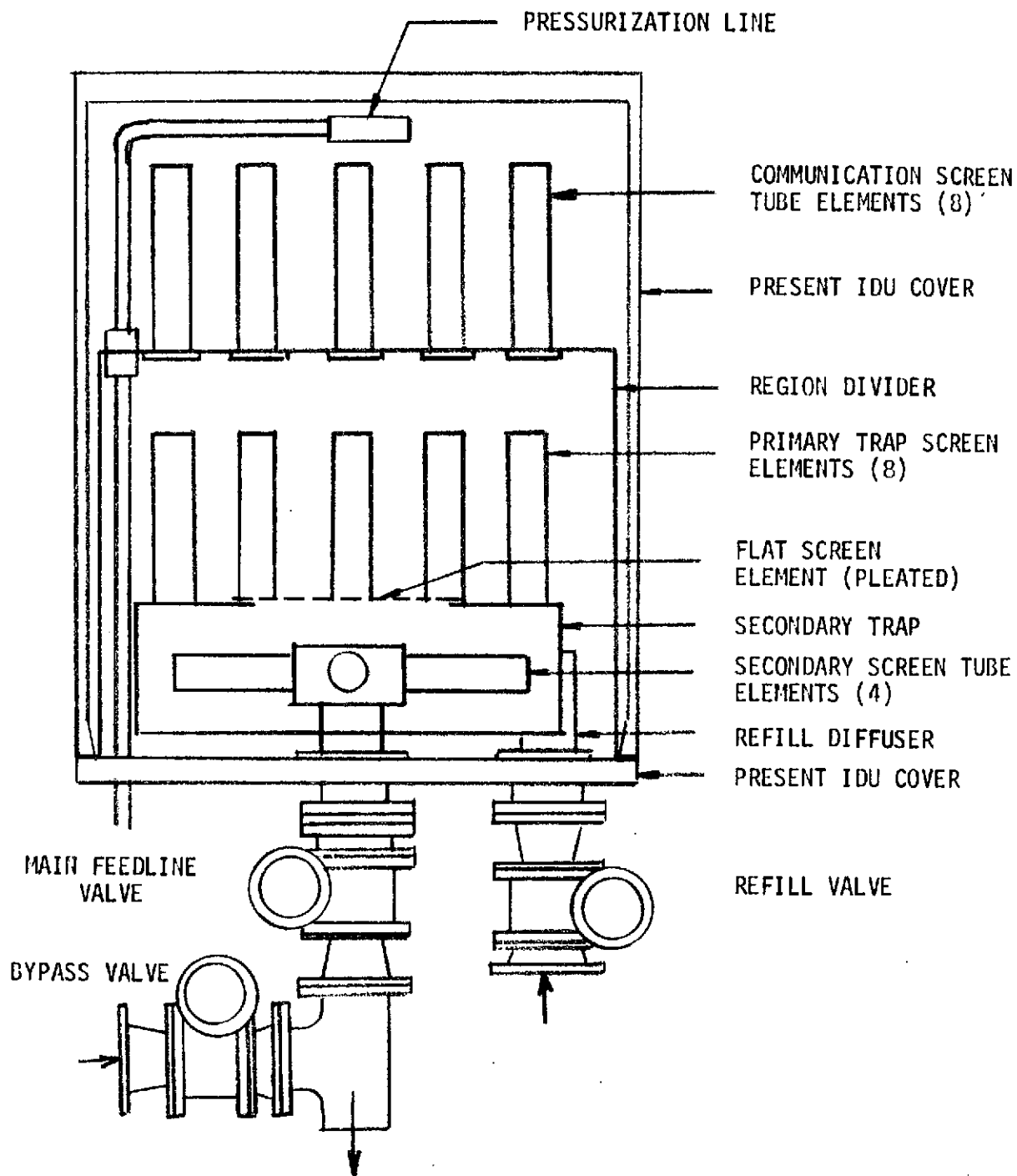
Figure 5.2.1. ASPM Test Prototype (Modified IDU)
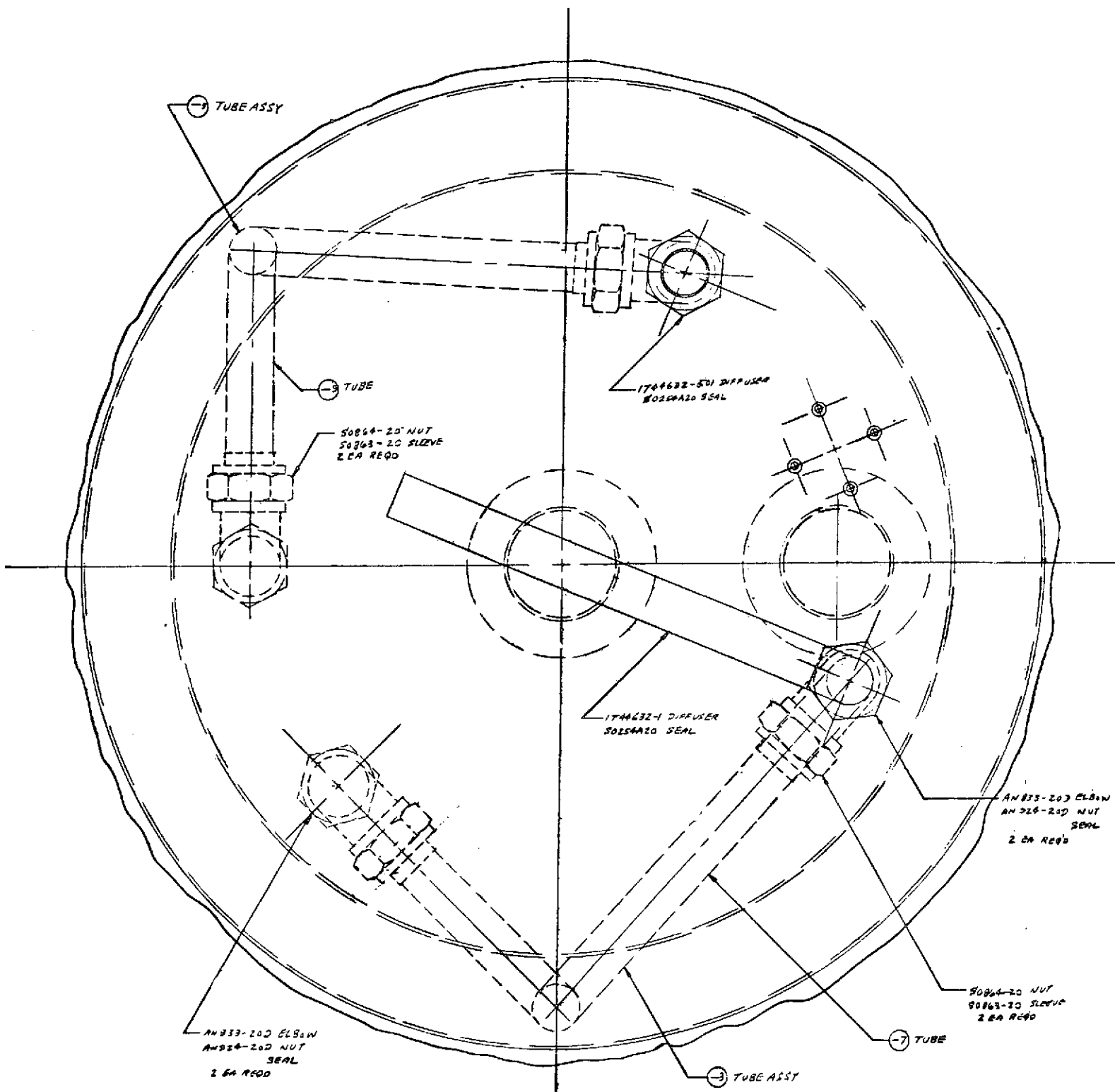
VIEW A-A
(FILTERS OMITTED FOR CLARITY)
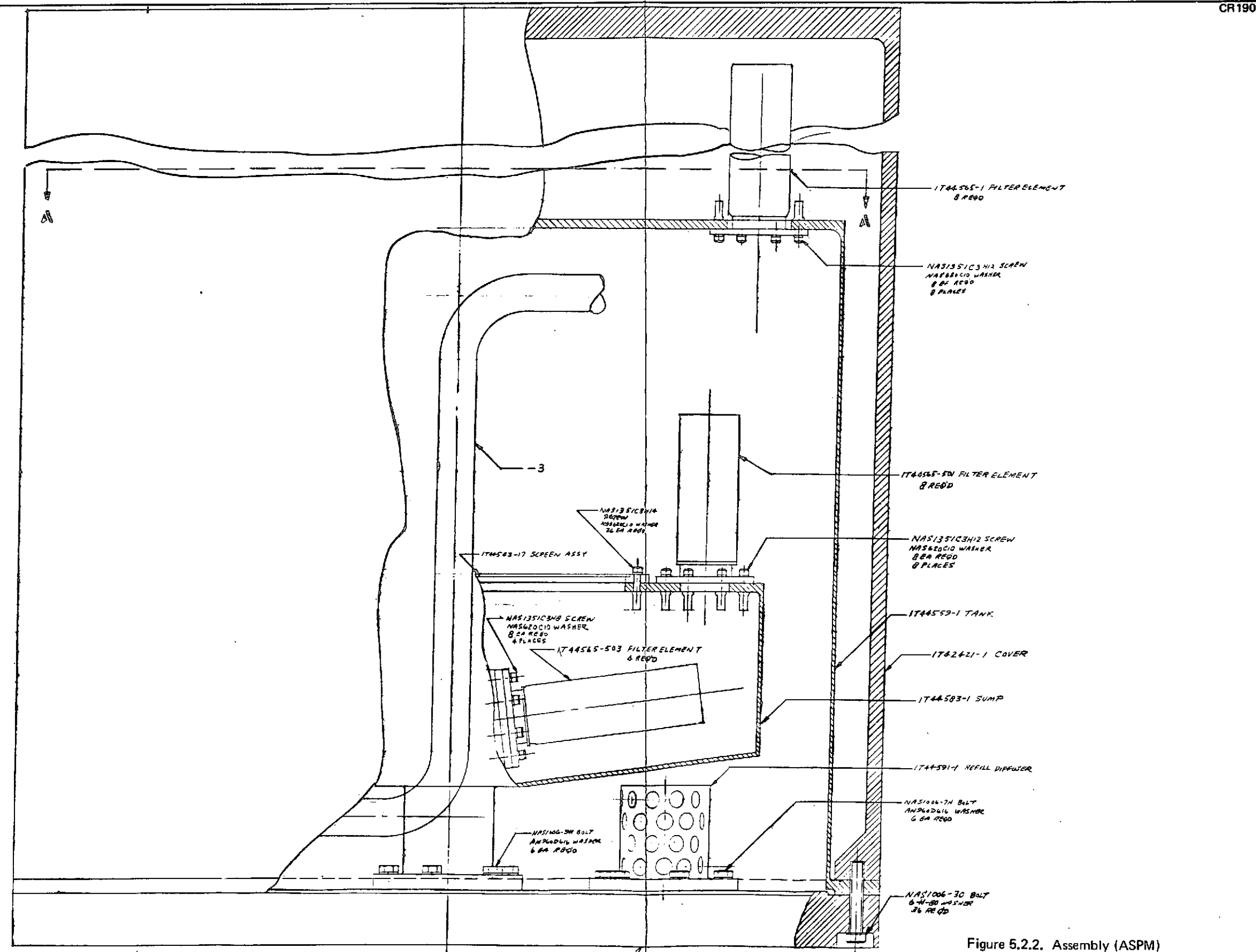
Figure 5.2.2. Assembly (ASPM)

NOTES:
UNLESS OTHERWISE SPECIFIED
1. TOLERANCES .XX ±.03, .XXX ±.010, ANGLES ±0° 30'
2. ALL MACHINED SURFACE ROUGHNESS ∇ PER ANSI B46.1.
3. FUSION WELD PER MPD 164, TYPE II
4. TEST TO 15 ±.50 INCHES OF WATER WITH HELIUM. NO LEAKAGE PERMITTED.
5. CLEAN FOR FUEL SERVICE PER MSFC-SPEC-164
6. INSTALL RIVNUTS .060 TO 0.005 LOW, PER DPS 13057.
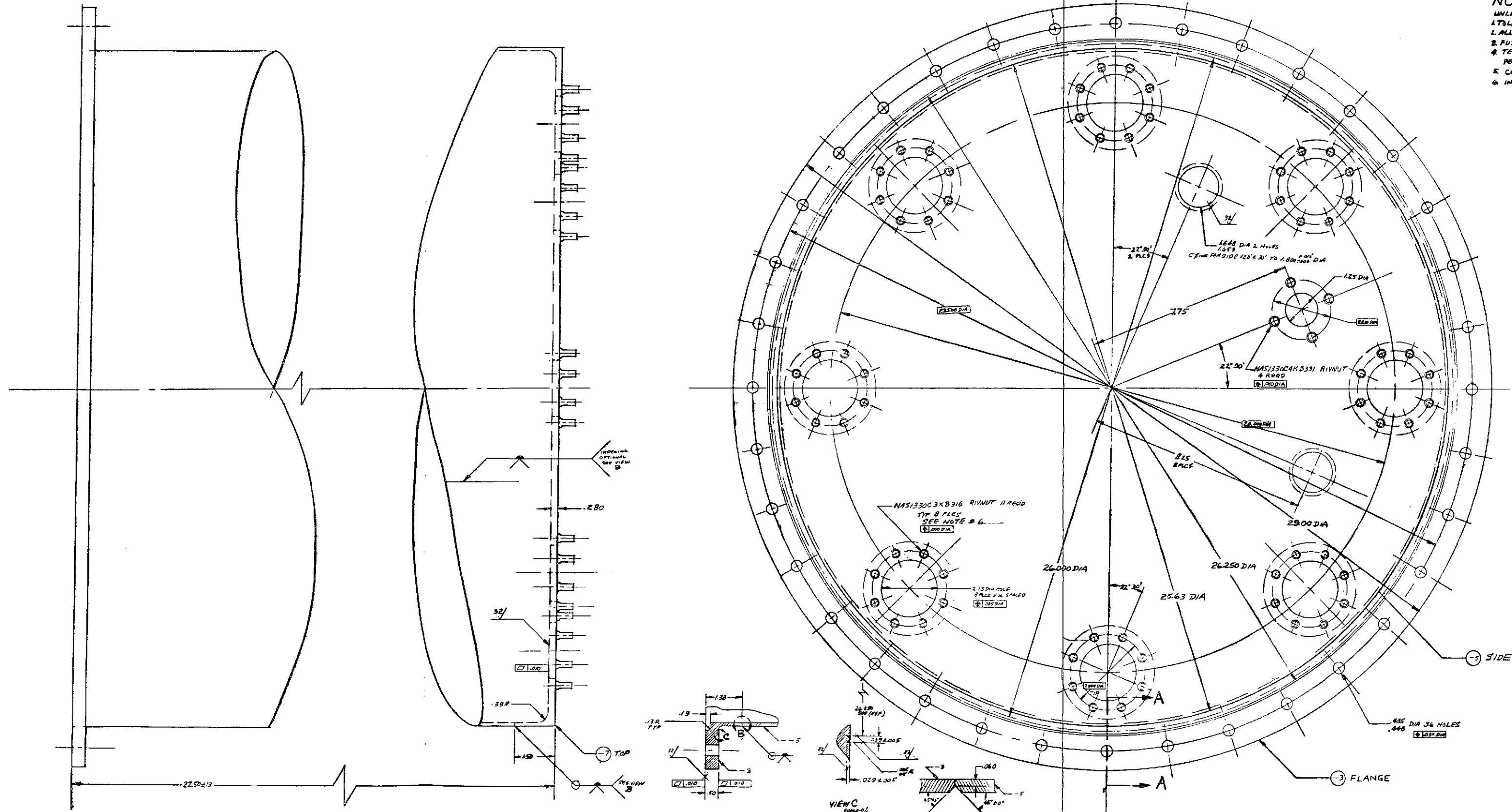
Figure 5.2.3. Tank Liner

VIEW C

VIEW B

⊖ TOP

⊖ SIDE

⊖ FLANGE

→ A

Page intentionally left blank

with alcohol tests, polyurethane repairs were necessary at the coined edtes where the pleated screen joined the end flanges. Care must be taken to make the radius at the coined edge relatively large (in the order of 2.54 cm) to prevent screen mesh distortion at this point.

Figure 5.2.5 shows a photo of the completed inner sump and baffle with the screen elements set in position. Figure 5.2.6 shows the same unit with the flat screen element in place and Figure 5.2.7 shows the top of the primary baffle with the long screen elements installed.

Figure 5.2.8 illustrates the integration of both prototypes into the "105-in." LH_2 tank as will be performed by NASA-MSFC.
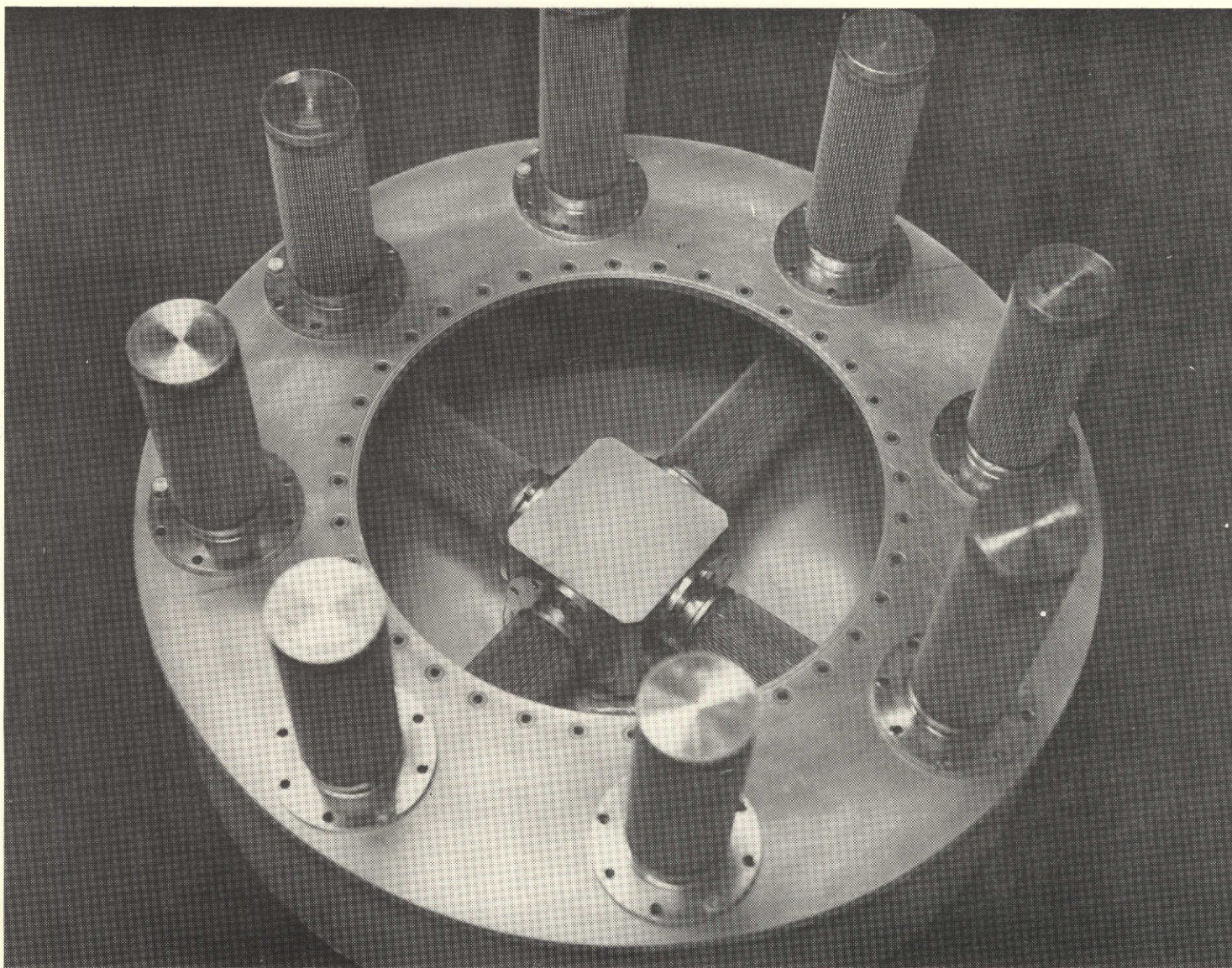
Figure 5.2.5. ASPM Prototype — Inner Sump (Flat Screen Removed)
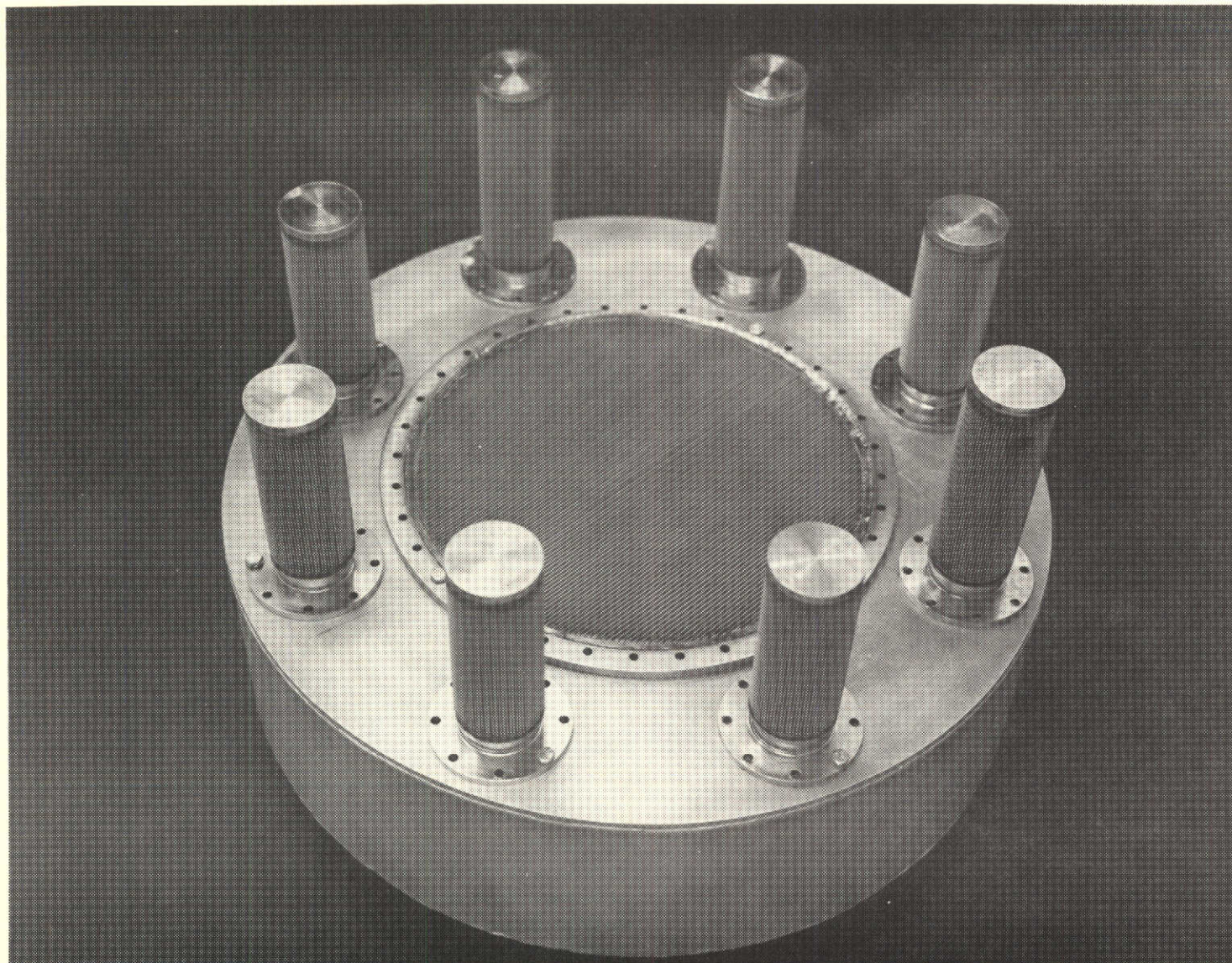
Figure 5.2.6. ASPM Prototype — Inner Sump Complete
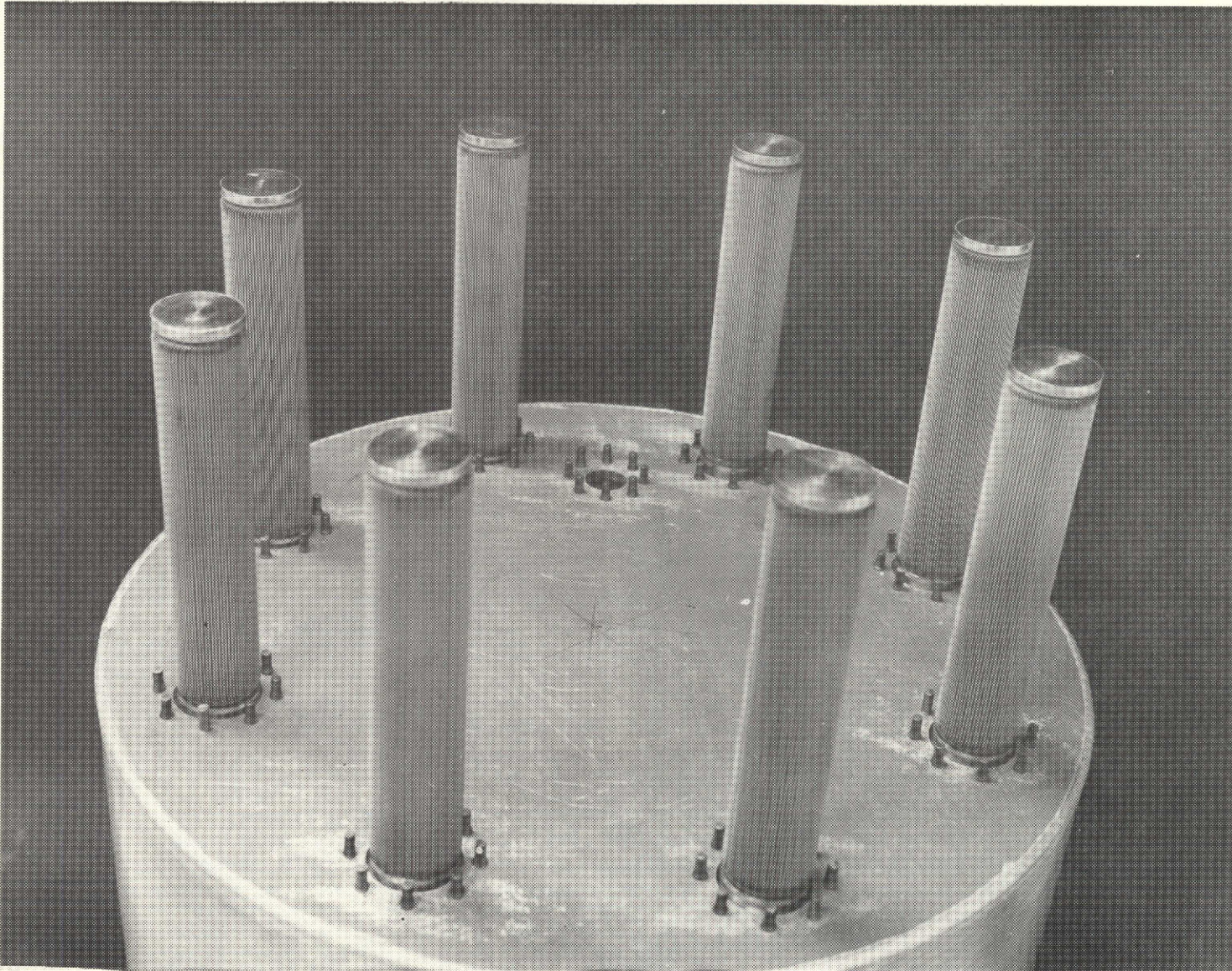
Figure 5.2.7. Top of Primary Baffle
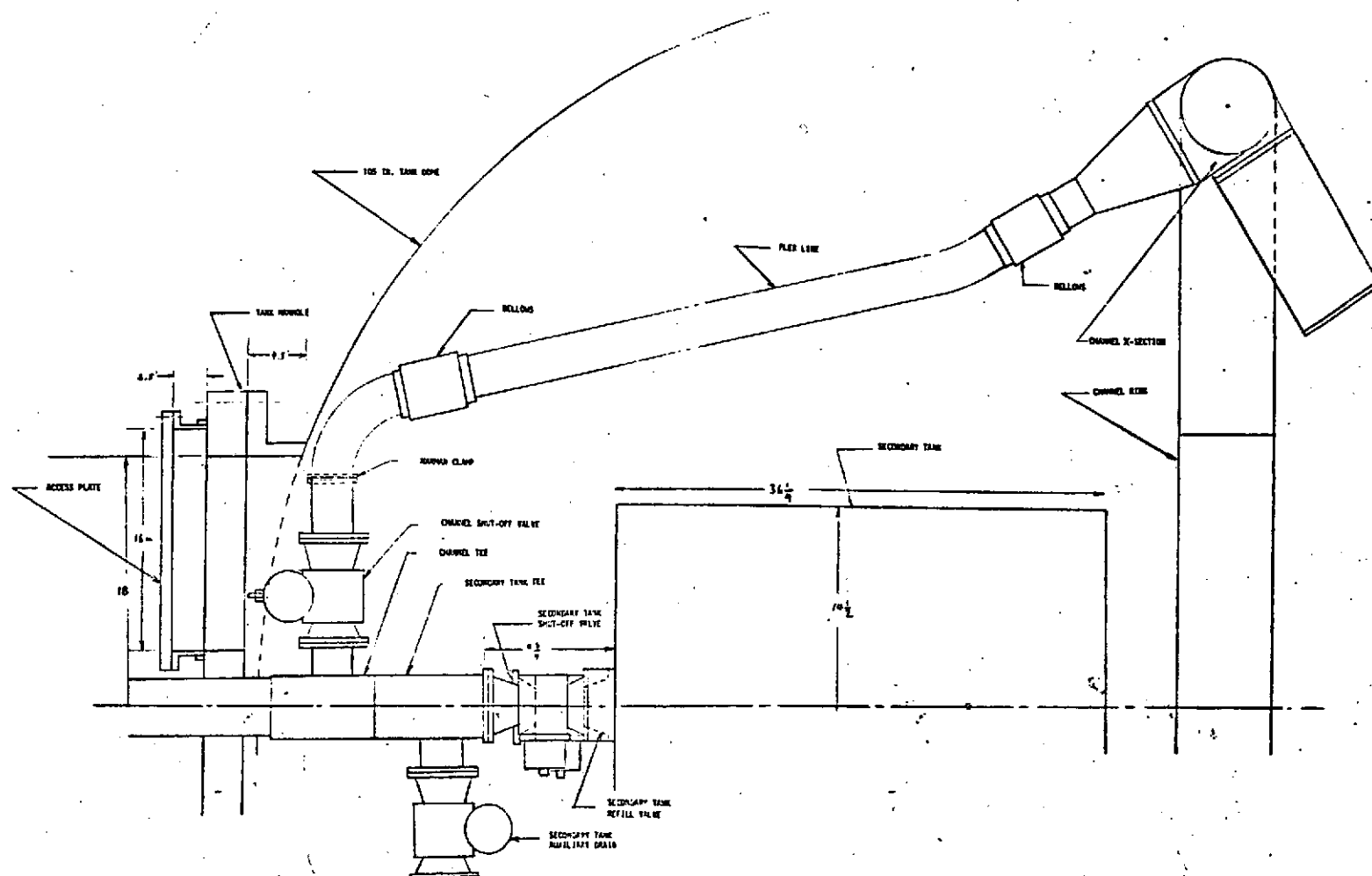
Figure 5.2.8. Propellant Acquisition Setup for NASA-MSFC APS Breadboard

Section 6.   ACCELERATION SETTLING STUDY

For propulsion systems requiring only a limited and fairly well defined number of engine firings, such as the ASPM, on-demand propellant flow may not be a strict requirement.   Under these conditions an alternate to surface tension acquisition as a propellant control technique is the use of complete vehicle acceleration to settle the cryogenic propellants prior to engine startup. Thus, a limited scope study of this concept was conducted and compared with the selected surface tension acquisition system for the ASPM.   It has been assumed that the acceleration settling is provided by firing auxiliary storable thrusters which employs positive expulsion tankage.

6.1   Settling Requirements Analysis

The MDAC H470 Propellant Settling Program was updated and minor modifications made in order to determine settling terms and settling propellant requirements for an ASPM.   It was assumed that the propellant settling time was composed of separate flow times associated with: liquid fall or ullage bubble rise time, turbulent dissipation time, and bubble rise time. Laminar dissipation times associated with slosh wave dissipation after settling were calculated, but not used in determining total settling time.   The total time was assumed to be equal to the sum of the turbulent dissipation and bubble rise times and the larger of the liquid fall or ullage rise times.   Adding the bubble rise time to the turbulent dissipation time is conservative in that bubbles can begin to rise while the liquid turbulent motion caused by impact is decreasing.   However, experiments reported in References 30 and 31 indicated that the turbulent motion does cause bubbles to be swept back towards the bottom of the tank.   There is currently no way of determining when bubbles will rise in low g, with significant turbulent motion, and therefore, it is assumed that some bubbles are near the bottom of the tank when the turbulent motion has decayed.

The equations for bubble rise or liquid fall times have been verified by both drop tower tests performed at NASA-LeRC (Reference 32) and by the 1-g tests performed at MDAC (Reference 31).

The turbulent dissipation factor associated with large tanks and cryogenic liquids has not been determined, but in all of the MDAC 1-g IRAD tests, the dissipation rates corresponded to a dissipation factor of 0.15 or less.   Consequently, the maximum turbulent dissipation factor used to calculate the dissipation time was taken as 0.15, and a minimum value equal to ten times the laminar dissipation factor is used for comparison.

The bubble rise velocity is automatically determined for the appropriate condition in the program, using equations for Stokes flow, the transition regime, spherical cap, and Harmathy regime.   The safe distance to which the bubble must rise is 1 m for both the LH_2 and LO_2 tanks; if the liquid depth is less than 1 m, the safe distance is equal to this depth.   The average bubble diameter is calculated using the equations given in Reference 31.   The bubble diameter is a function of an empirical parameter, n, the volume fraction of ullage gas entrained as bubbles in the liquid.   Preliminary computer runs indicated that for n varying between 10 to 50%, the bubble rise times were essentially the same since the bubbles were within the same flow regime, and the average diameter is not a strong function of n.

222

The assumed mission for the ASPM requires six high thrust burns demanding settling maneuvers with 95, 63, 42, and 16 percent liquid, and two maneuvers with only 5 percent liquid, approximately. Within the accuracy of the program, the last two cases are considered to have the same settling times, calculated for 5 percent liquid.

The individual settling times, total times, and propellant weights for LH_2 and LO_2 tank settling are summarized in Table 6-1, for which a constant settling acceleration of 1.55×10^{-3} g is used; the LH_2 results fix the design conditions, since LO_2 settling times are less than for LH_2. This case corresponds to a throttlable ACS engine with a thrust range from 111-445 Newtons (25-100 lbs). The total propellant required for settling is 54 kg (118 lbs).

Table 6-2 summarizes results for a constant vehicle acceleration, throttlable engine and a low turbulent dissipation factor. The total propellant consumption is significantly increased, resulting in a weight of 155 kg (341 lbs); this weight is considered to be an upper bound, and assumes that turbulent dissipation resulting from liquid impact with the tank bottom and within the bulk liquid itself is minimized by a relatively smoothly flowing asymmetric settling condition for which liquid sweeps down one side of the tank and up the other. These cases with asymmetric settling at high Bond numbers deserve additional study.

Use of a throttlable engine to maintain the same settling acceleration of the propellant for all six cases is probably not practical. If a constant thrust engine is used, the settling acceleration will, of course, increase as the percentage of main tank propellants is decreased. The settling time will also decrease, but the settling propellant required will increase. Table 6-3 summarizes the results and shows that settling propellant consumption is 76 kg (168 lbs) for the high turbulent dissipation case. Table 6-4 shows an additional increase in propellant consumption, to a total 237 kg (523 lbs), for the low turbulent dissipation factor assumption. The constant thrust settling requirements were also repeated with a thrust of 890 Newtons (200 lbs). The results are summarized in Tables 6-5 and 6-6.

Propellant consumption in Table 6-5 is seen to be increased approximately 60% over the comparable 445 Newton (100 lbs) thrust case for the high turbulent dissipation rate, resulting in a total propellant weight of 123 kg (270 lbs). The low turbulent dissipation rate case results in a 70% increase, to 394 kg (868 lbs) of propellant. Increasing the settling acceleration decreases the total settling time but increases the propellant consumption.

6.2 Thruster System Estimated Weights

Based on the above computed settling propellant requirements, weights were generated for an N_2O_4/MMH bipropellant APS system. The following conditions were assumed: Isp = 300 sec; densities = 1445 kg/M^3 (90.1 lb/ft^3) and 876 kg/M^3 (54.6 lb/ft^3) for N_2O_4 and MMH, respectively; chamber pressure = 965×10^3 N/M^2 (140 pgis) tank pressure = 1517×10^3 N/M^2 (220 psia) thrust = 445 N (100 lb) per engine with two engines operating;

Table 6.1

ASPM SETTLING SYSTEM PARAMETERS

Burn No.	Percent Liquid (%)	GAMTUR	$a_{Initial}/g$	a_{Final}/g	Rise Time (sec)	Drop Time (sec)	Turbulent Time (sec)	Bubble Time (sec)	Total Time (sec)	Propellant Weight (kg)	Thrust (lb)
1	95	0.15	1.55×10^{-3}	1.55×10^{-3}	47.5	9.8	37.3	23.8	108.7	16.2	(439)
2	63	0.15	1.55×10^{-3}	1.55×10^{-3}	27.9	17.4	79.7	23.8	131.5	14.2	(318)
3	42	0.15	1.55×10^{-3}	1.55×10^{-3}	18.5	20.2	80.8	23.8	124.9	10.2	(244)
4	16	0.15	1.55×10^{-3}	1.55×10^{-3}	7.4	23.6	65.2	23.8	112.6	6.1	(161)
5	5	0.15	1.55×10^{-3}	1.55×10^{-3}	2.5	25.4	37.3	16.9	79.5	3.2	(119)
6	5	0.15	1.55×10^{-3}	1.55×10^{-3}	2.5	25.4	37.3	16.9	79.5	3.2	(119)
					106.3	121.8	337.6	129.0	636.7	53.1	

Table 6.2

ASPM SETTLING SYSTEM PARAMETERS

Burn No.	Percent Liquid (%)	GAMTUR	$a_{Initial}/g$	a_{Final}/g	Rise Time (sec)	Drop Time (sec)	Turbulent Time (sec)	Bubble Time (sec)	Total Time (sec)	Propellant Weight (kg)	Thrust (lb)
1	95	0.032	1.55×10^{-3}	1.55×10^{-3}	47.5	9.8	175.0	23.8	246.4	37	(439)
2	63	0.032	1.55×10^{-3}	1.55×10^{-3}	27.9	17.4	374.0	23.8	425.9	46	(318)
3	42	0.032	1.55×10^{-3}	1.55×10^{-3}	18.5	20.2	379.5	23.8	423.6	35.1	(242)
4	16	0.032	1.55×10^{-3}	1.55×10^{-3}	7.4	23.6	306.1	23.8	353.5	19.3	(161)
5	5	0.032	1.55×10^{-3}	1.55×10^{-3}	2.5	25.4	175.0	16.9	217.3	8.9	(119)
6*	6	0.032	1.55×10^{-3}	1.55×10^{-3}	2.5	25.4	175.0	16.9	217.3	8.9	(119)
					106.3	121.8	1584.6	113.0	1884.0	155.2	

*Same as 5, to within accuracy of analysis

Table 6.3

ASPM SETTLING SYSTEM PARAMETERS

Burn No.	Percent Liquid (%)	GAMTUR	$a_{Initial}/g$	a_{Final}/g	Rise Time (sec)	Drop Time (sec)	Turbulent Time (sec)	Bubble Time (sec)	Total Time (sec)	Propellant Weight (kg)	Thrust (lb)
1	95	0.15	1.57×10^{-3}	1.57×10^{-3}	47.2	9.8	37.0	23.8	108.0	16.3	(445)
2	63	0.15	2.17×10^{-3}	2.17×10^{-3}	23.6	14.7	68.8	21.9	114.3	17.3	
3	42	0.14	2.83×10^{-3}	2.83×10^{-3}	13.7	15.0	65.3	20.5	100.8	15.3	
4	16	0.12	4.3×10^{-3}	4.3×10^{-3}	4.5	14.2	47.5	18.5	80.2	12.1	
5	5	0.115	5.8×10^{-3}	5.8×10^{-3}	1.3	13.1	25.2	12.1	50.5	7.6	
6*	5	0.115	5.8×10^{-3}	5.8×10^{-3}	1.3	13.1	25.2	12.1	50.5	7.6	
					92.6	79.9	269.0	108.9	504.3	76.2	

*Same as 5, to within accuracy of analysis

Table 6.4

ASPM SETTLING SYSTEM PARAMETERS

Burn No.	Percent Liquid (%)	GAMTUR	$a_{Initial}/g$	a_{Final}/g	Rise Time (sec)	Drop Time (sec)	Turbulent Time (sec)	Bubble Time (sec)	Total Time (sec)	Propellant Weight (kg)	Thrust (lb)
1	95	0.032	1.57×10^{-3}	1.57×10^{-3}	47.2	9.8	174.4	23.8	245.4	37.1	(445)
2	63	0.029	2.17×10^{-3}	2.17×10^{-3}	23.6	14.7	344.0	21.9	385.5	58.9	
3	42	0.027	2.8×10^{-3}	2.8×10^{-3}	13.7	15.0	326.0	20.5	362.1	54.8	
4	16	0.025	4.3×10^{-3}	4.3×10^{-3}	4.5	14.2	237.4	18.5	270.1	40.9	
5	5	0.023	5.8×10^{-3}	5.8×10^{-3}	1.3	13.1	126.0	12.1	151.3	22.9	
6*	5	0.023	5.8×10^{-3}	5.8×10^{-3}	1.3	13.1	126.0	12.1	151.3	22.9	
					92.6	79.9	1334.4	108.9	1565.7	237.5	

*Same as 5, to within accuracy of analysis

Table 6.5

ASPM SETTLING SYSTEM PARAMETERS

Burn No.	Percent Liquid (%)	GAMTUR	$a_{Initial}/g$	a_{Final}/g	Rise Time (sec)	Drop Time (sec)	Turbulent Time (sec)	Bubble Time (sec)	Total Time (sec)	Propellant Weight (kg)	Thrust (lb)
1	95	0.134	3.14×10^{-3}	3.14×10^{-3}	33.4	6.9	29.4	20.0	82.8	25.0	(890)
2	63	0.124	4.35×10^{-3}	4.35×10^{-3}	16.7	10.4	57.8	18.4	93.0	28.1	
3	42	0.116	5.65×10^{-3}	5.65×10^{-3}	9.7	10.6	54.9	17.3	82.8	25.0	
4	16	0.104	8.6×10^{-3}	8.6×10^{-3}	3.2	10.0	39.9	15.5	65.5	19.8	
5	5	0.097	1.16×10^{-2}	1.16×10^{-2}	0.9	9.3	21.2	10.2	40.7	12.3	
6	5	0.097	1.16×10^{-2}	1.16×10^{-2}	0.9	9.3	21.2	10.2	40.7	12.3	
					64.8	56.5	224.4	91.6	405.5	122.5	

Table 6.6

ASPM SETTLING SYSTEM PARAMETERS

Burn No.	Percent Liquid (%)	GAMTUR	$a_{Initial}/g$	a_{Final}/g	Rise Time (sec)	Drop Time (sec)	Turbulent Time (sec)	Bubble Time (sec)	Total Time (sec)	Weight (kg)	Thrust (lb)
1	95	0.027	3.14×10^{-3}	3.14×10^{-3}	33.4	6.9	146.8	20.0	200.3	60.3	(890)
2	63	0.025	4.35×10^{-3}	4.35×10^{-3}	16.7	10.4	289.2	18.4	324.4	98.1	(890)
3	42	0.023	5.65×10^{-3}	5.65×10^{-3}	9.7	10.6	274.7	17.3	302.6	91.4	(890)
4	16	0.021	8.6×10^{-3}	8.6×10^{-3}	3.2	10.0	199.5	15.5	225.1	68.1	(890)
5	5	0.019	1.16×10^{-2}	1.16×10^{-2}	0.9	9.3	105.9	10.2	125.4	38.0	(890)
6	5	0.019	1.16×10^{-2}	1.16×10^{-2}	0.9	9.3	105.9	10.2	125.4	38.0	(890)
					64.8	56.5	1122.0	91.6	1303.2	393.9	

Table 6.7
ESTIMATED ACCELERATION SETTLING SYSTEM WEIGHTS (kg)

	MINIMUM	MAXIMUM
N_2O_4 TANK	5	10.4
MMH TANK	5	10.4
HELIUM BOTTLE	1.8	4.5
HELIUM GAS	0.5	0.9
TANKAGE CONTROLS	4.5	4.5
TANKAGE SUPPORTS	1.8	3.2
PLUMBING	1.8	1.8
TOTAL TANKAGE	20.4	35.7
THRUSTERS (2)	4.5	4.5
ISOLATION VALVES	3.2	3.2
THRUST STRUCTURE	0.9	0.9
TOTAL INERTS	8.6	8.6
PROPELLANT*	127	407
TOTAL SYSTEM	156	451.3

*CONSTANT 890N (200 LBS) THRUST SETTLING WITH I_{sp} = 300 SEC

bladder expulsion tank; titanium tankage; helium pressurization. These values generally correspond with conditions being used on the NASA-MDAC Space Tug Study.

The calculated or estimated weights are summarized in Table 6-7.

6.3 Evaluation

The above results from the propallent settling analysis were used to generate a weight comparison between the selected LPIC acquisition system and the minimum and maximum weight settling systems for the ASPM application. The settling system is a separate N_2O_4/MMH subsystem consisting of bladder expulsion tanks and two separate thrusters which are not

used for attitude control; this function is performed by the integrated cryogenic ACS thrusters. It is assumed that the vehicle is preferentially oriented prior to the settling acceleration such that the ΔV settling is additive. Therefore, the principal penalty is due to the lower I_{sp} of the storable propulsion system (290 sec) compared to the cryogenic system (420 sec).

Three types of weight comparisons were considered and are summarized in Table 6.8: (1) the total system hardware and propellant weights; (2) the subsystem weight penalties; and (3) the payload weight penalties. The hardware and propellant weight numbers were taken from Table 6.6. The weight penalty accounts for the fact that the storable propellant have a lower I_{sp} than the cryogenic propellants, and thus the ΔV gained, although additive, requires a greater weight penalty than would be required if LH_2/LO_2 were used. The acquisition system weights shown include those system weights only associated with the provisions for acquisition. For example, the 74.5 kg indicated for the LH_2 system consists of 39.1 kg for the acquisition device plus 23 kg for components, plus 12.4 kg for pressurization hardware penalties. The 11.6 kg expendables is mainly helium pressurization gas.

The payload weight penalties are based on the sensitivity fraction (Δ PAYLOAD/Δ STAGE WEIGHT) generated for a Space Tug for three characteristic missions: D, deployment (6 restarts), R, retrieval (6 restarts), RT, and roundtrip (8 restarts). The roundtrip mission fits most closely to the baseline mission and design requirements for this study, which assumes 8 restarts for deployment/retrieval (see Section 2).

The values shown in Table 6.7 indicate that for vehicles with a limited number of defined burns and where on-demand flow is not a major requirement, pure acceleration settling is weight competitive with a surface tension acquisition system. For a deployment mission, pure settling results in a weight penalty of between 138 and 308 kg whereas an acquisition system has a weight penalty of 384 kg. For a roundtrip mission, pure settling results in a payload weight panelty of 59 to 146 kg whereas an acquisition system involves a weight penalty of 148 kg. However, stage flexibility requirements would probably still dictate the use of a surface tension acquisition system particularly for applications like the Space Tug vehicle.

Table 6.8

COMPARISON OF PURE SETTLING AND ACTIVE ACQUISITION (kg)
(ASPM APPLICATION)

	Sub-System Weight		Sub-System Weight Penalty		Payload Decrease		
	D-R	RT	D+R	RT	D	R	RT
Minimum Settling							
Hardware	29	29	29	29	80	46	29
Propellant	127	177	42	59	58	34	30
	156	206	71	88	138	80	59
Maximum Settling							
Hardware	44	44	44	44	121	70	44
Propellant	407	631	136	203	187	109	102
	451	675	180	247	308	179	149
Acquisition System							
LH$_2$ System	74.5	66.7	74.5	66.7	183	119	75
LO$_2$ System	67.4	67.4	67.4	67.4	185	108	67
Expendables	11.6	11.6	11.6	11.6	16	9	6
	153.5	145.7	153.5	145.7	384	236	148
Weight Sensitivities (ΔWt. Payload/ ΔWt Stage)					2.75	1.6	1
Inerts/ Expendables					1.375	0.8	0.5

228

Section 7

CONCLUSIONS

A number of important overall conclusions can be drawn from the con-
ducted in-depth design study of surface tension acquisition/expulsion systems.

1. It has been shown that practical screen surface tension acquisition
   devices can be designed and built to satisfy a broad range of appli-
   cations for cryogenic storage and transfer systems. Furthermore,
   these systems are relatively low in weight and can be designed
   using present technology to satisfy potential failure modes without
   relying on extensive in-orbit experimentation.

2. In order to arrive at valid acquisition concept selections, the
   evaluation must be conducted on an overall feed system basis.
   Each particular acquisition concept tends to place constraints
   or other interfacing subsystems, such as pressurization and
   thermal management, which involves their overall design and
   optimization. This in turn impacts the total feed system perfor-
   mance.

3. For a system with a limited number of defined expulsion steps, a
   pure acceleration liquid settling approach may be weight competi-
   tive with a surface tension acquisition system. This, however,
   does reduce system flexibility.

4. In order to further optimize and improve surface tension acquisi-
   tion system design, additional research is required to improve
   the qualitative and quantitative understanding of the influence of
   environmental conditions on surface tension device behavior and
   performance including pressurant gas heating, feed system vibra-
   tion and feed system flow dynamics. Techniques are currently
   available for designing around potential problems in these areas
   but this generally results in weight penalties and operational
   constraints that could be relieved with improved understanding.

Appendix A
NONUNIFORM FLOW IN AN ACQUISITION
SCREEN CHANNEL

A1. Problem Description

The pressure loss associated with propellant flow through the screen surfaces of a surface tension acquisition device contributes strongly to the sizing of the device. Losses throughout the system must be held to a small value so that surface tension forces (limited to approximately 0.09 psi in LH_2) can prevent the entrance of pressurant into the suction line.

In the past, the pressure loss through the screen was computed on the basis of an average and uniform velocity of flow (volume flow rate/screen area) through the submerged portions of the screen surface. Empirical techniques are available to relate velocity to a ΔP based on propellant and screen properties. However, the combination of viscous and dynamic effects can cause the flow velocity through the screen surface to be significantly non-uniform. When this is the case, the actual ΔP that must be used to size the acquisition device is larger than that ΔP which would be computed based on an average flow velocity through the screen. Therefore, it is important to determine the actual variation in flow. The analysis that flows is directed toward the situation where a propellant collection channel having part of its surface consisting of a porous material (which may or may not be woven screen) is submerged in the propellant while a known mass flow rate of liquid is being withdrawn from the channel. The variation in flow through the porous material will be computed.

A2. Analysis

Consider the channel shown schematically in Figure A-1. The mass outflow rate of an incompressible fluid is Q. The flow velocity in the channel (parallel to its centerline is assumed to be uniform over any cross section and is defined as u. The channel length is H, and the cross-sectional area is LD, where L is the width of the porous material on the channel. Viscous flow losses within the channel are computed using Darcy's equation with friction factor f and hydraulic radius $D_h/4$. The flow through the porous material is v. Two equations are developed based on a treatment of a small incremental element, Δx, of the fluid in the channel.
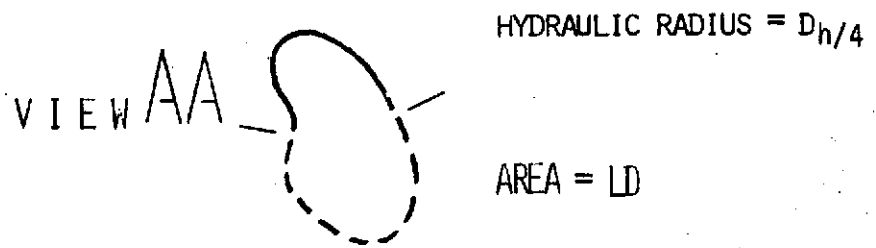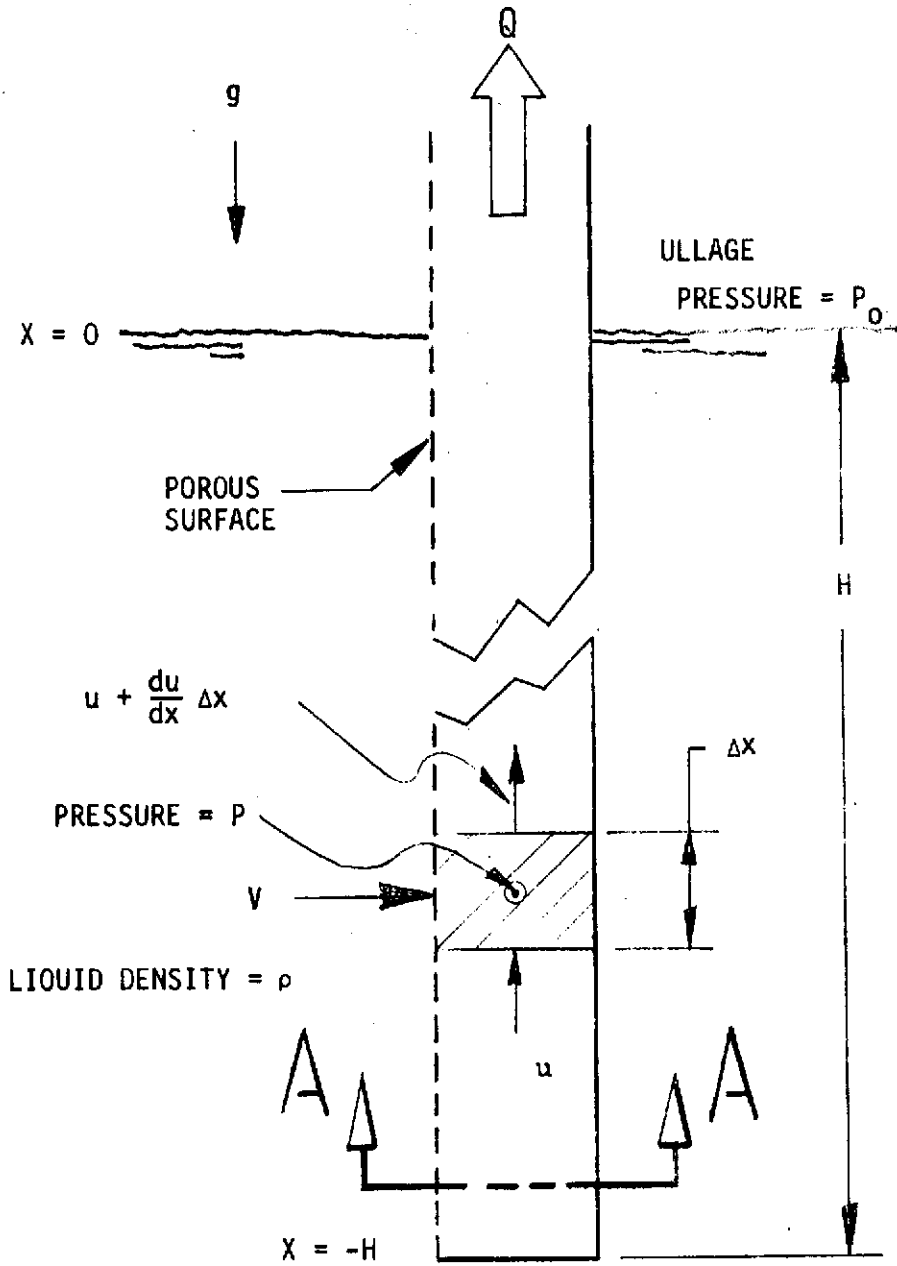
Figure A-1. Channel Configuration

Continuity:

$$\cdot V = D \frac{du}{dx}$$ (A1)

Momentum:

$$\frac{dP}{dx} + f \frac{\rho}{2D_h} u^2 + 2 \rho u \frac{du}{dx} + g = 0$$ (A2)

The flow loss through the porous material is assumed to be correlated by an equation of the form

$$K_o V = P_o - \rho g x - P$$ (A3)

where K_o is determined experimentally. Equation A3 is applicable for low v. In terms of Armour and Cannon's correlation (Reference 6), the relevant region is where $8.6/N_{Re} >> 0.52$. Three equations are not available to solve for the three unknowns (P, v, and u). The two boundary conditions are

$$x = -H, \quad u = 0$$

$$x = 0, \quad Q = LDu$$

The equations are nondimensionalized by substituting

$$u^* = \frac{u}{u_{max}} = \frac{\rho u D L}{Q}$$

$$v^* = \frac{v}{v_{avg}} = \frac{\rho V L H}{Q}$$

$$Z = \frac{X + H}{H}$$

$$\Delta P^* = \frac{P_o - P}{\Delta P_{avg}} = \frac{(P_o - P) \, LH}{K_o Q}$$

232

The three basic equations now become

$$v* = \frac{du*}{dZ} \qquad\qquad (A4)$$

$$v* = \Delta P* - \frac{\rho^2 LH^2 g}{K_o Q}(Z - 1) \qquad\qquad (A5)$$

$$\frac{d(\Delta P*)}{dZ} - \frac{fQH^2}{2D_h D^2 LK_o}u*^2 - \frac{\rho^2 LH^2 g}{K_o Q} = \frac{2QH}{D^2 LK_o}u* \frac{du*}{dZ} \qquad\qquad (A6)$$

These three equations can be combined into a single nonlinear equation for u*.

$$\frac{d^2 u*}{dZ^2} - F\phi u*^2 - \phi u* \frac{du*}{dZ} = 0 \qquad\qquad (A7)$$

where

$$F = \frac{fH}{4D_h}$$

$$\phi = \frac{2QH}{D^2 LK_o}$$

Boundary conditions:

$$Z = 0, \quad u* = 0$$

$$Z = 1, \quad u* = 1$$

Since g has no influence on the flow characteristics, the solutions for u and v are not dependent upon the channel being straight or perpendicular to the liquid surface.

Equation A7 is first solved by assuming that F = 0 in order to simplify the solution.

$$\frac{d^2 u^*}{dZ^2} - u^* \frac{du^*}{dZ.} = 0 \tag{A8}$$

Integrating yields

$$\frac{du^*}{dZ} = \frac{\phi}{2} u^{*2} + C_1^2 \tag{A9}$$

where C_1 is real and positive. This equation is of Riccati's form and is converted to linear form by the substitution

$$u^* = iC_1 \sqrt{\frac{2}{\phi}} + \frac{1}{U}$$

yielding

$$\frac{dU}{dZ} + iC_1 \sqrt{2\phi}U = -1 \frac{\phi}{2} \tag{A10}$$

Solving for U and then u^* and substituting for the boundary conditions results in

$$u = C_1 \sqrt{\frac{2}{\phi}} \tan\left(C_1 \sqrt{\frac{\phi}{2}} Z\right) \tag{A11}$$

where C_1 is given by the transcendal equation

$$C_1^1 \sqrt{\frac{\phi}{2}} = \tan\left(C_1 \sqrt{\frac{\phi}{2}}\right) \tag{A12}$$

This last equation has been solved numerically using Newton's method. Values found are shown in Figure A-2. Figure A-3 is a plot of v^* (flow velocity through the porous material) at $x = 0$ ($Z = 1$, v^* is a maximum) and $x = -H$ ($Z = 0$, v^* is a minimum). Figure A-4 shows the two constants, $C_1 \sqrt{2/\phi}$ and $C_1 \sqrt{\phi/2}$, that appear in Equation A11.

Nite in Figure A-3 that v^* begins to depart significantly from 1.0 (the average velocity) at both ends of the channel when ϕ exceeds approximately 1.0. Note also that according to Equation A5, $v^* = \Delta P^*$ when $Z = 1$. Therefore, Figure A-3 can be used directly to determine ΔP^*, and consequently the ΔP at $x = 0$, which is the value needed for channel sizing purposes.

NUMERICAL SOLUTION TO:

$$\frac{1}{C_1}\sqrt{\frac{\phi}{2}} = TAN\left(C_1\sqrt{\frac{\phi}{2}}\right)$$
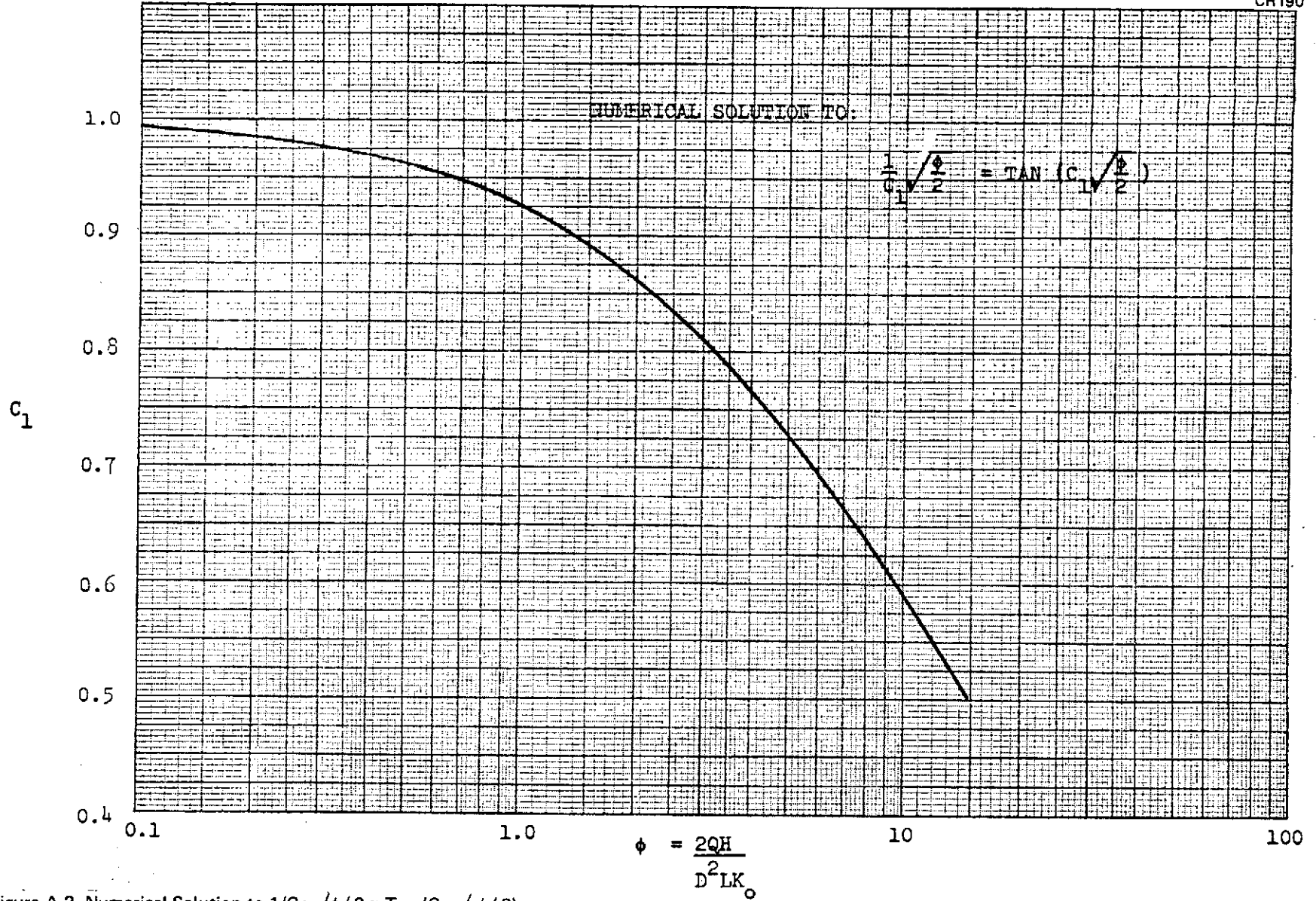
$$\phi = \frac{2QH}{D^2LK_o}$$

Figure A-2. Numerical Solution to $1/C_1\sqrt{\phi/2} = Tan(C_1\sqrt{\phi/2})$
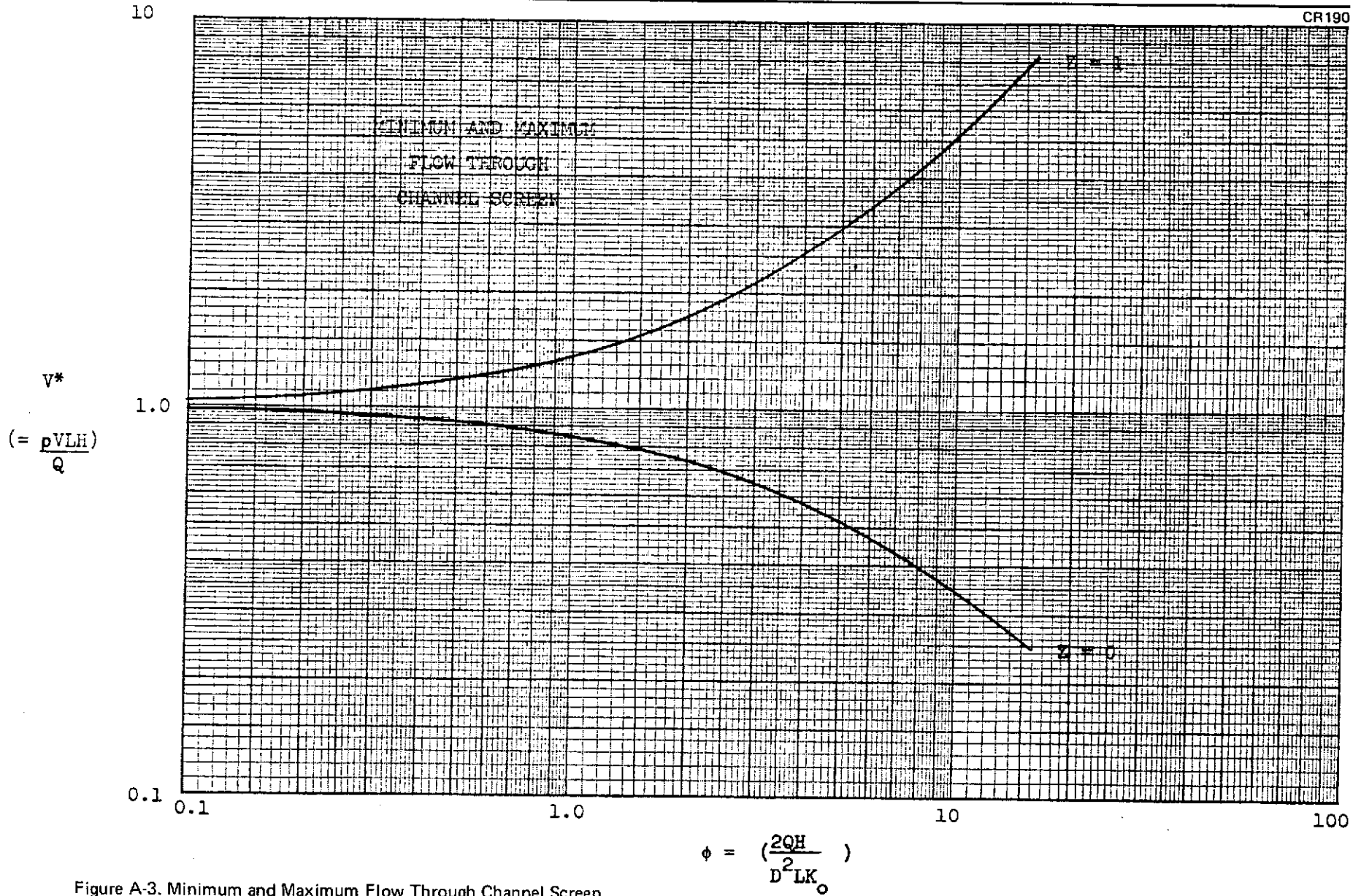
Figure A-3. Minimum and Maximum Flow Through Channel Screen

SOLUTION CONSTANTS

$$N = c_1 \sqrt{\frac{2}{\phi}} \; \tan \left(c_1 \sqrt{\frac{\phi}{2}} \right)$$

$c_1 \sqrt{\dfrac{2}{\phi}}$

$c_1 \sqrt{\dfrac{\phi}{2}}$

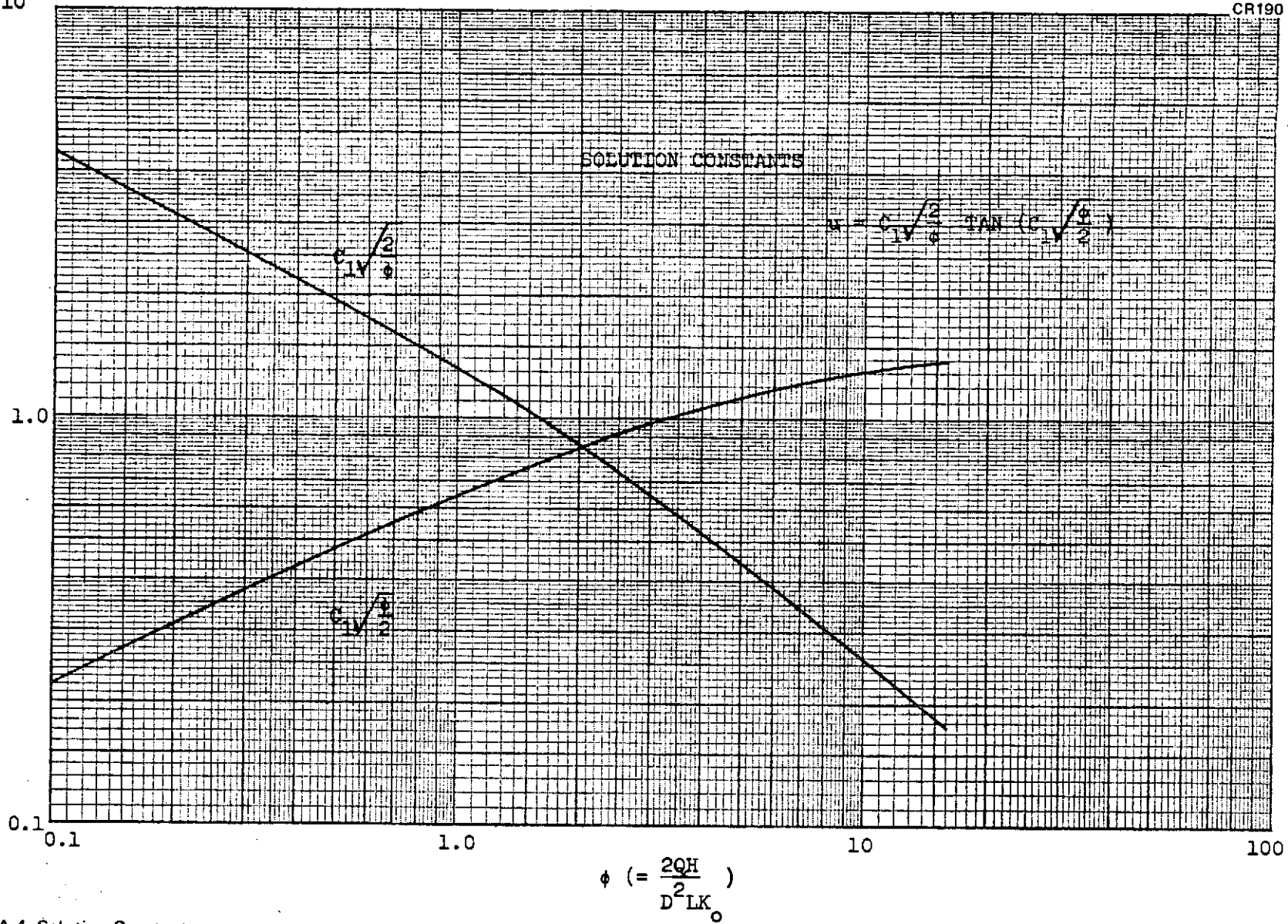$$\phi \; \left(= \frac{2QH}{D^2 L K_o} \right)$$

Figure A-4. Solution Constants

The relative influence of F on the solution can be investigated by comparing the magnitude of the second and third terms in Equation A7 using the solution of Equation A8 for u*. This ratio is plotted in Figure A-5 at Z = 1 (x = 0) as a function of ϕ (The ratios at Z = 0 are approximately five times as large). The largest value selected for F should encompass the practical cases of interest.

It is proposed that the solution for U* need not be improved by including a treatment of F. Two reasons are offered to support this conslusion. First, the solutions for v* and ΔP* do not differ from 1.0 significantly for $\phi < 1$, where the term containing F is largest in relation to the other terms. In the region $\phi < 1$, the two terms $F\phi u*^2$ and $\phi u*u'$ may have the same magnitude, but together they do not appreciably change v* and ΔP* from 1.0. Secondly, in practical applications, the ΔP becomes critical when H is small (i.e., when a small length of channel is covered). With small H, it should customarily be that F < 0.1, which renders the influence of the F $\phi u*^2$ term minor compared to $\phi u*u*'$ (<10 percent). As the solution becomes more important in the ΔP in increasing rapidly in size with dimishining H, the solution for u* and v* becomes more accurate because of diminishing F.
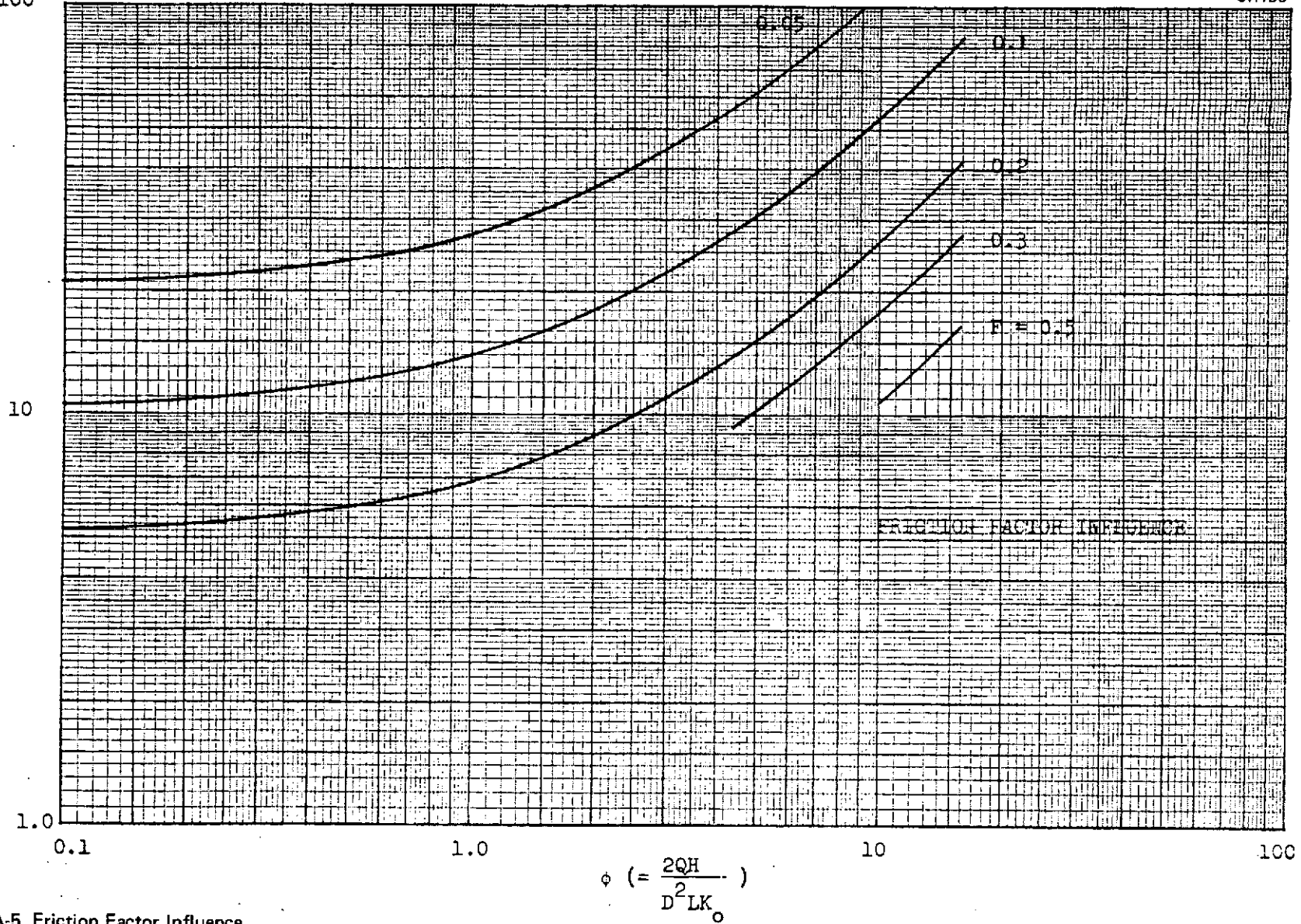
$$\frac{\phi u^{*du^{*}}/dZ}{F\phi u^{*2}}$$

(AT Z = 1)

$\phi \quad (= \frac{2QH}{D^{2}LK_{o}} \cdot)$

Figure A-5. Friction Factor Influence

Appendix B

ALL SCREEN CHANNEL DEVICE STABILITY
VERIFICATION TEST PROCEDURE

Two qualification test procedures are outlined below for the bubble point verification of large-scale all-screen devices. Both procedures are based on the principle that a film of liquid on the screens seals each screen pore and that the hydrostatic head, relative to a screen device filled with liquid, is negligible. Screen devices larger than the supportable heights of liquid columns can therefore be tested using films of wetting liquids. This procedure is practical with screen devices in tanks, whereas, submerging large screen devices in a test liquid and performing standard bubble point test (e. g. , SAE ARP 901) cannot be done with the large-scale screen devices assembled within propellant tanks. These procedures are used primarily to verify that a large-scale screen device maintains indefinitely a stable sealing interface at a pressure slightly less than the breakdown bubble point pressure of the screen. The procedures are used during the qualification testing of the tank final assembly and as a checkout test of the screen devices during routine maintenance. Failure of the screen device to meet the design capillary pressure difference would necessitate removal and replacement (or repair) of the screen device, which requires access to the tank. However, both procedures developed below do not require tank access, and can be performed with the vehicle in either a horizontal or vertical orientation.

1.   Isothermal Liquid Film Pressure Difference Test Procedure. The isothermal liquid film pressure difference test procedure is used for relatively small screen devices which can be initially surrounded with the test liquid in a practical manner. For example, filling a 1 to 3 m^3 secondary tank with the test liquid is practical, but completely filling the large-scale main tank with test liquid so as to wet the distributed all-screen channels is not recommended from a loading and cost standpoint.

Figure B1 is the schematic diagram for one method of screen device bubble point verification for the secondary tanks, which in principle would be used with other localized devices. Following tank cleaning procedures, the test liquid (e. g. , isopropyl alcohol, methanol, Freon 114) is pumped into the tank at ambient temperature through the connections upstream of the secondary tank main feed line valve, while the tank is vented through the auxiliary overboard vent. When full, the test liquid supply valve is closed. The supply gas (N_2, He, etc.) is then bubbled through the alcohol accumulator to displace the test liquid in the tank with a gas mixture saturated with alcohol vapor at the ambient temperature of the system. The drain valve is opened and test liquid is slowly displaced from the incoming gas mixture.

The gas enters the tank through the overboard vent line and throug the feedline so that there is no pressure difference between the inside of the

PRESSURE BOTTLE (N$_2$, He, etc.)

TEST
LIQUID

START TANK

CHANNEL

FEEDLINE

TEST LIQUID SUPPLY

AUXILIARY
OVERBOARD
VENT

PRESSURE REFERENCED
TO START TANK

MANUAL CONTROL
VALVE

PRESSURE
BOTTLE

PRESSURE
INSIDE
CHANNEL

TRANSPARENT
TANK OF
TEST LIQUID

MANOMETER #2
START TANK
GAUGE PRESSURE
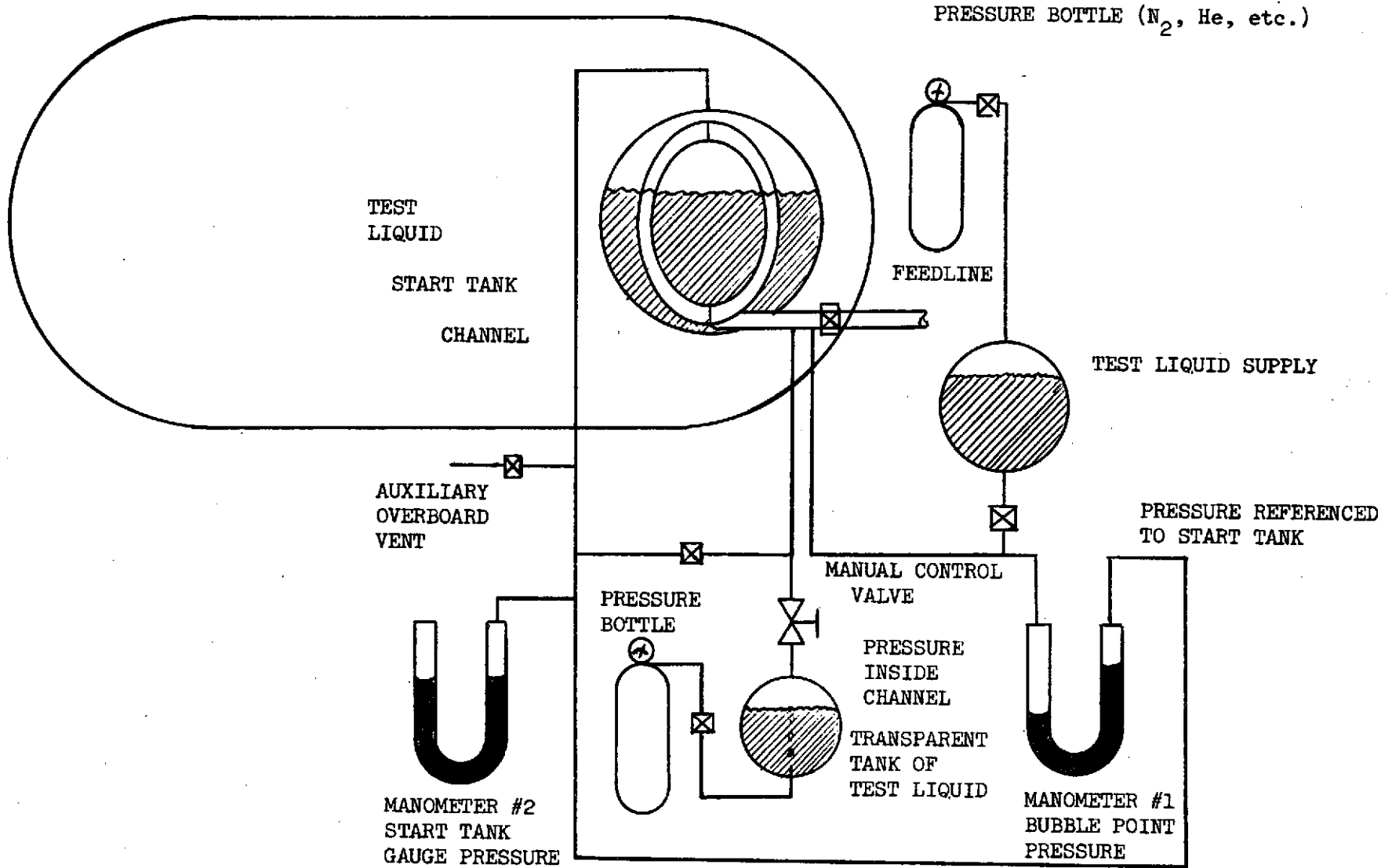
MANOMETER #1
BUBBLE POINT
PRESSURE

Figure B-1. Bubble Point Verification Test

channel device and the secondary tank which could break through the liquid film covering the screen. Since the system is isothermal and there are no test fluid concentration gradients in the ullage, the film of liquid remains on the screen as the bulk liquid drains from the tank.

When empty, the test liquid drain valve is closed and the bubble point pressure is checked by introducing a gas mixture through a transparent vessel containing the test liquid into the channel device. The gas entering the channel is saturated at the appropriate partial pressure of the test liquid to alleviate mass concentration gradients in the channels which could lead to evaporation of the liquid film. The transparent vessel allows direct observation of the gas bubbles entering the channel and thus can be used to verify that there is no leakage from the channel through unsealed screen pores into the tank. The pressure difference between the inside of the channels and the tank is monitored with manometer No. 1, and the gage pressure of the tank is monitored with manometer No. 2.

After reaching the design pressure for which screen stability must be assured, the transparent test vessel and tank gage pressures are observed for approximately 10 minutes to 1 hour; if no additional gas enters the channels and/or the secondary tank pressure is constant during this period, no leakage has occurred through the screen. The design pressure for screen stability is thus verified.

2. Condensing Liquid Film Pressure Difference Test. The condensing liquid film pressure difference test departs from the preceding isothermal test only in the manner in which the liquid film is formed on the screens. Rather than filling a tank to wet the screens, a saturated vapor flow of the test fluid is introduced into the tank at a temperature slightly above the tank temperature. Condensation thus occurs on the tank walls and screen device, as demonstrated by the test discussed in Section 3.2.9. During the condensation flow process, the vapor enters both through the channels and directly into the tank so as to maintain a negligibly small pressure difference across the screens. The fluid enters at the top of each channel so that the falling condensate film enhances the wetting of the screens.

Although the bench test described in Section 2.3.4 of Volume II demonstrated the feasibility of the condensing film technique, further tests are required to establish such parameters as the saturated vapor inflow rate and time required to totally wet the screen, and to determine the most appropriate test fluid. In addition, analyses are required of the interrelationships of the saturation temperature and pressure, heat transfer through the tank walls, and initial temperature of the tank.

A candidate procedure which eliminates much of the transient heat transfer problem involves initially cooling the tank below the ambient temperature. A saturated vapor having a vapor pressure equal to or greater than 1 atmosphere at the ambient temperature is then transferred into the tank at approximately 1 atmosphere or above. As condensation occurs, the tank internal temperature will rise, eventually reaching a steady-state temperature equal to the ambient temperature. This condition can be maintained indefinitely, thus allowing long-term bubble point tests to be conducted. Pressures equal to or greater than 1 atmosphere are used to avoid problems of crushing pressure loads on the tank wall.

Appendix C

PRESSURE DECAY INDUCED RETENSION BREAKDOWN
WITH AUTOGENOUS PRESSURIZATION

As discussed in Section 3.1.1.3, autogenous pressurization even with very low inlet temperatures, may be desirable from a weight standpoint. Interaction between autogenous pressurant gas and screen devices causes vapor condensation and ingestion into the screen device which can result in retention breakdown. The ingested liquid is warmer than that retained in the device, and pressure decay induced vaporization within the screen device can result in subsequent screen retention breakdown.

The screen device failure mode envisioned for cryogens results from the vapor pressure in the tank dropping below the saturation vapor pressure of liquid within the screen device, leading to a "boiling" (or, more precisely, vaporization) phenomenon. The rate of vaporization would be expected to increase rapidly as the tank vapor pressure drops further below the saturation vapor pressure of the liquid, because more superheat becomes available.

The existence of a stratified region of liquid would occur readily in a low-gravity environment with autogenous pressurization of propellant to a level necessary to meet practical NPSH requirements of the order of 13.8×10^3 to 69×10^3 N/M^2 (2 to 10 psi). For example, consider the autogenous pressurization of liquid hydrogen, initially at 20.3°K (36.5°R), to a tank pressure (i.e., hydrogen vapor pressure) of 2.07×10^5 N/M^2 (30 psia). The hydrogen vapor temperature in the ullage could vary from 4.15°R upward. Any free surface of liquid exposed to this vapor would essentially instantaneously reach a surface temperature of 41.5°R, corresponding to the vapor pressure of 2.07×10^5 N/M^2 (30 psia). Whether or not evaporation or condensation occurred at the interface would depend on the relative rates of heat transfer in the liquid and vapor regions, as shown by the following equation for the mass flux of condensed or evaporated liquid, $\rho_L v_L(t)$:

$$\rho_L v_L(t): = \frac{q_L}{L} - \frac{q_v}{L}$$

For $\rho_L v_L(t)$ positive, condensation occurs, whereas evaporation occurs for $\rho_L v_L(t)$ negative. Figures C-1 and C-2 illustrate a qualitative comparison of the temperature profiles with condensation and evaporation. For high heat fluxes in the vapor region relative to the liquid region, as a result of high vapor temperature, convection of the vapor, or radiation, evaporation would occur. For cases of high heat fluxes in the liquid region, relative to the vapor region, condensation would occur. This case corresponds to a dual screen, or channel, with liquid flow and/or natural convection. The vapor region
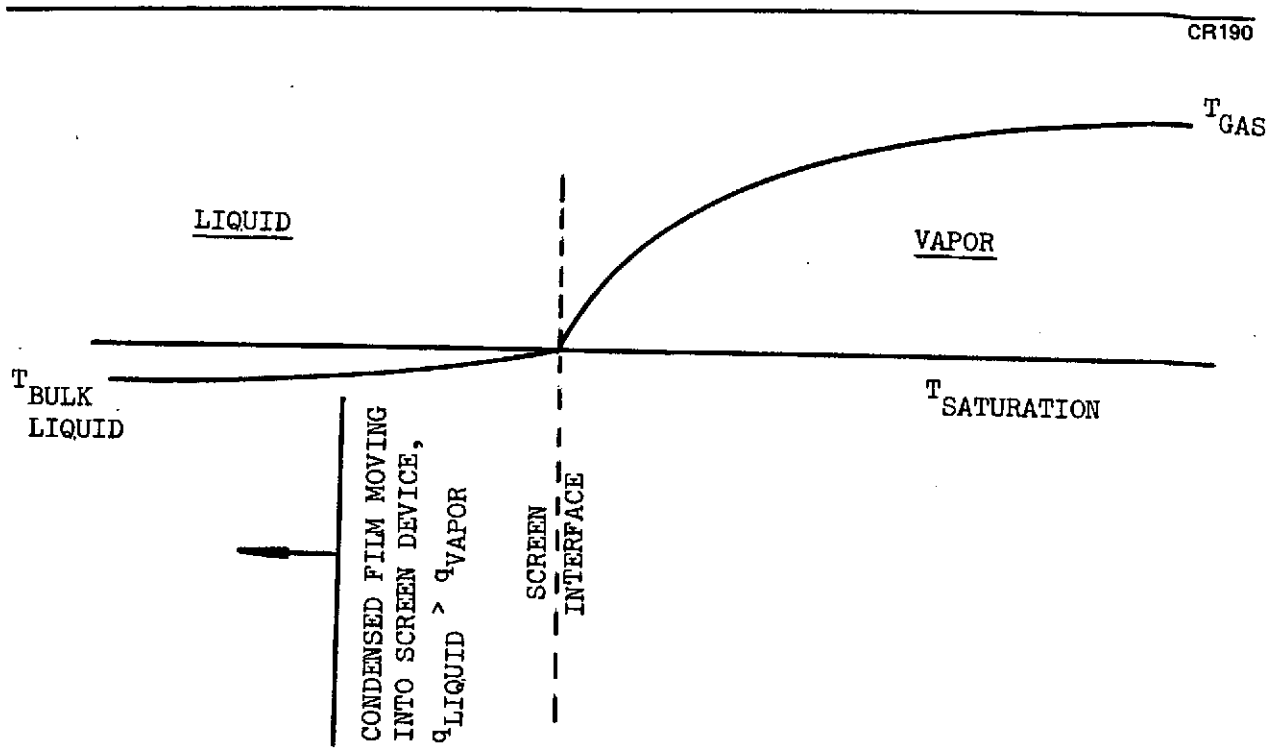
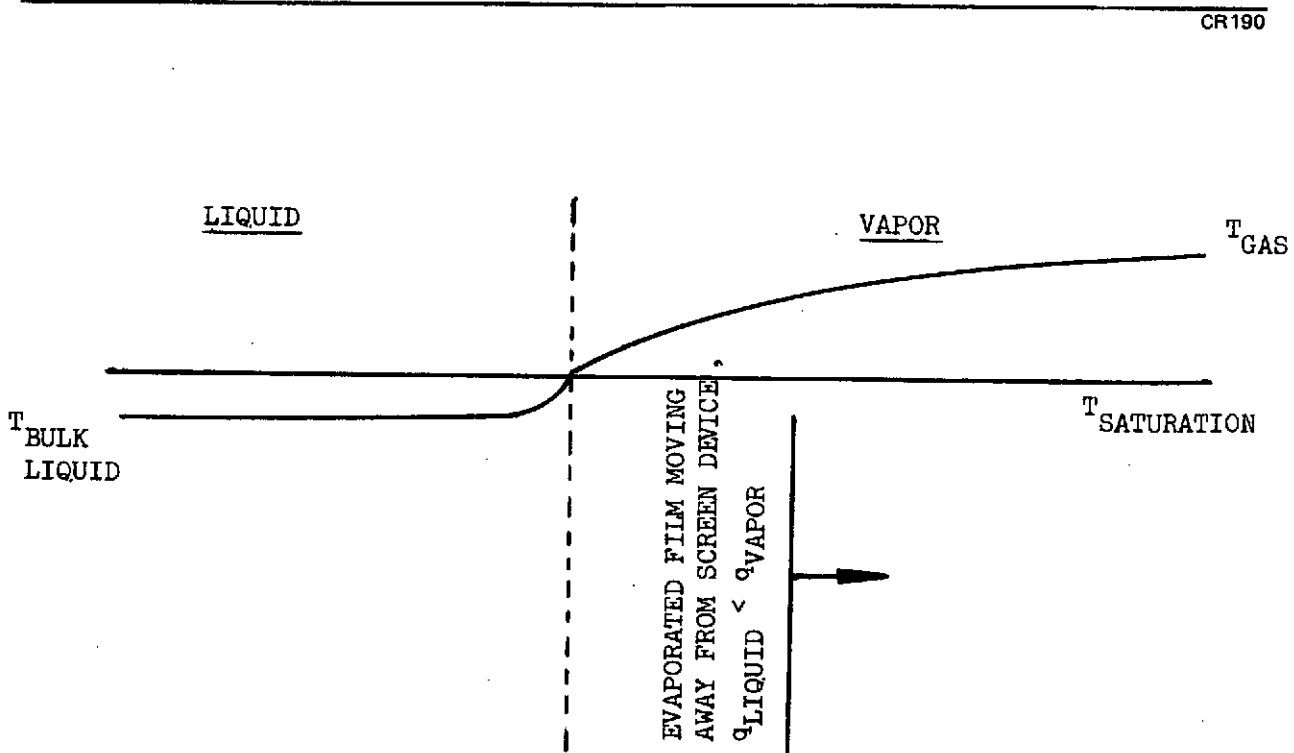Figure C-1. Temperature Profile for Condensation

Figure C-2. Temperature Profile for Evapoaration

could be almost motionless, if confined between the screen and a cold tank wall a few inches away. It should be noted that with acceleration loads on the system, the condensed film formed at the interface will be continuously drawn into the screen so as to maintain the capillary interface within the screen mesh.

The rate of evaporation or condensation for a one component system, initially at a uniform temperature, subjected to a sudden change in pressure has been determined analytically by Knuth (References A-1 and A-2); a specific case from this analysis for liquid hydrogen with autogenous pressurization is shown in Figure C-3. The results of References A-1 and A-2 apply only to a liquid and vapor which undergo no convective motion other than the one dimensional growth or receding of the interface. Figure C-3 shows typical results from the linearized analysis, which is valid if, for each phase, the difference in specific enthalpy of the initial state and saturated state for the system pressure is small compared to the latent heat. The volume condensed (or evaporated), per square foot, or the thickness of the condensed (or evaporated) region as a function of time is obtained in the linearized case; as

$$(t) = \theta_{\ell, i} \, (4 \, \alpha_\ell t/\pi)^{1/2}$$

where

$$\theta_{\ell, i} = C_{P\ell} \frac{(T_\ell - T_{o\ell})}{h_{v\ell}},$$

α_L is the thermal diffusivity of the liquid, $C_{P\ell}$ is the specific heat of the liquid, T_ℓ is the saturation temperature for the system pressure, $T_{o\ell}$ is the bulk liquid initial temperature, and Hv_ℓ is the latent heat of vaporization. Applying this result as shown in Figure C-3 for liquid hydrogen, it is seen that condensation is predicted to occur for conditions corresponding to the continuous autogenous pressurization of liquid hydrogen in orbit. Furthermore, in periods of the order of a day, significant portions of the exposed screen device will support condensed film thicknesses of the order of 1 to 3 cm. Under actual vehicle conditions, more rapid condensation rates are possible than those predicted by this idealized case. Another aspect of this envisioned screen failure mode concerns the rate of pressure decay in the tank. Slow pressure decay rates relative to the heat transfer rate in the liquid would not necessarily cause vapor bubbles to form within the screen. Consider the qualitative temperature profiles as a function of time during pressure decay shown in Figure C-4. If the difference between the maximum temperature in the liquid and the saturation temperature at the surface were always less than the superheat temperature differences required for the internal vaporization, no bubbles would form. Boiling data for liquid hydrogen shows that the superheat temperature need only be 0.1 to 0.5°R above the saturation temperature for boiling to initiate. Hence, it is expected that extremely low pressure decay rates would be required to alleviate this internal vaporization problem.
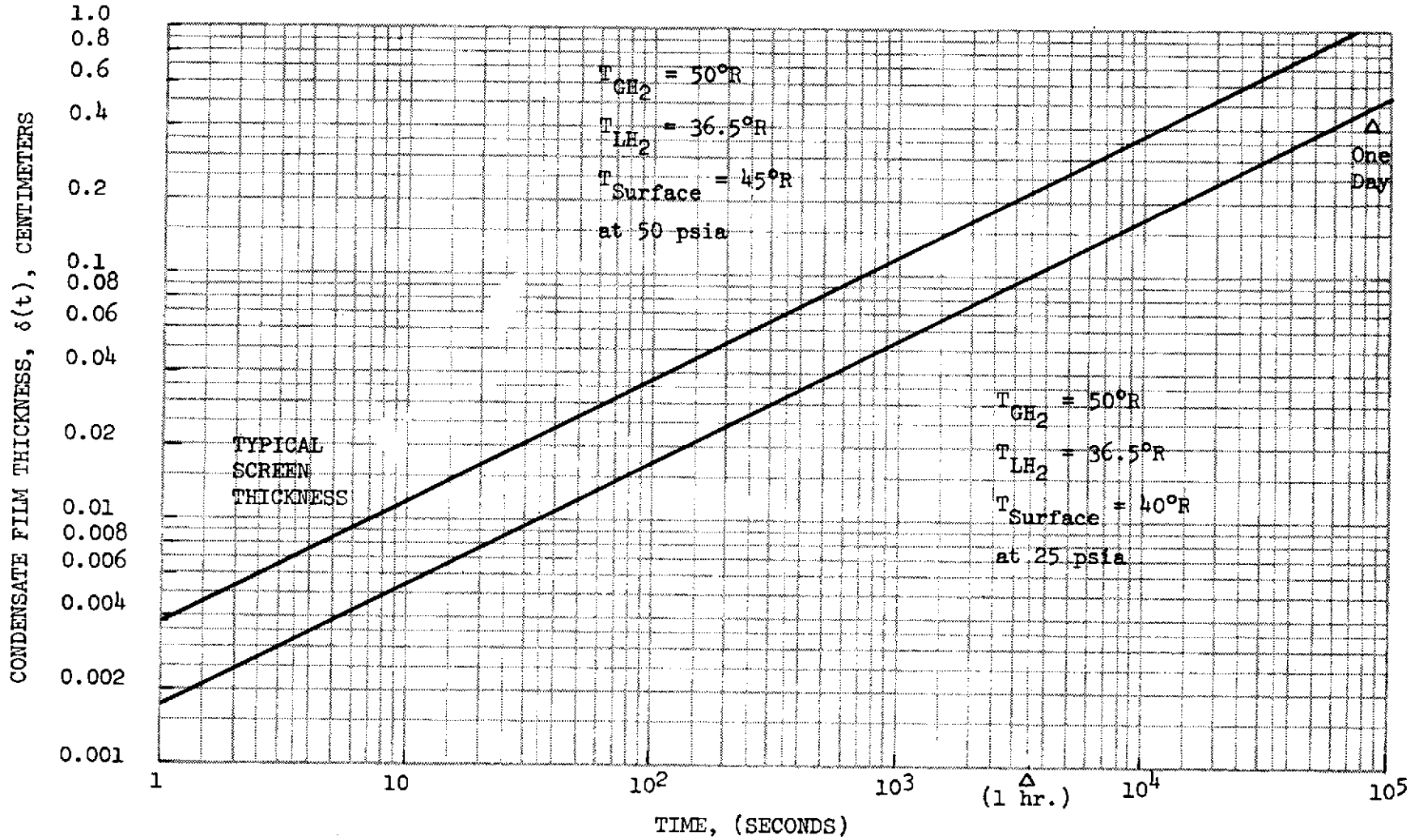
Figure C-3. Condensate Film Thickness Time Dependence — Small Temperature Difference Approximation

SCREEN
INTERFACE

GAS TEMPERATURE PROFILES

$T_{SATURATION}$ AT t = 0

$T_{LIQUID, MAX}$ AT t = t_1

$T_{SATURATION}$ AT t = t_1

LIQUID TEMPERATURE
PROFILES

$T_{LIQUID, MAX}$ AT t = t_2

$T_{SATURATION}$ AT t = t_2
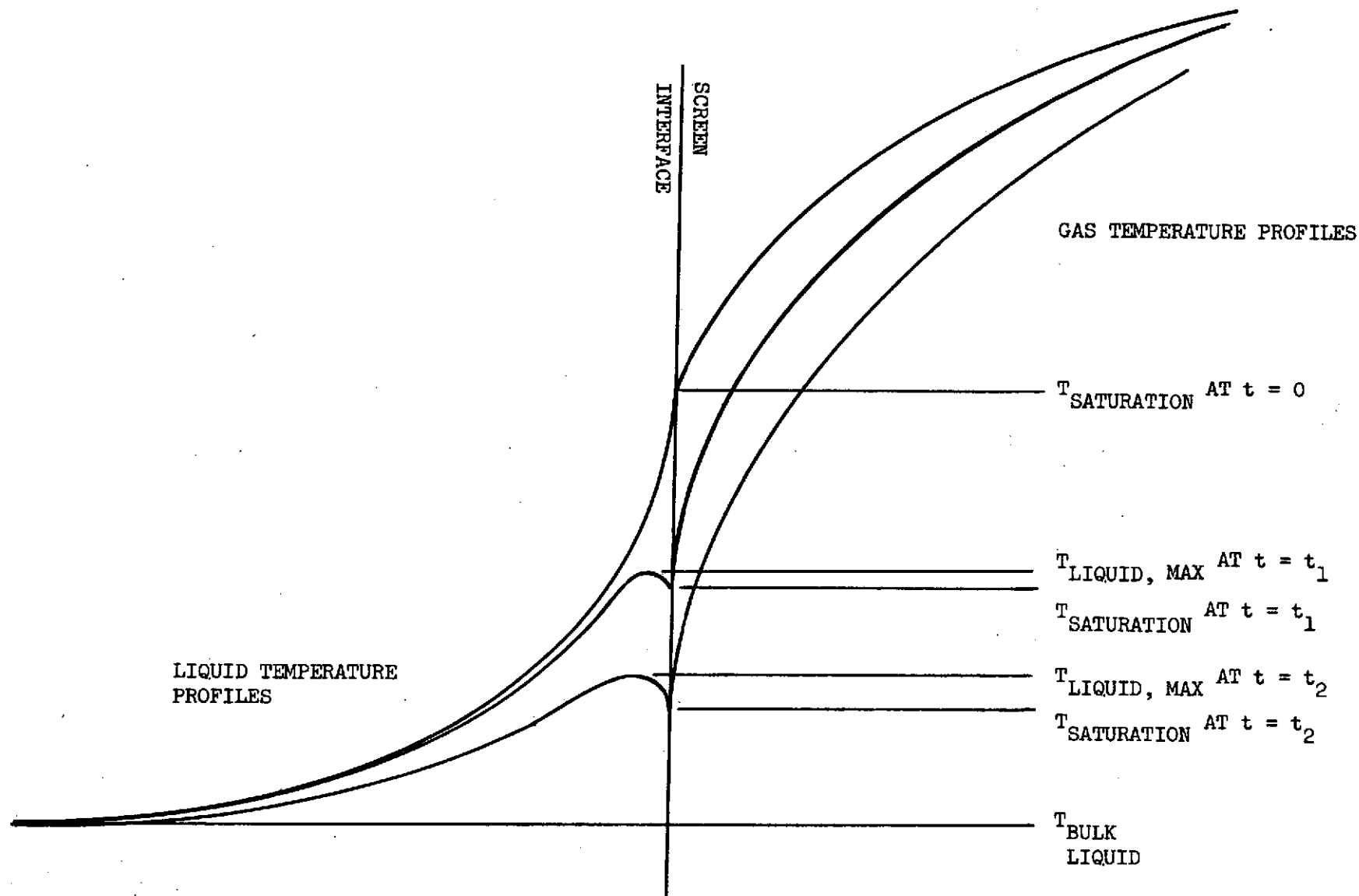
$T_{BULK \atop LIQUID}$

Figure C-4. Temperature Response During Pressure Decay of One-Component System

One estimate of the pressure decay rate that could occur with a Shuttle class liquid hydrogen tank with autogenous pressurization is obtained by assuming that ullage vapor condenses on a moving liquid interface induced by slosh wave amplification after engine shutdown. If condensation occurs on the exposed liquid surfaces, and the pressurization system has been shutdown, then a pressure decay will occur.* As the tank pressure drops below the vapor pressure corresponding to the temperature gradient within the screen device, boiling can occur within the device, leading to a possible screen drying and loss of retention capability.

One method of analyzing the condensation process is given by Sterbentz in Reference A-3, in which a modification of Nusselt's liquid film theory is used. This method is subject to question for the case of condensation on a subcooled liquid. In Nusselt's theory, it is assumed that the thermal resistance occurs in the condensate film flowing along a solid wall. In the case of condensation on a subcooled liquid, this assumption is not strictly valid. The presence of a screen further complicates the process. During the condensation, the liquid moves through the screen pores so as to maintain an interface at the screen which supports the liquid column in the screen.

In spite of these questions, the film condensation model is a reasonable method for estimating the severity of the problem of pressure decay. According to the modified Nusselt condensation model, the condensation rate is determined by the area of liquid exposed to the warm gas, the temperature difference, and the convective velocity. After engine shutdown, the slosh wave amplification and any ACS impulses will cause relative motion between the liquid and warm vapor which will increase the pressure decay rate by increasing the heat transfer coefficient and exposed area of liquid.

An approximate analysis has been performed by Sterbentz (Reference A-3) to determine the tank pressure decay rate, given by

$$\frac{dP}{dt} = \frac{\gamma P}{V g} \left(\frac{\rho_L}{\rho_v}\right) \left(\frac{\Delta T}{\rho_L \, h_{vL}}\right) A \, h_m$$

The condensation coefficient, h_m, is derived in Reference (3) for a zero-g field with a moving liquid interface in a manner analogous to Nusselt's derivation for film condensation in a gravity field. This zero gravity condensation heat transfer coefficient is derived as

$$h_m = \left[\frac{2 \, k_L \, \rho_L \, h_L \, u_o}{L \, \Delta T} \left(\frac{\bar{u}}{u_o}\right)\right]^{1/2}$$

---

*Continuous low-g pressurization could conceivably be used to maintain constant tank pressure, but if bulk liquid covered the pressurant inlet, as is likely in low-g, rapid cooling and condensation of the incoming vapor would occur. This procedure involves complicated low-g heat and mass transfer and has not been shown to be practical. It is therefore not considered a prove solution to the problem of low-g pressure decay induced vaporization.

The average velocity, $\bar{U}$, is 2/3 the maximum velocity, U_o, since a parabolic velocity profile is assumed. Thus, with the slight numerical error of Reference A-3 corrected, the condensation coefficient is found to be .

$$h_m = 1.16 \left(\frac{k_L \, \rho_L \, h_{vL} \, u_o}{L \Delta T} \right)^{1/2}$$

The pressure decay rate is also determined by the ratio of exposed liquid/vapor interface area to the ullage volume. Assuming that slosh wave amplification after engine shutdown results in a circular flow of liquid around the ullage volume, the exposed area, and length, L (or perimeter), is approximated by:

$$A = \pi D^2_{ullage}$$

$$L = \pi D_{ullage}$$

The corresponding ullage volume, V_{ullage}, is approximated by $\pi D^3/4$. Thus, the characteristic diameter of the ullage is:

$$D_{ullage} = \left(\frac{4 V_g}{\pi} \right)^{1/3}$$

The pressure decay rate is, therefore, determined by:

$$\frac{dP}{dt} = 2.32 \, \gamma P \left(\frac{\rho_L}{\rho_v} \right) \left(\frac{\Delta T}{\rho_L \, h_{vL}} \right) \left(\frac{k_L \, \rho_L \, h_{vL} \, u_o}{V_{ullage}} \right)^{1/2}$$

For small ullage volumes having large surface area to volume ratios, the decay rate increases. The decay rate is also proportional to both pressure and temperature difference, and is proportional to the square root of the liquid interface velocity, which is assumed here to be induced by slosh wave amplification.

Slosh wave amplification induced velocities occurring at engine shutdown are difficult to determine, especially in the presence of baffles and other internal hardware. However, if it is assumed, as a conservative estimate, that the maximum slosh wave velocity is the maximum velocity of the moving liquid/vapor interface, characteristic pressure decay rates can be determined.

A characteristic slosh wave velocity can be obtained as a function of the natural frequency, ω, as

$$v_{characteristic} = \eta \omega$$

where η, the half wave amplitude, is expected to be less than $0.1 - 0.2$ times the tank diameter. The natural frequency for a first mode asymmetric slosh wave in a right circular cylinder with a large liquid volume is

$$\omega^2 = \frac{1.84 \, g}{R_o}$$

For the Shuttle, having a tank diameter of 3.65 m (12 ft) and a maximum acceleration of 0.405 M/sec^2 (1.5 ft/sec^2), the maximum characteristic velocity (for $\eta = 0.4 \, R_o$) is

$$v_{characteristic} = 0.495 \, M/sec \, (1.63 \, ft/sec)$$

Table C-1 presents typical propellant properties for hydrogen and the important parameters for this problem. The average ullage temperature is assumed to be 100°R. Using the values in Table C-1, the pressure decay rate can be expressed as

$$\frac{dP}{dt} = 4.1 \left(\frac{u_o}{V_{ullage}} \right)^{1/2} \quad (psi/sec)$$

It is seen that for a characteristic velocity of 0.495 m/sec (1.6 ft/sec) and an ullage volume of 7 M^3 (245 ft^3) the maximum pressure decay rate is 55 N/M^2 sec (8 x 10^{-2} psi/sec). In two minutes, the pressure would drop approximately 66 N/M^2 (9.6 psi). A pressure drop of this magnitude would be expected to easily induce boiling inside a screen device. Assuming a less conservative case, for which the characteristic velocity is 0.0495 m/sec (0.16 ft/sec), and the ullage volume is 40 percent of the tank volume, the decay rate is reduced to approximately 9 N/M^2 sec (1.3 x 10^{-2} psi/sec), corresponding to a pressure drop of 10 N/m^2 (1.5 psi) in 2 minutes. Again, however, it is likely that boiling would occur within the screen device.

Another problem associated with the condensed liquid formed at the screen is that this higher temperature liquid would not meet the pump NPSH requirements. Ingestion of warmer liquid could lead to pump cavitation. To alleviate this problem, it would be possible to increase the tank pressure and mix the condensate with colder bulk liquid prior to expulsion into the pump. Increasing the tank pressure would increase the condensation rate, further complicating the problem as well as increasing tank and pressurization weight penalties. Furthermore, it would be necessary to monitor propellant temperatures upstream of the pumps and control tank pressure so as to maintain true NPSH to the pumps at all times. This true NPSH control operation would be more difficult for the case of autogenous pressurization since flow of the condensed liquid into the feedline could require increases in total tank pressure of the order of 5 psi within time periods of the order of 1 to 2 seconds, based on feedline velocities of the order of 30 ft/sec and feedlines of 15 to 30 ft in length. Maintaining continuous true NPSH control with screen condensation constitutes a significant problem area for autogenous pressurization, especially in a low-gravity environment.

Table C-1

PARAMETERS FOR SHUTTLE TANK PRESSURE DECAY

$\gamma = C_p/C_v = 1.6$ $\Delta T = 33°K (60°R)$

$P = 2.06 \times 10^5 \text{ N/m}^2 (30 \text{ psia})$ $h_{vL} = 4.41 \times 10^5 \text{ joule/kg}$ (190 Btu/lb)

$\rho_L = 70 \text{ kg/m}^3 (4.4 \text{ lb/ft}^3)$

$\rho_o = 1.6 \text{ kg/m}^3 (0.1 \text{ lb/ft}^3)$ $V_{TANK} = 69 \text{ m}^3 (2,450 \text{ ft}^3)$

$K_{liquid} = 9.050 \text{ joule/m-sec-°K} = 1.62 \times 10^5 \dfrac{\text{Btu}}{\text{ft sec °R}}$

REFERENCES FOR APPENDIX

C1   E. L. Knuth.   Evaporations and Condensations in One Component
        Systems.   ARS Journal.   September 1962, pp 1424-1426.

C2   E. L. Knuth.   Nonstationary Phase Changes Involving a Condensed
        Phase and a Saturated Vapor.   Physics of Fluids.   Vol. 2, No. 1
        Jan-Feb. 1959, pp 84-86.

C3   W. H. Sterbentz.   Liquid Propellant Thermal Conditioning System.
        NAS CR-72113, LMSC-A839783, pp B1-B4 and C1-C5, April 1967.

Appendix D
VACUUM VENT/REFILL SECONDARY TANK CONCEPT

When employing a local pressure isolated channel (LPIC) acquisition/ expulsion concept, a relatively large secondary tank is required when only the available long periods of high acceleration are used for dynamic refill. To reduce this tank size with minimum feed system weight penalty, a concept termed vacuum vent/refill has been evolved to accomplish low-g replenishment of the secondary tank. In the case of the CSS/APS this concept can reduce the secondary tank volume by about 80 percent and renders the LPIC concept essentially mission independent as long as time periods of 5 to 15 minutes can be allocated for the in-orbit refill operation. With high-pressure accumulators providing flow of gaseous propellant, the normal time to empty the accumulator is greater than practical start tank vacuum refill times, and therefore propellant flow demands for intermittent ACS maneuvers, life support, and fuel cells can be met while the start tank is refilled. This concept also provides the capability for re-establishing low-g fluid retention if the device should breakdown as a result of off-nominal environmental condition, such as abnormally high destabilizing acceleration loads.

1. Operation. An LPIC system with vacuum vent/refill capability is shown in Figure 1. The secondary tank is sized to contain the propellant required for control during the reentry maneuvers and landing. Assume that the secondary tank has been partially emptied by various low-g propellant expulsion, such as accumulator refill of the ACPS. (If engine restart were required, refill could be accomplished during the engine burn, which is the normal start tank refill mode.) The secondary tank pressure is first increased slightly above the main tank pressure. A bypass valve between the secondary tank channels and the main tank is then opened, thus flowing cryogen out of the secondary tank into the main tank until surface tension breakdown occurs in the screen device. The total residual liquid remaining in the secondary tank at this point is the liquid in the channels and the liquid on the tank walls. This liquid as well as the helium pressurant and hydrogen vapor, is then vented overboard to space. The secondary tank vent valve is closed and the refill valve, which is connected to a redundant screen device in the trap region, is opened causing liquid to flow into the secondary tank. This process involves essentially reversible evaporation and condensation and has been shown (References   and) to result in refill. It should be noted that in a low-g environment the principal problem with refill of a secondary tank or any localized screen device (e. g., start basket) is the difficulty in venting pure vapor, not liquid, overboard as the device is filled. The vacuum vent/ refill procedure discussed below is used in lieu of such techniques as liquid/ vapor separators (centrifugal, electrophoretic, dielectrophoretic, etc.) and vehicle acceleration.
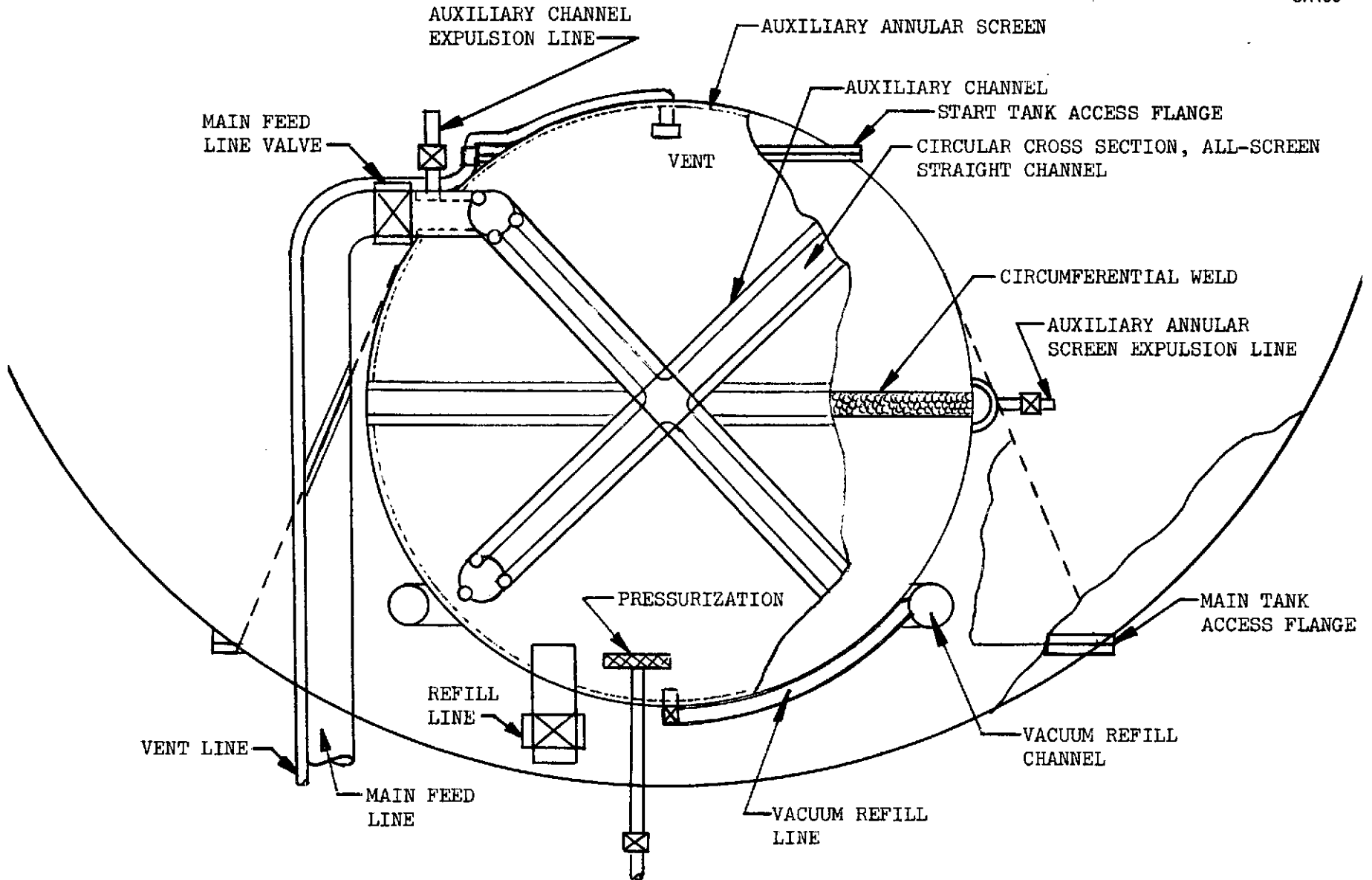
Figure D-1. Vacuum Vent/Refill LPIC Concept

As a refinement of the basic concept described above, auxiliary screen devices in the channel and on the inside secondary tank wall (shown in Figure 1) are used to transfer nearly all of the propellant back into the main tank before the vacuum vent operation. Details of the auxiliary screen device design are presented below.

Liquid propellant is supplied to the secondary tank during the vacuum refill operation by a separate main tank channel, submerged in a main tank screen "trap" region. One concept to accomplish this refill is illustrated in Figure 2. The primary trap region is maintained essentially full of liquid until the final deorbit engine burn. The screen mesh is sized so that breakdown does not occur for any of the acceleration magnitudes imposed on the vehicle during orbital coast. The secondary trap region serves two purposes; primary trap propellant replacement and propellant refill during vehicle positive accelerations.

During vacuum refill, propellant flowing from the primary trap region is replaced by propellant from the secondary trap region, which is filled by propellant in the main tank contacting the screen. If no main tank propellant contacts the upper screen of the secondary trap region, breakdown will occur. Although liquid could then flow out of the secondary region into the main tank, the g-levels would be so low that the outflow rate would be negligible, relative to that replacing liquid in the primary region. For this worst case operation, it is necessary that the propellant volume contained in the secondary region exceed the volume required for the maximum on-orbit propellant requirements between dynamic refills. For the baseline CSSI APS application,
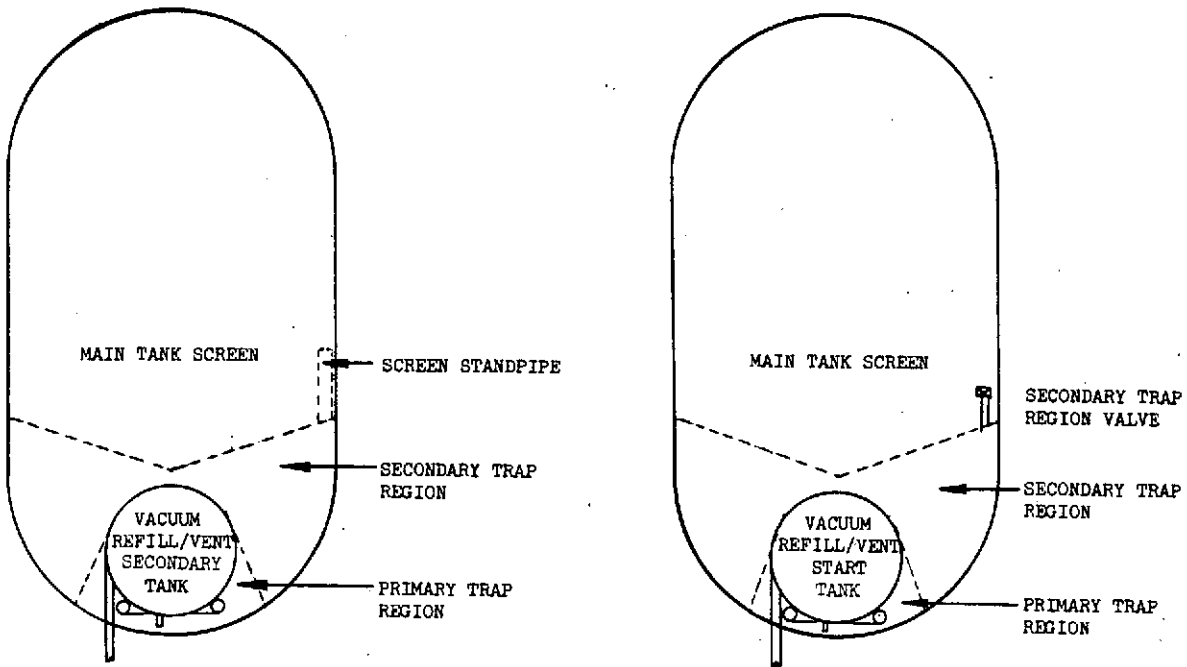
Figure D-2. Main Tank Propellant Acquisition for Start Tank Vacuum Refill

this requirement is met with the maximum liquid hydrogen volume required being of the order of 19.7 m^3 (700 ft^3). The total volume of liquid/hydrogen required for the on-orbit coast was conservatively determined to be 22 m^3 (778 ft^3) for the mission assumed in this study. Since 1.4 to 2.8 m^3 (50 to 100 ft^3) of LH$_2$ is contained in the secondary tank, the primary and secondary regions must contain the remainder.

After the secondary tank has been refilled, gas flow through the standpipe would cease and capillary attraction would then raise a column of liquid in the standpipe, closing off the screen. For this design, the screen mesh used on the standpipe has a lower bubble point than the secondary screen to provide for vapor flow and resealing. An an alternate, the standpipe and screen could be replaced with a valve. During start tank refill, the secondary trap region valve would be opened to allow gas to enter the secondary trap region, while the propellant replaced that withdrawn from the primary region. After refill, the secondary trap region valve would be closed and no liquid would be lost from the primary and secondary trap regions.

After some number of vacuum refill operations have occurred and the secondary trap region has been partially emptied, an engine burn occurs which settles propellant to the bottom of the tank at maximum acceleration. The secondary trap valve is then opened and vapor displaced up through the valve as liquid enters through the secondary trap region screen. It is not necessary during this operation to replace all of the vapor with liquid since any vapor present in the secondary trap region would not enter the primary trap region.

For the final reentry burn, liquid in the primary trap region would be used to fill the secondary tank. Vehicle acceleration would settle the remaining propellant which would dynamically refill the secondary tank through the main refill valve in the usual manner, while supplying continuous propellant flow to the ACPS accumulators.

2. Auxiliary Acquisition System Design. The principal additional weight associated with the vacuum vent/refill concept is the amount of residual liquid remaining in the start tank which cannot be transferred back into the main tank after screen breakdown occurs in the channel. It is therefore necessary to place auxiliary screens on the start tank wall and inside the channels to transfer nearly all of the start tank propellant back into the main tank. The residual liquid remaining in the channel and on the start tank wall after breakdown of the auxiliary screens is primarily a function of the outflow rate to the main tank and the size of the auxiliary screens. Lowering the outflow rate decreases the residual by allowing smaller screen flow areas to be used, but increases the transfer time. Determination of the maximum acceptable vent/refill operation time thus allows the outflow rate to be approximated, and the optimum auxiliary screen configuration to be designed.

The cold propellant vapor and helium that is vented overboard is not an additional penalty relative to the dynamic refill case, since this gas would be vented overboard during a dynamic refill. There could be a small amount of additional helium used to transfer the residual propellant back into the main tank, but in practice this amount is very small. After a normal propellant expulsion from the start tank, which requires cold helium pressurization,

equilibrium occurs such that the concentration of the hydrogen vapor in the start tank ullage reaches equilibrium; the hydrogen partial pressure thus adds to the helium initial pressure, raising the start tank ullage pressure. Furthermore, the main tank pressure decays, after engine cutoff, due to mixing of the propellant and warm pressurant. Thus, in practice negligible addittional helium is required to expel the 15 percent start tank residual back into the main tank. The design of an LPIC system using vacuum vent/refill provisions has been envolved for secondary tank volumes of 12.6 M^3 (450 ft^3), 2.83 M^3 (100 ft^3) and 1.42 m^3 (50 ft^3) on the LH$_2$ side and 1.84 m^3 (65 ft^3), 0.42 m^3 (16.7 ft^3) and 0.24 M^3 (8.3 ft^3) on the LO$_2$ side.

3. Main Tank Refill Channel. The design of this channel, which is placed along the outside of the secondary tank, is identical in design details to the basic channels in the secondary tank. It uses the 200 x 600 mesh screen to assure that liquid will be retained under all bad conditions for which the secondary tank channel is designed.

4. Secondary Tank Channel

a. Auxiliary Screens. A variety of possible auxiliary screen designs were examined to provide emptying of the secondary tank channels

The circular cross section all-screen straight channel, with the selected provisions for expelling the propellant back into the main tank through auxiliary screen tubes, is shown in Figure 3.1.3.6. The flow characteristics were determined using the acquisition device sizing computer program.

The purpose of the auxiliary channels and the annular screen device is to empty the secondary tanks and propellants into the main tank, in the absence of accelerating forces on the tanks, prior to the vacuum vent operation. The auxiliary channel concepts were initially evaluated for use in the 1.42 and 2.83 m^3 (50 and 100 ft^3) fuel tanks and the 0.236 and 0.471 m^3 (8.3 and 16.7 ft^3) oxidizer tanks with annulus sizes of 0.318 and 0.635 cm (0.125 and 0.25 inch) for the secondary tanks with the auxiliary channels indicated in Figure 1. The performance of these configurations was found to be acceptable at flowrates as great as 0.045 kg/sec (0.1 lb/sec) for the hydrogen and 0.545 kg/sec (1.2 lb/sec) for oxygen (see Table 1).

The main acquisition channels empty in from 6 to 8 minutes and from 2 to 3 minutes for worst design conditions, for LH$_2$ and LO$_2$ respectively. A time of up to 10 minutes should be acceptable.

b. Auxiliary Annular Screen Device. The purpose of the auxiliary annular screen is to transfer the 15% residual liquid remaining in the secondary tank back into the main tank prior to the vacuum vent/refill operation. This screen must be located around the tank wall to achieve this function. An appropriate auxiliary annular screen design is shown in Figures D-3 and D-4. The annular screen is designed in six or eight segments for each hemisphere. A separate annular screen is placed on the manhole cover. Each segment is formed by pleating a rectangular section of screen and then forming the segment on a mandrel. The screen segments are separately joined to the tank by several methods.
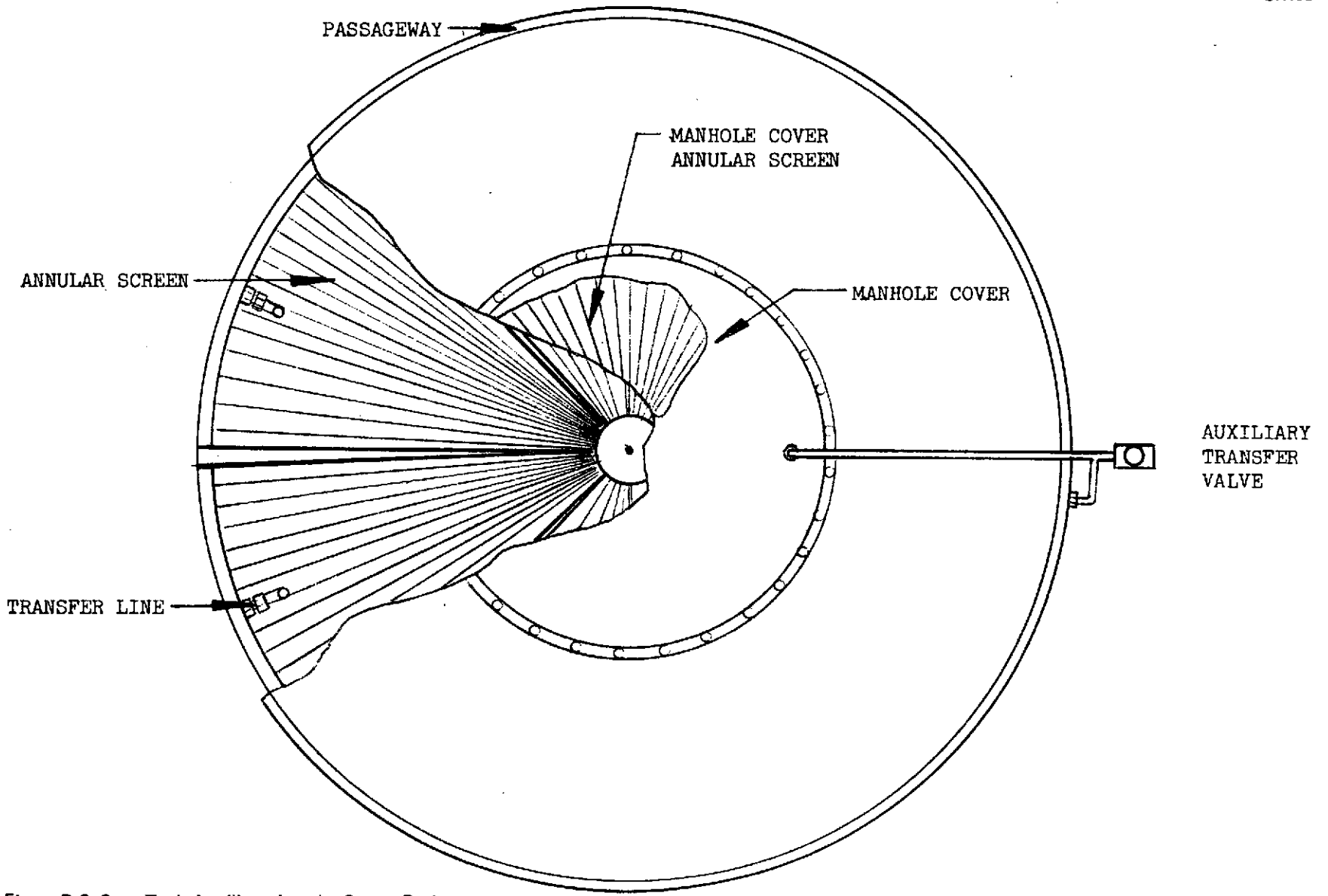
PASSAGEWAY

MANHOLE COVER
ANNULAR SCREEN

ANNULAR SCREEN

MANHOLE COVER

AUXILIARY
TRANSFER
VALVE

TRANSFER LINE

Figure D-3. Start Tank Auxiliary Annular Screen Design

ANNULAR SCREEN

LIQUID INFLOW INTO
ANNULAR SCREEN

MANIFOLD

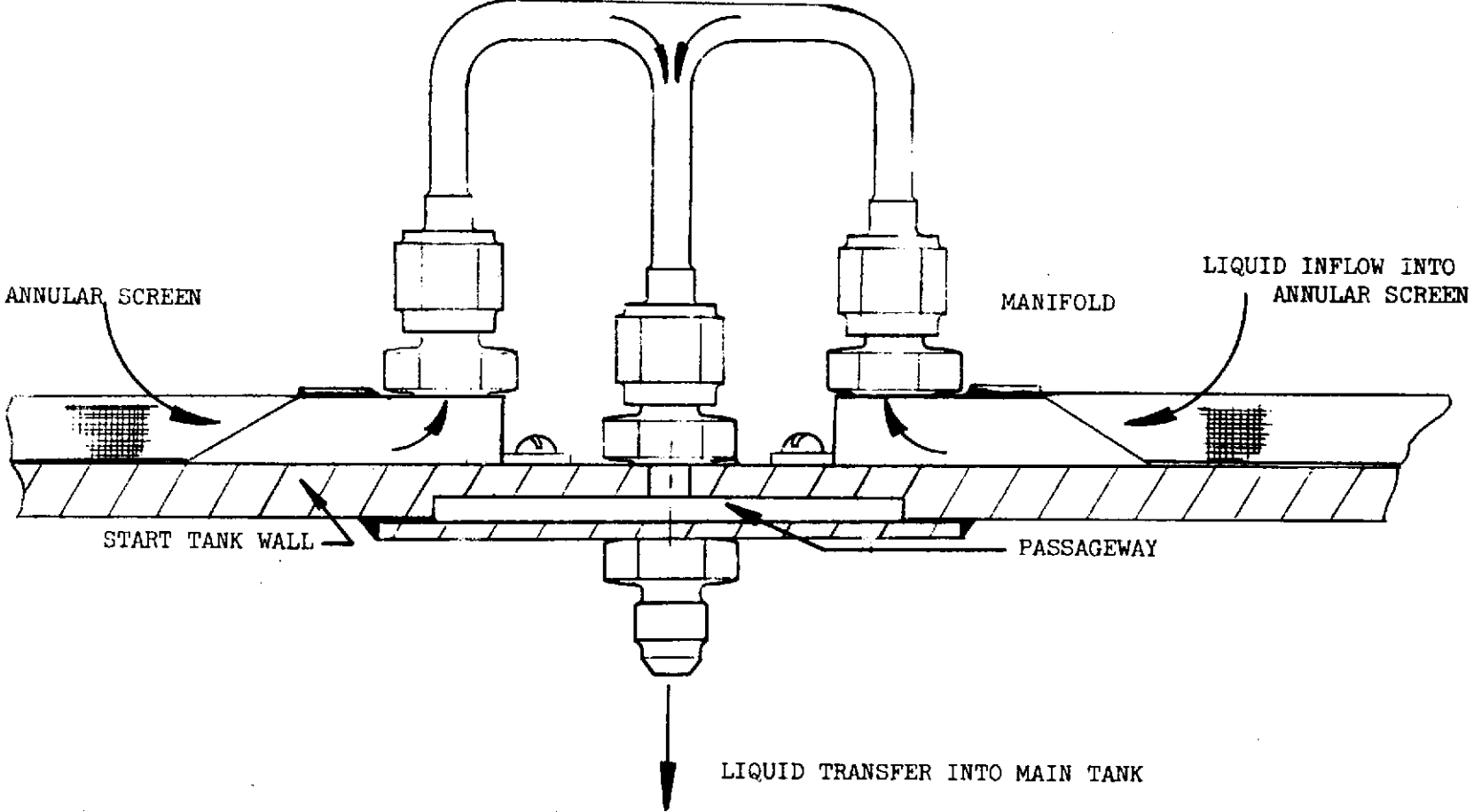START TANK WALL

PASSAGEWAY

LIQUID TRANSFER INTO MAIN TANK

Figure D-4. Start Tank Auxiliary Annular Screen Joining Details

AUXILIARY CHANNEL PERFORMANCE IN LIQUID PROPELLANT START TANKS

SCREEN SAFETY FACTORS = 2.0

Propellant	Tank Size, m³	(ft³)	Main Channel Diameter, cm	(in.)	Propellant Mass in Main Channels, kg	Mass Flowrate, kg/sec	Time to Empty Main Channel, sec	Residual Mass in Auxiliary Channels, kg
	1.42	(50)	16.5	(6.5)	5.3		235	0.16
	2.83	(100)	16.5	(6.5)	7.0	0.045	307	0.22
LH₂	12.72	(450)	17.8	(7.0)	14.0		308	0.39
						0.090		
	0.236	(8.33)	12.7	(5.0)	25.6		94	1.19
LO₂	0.471	(16.67)	12.7	(5.0)	34.2	0.545	126	1.71
	1.84	(65)	15.2	(6.0)	82.0		301	3.00

Figure D-4 illustrates how a segment is formed from two screens. The screen on the concave side is formed so as to lie very close to the start tank wall when assembled, and the pleated screen on the convex side provides the principal flow pathway for the residual liquid. Each segment can be bolted in place either before or after the hemispheres are welded together, since a manhole is provided for access with the larger start tanks.

After the screens are bolted into place, the tube fittings and lines shown in Figure 4 are routed together at the equator of the start tank. The flow path is as follows: The liquid enters the screen device and flows along the pleated passages to the equator. The base of each screen segment is welded to a manifold which is bolted to the start tank near the equator. Liquid enters this manifold, flows up through the tubing, and down into the passageway. The passageway is formed after the start tank hemispheres are welded together by welding a circular band to the start tank outer wall. The passageway is naturally formed due to the design of the isogrid hemispheres. All of the screen segments communicate liquid to this passageway band. Liquid exits through this fitting, which is connected to the valves controlling transfer from the secondary tank to the main tank. In addition, an external line is routed from the manhole cover to the valve inlet so that any liquid in the vicinity of the manhole cover can be transferred to the main tank.

The basic advantage of the separately formed segments is the ease with which they can be removed and replaced. If the bubble point of a segment were degraded, the segment could be removed and replaced through the manhole without removing the start tank or the primary channels.

Although the screens could be welded directly to the start tank wall, this concept offers an insignificant weight advantage while presenting problems of fabrication, assembly, and replacement. Since the volume of propellant contained inside the annular region is lost during the vacuum vent operation, it is necessary to minimize this volume. A range of annulus separation distances with both pleated and unpleated screens was considered. Pleated screens offer the advantage of increased wetted screen area and decreased screen flow loss, while being more practical to fabricate. Unpleated screens, however, reduce the pressure loss associated with flow in the annulus.

Tables 2 and 3 present the results for unpleated screens with annulus separation distances of 0.63 cm (0.25 in) and 0.32 cm (0.125 in.) for the 1.4 m³ (50 ft³) and 2.8 m³ (100 ft³) liquid hydrogen tanks. For the screen separation distance of 0.317 cm (0.125 in.), retention safety factors greater than 2.0 are achieved with residuals of approximately 1 percent for the two LH$_2$ tanks, and residuals of approximately 2 percent, with higher retention safety factors for the LO$_2$ start tanks. The pleated annular screen separation distance was determined for a safety factor of 2.0, which halved the percent residual of the unpleated screen. Therefore, pleated screens are selected for the design since the decreased residual weight penalty is much larger than the small increase in screen weight.

Hardware weights for the various vacuum vent/refil screen devices are summarized in Table 4.

Table D-2

ANNULAR SCREEN PERFORMANCE IN LIQUID HYDROGEN SECONDARY TANK

LH$_2$ FLOWRATE: 0.045 KG/SEC (0.1 LB/SEC)

200 x 600 MESH SCREEN - BUBBLE POINT PRESSURE = 181.9 N/M^2 (3.8 LB/FT^2)

Tank Volume		Separation Distance				Residual Mass	
m³	(ft³)	cm	(in.)	Screen Safety Factor	Percent Residual ①	kg	(lb)
UNPLEATED ANNULAR SCREEN							
2.83	(100)	0.317	(0.125)	2.85	1.08	2.14	(4.71)
		0.635	(0.25)	3.17	2.16	4.26	(9.39)
1.42	(50)	0.317	(0.125)	2.02	1.36	1.35	(2.97)
		0.635	(0.25)	2.17	2.71	2.68	(5.91)
PLEATED ANNULAR SCREEN (Pleated Area/Unpleated Area = 3)							
2.83	(100)	0.317	(0.125)	1.91	0.54	1.07	(2.36)
		0.330	(0.13)	2.10	0.56	1.11	(2.45)
		0.635	(0.25)	6.41	1.08	2.14	(4.71)
1.42	(50)	0.317	(0.125)	1.74	0.68	0.67	(1.48)
		0.343	(0.135)	2.06	0.74	0.73	(1.60)
		0.635	(0.25)	4.87	1.36	1.35	(2.97)

① Percent Residual = Residual Volume/Start Tank Volume x 100

Table 3

ANNULAR SCREEN PERFORMANCE IN LIQUID OXY EN SECONDARY TANK

LO$_2$ FLOWRATE: 1. 2 LB/SEC (0. 545 KG/SEC)

200 x 600 MESH SCREEN - BUBBLE POINT PRESSURE = 1250 N/M^2 (26. 1 LB/FT^2)

Tank Volume m³	(ft³)	Separation Distance cm	(in.)	Screen Safety Factor	Percent Residual	Residual Mass kg	(lb)
			UNPLEATED ANNULAR SCREEN				
0.471	(16.7)	0.317	(0.125)	3. 26	1. 96	10. 4	(23. 0)
		0.635	(0.25)	3. 91	3. 90	20. 7	(45. 7)
0.236	(8. 3)	0.317	(0.125)	2. 44	2. 46	6. 6	(14. 5)
		0.635	(0.25)	2. 78	4. 89	13. 1	(28. 8)
			PLEATED ANNULAR SCREEN (Pleated Area/Unpleated Area = 3)				
0.471	(16.7)	0.317	(0.125)	1. 47	0. 98	5. 2	(11. 5)
		0.368	(0.145)	2. 14	1. 14	6. 0	(13. 3)
		0.635	(0.25)	6. 30	1. 95	10. 4	(22. 9)
0.236	(8. 3)	0.317	(0.125)	1. 39	1. 23	3. 3	(7. 3)
		0.381	(0.15)	2. 14	1. 48	4. 0	(8. 7)
		0.635	(0.25)	5. 13	2. 44	6. 5	(14. 4)

Table 4

VACUUM VENT/REFILL ACQUISITION DEVICE HARDWARE WEIGHT (kg)

LH$_2$ Tank	Secondary Tank Values – M³(ft³)		
	1. 4(50)	28(100)	12. 6(450)
Auxiliary Channels	1. 0	1. 3	2. 6
Auxiliary Annular Screen	3. 5	4. 5	12. 4
Main Tank Refill Channel	6. 2	8. 2	16. 0
LO$_2$ Tank	0. 24(8. 3)	0. 47(16. 7)	1. 84(65)
Auxiliary Channels		1. 4	0. 5
Auxiliary Annular Screen		9. 0	9. 0
Main Tank Refill Channel		2. 2	3. 1

Appendix E

CONTROLLING PRESSURIZATION THERMODYNAMICS

When considering the relative merits of the alternate pressurization modes, it is helpful to understand the general thermodynamic behavior of the tankage system during the mission. The duty cycle events consist of removing a volume of liquid, adding a mass of pressurant, and adding heat with this pressurant. The response of the system varies widely, depending on whether the pressurant is vapor or helium and on its temperature.

E1 AUTOGENEOUS PRESSURIZATION

Using vaporized propellant as pressurant results in no net mass addition to the tank. The heat input to the tank is the latent heat of vaporization plus the sensible heat to raise the pressurant to the specified inlet temperature. The heating requirement per unit volume of GH_2 pressurant is shown in Figure E-1 as a function of inlet temperature. At low temperatures, the heat input per unit mass approaches the constant heat of vaporization as a limit. Since the gas density increases with decreasing temperature, the heat input per unit volume increases sharply. At high temperatures, the heat input per unit mass is dominated by the sensible heat, which is directly proportional to the temperature. With the density varying inversely with temperature, the heat input per unit volume approaches a constant.

The heat input to the tank with the pressurant is the determining factor in the autogeneous pressurization performance curves. The shape of the final ullage mass and final tank pressure curves in Figure 14 in Sub-section 3.1.3 is essentially the same as that in Figure E-1. The problem of pressurant heat input cannot be avoided by using "cold" autogeneous pressurization because the heat input is highest at near-liquid temperature. However, the calculated performance curves do not consider any heat sinks within the tank other than the tank wall heat loss.

E2 HELIUM PRESSURIZATION

When the liquid outflow volume is replaced by a pure helium pressurant, the equilibration process during the coast phase involves both heat and mass transfer. Propellant vapor must be added to the helium until the partial pressure equals the propellant vapor pressure. The system must also come to thermal equilibrium. The vaporization process cools the propellant, while the heat transfer from the ullage warms it. The net result depends on the pressurant inlet temperature.

Figure E-2 shows the NPSP at the final burn for helium pressurization of LH_2 at a fixed outflow pressure of 173×10^3 n/m^2 (25 psia). Only for the 18-burn curve at inlet temperatures greater than 263°K (500°R) does this pressurization mode fail to provide the desired NPSP. For most conditions,
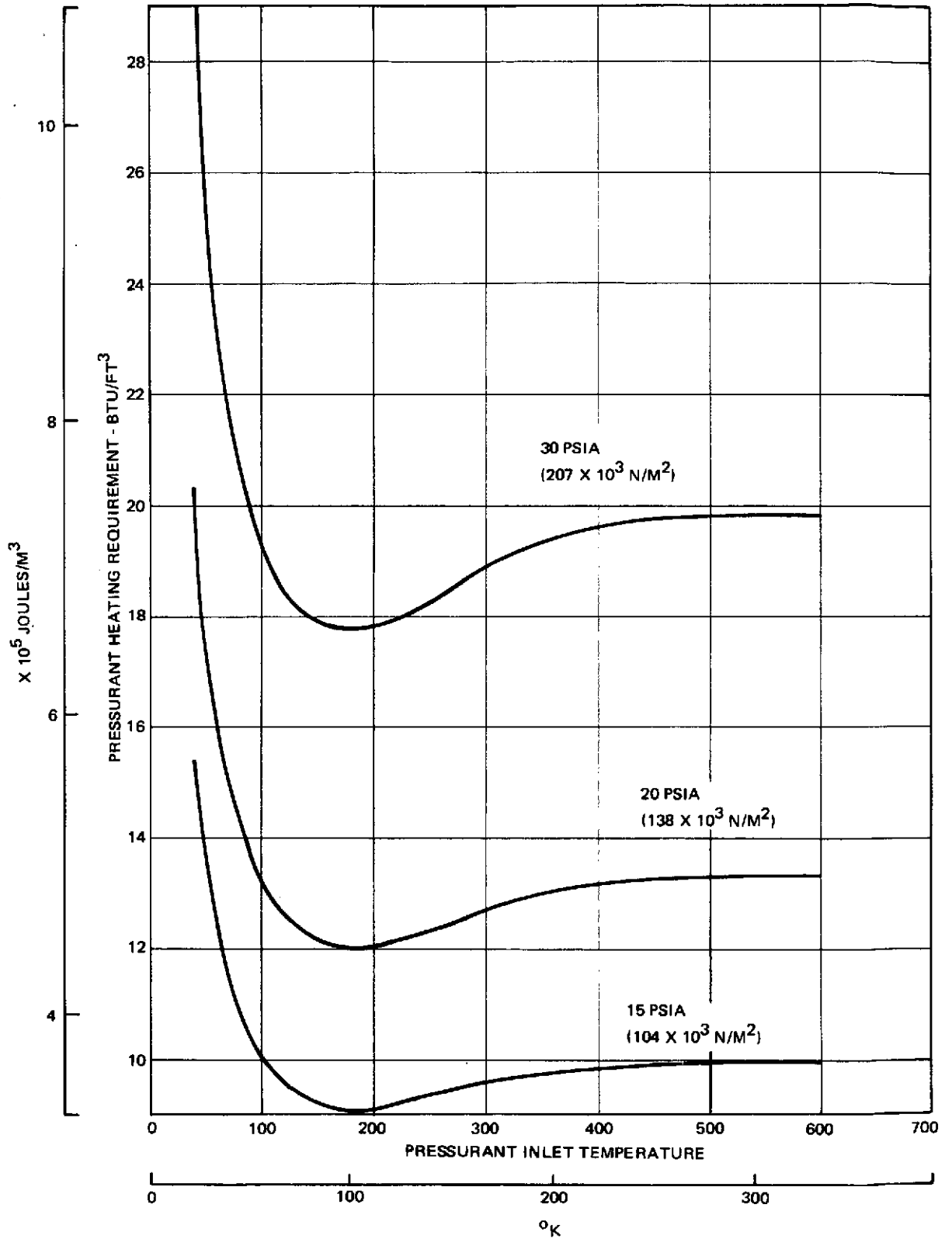
Figure E-1. LH$_2$ Autogenous Pressurant Heating Requirement
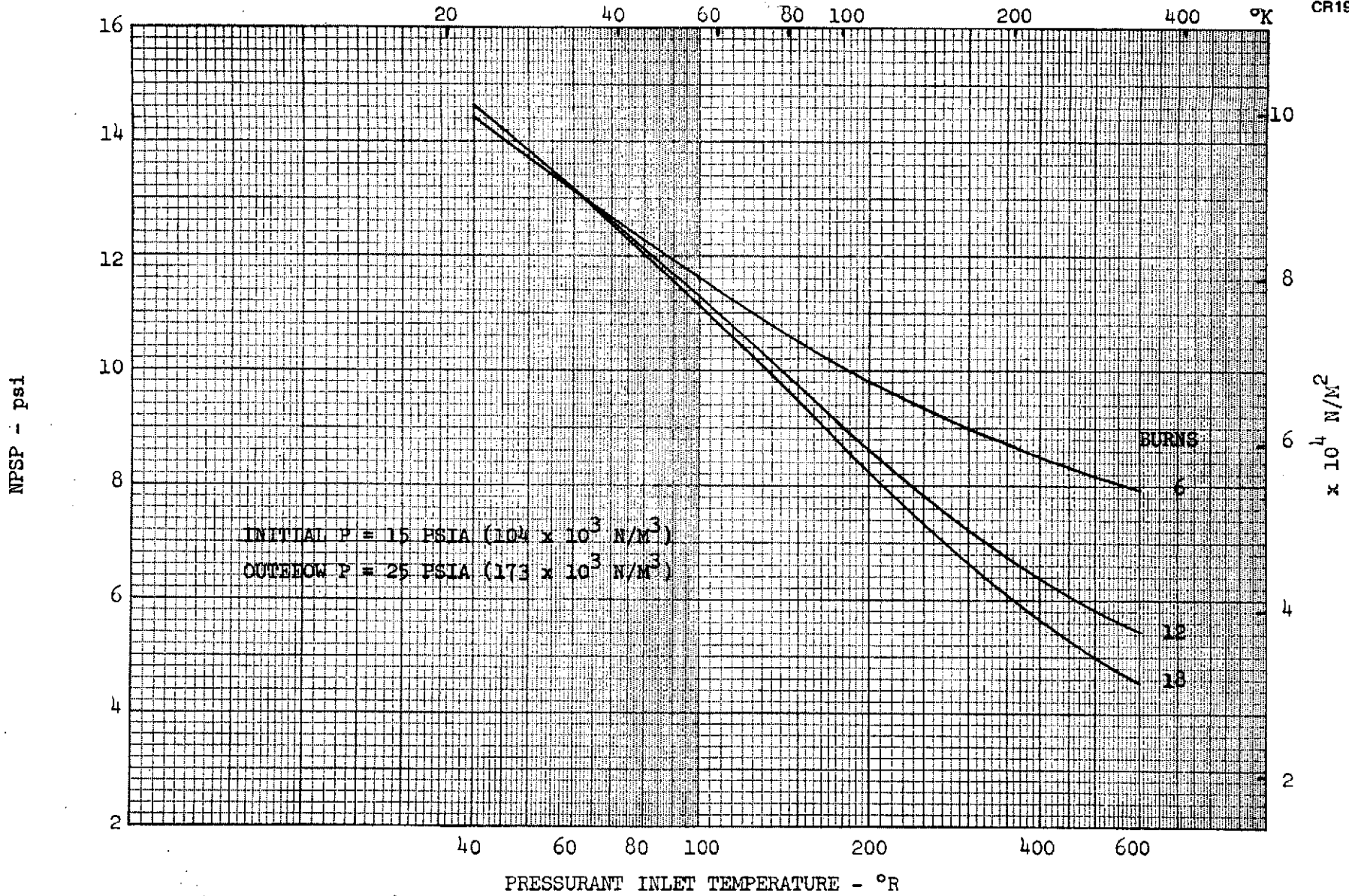
Figure E-2. Final Burn NPSP With Helium Pressurant — Fixed P

the tank is considerably overpressurized in excess of the NPSP requirement, which is an unnecessary consumption of pressurant. Figure E-3 shows the outflow pressure on the final burn when a true NPSP controller maintains the required 34.5 x 10^3 n/m^2 (5 psi) over the liquid vapor pressure. For the first burn, the tank pressure is always 138 x 10^3 n/m^2 (20 psia). At inlet temperatures below about 139°K (250°R), the helium pressurant has a net cooling effect on the tank. The liquid temperature decreases, giving a final pressure less than 138 x 10^3 n/m^2 (20 psia). At higher inlet temperatures, there is a net heating effect with a pressure increase during the mission.

The tank pressure increase due to heat input at the higher inlet temperatures is a cumulative effect that builds up during the mission. There is also a tank pressure increase due to the addition of propellant vapor during equilibration of the system after pressurization with low-temperature helium. This pressure increment is largest following the first burn, when the ratio of added helium volume to total ullage volume is largest. The magnitude of this effect is shown in Figure E-4 for the true NPSP example. This high pressure does not represent a waste of pressurant, since the pressure returns to the specified level during the next burn before more pressurant is added. However, this effect must be taken in account when setting the design pressure limit for the tank.
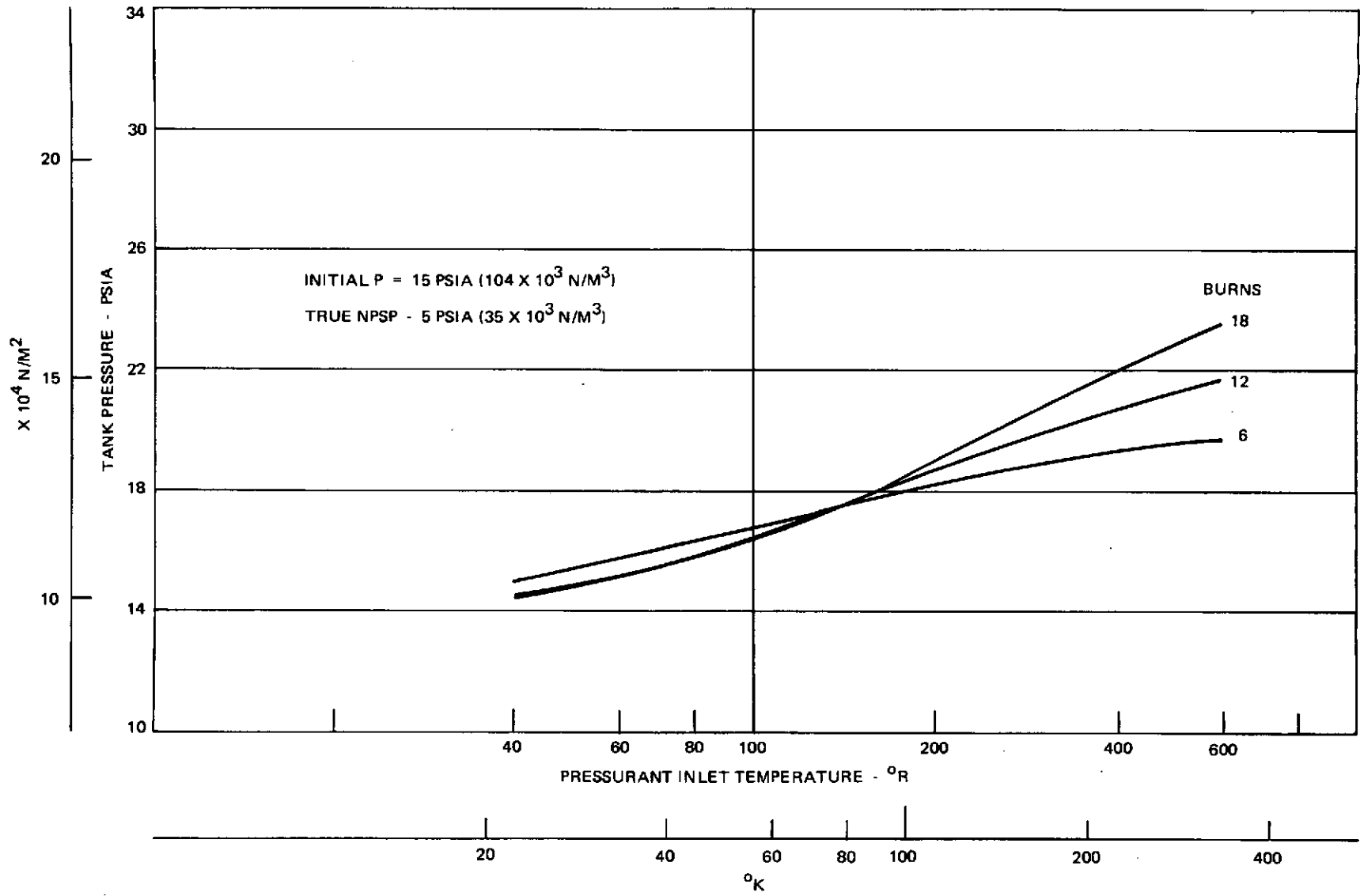
Figure E-3. Final Burn Outflow Pressure with Helium Pressurant - True NPSP
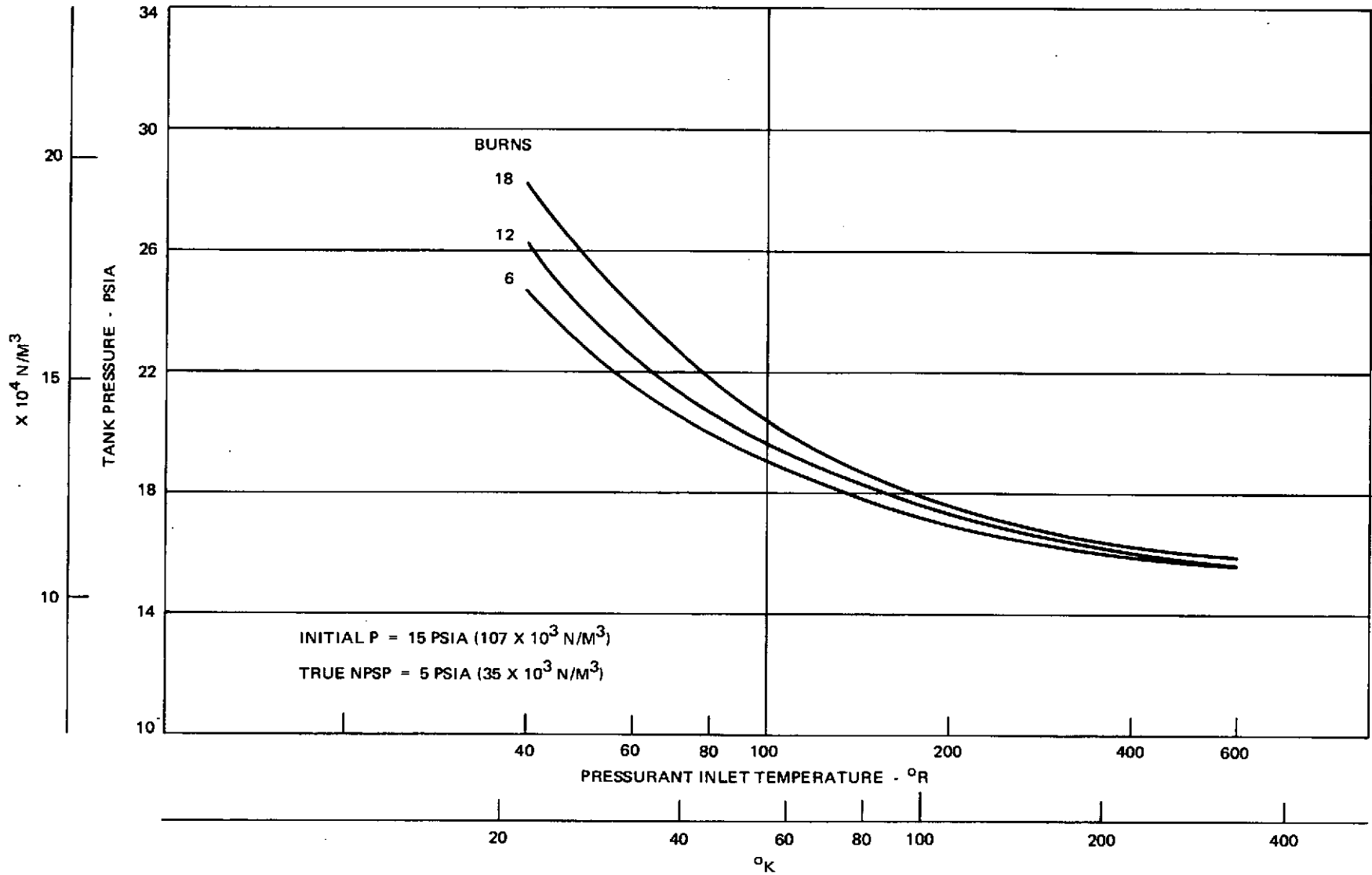
Figure E-4. Tank Pressure After First Burn with Helium Pressurant - True NPSP

Appendix F

THERMAL ENVIRONMENT PARAMETERS

The transient thermal environment assumed in this study is described by Figures F-1 through F-6. All curves shown were taken directly from Reference 18, which involved a tank insulation study for a Space Shuttle APS.
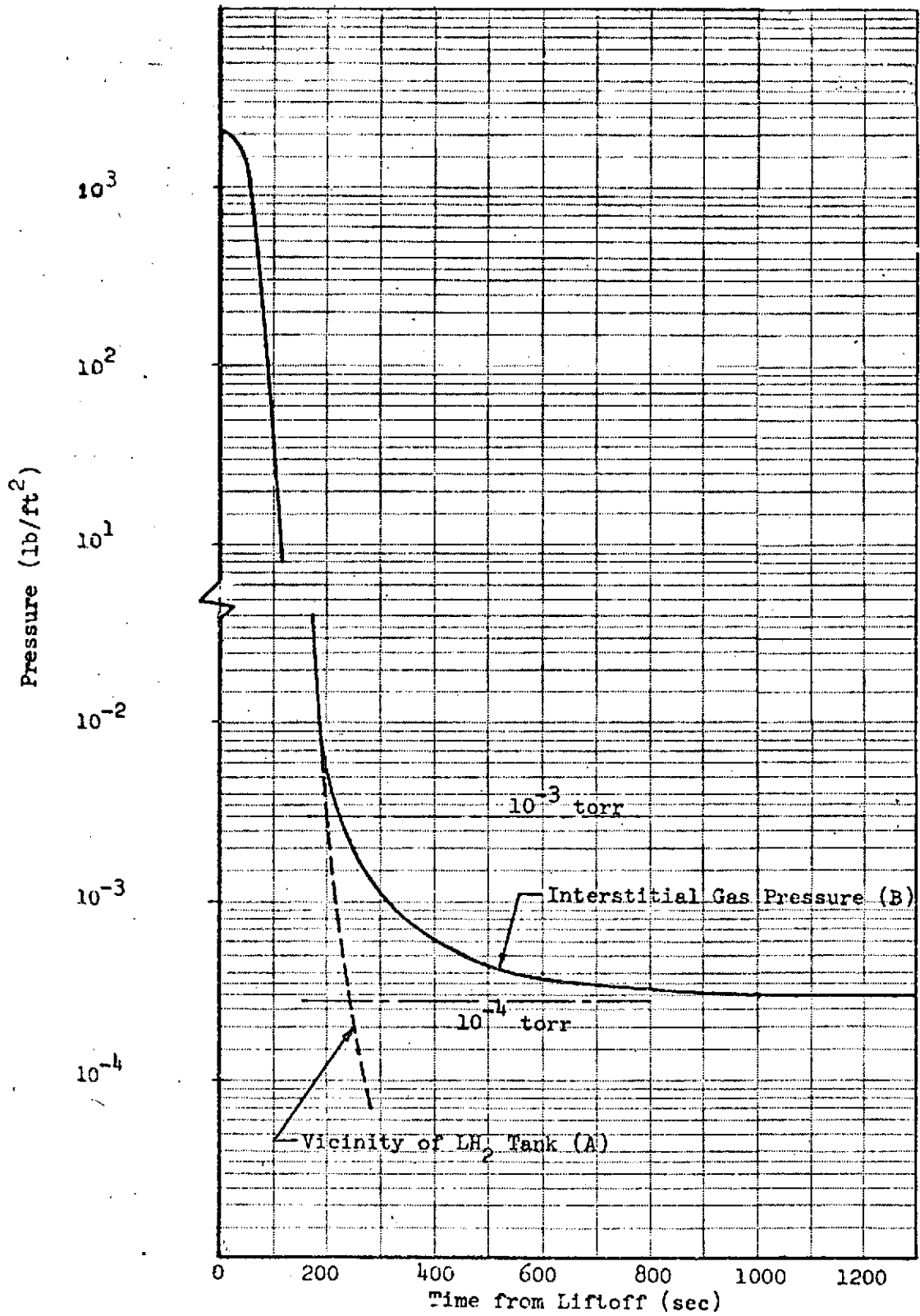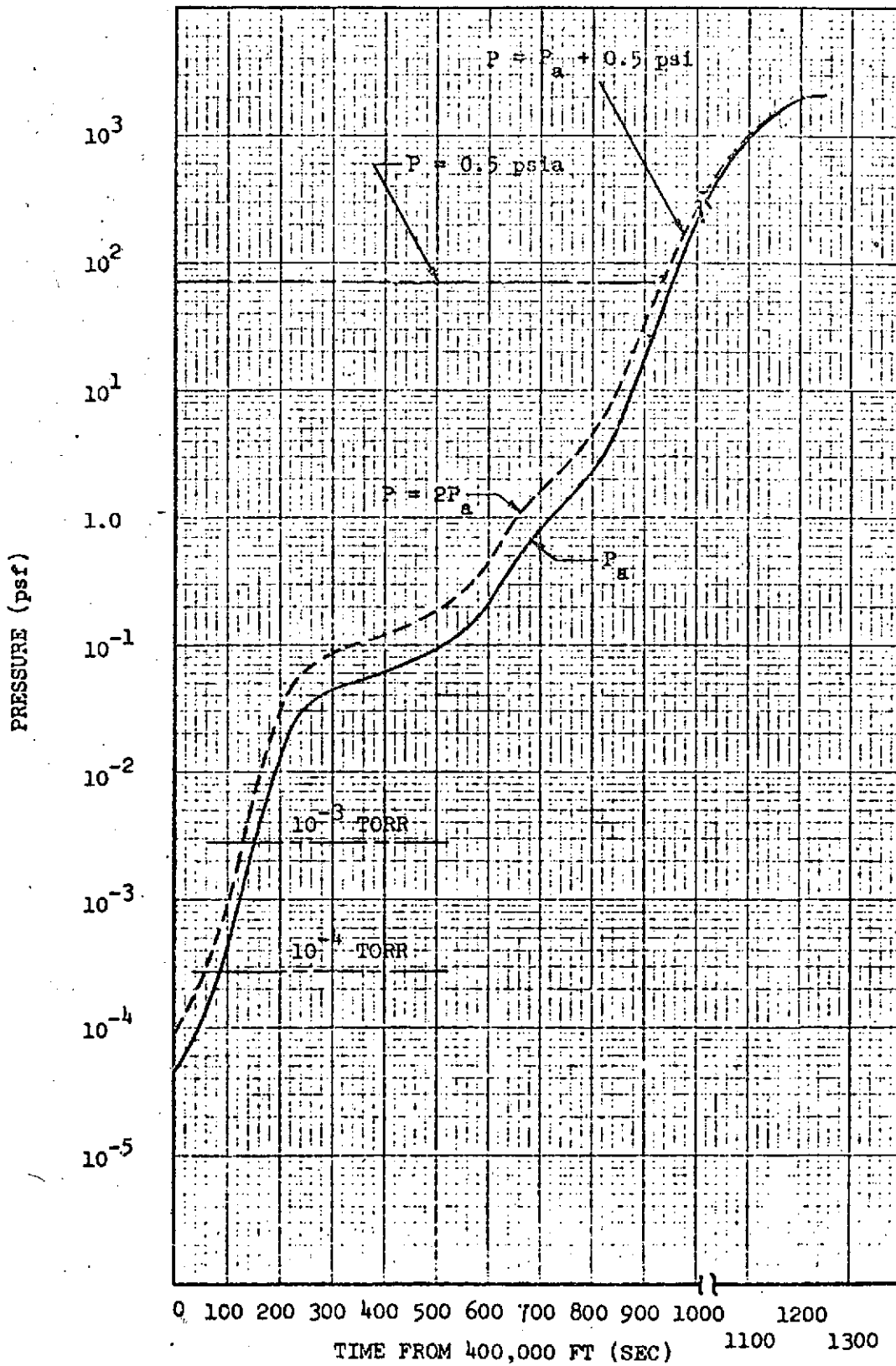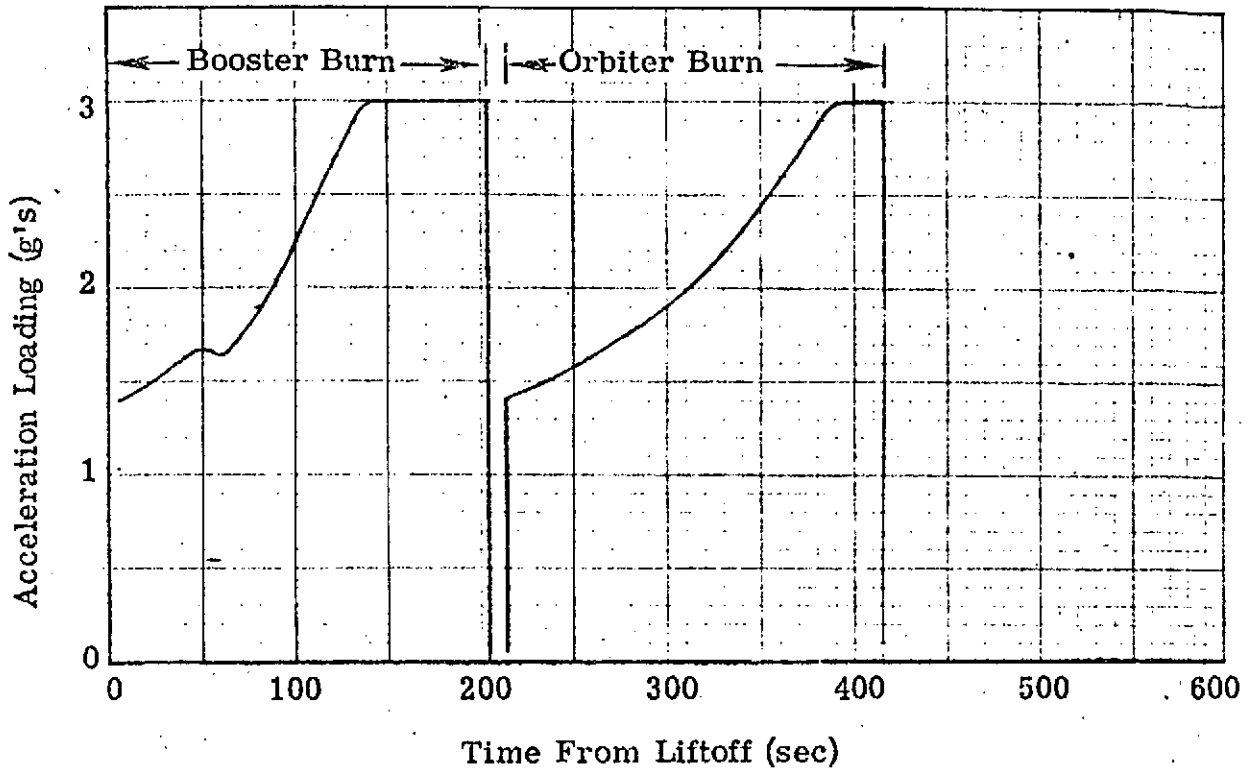
Figure F-1. Pressure Histories During Ascent

Figure F-2. Pressure History During Reentry

Figure F-3. Acceleration Loading History During Ascent
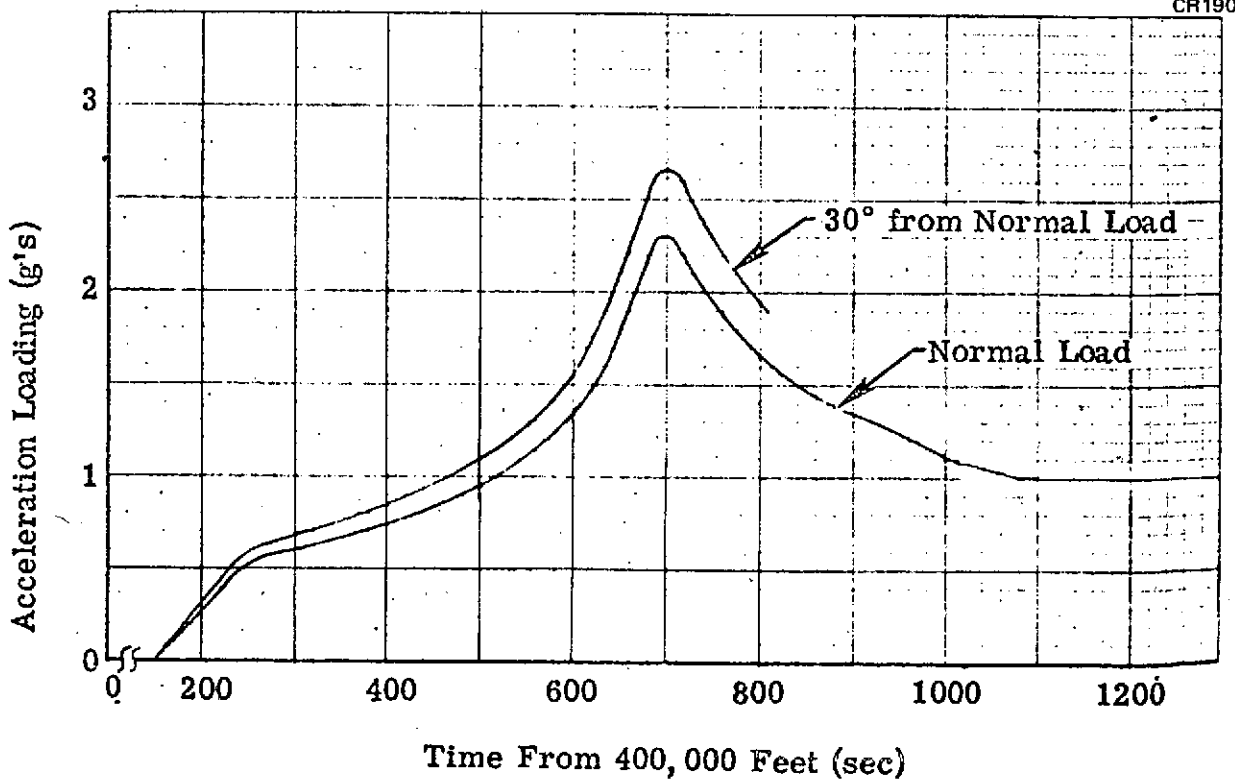
Figure F-4. Acceleration Loading History During Re-Entry
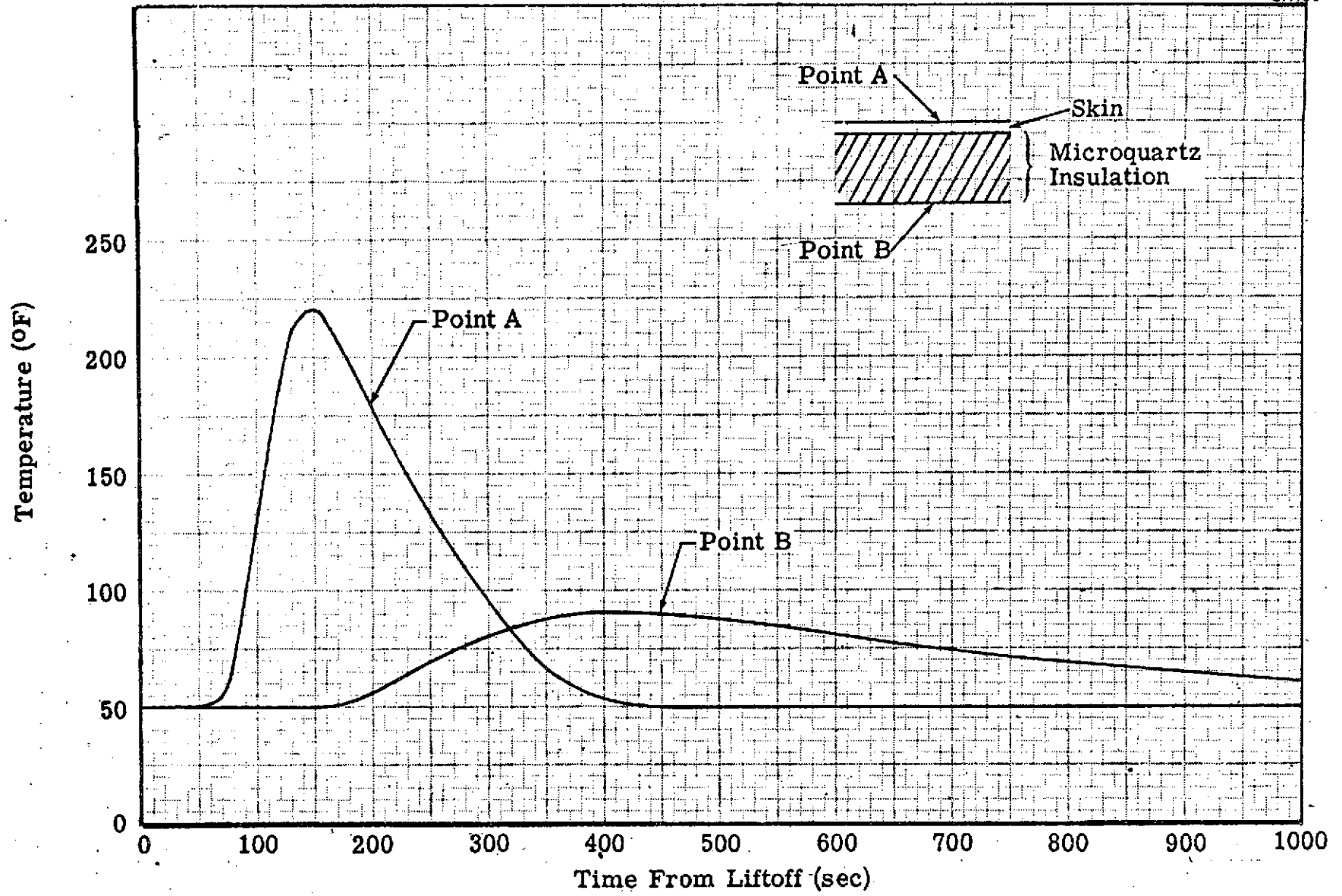
Figure F-5. Temperature Histories During Ascent — Vinicity of LH$_2$ Tank
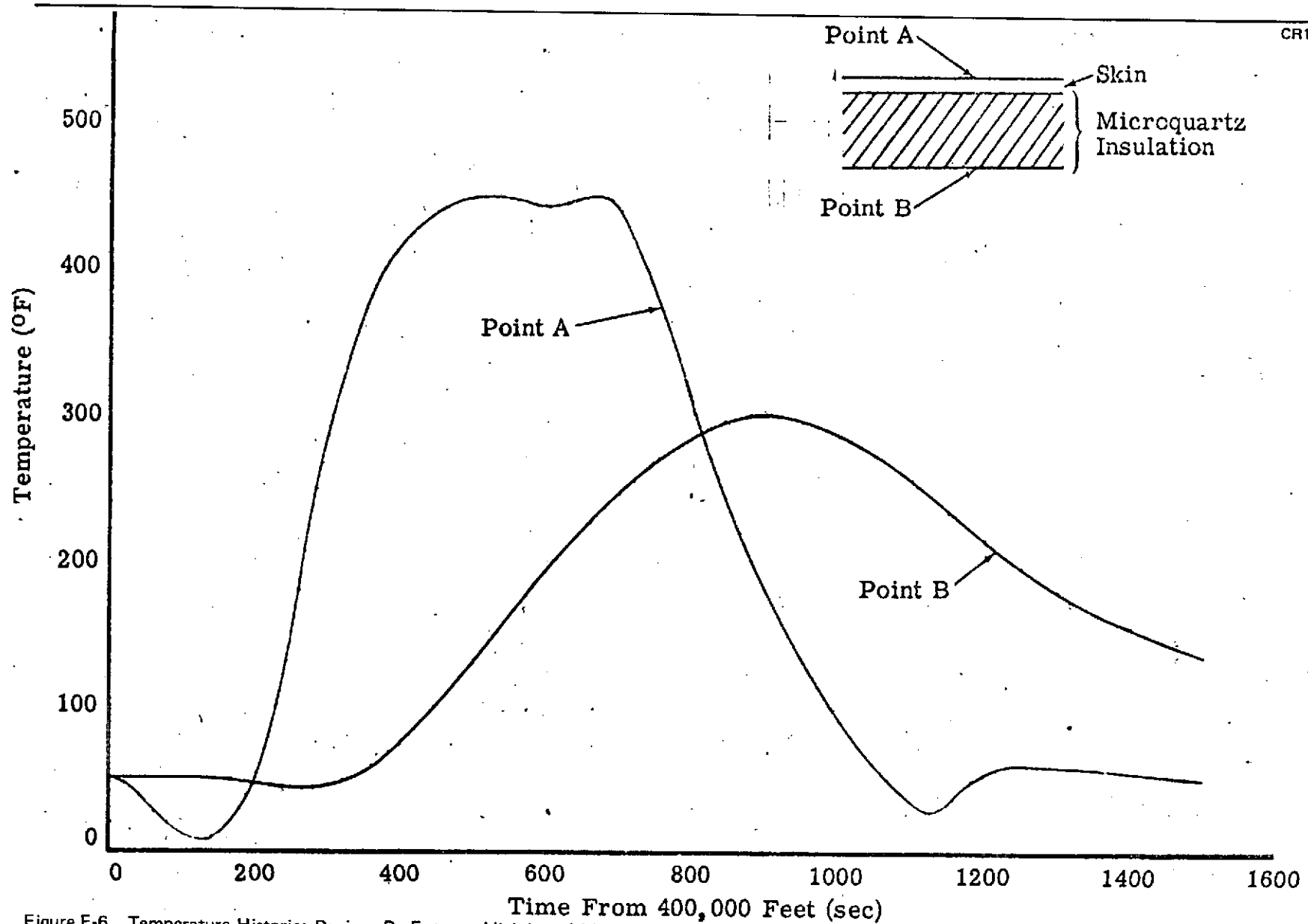
Figure F-6. Temperature Histories During Re-Entry — Vicinity of LH$_2$ Tank

Appendix G
RING CHANNEL INSTALLATION INSTRUCTIONS

All components for the ring channel system have been provided by
MDAC per the list shown in Table G-1. When assembled within the MSFC
105 in. tank this will result in a working acquisition system. The following
details are provided to assist in this installation. It is assumed that the
tank will be positioned in a vertical orientation with access through the
bottom manhole of the tank. The channel is attached only to the upper
circumferential ring which currently exists within the tank. Therefore,
other NASA supporting hardware can be freely attached to the lower ring
if desired.

Table G-1
TEST PROTOTYPE DRAWINGS

Number	Title	Comments
C551APS PROTOTYPE		
IT44517-B	Screen	13 cylindrical elements
IT44543	Clamp	Ring attachment
IT44514-A	Cross	Joint at ring intersection
IT44524-A	Bracket	Tank wall attachment
IT44535	Brace	Support rod
IT44516-A	Screen Assembly	
IT44538	Elbow Half	
IT44499-A	Screw Support Assembly	
SK50673	Installation	
SK21273	Bubble Point Test Tank	
SK22473	Blind Flange	
SK21673	Spring	
ES-10724	Coax Feed Thru	
ASPM PROTOTYPE		
IT44565	Filter Elements	20 cylindrical screens
IT44583	Sump	
IT44559	Tank, Inner	
IT44591	Refill Diffuser	
IT44593*	Installation	
ES-10725	Coax Feed Thru	For capacitance probe
IT44632	Vent, Pressurization Diffuser	

A. CLAMP PLACEMENT

Two 1T44543 clamps (one right and one left hand) are required at each of the six corners of the acquisition ring. A total of four are placed on each of the two 1T44516-3 components and two each on 1T44516-5 and 1T44516-7. The clamps are wrapped around the solid duct work at the elbow after the protective bagging has been slit. Each clamp is secured by a 1/2 inch long 10-32 machine screw. The ears of each clamp are orientated perpendicular to the plane of the ring. Figures 1 and 2 indicate the proper placement of the clamps. When tightening the 10-32 screws take care that the other 9/32 inch diameter holes align with each other.

B. BRACKET AND BRACE INSTALLATION

Twelve brackets (each consisting of one 1T44524-3 clip and either 1T44524-5 or 1T44524-6 clip) are slipped over the upper stabilizing ring within the 105-inch tank. A one-inch long 1/4-24 machine screw secures the two portions of the bracket together. Leave this screw loose so the bracket can be slid along the stabilizing ring. Figure 3 shows one of the brackets. The slotted end of a 1T44535 brace is loosely attached to each bracket (see Figure 4) with another one-inch long 1/4-24 machine screw. The twelve brackets are evenly placed about the perifery of the tank.

C. TEMPORARY -3 SUPPORT BRACKETS

Two brackets formed from tee shaped aluminum extrusions are now secured along the top of each end leg on the two 1T44516-3 ring components. These brackets can be placed on top of the protective bagging and secured by seven-inch diameter screw clamps placed over the two ends of the bracket. The brackets will be used to support the complete acquisition ring within the tank until the 12 braces are secured at which time the temporary brackets are removed. (Figure 5 shows the brackets secured by heavy tape rather than screw clamps.)

D. -5 BALANCING ACT

A trial and error process is used to determine a point along each of the two temporary brackets secured to the -3 ring component from which the component can be suspended and rest in a horizontal plane. The telescoping handling aid is attached to successive holes in the two brackets until the balance point is formed. Figure 5 indicates the desired result. The points selected should be approximately 15-3/4 inches from either end of the -3 component. The selected holes are marked and the handling aids removed.

E. HANDLING AID PLACEMENT

The two telescoping handling aids are passed into the tank and placed parallel to one another while resting on the top tank stabilizing ring. Figure 6 shows the proper orientation of the two aids. The aids should be placed as far apart as the telescoping mechanism permits.

Figure G-1. Elbow Zone Details Showing Rivets and Support Clamps
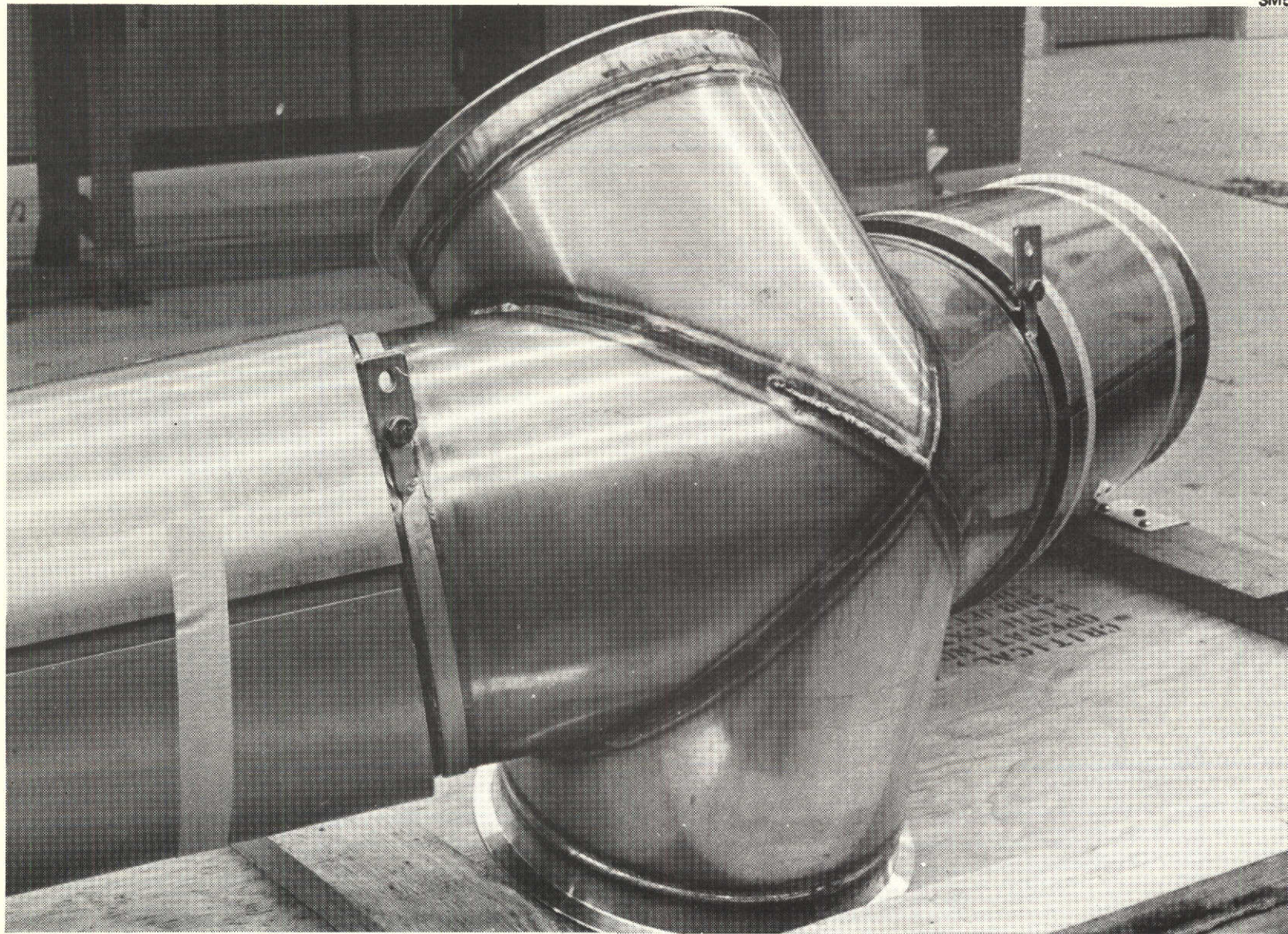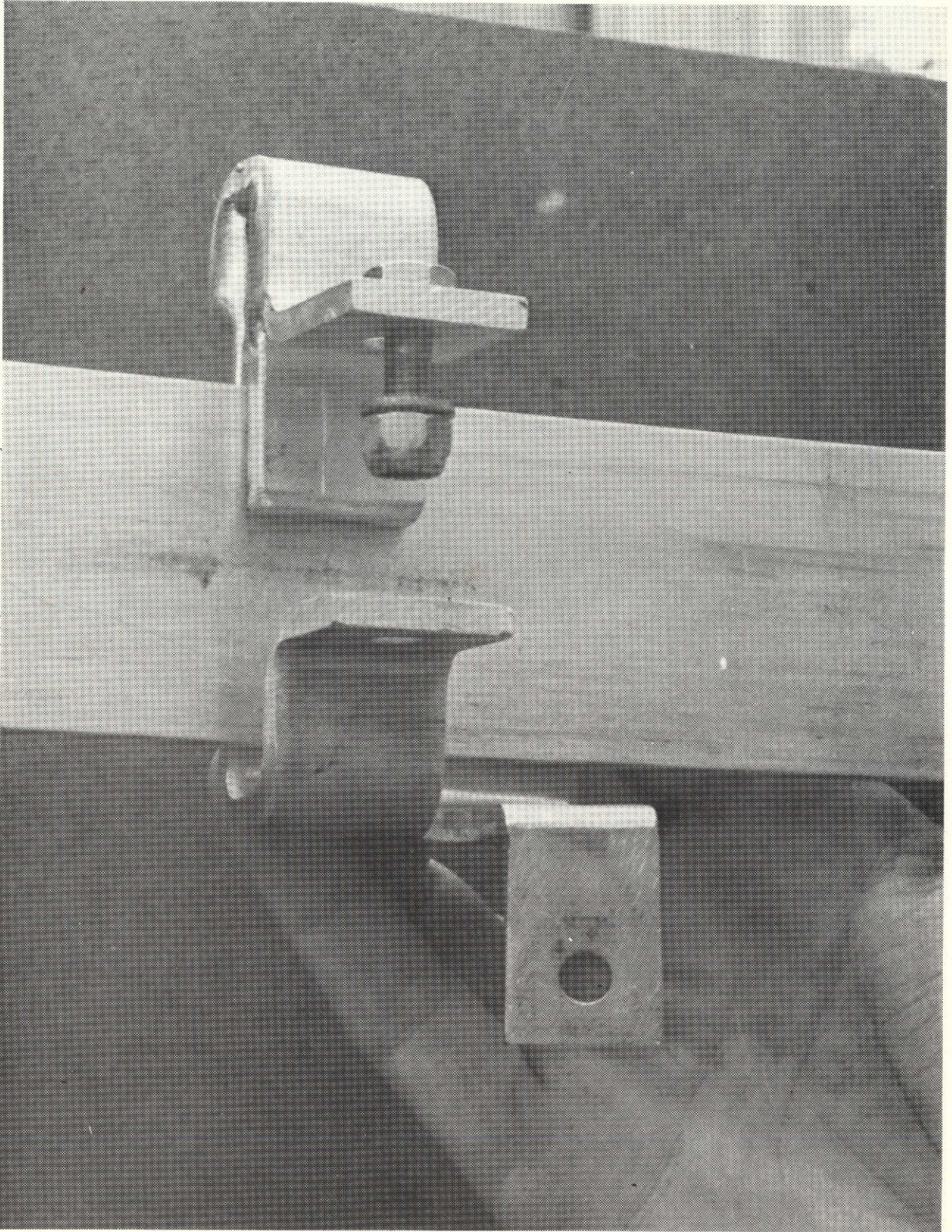
Figure G-2. Cross Area Details
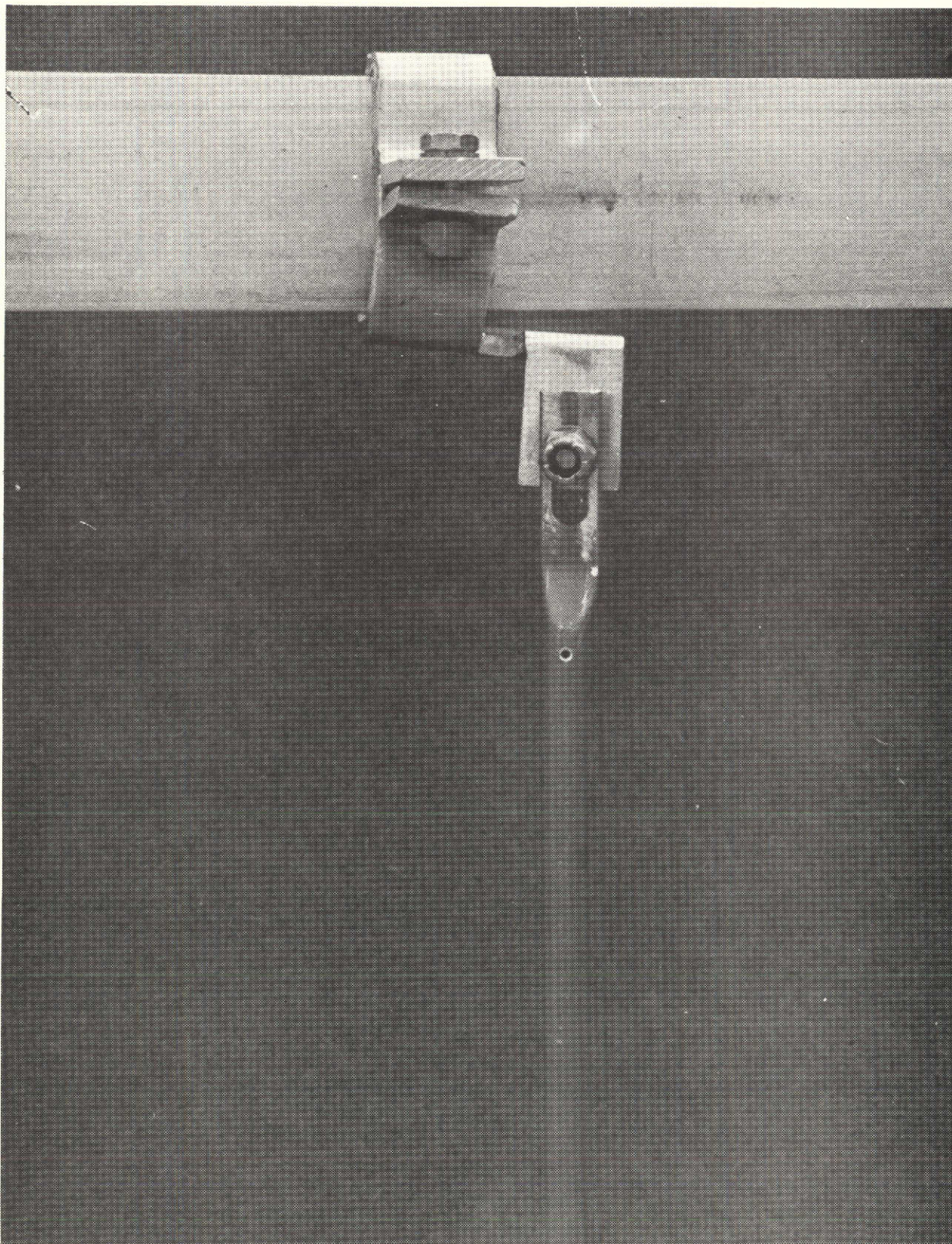
Figure G-3. Tank Ring Support Attachment Brackets

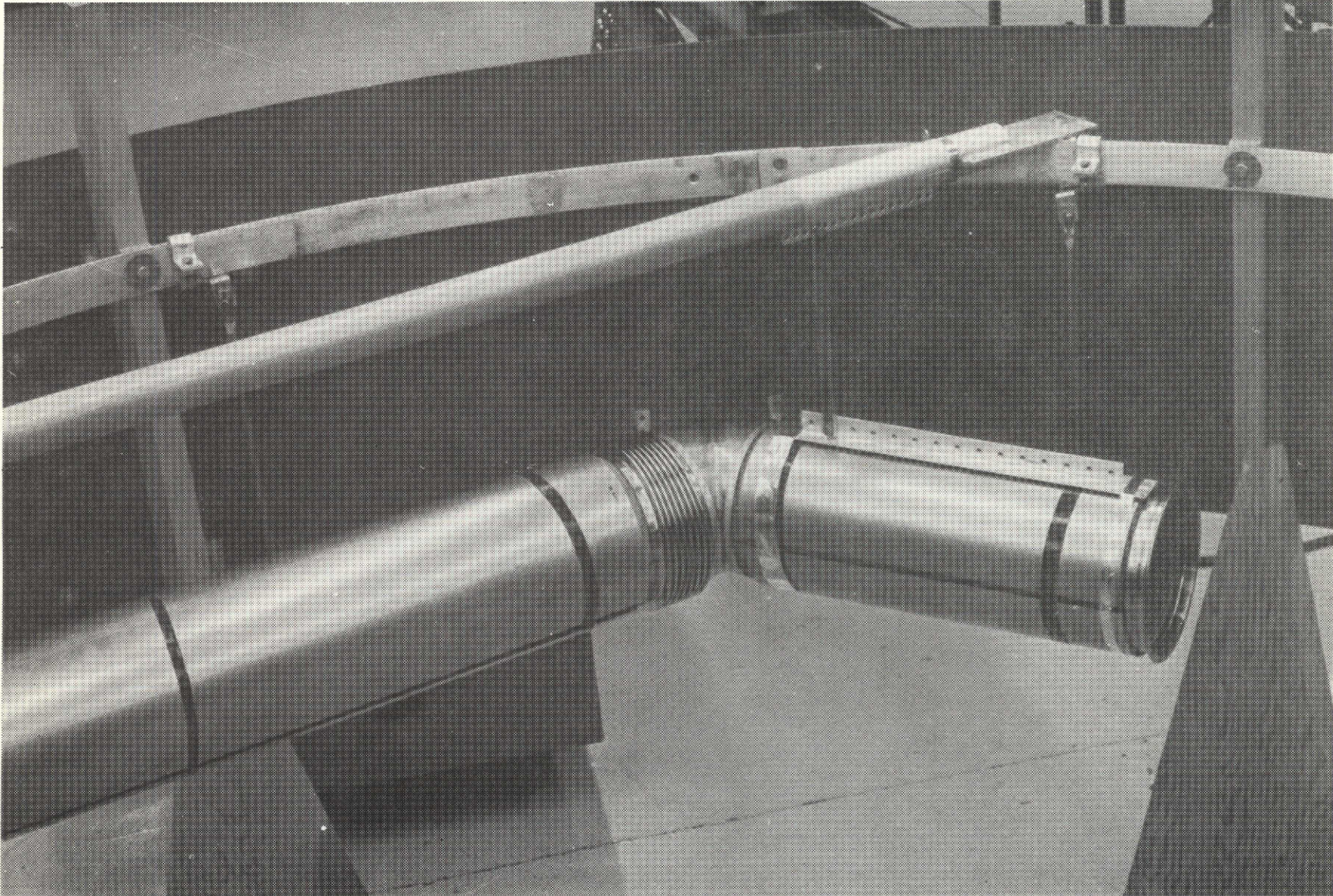Figure G-4. Attachment of Support Rod to Ring Bracket

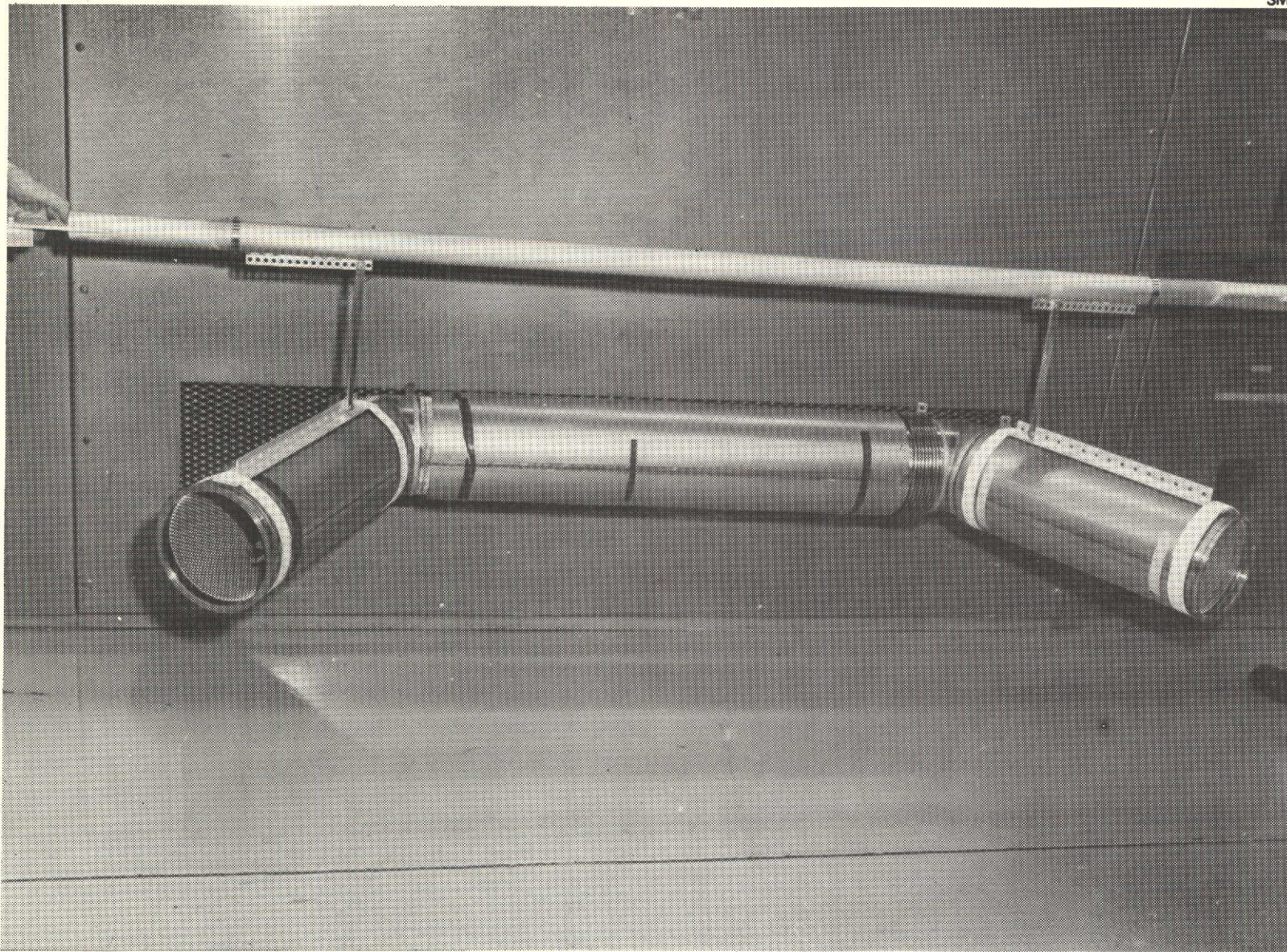Figure G-5. Installation of Support Brackets to Channel

Figure G-6. Balancing of Channel Sections on Support Pad

F.   -3 INSTALLATION

The two 1T44516-5 ring components are taken into the tank and suspended from the handling aids. Both ends of this component need to be carried because of the bellows segment. The vertical legs on the aids are of such a length that the ring lies midway between the two stabilizing rings within the tank. Figure 8 shows one of the -3 components as it should appear within the tank. The ends of the protective bags should be out away at this time.

G.   -5 INSTALLATION

The ends of the bag on the 1T44516-5 component should be removed and a Creavey seal (AS300-7.360) placed in the gland on either end. -5 is taken into the tank and joined to the two -3 components. V-bands secure the joints once the -5 component has been leveled. The torque value for the T-bolts is stamped onto the V-band.

H.   -7 INSTALLATION

1T44516-7 is treated the same as -5. Small misalignments in making the final joint can be accommodated by the action of the two bellows and flexure of the screen material. The telescoping aids can be slid along the stabilizing ring to place the ring in the proper orientation with respect to the tank center-line and outlet. Figure 9 shows the complete ring suspended from the two handling aids.

I.   BRACE PLACEMENT

The twelve brackets on the stabilizing ring can be moved as required so that the lower end of each 1T44535 brace can be joined to a corresponding 1T44543 clamp on the acquisition ring (using a one-inch long 1/4-24 machine screw). Figure 10 illustrates the orientation of the braces. When all the braces have been tightened the telescoping handling aids and the tee shaped brackets on the -3 components can be removed and taken out of the tank.

J.   -11 INSTALLATION

The short 1T44516-11 segment can now be joined to the top leg of the -7 component. Figure 11 shows the complete acquisition ring with -11 in place.

K.   COVER REMOVAL

The final step in the installation is to remove the protective covers by loosening the tape and slowly and carefully lifting off the foam lined aluminum covers. This step should be delayed as long as possible.
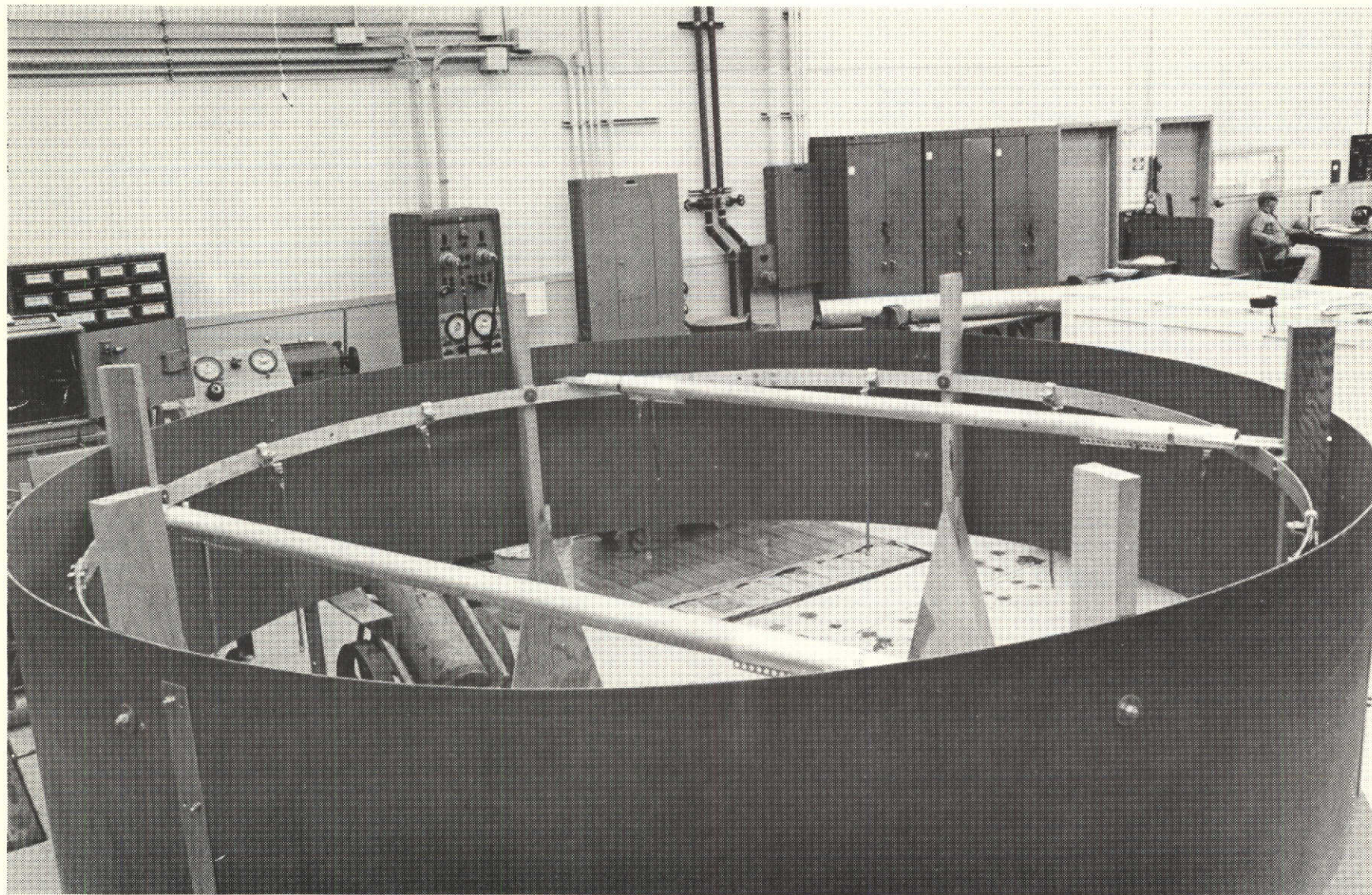
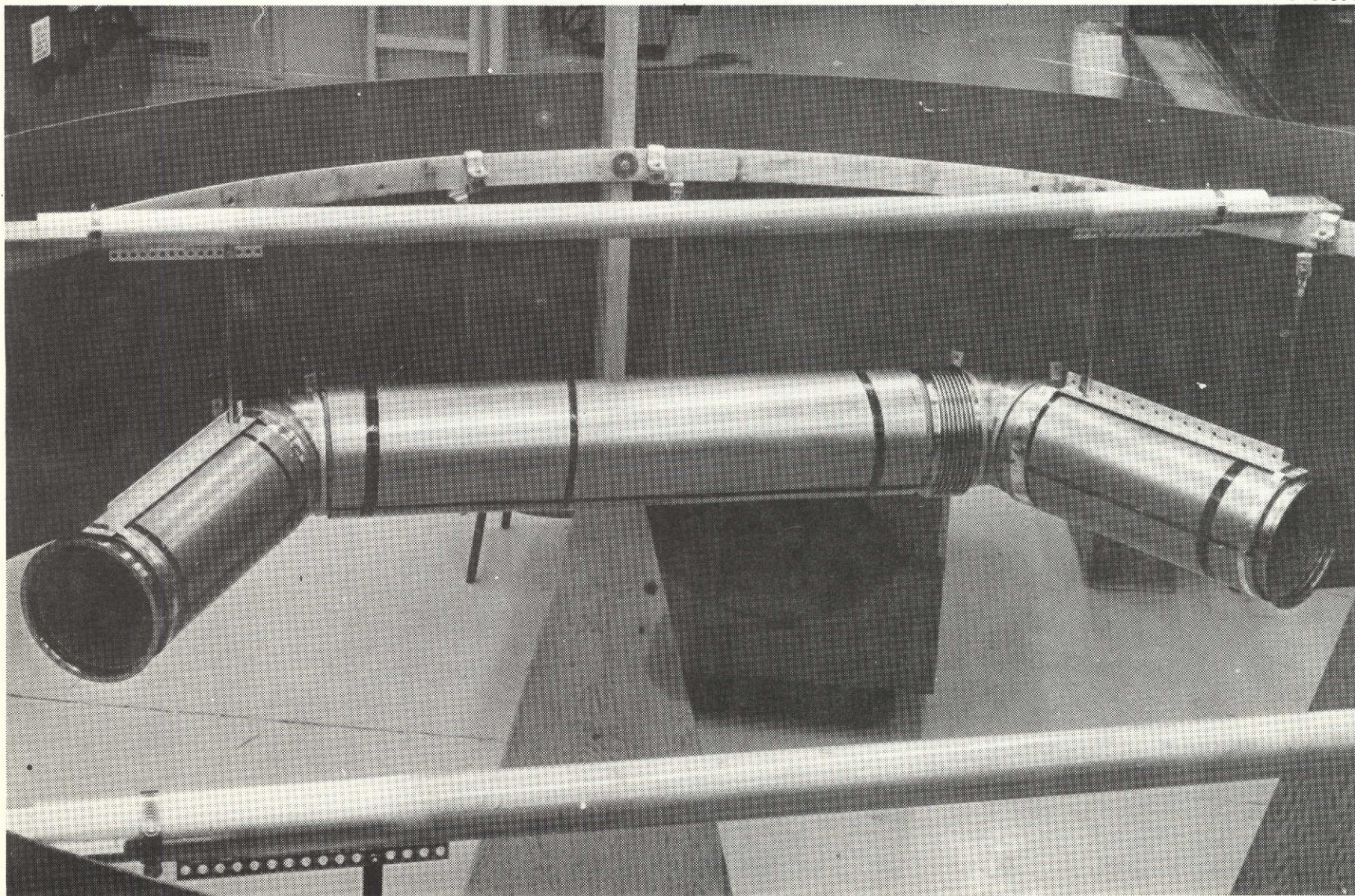Figure G-7. Installation of In-Tank Handling Aids

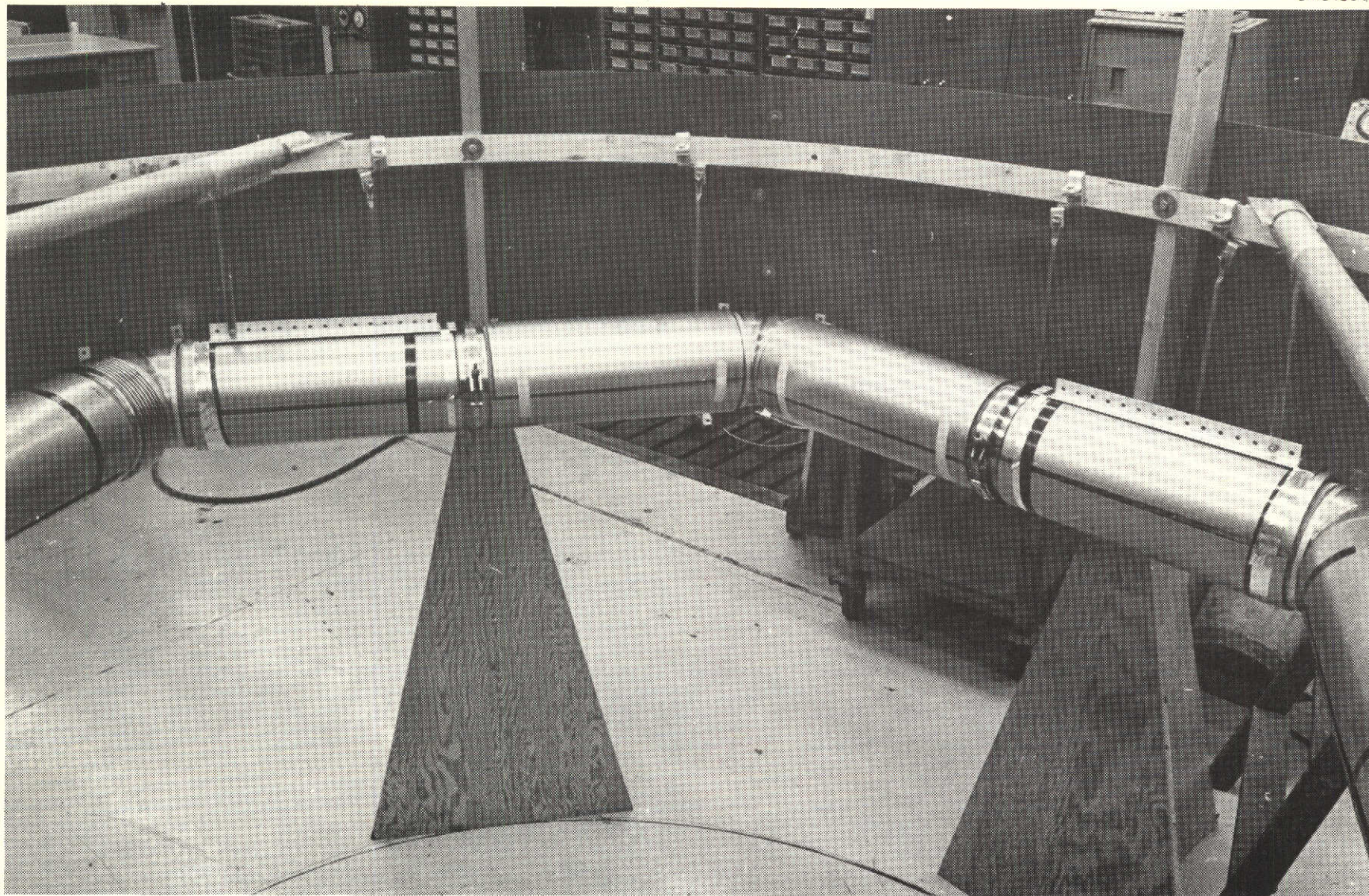Figure G-8. Initial Hanging of Primary Channel

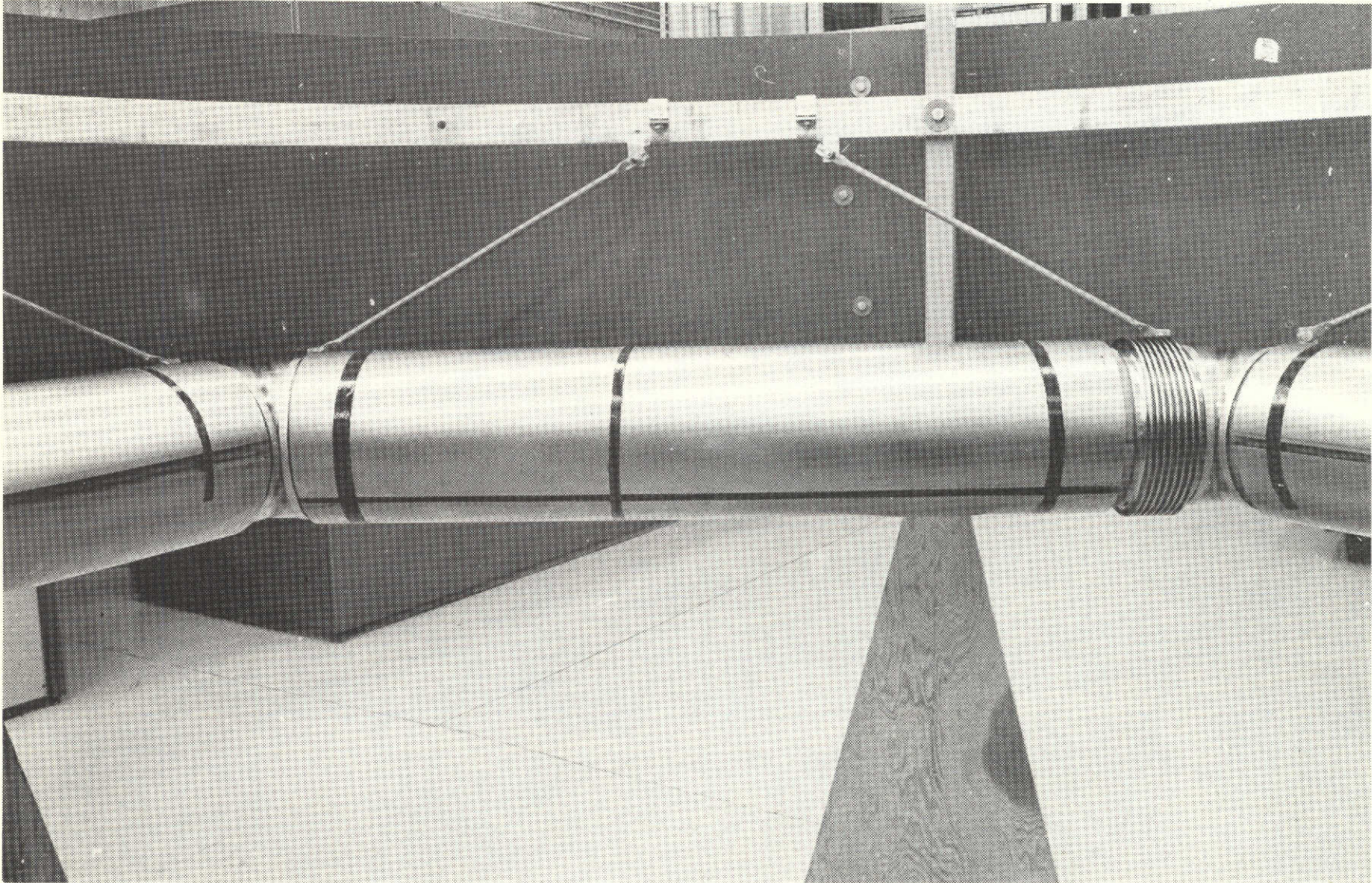Figure G-9. Primary Channel Clamp Installation

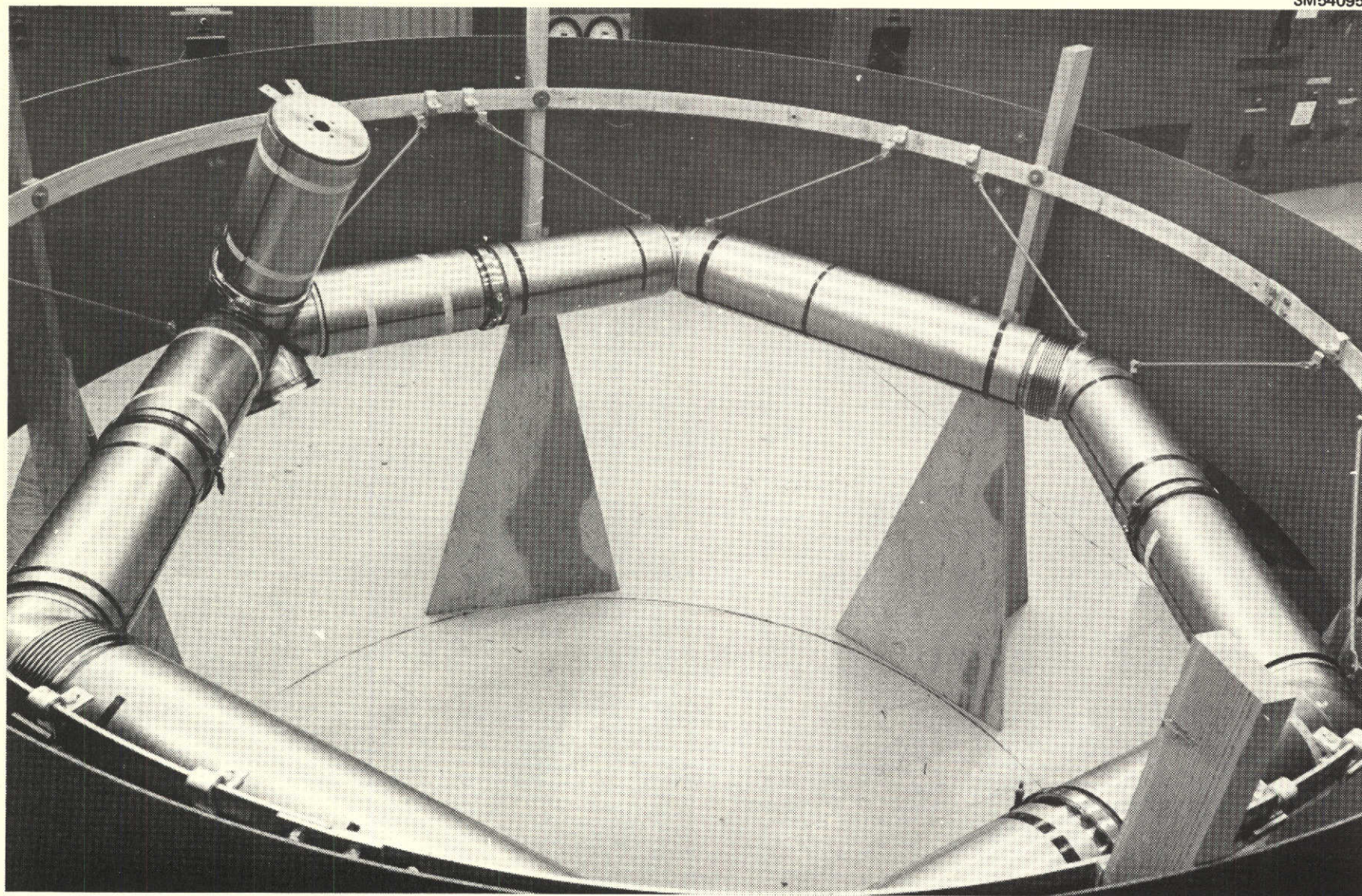Figure G-10. Support Rod Installation

Figure G-11. Completed Installation Including Protection Covers

REFERENCES

1. "Space Shuttle High Pressure Auxiliary Propulsion Subsystem Definition Study," Contract NAS8-26248, Subtask B Report, MDC E0298, February 1971.

2. Baseline Tug Definition Document Rev. A—Preliminary Design Office, Program Development. NASA-MSFC, June 26, 1972.

3. DOD Upper Stage/Shuttle System Preliminary Requirements Study. SAMSO-TR-72-202, MDAC Final Contract Report, August 1972.

4. J. C. Armour and J. N. Cannon, "Fluid Flow Through Woven Screens," AIChE Journal, May 1968, pp 415-420.

5. "Low Gravity Propellant Control Using Capillary Devices in Large Scale Cryogen Devices—Related IRAD Studies," General Dynamics GDC-DDB70-009, August 1970.

6. J. N. Castle, "Heat Transfer Effects or Bubble Point Tests in Liquid Nitrogen," MDAC MDC G-2653, January 1972.

7. Letter in Reply to 71RC7134 by Rocketdyne, Division of North American Rockwell Corporation, 27 September 1971.

8. J. Parmakian, "Waterhammer Analysis," Dover Publications, 1963.

9. G. W. Burge, "System Effects on Propellant Storability and Vehicle Performance," DAC Report 59314 (AFRPL TR-66-254), October 1966.

10. J. N. Castle, "Preliminary Experimental Evaluation in LH_2 of a Screen Surface Tension Acquisition Device," McDonnell Douglas Report MDC G2452, August 1971.

11. J. N. Castle, Performance Testing of an Integrated Liquid Hydrogen Storage, Acquisition, and Vent System, MDC G3092, June 1972.

12. Space Shuttle Isogrid Tank Buckling Test Volume 1, Design and Analysis, NAS8-26016, February 1972 McDonnell Douglas Report MDC

13. G. W. Burge, System Effects on Propellant Storability and Vehicle Performance—Supplemental Technical Report AFRPL-TR-68-277 (DAC 63061), December 1968.

14. W. J. Wachtler and J. Tobolski, "Pressure Sensing and Control Development for Pressurization and Venting Systems," Final Report, Contract NAS3-13310, MDAC MDC G0933, NASA CR 72748.

15. J. A. Start and M. H. Blatt, "Cryogenic Zero-Gravity Prototype Vent System," GD/C Report GDC-DDB67-006, October 1967.

16. W. H. Sterbentz, "Liquid Propellant Thermal Conditioning System," LMSC Report LMSC-A839783, (NAS CR-72113), April 1967.

17. "Passive Retention/Expulsion Methods for Subcritical Storage of Cryogens," Final Report, Martin Marietta Corporation, Denver, Colorado, March 1971.

18. D. R. Krause, Development of Lightweight Material Composites to Insulate Cryogenic Tanks for 30-Day Storage in Outer Space, Second Quarterly Report, Contract NAS8-26006, McDonnell Douglas Astronautics Report No. MDC G0775, December 1970.

19. Investigation of High Performance Insulation Application Problems, Final Report, MDC G4722, August 1973.

20. Space LOX Vent System, 2nd Quarterly Report, GDC 632-1-17, December 1971.

21. Study of a Combined External Insulation System Consisting of a Klegecall Foam Covered by MLI CEC/SES/FM/BF/CM/CP/21-860 L'air Liquide (France), July 1972.

22. "Lightweight Evacuated Multilayer Insulation Systems for the Space Shuttle Vehicle," Quarterly Technical Progress Report No. 2, Contract NAS 3-14369, Boeing Report, October 1, 1971.

23. D. W. Murphy et al, Vent-Free Fluorine Feed System, Martin Marietta Corp., MCR-67-415, Vol. I, AFRPL-TR-67-323, March 1968.

24. D. W. Murphy et al, Vent-Free Fluorine Feed System, Martin Marietta Corp., MCR-67-416, Vol. II, June 1968.

25. "Low Gravity Propellant Control Using Capillary Devices in Large Cryogenic Vehicles," Final Report, Contract NAS8-21465, Report No. GDCD DB7D-008, August 1970.

26. L. J. Poth et al, "A Study of Cryogenic Propellant Stratification Reduction Techniques," GD/FW FZA-419-1, NAS8-20330, September 15, 1967.

27. J. C. Chen, A Correlation for Boiling Heat Transfer to Saturated Fluids in Convective Flow, ASME Paper 63-HT-34, 1963.

28. B. R. Heckman, Bubble Point Characteristics of Multi-Layer Screen Elements, MDAC Report MDC G2656, December 1971.

29. Space Tug Point Design Study, Vol. II, Report MDC G2818, February 1972.

30. Analytical Approaches for the Design of Orbital Refueling Systems, G. W. Burge, J. B. Blackmon, and R. A. Madsen, AIAA Paper No. 69-567.

31. Propellant Settling, J. B. Blackmon, J. N. Castle, and B. R. Heckma Douglas Report No. DAC-62263, May 1968.

32. Low-Gravity Reorientation in a Scale-Model Centaur Liquid-Hydrogen Tank, J. A. Salzman, W. J. Masica, and R. F. Lacovic, NASA TN D-7168, February 1973.